

**$\pi$ -Complex Behavior in  
Catalyst-Transfer  
Condensation Polymerizations**

by

Peter Keith Goldberg

A dissertation submitted in partial fulfillment  
of the requirements for the degree of  
Doctor of Philosophy  
(Chemistry)  
in the University of Michigan  
2017

Doctoral Committee:

Professor Anne J. McNeil, Chair  
Professor Jinsang Kim  
Professor Adam J. Matzger  
Assistant Professor Paul Zimmerman

“This life is nothing short of an invocation lightning bolt of sensual synchronicity. Intuition is the growth of stardust, and of us. By condensing, we reflect. We must empower ourselves and strengthen others.”

- **Seb Pearce**

Peter Keith Goldberg

[pkgold@umich.edu](mailto:pkgold@umich.edu)

ORCID iD: 0000-0003-0655-6766

© Peter Keith Goldberg 2017

## **Dedication**

To my wife, family, and friends for offering advice, encouragement, and support.

## Acknowledgements

This thesis is the culmination of many years of personal and intellectual training. I am deeply indebted to all the educators, coaches, family, friends, and colleagues that have invested their time in me throughout the years. I would like to thank my advisor, Dr. Anne McNeil, for encouraging me to pursue my passions during graduate school and cultivating an attention to detail that I will carry with me into my next adventure. Thanks to my committee members and collaborators, who have heard about my work too many times but continue to provide feedback and help me improve.

My efforts were enabled by all the McNeil lab members that came before me, and especially those that worked alongside me. I must thank Dr. Jonas Locke, Yash Adhia, Dr. Jing Chen, Dr. Cheryl Moy, Dr. Ed Palermo, Dr. Kelsey Carter, Dr. Zack Bryan, Dr. Danielle Zurcher, Dr. Mitchell Smith, Dr. Ariana Hall, Kendra Souther, Amanda Leone, Dr. Gesine Veits, and Dr. Chen Kong. This lab has been a great place to learn, and my mentees Xinyu Liu, Jacob Lueck, Aryeh Blumenreich, and Matthew Bagazinski challenged me to learn in an entirely new way.

Taylor Tinkham has been my inspiration, support, baker/cook, girlfriend/fiancé/wife, and everything in between during my time here at Michigan. Not a single letter of this thesis could have been typed without you. My family has been a source of unrelenting and unconditional support, and they compel me to keep moving forward.

I have had my share of valuable experiences at the University of Michigan, enabled by many great people and in some great organizations. For brevity, I acknowledge the substantial impact of the following organizations and groups: RELATE, CPDO, CALC|UM, CSEI|UM, Rackham GSS, FEMMES, all the chemistry staff (office, building, and technical), chemistry janitorial staff, and the Matzger group.

## Table of Contents

Dedication	ii
Acknowledgements	iii
List of Figures	v
List of Tables	xiv
List of Schemes	xviii
List of Charts	xx
List of Appendices	xxi
Abstract	xxii
<b>Chapter 1.</b> Introduction	1
<b>Chapter 2.</b> Long-distance catalyst migration across poly(3-alkylthiophene)	26
<b>Chapter 3.</b> Catalyst-dependent migration in polyphenylene synthesis	49
<b>Chapter 4.</b> Optimizing NHC-precatalysts for end-functionalized (co)polymers	75
<b>Chapter 5.</b> Conclusions and future directions	98
<b>Appendices.</b>	109

## List of Figures

**Figure 1-1.** Phase evolution and charge generation/transport of a bulk-heterojunction solar cell with heating/extended use. 2

**Figure 1-2.** Chemical structures and optical microscope images of a poly(3-hexylthiophene)/PC<sub>61</sub>BM blend after annealing at 150 °C with (A) no (control), (B) 5 wt %, or (C) 10 wt % of a gradient copolymer additive. The scale bar represents 25 μm. 3

**Figure 2-1.** Mass spectrum of **P3DT** produced by **4a** after end-capping with **2** (15 equiv) and **3** (30 equiv). Migration (cap/cap, **—**) and dissociation (cap/Br, **—**) product peaks are highlighted from all other masses (**—**). Insets (right) show **P3DT** end-groups at DP = 34 (top) and DP = 52 (bottom). 35

**Figure 2-2.** MALDI-TOF mass spectra of **P3DT** produced by **4c** post end-capping with **2** (15 equiv) and **3** (30 equiv). Migration (cap/cap, **—**) and dissociation (cap/Br, **—**) product peaks are highlighted from all other masses (**—**). Insets (right) show **P3DT** end-groups at DP = 34 (top) and DP = 52 (bottom). 37

**Figure 2-3.** Mass spectrum of **P3DT** produced by **4d** after end-capping with **2** (15 equiv) and **3** (30 equiv). Migration (cap/cap, **—**) and dissociation (cap/Br, **—**) product peaks are highlighted from all other masses (**—**). Insets (right) show **P3DT** end-groups at DP = 34 (top) and DP = 52 (bottom). 39

**Figure 2-4.** Migration percent at each DP for precatalysts **4a–4d** tested in the end-capping model system. The migration pathway was calculated from peak areas of the cap/cap and cap/Br peaks (at each DP) determined by MALDI-TOF MS (Appendix 1). 41

**Figure 2-5.** (A) Cumulative distribution function for a random walk on a polymer with DP = 14 with guiding lines (**—**) drawn at 95% migration product (2,204 steps, **◆**). (B) The number of steps calculated from the cumulative distribution function are plotted versus DP (**◆**). A quadratic fit ( $r^2 = 1.0000$ , **—**) is used to extrapolate the # of steps due to the high computational workload required at high DP. 42

**Figure 3-1.** MALDI-TOF mass spectra of **P1** produced by **4a** after end-capping with **3a** (15 equiv) and **3b** (50 equiv). Migration (cap/cap, **—**) and dissociation (cap/Br, **—**) product peaks are highlighted from all other masses (**—**). Insets (right) show **P1** end-groups at DP = 3 (top) and DP = 7 (bottom). 55

**Figure 3-2.** MALDI-TOF mass spectra of **P1** produced by **4b** after end-capping with **3a** (15 equiv) and **3b** (50 equiv). Migration (cap/cap, **—**) and dissociation (cap/Br, **—**) product peaks are

highlighted from all other masses (—). Insets (right) show **P1** end-groups at DP = 3 (top) and DP = 7 (bottom). 56

**Figure 3-3.** MALDI-TOF mass spectra of **P1** produced by **4c** after end-capping with **3a** (15 equiv) and **3b** (50 equiv). Migration (cap/cap, —) and dissociation (cap/Br, —) product peaks are highlighted from all other masses (—). Insets (right) show **P1** end-groups at DP = 18 (top) and DP = 33 (bottom). 58

**Figure 3-4.** MALDI-TOF mass spectra of **P1** produced by **4d** after end-capping with **3a** (15 equiv) and **3b** (50 equiv). Migration (cap/cap, —) and dissociation (cap/Br, —) product peaks are highlighted from all other masses (—). Insets (right) show **P1** end-groups at DP = 7 (top) and DP = 18 (bottom). 59

**Figure 3-5.** MALDI-TOF mass spectra of **P1** produced by **4e** after end-capping with **3a** (15 equiv) and **3b** (50 equiv). Migration (cap/cap, —) and dissociation (cap/Br, —) product peaks are highlighted from all other masses (—). Insets (right) show **P1** end-groups at DP = 7 (top) and DP = 18 (bottom). 61

**Figure 3-6.** Migration pathway percent calculated at each DP for precatalysts **4a–d** across **P1** in the end-capping model experiments. Migration pathway percent was calculated from peak areas determined by MALDI-TOF MS. Error bars represent one standard deviation. 62

**Figure 3-7.** Catalyst-polymer  $\pi$ -complex between a polymer with a DP of 4 and a capping agent at the  $\omega$  end (left) with the catalyst at location 2. The cumulative distribution function (right) depicts how the probability of the catalyst reaching position 10 (i.e., the migration pathway) increases with an increasing number of steps (for detailed explanation of the calculation, see Appendix 2). 63

**Figure 3-8.** (A) Experimental values for the migration pathway are plotted against molecular weight/DP for **4d** (●) and statistical calculations (◆) at 520 steps. (B) Plots of cumulative distribution function for DP = 7, 9, 11, 13, 15, and 17 for 0–700 steps are overlaid with the end-capping data [plotted in (A)] from **4d** (●) and the statistical calculations points (◆). A reference line at 520 steps (---) is provided to illustrate the experimental deviation from the random-walking calculation. (C) Logistic function fit to migration percent across DP = 5–18 for **4d**. 65

**Figure 4-1.** GPC chromatogram of (A) **P2** catalyzed by **5a** (—), **5b** (—), or **5c** (—) or (B) **P1** catalyzed by **5a** using 57 (—) or 25 (—) equiv of **1** relative to **5a**. 84

**Figure 4-2.** GPC chromatogram and scheme of **P2** produced by **6b** with 0 equiv (—), 0.5 equiv (—), 1 equiv (—), or 2 equiv (—) of 3-chloropyridine (relative to precatalyst). 86

**Figure 4-3.** MALDI-TOF mass spectrum of **P2** produced by **6b** with 1 equiv of 3-chloropyridine. Inset shows a zoomed in view at DP = 73 with cinnamyl/H (83% area ratio) and H/H (17 % area ratio) end-groups. 88

**Figure 4-4.** GPC chromatogram of **P2** produced by **6b** with (A) 65 equiv of **2** without LiCl (—) or with 1.0 equiv LiCl (—). (B) 18 equiv of **2** with 0 equiv LiCl (—), 0.33 equiv LiCl (—),



0.66 equiv LiCl (—), or 1.0 equiv LiCl (—). Equiv LiCl is relative to *i*PrMgCl used to generate **2**. 89

**Figure 5-1.** Multi-aryl monomers could be used to block coordination to groups (like vinyl) that are perform poorly in CTCP. 102

**Figure A1-1.** <sup>1</sup>H and <sup>13</sup>C NMR spectra for **S1**. 115

**Figure A1-2.** Average percent conversion of **3** (■), and 2-bromo-3-hexylthiophene (■) in cross-coupling competition experiments with **2** sorted by precatalyst. Error bars represent one standard deviation. 117

**Figure A1-3.** GPC chromatogram (prior to precipitation) of **P3DT** produced by **4a** with 0 (—) or 30 equiv (—) of **3**. 120

**Figure A1-4.** GPC chromatogram (prior to precipitation) of **P3DT** produced by **4b** with 0 (—) or 30 equiv (—) of **3**. 121

**Figure A1-5.** GPC chromatogram (prior to precipitation) of **P3DT** produced by **4c** with 0 (—) or 30 equiv (—) of **3**. 122

**Figure A1-6.** GPC chromatogram (prior to precipitation) of **P3DT** produced by **4d** with 0 (—) or 30 equiv (—) of **3**. 123

**Figure A1-7.** GPC chromatogram (prior to precipitation) of **P3DT** produced by **4e** with 0 (—) or 30 equiv (—) of **3**. 124

**Figure A1-8.** GPC chromatogram of **P3DT** produced by **4a** pre (—) or post (—) end-capping with **2** (15 equiv) and **3** (30 equiv). 128

**Figure A1-9.** MALDI-TOF mass spectra of **P3DT** produced by **4a** pre end-capping (—). Insets (right) show **P3DT** end-groups at DP = 34 (top) and DP = 52 (bottom). 129

**Figure A1-10.** MALDI-TOF mass spectra of **P3DT** produced by **4a** post end-capping with **2** (15 equiv) and **3** (30 equiv). Migration (cap/cap, —) and dissociation (cap/Br, —) product peaks are highlighted from all other masses (—). Insets (right) show **P3DT** end-groups at DP = 34 (top) and DP = 52 (bottom). 130

**Figure A1-11.** GPC chromatogram of **P3DT** produced by **4b** pre (—) or post (—) end-capping with **2** (15 equiv) and **3** (30 equiv). 132

**Figure A1-12.** MALDI-TOF mass spectra of **P3DT** produced by **4b** pre end-capping (—). Insets (right) show **P3DT** end-groups at DP = 34 (top) and DP = 43 (bottom). 133

**Figure A1-13.** MALDI-TOF mass spectra of **P3DT** produced by **4b** post end-capping with **2** (15 equiv) and **3** (30 equiv). Migration (cap/cap, —) and dissociation (cap/Br, —) product peaks are highlighted from all other masses (—). Insets (right) show **P3DT** end-groups at DP = 34 (top) and DP = 43 (bottom). 134

**Figure A1-14.** GPC chromatogram of **P3DT** produced by **4c** pre (—) or post (—) end-capping with **2** (15 equiv) and **3** (30 equiv). 137

**Figure A1-15.** MALDI-TOF mass spectra of **P3DT** produced by **4c** pre end-capping (—). Insets (right) show **P3DT** end-groups at DP = 34 (top) and DP = 52 (bottom). 138

**Figure A1-16.** MALDI-TOF mass spectra of **P3DT** produced by **4c** post end-capping with **2** (15 equiv) and **3** (30 equiv). Migration (cap/cap, —) and dissociation (cap/Br, —) product peaks are highlighted from all other masses (—). Insets (right) show **P3DT** end-groups at DP = 34 (top) and DP = 52 (bottom). 139

**Figure A1-17.** GPC chromatogram of **P3DT** produced **4d** pre (—) or post (—) end-capping with **2** (15 equiv) and **3** (30 equiv). 141

**Figure A1-18.** MALDI-TOF mass spectra of **P3DT** produced by **4d** pre end-capping (—). Insets (right) show **P3DT** end-groups at DP = 34 (top) and DP = 52 (bottom). 142

**Figure A1-19.** MALDI-TOF mass spectra of **P3DT** from end-capping model system using **4d**. Migration (cap/cap, —) and dissociation (cap/Br, —) product peaks are highlighted from all other masses (—). Insets (right) show **P3DT** end-groups at DP = 34 (top) and DP = 52 (bottom). 143

**Figure A1-20.** GPC chromatogram of **P3DT** produced **4e** pre (—) or post (—) end-capping with **2** (15 equiv) and **3** (30 equiv). 145

**Figure A1-21.** MALDI-TOF mass spectra of **P3DT** produced by **4e** pre end-capping (—). Insets (right) show **P3DT** end-groups at DP = 25 (top) and DP = 34 (bottom). 146

**Figure A1-22.** MALDI-TOF mass spectra of **P3DT** from end-capping model system using **4e**. Migration (cap/cap, —) and dissociation (cap/Br, —) product peaks are highlighted from all other masses (—). Insets (right) show **P3DT** end-groups at DP = 25 (top) and DP = 34 (bottom). 147

**Figure A1-23.** Migration percent at each DP for catalysts **4a–4e** tested in the end-capping experiments. Migration pathway was calculated from peak areas of the cap/cap and cap/Br peaks (at each DP) determined by MALDI-TOF MS. 150

**Figure A1-24.** Numerical representation of catalyst binding to the cap of **P3DT** (DP = 4) with cap/Br end-groups for use in the random-walking calculations. Zeroes represent unoccupied  $\pi$ -binding sites, while a one identifies the catalyst location in the position matrix. 151

**Figure A1-25.** Plot of the probability distribution function of the *first passage distribution* for a purely random walk across 10 locations (corresponding to a DP of 4). 153

**Figure A1-26.** Plot of the cumulative distribution function of the *first passage distribution* for a purely random walk across 10 locations (corresponding to a DP of 4). 153

**Figure A1-27.** The number of steps calculated from the cumulative distribution functions are plotted versus DP (◆). A quadratic fit (—,  $r^2 = 1.0000$ , (# of steps =  $-0.5874 \times \text{DP}^2 + 10.7004 \times$

DP + 10.4878) is used to extrapolate the number of steps due to the high computational workload required at high DP. <sup>a</sup>Steps were calculated from the quadratic fit. 154

**Figure A1-28.** Plot of the cumulative distribution function of the *first passage distribution* for a purely random walk across 10 locations (corresponding to a DP of 4). The number of steps required to match 80% migration is 118. 155

**Figure A2-1.** <sup>1</sup>H and <sup>13</sup>C NMR spectra for **S1**. 164

**Figure A2-2.** <sup>1</sup>H and <sup>13</sup>C NMR spectra for **S2**. 165

**Figure A2-3.** Percent conversion of **3b** (■), and 2-bromo-1,4-bis(methoxy)phenylene (■) in cross-coupling competition experiments with **3a** sorted by catalyst. 167

**Figure A2-4.** GPC chromatogram of **P1** produced by **4a** pre (—) or post (—) end-capping with **3a** (15 equiv) and **3b** (50 equiv). 170

**Figure A2-5.** MALDI-TOF mass spectra of **P1** produced by **4a** before end-capping. Insets (right) show **P1** end-groups at DP = 3 (top) and DP = 7 (bottom). 171

**Figure A2-6.** MALDI-TOF mass spectra of **P1** produced by **4a** after end-capping with **3a** (15 equiv) and **3b** (50 equiv). Migration (cap/cap, —) and dissociation (cap/Br, —) product peaks are highlighted from all other masses (—). Insets (right) show **P1** end-groups at DP = 3 (top) and DP = 7 (bottom). 172

**Figure A2-7.** GPC chromatogram of **P1** produced by **4b** pre (—) or post (—) end-capping with **3a** (15 equiv) and **3b** (50 equiv). 173

**Figure A2-8.** MALDI-TOF mass spectra of **P1** produced by **4b** before end-capping. Insets (right) show **P1** end-groups at DP = 3 (top) and DP = 7 (bottom). 174

**Figure A2-9.** MALDI-TOF mass spectra of **P1** produced by **4b** after end-capping with **3a** (15 equiv) and **3b** (50 equiv). Migration (cap/cap, —) and dissociation (cap/Br, —) product peaks are highlighted from all other masses (—). Insets (right) show **P1** end-groups at DP = 3 (top) and DP = 7 (bottom). 175

**Figure A2-10.** GPC chromatogram of **P1** produced by **4c** pre (—) or post (—) end-capping with **3a** (15 equiv) and **3b** (50 equiv). 177

**Figure A2-11.** MALDI-TOF mass spectra of **P1** produced by **4c** before end-capping. Insets (right) show **P1** end-groups at DP = 18 (top) and DP = 33 (bottom). 178

**Figure A2-12.** MALDI-TOF mass spectra of **P1** produced by **4c** after end-capping with **3a** (15 equiv) and **3b** (50 equiv). Migration (cap/cap, —) and dissociation (cap/Br, —) product peaks are highlighted from all other masses (—). Insets (right) show **P1** end-groups at DP = 18 (top) and DP = 33 (bottom). 179

**Figure A2-13.** GPC chromatogram of **P1** produced **4d** pre (—) or post (—) end-capping with **3a** (15 equiv) and **3b** (50 equiv). 181

**Figure A2-14.** MALDI-TOF mass spectra of **P1** produced by **4d** before end-capping. Insets (right) show **P1** end-groups at DP = 7 (top) and DP = 18 (bottom). 182

**Figure A2-15.** MALDI-TOF mass spectra of **P1** produced by **4d** after end-capping with **3a** (15 equiv) and **3b** (50 equiv). Migration (cap/cap, —) and dissociation (cap/Br, —) product peaks are highlighted from all other masses (—). Insets (right) show **P1** end-groups at DP = 7 (top) and DP = 18 (bottom). 183

**Figure A2-16.** GPC chromatogram of **P1** produced **4e** pre (—) or post (—) end-capping with **3a** (15 equiv) and **3b** (50 equiv). 185

**Figure A2-17.** MALDI-TOF mass spectra of **P1** produced by **4e** before end-capping. Insets (right) show **P1** end-groups at DP = 7 (top) and DP = 18 (bottom). 186

**Figure A2-18.** MALDI-TOF mass spectra of **P1** produced by **4e** after end-capping with **3a** (15 equiv) and **3b** (50 equiv). Migration (cap/cap, —) and dissociation (cap/Br, —) product peaks are highlighted from all other masses (—). Insets (right) show **P1** end-groups at DP = 7 (top) and DP = 18 (bottom). 187

**Figure A2-19.** Migration pathway percent calculated at each DP for precatalysts **4a–e** across **P1** in the end-capping model experiments. Migration pathway percent was calculated from peak areas determined by MALDI-TOF MS. Error bars represent one standard deviation. 190

**Figure A2-20.** Numerical representation of catalyst binding to the cap of **P1** (DP = 4) with cap/Br end-groups for use in the random-walking calculations. Zeroes represent unoccupied  $\pi$ -binding sites, while a one identifies the catalyst location in the position matrix. 191

**Figure A2-21.** Plot of the probability distribution function of the *first passage distribution* for a purely random walk across 10 locations (corresponding to a DP of 4). 193

**Figure A2-22.** Plot of the cumulative distribution function of the *first passage distribution* for a purely random walk across 10 locations (corresponding to a DP of 4). 193

**Figure A2-23.** Plot of the cumulative distribution function of the *first passage distribution* for a purely random walk across 10 locations (corresponding to a DP of 4). The number of steps required to match 80% migration is 118. 194

**Figure A2-24.** (A) Experimental values for the migration pathway are plotted against molecular weight/DP for **4d** (●) and statistical calculations (◆) at 520 steps. (B) Plots of cumulative distribution function for DP = 7, 9, 11, 13, 15, and 17 for 0–700 steps are overlaid with the end-capping data [plotted in (A)] from **4d** (●) and the statistical calculations points (◆). A reference line at 520 steps (---) is provided to illustrate the experimental deviation from the random-walking calculation. (C) Logistic function fit to migration percent across DP = 5–18 for **4d**. 196

<b>Figure A2-25.</b> Experimental values for the migration pathway are plotted against molecular weight/DP for <b>4d</b> (●) and statistical calculations for a purely random walk (520 steps, ◆) or a random walk that is biased towards the cap ( $C = 3$ ) and neutral to phenylene-Br ( $B = 2$ ) (816 steps, ▼).	198
<b>Figure A3-1.</b> $^1\text{H}$ and $^{13}\text{C}$ NMR spectra for <b>S1</b> .	214
<b>Figure A3-2.</b> $^1\text{H}$ and $^{13}\text{C}$ NMR spectra for <b>S2</b> .	215
<b>Figure A3-3.</b> $^1\text{H}$ and $^{13}\text{C}$ NMR spectra for <b>S3</b> .	216
<b>Figure A3-4.</b> $^1\text{H}$ and $^{13}\text{C}$ NMR spectra for <b>3a</b> .	217
<b>Figure A3-5.</b> $^1\text{H}$ and $^{13}\text{C}$ NMR spectra for <b>S4</b> .	218
<b>Figure A3-6.</b> $^1\text{H}$ and $^{13}\text{C}$ NMR spectra for <b>S5</b> .	219
<b>Figure A3-7.</b> $^1\text{H}$ and $^{31}\text{P}$ NMR spectra for <b>4a</b> .	220
<b>Figure A3-8.</b> $^1\text{H}$ and $^{13}\text{C}$ NMR spectra for <b>5a</b> .	221
<b>Figure A3-9.</b> $^1\text{H}$ and $^{13}\text{C}$ NMR spectra for <b>5b</b> .	222
<b>Figure A3-10.</b> $^1\text{H}$ and $^{13}\text{C}$ NMR spectra for <b>5c</b> .	223
<b>Figure A3-11.</b> $^1\text{H}$ and $^{13}\text{C}$ NMR spectra for <b>S6</b> .	224
<b>Figure A3-12.</b> $^1\text{H}$ and $^{13}\text{C}$ NMR spectra for <b>6b</b> .	225
<b>Figure A3-13.</b> GPC chromatogram of <b>P(1-co-2)</b> catalyzed by <b>3a</b> at 254 nm (—) and 427 nm (---). All aryl groups absorb light at 254 nm, but only <b>P1</b> segments absorb at 427 nm.	227
<b>Figure A3-14.</b> (A) number average molecular weight (●) and dispersity (◆) versus percent conversion ( <b>1</b> and <b>2</b> combined) for the copolymerization of <b>1</b> and <b>2</b> using <b>3a</b> . (B) Percent total conversion (◆), conversion of <b>1</b> (●), and conversion of <b>2</b> (●) versus time.	227
<b>Figure A3-15.</b> Selected regions of the $^1\text{H}$ NMR spectra of Trial 1 in THF. Bottom ( <b>3a</b> ) and top (MeOPhMgCl) spectra correspond to the two starting materials prior to mixing. The middle three spectra show the reaction progress at 1, 5, and 25 min after mixing (bottom to top). Prominent peaks are highlighted in the reaction spectrum from the starting materials [ <b>3a</b> (—), MeOPhMgCl (—)] and the reaction product (—)].	230
<b>Figure A3-16.</b> $^1\text{H}$ NMR spectrum in $\text{CDCl}_3$ of Trial 1 after workup. The integrals highlighted (dark red) correspond to 2,2'-dimethoxybiphenyl.	231
<b>Figure A3-17.</b> $^1\text{H}$ NMR spectra in $\text{CDCl}_3$ of analytically pure <b>3a</b> (top) and recovered <b>3a</b> from Trial 3 (bottom).	234
<b>Figure A3-18.</b> $^1\text{H}$ and $^{31}\text{P}$ spectra of <b>4c</b> .	239

<b>Figure A3-19.</b> $^{13}\text{C}$ NMR spectrum of <b>4c</b> .	240
<b>Figure A3-20.</b> HSQCAD NMR spectrum of <b>4c</b> .	241
<b>Figure A3-21.</b> HSQCAD NMR spectrum highlighting the $^1\text{H}/^{13}\text{C}$ correlations of the CH (—) and $\text{CH}_3$ (—) of the <i>i</i> Pr groups on the IPr ligand and $\text{CH}_3$ (—) of the tolyl ligand of <b>4c</b> .	242
<b>Figure A3-22.</b> GPC chromatogram of <b>P2</b> catalyzed by <b>4c</b> (—) and <b>3a</b> (—).	244
<b>Figure A3-23.</b> GPC chromatogram of <b>P2</b> catalyzed by <b>3c</b> after pre-initiating with 2-chlorotoluene (10 equiv) and <i>p</i> -tolylmagnesium chloride for 1 (—), 10 (—), or 90 (—) min.	247
<b>Figure A3-24.</b> MALDI-TOF mass spectrum of <b>P2</b> produced by <b>3c</b> after pre-initiating for 1 min. Inset shows a zoomed in view at DP = 37.	248
<b>Figure A3-25.</b> MALDI-TOF mass spectrum of <b>P2</b> produced by <b>3c</b> after pre-initiating for 10 min. Inset shows a zoomed in view at DP = 37.	248
<b>Figure A3-26.</b> MALDI-TOF mass spectrum of <b>P2</b> produced by <b>3c</b> after pre-initiating for 90 min. Inset shows a zoomed in view at DP = 37.	249
<b>Figure A3-27.</b> GPC chromatogram of <b>P2</b> catalyzed by <b>5a</b> (—), <b>5b</b> (—), or <b>5c</b> (—).	251
<b>Figure A3-28.</b> GPC chromatogram of <b>P1</b> catalyzed by <b>5a</b> using 57 (—) or 25 (—) equiv of <b>1</b> relative to <b>5a</b> .	253
<b>Figure A3-29.</b> GPC chromatogram of <b>P1</b> catalyzed by <b>5a</b> with 1 equiv of 3-chloropyridine using 63 (—) or 20 (—) equiv of <b>1</b> relative to <b>5a</b> .	255
<b>Figure A3-30.</b> GPC chromatogram of <b>P2</b> catalyzed by <b>3a</b> (—), <b>6a</b> (—), or <b>6b</b> (—).	257
<b>Figure A3-31.</b> GPC chromatogram of <b>P2</b> produced by <b>6b</b> with 0 equiv (—), 0.5 equiv (—), 1 equiv (—), or 2 equiv (—) of 3-chloropyridine (relative to catalyst).	260
<b>Figure A3-32.</b> GPC chromatogram of <b>P2</b> produced by <b>6b</b> with 0.5 equiv (—), 0.9 equiv (—), 1 equiv (—), or 1.1 equiv (—) of 3-chloropyridine (relative to catalyst).	262
<b>Figure A3-33.</b> GPC chromatogram of <b>P2</b> produced by <b>6b</b> with 1.05 equiv of 3-chloropyridine (—), 3-fluoropyridine (—), or pyridine (—) (relative to catalyst).	264
<b>Figure A3-34.</b> GPC chromatogram of <b>P2</b> produced by <b>6b</b> with 1.0 equiv LiCl (—) or without LiCl (—).	267
<b>Figure A3-35.</b> MALDI-TOF mass spectrum of <b>P2</b> produced by <b>6b</b> with 1 equiv of 3-chloropyridine. Inset shows a zoomed in view at DP = 73 with cinnamyl/H (83% area ratio) and H/H (17% area ratio) end-groups.	268
<b>Figure A3-36.</b> GPC chromatogram of <b>P2</b> produced by <b>6b</b> with 0 equiv LiCl (—), 0.33 equiv LiCl (—), 0.66 equiv LiCl (—), or 1 equiv LiCl (—).	271

**Figure A3-37.** MALDI-TOF mass spectrum of **P2** produced by **6b** without LiCl. Inset shows a zoomed in view at DP = 14. 272

**Figure A3-38.** MALDI-TOF mass spectrum of **P2** produced by **6b** with 0.33 equiv LiCl (relative to iPrMgCl used to generate **2**). Inset shows a zoomed in view at DP = 14. 272

**Figure A3-39.** MALDI-TOF mass spectrum of **P2** produced by **6b** with 0.66 equiv LiCl (relative to iPrMgCl used to generate **2**). Inset shows a zoomed in view at DP = 14. 273

**Figure A3-40.** MALDI-TOF mass spectrum of **P2** produced by **6b** with 1.0 equiv LiCl (relative to iPrMgCl used to generate **2**). Inset shows a zoomed in view at DP = 14. 273

## List of Tables

- Table 2-1.** Percent migration (experimental data) and calculated # of steps at each DP for **4a**. 43
- Table 4-1.** Percent end-groups of **P2** produced by **6b** as determined by MALDI-TOF MS.  $M_n$  and dispersity for **P2** ranged from 3.7–4.6 kDa and 1.16–1.17, respectively, and are plotted in Figure 4-4B. <sup>a</sup>Equiv LiCl is relative to iPrMgCl used to generate **2**. 89
- Table A1-1.** Conversion data plotted in Figure A1-2. 117
- Table A1-2.** Data for **P3DT** produced by **4a** with 0 or 30 equiv of **3**. <sup>a</sup>Determined by GC analysis. <sup>b</sup>Determined by GPC analysis. <sup>c</sup>Calculated from the average peak area ratios (at each DP) from the five most intense peaks observed by MALDI-TOF MS analysis. 120
- Table A1-3.** Data for **P3DT** produced by **4b** with 0 or 30 equiv of **3**. <sup>a</sup>Determined by GC analysis. <sup>b</sup>Determined by GPC analysis. <sup>c</sup>Calculated from the average peak area ratios (at each DP) from the five most intense peaks observed by MALDI-TOF MS analysis. 121
- Table A1-4.** Data for **P3DT** produced by **4c** with 0 or 30 equiv of **3**. <sup>a</sup>Determined by GC analysis. <sup>b</sup>Determined by GPC analysis. <sup>c</sup>Calculated from the average peak area ratios (at each DP) from the five most intense peaks observed by MALDI-TOF MS analysis. 122
- Table A1-5.** Data for **P3DT** produced by **4d** with 0 or 30 equiv of **3**. <sup>a</sup>Determined by GC analysis. <sup>b</sup>Determined by GPC analysis. <sup>c</sup>Calculated from the average peak area ratios (at each DP) from the five most intense peaks observed by MALDI-TOF MS analysis. 123
- Table A1-6.** Data for **P3DT** produced by **4e** with 0 or 30 equiv of **3**. <sup>a</sup>Determined by GC analysis. <sup>b</sup>Determined by GPC analysis. <sup>c</sup>Calculated from the average peak area ratios (at each DP) from the five most intense peaks observed by MALDI-TOF MS analysis. The major end-group for both conditions was Br/Br. 124
- Table A1-7.** Data for **P3DT** produced by **4a** pre or post end-capping with **2** (15 equiv) and **3** (30 equiv). <sup>a</sup>Determined by GC analysis. <sup>b</sup>Determined by GPC analysis. <sup>c</sup>Calculated from the average peak area ratios (at each DP) from the five most intense peaks observed by MALDI-TOF MS analysis. 128
- Table A1-8.** Catalyst migration values for **4a** from Run 1–4. Avg and STD values are plotted in Figure A1-23. 131
- Table A1-9.** Data for **P3DT** produced by **4b** pre or post end-capping with **2** (15 equiv) and **3** (30 equiv). <sup>a</sup>Determined by GC analysis. <sup>b</sup>Determined by GPC analysis. <sup>c</sup>Calculated from the average peak area ratios (at each DP) from the five most intense peaks observed by MALDI-TOF MS analysis. 132



**Table A1-10.** Catalyst migration values for **4b** from Run 1–4. Avg and STD values are plotted in Figure A1-23. 136

**Table A1-11.** Data for **P3DT** produced by **4c** pre or post end-capping with **2** (15 equiv) and **3** (30 equiv). <sup>a</sup>Determined by GC analysis. <sup>b</sup>Determined by GPC analysis. <sup>c</sup>Calculated from the average peak area ratios (at each DP) from the five most intense peaks observed by MALDI-TOF MS analysis. 137

**Table A1-12.** Catalyst migration values for **4c** from Run 1. Avg and STD values are plotted in Figure A1-23. 140

**Table A1-13.** Data for **P3DT** produced by **4d** pre or post end-capping with **2** (15 equiv) and **3** (30 equiv). <sup>a</sup>Determined by GC analysis. <sup>b</sup>Determined by GPC analysis. <sup>c</sup>Calculated from the average peak area ratios (at each DP) from the five most intense peaks observed by MALDI-TOF MS analysis. 141

**Table A1-14.** Catalyst migration values for **4d** from Run 1. Avg and STD values are plotted in Figure A1-23. 144

**Table A1-15.** Data for **P3DT** produced by **4e** pre or post end-capping with **2** (15 equiv) and **3** (30 equiv). <sup>a</sup>Determined by GC analysis. <sup>b</sup>Determined by GPC analysis. <sup>c</sup>Calculated from the average peak area ratios (at each DP) from the five most intense peaks observed by MALDI-TOF MS analysis. 145

**Table A1-16.** Catalyst migration values for **4e** from Run 1. Avg and STD values are plotted in Figure A1-23. 148

**Table A1-17.** Transition matrix for a random walk with 10 linear steps from chain-end to chain-end (i.e., DP = 4 with cap/Br end-groups). 152

**Table A1-18.** Percent migration (experimental data) and calculated # of steps at each DP for **4a**. 156

**Table A2-1.** Conversion data plotted in Figure A2-3. 167

**Table A2-2.** Data for **P1** produced by **4a** pre or post end-capping with **3a** (15 equiv) and **3b** (50 equiv). <sup>a</sup>Determined by GC analysis. <sup>b</sup>Determined by GPC analysis. <sup>c</sup>Calculated from the average peak area ratios (at each DP) from the five most intense peaks observed by MALDI-TOF MS analysis. 170

**Table A2-3.** Catalyst migration values for **4a** from Run 1–3. Avg and STD values are plotted in Figure A2-19. 172

**Table A2-4.** Data for **P1** produced by **4a** pre or post end-capping with **3a** (15 equiv) and **3b** (50 equiv). <sup>a</sup>Determined by GC analysis. <sup>b</sup>Determined by GPC analysis. <sup>c</sup>Calculated from the average peak area ratios (at each DP) from the five most intense peaks observed by MALDI-TOF MS analysis. 173

**Table A2-5.** Catalyst migration values for **4b** from Run 1–5. Avg and STD values are plotted in Figure A2-19. 176

**Table A2-6.** Data for **P1** produced by **4c** pre or post end-capping with **3a** (15 equiv) and **3b** (50 equiv). <sup>a</sup>Determined by GC analysis. <sup>b</sup>Determined by GPC analysis. <sup>c</sup>Calculated from the average peak area ratios (at each DP) from the five most intense peaks observed by MALDI-TOF MS analysis. 177

**Table A2-7.** Catalyst migration values for **4c** from Run 1–3. Avg and STD values are plotted in Figure A2-19. 180

**Table A2-8.** Data for **P1** produced by **4d** pre or post end-capping with **3a** (15 equiv) and **3b** (50 equiv). <sup>a</sup>Determined by GC analysis. <sup>b</sup>Determined by GPC analysis. <sup>c</sup>Calculated from the average peak area ratios (at each DP) from the five most intense peaks observed by MALDI-TOF MS analysis. 181

**Table A2-9.** Catalyst migration values for **4d** from Run 1–3. Avg and STD values are plotted in Figure A2-19. 184

**Table A2-10.** Data for **P1** produced by **4e** pre or post end-capping with **3a** (15 equiv) and **3b** (50 equiv). <sup>a</sup>Determined by GC analysis. <sup>b</sup>Determined by GPC analysis. <sup>c</sup>Calculated from the average peak area ratios (at each DP) from the five most intense peaks observed by MALDI-TOF MS analysis. 185

**Table A2-11.** Catalyst migration values for **4e** from Run 1–4. Avg and STD values are plotted in Figure A2-19. 188

**Table A2-12.** Transition matrix for a random walk with 10 linear steps from chain-end to chain-end (i.e., DP = 4 with cap/Br end-groups). 192

**Table A2-13.** Transition matrix used for DP = 4 to account for *sticky*, *neutral*, or *repulsive* chain-ends (C = cap end, Br = phenylene-Br end) where B/C could each have values of 3, 2, or 1. 197

**Table A2-14.** Migration and molecular weight values plotted in Figure A2-25. 198

**Table A3-1.** Molecular weight, dispersity, and conversion values as plotted in Figure A3-14. 228

**Table A3-2.** Molecular weight, dispersity, and conversion values of **P2** catalyzed by **4c**.<sup>a</sup>  $M_n$  and  $\bar{D}$  could not be calculated due to the low molecular weight peak tail that extended beyond the lower limit of the GPC calibration curve. 244

**Table A3-3.** Molecular weight, dispersity, and conversion values for polymerizing **2** using **3c** as plotted in Figure A3-23. 247

**Table A3-4.** Percent end-groups for **P2** catalyzed by **3c** after pre-initiating with 2-chlorotoluene (10 equiv) and *p*-tolylmagnesium chloride for 1, 10, or 90 min as determined by MALDI-TOF MS and as plotted in Figure A3-24, Figure A3-25, and Figure A3-26. 249

<b>Table A3-5.</b> Molecular weight, dispersity, and conversion values for polymerizing <b>2</b> using <b>5a</b> , <b>5b</b> , or <b>5c</b> .	251
<b>Table A3-6.</b> Molecular weight, dispersity, and conversion values for polymerizing <b>1</b> using <b>5a</b> as plotted in Figure A3-28.	253
<b>Table A3-7.</b> Molecular weight, dispersity, and conversion values for polymerizing <b>1</b> using <b>5a</b> as plotted in Figure A3-29.	255
<b>Table A3-8.</b> Molecular weight, dispersity, and conversion values for polymerizing <b>2</b> using <b>3a</b> , <b>6a</b> , or <b>6b</b> as plotted in Figure A3-30.	257
<b>Table A3-9.</b> Molecular weight, dispersity, and conversion of <b>2</b> for <b>P2</b> produced by <b>6b</b> with different amounts of 3-chloropyridine (relative to catalyst) as plotted in Figure A3-31.	260
<b>Table A3-10.</b> Molecular weight, dispersity, and conversion of <b>2</b> for <b>P2</b> produced by <b>6b</b> with different amounts of 3-chloropyridine (relative to catalyst) as plotted in Figure A3-32.	262
<b>Table A3-11.</b> Molecular weight, dispersity, and conversion of <b>2</b> for <b>P2</b> produced by <b>6b</b> with 1.05 equiv of 3-chloropyridine, 3-fluoropyridine, or pyridine as plotted in Figure A3-33.	264
<b>Table A3-12.</b> Molecular weight, dispersity, and conversion of <b>2</b> for <b>P2</b> produced by <b>6b</b> with or without added LiCl as plotted in Figure A3-34. <sup>a</sup> Equiv LiCl is relative to iPrMgCl used to generate <b>2</b> .	267
<b>Table A3-13.</b> Molecular weight, dispersity, and conversion of <b>2</b> for <b>P2</b> produced by <b>6b</b> with or without added LiCl as plotted in Figure A3-36. <sup>a</sup> Equiv LiCl is relative to iPrMgCl used to generate <b>2</b> .	271
<b>Table A3-14.</b> Percent end-groups of <b>P2</b> from polymerizing <b>2</b> with <b>6b</b> and added LiCl as determined by MALDI-TOF MS as plotted in Figure A3-37, Figure A3-38, Figure A3-39, and Figure A3-40. <sup>a</sup> Equiv LiCl is relative to iPrMgCl used to generate <b>2</b> .	274

## List of Schemes

- Scheme 1-1.** Catalytic cycle for the polymerization of 3-alkylthiophene using Kumada CTCP. 5
- Scheme 1-2.** Block copolymerization of phenylene and thiophene monomers. Block copolymer is achieved when (A) phenylene is polymerized as the first block, but a mixture of products is formed when the order of addition is reversed. (B) The proposed mechanism to form polythiophene capped with phenylene-Br. 7
- Scheme 1-3.** Initiator enchainment provides evidence for catalyst migration. 10
- Scheme 1-4.** General end-capping experiments performed in Chapter 2 and 3. 12
- Scheme 1-5.** General products from initiation and propagation using precatalysts. Dihalide precatalysts (top) generate a polymer that could propagate from both C-Br to yield ill-defined copolymers. Functionalized precatalysts (bottom) transfer a reactive-ligand (●) to the polymer to prevent propagation from the  $\alpha$  end. 13
- Scheme 2-1.** Catalytic cycle for the polymerization of 3-alkylthiophene using Kumada CTCP. 27
- Scheme 2-2.** (A) Initiator enchainment and (B) capping at both ends of poly(3-alkylthiophene) provide evidence for catalyst migration. 28
- Scheme 2-3.** Ni(dppp)Cl<sub>2</sub> catalyzed polymerization of a quarterthiophene monomer requires catalyst migration across four thiophene units for intramolecular oxidative addition (right) to realize a chain-growth polymerization. 29
- Scheme 2-4.** End-capping observed at both ends of poly(3-hexylthiophene) polymerized by Ni(dppe)Cl<sub>2</sub>. 29
- Scheme 2-5.** End-capping reaction with unassociated catalyst generates *false positive* (i.e. migration product) if competitive agent is absent or not sufficiently reactive (intermolecular reaction). 31
- Scheme 2-6.** Small molecule cross-coupling to verify that competitive agent outcompetes polymer C-Br (2-bromo-3-hexylthiophene is used as a proxy). 32
- Scheme 2-7.** Polymerizing **1** with or without added competitive agent. <sup>a</sup>Determined by GPC analysis. <sup>b</sup>Calculated from the average peak area ratios (at each DP) from the five most intense peaks observed by MALDI-TOF MS analysis. 33
- Scheme 2-8.** End-capping model system to detect catalyst migration by reaction with **2** at both ends. 33

**Scheme 2-9.** Unassociated Ni(PPh<sub>3</sub>)<sub>m</sub> catalyst yields coupling product of **2** and **3** rather than end-capping **P3DT**. 40

**Scheme 3-1.** Small molecule competition experiment where an associative complex directs oxidative addition with the biaryl formed in situ (intramolecular pathway) rather than through the intermolecular pathway with a more reactive competitive agent (2-bromobenzonitrile, present in excess amounts). L<sub>2</sub> = 1,2-bis(diethylphosphino)ethane, 1,2-bis(*p*-methoxyphenylphosphino)ethane, dppe or 2 PPh<sub>3</sub> (dppe = 1,2-bis(diphenylphosphino)ethane, PPh<sub>3</sub> = triphenylphosphine). 50

**Scheme 3-2.** Block copolymerization of **2** (**P2** M<sub>n</sub> = 4.1 kDa, Đ = 1.33) then **1** (M<sub>n</sub> = 6.7 kDa, Đ = 1.44) to yield **P(2-block-1)** and **1-P2-1** as the major species.<sup>32</sup> 51

**Scheme 3-3.** End-capping model system to detect catalyst migration by capping with **3a**. 54

**Scheme 4-1.** Gradient sequence copolymer prepared via a semi-batch polymerization where **1** is added to a solution of **2** and precatalyst. 76

**Scheme 4-2.** Block copolymerizing **1** (**P1** M<sub>n</sub> = 4.1 kDa, Đ = 1.33) then **2** (M<sub>n</sub> = 6.7 kDa, Đ = 1.44) yields **P(1-block-2)** and **2-P1-2** as the major species.<sup>23</sup> 77

**Scheme 4-3.** General products from initiation and propagation using precatalysts. Dihalide precatalysts (top) generate a polymer that could propagate from both C-Br to yield ill-defined copolymers. Functionalized precatalysts (bottom) transfer a reactive ligand (●) to the polymer to prevent propagation from the α end. 78

**Scheme 4-4.** General routes to an IPrPd precatalyst with a reactive ligand (red). 79

**Scheme 4-5.** Transmetalating **3a** with 2-methoxyphenylmagnesium chloride to generate the biaryl coupling product observed by <sup>1</sup>H NMR spectroscopy. 80

**Scheme 4-6.** Oxidative addition of iodobenzene or *o*-iodotoluene into **4a** to yield **4b/4c**. When R = H, the precatalyst decomposed to yield IPrPhI 81

**Scheme 4-7.** Proposed in situ generation of **3c** from **3a** using *p*-tolylmagnesium chloride and *o*-chlorotoluene (biaryl cross-coupling products also shown). Adding **2** would initiate the polymerization, transferring the *o*-tolyl reactive ligand to the polymer 82

**Scheme 4-8.** Polymerizing **2** with **5a–c**. 83

**Scheme 4-9.** GPC chromatogram and scheme of **P2** catalyzed by **6a** (—) or **6b** (—). 85

**Scheme 4-10.** Polymerizing **1** using **6b** and added 3-chloropyridine failed to yield the expected **P1**. Block copolymerization of **2** then **1** extended **P2** to yield **P(2-block-1)**, demonstrating that the propagation of **1** can occur. 90

**Scheme 5-1.** End-capping to screen building blocks used in high-efficiency solar cells for π-binding issues that could occur during copolymerizations. 101

## List of Charts

**Chart 2-1.** Structures and names of the dihalide precatalysts investigated in the end-capping model system. 32

**Chart 3-1.** Structures and names of the dihalide precatalysts investigated in the end-capping model system. 53

## List of Appendices

<b>Appendix 1.</b> Supporting Information for Chapter 2.	
Long-distance catalyst migration across poly(3-alkylthiophene)	109
<b>Appendix 2.</b> Supporting Information for Chapter 3.	
Catalyst-dependent migration in poly(phenylene) synthesis	158
<b>Appendix 3.</b> Supporting Information for Chapter 4.	
Optimizing NHC-precatalysts for end-functionalized (co)polymers	200

## Abstract

Conjugated polymers combine mechanical flexibility with light absorption/emission and charge conductivity, stimulating their use in transistors, light emitting diodes, and solar cells. Living, chain-growth methods enable polymeric properties (e.g., miscibility, morphology, charge transport) to be tailored by controlling molecular weight, end-groups, and copolymer sequence. However, synthetic challenges have limited the scope of conjugated copolymers produced in this fashion. The distinguishing feature of chain-growth polymerizations of conjugated monomers is that the catalyst remains associated with a single polymer chain during the polymerization. This association is due to a catalyst-polymer  $\pi$ -complex, which may be able to migrate along the polymer to react at both ends—preventing sequence and end-group control. We have recently demonstrated that IPrPd(3-chloropyridine)Cl<sub>2</sub> is a promising catalyst for thiophene and phenylene copolymers, which were previously inaccessible. However, control over polymer sequence can only be exerted if the catalyst reacts at a single polymer end. This thesis details how the  $\pi$ -complex directs intramolecular reactivity using four popular precatalysts in catalyst-transfer condensation polymerizations, how  $\pi$ -complex reactivity is heavily influenced by the polymer, and catalyst design strategies to overcome reactions at both polymer ends.

Chapter 1 discusses the advantages of chain-growth polymerization over conventional, step-growth polymerizations to control polymer  $M_n$ ,  $\mathcal{D}$ , and copolymer sequence. Despite the limited monomer scope, several examples are discussed that illustrate how copolymer sequence can improve solar cell stability when employed as the main component or an additive. We introduce how preferential  $\pi$ -binding and catalyst migration present major obstacles to copolymerizations, but that the relationship between catalyst/polymer properties and their  $\pi$ -complex behavior is limited.

Chapter 2 details an end-capping model system that investigates the strength of catalyst-polymer  $\pi$ -complexes in catalyst-transfer condensation polymerization. The  $\pi$ -complex is *challenged* by forcing end-to-end migration across a poly(3-alkylthiophene) backbone with an excess of highly reactive competitive agent in the reaction mixture. Near quantitative migration



products suggest that all catalysts bind to the polymer tight enough to resist chain-transfer, but the catalyst is highly mobile and can migrate across many repeat units to react at both ends.

Chapter 3 expands our investigation into end-to-end catalyst migration by changing the polymer. Here we observe large differences in the interactions between the different catalysts and poly(phenylene) that are influenced by the ligand identity and transition metal. The random-walking statistical model, commonly used to describe migration, provides an incomplete fit with our experimental results.

Chapter 4 investigates precatalysts that transfer a reactive ligand to the polymer during initiation to prevent reaction on both polymer ends (enabled by end-to-end migration). We identify and optimize a promising lead, but reactive ligand transfer during initiation was incomplete. Polymerization additives improved precatalyst control over molecular weight and dispersity, but had little effect on reactive ligand transfer during initiation.

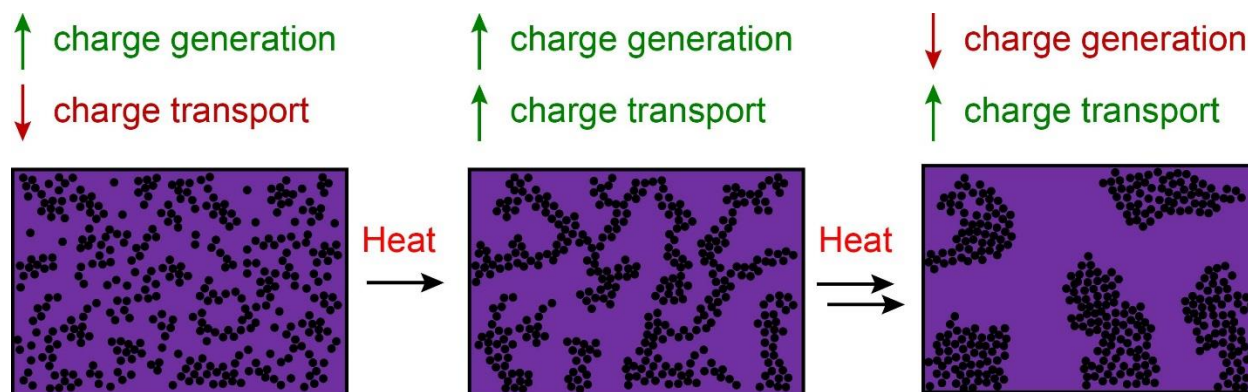
Chapter 5 describes how our investigations into  $\pi$ -complex stability/catalyst mobility could relate to polymerization and/or copolymerization behavior. We note that catalyst migration can be a highly desirable trait for expanding the monomer and comonomer scope, which are major limitations in catalyst-transfer condensation polymerizations. Continued efforts are required to elevate these living, chain-growth methods into widespread use for conjugated polymer synthesis.

## Chapter 1

### Introduction

Conjugated polymers (CPs) have garnered significant interest since the Nobel prize winning work of Heeger,<sup>1</sup> MacDiarmid,<sup>2</sup> and Shirakawa<sup>3</sup> revealed that polymers with extended conjugation can be electrically conductive. Flexible and stretchable semi-conductors, such as CPs, enable new applications in bio-electronic interfaces for sensing and/or stimulation.<sup>4-6</sup> CPs potential for low-cost, high-throughput manufacturing also makes them attractive materials to replace their inorganic counterparts in light-emitting-diodes,<sup>7-11</sup> field-effect-transistors,<sup>12-14</sup> chemical sensors,<sup>15-17</sup> and photovoltaic devices.<sup>18-21</sup>

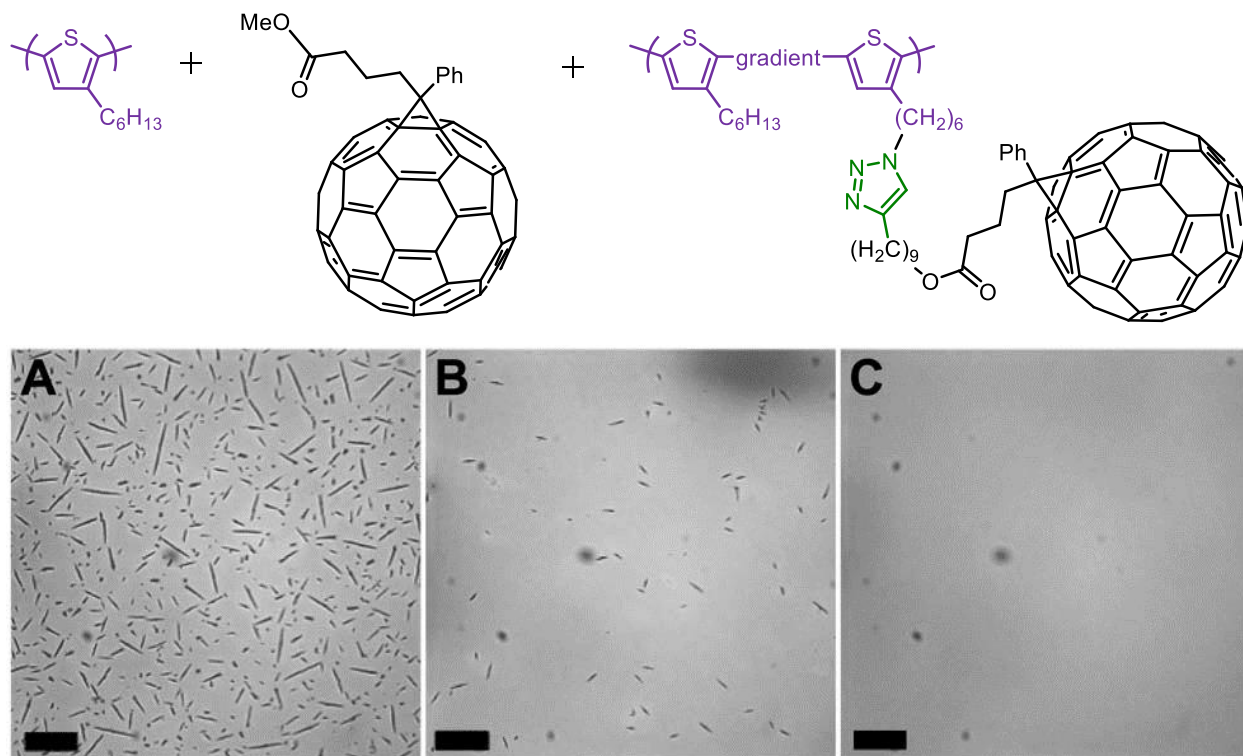
Organic photovoltaics (OPVs) are typically fabricated using a blend of two materials in the active layer. The solid-state organization of these two materials, the electron donor (CP) and electron acceptor (small molecule or CP), plays a critical role in device performance.<sup>22,23</sup> Intimate mixing of the donor and acceptor promotes charge separation, while distinct domains of each component facilitate charge conduction to the respective electrodes.<sup>24,25</sup> Balancing these conflicting morphology requirements to maximize performance has been the focus of many studies. Deposition technique (and solvent),<sup>26-29</sup> annealing conditions,<sup>30-33</sup> and high-boiling point additives<sup>34-37</sup> can influence the peak efficiency, but phase separation in the active layer leads to deteriorating performance after extended use (Figure 1-1). With maximum power conversion efficiencies (PCEs) eclipsing 12%,<sup>38,39</sup> OPV lifetime has emerged as one of the top parameters limiting commercial feasibility.<sup>40-45</sup>



**Figure 1-1.** Phase evolution and charge generation/transport of a bulk-heterojunction solar cell with heating/extended use.

### *Gradient copolymer additives*

Strategies that target thermodynamic rather than kinetic control over mixing, such as changing the polymer mobility (via molecular weight, side-chain substitution, or cross-linking),<sup>46–51</sup> donor and/or acceptor crystallinity,<sup>52–54</sup> and additives<sup>55–60</sup> such as copolymers can all stabilize OPV performance. Copolymer additives are particularly attractive because they can be added to donor/acceptor blends that have already been optimized over many parameters. The beneficial role of copolymer additives to effect active layer morphology was recently demonstrated in solar cells made from poly(3-hexylthiophene)/PC<sub>61</sub>BM using a poly(thiophene) gradient copolymer (Figure 1-2).<sup>61</sup> Extended thermal annealing of control devices, made without the additive, produced  $\mu$ -sized PC<sub>61</sub>BM crystallites visible by optical microscopy. These morphological changes were correlated with a reduction in PCE from 2.4% to 1.8%. Adding 1 wt% copolymer additive greatly reduced the quantity of crystallites, and with 10 wt% no crystallites were observed (Figure 1-2).

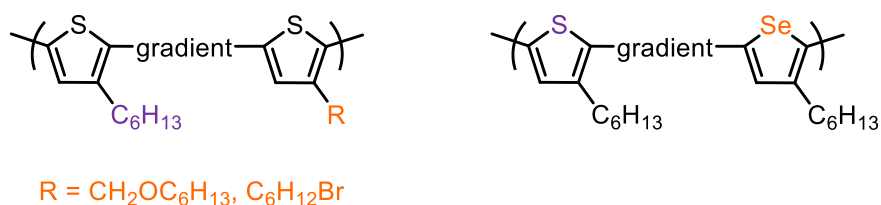


**Figure 1-2.** Chemical structures and optical microscope images of a poly(3-hexylthiophene)/PC<sub>61</sub>BM blend after annealing at 150 °C with (A) no (control), (B) 5 wt %, or (C) 10 wt % of a gradient copolymer additive.<sup>61</sup> The scale bar represents 25 μm.

Copolymers can also be used as the sole electron donor in OPVs to achieve stable morphologies. One study compared the PCE of OPVs fabricated using either poly(3-hexylthiophene), poly(3-hexylselenophene), a 1:1 blend, or a gradient/block sequence copolymer containing 50 mol% of each.<sup>62</sup> Solar cells featuring both thiophene and selenophene repeat units in the polymers exhibited broader optical absorption, but polymer aggregation and phase separation (driven by poorly soluble selenophene units) hampered charge extraction. Significant PCE decreases were observed for all the devices except those fabricated using gradient copolymers, where performance remained high after extended thermal annealing. The superior device stability using the gradient copolymer was attributed to balanced mixing and separation resulting from the gradient sequence—the gradual composition change from 3-hexylthiophene to 3-hexylselenophene creates a largely random composition segment in the middle of gradient copolymer that promotes mixing, while the relatively pure segments at either chain-end drive polymer crystallization and separation.

The examples above demonstrate that conjugated gradient copolymers can stabilize the active layer morphology in solar cells, but the maximum PCE was decreased in both cases. In theory, controlling morphology by adding copolymers could lead to improved PCE—several copolymer properties could be optimized to achieve this goal. (1) Molecular weight can influence copolymer diffusion, the propensity to form micelles, the relative stabilization at the interface, and the stiffness of the interface.<sup>63,64</sup> Likewise, (2) copolymer sequence and (3) gradient strength can have a profound effect by influencing copolymer conformation and penetration across the interface.<sup>65–68</sup> There are numerous examples of non-conjugated gradient copolymer additives, but conjugated gradient copolymers are rare. Conjugated polymers exhibit distinct morphologies (from their non-conjugated analogues) that influence mixing in solution and thin-film due to their backbone rigidity and semi-crystallinity. Systematic studies to identify the relationships between compatibilization and molecular weight, gradient strength, or composition in conjugated gradient copolymers are sorely needed—a streamlined process to optimize gradient copolymers for each application should expedite their development.

Sterically and electronically differentiated comonomers are desired to address the lack of information on conjugated gradient copolymers. The differentiated properties of each comonomer would amplify subtle differences in film morphology and the subsequent impact on electronic properties—thereby facilitating quantitative comparisons of polymer blends. However, the three conjugated gradient polymers directly prepared thus far differ only in the side-chain or heteroatom (Chart 1-1). Work presented in this thesis aims to expand the comonomers used for gradient copolymerizations.

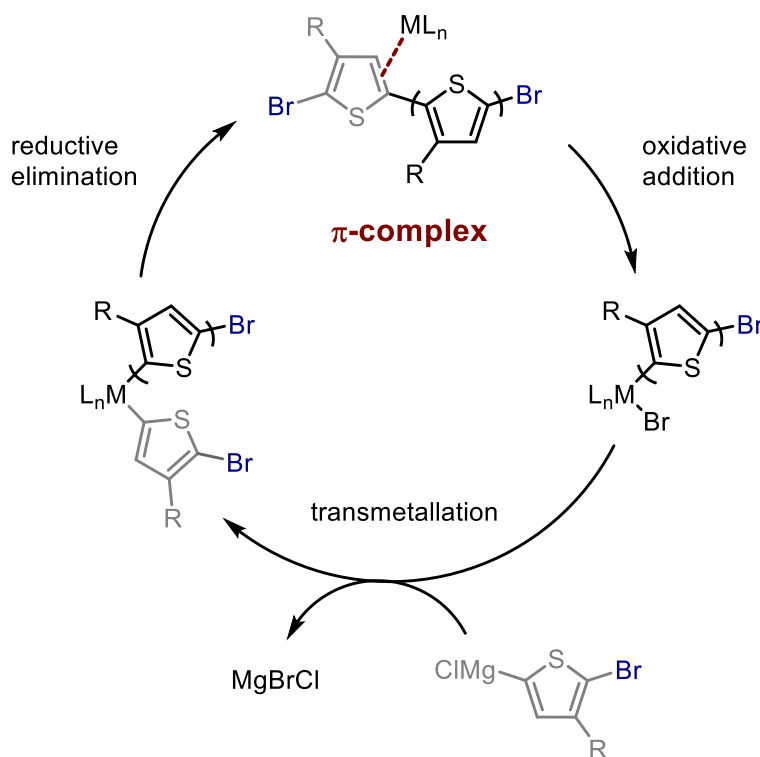


**Chart 1-1.** Only a limited number of conjugated gradient copolymers have been directly prepared with  $M_n > 15$  kDa and  $\bar{D} < 1.3$ .

### *Living, chain-growth polymerizations*

Gradient copolymers require living, chain-growth copolymerizations, which were first realized for CPs using catalyst-transfer condensation polymerization (CTCP) to produce poly(3-

hexylthiophene.<sup>69,70</sup> A catalyst-polymer  $\pi$ -complex was invoked to explain the preference for catalyst reaction with the same polymer during the polymerization. The  $\pi$ -complex, formed following reductive elimination, generates an associative pair that directs *intramolecular* oxidative addition (Scheme 1-1). Living, chain-growth polymerizations are distinguished from step-growth polymerization in several ways: living, chain-growth methods generate polymer with (1) a linear increase in  $M_n$  with monomer conversion where the (2)  $M_n$  at complete conversion is governed by the  $[\text{monomer}]_0/[\text{initiator}]_0$ . (3) Adding a second aliquot of monomer (after the original portion was consumed) extends the polymer with the same dependence on  $[\text{initiator}]_0$  because the chain-end remains active until the reaction is terminated to yield (4) well-defined end-groups. CPs prepared using living chain-growth methods typically have low dispersities ( $<1.3$ ), although higher dispersities are observed if initiation is slow or side-reactions are present.

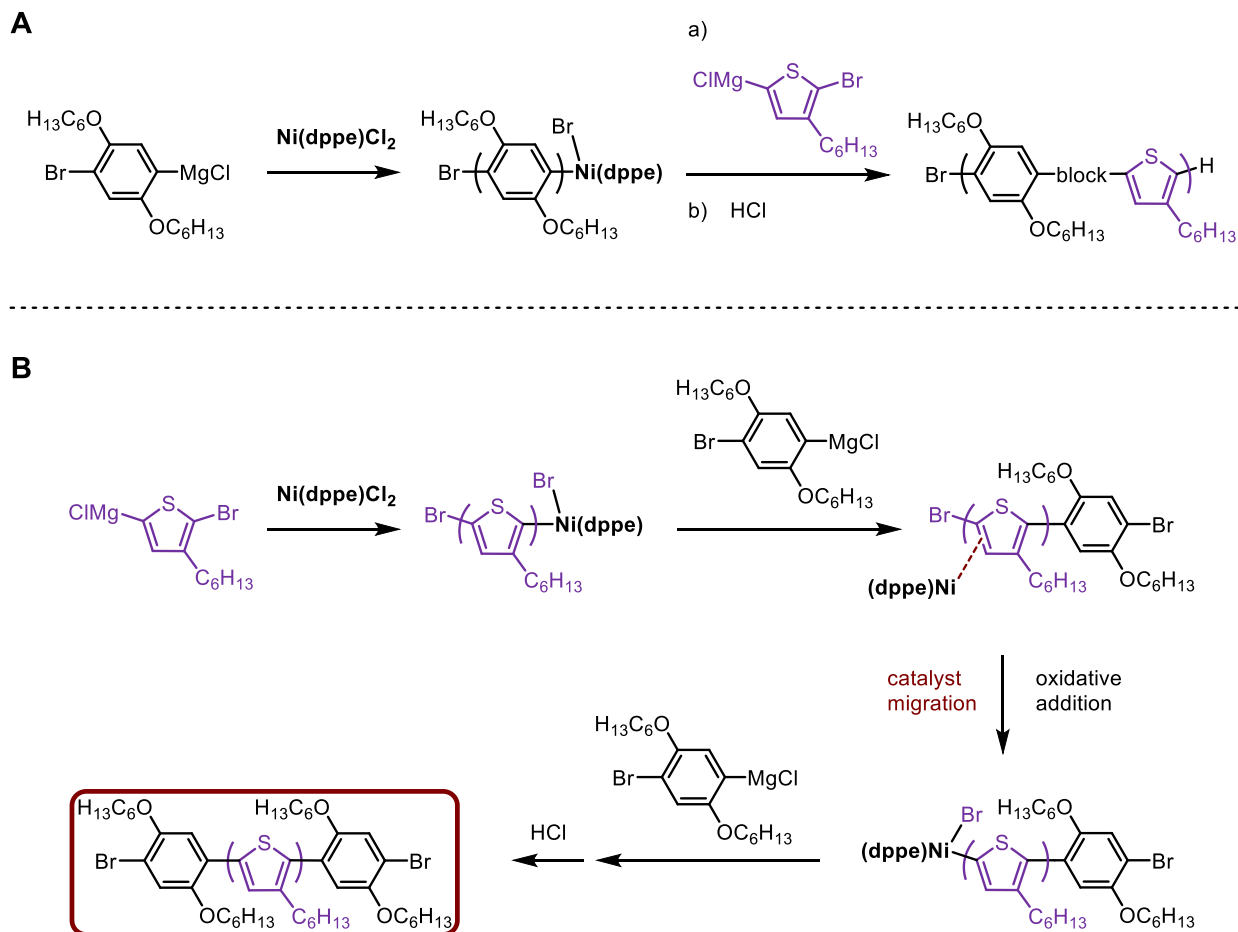


**Scheme 1-1.** Catalytic cycle for the polymerization of 3-alkylthiophene using Kumada CTCP.

### Copolymerizations using CTCP

CTCP has been expanded beyond thiophene to include other (hetero)aryls such as phenylene,<sup>71</sup> pyridine,<sup>72</sup> pyrrole,<sup>73</sup> selenophene,<sup>74</sup> and thiazole<sup>75</sup> among others. A great number of

copolymers can be envisaged from this limited monomer set—in stark contrast to the merely three gradient copolymers (Chart 1-1). The dearth of gradient copolymers can be attributed to copolymerization issues in CTCP, which are best exemplified in the synthesis of poly(thiophene-block-phenylene) using Ni(dppe)Cl<sub>2</sub> as the precatalyst.<sup>76</sup> Both thiophene and phenylene monomers can be polymerized separately under the same conditions to yield polymers with targeted  $M_n$  and low Đ. Copolymerizing phenylene and thiophene is also successful when phenylene is polymerized first, and then adding thiophene yields the block copolymer. If thiophene is polymerized first, however, then phenylene addition produces a complex mixture of copolymers and homopolymers.<sup>76,77</sup> One notable product is polythiophene with a phenylene-Br unit on both ends (Scheme 1-2). This product is likely generated via transmetallation of phenylene monomer with Ni(dppe)(polythiophene)Br. Next, reductive elimination yields a Ni(0) species that preferentially forms a  $\pi$ -complex with the polythiophene segment of the polymer (rather than to the phenylene-Br). Catalyst migration across the conjugated backbone directs intramolecular oxidative addition into the thiophene-Br bond at the  $\alpha$  terminus. Reaction with additional phenylene monomer incorporates a second phenylene-Br, but oxidative at either reactive terminus does not occur. Catalyst complexation to the internal thiophene repeat units inhibits catalyst-transfer to phenylene, yielding Br-phenylene-capped polythiophene after a standard acid quench.



**Scheme 1-2.** Block copolymerization of phenylene and thiophene monomers. Block copolymer is achieved when (A) phenylene is polymerized as the first block, but a mixture of products is formed when the order of addition is reversed. (B) The proposed mechanism to form polythiophene capped with phenylene-Br.

This side-product highlights two key processes in polymerizations. First, the  $\pi$ -complex can be greatly influenced by the repeat unit. Different  $\pi$ -binding affinities can direct the  $\pi$ -complex to form preferentially on repeat unit over another, obstructing catalyst-transfer to the  $\omega$  terminus for oxidative addition and directional propagation. Chain-transfer or dissociation can become competitive pathways from this unproductive binding intermediate, generating homopolymers. Second, catalyst migration across the CP backbone can generate a copolymer that has reacted from both ends. Catalyst migration during copolymerizations would scramble the desired copolymer sequence and could greatly influence the copolymer properties.



### *Investigating the catalyst-polymer $\pi$ -complex*

Initial reports of living, chain-growth polymerizations used Ni(dppp)Cl<sub>2</sub> or Ni(dppe)Cl<sub>2</sub> precatalysts, and they remain the most commonly used precatalysts. Ni phosphine precatalysts have been used extensively in Kumada cross-couplings due to their facile oxidative addition into a variety of aryl halides. The abundance of Ni makes these catalysts the economical choice over Pd, and their successful coupling of lower-cost aryl chlorides bolsters their appeal. Their facile oxidative addition is a result of Ni's location in the periodic table. Within the group 10 metals, the M-C bond strength is lowest for Ni, contributing to the lowest reductive and oxidative elimination barriers.<sup>78</sup> Ni also coordinates to alkene, alkyne, and aryl substrates, primarily through  $\pi$ -backbonding to C=C.<sup>79,80</sup> This well-known coordination forms the foundation for the catalyst-polymer  $\pi$ -complex, and can promote reactivity with unactivated substrates or with unique selectivity. The facile oxidative addition/reductive elimination, strong coordination, and more accessible radical pathways make Ni an attractive choice for many reactions. However, this complexity makes reactions less predictable and mechanistic investigations more difficult, which has limited the development of Ni. On the other hand, Pd is one of the most versatile and widely used transition metals on industrial and lab scales.<sup>81,82</sup> Pd catalysts offer predictable reactivity through well-defined pathways that often proceed through a mono-ligated Pd intermediate.<sup>83</sup> Ligands designed specifically for these catalytic requirements have elevated Pd precatalysts into prominence/popularity.<sup>84</sup>

Phosphine ligands are popular in both Ni and Pd catalysis due to the wide variety of steric and electronic properties that are accessible.<sup>85</sup> Mono-dentate phosphines bearing bulky <sup>t</sup>Bu or cyclohexyl groups are frequently employed in Pd catalysis, while bi-dentate phosphines are much more common using Ni.<sup>78,86</sup> The sp<sup>3</sup> hybridization of the phosphorous atom results in a cone-shaped arrangement of steric bulk that is frequently measured by cone angle.<sup>87</sup> In addition to their high efficiencies in reactions, <sup>31</sup>P NMR spectroscopy has been an extremely valuable tool to investigate the mechanisms of transition metal catalyzed reactions. N-heterocyclic carbene (NHC) ligands were initially considered phosphine mimics, acting as strong  $\sigma$ -donors and comparatively weak  $\pi$ -acceptors, but extensive studies have uncovered key differences between the two ligands. NHCs are generally stronger electron-donors, leading to thermodynamically stronger metal-ligand bonds that increase catalyst stability. Additionally, the steric bulk of NHCs is fan or umbrella

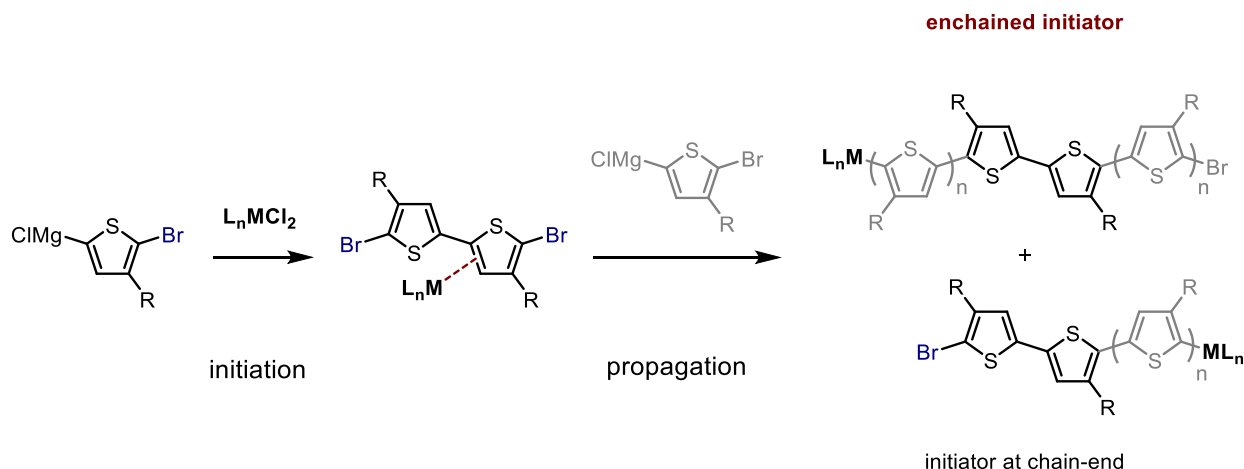
shaped, which is more aptly described by percent buried volume calculations. The percent buried volume of a ligand is the occupied volume of a sphere around the metal center which is occupied by the ligand—for dppe, dppp, and 2 IPr ligands on PdCl<sub>2</sub> the percent buried volume is 51.4%, 52.2%, and 34%, respectively (for a Pd-ligand bond of 2.00 Å, dppe = 1,2-bis(diphenylphosphino)ethane, dppp = 1,3-bis(diphenylphosphino)propane, IPr = 1,3-bis(2,6-diisopropylphenyl)imidazole).<sup>85</sup> For both ligands, the combination of strongly donating and sterically bulky ligands in M<sup>0</sup>/M<sup>2</sup> cross-couplings facilitates oxidative addition and reductive elimination, respectively. Both sterics and electronics also play an important role in generating a coordinatively unsaturated, highly active catalyst that is stable throughout the reaction.

To expand the scope of monomers and conditions, researchers are exploring different ligands and transition metals. NHCs<sup>88-90</sup> and diimine ligands<sup>91,92</sup> have achieved some success using Ni, and NHCs<sup>93-95</sup> or monodentate phosphine<sup>96-98</sup> ligands have been explored with Pd. A major breakthrough was reported in 2012, when phenylene and thiophene block copolymers were prepared from either direction using IPrPd(3-chloropyridine)Cl<sub>2</sub>.<sup>93</sup> Batch copolymerizations verified that multiple cross-propagations can occur (Chapter 4), suggesting that IPrPd-based precatalysts would be promising candidates for copolymerizations.

Improved phenylene/thiophene copolymerization results using IPrPd(3-chloropyridine)Cl<sub>2</sub> (relative to Ni(dppe)Cl<sub>2</sub>) suggests that preferential  $\pi$ -binding is not an issue. A detailed investigation of the  $\pi$ -complex between each catalyst/monomer is warranted to extend this successful CTCP copolymerization to other monomers. However, the catalyst-polymer  $\pi$ -complex has not been directly observed in phenylene and/or thiophene polymerizations. Several groups have reported  $\pi$ -complexes when polymerizing monomers with larger aromatic systems than thiophene or phenylene.<sup>99,100</sup> These polymerizations generated polymer with low  $M_n$  and higher  $\bar{D}$ , deviating significantly from the controlled polymerizations using thiophene or phenylene. Computational studies support that very strong binding interactions can interfere with catalyst transfer to the reactive polymer end, making chain-transfer to monomer viable alternative pathways.<sup>101</sup> These results suggest that a balance between  $\pi$ -complex strength and catalyst mobility is critical for chain-growth polymerizations. Catalysts with strong binding (to prevent dissociation/chain-transfer) that also migrate to the  $\omega$  chain end for oxidative addition are highly

desirable—this work aims to identify key attributes of the catalyst and monomer that will aid in the design of future, high-performing CTCP catalyst/(co)monomer combinations.

The chain-growth behavior of CTCP polymerizations provides support for a  $\pi$ -complex intermediate. Intramolecular oxidative addition, facilitated by the  $\pi$ -complex, occurs despite the presence of competing monomer groups. Many polymerizations are also insensitive to externally added aryl halide or strong  $\pi$ -binding groups (Appendix 1).<sup>93,99,102–104</sup> Catalyst is not restricted to the  $\omega$  chain-end, however. Initiating dihalide precatalysts using 3-alkylthiophene monomer proceeds through a 5,5'-dibromo-4,4'-dialkyl-2,2'-bithiophene initiator that can react at either C-Br bond. Propagating from a single end would place the bithiophene initiator at the  $\alpha$  chain-end, whereas reaction at both ends enchain the initiator into the polymer backbone (Scheme 1-3) and generates unique signals identifiable by <sup>1</sup>H NMR spectroscopy.<sup>105</sup> The amount of initiator that is enchain into the polymer backbone varies with catalyst and monomer, but can be quantitative in some cases.<sup>94,106</sup> Catalyst migration to react at both ends of the polymer occurs via a series of  $\pi$ -complexes in a process termed chain-walking. The catalyst maintains association, despite traveling between chain-ends, to generate polymer with targeted  $M_n$  and low  $\mathcal{D}$ .



**Scheme 1-3.** Initiator enchainment provides evidence for catalyst migration.

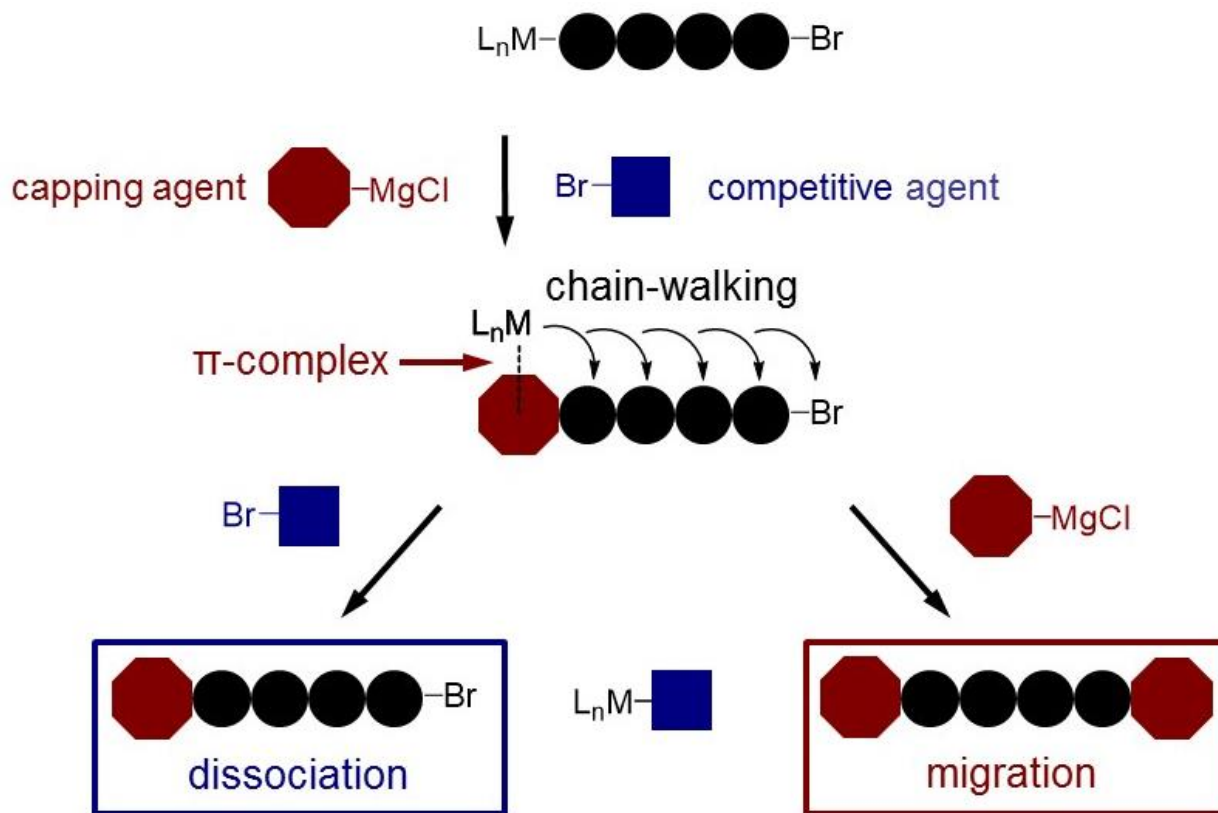
Catalyst migration can also direct reactions on polymer ends during termination. Adding excess mono-functional Grignard reagent (i.e., capping agent), initially terminates the  $\omega$  chain-end, then migrates to the  $\alpha$  end to install a second equivalent of capping agent. Near exclusive di-capping is observed for a variety of aryl/heteroaryl Grignard reagents using  $Ni(dppe)Cl_2$  or  $Ni(dppp)Cl_2$  as the precatalyst,<sup>107–110</sup> but could occur via an intramolecular and/or intermolecular

pathway. Excluding the intermolecular pathway is essential to applying end-capping results towards future catalyst development.

Competitive agents have been frequently used in small-molecule cross-coupling reactions. Selective reactions on a multi-functional aryl halide, despite an excess of reactive aryl-halogen bonds (on the competitive agent), provides evidences for intramolecular reactivity.<sup>69,94,111–113</sup> These small-molecule experiments can be a modular approach to quickly screen conditions for CTCP, but the reactivity of the substrate can change substantially as coupling proceeds.<sup>114</sup> Selectivity for a multi-functional product—presumably through a  $\pi$ -complex—does not necessarily translate to chain-growth CTCP.<sup>114,115</sup>

The end-capping experiments documented in this thesis combine the benefits of polymer end-capping (polymerization relevant conditions, multiple polymer lengths in each experiment) with small molecular cross-coupling experiments (modular, intramolecular reactivity due to competitive agent) (Chapters 2 and 3). CTCP reactions were terminated by introducing capping agent and excess competitive agent—capping agent labelled the location of the catalyst on each polymer and competitive agent consumed diffuse catalyst to limit intermolecular reactions (Scheme 1-4). We evaluated how different ligands and transition metals of four popular Kumada CTCP catalysts influence the migration behavior across either polythiophene or polyphenylene.

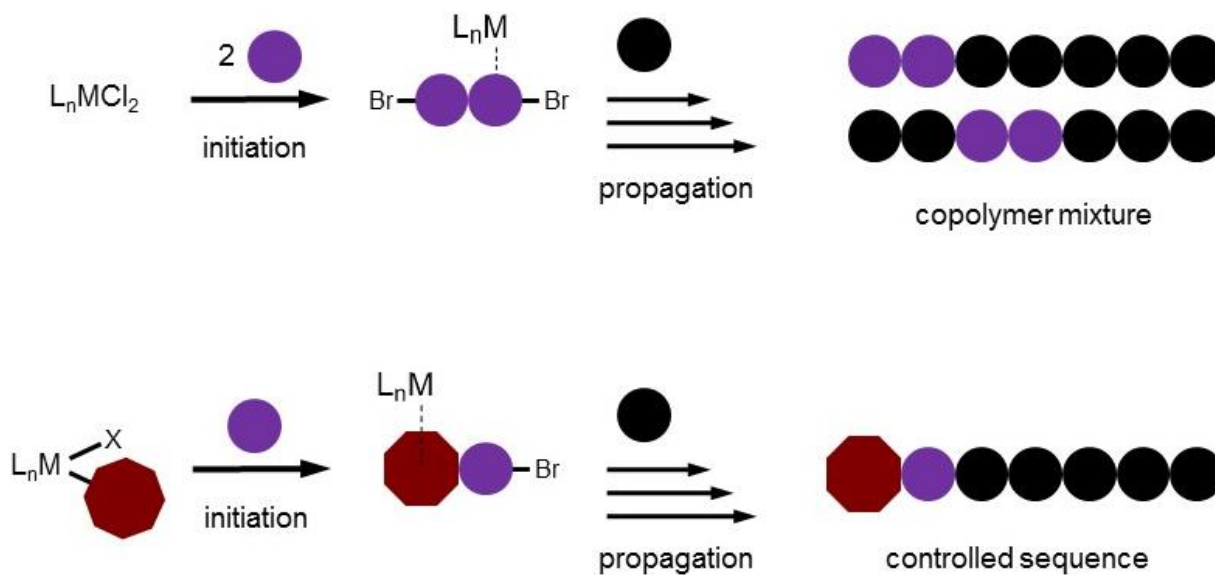
Products were analyzed across a range of polymer lengths using matrix-assisted laser desorption/ionization time-of-flight mass spectrometry (MALDI-TOF MS) to investigate the role of polymer length on migration. The ratio of polythiophene that had reacted at both ends was over 85% for all catalysts up to a DP of 50, but almost no migration was observed across phenylene using Ni(dppe)Cl<sub>2</sub> and Ni(dppp)Cl<sub>2</sub>. Changes in migration behavior of Ni phosphines by switching monomers is particularly interesting considering their poor copolymerizations of thiophene/phenylene, but the connection between these results is unexplored. The end-capping experiments provide a modular method to probe  $\pi$ -complex stability/catalyst mobility (but cannot differentiate the two) that offers a glimpse into how the  $\pi$ -complex for CTCP directs reactivity. Due to the fundamental nature of the  $\pi$ -complex, insights gained by investigating new catalyst, monomer, and/or comonomer combinations could have far-reaching impacts in CTCP.



**Scheme 1-4.** General end-capping experiments performed in Chapter 2 and 3.

*Addressing migration through precatalyst design*

For the commonly used Ni(dppe) catalysts, migration can be addressed using a precatalyst that transfers a reactive ligand (RL) to the  $\alpha$  end of the polymer end during initiation (Scheme 1-5).<sup>116</sup> Even if the catalyst does migrate between chain-ends, propagation can only occur from the  $\omega$  terminus. Reactive ligands can also be selected to improve precatalyst solubility (relative to the dihalide salt),<sup>104,117</sup> influence the initiation rate,<sup>118,119</sup> initiate from surfaces,<sup>120-124</sup> and/or incorporate a desired functional group.<sup>125-127</sup> Changing the reactive ligand does not alter the poor polymerization behavior; the same cross-propagation difficulty was observed using Ni(dppe)(*o*-PhOMe)Br.<sup>128</sup> Chapter 4 identifies IPrPd(3-chloropyridine)Cl<sub>2</sub> as a precatalyst with desirable reactivity in copolymerizations, but does not transfer a reactive ligand to the polymer. We considered the following strategies to identify a precatalyst suitable for copolymerizations.



**Scheme 1-5.** General products from initiation and propagation using precatalysts. Dihalide precatalysts (top) generate a polymer that could propagate from both C-Br to yield ill-defined copolymers. Functionalized precatalysts (bottom) transfer a reactive-ligand (●) to the polymer to prevent propagation from the  $\alpha$  end.

Precatalysts that transferred reactive ligands to the  $\alpha$  end of CPs were first prepared using an in situ approach. These precatalysts could be generated A) via oxidative addition from a Ni(0) triphenylphosphine precatalyst, or from a Ni(II) triphenylphosphine precatalyst using B) transmetalation with an aryl-lithium reagent, or C) in situ reduction from nBuLi followed by oxidative addition into an aryl halide. Each strategy yielded different amounts of end-group incorporation, polymer yield, dispersity, with the highest end-group incorporation achieved via in situ reduction of Ni(II).<sup>104</sup> Unreacted precatalyst, in situ catalyst decomposition, initiation products, and/or excess ligands can all effect the polymerization and are difficult to control/quantify.

Precatalysts have undergone rapid development in the past few years – catalyst systems using palladium (from PdCl<sub>2</sub> or Pd<sub>2</sub>(dba)<sub>3</sub>) with added ancillary ligand (usually 2-3 equiv) are being replaced by discrete precatalysts that combine the transition metal, ancillary ligand, and reactive ligand(s). Discrete precatalysts are attractive because many undergo facile activation and the amount of ligand on each catalyst can be controlled. Common precatalysts feature palladacycles (Buchwald precatalysts) or allyl precatalysts (developed by Nolan). These catalysts are highly active in a variety of reactions, but have mainly been developed for Buchwald-Hartwig

aminations and Suzuki cross-couplings. Precatalysts are activated by excess base, present in the reaction solution, followed by reductive elimination of the reactive ligand to generate the active catalyst. The reactive ligand by-product, present in only small amounts due to low catalyst loading, is removed during purification. Our precatalyst requirements and reaction conditions differ from conventional cross-coupling reactions. Precatalyst should be activated by transmetalation with monomer (rather than base), and incorporate reactive ligand into the desired product (polymer). Buchwald precatalysts were excluded from our catalyst screening because activation involves a cyclization reaction rather than a cross-coupling product.

We explored IPrPd derivatives that could combine efficient copolymerizations with control over sequence, and investigated the role of polymerization additives to improve end-group transfer. Precatalysts featuring a cinnamyl reactive ligand gave the highest levels of  $M_n$  control and low  $\mathcal{D}$ , but reactive ligand transfer to polymer was not quantitative. Efforts to improve reactive ligand transfer using small molecule additives or initiating with thiophene (rather than phenylene) were unsuccessful. Despite the challenges, identifying a precatalyst with a broad copolymerization scope that transfers a reactive ligand to the copolymer would be a rewarding pursuit. Examples of conjugated gradient copolymers hint at their vast potential, but synthetic methods have limited their use to only a handful of systems.

## Conclusion

CTCP methods are an attractive method for the synthesis of CPs to manipulate polymeric properties ( $M_n$ ,  $\mathcal{D}$ , end-groups, and copolymer sequence), develop structure-property relationships, and ultimately improve performance for a specific application. Examples of gradient copolymers, which can only be prepared via living, chain-growth methods, illustrate the importance of copolymer sequence for effecting polymer morphology. In practice, only a handful of monomers can be polymerized via CTCP. This thesis details our efforts to understand CTCP by indirectly probing the metal-polymer  $\pi$ -complex responsible for chain-growth behavior. Using end-capping experiments, we quantified the intramolecular migration of four CTCP catalysts across two polymers relative to a competitive chain-transfer/dissociation pathway. Although all catalysts perform similarly in polymerizations, drastically different migration results were observed based on the catalyst and monomer used. We sought to overcome catalyst migration during copolymerization by preparing Pd precatalysts that transfer a reactive ligand to the polymer, but

unstable precatalysts, slow initiation, and/or incomplete end-group transfer make catalyst development challenging. Continued iterations of mechanistic studies and catalyst development are necessary to expand the benefits of CTCP to a broader audience in the burgeoning field of organic electronics.



## References

- (1) Heeger, A. J. Nobel Lecture: Semiconducting and Metallic Polymers: The Fourth Generation of Polymeric Materials. *Rev. Mod. Phys.* **2001**, *73*, 681–700.
- (2) Chiang, C. K.; Fincher, C. R.; Park, Y. W.; Heeger, A. J.; Shirakawa, H.; Louis, E. J.; Gau, S. C.; MacDiarmid, A. G. Electrical Conductivity in Doped Polyacetylene. *Phys. Rev. Lett.* **1977**, *39*, 1098–1101.
- (3) Shirakawa, H.; Louis, E. J.; MacDiarmid, A. G.; Chiang, C. K.; Heeger, A. J. Synthesis of Electrically Conducting Organic Polymers: Halogen Derivatives of Polyacetylene, (CH) X. *J. Chem. Soc. Chem. Commun.* **1977**, 578–580.
- (4) Manouras, T.; Vamvakaki, M. Field Responsive Materials: Photo-, Electro-, Magnetic- and Ultrasound-Sensitive Polymers. *Polym. Chem.* **2017**, *8*, 74–96.
- (5) Chen, R.; Canales, A.; Anikeeva, P. Neural Recording and Modulation Technologies. *Nat. Rev. Mater.* **2017**, *2*, 16093.
- (6) Rim, Y. S.; Bae, S.-H. H.; Chen, H.; De Marco, N.; Yang, Y. Recent Progress in Materials and Devices toward Printable and Flexible Sensors. *Adv. Mater.* **2016**, *28*, 4415–4440.
- (7) Grimsdale, A. C.; Chan, K. L.; Martin, R. E.; Jokisz, P. G.; Holmes, A. B. Synthesis of Light-Emitting Conjugated Polymers for Applications in Electroluminescent Devices. *Chem. Rev.* **2009**, *109*, 897–1091.
- (8) Botiz, I.; Astilean, S.; Stingelin, N. Altering the Emission Properties of Conjugated Polymers. *Polym. Int.* **2016**, *65*, 157–163.
- (9) Facchetti, A.  $\pi$ -Conjugated Polymers for Organic Electronics and Photovoltaic Cell Applications. *Chem. Mater.* **2011**, *23*, 733–758.
- (10) Guo, X.; Baumgarten, M.; Müllen, K. Designing  $\pi$ -Conjugated Polymers for Organic Electronics. *Prog. Polym. Sci.* **2013**, *38*, 1832–1908.
- (11) Farinola, G. M.; Ragni, R. Electroluminescent Materials for White Organic Light Emitting Diodes. *Chem. Soc. Rev.* **2011**, *40*, 3467–3482.
- (12) Sirringhaus, H. 25Th Anniversary Article: Organic Field-Effect Transistors: The Path Beyond Amorphous Silicon. *Adv. Mater.* **2014**, *26*, 1319–1335.
- (13) Wang, C.; Dong, H.; Hu, W.; Liu, Y.; Zhu, D. Semiconducting  $\pi$ -Conjugated Systems in Field-Effect Transistors: A Material Odyssey of Organic Electronics. *Chem. Rev.* **2012**, *112*, 2208–2267.
- (14) Dou, L.; Liu, Y.; Hong, Z.; Li, G.; Yang, Y. Low-Bandgap Near-IR Conjugated Polymers/Molecules for Organic Electronics. *Chem. Rev.* **2015**, *115*, 12633–12665.
- (15) Rochat, S.; Swager, T. M.; Rochat, S.; Swager, T. M. Conjugated Amplifying Polymers for Optical Sensing Applications. *ACS Appl. Mater. Interfaces* **2013**, *5*, 4488–4502.
- (16) Lee, K.; Povlich, L. K.; Kim, J. Recent Advances in Fluorescent and Colorimetric Conjugated Polymer-Based Biosensors. *Analyst* **2010**, *135*, 2179–2189.

- (17) Peng, H.-Q.; Niu, L.-Y.; Chen, Y.-Z.; Wu, L.-Z.; Tung, C.-H.; Yang, Q.-Z. Biological Applications of Supramolecular Assemblies Designed for Excitation Energy Transfer. *Chem. Rev.* **2015**, *115*, 7502–7542.
- (18) Mazzio, K. a.; Luscombe, C. K. The Future of Organic Photovoltaics. *Chem. Soc. Rev.* **2015**, *44*, 78–90.
- (19) Lu, L.; Zheng, T.; Wu, Q.; Schneider, A. M.; Zhao, D.; Yu, L. Recent Advances in Bulk Heterojunction Polymer Solar Cells. *Chem. Rev.* **2015**, *115*, 12666–12731.
- (20) Wang, K.; Liu, C.; Meng, T.; Yi, C.; Gong, X. Inverted Organic Photovoltaic Cells. *Chem. Soc. Rev.* **2016**, *45*, 2937–2975.
- (21) Yu, J.; Zheng, Y.; Huang, J. Towards High Performance Organic Photovoltaic Cells: A Review of Recent Development in Organic Photovoltaics. *Polymers* **2014**, *6*, 2473–2509.
- (22) Diao, Y.; Shaw, L.; Bao, Z.; Mannsfeld, S. C. B. Morphology Control Strategies for Solution-Processed Organic Semiconductor Thin Films. *Energy Environ. Sci.* **2014**, *7*, 2145.
- (23) Deshmukh, K. D.; Qin, T.; Gallaher, J. K.; Liu, A. C. Y.; Gann, E.; O'Donnell, K.; Thomsen, L.; Hodgkiss, J. M.; Watkins, S. E.; McNeill, C. R. Performance, Morphology and Photophysics of High Open-Circuit Voltage, Low Band Gap All-Polymer Solar Cells. *Energy Environ. Sci.* **2015**, *8*, 332–342.
- (24) Mukherjee, S.; Proctor, C. M.; Bazan, G. C.; Nguyen, T.-Q.; Ade, H. Significance of Average Domain Purity and Mixed Domains on the Photovoltaic Performance of High-Efficiency Solution-Processed Small-Molecule BHJ Solar Cells. *Adv. Energy Mater.* **2015**, *5*, 1500877.
- (25) Lee, C.; Li, Y.; Lee, W.; Lee, Y.; Choi, J.; Kim, T.; Wang, C.; Gomez, E. D.; Woo, H. Y.; Kim, B. J. Correlation between Phase-Separated Domain Sizes of Active Layer and Photovoltaic Performances in All-Polymer Solar Cells. *Macromolecules* **2016**, *49*, 5051–5058.
- (26) van Franeker, J. J.; Kouijzer, S.; Lou, X.; Turbiez, M.; Wienk, M. M.; Janssen, R. A. J. Depositing Fullerenes in Swollen Polymer Layers via Sequential Processing of Organic Solar Cells. *Adv. Energy Mater.* **2015**, *5*, 1500464.
- (27) Perelaer, J.; Jena, F.; Schubert, U. S.; Jcsm, M. Ink-Jet Printing of Functional Polymers for Advanced Applications. In *Polymer Science: A Comprehensive Reference*; Matyjaszewski, K.; Möller, M., Eds.; Elsevier B.V., 2012; Vol. 8, pp. 147–175.
- (28) Chen, Y.; Zhang, X.; Zhan, C.; Yao, J. Origin of Effects of Additive Solvent on Film-Morphology in Solution-Processed Nonfullerene Solar Cells. *ACS Appl. Mater. Interfaces* **2015**, *7*, 6462–6471.
- (29) Kwon, S.; Kang, H.; Lee, J.-H.; Lee, J.; Hong, S.; Kim, H.; Lee, K. Effect of Processing Additives on Organic Photovoltaics: Recent Progress and Future Prospects. *Adv. Energy Mater.* **2016**, 1601496.
- (30) Qadir, K. W.; Ahmad, Z.; Sulaiman, K. Thermal Annealing Effect on the Optical, Electrical

- and Morphological Properties of the PBTTT-C<sub>12</sub>:PC<sub>71</sub> BM Blend Films. *J. Sol. Energy Eng.* **2015**, *137*, 34503.
- (31) Wang, T.; Pearson, A. J.; Lidzey, D. G.; Jones, R. a. L. Evolution of Structure, Optoelectronic Properties, and Device Performance of Polythiophene:Fullerene Solar Cells During Thermal Annealing. *Adv. Funct. Mater.* **2011**, *21*, 1383–1390.
- (32) Smith, K. a.; Stewart, B.; Yager, K. G.; Strzalka, J.; Verduzco, R. Control of All-Conjugated Block Copolymer Crystallization via Thermal and Solvent Annealing. *J. Polym. Sci. Part B Polym. Phys.* **2014**, *52*, 900–906.
- (33) Li, M.; Liu, F.; Wan, X.; Ni, W.; Kan, B.; Feng, H.; Zhang, Q.; Yang, X.; Wang, Y.; Zhang, Y.; *et al.* Subtle Balance between Length Scale of Phase Separation and Domain Purification in Small-Molecule Bulk-Heterojunction Blends under Solvent Vapor Treatment. *Adv. Mater.* **2015**, *27*, 6296–6302.
- (34) Foster, S.; Deledalle, F.; Mitani, A.; Kimura, T.; Kim, K.-B.; Okachi, T.; Kirchartz, T.; Oguma, J.; Miyake, K.; Durrant, J. R.; *et al.* Electron Collection as a Limit to Polymer:PCBM Solar Cell Efficiency: Effect of Blend Microstructure on Carrier Mobility and Device Performance in PTB7:PCBM. *Adv. Energy Mater.* **2014**, *4*, 1400311.
- (35) Kaake, L. G.; Welch, G. C.; Moses, D.; Bazan, G. C.; Heeger, A. J. Influence of Processing Additives on Charge-Transfer Time Scales and Sound Velocity in Organic Bulk Heterojunction Films. *J. Phys. Chem. Lett.* **2012**, *3*, 1253–1257.
- (36) Chen, K.-S.; Yip, H.-L.; Schlenker, C. W.; Ginger, D. S.; Jen, A. K.-Y. Halogen-Free Solvent Processing for Sustainable Development of High Efficiency Organic Solar Cells. *Org. Electron.* **2012**, *13*, 2870–2878.
- (37) Lee, J. K.; Ma, W. L.; Brabec, C. J.; Yuen, J.; Moon, J. S.; Kim, J. Y.; Lee, K.; Bazan, G. C.; Heeger, A. J. Processing Additives for Improved Efficiency from Bulk Heterojunction Solar Cells. *J. Am. Chem. Soc.* **2008**, *130*, 3619–3623.
- (38) Li, S.; Ye, L.; Zhao, W.; Zhang, S.; Mukherjee, S.; Ade, H.; Hou, J. Energy-Level Modulation of Small-Molecule Electron Acceptors to Achieve over 12% Efficiency in Polymer Solar Cells. *Adv. Mater.* **2016**, *28*, 9423–9429.
- (39) Zhao, F.; Dai, S.; Wu, Y.; Zhang, Q.; Wang, J.; Jiang, L.; Ling, Q.; Wei, Z.; Ma, W.; You, W.; *et al.* Single-Junction Binary-Blend Nonfullerene Polymer Solar Cells with 12.1% Efficiency. *Adv. Mater.* **2017**, *29*, 1700144.
- (40) Po, R.; Bernardi, A.; Calabrese, A.; Carbonera, C.; Corso, G.; Pellegrino, A. From Lab to Fab: How Must the Polymer Solar Cell Materials Design Change? – an Industrial Perspective. *Energy Environ. Sci.* **2014**, *7*, 925–943.
- (41) Krebs, F. C.; Jørgensen, M. Polymer and Organic Solar Cells Viewed as Thin Film Technologies: What It Will Take for Them to Become a Success Outside Academia. *Sol. Energy Mater. Sol. Cells* **2013**, *119*, 73–76.
- (42) Wu, C.-H. H.; Chueh, C.-C. C.; Xi, Y.-Y. Y.; Zhong, H.-L. L.; Gao, G.-P. P.; Wang, Z.-H. H.; Pozzo, L. D.; Wen, T.-C. C.; Jen, A. K.-Y. Y. Influence of Molecular Geometry of Perylene Diimide Dimers and Polymers on Bulk Heterojunction Morphology Toward High-

- Performance Nonfullerene Polymer Solar Cells. *Adv. Funct. Mater.* **2015**, *25*, 5326–5332.
- (43) Polman, A.; Knight, M.; Garnett, E. C.; Ehrler, B.; Sinke, W. C. Photovoltaic Materials: Present Efficiencies and Future Challenges. *Science*. **2016**, *352*, aad4424–aad4424.
- (44) Machui, F.; Hösel, M.; Li, N.; Spyropoulos, G. D.; Ameri, T.; Søndergaard, R. R.; Jørgensen, M.; Scheel, A.; Gaiser, D.; Kreul, K.; *et al.* Cost Analysis of Roll-to-Roll Fabricated ITO Free Single and Tandem Organic Solar Modules Based on Data from Manufacture. *Energy Environ. Sci.* **2014**, *7*, 2792.
- (45) Jepsen, T. H.; Larsen, M.; Jørgensen, M.; Solanko, K. a.; Bond, A. D.; Kadziola, A.; Nielsen, M. B. Synthesis of Functionalized Dibenzothiophenes - An Efficient Three-Step Approach Based on Pd-Catalyzed C-C and C-S Bond Formations. *European J. Org. Chem.* **2011**, *2011*, 53–57.
- (46) Diacon, A.; Derue, L.; Lecourtier, C.; Dautel, O.; Wantz, G.; Hudhomme, P. Cross-Linkable Azido C 60 -Fullerene Derivatives for Efficient Thermal Stabilization of Polymer Bulk-Heterojunction Solar Cells. *J. Mater. Chem. C* **2014**, *2*, 7163–7167.
- (47) Brotas, G.; Farinhas, J.; Ferreira, Q.; Morgado, J.; Charas, A. Nanostructured Layers of a New Cross-Linkable poly(3-Hexylthiophene) in Organic Photovoltaic Cells. *Synth. Met.* **2012**, *162*, 2052–2058.
- (48) Zhou, N.; Dudnik, A. S.; Li, T. I. N. G.; Manley, E. F.; Aldrich, T. J.; Guo, P.; Liao, H.-C.; Chen, Z.; Chen, L. X.; Chang, R. P. H.; *et al.* All-Polymer Solar Cell Performance Optimized via Systematic Molecular Weight Tuning of Both Donor and Acceptor Polymers. *J. Am. Chem. Soc.* **2016**, *138*, 1240–1251.
- (49) Xiao, Z.; Sun, K.; Subbiah, J.; Qin, T.; Lu, S.; Purushothaman, B.; Jones, D. J.; Holmes, A. B.; Wong, W. W. H. Effect of Molecular Weight on the Properties and Organic Solar Cell Device Performance of a Donor–acceptor Conjugated Polymer. *Polym. Chem.* **2015**, *6*, 2312–2318.
- (50) Huang, W.; Li, M.; Zhang, L.; Yang, T.; Zhang, Z.; Zeng, H.; Zhang, X.; Dang, L.; Liang, Y. Molecular Engineering on Conjugated Side Chain for Polymer Solar Cells with Improved Efficiency and Accessibility. *Chem. Mater.* **2016**, *28*, 5887–5895.
- (51) Kuo, C.; Huang, Y.-C.; Hsiow, C.; Yang, Y.; Huang, C.; Rwei, S.; Wang, H.-L.; Wang, L. Effect of Side-Chain Architecture on the Optical and Crystalline Properties of Two-Dimensional Polythiophenes. *Macromolecules* **2013**, *46*, 5985–5997.
- (52) Kim, Y.; Cook, S.; Tuladhar, S. M.; Choulis, S. A.; Nelson, J.; Durrant, J. R.; Bradley, D. D. C.; Giles, M.; McCulloch, I.; Ha, C.-S.; *et al.* A Strong Regioregularity Effect in Self-Organizing Conjugated Polymer Films and High-Efficiency Polythiophene:fullerene Solar Cells. *Nat. Mater.* **2006**, *5*, 197–203.
- (53) Kim, J.-S.; Kim, J.-H.; Lee, W.; Yu, H.; Kim, H. J.; Song, I.; Shin, M.; Oh, J. H.; Jeong, U.; Kim, T.-S.; *et al.* Tuning Mechanical and Optoelectrical Properties of Poly(3-Hexylthiophene) through Systematic Regioregularity Control. *Macromolecules* **2015**, *48*, 4339–4346.
- (54) Noriega, R.; Rivnay, J.; Vandewal, K.; Koch, F. P. V; Stingelin, N.; Smith, P.; Toney, M.

- F.; Salleo, A. A General Relationship between Disorder, Aggregation and Charge Transport in Conjugated Polymers. *Nat. Mater.* **2013**, *12*, 1038–1044.
- (55) Kim, H. J.; Kim, J.-H. H.; Ryu, J. H.; Kim, Y.; Kang, H.; Lee, W. B.; Kim, T.-S. S.; Kim, B. J. Architectural Engineering of Rod–Coil Compatibilizers for Producing Mechanically and Thermally Stable Polymer Solar Cells. *ACS Nano* **2014**, *8*, 10461–10470.
- (56) Kipp, D.; Verduzco, R.; Ganesan, V. Block Copolymer Compatibilizers for Ternary Blend Polymer Bulk Heterojunction Solar Cells – an Opportunity for Computation Aided Molecular Design. *Mol. Syst. Des. Eng.* **2016**, *1*, 353–369.
- (57) Li, A.; Amonoo, J.; Huang, B.; Goldberg, P. K.; McNeil, A. J.; Green, P. F. Enhancing Photovoltaic Performance Using an All-Conjugated Random Copolymer to Tailor Bulk and Interfacial Morphology of the P3HT:ICBA Active Layer. *Adv. Funct. Mater.* **2014**, *24*, 5594–5602.
- (58) Renaud, C. C.; Mougner, S.-J. J. S. J.; Pavlopoulou, E.; Brochon, C.; Fleury, G.; Deribew, D.; Portale, G.; Cloutet, E.; Chambon, S.; Vignau, L.; *et al.* Block Copolymer as a Nanostructuring Agent for High-Efficiency and Annealing-Free Bulk Heterojunction Organic Solar Cells. *Adv. Mater.* **2012**, *24*, 2196–2201.
- (59) Zhu, M.; Kim, H.; Jang, Y. J.; Park, S.; Ryu, D. Y.; Kim, K.; Tang, P.; Qiu, F.; Kim, D. H.; Peng, J. Toward High Efficiency Organic Photovoltaic Devices with Enhanced Thermal Stability Utilizing P3HT-B-P3PHT Block Copolymer Additives. *J. Mater. Chem. A* **2016**, *4*, 18432–18443.
- (60) Liu, J.; Zhu, X.; Li, J.; Shen, J.; Tu, G. Enhancing the Thermal Stability of the Bulk-Heterojunction Photovoltaics Based on P3HT/PCBM by Incorporating Diblock Amphiphilic P3HT–PEO at D/A Interface. *RSC Adv.* **2016**, *6*, 61934–61943.
- (61) Palermo, E. F.; Darling, S. B.; McNeil, A. J.  $\pi$ -Conjugated Gradient Copolymers Suppress Phase Separation and Improve Stability in Bulk Heterojunction Solar Cells. *J. Mater. Chem. C* **2014**, *2*, 3401–3406.
- (62) Amonoo, J. a.; Li, A.; Purdum, G. E.; Sykes, M. E.; Huang, B.; Palermo, E. F.; McNeil, A. J.; Shtein, M.; Loo, Y.-L.; Green, P. F. An All-Conjugated Gradient Copolymer Approach for Morphological Control of Polymer Solar Cells. *J. Mater. Chem. A* **2015**, *3*, 20174–20184.
- (63) Fink, J. K. Compatibilization. In *Reactive Polymers Fundamentals and Applications*; Elsevier, 2013; pp. 373–409.
- (64) Galloway, J. a.; Jeon, H. K.; Bell, J. R.; MacOsco, C. W. Block Copolymer Compatibilization of Cocontinuous Polymer Blends. *Polymer* **2005**, *46*, 183–191.
- (65) Bergman, J. a.; Cochran, E. W.; Heinen, J. M. Role of the Segment Distribution in the Microphase Separation of Acrylic Diblock and Triblock Terpolymers. *Polymer* **2014**, *55*, 4206–4215.
- (66) Luo, M.; Brown, J. R.; Remy, R. A.; Scott, D. M.; Mackay, M. E.; Hall, L. M.; Epps, T. H. Determination of Interfacial Mixing in Tapered Block Polymer Thin Films: Experimental and Theoretical Investigations. *Macromolecules* **2016**, *49*, 5213–5222.

- (67) Palermo, E. F.; McNeil, A. J. Impact of Copolymer Sequence on Solid-State Properties for Random, Gradient and Block Copolymers Containing Thiophene and Selenophene. *Macromolecules* **2012**, *45*, 5948–5955.
- (68) Palermo, E. F.; van der Laan, H. L.; McNeil, A. J. Impact of  $\pi$ -Conjugated Gradient Sequence Copolymers on Polymer Blend Morphology. *Polym. Chem.* **2013**, *4*, 4606–4611.
- (69) Sheina, E. E.; Liu, J.; Iovu, M. C.; Laird, D. W.; McCullough, R. D. Chain Growth Mechanism for Regioregular Nickel-Initiated Cross-Coupling Polymerizations. *Macromolecules* **2004**, *37*, 3526–3528.
- (70) Yokoyama, A.; Miyakoshi, R.; Yokozawa, T. Chain-Growth Polymerization for Poly(3-Hexylthiophene) with a Defined Molecular Weight and a Low Polydispersity. *Macromolecules* **2004**, *37*, 1169–1171.
- (71) Miyakoshi, R.; Shimono, K.; Yokoyama, A.; Yokozawa, T. Catalyst-Transfer Polycondensation for the Synthesis of Poly(p-Phenylene) with Controlled Molecular Weight and Low Polydispersity. *J. Am. Chem. Soc.* **2006**, *128*, 16012–16013.
- (72) Nanashima, Y.; Yokoyama, A.; Yokozawa, T. Synthesis of Well-Defined Poly(2-Alkoxy-pyridine-3,5-Diyl) via Ni-Catalyst-Transfer Condensation Polymerization. *Macromolecules* **2012**, *45*, 2609–2613.
- (73) Yokoyama, A.; Kato, A.; Miyakoshi, R.; Yokozawa, T. Precision Synthesis of Poly(N-Hexylpyrrole) and Its Diblock Copolymer with Poly(p-Phenylene) via Catalyst-Transfer Polycondensation. *Macromolecules* **2008**, *41*, 7271–7273.
- (74) Heeney, M.; Zhang, W.; Crouch, D. J.; Chabinyc, M. L.; Gordeyev, S.; Hamilton, R.; Higgins, S. J.; McCulloch, I.; Skabara, P. J.; Sparrowe, D.; *et al.* Regioregular poly(3-Hexyl)selenophene: A Low Band Gap Organic Hole Transporting Polymer. *Chem. Commun.* **2007**, 5061–5063.
- (75) Pammer, F.; Jäger, J.; Rudolf, B.; Sun, Y.; Jager, J.; Rudolf, B.; Sun, Y.; Jäger, J.; Rudolf, B.; Sun, Y.; *et al.* Soluble Head-to-Tail Regioregular Polythiazoles: Preparation, Properties, and Evidence for Chain-Growth Behavior in the Synthesis via Kumada-Coupling Polycondensation. *Macromolecules* **2014**, *47*, 5904–5912.
- (76) Miyakoshi, R.; Yokoyama, A.; Yokozawa, T. Importance of the Order of Successive Catalyst-Transfer Condensation Polymerization in the Synthesis of Block Copolymers of Polythiophene and Poly(p-Phenylene). *Chem. Lett.* **2008**, *37*, 1022–1023.
- (77) Wu, S.; Bu, L.; Huang, L.; Yu, X.; Han, Y.; Geng, Y.; Wang, F. Synthesis and Characterization of Phenylene-Thiophene All-Conjugated Diblock Copolymers. *Polymer* **2009**, *50*, 6245–6251.
- (78) Ananikov, V. P. Nickel: The “Spirited Horse” of Transition Metal Catalysis. *ACS Catal.* **2015**, *5*, 1964–1971.
- (79) Massera, C.; Frenking, G. Energy Partitioning Analysis of the Bonding in L2TM–C2H2 and L2TM–C2H4 (TM = Ni, Pd, Pt; L2 = (PH3)2, (PMe3)2, H2 PCH2PH2, H2P(CH2)2PH2)†. *Organometallics* **2003**, *22*, 2758–2765.

- (80) Bilbrey, J. A.; Bootsma, A. N.; Bartlett, M. A.; Locklin, J.; Wheeler, S. E.; Allen, W. D. Ring-Walking of Zerovalent Nickel on Aryl Halides. *J. Chem. Theory Comput.* **2017**, *13*, 1706–1711.
- (81) Köhler, K.; Wussow, K.; Wirth, A. S. Palladium-Catalyzed Cross-Coupling Reactions - A General Introduction. In *Palladium-Catalyzed Coupling Reactions*; Wiley-VCH Verlag GmbH & Co. KGaA: Weinheim, Germany, 2013; pp. 1–30.
- (82) Tsuji, J. The Basic Chemistry of Organopalladium Compounds. *Palladium Reagents Catal.* **2005**, *9*, 1–26.
- (83) Echavarren, A. M.; Crdenas, D. J. Mechanistic Aspects of Metal-Catalyzed C,C- and C,X-Bond-Forming Reactions. In *Metal-Catalyzed Cross-Coupling Reactions*; Wiley-VCH Verlag GmbH: Weinheim, Germany, 2004; pp. 1–40.
- (84) Hazari, N.; Melvin, P. R.; Beromi, M. M. Well-Defined Nickel and Palladium Precatalysts for Cross-Coupling. *Nat. Rev. Chem.* **2017**, *1*, 25.
- (85) Clavier, H.; Nolan, S. P. Percent Buried Volume for Phosphine and N-Heterocyclic Carbene Ligands: Steric Properties in Organometallic Chemistry. *Chem. Commun.* **2010**, *46*, 841.
- (86) Surry, D. S.; Buchwald, S. L. Dialkylbiaryl Phosphines in Pd-Catalyzed Amination: A User's Guide. *Chem. Sci.* **2011**, *2*, 27–50.
- (87) Tolman, C. a. Steric Effects of Phosphorus Ligands in Organometallic Chemistry and Homogeneous Catalysis. *Chem. Rev.* **1977**, *77*, 313–348.
- (88) Tamba, S.; Fuji, K.; Nakamura, K.; Mori, A. Nickel(II)-Catalyzed Cross-Coupling Polycondensation of Thiophenes via C–S Bond Cleavage. *Organometallics* **2014**, *33*, 12–15.
- (89) Shi, X.; Sui, A.; Wang, Y.; Li, Y. S.; Geng, Y.; Wang, F.; Shi, X.; Sui, A.; Wang, Y.; Li, Y. S.; *et al.* Controlled Synthesis of High Molecular Weight poly(3-Hexylthiophene)s via Kumada Catalyst Transfer Polycondensation with Ni(IPr)(acac) 2 as the Catalyst. *Chem. Commun.* **2015**, *51*, 2138–2140.
- (90) Fujita, K.; Sumino, Y.; Ide, K.; Tamba, S.; Shono, K.; Shen, J.; Nishino, T.; Mori, A.; Yasuda, T. Synthesis of Poly(3-Substituted Thiophene)s of Remarkably High Solubility in Hydrocarbon via Nickel-Catalyzed Deprotonative Cross-Coupling Polycondensation. *Macromolecules* **2016**, *49*, 1259–1269.
- (91) Bridges, C. R.; Yan, H.; Pollit, A. A.; Seferos, D. S. Controlled Synthesis of Fully  $\pi$ -Conjugated Donor–Acceptor Block Copolymers Using a Ni(II) Diimine Catalyst. *ACS Macro Lett.* **2014**, *3*, 671–674.
- (92) Bridges, C. R.; McCormick, T. M.; Gibson, G. L.; Hollinger, J.; Seferos, D. S. Designing and Refining Ni(II)diimine Catalysts Towards the Controlled Synthesis of Electron-Deficient Conjugated Polymers. *J. Am. Chem. Soc.* **2013**, *135*, 13212–13219.
- (93) Bryan, Z. J.; Smith, M. L.; McNeil, A. J. Chain-Growth Polymerization of Aryl Grignards Initiated by a Stabilized NHC-Pd Precatalyst. *Macromol. Rapid Commun.* **2012**, *33*, 842–847.

- (94) Qiu, Y.; Mohin, J.; Tsai, C.-H.; Tristram-Nagle, S.; Gil, R. R.; Kowalewski, T.; Noonan, K. J. T. Stille Catalyst-Transfer Polycondensation Using Pd-PEPPSI-IPr for High-Molecular-Weight Regioregular Poly(3-Hexylthiophene). *Macromol. Rapid Commun.* **2015**, *36*, 840–844.
- (95) Sui, A.; Shi, X.; Tian, H.; Geng, Y.; Wang, F. Suzuki–Miyaura Catalyst-Transfer Polycondensation with Pd(IPr)(OAc)<sub>2</sub> as the Catalyst for the Controlled Synthesis of Polyfluorenes and Polythiophenes. *Polym. Chem.* **2014**, *5*, 7072–7080.
- (96) Elmalem, E.; Biedermann, F.; Johnson, K.; Friend, R. H.; Huck, W. T. S. Synthesis and Photophysics of Fully  $\pi$ -Conjugated Heterobis-Functionalized Polymeric Molecular Wires via Suzuki Chain-Growth Polymerization. *J. Am. Chem. Soc.* **2012**, *134*, 17769–17777.
- (97) Zhang, H.-H.; Peng, W.; Dong, J.; Hu, Q.-S. T -Bu<sub>3</sub>P-Coordinated 2-Phenylaniline-Based Palladacycle Complex/ArBr as Robust Initiators for Controlled Pd(0)/T -Bu<sub>3</sub>P-Catalyzed Suzuki Cross-Coupling Polymerization of AB-Type Monomers. *ACS Macro Lett.* **2016**, *5*, 656–660.
- (98) Verswyvel, M.; Verstappen, P.; De Cremer, L.; Verbiest, T.; Koeckelberghs, G. Development of a Universal Chain-Growth Polymerization Protocol of Conjugated Polymers: Toward a Variety of All-Conjugated Block-Copolymers. *J. Polym. Sci. Part A Polym. Chem.* **2011**, *49*, 5339–5349.
- (99) Willot, P.; Koeckelberghs, G. Evidence for Catalyst Association in the Catalyst Transfer Polymerization of Thieno[3,2- B]thiophene. *Macromolecules* **2014**, *47*, 8548–8555.
- (100) Komber, H.; Senkovskyy, V.; Tkachov, R.; Johnson, K.; Kiriya, A.; Huck, W. T. S.; Sommer, M. Ring Walking versus Trapping of Nickel(0) during Kumada Catalyst Transfer Polycondensation Using Externally Initiated Electron-Accepting Thiophene–Benzothiadiazole–Thiophene Precursors. *Macromolecules* **2011**, *44*, 9164–9172.
- (101) Smith, M. L.; Leone, A. K.; Zimmerman, P. M.; McNeil, A. J. Impact of Preferential  $\pi$ -Binding in Catalyst-Transfer Polycondensation of Thiazole Derivatives. *ACS Macro Lett.* **2016**, *5*, 1411–1415.
- (102) Yokoyama, A.; Suzuki, H.; Kubota, Y.; Ohuchi, K.; Higashimura, H.; Yokozawa, T. Chain-Growth Polymerization for the Synthesis of Polyfluorene via Suzuki–Miyaura Coupling Reaction from an Externally Added Initiator Unit. *J. Am. Chem. Soc.* **2007**, *129*, 7236–7237.
- (103) Beryozkina, T.; Senkovskyy, V.; Kaul, E.; Kiriya, A. Kumada Catalyst-Transfer Polycondensation of Thiophene-Based Oligomers: Robustness of a Chain-Growth Mechanism. *Macromolecules* **2008**, *41*, 7817–7823.
- (104) Doubina, N.; Ho, A.; Jen, A. K.-Y. Y.; Luscombe, C. K. Effect of Initiators on the Kumada Catalyst-Transfer Polycondensation Reaction. *Macromolecules* **2009**, *42*, 7670–7677.
- (105) Kohn, P.; Huettner, S.; Komber, H.; Senkovskyy, V.; Tkachov, R.; Kiriya, A.; Friend, R. H.; Steiner, U.; Huck, W. T. S.; Sommer, J.-U. U.; *et al.* On the Role of Single Regiodefects and Polydispersity in Regioregular poly(3-Hexylthiophene): Defect Distribution, Synthesis of Defect-Free Chains, and a Simple Model for the Determination of Crystallinity. *J. Am. Chem. Soc.* **2012**, *134*, 4790–4805.



- (106) Hardeman, T.; De Becker, J.; Koeckelberghs, G. Influence of the Halogen and Organometallic Function in a KCTP (Co)polymerization. *J. Polym. Sci. Part A Polym. Chem.* **2016**, *54*, 3701–3706.
- (107) Jeffries-EL, M.; Sauv , G.; McCullough, R. D.; Malika, J. E. L.; Sauv , G.; McCullough, R. D.; Jeffries-EL, M.; Sauv , G.; McCullough, R. D. In-Situ End-Group Functionalization of Regioregular Poly(3-Alkylthiophene) Using the Grignard Metathesis Polymerization Method. *Adv. Mater.* **2004**, *16*, 1017–1019.
- (108) Jeffries-El, M.; Sauv , G.; McCullough, R. D. Facile Synthesis of End-Functionalized Regioregular Poly(3-Alkylthiophene)s via Modified Grignard Metathesis Reaction. *Macromolecules* **2005**, *38*, 10346–10352.
- (109) Kochemba, W. M.; Pickel, D. L.; Sumpter, B. G.; Chen, J.; Kilbey, S. M. In Situ Formation of Pyridyl-Functionalized Poly(3-Hexylthiophene)s via Quenching of the Grignard Metathesis Polymerization: Toward Ligands for Semiconductor Quantum Dots. *Chem. Mater.* **2012**, *24*, 4459–4467.
- (110) Kochemba, W. M.; Kilbey, S. M.; Pickel, D. L. End-Group Composition of poly(3-Hexylthiophene)s Prepared by in Situ Quenching of the Grignard Metathesis Polymerization: Influence of Additives and Reaction Conditions. *J. Polym. Sci. Part A Polym. Chem.* **2012**, *50*, 2762–2769.
- (111) Huddleston, N. E.; Sontag, S. K.; Bilbrey, J. a.; Sheppard, G. R.; Locklin, J. Palladium-Mediated Surface-Initiated Kumada Catalyst Polycondensation: A Facile Route Towards Oriented Conjugated Polymers. *Macromol. Rapid Commun.* **2012**, *33*, 2115–2120.
- (112) Bryan, Z. J.; McNeil, A. J. Evidence for a Preferential Intramolecular Oxidative Addition in Ni-Catalyzed Cross-Coupling Reactions and Their Impact on Chain-Growth Polymerizations. *Chem. Sci.* **2013**, *4*, 1620–1624.
- (113) Larrosa, I.; Somoza, C.; Banquy, A.; Goldup, S. M. Two Flavors of PEPPSI-IPr: Activation and Diffusion Control in a Single NHC-Ligated Pd Catalyst? *Org. Lett.* **2011**, *13*, 146–149.
- (114) Bryan, Z. J.; Hall, A. O.; Zhao, C. T.; Chen, J.; McNeil, A. J. Limitations of Using Small Molecules to Identify Catalyst-Transfer Polycondensation Reactions. *ACS Macro Lett.* **2016**, *5*, 69–72.
- (115) Tokita, Y.; Katoh, M.; Ohta, Y.; Yokozawa, T. Mechanistic Investigation of Catalyst-Transfer Suzuki-Miyaura Condensation Polymerization of Thiophene-Pyridine Biaryl Monomers with the Aid of Model Reactions. *Chem. Eur. J.* **2016**, *22*, 17436–17444.
- (116) Locke, J. R.; McNeil, A. J. Syntheses of Gradient  $\pi$ -Conjugated Copolymers of Thiophene. *Macromolecules* **2010**, *43*, 8709–8710.
- (117) Smeets, A.; Van den Bergh, K.; De Winter, J.; Gerbaux, P.; Verbiest, T.; Koeckelberghs, G. Incorporation of Different End Groups in Conjugated Polymers Using Functional Nickel Initiators. *Macromolecules* **2009**, *42*, 7638–7641.
- (118) Lee, S. R.; Bloom, J. W. G.; Wheeler, S. E.; McNeil, A. J. Accelerating Ni(ii) Precatalyst Initiation Using Reactive Ligands and Its Impact on Chain-Growth Polymerizations. *Dalt. Trans.* **2013**, *42*, 4218–4222.

- (119) Hall, A. O.; Lee, S. R.; Bootsma, A. N.; Bloom, J. W. G.; Wheeler, S. E.; McNeil, A. J. Reactive Ligand Influence on Initiation in Phenylene Catalyst-Transfer Polymerization. *J. Polym. Sci. Part A Polym. Chem.* **2017**, *55*, 1530–1535.
- (120) Tkachov, R.; Senkovskyy, V.; Horecha, M.; Oertel, U.; Stamm, M.; Kiriya, A. Surface-Initiated Kumada Catalyst-Transfer Polycondensation of poly(9,9-Dioctylfluorene) from Organosilica Particles: Chain-Confinement Promoted  $\beta$ -Phase Formation. *Chem. Commun.* **2010**, *46*, 1425–1427.
- (121) Sontag, S. K.; Marshall, N.; Locklin, J. Formation of Conjugated Polymer Brushes by Surface-Initiated Catalyst-Transfer Polycondensation. *Chem. Commun.* **2009**, 3354.
- (122) Doubina, N.; Jenkins, J. L.; Paniagua, S. a; Mazzio, K. a; MacDonald, G. a; Jen, A. K.-Y.; Armstrong, N. R.; Marder, S. R.; Luscombe, C. K. Surface-Initiated Synthesis of poly(3-Methylthiophene) from Indium Tin Oxide and Its Electrochemical Properties. *Langmuir* **2012**, *28*, 1900–1908.
- (123) Kang, S.; Ono, R. J.; Bielawski, C. W. Controlled Catalyst Transfer Polycondensation and Surface-Initiated Polymerization of a P-Phenyleneethynylene-Based Monomer. *J. Am. Chem. Soc.* **2013**, *135*, 4984–4987.
- (124) Senkovskyy, V.; Tkachov, R.; Beryozkina, T.; Komber, H.; Oertel, U.; Horecha, M.; Bocharova, V.; Stamm, M.; Gevorgyan, S. a; Krebs, F. C.; *et al.* “Hairy” poly(3-Hexylthiophene) Particles Prepared via Surface-Initiated Kumada Catalyst-Transfer Polycondensation. *J. Am. Chem. Soc.* **2009**, *131*, 16445–16453.
- (125) Smeets, A.; Willot, P.; De Winter, J.; Gerbaux, P.; Verbiest, T.; Koeckelberghs, G. End Group-Functionalization and Synthesis of Block-Copolythiophenes by Modified Nickel Initiators. *Macromolecules* **2011**, *44*, 6017–6025.
- (126) Monnaie, F.; Brullot, W.; Verbiest, T.; De Winter, J.; Gerbaux, P.; Smeets, A.; Koeckelberghs, G. Synthesis of End-Group Functionalized P3HT: General Protocol for P3HT/Nanoparticle Hybrids. *Macromolecules* **2013**, *46*, 8500–8508.
- (127) Yuan, M.; Okamoto, K.; Bronstein, H. a.; Luscombe, C. K. Constructing Regioregular Star Poly(3-Hexylthiophene) via Externally Initiated Kumada Catalyst-Transfer Polycondensation. *ACS Macro Lett.* **2012**, *1*, 392–395.
- (128) Locke, J. R.  $\pi$ -Conjugated Copolymers of Controlled Sequence, University of Michigan, 2012.

## Chapter 2

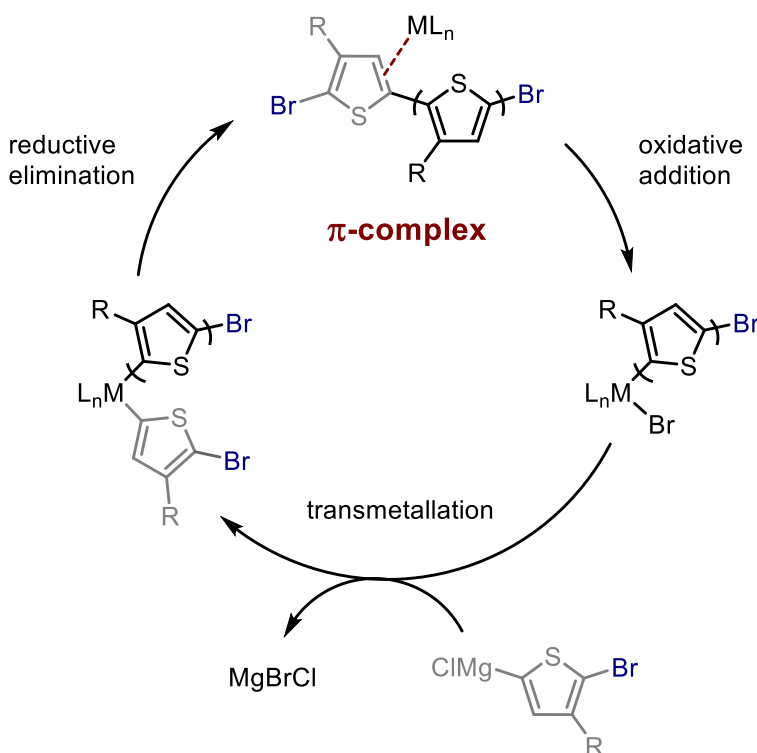
### Long-distance catalyst migration across poly(3-alkylthiophene)

#### Introduction

Conjugated polymers have garnered significant interest due to their flexibility and potential application in low-cost sensors,<sup>1-3</sup> light-emitting diodes,<sup>4-8</sup> transistors,<sup>9-11</sup> and solar cells.<sup>12-15</sup> Electronic and morphological properties can be tuned by modifying the chemical structure, leading to a diverse array of monomer combinations that have been evaluated in thin-films and devices. However, it is challenging to dictate molecular weight and end-groups for most polymers using existing step-growth polymerizations. The enhanced synthetic control offered by living, chain-growth polymerizations was first realized for conjugated polymer synthesis in 2004 when catalyst-transfer condensation polymerization (CTCP) was employed to prepare poly(3-hexylthiophene).<sup>16,17</sup> The discovery of CTCP has enabled new materials to be prepared that demonstrate the importance of molecular weight, copolymer sequence, and end-groups on physical and electronic properties.<sup>18-22</sup> Despite the clear advantages, CTCP has only been applied to a limited number of monomers because most attempts to polymerize extended macrocycles and/or electron deficient monomers have failed.<sup>23-29</sup> Understanding what separates the successes from failures is critical to developing new catalysts to polymerize monomers with tailored electronic levels, better absorption/emission properties, and higher charge mobility. A more versatile method capable of incorporating the diverse monomer scope associated with step-growth polymerizations with the molecular weight and sequence control of CTCP would be invaluable for systematically optimizing electronic structure and morphology of conjugated polymers for each application.

The key feature that distinguishes CTCP from conventional cross-coupling polymerizations is an associative complex that forms following reductive elimination, where the electron-rich transition metal binds to the  $\pi$ -system of the conjugated polymer. This  $\pi$ -complex predisposes the catalyst to intramolecular oxidative addition, which leads to a chain-growth

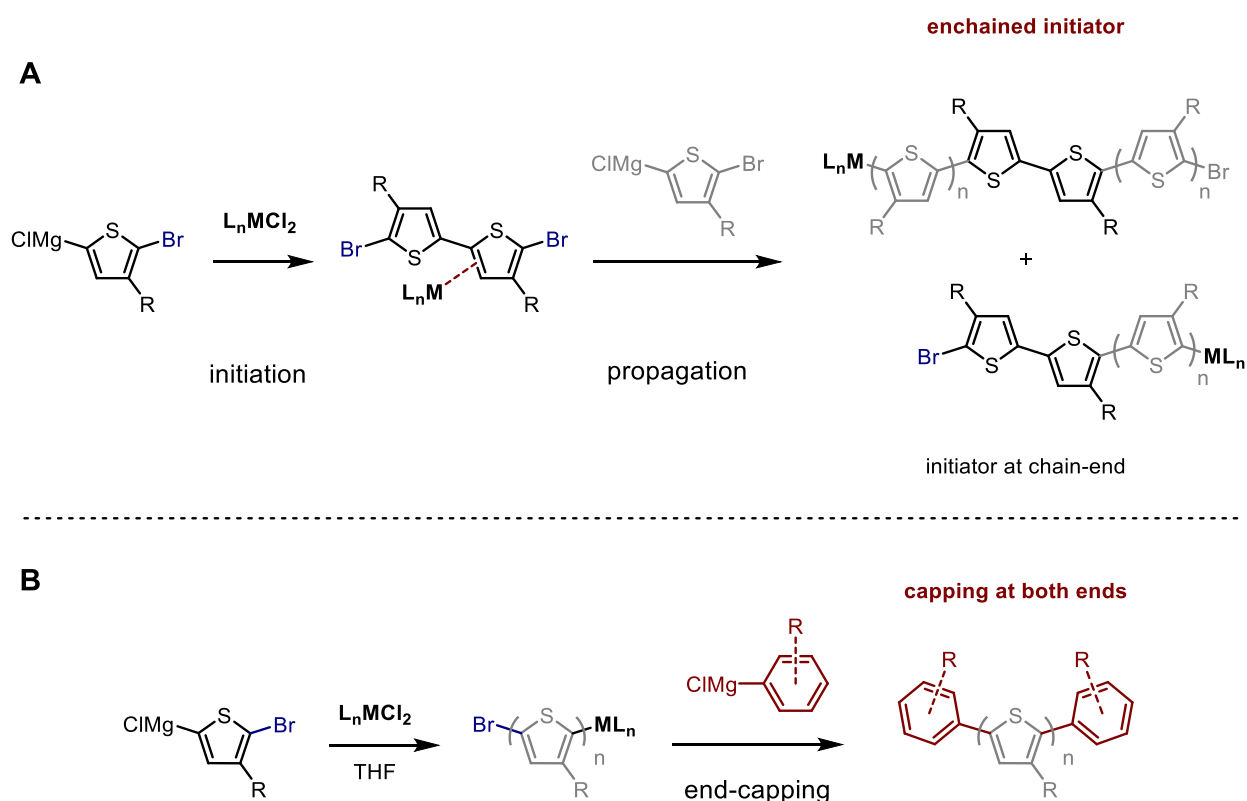
polymerization (Scheme 2-1). Studying how the catalyst-polymer  $\pi$ -complex directs intramolecular oxidative addition could help researchers target promising monomer/catalyst combinations and identify when complex formation is problematic. Unfortunately, the  $\pi$ -complex is difficult to study because it is not an observable intermediate in well-controlled systems.<sup>18</sup>



**Scheme 2-1.** Catalytic cycle for the polymerization of 3-alkylthiophene using Kumada CTCP.

Many researchers have investigated thiophene polymerizations because of the high degree of control over molecular weight and dispersity, which affect structure-property relationships and solar cell performance. Compelling indirect evidence for the  $\pi$ -complex has been documented in reports of initiator enchainment,<sup>30–33</sup> monomer scope,<sup>34–42</sup> and end-capping experiments.<sup>43–46</sup> Dihalide precatalysts are commonly employed in CTCP due to their stability and commercial availability. Initiating dihalide precatalysts using thiophene monomer proceeds through a 5,5'-dibromo-4,4'-dialkyl-2,2'-bithiophene initiator that can react at both C-Br bonds. Propagation from both ends with a single catalyst is observed, but chain-growth behavior is maintained through a series of  $\pi$ -complexes where the catalyst “walks” from monomer to monomer to migrate between chain-ends. This dynamic process, referred to herein as chain-walking, enables the catalyst to

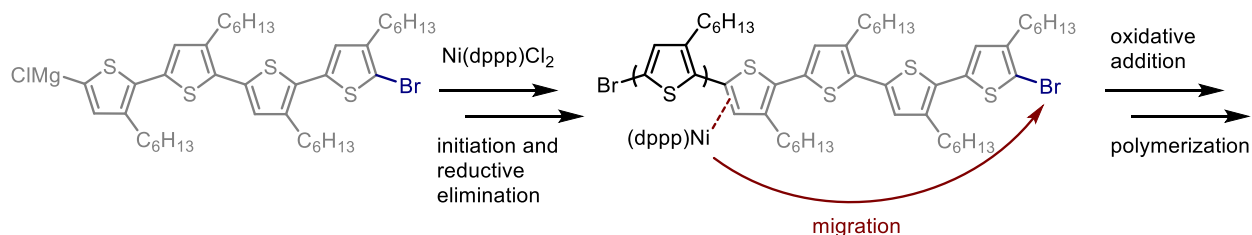
migrate across the conjugated backbone without chain-transfer or dissociation (which would lead to a step-growth polymerization). Catalyst chain-walking is the process through which the catalyst moves along the conjugated polymer through a series of  $\pi$ -complexes, while catalyst migration quantifies end-to-end movement. Propagating from both ends enchains the bithiophene initiator into the polymer backbone (Scheme 2-2).<sup>30</sup> Initiator enchainment has been independently reported for several catalysts, but a meaningful comparison between catalysts requires identical polymerization conditions. Additionally, initiator enchainment can only be calculated from the bulk polymer sample (using NMR spectroscopy), whereas enchainment should increase with increasing degree of polymerization (DP).<sup>30,33</sup>



**Scheme 2-2.** (A) Initiator enchainment and (B) capping at both ends of poly(3-alkylthiophene) provide evidence for catalyst migration.

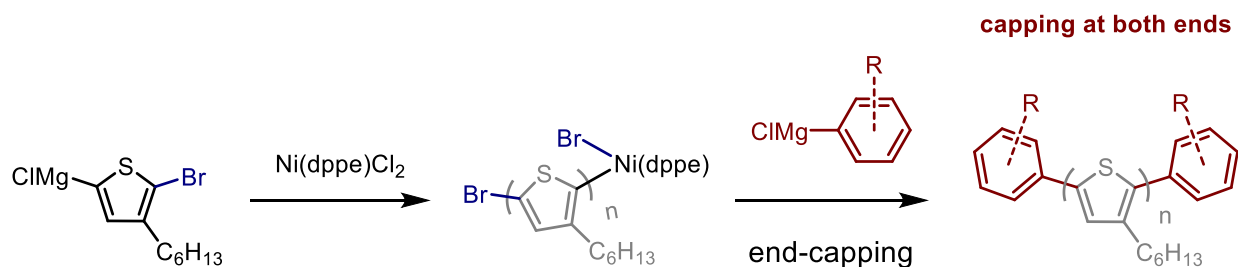
Catalyst chain-walking has been exploited using monomers containing multiple aryl groups, such as tetramers of 3-hexylthiophene, that place the reactive C-Br bond three thiophene rings away from the catalyst after reductive elimination and  $\pi$ -complex formation (Scheme 2-3). To maintain chain-growth behavior, the catalyst must chain-walk across the large repeating unit

for intramolecular oxidative addition. Even for polymers with 100 thiophene units, there is no apparent difference in dispersity when quarterthiophene monomers were used to produce poly(3-hexylthiophene) using Ni(dppp)Cl<sub>2</sub> relative to bithiophene or thiophene monomers targeting the same molecular weight (dppp = 1,3-bis(diphenylphosphine)propane).<sup>34</sup> Catalysts that are less efficient at CTCP, such as Ni(PPh<sub>3</sub>)<sub>2</sub>(Ph)Br, show an increase in dispersity with increasing monomer size (PPh<sub>3</sub> = triphenylphosphine).<sup>41</sup>



**Scheme 2-3.** Ni(dppp)Cl<sub>2</sub> catalyzed polymerization of a quarterthiophene monomer requires catalyst migration across four thiophene units for intramolecular oxidative addition (right) to realize a chain-growth polymerization.

Catalyst migration has also been examined by end-capping polymerizations with an excess of mono-functional Grignard reagent (i.e., capping agent). The capping agent (cap) transmetalates with the catalyst on the active ( $\omega$ ) chain end, yielding cap/Br end-groups and (associated) catalyst. Catalyst migration followed by oxidative addition into the  $\alpha$  C-Br terminus enables further reaction with the capping agent to give cap/cap end-groups. End-capping at both ends of poly(3-hexylthiophene) has been observed using a variety of aryl capping agents, indicating that the catalyst migrates between polymer ends (Scheme 2-4).<sup>43-46</sup>



**Scheme 2-4.** End-capping observed at both ends of poly(3-hexylthiophene) polymerized by Ni(dppe)Cl<sub>2</sub>.

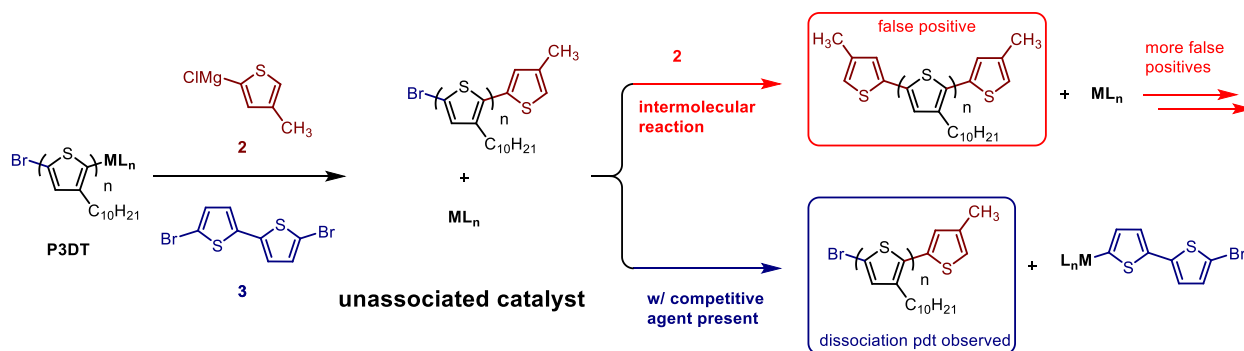
Collectively, initiator enchainment, monomer scope, and end-capping experiments all demonstrate that catalyst migration occurs during a typical polymerization and can be quantitative by end-capping (when migration is “forced”). Because the  $\pi$ -complex is fundamental to CTCP and

catalyst migration has been observed, rigorous investigations of the chain-walking process could identify how catalyst parameters affect migration and the subsequent influence on dispersity as well as molecular weight/sequence/end-group control. Existing information about the  $\pi$ -complex is limited— (1) The amount of initiator enchainment only indicates migration frequency (not  $\pi$ -complex stability). (2) End-capping experiments provide a modular system for examining catalyst migration, but reactions at both polymer ends could occur through intermolecular and/or intramolecular pathways. If the intermolecular reactions are suppressed, end-capping experiments can provide insights about the catalyst-polymer  $\pi$ -complex beyond the scope of standard polymerizations. Using conditions with clear evidence for  $\pi$ -complexation, such as poly(3-alkylthiophene) with Ni(dppp)Cl<sub>2</sub> and Ni(dppe)Cl<sub>2</sub>, we can push the limits of  $\pi$ -complex stability/catalyst mobility by forcing migration across long-distances. By stressing the system beyond the typical requirements for CTCP, we aim to identify catalyst/monomer parameters that influence migration and can be leveraged to expand CTCP to new monomers.

Herein, we present a model system based on end-group labeling to evaluate the role of ligand and transition metal identity on catalyst migration across poly(3-decylthiophene). Adding capping agent to the polymerization terminates the  $\omega$  chain-end and forms a catalyst-polymer  $\pi$ -complex. If the  $\pi$ -complex is sufficiently strong and the catalyst is mobile, the catalyst migrates to the  $\alpha$  end via chain-walking to react with a second capping agent. Polymers where the catalyst has reacted at both ends (i.e., the migration product) are labelled with a capping agent on both ends. In contrast to previous investigations, we employed an excess of reactive aryl halide (competitive agent) to minimize diffusion/chain-transfer products by sequestering Ni<sup>0</sup>/Pd<sup>0</sup> without disrupting polymerization behavior. The migration product dominated across all molecular weights for all four tested CTCP catalysts, indicating that the catalyst-polymer  $\pi$ -complex can chain-walk across over 60 repeat units to direct intramolecular oxidative addition into terminal C-Br bonds. The observation that Ni *and* Pd catalysts demonstrate this remarkable migration behavior is striking considering reports of their different complexation behavior.<sup>47-49</sup> Furthermore, both bidentate phosphine and N-heterocyclic carbene (NHC) ligated Ni catalysts yield similar results. This shared behavior suggests that migration ability could be important for efficient CTCP catalysts and should be considered when evaluating new monomer/catalyst combinations.

## Results and Discussion

We established an end-capping system where intermolecular reactivity was minimized by using a competitive agent to sequester unassociated catalyst. In the end-capping experiments, a capping agent was incorporated into all polymers via transmetalation then reductive elimination, forming a catalyst-polymer  $\pi$ -complex. Ultimately, the catalyst will either migrate to the  $\alpha$  end to install a second capping agent or dissociate/chain-transfer from the parent polymer to react with competitive agent. Characterizing polymers by end-group mass at each DP allowed us to determine the effect of chain-length on catalyst migration and easily compare catalysts at identical polymer molecular weights. Chain-walking, especially across long polymers, could lead to an increase in termination or chain-transfer as the catalyst would spend increasing amounts of time migrating between chain-ends. Therefore, identifying catalyst migration at each chain-length should provide valuable insight into polymerization relevant behavior. Dissociated catalyst and/or catalyst that has reacted at both ends was sequestered by an excess of competitive agent (i.e., reactive aryl halide). Removing unassociated catalyst is critical to properly assigning reaction products—false positives could be produced catalytically in the absence of competitive agent (Scheme 2-5).

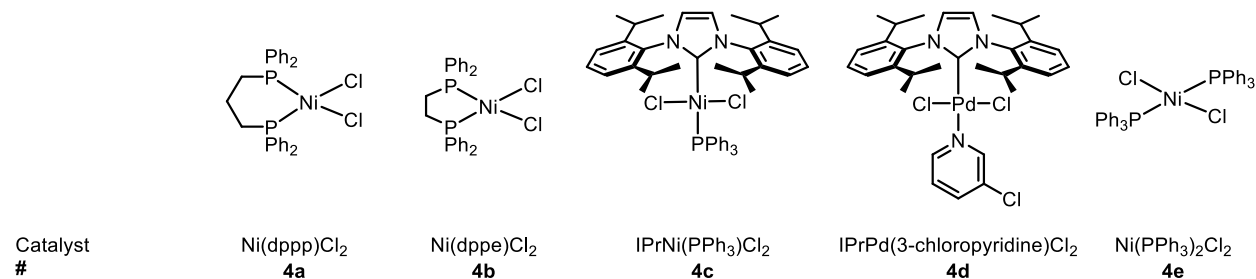


**Scheme 2-5.** End-capping reaction with unassociated catalyst generates *false positive* (i.e. migration product) if competitive agent is absent or not sufficiently reactive (intermolecular reaction).

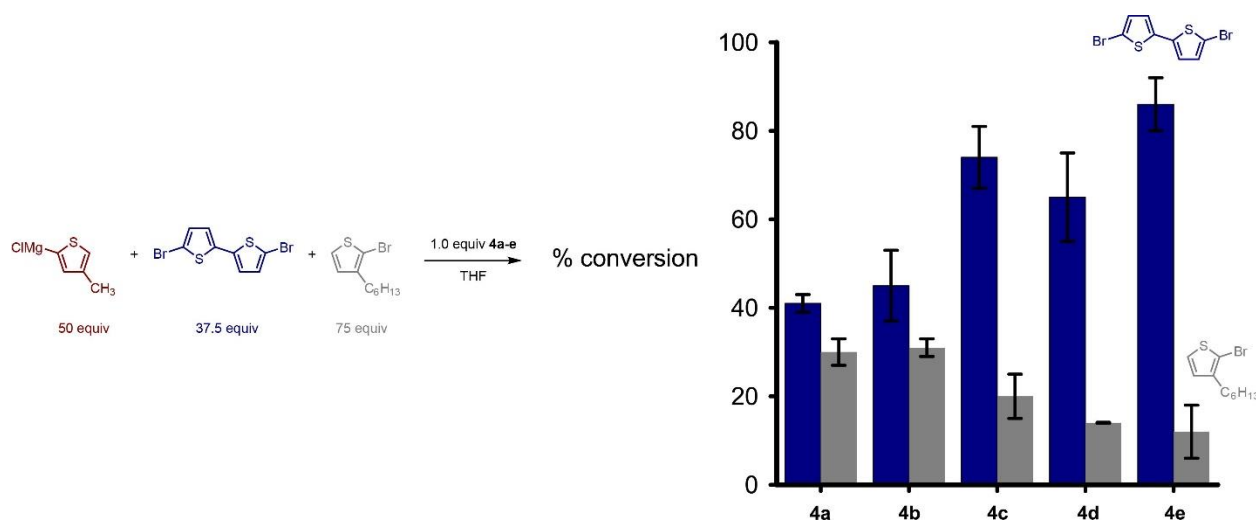
Small molecule cross-coupling competition experiments and polymerizations conducted in the presence of competitive agents were used to identify 5,5'-dibromo-2,2'-bithiophene, **3**, as a suitable competitive agent from a small library of (hetero)aryl bromides and iodides. We demonstrate that **3** is capable of sequestering unassociated catalyst (Scheme 2-6) without disrupting polymerization (i.e., **3** does not interfere with the  $\pi$ -complex or undergo Grignard exchange)—polymerizing (5-bromo-4-decylthiophen-2-yl)magnesium chloride, **1**, in the presence



of **3** (30 equiv) has a negligible impact on molecular weight,  $\mathcal{D}$ , and end-group control (Scheme 2-7, Appendix 1). Using **3**, the intermolecular pathway can be minimized so that we can correlate the end-capping behavior with chain-walking and the catalyst-polymer  $\pi$ -complex.



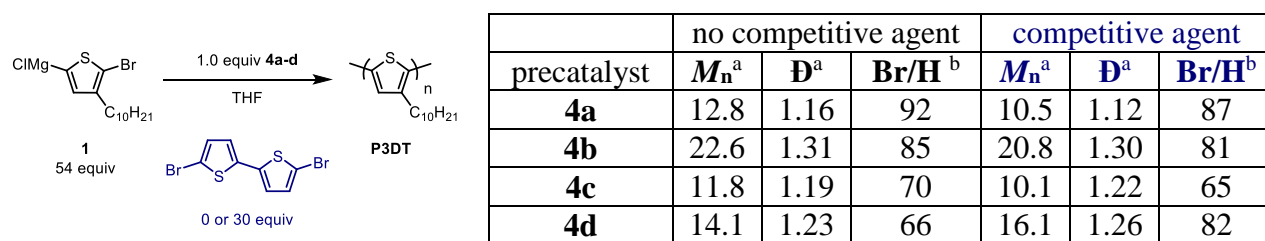
**Chart 2-1.** Structures and names of the dihalide precatalysts investigated in the end-capping model system.



**Scheme 2-6.** Small molecule cross-coupling to verify that competitive agent outcompetes polymer C-Br (2-bromo-3-hexylthiophene is used as a proxy).

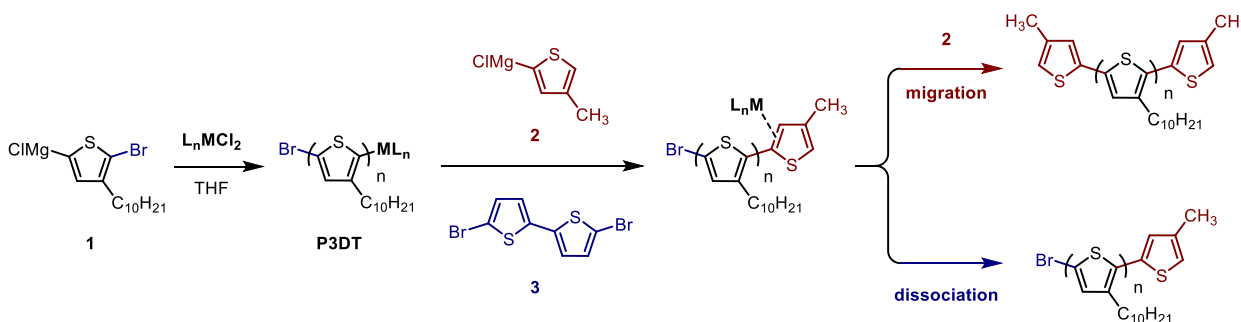
We evaluated the migration behavior across poly(3-decylthiophene) using the most commonly employed CTCP precatalysts: Ni(dppp)Cl<sub>2</sub>, **4a**, Ni(dppe)Cl<sub>2</sub>, **4b**, IPrNi(PPh<sub>3</sub>)Cl<sub>2</sub>, **4c**, and IPrPd(3-chloropyridine)Cl<sub>2</sub>, **4a**, (IPr = 1,3-bis(2,6-diisopropylphenyl)imidazole, Chart 2-1). All four catalysts mediate a living, chain-growth polymerization of **1** with low dispersities and  $M_n$  dependent on the monomer/catalyst ratio (Appendix 1). We also evaluated Ni(PPh<sub>3</sub>)<sub>2</sub>Cl<sub>2</sub>, which has seen limited use in CTCP because chain-transfer side-reactions compete with the desired chain-growth pathway.<sup>41,50</sup> Correlating ligand identity and transition metal with migration

behavior *may* provide important insight for the design of catalysts to polymerize more complex multi-aryl monomers.



**Scheme 2-7.** Polymerizing **1** with or without added competitive agent. <sup>a</sup>Determined by GPC analysis. <sup>b</sup>Calculated from the average peak area ratios (at each DP) from the five most intense peaks observed by MALDI-TOF MS analysis.

Polymerizations in the end-capping model system were conducted under typical conditions for CTCP with monomer concentrations adjusted to target molecular weights suitable for MALDI-TOF MS analysis (DP = 54). After monomer consumption slowed (~ 90% conversion), the polymerization solution was added to a mixture of the capping and competitive agents (2-chloromagnesio-4-methylthiophene, **2**, and **3**, respectively, Scheme 2-8). Molecular weight, monomer conversion, and polymer end-groups were compared before and after adding capping/competitive agent. We only examined data if aliquots removed prior to adding capping/competitive agent showed end-groups consistent with a living polymerization (i.e., Br/H) and no further polymerization occurred during end-capping (i.e., the molecular weight and monomer conversion were constant). For this reason, only catalysts that exhibit living, chain-growth behavior were the focus of this model system. Precatalyst **4e** was also investigated to contrast end-capping results with a more step-growth system. Lower levels of end-group control in the polymerization yielded **P3DT** with a majority of Br/Br end-groups, which did not react with capping agent during the end-capping procedure.



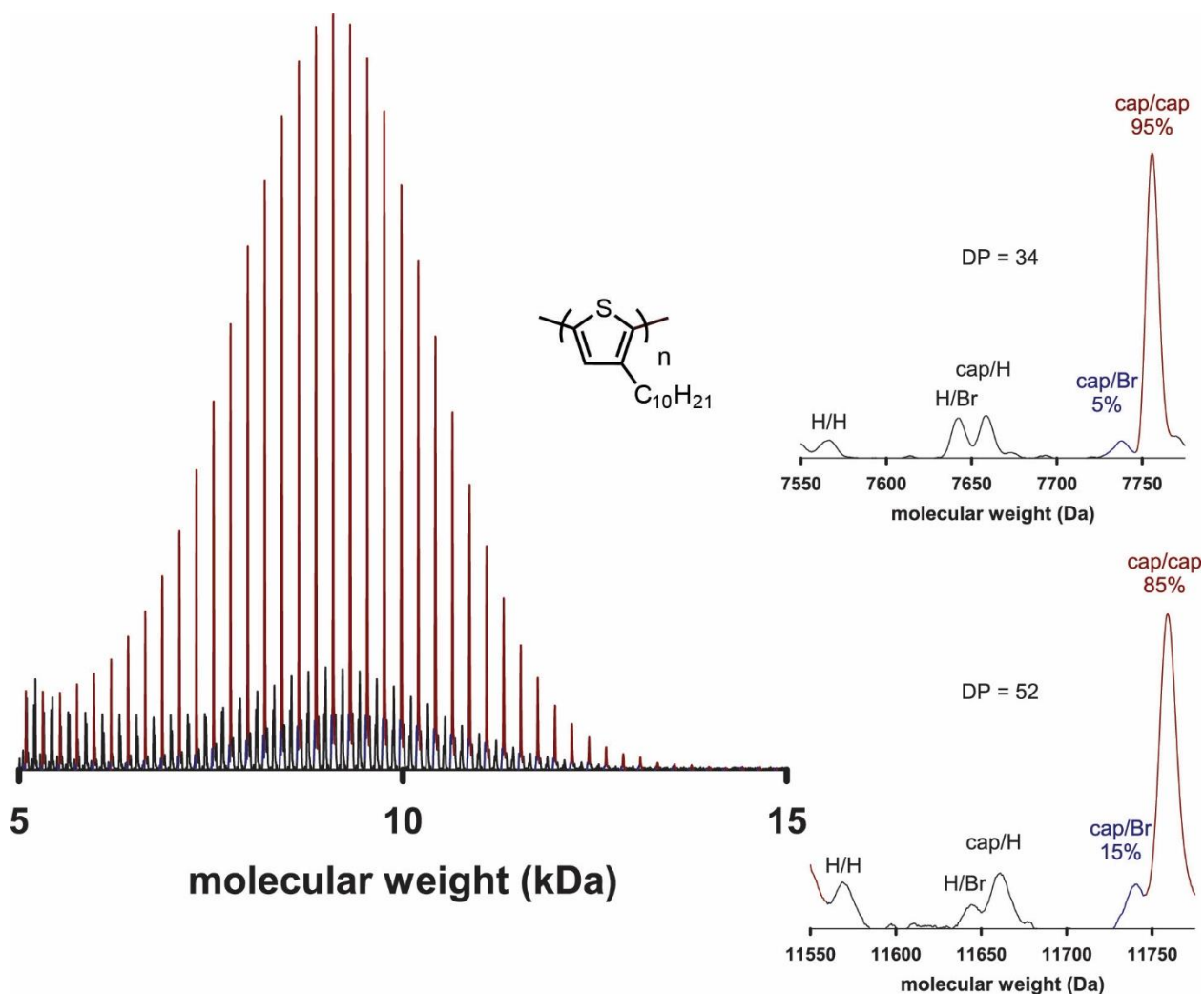
**Scheme 2-8.** End-capping model system to detect catalyst migration by reaction with **2** at both ends.

### *End-capping using Ni bi-dentate phosphine catalysts*

The most frequently used precatalyst for the synthesis of poly(3-hexylthiophene) is **4a**, and migration has been implicated in initiator enchainment,<sup>30,32</sup> monomer scope,<sup>34-36</sup> and end-capping.<sup>43-46</sup> Selective di-capping of poly(3-hexylthiophene) has been observed using alkyl or aryl capping agents, indicating catalyst migration, but end-capping without competitive agent cannot distinguish the intramolecular from the intermolecular pathways.<sup>43,44</sup> In separate experiments, 1-pentene has been used as a competitive agent to partially stall end-capping of poly(3-hexylthiophene) after the introduction of pyridine at only one end.<sup>45,46</sup> The use of 1,000 equivalents 1-pentene as a competitive agent should sequester unassociated Ni<sup>0</sup>, but olefins and non-conjugated double bonds have been shown to compete with the catalyst-polymer  $\pi$ -complex.<sup>19,20,51,52</sup> The disruptive nature of 1-pentene as a competitive agent means that these results may not be reflective of chain-walking under polymerization conditions. Therefore the previous studies provide an incomplete investigation of chain-walking.

Using **3** in our end-capping model system as a highly reactive competitive agent that does not disrupt polymerization behavior, we investigated catalyst migration under relevant conditions for polymerizations (Appendix 1). Employing **4a** as the precatalyst produced poly(3-decylthiophene), **P3DT**, with clearly identifiable end-groups with a DP from 24–52 repeat units. The migration product was the major species at all chain lengths, although a small portion of dissociation product was also observed. The percent migration decreased slightly with increasing DP, going from 96% at DP = 30 to 89% at DP = 50 (Figure 2-1, Figure 2-4, Appendix 1). Prevalent migration suggests that the Ni-**P3DT**  $\pi$ -complex is robust and the catalyst is mobile across the polymer backbone across even greater distances than previously reported.<sup>43</sup> Importantly, using a competitive agent in our studies confirms the intramolecular nature of migration. The different amount of di-capping observed using **3** in our system (~100% migration when DP <20) relative to literature reports using 1-pentene as a competitive agent (45% migration) are quite dramatic,<sup>45,46</sup> supporting our hypothesis that 1-pentene promotes chain-transfer from the catalyst-polymer  $\pi$ -complex rather than only sequestering catalyst that has already dissociated.<sup>46</sup> Previous reports of the strong association between Ni<sup>0</sup> and vinyl groups in end-capping with vinyl Grignard reagents<sup>43,44</sup> and the polymerization of vinyl containing monomers<sup>24,51,52</sup> support this conclusion. The structurally similar **4b** yielded similarly high levels of migration (~95%), but these amounts were

insensitive to chain-length (Appendix 1). Migration products were even detected at >80 repeat units, but the signal overlap due to broad isotopic distributions at high molecular weight make quantifying migration difficult. For Ni-phosphine catalysts, the  $\pi$ -complex is sufficiently strong to maintain association with **P3DT**, and the catalyst is mobile enough to chain-walk the many steps required for intramolecular, end-to-end catalyst migration.



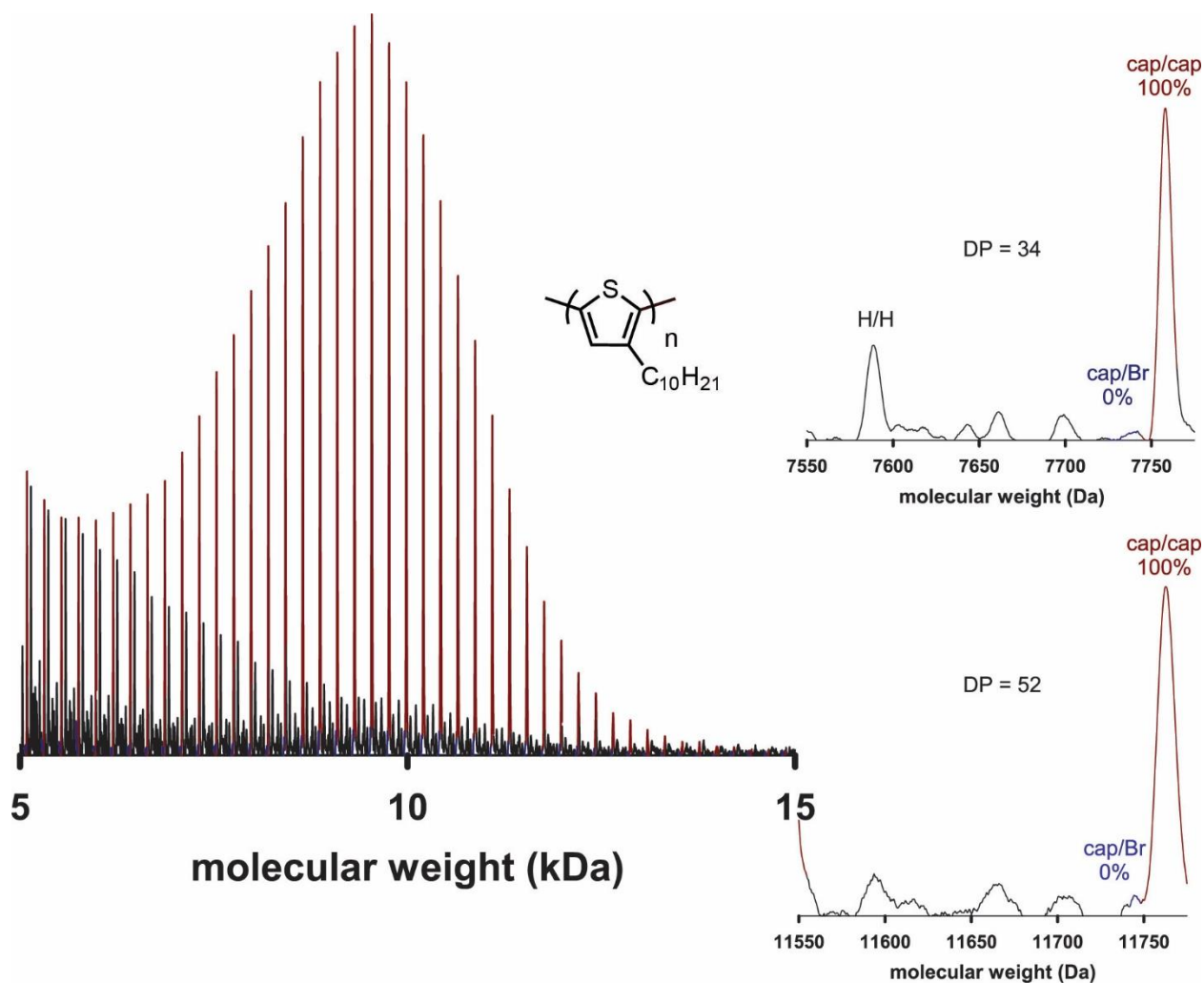
**Figure 2-1.** Mass spectrum of **P3DT** produced by **4a** after end-capping with **2** (15 equiv) and **3** (30 equiv). Migration (cap/cap, █) and dissociation (cap/Br, █) product peaks are highlighted from all other masses (█). Insets (right) show **P3DT** end-groups at DP = 34 (top) and DP = 52 (bottom).

#### *Ligand effects: phosphine v. N-heterocyclic carbene*

We next evaluated precatalyst **4c** to determine the effect of the ancillary ligand on the Ni-**P3DT**  $\pi$ -complex. We have previously demonstrated that increasing the  $\sigma$ -donating ability of

phosphine ligands on Ni promotes chain-growth behavior through a stronger  $\pi$ -complex and/or faster oxidative addition.<sup>53,54</sup> N-heterocyclic carbenes (NHCs) are strong  $\alpha$ -donors and weak  $\pi$ -acceptors relative to their phosphine counterparts, making them attractive candidates for chain-growth polymerizations.<sup>55-57</sup> Precatalyst **4c** has recently been identified as an efficient CTCF catalyst for poly(3-alkylthiophenes)<sup>58-60</sup> and generates lower amounts of initiator enchainment (66%) relative to **4a** (72%).<sup>32</sup> The lower reported levels of initiator enchainment using **4c** could be the result of lower energy barriers for oxidative addition, a greater attraction towards the  $\omega$  chain-end, or weaker  $\pi$ -complex that increases chain-transfer or dissociation during chain-walking. Using **4c** in our end-capping model system could allow us to identify whether the enchainment differences between catalysts are related to  $\pi$ -complex stability/catalyst mobility.

Despite differences in end-to-end migration during thiophene polymerizations (observed by initiator enchainment),<sup>32</sup> the chain-walking ability of Ni catalysts **4a-c** are similar in the end-capping experiments. Precatalyst **4c** yields nearly exclusive migration products (migration is 100% at DP = 50), as compared to >89% migration for **4a** and 97% for **4b**. A minor amount of dissociation product can be observed in the mass spectrum, but these peaks were too small to be selected during peak picking (Figure 2-2, Appendix 1). Our end-capping experiments demonstrate catalyst **4c** can migrate along **P3DT**, indicating that the mono-dentate ligands are sufficiently donating/bulky to form a  $\pi$ -complex that is resistant to chain-transfer or dissociation.



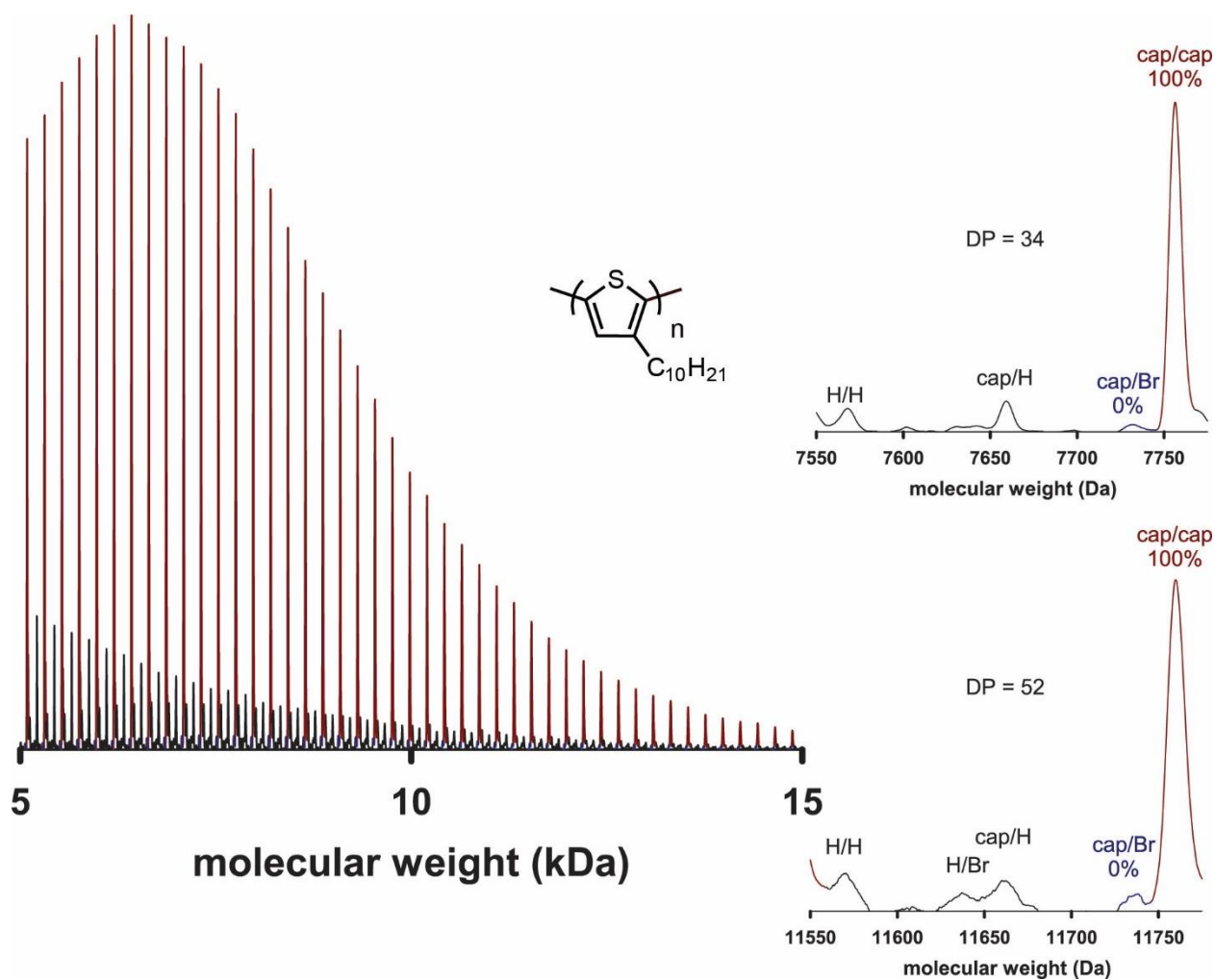
**Figure 2-2.** MALDI-TOF mass spectra of **P3DT** produced by **4c** post end-capping with **2** (15 equiv) and **3** (30 equiv). Migration (cap/cap, █) and dissociation (cap/Br, █) product peaks are highlighted from all other masses (█). Insets (right) show **P3DT** end-groups at DP = 34 (top) and DP = 52 (bottom).

### *Metal effects: Ni versus Pd*

Direct comparisons between Ni and Pd CTCP catalysts are scarce because living, chain-growth polymerizations using Ni involve bi-dentate phosphines, while Pd is typically ligated by bulky, mono-dentate phosphines or NHCs.<sup>18–20</sup> To isolate the role of the metal identity from ligand effects in CTCP, we compared **4c** with IPrPd(3-chloropyridine)Cl<sub>2</sub> (**4d**). Both catalysts have the same IPr ancillary ligand and differ only in the transition metal and labile ligands. The labile ligands, PPh<sub>3</sub> and 3-chloropyridine, are not expected to be coordinated to the catalyst during the chain-walking and subsequent oxidative addition due to steric constraints.<sup>61,62</sup> As a consequence, any differences in migration behavior should be attributed to changing the transition metal. The

migration behavior of **4d** has been previously observed by initiator enchainment using Kumada or Stille CTCP, where poly(3-hexylthiophene) that had polymerized from both ends was 80%<sup>62</sup> or 100%<sup>31</sup> of the reaction product, respectively. Chain-walking of **4d** has also been analyzed computationally, and  $\pi$ -binding followed by chain-walking directs intramolecular oxidative addition.<sup>61,62</sup>

Consistent with the enchainment results, precatalyst **4d** also yielded the migration product as the nearly exclusive product of the end-capping experiments. The migration products were the sole peak series for DP of 40–60, and were even observed up to 80 repeat units (Figure 2-3). Observing migration products on such long polymers reveals that the Pd-**P3DT**  $\pi$ -complex is strong enough to maintain association during chain-walking to yield the di-functionalized products. This result is surprising, giving that comparisons in small molecule cross-couplings suggest that Pd<sup>0</sup> binds more weakly to aryl groups prior to oxidative addition (relative to Ni<sup>0</sup>).<sup>47,48</sup> Weaker binding in the Pd-polymer  $\pi$ -complex could result in catalyst dissociation during catalyst chain-walking, but that is not observed in these experiments.



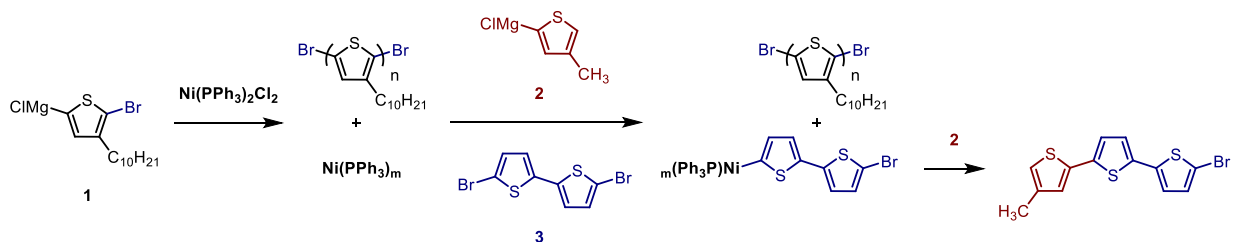
**Figure 2-3.** Mass spectrum of **P3DT** produced by **4d** after end-capping with **2** (15 equiv) and **3** (30 equiv). Migration (cap/cap, ■) and dissociation (cap/Br, ■) product peaks are highlighted from all other masses (■). Insets (right) show **P3DT** end-groups at DP = 34 (top) and DP = 52 (bottom).

#### *Uncontrolled CTCP catalyst Ni(PPh<sub>3</sub>)<sub>2</sub>Cl<sub>2</sub>*

Because all tested CTCP catalysts displayed impressive levels of migration in the end-capping experiments, we investigated whether migration would also be observed using a lower performing catalyst. Test polymerizations with Ni(PPh<sub>3</sub>)<sub>2</sub>Cl<sub>2</sub> yielded polymers with higher dispersity and lower molecular weight, which suggests that chain-transfer and termination events occur during the predominantly chain-growth polymerization.<sup>41,63</sup> These results are consistent with literature reports that identify increased dispersity for poly(3-alkylthiophene) above DP ~40.<sup>41,63</sup> Less efficient migration (relative to **4a**) has also been observed when polymerizing thiophene



trimers, resulting in a significant increase in dispersity and reduced molecular weight.<sup>34,41</sup> Differences in polymerization behavior between  $\text{Ni}(\text{PPh}_3)_2\text{Cl}_2$  and the other CTCP catalysts were amplified in our end-capping system, where  $\text{Ni}(\text{PPh}_3)_2\text{Cl}_2$  yielded a mixture of dissociation and migration products (~50% each). However, clear interpretation of this product distribution is confounded by the small amount of end-capped products (~15% of the polymers at each DP). The major end-groups at all molecular weight corresponds to Br/Br for both the pre- and post-capping polymers. Halogens at both polymer ends suggest that the catalyst does not stay associated with the polymer during the polymerization or end-capping. With this non-chain-growth character, oxidative addition of the unassociated catalyst into **3** could outcompete reaction with **P3DT** to produce mainly small-molecule cross-coupling products rather than end-functionalized polymer (Scheme 2-9). The small number of end-capping products validates our focus on CTCP catalysts.

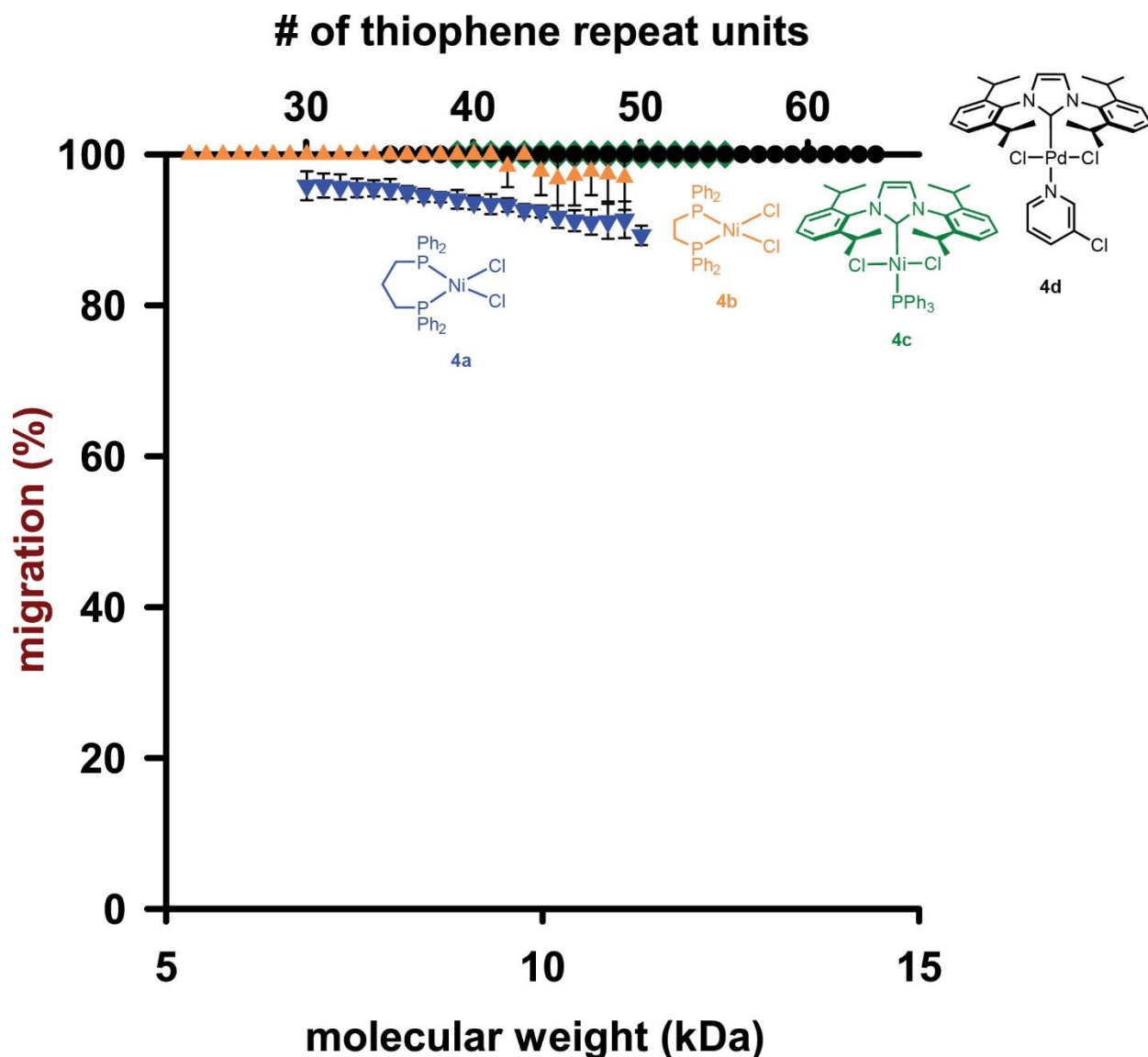


**Scheme 2-9.** Unassociated  $\text{Ni}(\text{PPh}_3)_m$  catalyst yields coupling product of **2** and **3** rather than end-capping **P3DT**.

### *Trends in catalyst migration*

The end-capping experiments reveal that all four CTCP precatalysts can migrate large distances when migration is forced. For **4b-d**, migration is near quantitative and is insensitive to chain-length. Using precatalyst **4a**, however, the ratio of migration products decreases slightly as chain-length increases. Since this trend does not occur with the electronically similar **4b**, we propose that the greater steric bulk of dppp on **4a** (relative to dppe on **4b**) increases the energy barrier to catalyst migration, while the binding stabilization remains the same. Migration barriers are more likely to be effected by increased steric hindrance than the  $\pi$ -complex stability due to the dihedral angle between the planar thiophene repeat units. Each repeat unit should be accessible to the catalyst, for all ligands tested, but rotation between thiophene rings (with alkyl side-chains jutting out) could cause steric repulsion during chain-walking for bulkier catalysts. While the

overall effect on migration across **P3DT** is minor, migration differences could be amplified using other monomers.

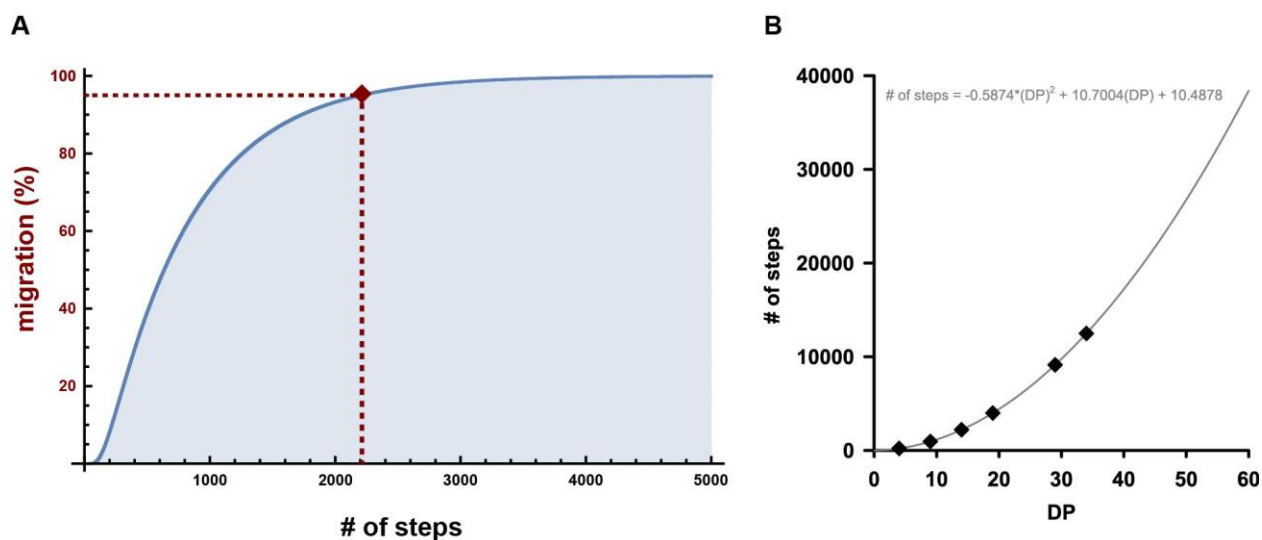


**Figure 2-4.** Migration percent at each DP for pre-catalysts **4a–4d** tested in the end-capping model system. The migration pathway was calculated from peak areas of the cap/cap and cap/Br peaks (at each DP) determined by MALDI-TOF MS (Appendix 1).

*Statistical analysis using a random-walk model*

The large number of repeat units that the CTCP catalysts traverse during migration is especially remarkable given that the most widely accepted model for chain-walking assumes a random walk along the polymer backbone.<sup>30,33</sup> A catalyst in the middle of the polymer has an equal

probability of moving left or right, treating all repeat units identically. Chain-walking across each repeat unit involves an inter- and intra-ring walking step from the most energetically favorable  $\eta$ -2 coordination.<sup>54,61</sup> Because end-group effects are relatively minor on long polymers, we considered the simplest case where there is an equal probability to chain-walk between all repeat units and capping agent. We calculated the probability for catalysts to reach the  $\alpha$  chain-end (where it was assumed to react immediately), with the cumulative probability at a given number of steps being equal to the migration percent (Appendix 1). For 95% of the catalyst to migrate across 14 and 50 repeat units, the threshold number of steps is 2,204 and 26,754. Three out of four high-performing CTCF catalysts (**4b–4d**) chain-walk this incredible number of steps with little change in the migration product, while Ni(PPh<sub>3</sub>)<sub>2</sub>Cl<sub>2</sub> yielded a mixture of migration and dissociation products. The percent migration diminishes from 96% to 89% with increasing DP (34 and 50, respectively) using precatalyst **4a**, which allows us to fit the random-walking across multiple data points. We calculated the number of chain-walking steps required for 95% migration at DP = 36 (and so on), then compared the calculated number of steps (Table 2-1). The wide variation in the number of steps, albeit over a very limited percent migration range, suggests that the random-walking model does not completely describe the migration behavior for **4a**.



**Figure 2-5.** (A) Cumulative distribution function for a random walk on a polymer with DP = 14 with guiding lines ( ■ ■ ■ ) drawn at 95% migration product (2,204 steps, ◆ ). B) The number of steps calculated from the cumulative distribution function are plotted versus DP (◆ ). A quadratic fit ( $r^2 = 1.0000$ , — ) is used to extrapolate the # of steps due to the high computational workload required at high DP.

DP	Migration (%)	Calculated # of steps
36	95	13977
42	93	17056
47	91	19369
50	89	20514

**Table 2-1.** Percent migration (experimental data) and calculated # of steps at each DP for **4a**.

## Conclusions

Overall, the end-capping system provides an indirect route to probe the catalyst-polymer  $\pi$ -complex by detecting products of catalyst migration. Using highly reactive **3** as a competitive agent minimized interpolymer reactions, enabling us to assign migration products to chain-walking via a  $\pi$ -complex. Although migration was forced by adding the capping agent (**2**), our results reveal the impressive stability of metal-**P3DT**  $\pi$ -complexes and the high mobility of catalysts to chain-walk >26,700 steps across 50 repeat units to react at both polymer ends. Efficient migration behavior was observed for all the high performing CTCP catalysts examined, using Pd or Ni catalysts ligated by NHCs as well as Ni ligated by bidentate phosphines. The shared ability to migrate with minimal dissociation suggests that efficient migration could be indicative of CTCP catalysts. In typical thiophene polymerizations, end-to-end migration is rare relative to oxidative addition into the adjacent C-Br and our end-capping experiments suggest that chain-transfer from migrating CTCP catalysts should be minimal. Chapter 3 investigates whether chain-walking is similarly robust across poly(phenylene), and whether migration behavior is a diagnostic parameter to evaluate CTCP for new catalyst/monomer combinations. Catalysts with a high affinity for chain-walking will be targeted for expanding CTCP monomer scope to multi-aryl monomers. Initial investigations by Noonan<sup>34</sup> and Mori<sup>40</sup> (among others) using **4a** and **4c** suggest that polymerizing multi-aryl monomers is a promising approach to access new polymers for high-performing devices.

## References

- (1) Rochat, S.; Swager, T. M.; Rochat, S.; Swager, T. M. Conjugated Amplifying Polymers for Optical Sensing Applications. *ACS Appl. Mater. Interfaces* **2013**, *5*, 4488–4502.
- (2) Lee, K.; Povlich, L. K.; Kim, J. Recent Advances in Fluorescent and Colorimetric Conjugated Polymer-Based Biosensors. *Analyst* **2010**, *135*, 2179–2189.
- (3) Peng, H.-Q.; Niu, L.-Y.; Chen, Y.-Z.; Wu, L.-Z.; Tung, C.-H.; Yang, Q.-Z. Biological Applications of Supramolecular Assemblies Designed for Excitation Energy Transfer. *Chem. Rev.* **2015**, *115*, 7502–7542.
- (4) Grimsdale, A. C.; Chan, K. L.; Martin, R. E.; Jokisz, P. G.; Holmes, A. B. Synthesis of Light-Emitting Conjugated Polymers for Applications in Electroluminescent Devices. *Chem. Rev.* **2009**, *109*, 897–1091.
- (5) Botiz, I.; Astilean, S.; Stingelin, N. Altering the Emission Properties of Conjugated Polymers. *Polym. Int.* **2016**, *65*, 157–163.
- (6) Facchetti, A.  $\pi$ -Conjugated Polymers for Organic Electronics and Photovoltaic Cell Applications. *Chem. Mater.* **2011**, *23*, 733–758.
- (7) Guo, X.; Baumgarten, M.; Müllen, K. Designing  $\pi$ -Conjugated Polymers for Organic Electronics. *Prog. Polym. Sci.* **2013**, *38*, 1832–1908.
- (8) Farinola, G. M.; Ragni, R. Electroluminescent Materials for White Organic Light Emitting Diodes. *Chem. Soc. Rev.* **2011**, *40*, 3467–3482.
- (9) Sirringhaus, H. 25Th Anniversary Article: Organic Field-Effect Transistors: The Path Beyond Amorphous Silicon. *Adv. Mater.* **2014**, *26*, 1319–1335.
- (10) Wang, C.; Dong, H.; Hu, W.; Liu, Y.; Zhu, D. Semiconducting  $\pi$ -Conjugated Systems in Field-Effect Transistors: A Material Odyssey of Organic Electronics. *Chem. Rev.* **2012**, *112*, 2208–2267.
- (11) Dou, L.; Liu, Y.; Hong, Z.; Li, G.; Yang, Y. Low-Bandgap Near-IR Conjugated Polymers/Molecules for Organic Electronics. *Chem. Rev.* **2015**, *115*, 12633–12665.
- (12) Mazziro, K. a.; Luscombe, C. K. The Future of Organic Photovoltaics. *Chem. Soc. Rev.* **2015**, *44*, 78–90.
- (13) Lu, L.; Zheng, T.; Wu, Q.; Schneider, A. M.; Zhao, D.; Yu, L. Recent Advances in Bulk Heterojunction Polymer Solar Cells. *Chem. Rev.* **2015**, *115*, 12666–12731.
- (14) Wang, K.; Liu, C.; Meng, T.; Yi, C.; Gong, X. Inverted Organic Photovoltaic Cells. *Chem. Soc. Rev.* **2016**, *45*, 2937–2975.
- (15) Yu, J.; Zheng, Y.; Huang, J. Towards High Performance Organic Photovoltaic Cells: A Review of Recent Development in Organic Photovoltaics. *Polymers* **2014**, *6*, 2473–2509.
- (16) Yokoyama, A.; Miyakoshi, R.; Yokozawa, T. Chain-Growth Polymerization for Poly(3-Hexylthiophene) with a Defined Molecular Weight and a Low Polydispersity. *Macromolecules* **2004**, *37*, 1169–1171.
- (17) Sheina, E. E.; Liu, J.; Iovu, M. C.; Laird, D. W.; McCullough, R. D. Chain Growth

- Mechanism for Regioregular Nickel-Initiated Cross-Coupling Polymerizations. *Macromolecules* **2004**, *37*, 3526–3528.
- (18) Bryan, Z. J.; McNeil, A. J. Conjugated Polymer Synthesis via Catalyst-Transfer Polycondensation (CTP): Mechanism, Scope, and Applications. *Macromolecules* **2013**, *46*, 8395–8405.
- (19) Verheyen, L.; Leysen, P.; Van Den Eede, M.-P.; Ceunen, W.; Hardeman, T.; Koeckelberghs, G. Advances in the Controlled Polymerization of Conjugated Polymers. *Polymer* **2017**, *108*, 521–546.
- (20) Yokozawa, T.; Ohta, Y. Transformation of Step-Growth Polymerization into Living Chain-Growth Polymerization. *Chem. Rev.* **2016**, *116*, 1950–1968.
- (21) Peter, F.; Koch, V.; Rivnay, J.; Foster, S.; Müller, C.; Downing, J. M.; Buchaca-domingo, E.; Heeney, M.; Rumbles, G.; Silva, C.; *et al.* The Impact of Molecular Weight on Microstructure and Charge Transport in Semicrystalline Polymer semiconductors—poly(3-Hexylthiophene), a Model Study. *Prog. Polym. Sci.* **2013**, *38*, 1978–1989.
- (22) Kim, J. S. J. K.; Lee, Y.; Lee, J. H.; Park, J. H.; Kim, J. S. J. K.; Cho, K. High-Efficiency Organic Solar Cells Based on End-Functional-Group-Modified Poly(3-Hexylthiophene). *Adv. Mater.* **2010**, *22*, 1355–1360.
- (23) Willot, P.; Koeckelberghs, G. Evidence for Catalyst Association in the Catalyst Transfer Polymerization of Thieno[3,2- B]thiophene. *Macromolecules* **2014**, *47*, 8548–8555.
- (24) Nojima, M.; Ohta, Y.; Yokozawa, T. Structural Requirements for Palladium Catalyst Transfer on a Carbon–Carbon Double Bond. *J. Am. Chem. Soc.* **2015**, *137*, 5682–5685.
- (25) Nojima, M.; Ohta, Y.; Yokozawa, T. Investigation of Catalyst-Transfer Condensation Polymerization for Synthesis of Poly(P-Phenylenevinylene). *J. Polym. Sci. Part A Polym. Chem.* **2014**, *52*, 2643–2653.
- (26) Bryan, Z. J.; Hall, A. O.; Zhao, C. T.; Chen, J.; McNeil, A. J. Limitations of Using Small Molecules to Identify Catalyst-Transfer Polycondensation Reactions. *ACS Macro Lett.* **2016**, *5*, 69–72.
- (27) Yokozawa, T.; Nanashima, Y.; Nojima, M.; Ohta, Y. Catalyst-Transfer Condensation Polymerization of Acceptor Aromatic Monomers and of Donor Carbon-Carbon Double Bond-Containing Monomers. *Macromol. Symp.* **2015**, *350*, 22–33.
- (28) Verswyvel, M.; Hoebens, C.; De Winter, J.; Gerbaux, P.; Koeckelberghs, G. Study of the Controlled Chain-Growth Polymerization of poly(3,6- Phenanthrene). *J. Polym. Sci. Part A Polym. Chem.* **2013**, *51*, 5067–5074.
- (29) Grisorio, R.; Suranna, G. P. Intramolecular Catalyst Transfer Polymerisation of Conjugated Monomers: From Lessons Learned to Future Challenges. *Polym. Chem.* **2015**, *6*, 7781–7795.
- (30) Kohn, P.; Huettner, S.; Komber, H.; Senkovskyy, V.; Tkachov, R.; Kiriya, A.; Friend, R. H.; Steiner, U.; Huck, W. T. S.; Sommer, J.-U. U.; *et al.* On the Role of Single Regiodefects and Polydispersity in Regioregular poly(3-Hexylthiophene): Defect Distribution, Synthesis of Defect-Free Chains, and a Simple Model for the Determination of Crystallinity. *J. Am.*

*Chem. Soc.* **2012**, *134*, 4790–4805.

- (31) Qiu, Y.; Mohin, J.; Tsai, C.-H.; Tristram-Nagle, S.; Gil, R. R.; Kowalewski, T.; Noonan, K. J. T. Stille Catalyst-Transfer Polycondensation Using Pd-PEPPSI-IPr for High-Molecular-Weight Regioregular Poly(3-Hexylthiophene). *Macromol. Rapid Commun.* **2015**, *36*, 840–844.
- (32) Hardeman, T.; De Becker, J.; Koeckelberghs, G. Influence of the Halogen and Organometallic Function in a KCTP (Co)polymerization. *J. Polym. Sci. Part A Polym. Chem.* **2016**, *54*, 3701–3706.
- (33) Tkachov, R.; Senkovskyy, V.; Komber, H.; Sommer, J. U.; Kiriy, A. Random Catalyst Walking along Polymerized Poly(3-Hexylthiophene) Chains in Kumada Catalyst-Transfer Polycondensation. *J. Am. Chem. Soc.* **2010**, *132*, 7803–7810.
- (34) Tsai, C.-H.; Fortney, A.; Qiu, Y.; Gil, R. R.; Yaron, D.; Kowalewski, T.; Noonan, K. J. T. Conjugated Polymers with Repeated Sequences of Group 16 Heterocycles Synthesized through Catalyst-Transfer Polycondensation. *J. Am. Chem. Soc.* **2016**, *138*, 6798–6804.
- (35) Qiu, Y.; Fortney, A.; Tsai, C.-H. H.; Baker, M. A.; Gil, R. R.; Kowalewski, T.; Noonan, K. J. T. Synthesis of Polyfuran and Thiophene-Furan Alternating Copolymers Using Catalyst-Transfer Polycondensation. *ACS Macro Lett.* **2016**, *5*, 332–336.
- (36) Ono, R. J.; Kang, S.; Bielawski, C. W. Controlled Chain-Growth Kumada Catalyst Transfer Polycondensation of a Conjugated Alternating Copolymer. *Macromolecules* **2012**, *45*, 2321–2326.
- (37) Todd, A. D.; Bielawski, C. W. Controlled Synthesis of an Alternating Donor–Acceptor Conjugated Polymer via Kumada Catalyst-Transfer Polycondensation. *ACS Macro Lett.* **2015**, *4*, 1254–1258.
- (38) Tanaka, S.; Tanaka, D.; Tatsuta, G.; Murakami, K.; Tamba, S.; Sugie, A.; Mori, A. Concise Synthesis of Well-Defined Linear and Branched Oligothiophenes with Nickel-Catalyzed Regiocontrolled Cross-Coupling of 3-Substituted Thiophenes by Catalytically Generated Magnesium Amide. *Chem. Eur. J.* **2013**, *19*, 1658–1665.
- (39) Scheuble, M.; Richter, T. V.; Goll, M.; Link, S.; López Navarrete, J. T.; Ruff, A.; Ruiz Delgado, M. C.; Ludwigs, S. Branched Polythiophenes by Ni-Catalyzed Kumada Coupling. *Polym. Chem.* **2014**, *5*, 6824–6833.
- (40) Murakami, K.; Tanaka, S.; Mori, A. Linear-Selective Cross-Coupling Polymerization of Branched Oligothiophene by Deprotonative Metalation and Cross-Coupling. *Polym. Chem.* **2015**, *6*, 6573–6578.
- (41) Beryozkina, T.; Senkovskyy, V.; Kaul, E.; Kiriy, A. Kumada Catalyst-Transfer Polycondensation of Thiophene-Based Oligomers: Robustness of a Chain-Growth Mechanism. *Macromolecules* **2008**, *41*, 7817–7823.
- (42) Wu, S.; Sun, Y.; Huang, L.; Wang, J.; Zhou, Y.; Geng, Y.; Wang, F. Grignard Metathesis Chain-Growth Polymerization for Poly(bithienylmethylene)s: Ni Catalyst Can Transfer across the Nonconjugated Monomer. *Macromolecules* **2010**, *43*, 4438–4440.
- (43) Jeffries-EL, M.; Sauvé, G.; McCullough, R. D.; Malika, J. E. L.; Sauvé, G.; McCullough,

- R. D.; Jeffries-EL, M.; Sauvé, G.; McCullough, R. D. In-Situ End-Group Functionalization of Regioregular Poly(3-Alkylthiophene) Using the Grignard Metathesis Polymerization Method. *Adv. Mater.* **2004**, *16*, 1017–1019.
- (44) Jeffries-El, M.; Sauvé, G.; McCullough, R. D. Facile Synthesis of End-Functionalized Regioregular Poly(3-Alkylthiophene)s via Modified Grignard Metathesis Reaction. *Macromolecules* **2005**, *38*, 10346–10352.
- (45) Kochemba, W. M.; Pickel, D. L.; Sumpter, B. G.; Chen, J.; Kilbey, S. M. In Situ Formation of Pyridyl-Functionalized Poly(3-Hexylthiophene)s via Quenching of the Grignard Metathesis Polymerization: Toward Ligands for Semiconductor Quantum Dots. *Chem. Mater.* **2012**, *24*, 4459–4467.
- (46) Kochemba, W. M.; Kilbey, S. M.; Pickel, D. L. End-Group Composition of poly(3-Hexylthiophene)s Prepared by in Situ Quenching of the Grignard Metathesis Polymerization: Influence of Additives and Reaction Conditions. *J. Polym. Sci. Part A Polym. Chem.* **2012**, *50*, 2762–2769.
- (47) Yoshikai, N.; Matsuda, H.; Nakamura, E. Ligand Exchange as the First Irreversible Step in the Nickel-Catalyzed Cross-Coupling Reaction of Grignard Reagents. *J. Am. Chem. Soc.* **2008**, *130*, 15258–15259.
- (48) Bahri-Laleh, N.; Poater, A.; Cavallo, L.; Mirmohammadi, S. A.; Yokoyama, A.; Miyakoshi, R.; Yokozawa, T.; Savagatrup, S.; Printz, A. D.; Rodriguez, D.; *et al.* Exploring the Mechanism of Grignard Metathesis Polymerization of 3-Alkylthiophenes. *Dalton Trans.* **2014**, *43*, 15143–15150.
- (49) Sontag, S. K.; Bilbrey, J. A.; Huddleston, N. E.; Sheppard, G. R.; Allen, W. D.; Locklin, J.  $\Pi$ -Complexation in Nickel-Catalyzed Cross-Coupling Reactions. *J. Org. Chem.* **2014**, *79*, 1836–1841.
- (50) Khanduyeva, N.; Senkovskyy, V.; Beryozkina, T.; Bocharova, V.; Simon, F.; Nitschke, M.; Stamm, M.; Grötzschel, R.; Kiriya, A. Grafting of Poly(3-Hexylthiophene) from Poly(4-Bromostyrene) Films by Kumada Catalyst-Transfer Polycondensation: Revealing of the Composite Films Structure. *Macromolecules* **2008**, *41*, 7383–7389.
- (51) Bedi, A.; De Winter, J.; Gerbaux, P.; Koeckelberghs, G. Detrimental Ni(0) Transfer in Kumada Catalyst Transfer Polycondensation of benzo[2,1-b:3,4-b']dithiophene. *J. Polym. Sci. Part A Polym. Chem.* **2016**, *54*, 1706–1712.
- (52) Hundt, N.; Palaniappan, K.; Sista, P.; Murphy, J. W.; Hao, J.; Nguyen, H.; Stein, E.; Biewer, M. C.; Gnade, B. E.; Stefan, M. C. Synthesis and Characterization of Polythiophenes with Alkenyl Substituents. *Polym. Chem.* **2010**, *1*, 1624.
- (53) Lee, S. R.; Bryan, Z. J.; Wagner, A. M.; McNeil, A. J. Effect of Ligand Electronic Properties on Precatalyst Initiation and Propagation in Ni-Catalyzed Cross-Coupling Polymerizations. *Chem. Sci.* **2012**, *3*, 1562–1566.
- (54) Bryan, Z. J.; McNeil, A. J. Evidence for a Preferential Intramolecular Oxidative Addition in Ni-Catalyzed Cross-Coupling Reactions and Their Impact on Chain-Growth Polymerizations. *Chem. Sci.* **2013**, *4*, 1620–1624.
- (55) Egbert, J. D.; Chartoire, A.; Slawin, A. M. Z.; Nolan, S. P. Synthesis, Characterization, and



- Reactivity of N-Heterocyclic Carbene Palladium(II) Hydroxide Dimers. *Organometallics* **2011**, *30*, 4494–4496.
- (56) Kantchev, E. A. B.; O'Brien, C. J.; Organ, M. G. Palladium Complexes of N-Heterocyclic Carbenes as Catalysts for Cross-Coupling Reactions--a Synthetic Chemist's Perspective. *Angew. Chem., Int. Ed.* **2007**, *46*, 2768–2813.
- (57) Nelson, D. J.; Nolan, S. P. Quantifying and Understanding the Electronic Properties of N-Heterocyclic Carbenes. *Chem. Soc. Rev.* **2013**, *42*, 6723–6753.
- (58) Fujita, K.; Sumino, Y.; Ide, K.; Tamba, S.; Shono, K.; Shen, J.; Nishino, T.; Mori, A.; Yasuda, T. Synthesis of Poly(3-Substituted Thiophene)s of Remarkably High Solubility in Hydrocarbon via Nickel-Catalyzed Deprotonative Cross-Coupling Polycondensation. *Macromolecules* **2016**, *49*, 1259–1269.
- (59) Tanaka, S.; Tamba, S.; Tanaka, D.; Sugie, A.; Mori, A. Synthesis of Well-Defined Head-to-Tail-Type Oligothiophenes by Regioselective Deprotonation of 3-Substituted Thiophenes and Nickel-Catalyzed Cross-Coupling Reaction. *J. Am. Chem. Soc.* **2011**, *133*, 16734–16737.
- (60) Fuji, K.; Tamba, S.; Shono, K.; Sugie, A.; Mori, A. Murahashi Coupling Polymerization: Nickel(II)-N-Heterocyclic Carbene Complex-Catalyzed Polycondensation of Organolithium Species of (Hetero)arenes. *J. Am. Chem. Soc.* **2013**, *135*, 12208–12211.
- (61) Zhao, Y.; Nett, A. J.; McNeil, A. J.; Zimmerman, P. M. Computational Mechanism for Initiation and Growth of Poly(3-Hexylthiophene) Using Palladium N-Heterocyclic Carbene Precatalysts. *Macromolecules* **2016**, *49*, 7632–7641.
- (62) Mikami, K.; Nojima, M.; Masumoto, Y.; Mizukoshi, Y.; Takita, R.; Yokozawa, T.; Uchiyama, M. Catalyst-Dependent Intrinsic Ring-Walking Behavior on  $\pi$ -Face of Conjugated Polymers. *Polym. Chem.* **2017**, *8*, 1708–1713.
- (63) Senkovskyy, V.; Khanduyeva, N.; Komber, H.; Oertel, U.; Stamm, M.; Kuckling, D.; Kiriy, A. Conductive Polymer Brushes of Regioregular Head-to-Tail poly(3-Alkylthiophenes) via Catalyst-Transfer Surface-Initiated Polycondensation. *J. Am. Chem. Soc.* **2007**, *129*, 6626–6632.

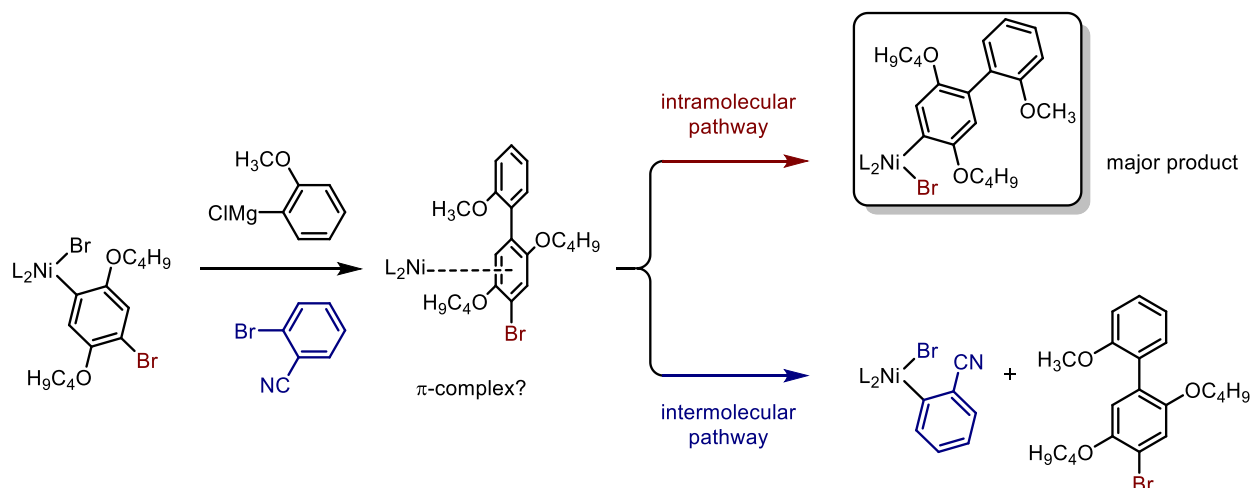
## Chapter 3

### Catalyst-dependent migration in polyphenylene synthesis

#### Introduction

Conjugated polymers (CPs) have attracted considerable interest for use in organic electronics due in part to their highly tunable optical, electrical, and mechanical properties. Copolymerizations have emerged as the primary route to fine-tune CPs for high-performing transistors,<sup>1-3</sup> light-emitting diodes,<sup>4-7</sup> and solar cells.<sup>8-10</sup> However, most one-pot CP copolymerizations are limited to alternating or random sequences, and offer little control over polymer molecular weight and dispersity.<sup>11,12</sup> These limitations hinder our ability to control and stabilize CP morphology, which plays a critical role in device performance.<sup>13-16</sup> Living, chain-growth polymerizations via catalyst-transfer condensation polymerization (CTCP) provide a route to access CPs with control over sequence, molecular weight, and end-groups, but the narrow monomer scope limits its application. Insights gained through detailed mechanistic investigations have enhanced polymerization control, and should hold the key for developing CTCP for commercial applications.

The chain-growth nature of CTCP is enabled by a catalyst-polymer  $\pi$ -complex that predisposes the catalyst to intramolecular oxidative addition. Compelling evidence for an associative intermediate has been offered in several small molecule competition experiments.<sup>17-19</sup> In one experiment, an associative intermediate justifies the selectivity for an intramolecular pathway over the stoichiometric and reactivity favored intermolecular pathway (Scheme 3-1). Importantly, the results from this model system translated to polymerizing (1-bromo-2,5-bis[hexyloxy]phenyl)magnesium chloride (**1**)—catalysts that were most selective for the intramolecular reaction pathway produced polymers with lower dispersities in the presence of a competitive agent. These results further corroborate other studies which indicate that more electron-rich ligands, which should strengthen the catalyst-polymer  $\pi$ -complex, can improve chain-growth behavior to yield polymers with lower dispersities.<sup>20,21</sup>

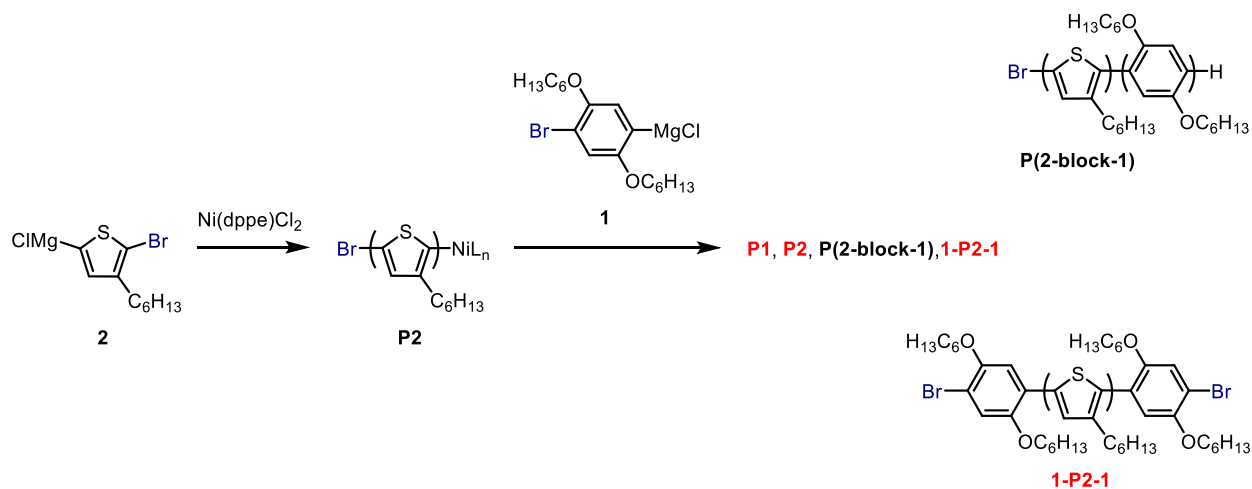


**Scheme 3-1.** Small molecule competition experiment where an associative complex directs oxidative addition with the biaryl formed in situ (intramolecular pathway) rather than through the intermolecular pathway with a more reactive competitive agent (2-bromobenzonitrile, present in excess amounts).  $L_2$  = 1,2-bis(diethylphosphino)ethane, 1,2-bis(*p*-methoxyphenylphosphino)ethane, dppe or 2  $PPh_3$  (dppe = 1,2-bis(diphenylphosphino)ethane,  $PPh_3$  = triphenylphosphine).

Since the discovery of CTCP in 2004,<sup>22,23</sup> only a handful of monomers have been polymerized in a living, chain-growth fashion where the molecular weight was determined by the  $[monomer]_0/[initiator]_0$  and dispersities ( $\mathcal{D}$ ) were below 1.25.<sup>24</sup> These successful examples use a variety of electron-rich 5- and 6-membered arenes, but examples of polymerizing electron deficient moieties are rare.<sup>24</sup> Recent accounts have implicated the catalyst-polymer  $\pi$ -complex as the problematic step,<sup>25–30</sup> where a strong  $\pi$ -complex retards catalyst-transfer to the reactive termini for oxidative addition. Instead, chain-transfer can become prevalent and only low molecular weight oligomers are formed.

Issues with the  $\pi$ -complex can also obstruct copolymerizations, even when each comonomer can be polymerized separately under the same conditions. Incorporating each comonomer into a statistical copolymer requires many cross-propagation events where the catalyst must migrate across the terminal unit for oxidative addition. Differences in  $\pi$ -binding with each monomer can direct the catalyst away from the active terminus and obstruct oxidative addition. This pathway has been identified in block copolymerizations of phenylene (**1**) with thiophene (**2**) using  $Ni(dppe)Cl_2$ , where the order of block formation is critical to polymerization control (Scheme 3-2).<sup>31,32</sup> The block copolymerization from **2** to **1** fails because the catalyst “sticks” to the block of **2**. This failure results in chain-transfer (to yield **P1** and **P2**) and end-capping **P2** with a single unit of **1** on both ends. Changing the donor strength of the phosphine ligand, which yields

dramatic differences in polymerizing **1**,<sup>20</sup> offered no improvement in the molecular weight or dispersity of **P(2-block-1)**.<sup>33</sup> Although chain-growth protocols to access **P2** and **P1** were developed in 2004<sup>22,23</sup> and 2006,<sup>34</sup> respectively, alternative copolymerization methods using Ni phosphine catalysts have all failed—prompting research into other transition metals and ligands.



**Scheme 3-2.** Block copolymerization of **2** (**P2**  $M_n = 4.1$  kDa,  $\mathcal{D} = 1.33$ ) then **1** ( $M_n = 6.7$  kDa,  $\mathcal{D} = 1.44$ ) to yield **P(2-block-1)** and **1-P2-1** as the major species.<sup>32</sup>

Recent developments in CTCP have expanded the precatalyst scope beyond Ni phosphine catalysts to include diamine<sup>35,36</sup> and N-heterocyclic carbene (NHC)<sup>37–39</sup> ligands as well as Pd precatalysts ligated by mono dentate phosphines<sup>40–46</sup> or NHCs.<sup>47–49</sup> The first batch copolymerization of **1** and **2** to yield copolymers with high molecular weight and low dispersity used  $\text{IPrPd}(\text{3-chloropyridine})\text{Cl}_2$ , **4d** (IPr = 1,3-bis[2,6-di-*i*-propylphenyl]imidazol-2-ylidene, Chapter 4). The mechanism of **4d** catalyzed polymerizations has not been determined experimentally, but computations suggest that chain-growth characteristics are achieved through a Pd-polymer  $\pi$ -complex.<sup>19,47,50,51</sup> Alternatively, Koeckelberghs has targeted Pd with a RuPhos ligand to minimize  $\pi$ -binding with electronically distinct monomers (RuPhos = 2-dicyclohexylphosphino-2',6'-diisopropoxybiphenyl), polymerizing through a reactivity-based pathway. The first tri-block copolymers of 3-hexylthiophene, 3-octyselenophene, and 9,9-dioctylfluorene were prepared (from all orders of monomer addition) using the PdRuPhos system,<sup>44,46</sup> but this drastic increase in cross-propagation comes at a cost—higher dispersity in both homo- and copolymerizations. Dispersities were  $\sim 1.7$  under optimized conditions for **P2**, as opposed to the commonly reported values of  $\sim 1.25$  when **4b** is used as the precatalyst.<sup>52,53</sup>

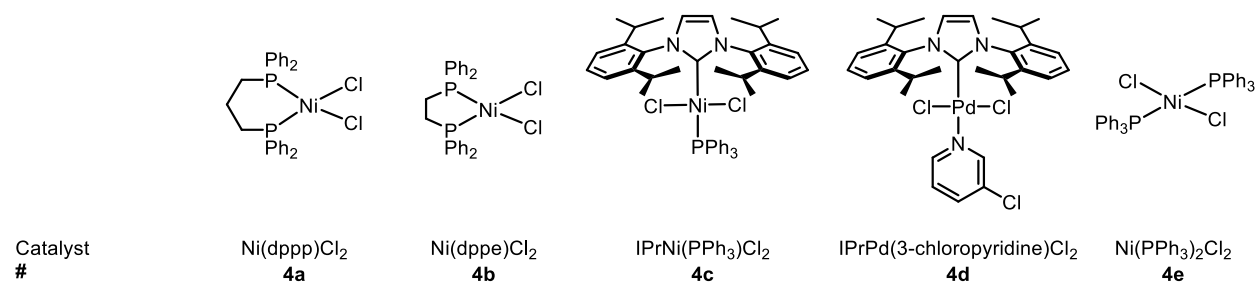
The examples above illustrate the importance of precatalyst choice on polymerizations and copolymerizations. We hypothesized that studying the catalyst-polymer  $\pi$ -complex, the defining feature of chain-growth polymerizations, is integral to understanding the different polymerization behavior of the precatalysts. A catalyst that forms a strong  $\pi$ -complex (for controlled polymerizations), but that can migrate across varied aryl groups (to cross-propagate with different monomers) would be highly desirable. However, design principles to tailor copolymerization behavior have not been established. Catalyst-polymer  $\pi$ -complexes have not been directly observed, despite numerous small-molecule examples.<sup>26,27,52</sup> The importance of the  $\pi$ -complex, combined with the difficulty of studying it, has created a large knowledge gap. To partially fill this gap, we developed an indirect method to probe differences in the catalyst-polymer  $\pi$ -complexes by detecting end-to-end catalyst migration. This system, based on end-group labelling, forces migration after the first end-cap is incorporated. A mobile catalyst that forms strong  $\pi$ -complexes can transfer across the polymer through a series of  $\pi$ -complexation events. This process, referred to herein as chain-walking, enables the catalyst to react at both polymer ends without chain-transfer (migration). If the  $\pi$ -complex is weak or fleeting, then the catalyst would dissociate (to react with excess competitive agent), leaving a polymer with an unreacted  $\alpha$  chain-end. High chain-walking barriers that restrict the catalyst to the  $\omega$  chain-end could also lead to dissociation products. In this way, the  $\pi$ -complex behavior determines the ratios of polymers with one or two capping agents (analyzed by mass spectrometry) and enables us to compare different catalysts and polymers under similar conditions.

Results from the end-capping experiments with thiophene (Chapter 2) revealed that the  $\pi$ -complex can be robust for a broad range of catalysts, producing nearly quantitative migration products across more than 50 repeat units. However, these experiments examine only one piece of the catalyst-polymer  $\pi$ -complex—the catalyst. Understanding how changing the monomer/polymer influences the  $\pi$ -complex is critical to developing copolymerization methods that enable cross-propagation. Herein, we explore the end-capping model system using **1** with four popular CTCP catalysts and evaluate how the end-capping results relate to the current theories of random catalyst chain-walking.

## Results and discussion

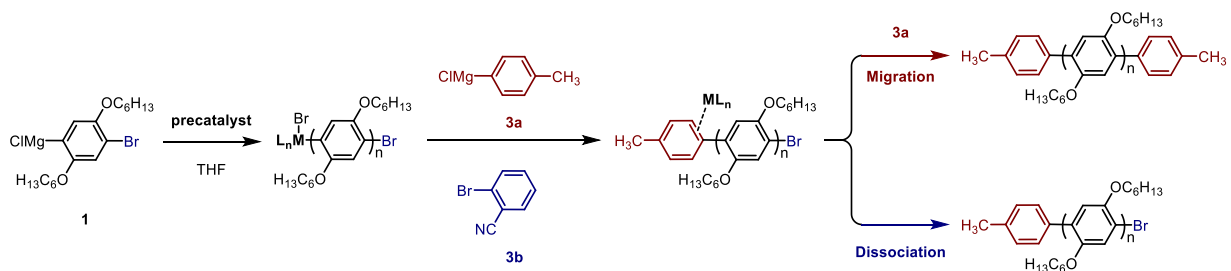
### End-capping model system

The experiments below are similar to the end-capping model system described in detail in Chapter 2. Sample reactions show **4a–d** polymerize **1** in a living, chain-growth fashion, as evidenced by targeted  $M_n$  and low  $\bar{D}$  (Appendix 2). Therefore, results obtained in the model system are more reflective of subtle mechanistic differences between catalysts rather than polymerization efficiency. The selected catalysts vary over several parameters including ligand bite angle, ligand identity/coordination, and transition metal.



**Chart 3-1.** Structures and names of the dihalide precatalysts investigated in the end-capping model system.

The main differences between the end-capping experiments using **1** or **2** is the identity of the capping and competitive agents. An excess of competitive agent during end-capping is essential for identifying the  $\pi$ -complex stability/mobility of each catalyst. The competitive agent reacts with diffuse  $M^0$  and preserve the dissociation product. However, competitive agent that is too reactive could undergo Grignard exchange with monomer or induce chain-transfer from the polymer. After evaluating several competitive agents, it was found that 2-bromobenzonitrile, **3b**, could be used as a competitive agent that did not disrupt polymerizations. Small molecule cross-coupling competition experiments were performed to demonstrate that **3b** is substantially more reactive than **S1** (Appendix 2). Therefore, **3b** should sequester  $M^0$  generated during end-capping experiments and prevent catalyst diffusion between polymers. The capping agent was also optimized to resemble chain-walking across **P1**. As discussed above, differences in the  $\pi$ -binding affinity between different aryl groups can cause a catalyst to “stick” to a segment of the polymer and hinder oxidative addition. We identified (p-tolyl)magnesium chloride, **3a**, as capping agent with similar electronic properties to **1** that is easily identified by mass spectrometry (using matrix-assisted laser desorption/ionization time-of-flight mass spectrometry, MALDI-TOF MS).



**Scheme 3-3.** End-capping model system to detect catalyst migration by capping with **3a**.

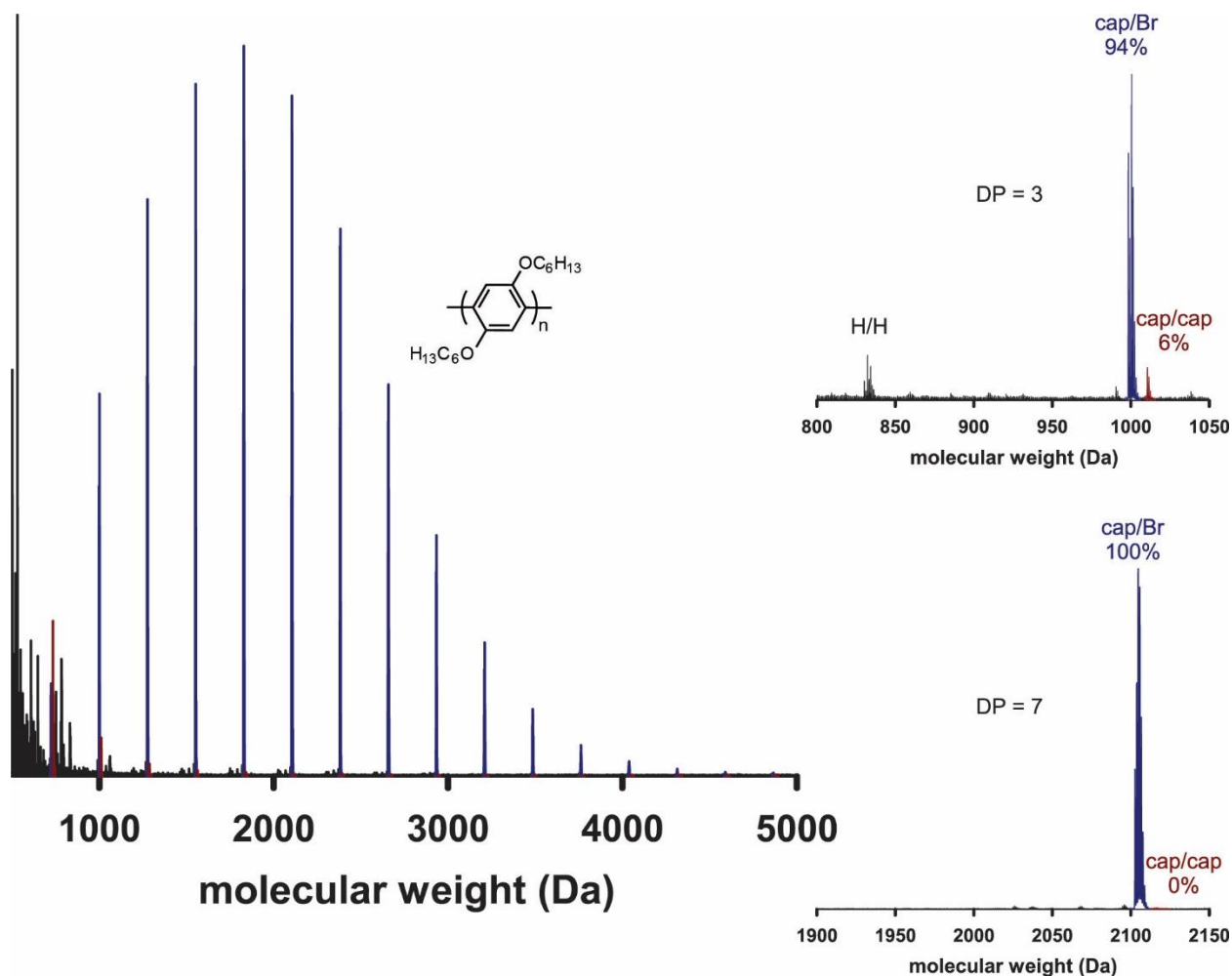
### *End-capping using Ni bidentate phosphine ligands*

The most common precatalyst employed in Kumada CTCP is Ni(dppp)Cl<sub>2</sub>, **4a** (dppp = 1,3-bis(diphenylphosphino)propane),<sup>24,54</sup> but examples of migration across **1** are limited to copolymerizing **1** and **2** where preferential  $\pi$ -binding to **2** restricts block copolymer synthesis to a single direction. Using precatalyst **4a** in our end-capping experiments, the majority of polymers had cap/Br end-groups from the dissociation pathway. The migration product was only prevalent at very short chain-lengths (DP of two). At a DP of three, however, the migration product is only 6% by area (Figure 3-1, Appendix 2). The low level of migration is surprising, given the extensive migration across **P3DT**, but does not directly contradict typical polymerization results (**P3DT** = poly(3-decylthiophene)).

Limited migration of **4a** across **P1** could originate from two different scenarios. The first possibility is that Ni-**P1**  $\pi$ -complex is not stable. The complex that is formed is fleeting, so the catalyst dissociates from the polymer shortly after it is formed. The catalyst could be localized at the  $\omega$  end throughout the entire polymerization (i.e., no migration), where rapid oxidative addition into the  $\omega$  chain-end could occur (before dissociation/chain-transfer) to achieve a chain-growth mechanism.

An alternative mechanism is that there is high energy barrier to chain-walking due to steric repulsion between the dppp ligand and the twisted phenyl rings or hexyloxy side-chains of the polymer. In the end-capping experiments, the catalyst would be localized at the capped-end and dissociation/chain-transfer to excess competitive agent occurs before migration to the  $\alpha$  chain-end—even though a strong  $\pi$ -complex is formed. With a high barrier to chain-walking, the catalyst-polymer  $\pi$ -complex would remain at the  $\omega$  terminus during polymerizations. Catalyst would be well positioned for intramolecular oxidative addition at the  $\omega$  terminus, thereby reducing

chain-transfer or dissociation (relative to otherwise identical catalyst that migrates). Either scenario (strong binding with high chain-walking barriers or weak binding with low oxidative addition barriers) could explain the limited migration products but living, chain-growth polymerizations.



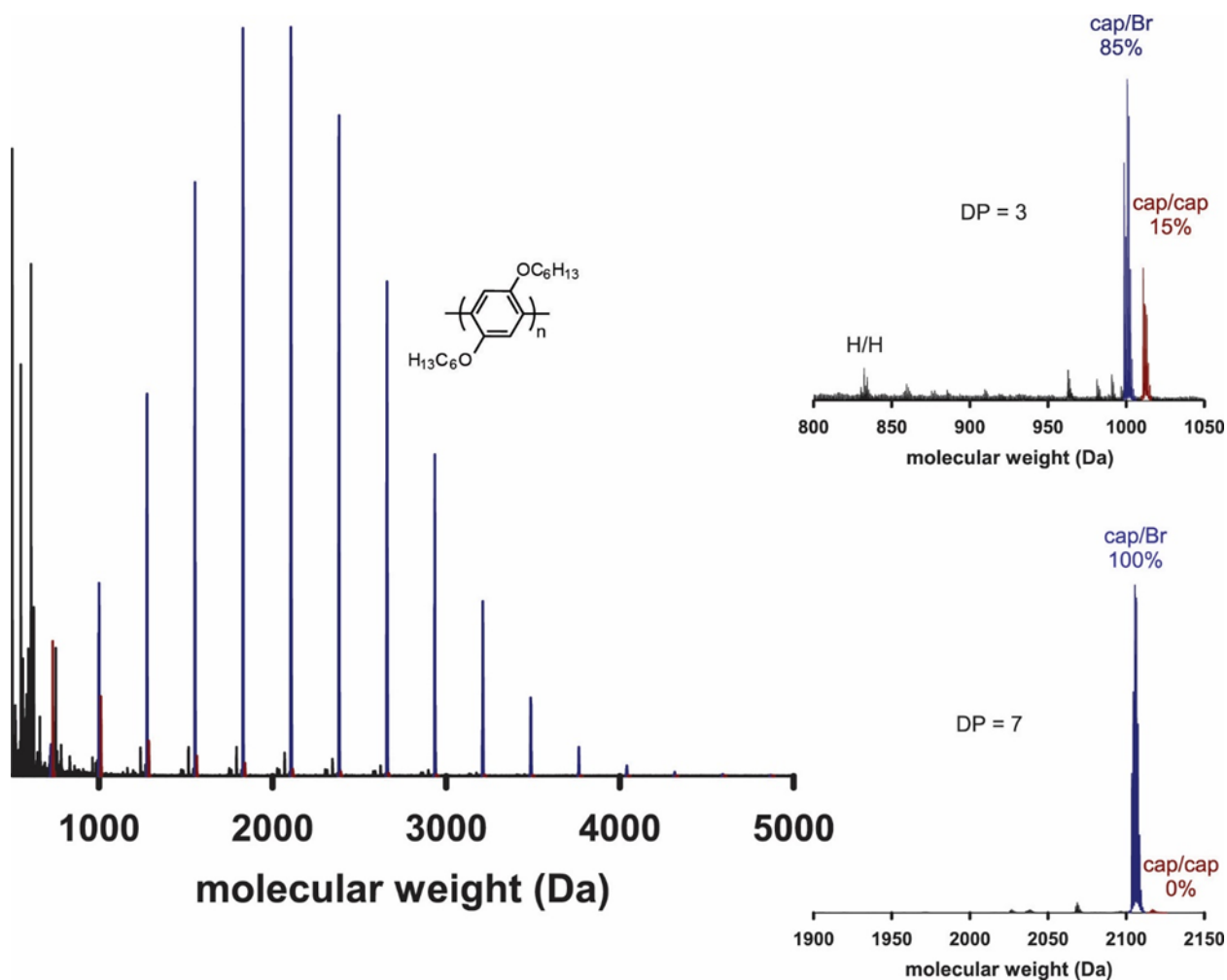
**Figure 3-1.** MALDI-TOF mass spectra of **P1** produced by **4a** after end-capping with **3a** (15 equiv) and **3b** (50 equiv). Migration (cap/cap, ■) and dissociation (cap/Br, ■) product peaks are highlighted from all other masses (■). Insets (right) show **P1** end-groups at DP = 3 (top) and DP = 7 (bottom).

#### *Ligand effects: phosphine bite-angle*

Precatalyst **4b** has received considerable interest for polymerizing **1** due to the ability to prepare aryl-functionalized precatalysts to study polymerization behavior,<sup>20</sup> accelerate initiation,<sup>55</sup> and functionalize polymers.<sup>56</sup> Convincing evidence for Ni(dppe) migration is presented in small molecule experiments,<sup>17</sup> but catalyst migration across polyphenylene has not been documented. While the bidentate phosphine is electronically similar to dppp, the shorter alkyl linker decreases



the ligand bite angle for the  $L_nNiCl_2$  complex from  $91^\circ$  to  $85^\circ$  and changes the rate-determining step in the polymerization from transmetallation to reductive elimination.<sup>21,57</sup> If steric repulsion is a major deterrent to chain-walking for **4a**, then migration using **4b** should be higher. End-capping experiments using **4b** yielded results similar to **4a**. The dissociation product was favored at  $DP > 2$ , and was detected at all chain-lengths. The steric differences between dppp/dppe and different polymerization rate-limiting steps (i.e., reductive elimination versus transmetallation) have only a minor impact on the end-capping results.



**Figure 3-2.** MALDI-TOF mass spectra of **P1** produced by **4b** after end-capping with **3a** (15 equiv) and **3b** (50 equiv). Migration (cap/cap, ■) and dissociation (cap/Br, ■) product peaks are highlighted from all other masses (■). Insets (right) show **P1** end-groups at DP = 3 (top) and DP = 7 (bottom).

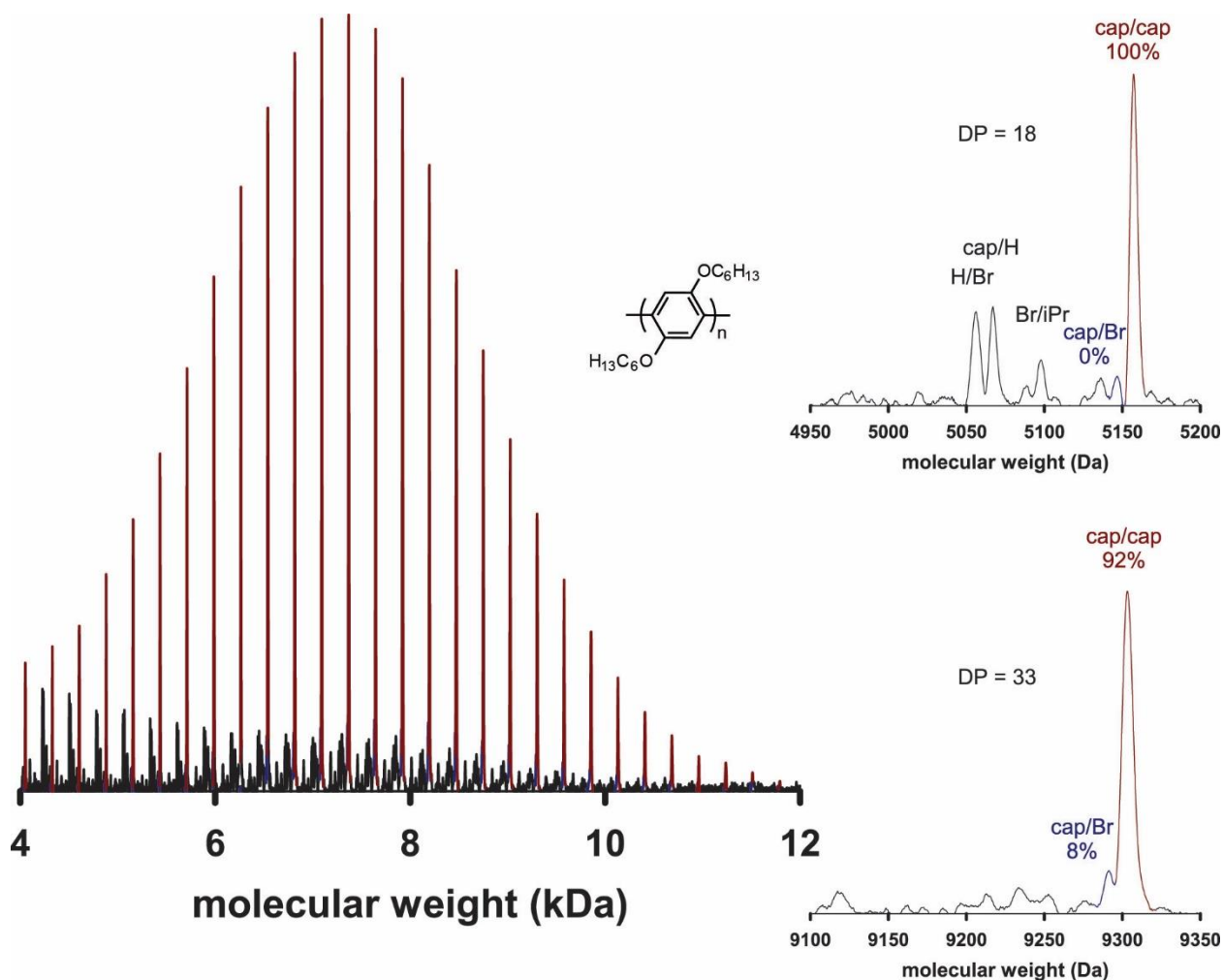
These results are surprising based on the success and ubiquity of **4b** in CTCP, and from cross-coupling examples of selective “di-capping” between an aryl Grignard with an excess of aryl dihalide.<sup>58</sup> In small-molecule competition experiments by McNeil and coworkers (Scheme 3-1), 1

equiv of a capping agent (*o*-methoxyphenylmagnesium chloride) and 1–100 equiv of competitive agent (**3b**) were mixed with Ni(dppe)(4-bromo-2,5-bis(butoxy)phenylene)Br.<sup>17</sup> The ratio of the intramolecular to intermolecular reaction changes from 95:5 to 40:60 in going from 1–50 equiv of **3b**. The similarity between this reported system and the end-capping experiments described herein warrants a thorough comparison, with their results serving as a data point for DP = 1. Comparing at 50 equivalents of **3b**, their results give less migration product (40%) than what we observe at DP = 2 (64%). The two major differences are the capping agent (*p*-tolylmagnesium chloride versus *o*-methoxyphenylmagnesium chloride) and the catalyst/competitive agent concentration (their system was over 26 times more concentrated). The increased concentration of competitive agent (at the same 50 equiv) should accelerate the rate of the reaction with competitive agent (via chain-transfer or after dissociation), while the intramolecular reaction will remain the same. The end-capping experiments performed in our studies were conducted under dilute conditions (within the typical range of CTCP) to limit catalyst diffusion polymers (intermolecular pathway), which would convert the dissociation product (cap/Br polymer) to the migration product (cap/cap polymer) or cap/H polymer. Despite the different values, both experiments demonstrate that the  $\pi$ -complex biases but does not guarantee intramolecular reactivity across short chains.

#### *Ligand effects: phosphine v. N-heterocyclic carbene*

We next evaluated the precatalyst IPrNi(PPh<sub>3</sub>)Cl<sub>2</sub>, **4c**, to determine the effect of the donor/acceptor capabilities and steric differences of the ancillary ligand. N-heterocyclic carbenes (NHCs) are known to be strong  $\sigma$ -donors and weak  $\pi$ -acceptors relative to their phosphine counterparts.<sup>59–63</sup> Literature polymerizations of **2** with **4c** indicate a controlled chain-growth mechanism,<sup>37,64</sup> but phenylene derivatives have received little attention.<sup>65,66</sup> In our hands, polymerizing **1** resulted in high molecular weight polymer with low dispersity and H/Br end-groups consistent with a chain-growth polymerization (Appendix 2). Evaluating precatalyst **4c** in the end-capping experiments yielded drastically different results compared to the phosphine-ligated precatalysts. The migration product was produced almost exclusively through DP of 35 (Figure 3-3). The migration product is observed at longer polymer lengths, but low signal-to-noise and peak broadening make quantitative comparisons challenging. The complete reversal in the product distribution, with Ni-bidentate phosphine catalysts generating nearly exclusive

dissociation products and Ni-NHC yielding the migration product, illustrates the remarkable effect of the ligand on the catalyst-**P1**  $\pi$ -complex.



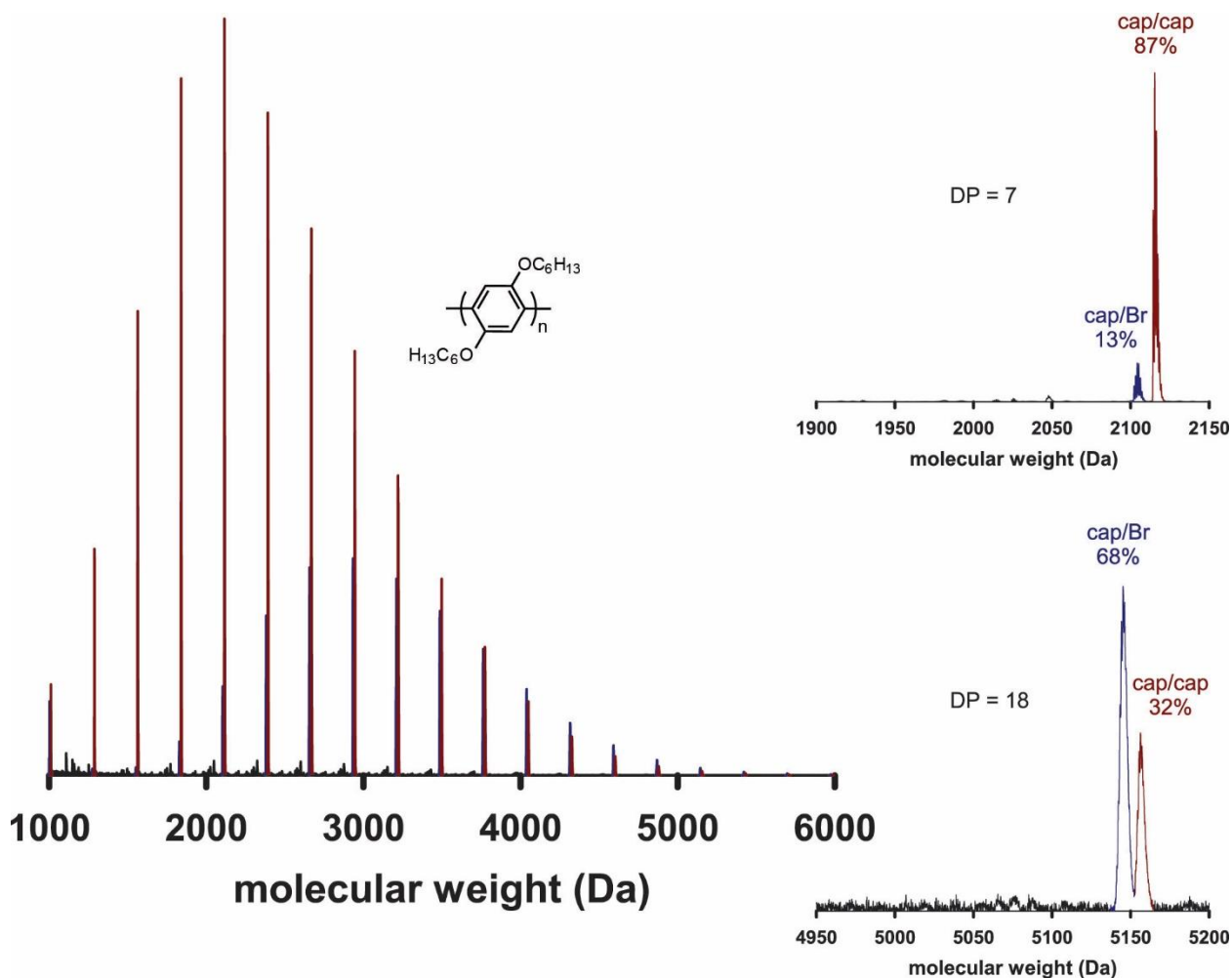
**Figure 3-3.** MALDI-TOF mass spectra of **P1** produced by **4c** after end-capping with **3a** (15 equiv) and **3b** (50 equiv). Migration (cap/cap, ■) and dissociation (cap/Br, ■) product peaks are highlighted from all other masses (■). Insets (right) show **P1** end-groups at DP = 18 (top) and DP = 33 (bottom).

#### *Metal effects: Ni versus Pd*

Pd catalysts are attractive for CTCP due to their broad substrate scope and high performance in a variety of cross-coupling procedures.<sup>61,67–69</sup> CTCP methods have been developed for a limited number of Pd catalysts ligated by either a mono dentate phosphine or NHC.<sup>43,46,47,49</sup> To isolate the role of the metal identity from ligand effects, we evaluated NHC-ligated **4d**. Both **4c** and **4d** use the same IPr ligand, differing only in the metal center and labile ligands. The labile ligands, PPh<sub>3</sub> and 3-chloropyridine, are not expected to be associated with the catalyst during

chain-walking and subsequent oxidative addition due to steric constraints.<sup>50,51</sup> If migration differences are observed, they should be attributed to changing the transition metal.

End-capping experiments using **4d** showed migration that was unique from the Ni-bidentate phosphine (**4a/4b**) and Ni-NHC (**4c**) catalysts. At low molecular weights (DP < 5), the migration product was observed almost exclusively. The migration percent diminishes with longer polymers until the dissociation product is the major species at DP = 13 and above (Figure 3-4).



**Figure 3-4.** MALDI-TOF mass spectra of **P1** produced by **4d** after end-capping with **3a** (15 equiv) and **3b** (50 equiv). Migration (cap/cap, —) and dissociation (cap/Br, —) product peaks are highlighted from all other masses (—). Insets (right) show **P1** end-groups at DP = 7 (top) and DP = 18 (bottom).

The shorter lengths that **4d** can selectively migrate across (relative to **4c**) is qualitatively consistent with reports of weaker  $\pi$ -binding of Pd to arenes.<sup>70,71</sup> Previous comparisons between Ni and Pd (ligated by dppp) using kinetic isotope effects indicated that the first irreversible step in

Kumada cross-couplings is  $\pi$ -complexation of Ni catalysts to the haloarene.<sup>70</sup> The Ni(dppp)-PhBr  $\pi$ -complex is energetically favorable (~17 kcal/mol downhill in energy), and facilitates oxidative addition. Alternatively, complexation with Pd is much weaker (~ 7 kcal/mol), affording a fleeting interaction that has a negligible influence on the product isotopes. Koeckelberghs utilized weaker binding with Pd to prepare ABC block copolymers using thiophene, selenophene, and fluorene monomers in all possible combinations and orders of addition using a Pd phosphine catalyst.<sup>46</sup> Chain-growth behavior was proposed to occur by making the polymer C-Br more reactive than monomer C-Br. Without the strong-complexation typical of CTCP catalysts, elevated dispersities ( $\mathcal{D} = 1.4\text{--}1.7$ ) were observed for all copolymer, even after precipitation and Soxhlet extraction to remove low molecular weight polymers.

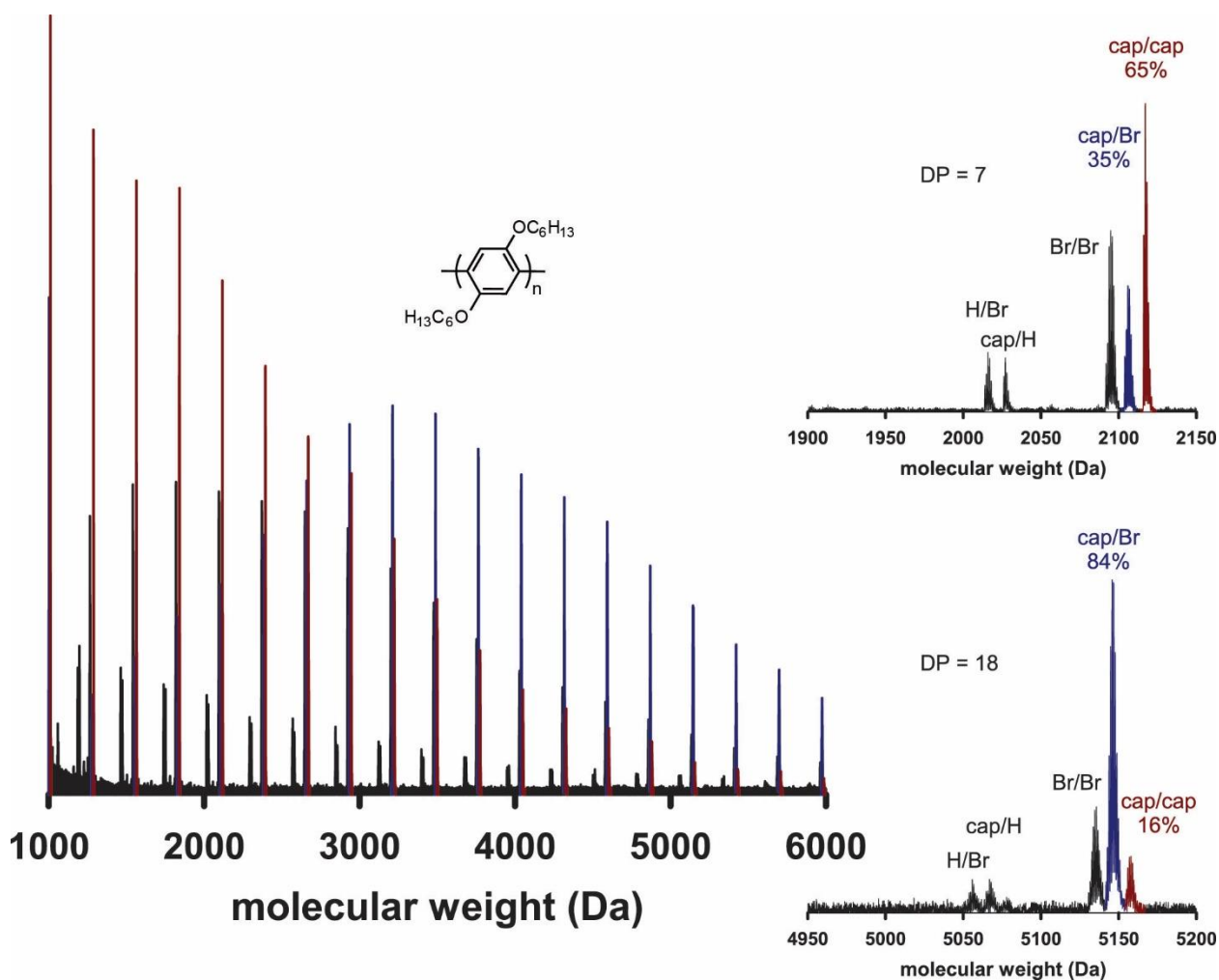
The end-capping experiments performed herein suggest that the Pd-**P1**  $\pi$ -complex is strong enough to direct subsequent oxidative addition into **P1** rather than reacting with **3b**. The migration pathway is >50% up to DP = 12. In Chapter 4, we show that **4d** is a promising precatalyst for copolymerizing **1** and **2** with the high levels of control expected from CTCP. This efficient copolymerization behavior occurs despite the differences in migration for **4d** across **P3DT** and **1** (in Chapter 2 and Chapter 3, respectively). The end-capping and copolymerizations results indicate that  $\pi$ -binding does not inhibit cross-propagation.

#### *Uncontrolled CTCP precatalyst Ni(PPh<sub>3</sub>)<sub>2</sub>Cl<sub>2</sub>*

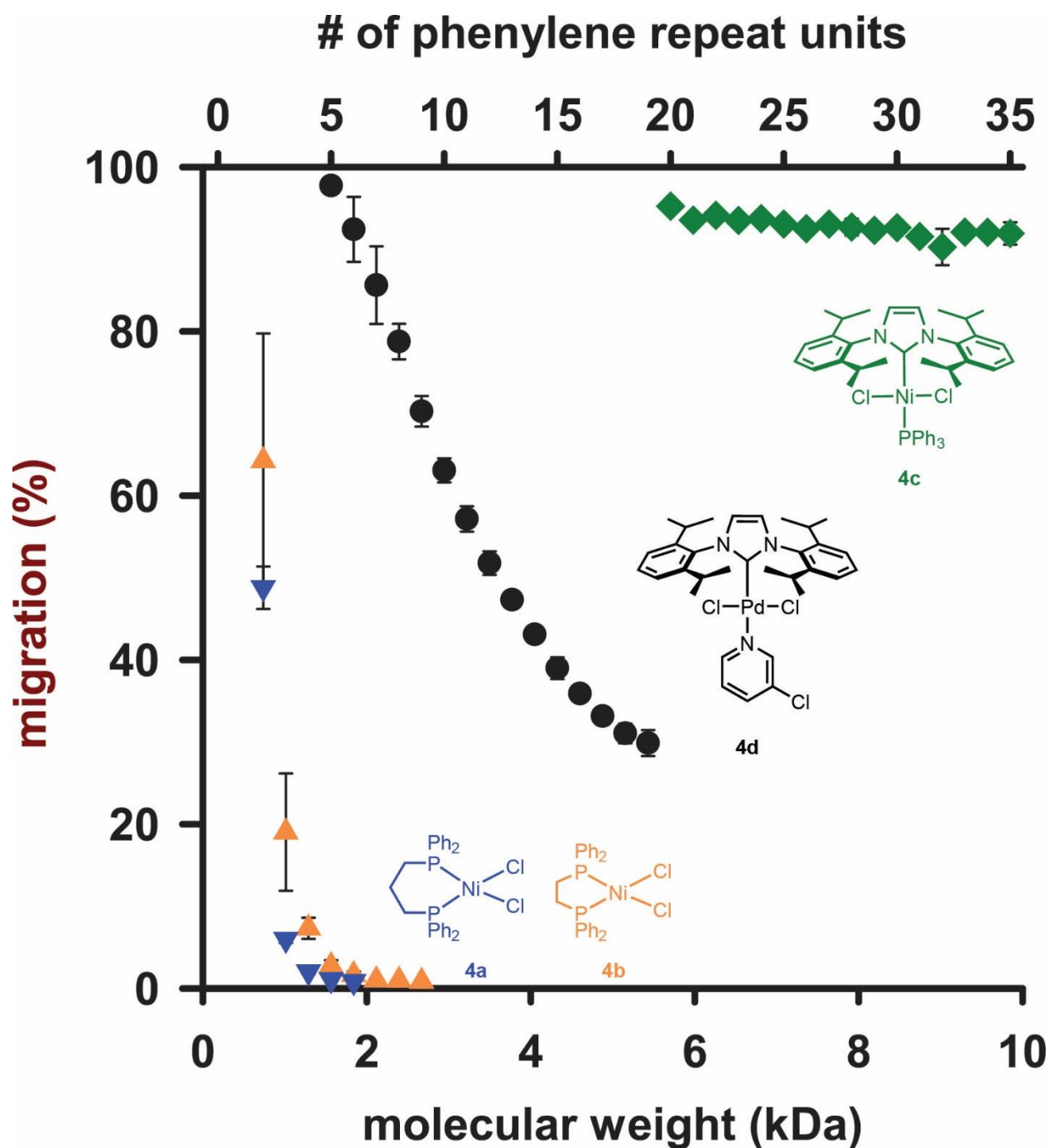
The final precatalyst evaluated in the end-capping experiments, **4e**, displays high activity in Kumada cross-couplings but is prone to chain-transfer/dissociation during CTCP of **2**.<sup>72,73</sup> Control polymerizations with **1** are consistent with these reports, producing polymers of reduced molecular weight and higher dispersities with high conversion of **1** (relative to polymerizing using precatalyst **4a/4b**, Appendix 2). Additionally, prominent Br/Br end-groups indicate that the catalyst is not present on the  $\omega$  chain-end during the acid quench. Using **4e** in the end-capping system serves as an important control due to the documented chain-transfer events with this catalyst. Understanding how end-capping correlates to known polymerization results could make these experiments an important tool to diagnose  $\pi$ -complex deficiencies.

Consistent with polymerization controls, the end-capping results using **4e** are distinct from the four CTCP precatalysts—a mixture of dissociation and migration products were observed from DP of 4–18 (Figure 3-5). The migration product was prominent at short chain-lengths, in addition

to prominent Br/Br peaks from unassociated catalyst. Migration decreased similar to the sigmoidal decay observed with precatalyst **4d**, but the percent migration was consistently ~ 25% lower. The percentage of Br/Br peaks also decreased with increasing molecular weight, but they decayed much more slowly. It is unclear whether Ni(PPh<sub>3</sub>), Ni(PPh<sub>3</sub>)<sub>2</sub>, or a combination of the two are responsible for the migration behavior using **4e**. Due to the presence of cap/H, which could arise from either the migration pathway (H is derived from HCl quench) or dissociation pathway (H derived from termination prior to capping), quantitative comparison with **4a–d** was not conducted.



**Figure 3-5.** MALDI-TOF mass spectra of **P1** produced by **4e** after end-capping with **3a** (15 equiv) and **3b** (50 equiv). Migration (cap/cap, █) and dissociation (cap/Br, █) product peaks are highlighted from all other masses (█). Insets (right) show **P1** end-groups at DP = 7 (top) and DP = 18 (bottom).

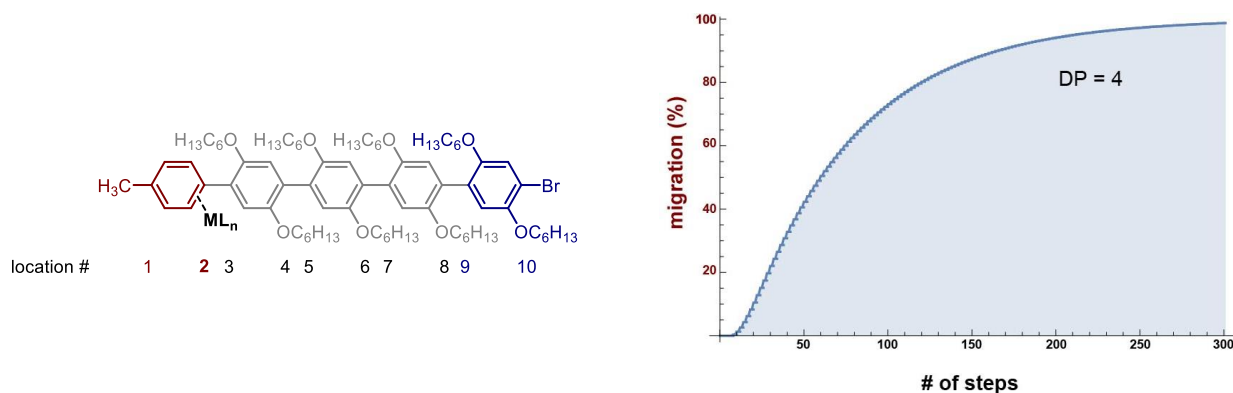


**Figure 3-6.** Migration pathway percent calculated at each DP for precatalysts **4a–d** across **P1** in the end-capping model experiments. Migration pathway percent was calculated from peak areas determined by MALDI-TOF MS. Error bars represent one standard deviation.

*Statistical analysis using a random-walk model*

The decay of migration product ratios is qualitatively intuitive—more aryl groups to chain-walk across provides a greater number of chances to dissociate before reaching the chain-end. The

most widely accepted model for chain-walking assumes a random walk along the polymer backbone.<sup>74–77</sup> We calculated the number of chain-walking steps required to migrate from one end of the polymer to the other in the simplest case where there is an equal probability to chain-walk between all monomer and capping agent units. Computational modeling for **4a** with phenylene indicates  $\eta$ -2 coordination,<sup>78</sup> in line with numerous calculations for **4a**, **4c**, and **4d** with **2**.<sup>35,50,63</sup> From an  $\eta$ -2  $\pi$ -complex, migration across each repeat unit takes two linear steps. Catalyst started one step in on the capped chain-end (location 2) and chain-walking proceeded until the catalyst reached the reactive termini (location 10) where it was assumed to react immediately (Figure 3-7).



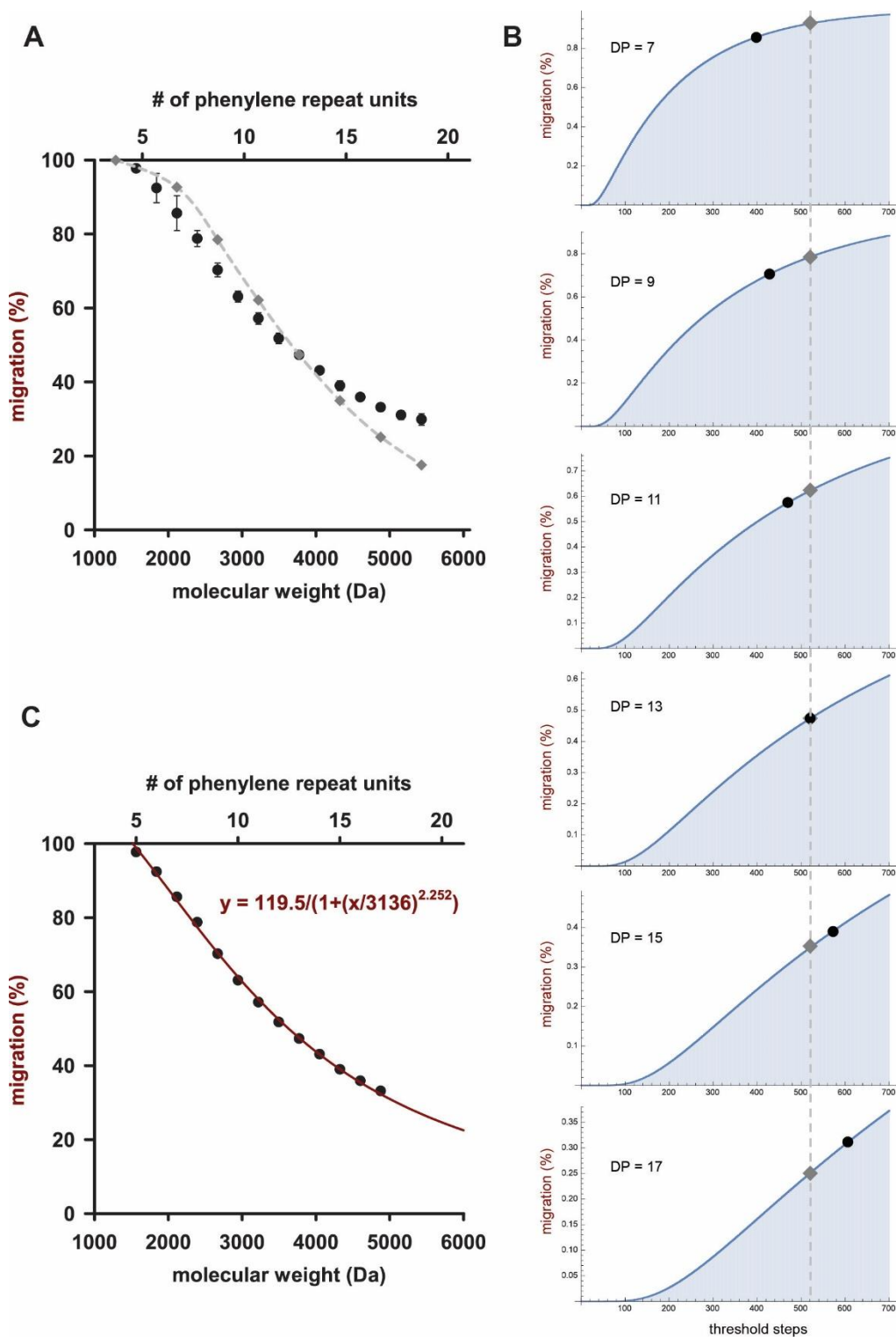
**Figure 3-7.** Catalyst-polymer  $\pi$ -complex between a polymer with a DP of 4 and a capping agent at the  $\omega$  end (left) with the catalyst at location 2. The cumulative distribution function (right) depicts how the probability of the catalyst reaching position 10 (i.e., the migration pathway) increases with an increasing number of steps (for detailed explanation of the calculation, see Appendix 2).

Mathematica software was used to calculate the cumulative probability of reaching the  $\alpha$  chain-end (based on a purely random walk) at each DP. The cumulative probability for catalysts to migrate to the  $\alpha$  end (position 10 for DP = 4 in Figure 3-7) is analogous to the migration percent in the end-capping experiments. Therefore, we used the percent migration from end-capping experiments to determine the number of steps required for catalyst migration. In the example shown above where DP = 4, experimental data for each catalyst would be fit separately (Figure 3-7). For **4a**, 12 steps are required to match the 2% migration observed. Using the same cumulative probability calculation, we calculate that 16 steps are required for 7% migration using precatalyst **4b**. The number of steps for **4c** and **4d** could not be calculated at such short chain-lengths because the migration product was 100% (corresponding to an infinite number of steps).



The cumulative probability of chain-transfer or dissociation events should be dependent on the number of steps that the catalyst chain-walks between chain-ends, but the probability for dissociation at each step should independent of DP or location on the polymer. If we analyze **4d** at DP = 13 (migration  $\approx$  dissociation), 520 steps are required to achieve 47% migration. For each catalyst, a similar number of steps at each chain-length indicates that the random-walk calculation (vide supra) accounts for catalyst behavior during end-capping. Catalysts would walk this consistent number of steps before dissociation. For a catalyst to walk the same 520 steps across polymers with a DP of 7 and 17, the predicted migration values would 93% and 25% migration, respectively (Figure 3-8). These predicted values (from a purely statistical random-walk) are compared to the experimentally determined migration values for **4d** (Figure 3-8). This comparison is shown from two perspectives—Figure 3-8A plots the predicted migration values on top of end-capping experimental data. The second perspective plots experimental data on top of the cumulative distribution function at various DP (Figure 3-8B). At DP = 7, the experimentally determined 86% migration corresponds to 398 steps, and 604 steps are required to match the experimental migration at DP = 17. Both Figure 3-8A and Figure 3-8A intersect at 47% migration (for DP = 13) because this point was used to calculate 520 steps. The large variation in steps suggests that the random-walking model does not fully capture the migration of **4d**. A logistic function matches the experimental data quite well, although the reasons are unclear (Figure 3-8C).

Based on the differences between catalysts in the end-capping experiments, we would expect a different number of steps for each catalyst. Moderate preferences for the chain-end have been used by other groups to improve the fit between experimental data and the random-walking model,<sup>74,75</sup> but the influence of end-groups is minor above DP  $\sim$  10. Making the cap or phenylene-Br more attractive/repulsive has only a small effect with **4c/d**, but dominates the fit to data from **4a/b** (Appendix 2). Migration is insensitive to DP with **4c** *within our data range* (similar to **4b-d** in Chapter 2). Because the number of steps required to reach the chain-end will always increase with chain length, migration that is insensitive to DP cannot be used to evaluate the validity of the random chain-walking model. Nevertheless, the random-chain-walking model calculates that over 10,700 steps are required for 92% of the **4c** catalyst to migrate across a polymer with DP = 34.



**Figure 3-8.** (A) Experimental values for the migration pathway are plotted against molecular weight/DP for **4d** (●) and statistical calculations (◆) at 520 steps. (B) Plots of cumulative distribution function for DP = 7, 9, 11, 13, 15, and 17 for 0–700 steps are overlaid with the end-capping data [plotted in (A)] from **4d** (●) and the statistical calculations points (◆). A reference line at 520 steps (■ ■ ■) is provided to illustrate the experimental deviation from the random-walking calculation. (C) Logistic function fit to migration percent across DP = 5–18 for **4d**.

### *Monomer effects: phenylene versus thiophene*

End-capping experiments revealed large differences in the  $\pi$ -complex stability/catalyst mobility between **4a–d** and **P1** (Figure 3-6). Migration proceeded nearly quantitatively with **4c** across over 35 repeat units, while **4a/b** migration plummeted below 5% after a DP of only 3. Precatalyst **4d** yielded an intermediate amount of chain-walking, with a gradual transition from migration to dissociation products at 12 repeat units or more. This behavior contrasts end-capping of **P3DT**, where the migration percent exceeded 95% up to 36 repeat units (or more) for all four CTCP catalysts (Chapter 2). Catalyst migration requires a combination of strong  $\pi$ -binding (electronics) and low chain-walking barriers (sterics). The two polymers studied in this thesis vary considerably in both categories. Polythiophenes like **P3DT** exhibit flexible-rod characteristics in solution due to two planar conformations that maintain conjugation. As such, effective conjugation lengths approach  $\sim 10$  units.<sup>79</sup> Alternatively, **P1** exhibits a rigid-rod architecture, but the steric interactions between phenyl rings “force” a twisting of  $\sim 40^\circ$  between each ring. With two hexyloxy side-chains AND significant twisting between each repeat unit, migration across phenylene for bulkier catalysts could be challenging. The resulting effective conjugation length of 5 units gives **P1** a higher energy LUMO that provides a vastly different electronic landscape for interacting with the catalysts.<sup>80,81</sup> Differences in  $\pi$ -binding has been investigated computationally, with the ground state stabilization of Ni(dppp) complexed to thiophene being significantly more stabilizing than to phenylene (binding to a single aryl group of each).<sup>78</sup> While both electronic and steric considerations suggest that migration should be higher across phenylene, the magnitude of these differences with Ni phosphine catalysts is surprising.

### **Conclusion**

End-capping experiments across **P1** revealed stark differences in catalyst migration between phosphine/NHC ligands and Ni/Pd transition metals. The use of 2-bromobenzonitrile, **3b**, as a competitive agent minimized intermolecular reactions between polymers and enabled us to attribute the migration products to catalyst chain-walking via the  $\pi$ -complex. Bidentate phosphine-ligated Ni catalysts **4a/b** favored dissociation products at all DP > 2, but switching ligands to IPr with **4c** yielded over 90% migration up to the limits of our data range (DP  $\sim 35$ ). Changing the transition metal to Pd yields migration behavior that varied with chain-length. The results are incompletely described by purely statistical calculations based on random catalyst chain-walking

(particularly for **4d**), which suggests that an additional driving force for chain-walking might be operative.

The end-capping system has been used to expose the underlying mechanistic differences between equally competent polymerizations of **1** and **2**. These results suggest that developing catalysts for CTCP polymerizations is highly influenced by the monomers studied, but NHC-ligated catalysts may exhibit more general migration. Catalysts that exhibit limited chain-walking are desirable to minimize sequence scrambling due to migration during copolymerizations—undesired chain-walking or preferential  $\pi$ -binding have also been attributed to copolymerization failures. These studies reveal how catalyst design and monomer choice influences migration, and should be fruitful for developing new catalysts that either leverage the benefits of chain-walking or mitigate its effect.

## References

- (1) Wang, C.; Dong, H.; Hu, W.; Liu, Y.; Zhu, D. Semiconducting  $\pi$ -Conjugated Systems in Field-Effect Transistors: A Material Odyssey of Organic Electronics. *Chem. Rev.* **2012**, *112*, 2208–2267.
- (2) Nielsen, C. B.; Turbiez, M.; McCulloch, I. Recent Advances in the Development of Semiconducting DPP-Containing Polymers for Transistor Applications. *Adv. Mater.* **2013**, *25*, 1859–1880.
- (3) Holliday, S.; Donaghey, J. E.; McCulloch, I. Advances in Charge Carrier Mobilities of Semiconducting Polymers Used in Organic Transistors. *Chem. Mater.* **2014**, *26*, 647–663.
- (4) Gong, S.; Sun, N.; Luo, J.; Zhong, C.; Ma, D.; Qin, J.; Yang, C. Highly Efficient Simple-Structure Blue and All-Phosphor Warm-White Phosphorescent Organic Light-Emitting Diodes Enabled by Wide-Bandgap Tetraarylsilane-Based Functional Materials. *Adv. Funct. Mater.* **2014**, *24*, 5710–5718.
- (5) Guo, X.; Baumgarten, M.; Müllen, K. Designing  $\pi$ -Conjugated Polymers for Organic Electronics. *Prog. Polym. Sci.* **2013**, *38*, 1832–1908.
- (6) Grimsdale, A. C.; Chan, K. L.; Martin, R. E.; Jokisz, P. G.; Holmes, A. B. Synthesis of Light-Emitting Conjugated Polymers for Applications in Electroluminescent Devices. *Chem. Rev.* **2009**, *109*, 897–1091.
- (7) Ying, L.; Ho, C.-L.; Wu, H.; Cao, Y.; Wong, W.-Y. White Polymer Light-Emitting Devices for Solid-State Lighting: Materials, Devices, and Recent Progress. *Adv. Mater.* **2014**, *26*, 2459–2473.
- (8) Junwu, C. A.; Yong, C.; Chen, J.; Cao, Y.; Junwu, C. A.; Yong, C. Development of Novel Conjugated Donor Polymers for High-Efficiency Bulk-Heterojunction Photovoltaic Devices. *Acc. Chem. Res.* **2009**, *42*, 1709–1718.
- (9) Gibson, G. L.; McCormick, T. M.; Seferos, D. S. Atomistic Band Gap Engineering in Donor-Acceptor Polymers. *J. Am. Chem. Soc.* **2012**, *134*, 539–547.
- (10) Carsten, B.; Szarko, J. M.; Son, H. J.; Wang, W.; Lu, L.; He, F.; Rolczynski, B. S.; Lou, S. J.; Chen, L. X.; Yu, L. Examining the Effect of the Dipole Moment on Charge Separation in Donor-Acceptor Polymers for Organic Photovoltaic Applications. *J. Am. Chem. Soc.* **2011**, *133*, 20468–20475.
- (11) Marzano, G.; Ciasca, C. V.; Babudri, F.; Bianchi, G.; Pellegrino, A.; Po, R.; Farinola, G. M. Organometallic Approaches to Conjugated Polymers for Plastic Solar Cells: From Laboratory Synthesis to Industrial Production. *European J. Org. Chem.* **2014**, *2014*, 6583–6614.
- (12) Odian, G. Step Polymerization. In *Principles of Polymerization*; John Wiley & Sons, Inc.: Hoboken, NJ, USA, 2004; pp. 39–197.
- (13) Chen, L.-M.; Hong, Z.; Li, G.; Yang, Y. Recent Progress in Polymer Solar Cells: Manipulation of Polymer:Fullerene Morphology and the Formation of Efficient Inverted Polymer Solar Cells. *Adv. Mater.* **2009**, *21*, 1434–1449.
- (14) Van Bavel, S.; Veenstra, S.; Loos, J. On the Importance of Morphology Control in Polymer

- Solar Cells. *Macromol. Rapid Commun.* **2010**, *31*, 1835–1845.
- (15) Lu, L.; Yu, L. Understanding Low Bandgap Polymer PTB7 and Optimizing Polymer Solar Cells Based on It. *Adv. Mater.* **2014**, *26*, 4413–4430.
- (16) Jones, M. L.; Huang, D. M.; Chakrabarti, B.; Groves, C. Relating Molecular Morphology to Charge Mobility in Semicrystalline Conjugated Polymers. *J. Phys. Chem. C* **2016**, *120*, 4240–4250.
- (17) Bryan, Z. J.; McNeil, A. J. Evidence for a Preferential Intramolecular Oxidative Addition in Ni-Catalyzed Cross-Coupling Reactions and Their Impact on Chain-Growth Polymerizations. *Chem. Sci.* **2013**, *4*, 1620–1624.
- (18) Zenkina, O. V.; Karton, A.; Freeman, D.; Shimon, L. J. W.; Martin, J. M. L.; van der Boom, M. E. Directing Aryl–I versus Aryl–Br Bond Activation by Nickel via a Ring Walking Process. *Inorg. Chem.* **2008**, *47*, 5114–5121.
- (19) Larrosa, I.; Somoza, C.; Banquy, A.; Goldup, S. M. Two Flavors of PEPPSI-IPr: Activation and Diffusion Control in a Single NHC-Ligated Pd Catalyst? *Org. Lett.* **2011**, *13*, 146–149.
- (20) Lee, S. R.; Bryan, Z. J.; Wagner, A. M.; McNeil, A. J. Effect of Ligand Electronic Properties on Precatalyst Initiation and Propagation in Ni-Catalyzed Cross-Coupling Polymerizations. *Chem. Sci.* **2012**, *3*, 1562–1566.
- (21) Lanni, E. L.; Locke, J. R.; Gleave, C. M.; McNeil, A. J. Ligand-Based Steric Effects in Ni-Catalyzed Chain-Growth Polymerizations Using Bis(dialkylphosphino)ethanes. *Macromolecules* **2011**, *44*, 5136–5145.
- (22) Sheina, E. E.; Liu, J.; Iovu, M. C.; Laird, D. W.; McCullough, R. D. Chain Growth Mechanism for Regioregular Nickel-Initiated Cross-Coupling Polymerizations. *Macromolecules* **2004**, *37*, 3526–3528.
- (23) Yokoyama, A.; Miyakoshi, R.; Yokozawa, T. Chain-Growth Polymerization for Poly(3-Hexylthiophene) with a Defined Molecular Weight and a Low Polydispersity. *Macromolecules* **2004**, *37*, 1169–1171.
- (24) Leone, A. K.; McNeil, A. J. Matchmaking in Catalyst-Transfer Polycondensation: Optimizing Catalysts Based on Mechanistic Insight. *Acc. Chem. Res.* **2016**, *49*, 2822–2831.
- (25) Smith, M. L.; Leone, A. K.; Zimmerman, P. M.; McNeil, A. J. Impact of Preferential  $\pi$ -Binding in Catalyst-Transfer Polycondensation of Thiazole Derivatives. *ACS Macro Lett.* **2016**, *5*, 1411–1415.
- (26) Willot, P.; Koeckelberghs, G. Evidence for Catalyst Association in the Catalyst Transfer Polymerization of Thieno[3,2- B]thiophene. *Macromolecules* **2014**, *47*, 8548–8555.
- (27) Komber, H.; Senkovskyy, V.; Tkachov, R.; Johnson, K.; Kiriya, A.; Huck, W. T. S.; Sommer, M. Ring Walking versus Trapping of Nickel(0) during Kumada Catalyst Transfer Polycondensation Using Externally Initiated Electron-Accepting Thiophene–Benzothiadiazole–Thiophene Precursors. *Macromolecules* **2011**, *44*, 9164–9172.
- (28) Nojima, M.; Kosaka, K.; Kato, M.; Ohta, Y.; Yokozawa, T. Alternating Intramolecular and Intermolecular Catalyst-Transfer Suzuki-Miyaura Condensation Polymerization: Synthesis of Boronate-Terminated  $\pi$ -Conjugated Polymers Using Excess Dibromo Monomers.

- Macromol. Rapid Commun.* **2016**, *37*, 79–85.
- (29) Bedi, A.; De Winter, J.; Gerbaux, P.; Koeckelberghs, G. Detrimental Ni(0) Transfer in Kumada Catalyst Transfer Polycondensation of benzo[2,1-b:3,4-B']dithiophene. *J. Polym. Sci. Part A Polym. Chem.* **2016**, *54*, 1706–1712.
- (30) Yokozawa, T.; Nanashima, Y.; Nojima, M.; Ohta, Y. Catalyst-Transfer Condensation Polymerization of Acceptor Aromatic Monomers and of Donor Carbon-Carbon Double Bond-Containing Monomers. *Macromol. Symp.* **2015**, *350*, 22–33.
- (31) Miyakoshi, R.; Yokoyama, A.; Yokozawa, T. Importance of the Order of Successive Catalyst-Transfer Condensation Polymerization in the Synthesis of Block Copolymers of Polythiophene and Poly(p-Phenylene). *Chem. Lett.* **2008**, *37*, 1022–1023.
- (32) Wu, S.; Bu, L.; Huang, L.; Yu, X.; Han, Y.; Geng, Y.; Wang, F. Synthesis and Characterization of Phenylene-Thiophene All-Conjugated Diblock Copolymers. *Polymer* **2009**, *50*, 6245–6251.
- (33) Locke, J. R.  $\pi$ -Conjugated Copolymers of Controlled Sequence, University of Michigan, 2012.
- (34) Miyakoshi, R.; Shimono, K.; Yokoyama, A.; Yokozawa, T. Catalyst-Transfer Polycondensation for the Synthesis of Poly(p-Phenylene) with Controlled Molecular Weight and Low Polydispersity. *J. Am. Chem. Soc.* **2006**, *128*, 16012–16013.
- (35) Bridges, C. R.; McCormick, T. M.; Gibson, G. L.; Hollinger, J.; Seferos, D. S. Designing and Refining Ni(II)diimine Catalysts Towards the Controlled Synthesis of Electron-Deficient Conjugated Polymers. *J. Am. Chem. Soc.* **2013**, *135*, 13212–13219.
- (36) Bridges, C. R.; Yan, H.; Pollit, A. A.; Seferos, D. S. Controlled Synthesis of Fully  $\pi$ -Conjugated Donor–Acceptor Block Copolymers Using a Ni(II) Diimine Catalyst. *ACS Macro Lett.* **2014**, *3*, 671–674.
- (37) Fujita, K.; Sumino, Y.; Ide, K.; Tamba, S.; Shono, K.; Shen, J.; Nishino, T.; Mori, A.; Yasuda, T. Synthesis of Poly(3-Substituted Thiophene)s of Remarkably High Solubility in Hydrocarbon via Nickel-Catalyzed Deprotonative Cross-Coupling Polycondensation. *Macromolecules* **2016**, *49*, 1259–1269.
- (38) Tamba, S.; Fuji, K.; Nakamura, K.; Mori, A. Nickel(II)-Catalyzed Cross-Coupling Polycondensation of Thiophenes via C–S Bond Cleavage. *Organometallics* **2014**, *33*, 12–15.
- (39) Qiu, Y.; Worch, J. C.; Fortney, A.; Gayathri, C.; Gil, R. R.; Noonan, K. J. T. Nickel-Catalyzed Suzuki Polycondensation for Controlled Synthesis of Ester-Functionalized Conjugated Polymers. *Macromolecules* **2016**, *49*, 4757–4762.
- (40) Tkachov, R.; Senkovskyy, V.; Beryozkina, T.; Boyko, K.; Bakulev, V.; Lederer, A.; Sahre, K.; Voit, B.; Kiriya, A. Palladium-Catalyzed Chain-Growth Polycondensation of AB-Type Monomers: High Catalyst Turnover and Polymerization Rates. *Angew. Chemie* **2014**, *126*, 2434–2439.
- (41) Zhang, H.; Xing, C.; Tsemo, G. B.; Hu, Q. T-Bu 3 P-Coordinated 2-Phenylaniline-Based Palladacycle Complex as a Precatalyst for the Suzuki Cross-Coupling Polymerization of Aryl Dibromides with Aryldiboronic Acids. *ACS Macro Lett.* **2013**, *9*, 10–13.

- (42) Yokozawa, T.; Suzuki, R.; Nojima, M.; Ohta, Y.; Yokoyama, A. Precision Synthesis of poly(3-Hexylthiophene) from Catalyst-Transfer Suzuki-Miyaura Coupling Polymerization. *Macromol. Rapid Commun.* **2011**, *32*, 801–806.
- (43) Elmalem, E.; Biedermann, F.; Johnson, K.; Friend, R. H.; Huck, W. T. S. Synthesis and Photophysics of Fully  $\pi$ -Conjugated Heterobis-Functionalized Polymeric Molecular Wires via Suzuki Chain-Growth Polymerization. *J. Am. Chem. Soc.* **2012**, *134*, 17769–17777.
- (44) Verswyvel, M.; Verstappen, P.; De Cremer, L.; Verbiest, T.; Koeckelberghs, G. Development of a Universal Chain-Growth Polymerization Protocol of Conjugated Polymers: Toward a Variety of All-Conjugated Block-Copolymers. *J. Polym. Sci. Part A Polym. Chem.* **2011**, *49*, 5339–5349.
- (45) Hardeman, T.; Koeckelberghs, G. The Synthesis of Poly(thiophene- Co -Fluorene) Gradient Copolymers. *Macromolecules* **2015**, *48*, 6987–6993.
- (46) Verswyvel, M.; Steverlyncx, J.; Hadj Mohamed, S.; Trabelsi, M.; Champagne, B.; Koeckelberghs, G. All-Conjugated ABC- Block -Copolymer Formation with a Varying Sequence via an Unassociated Catalyst. *Macromolecules* **2014**, *47*, 4668–4675.
- (47) Bryan, Z. J.; Smith, M. L.; McNeil, A. J. Chain-Growth Polymerization of Aryl Grignards Initiated by a Stabilized NHC-Pd Precatalyst. *Macromol. Rapid Commun.* **2012**, *33*, 842–847.
- (48) Qiu, Y.; Mohin, J.; Tsai, C.-H.; Tristram-Nagle, S.; Gil, R. R.; Kowalewski, T.; Noonan, K. J. T. Stille Catalyst-Transfer Polycondensation Using Pd-PEPPSI-IPr for High-Molecular-Weight Regioregular Poly(3-Hexylthiophene). *Macromol. Rapid Commun.* **2015**, *36*, 840–844.
- (49) Sui, A.; Shi, X.; Tian, H.; Geng, Y.; Wang, F. Suzuki–Miyaura Catalyst-Transfer Polycondensation with Pd(IPr)(OAc)<sub>2</sub> as the Catalyst for the Controlled Synthesis of Polyfluorenes and Polythiophenes. *Polym. Chem.* **2014**, *5*, 7072–7080.
- (50) Zhao, Y.; Nett, A. J.; McNeil, A. J.; Zimmerman, P. M. Computational Mechanism for Initiation and Growth of Poly(3-Hexylthiophene) Using Palladium N-Heterocyclic Carbene Precatalysts. *Macromolecules* **2016**, *49*, 7632–7641.
- (51) Mikami, K.; Nojima, M.; Masumoto, Y.; Mizukoshi, Y.; Takita, R.; Yokozawa, T.; Uchiyama, M. Catalyst-Dependent Intrinsic Ring-Walking Behavior on  $\pi$ -Face of Conjugated Polymers. *Polym. Chem.* **2017**, *8*, 1708–1713.
- (52) Lanni, E. L.; McNeil, A. J. Mechanistic Studies on Ni(dppe)Cl<sub>2</sub>-Catalyzed Chain-Growth Polymerizations: Evidence for Rate-Determining Reductive Elimination. *J. Am. Chem. Soc.* **2009**, *131*, 16573–16579.
- (53) Tkachov, R.; Senkovskyy, V.; Komber, H.; Kiriya, A. Influence of Alkyl Substitution Pattern on Reactivity of Thiophene-Based Monomers in Kumada Catalyst-Transfer Polycondensation. *Macromolecules* **2011**, *44*, 2006–2015.
- (54) Verheyen, L.; Leysen, P.; Van Den Eede, M.-P.; Ceunen, W.; Hardeman, T.; Koeckelberghs, G. Advances in the Controlled Polymerization of Conjugated Polymers. *Polymer* **2017**, *108*, 521–546.
- (55) Lee, S. R.; Bloom, J. W. G.; Wheeler, S. E.; McNeil, A. J. Accelerating Ni(ii) Precatalyst



- Initiation Using Reactive Ligands and Its Impact on Chain-Growth Polymerizations. *Dalt. Trans.* **2013**, *42*, 4218–4222.
- (56) Marshall, N.; Sontag, S. K.; Locklin, J. Substituted Poly( P -Phenylene) Thin Films via Surface-Initiated Kumada-Type Catalyst Transfer Polycondensation. *Macromolecules* **2010**, *43*, 2137–2144.
- (57) Lanni, E. L.; McNeil, A. J. Evidence for Ligand-Dependent Mechanistic Changes in Nickel-Catalyzed Chain-Growth Polymerizations. *Macromolecules* **2010**, *43*, 8039–8044.
- (58) Tamao, K.; Sumitani, K.; Kiso, Y.; Zembayashi, M.; Fujioka, A.; Kodama, S.; Nakajima, I.; Minato, A.; Kumada, M. Nickel-Phosphine Complex-Catalyzed Grignard Coupling. I. Cross-Coupling of Alkyl, Aryl, and Alkenyl Grignard Reagents with Aryl and Alkenyl Halides: General Scope and Limitations. *Bull. Chem. Soc. Jpn.* **1976**, *49*, 1958–1969.
- (59) Nelson, D. J.; Nolan, S. P. Quantifying and Understanding the Electronic Properties of N-Heterocyclic Carbenes. *Chem. Soc. Rev.* **2013**, *42*, 6723–6753.
- (60) Díez-González, S.; Marion, N.; Nolan, S. P.; Díez-González, S.; Marion, N.; Nolan, S. P.; Díez-González, S.; Marion, N.; Nolan, S. P. N-Heterocyclic Carbenes in Late Transition Metal Catalysis. *Chem. Rev.* **2009**, *109*, 3612–3676.
- (61) Fortman, G. C.; Nolan, S. P. N-Heterocyclic Carbene (NHC) Ligands and Palladium in Homogeneous Cross-Coupling Catalysis: A Perfect Union. *Chem. Soc. Rev.* **2011**, *40*, 5151–5169.
- (62) Jacobsen, H.; Correa, A.; Poater, A.; Costabile, C.; Cavallo, L. Understanding the M(NHC) (NHC=N-Heterocyclic Carbene) Bond. *Coord. Chem. Rev.* **2009**, *253*, 687–703.
- (63) Shi, X.; Sui, A.; Wang, Y.; Li, Y. S.; Geng, Y.; Wang, F.; Shi, X.; Sui, A.; Wang, Y.; Li, Y. S.; *et al.* Controlled Synthesis of High Molecular Weight poly(3-Hexylthiophene)s via Kumada Catalyst Transfer Polycondensation with Ni(IPr)(acac) 2 as the Catalyst. *Chem. Commun.* **2015**, *51*, 2138–2140.
- (64) Tamba, S.; Shono, K.; Sugie, A.; Mori, A. C–H Functionalization Polycondensation of Chlorothiophenes in the Presence of Nickel Catalyst with Stoichiometric or Catalytically Generated Magnesium Amide. *J. Am. Chem. Soc.* **2011**, *133*, 9700–9703.
- (65) Fuji, K.; Tamba, S.; Shono, K.; Sugie, A.; Mori, A. Murahashi Coupling Polymerization: Nickel(II)–N-Heterocyclic Carbene Complex-Catalyzed Polycondensation of Organolithium Species of (Hetero)arenes. *J. Am. Chem. Soc.* **2013**, *135*, 12208–12211.
- (66) Hardeman, T.; De Becker, J.; Koeckelberghs, G. Influence of the Halogen and Organometallic Function in a KCTP (Co)polymerization. *J. Polym. Sci. Part A Polym. Chem.* **2016**, *54*, 3701–3706.
- (67) Li, H.; Johansson Seechurn, C. C. C.; Colacot, T. J. Development of Preformed Pd Catalysts for Cross-Coupling Reactions, Beyond the 2010 Nobel Prize. *ACS Catal.* **2012**, *2*, 1147–1164.
- (68) Valente, C.; Çalimsiz, S.; Hoi, K. H.; Mallik, D.; Sayah, M.; Organ, M. G. The Development of Bulky Palladium NHC Complexes for the Most-Challenging Cross-Coupling Reactions. *Angew. Chemie Int. Ed.* **2012**, *51*, 3314–3332.

- (69) Surry, D. S.; Buchwald, S. L. Dialkylbiaryl Phosphines in Pd-Catalyzed Amination: A User's Guide. *Chem. Sci.* **2011**, *2*, 27–50.
- (70) Yoshikai, N.; Matsuda, H.; Nakamura, E. Ligand Exchange as the First Irreversible Step in the Nickel-Catalyzed Cross-Coupling Reaction of Grignard Reagents. *J. Am. Chem. Soc.* **2008**, *130*, 15258–15259.
- (71) Bilbrey, J. A.; Bootsma, A. N.; Bartlett, M. A.; Locklin, J.; Wheeler, S. E.; Allen, W. D. Ring-Walking of Zerovalent Nickel on Aryl Halides. *J. Chem. Theory Comput.* **2017**, *13*, 1706–1711.
- (72) Khanduyeva, N.; Senkovskyy, V.; Beryozkina, T.; Bocharova, V.; Simon, F.; Nitschke, M.; Stamm, M.; Grötzschel, R.; Kiriy, A. Grafting of Poly(3-Hexylthiophene) from Poly(4-Bromostyrene) Films by Kumada Catalyst-Transfer Polycondensation: Revealing of the Composite Films Structure. *Macromolecules* **2008**, *41*, 7383–7389.
- (73) Senkovskyy, V.; Khanduyeva, N.; Komber, H.; Oertel, U.; Stamm, M.; Kuckling, D.; Kiriy, A. Conductive Polymer Brushes of Regioregular Head-to-Tail poly(3-Alkylthiophenes) via Catalyst-Transfer Surface-Initiated Polycondensation. *J. Am. Chem. Soc.* **2007**, *129*, 6626–6632.
- (74) Tkachov, R.; Senkovskyy, V.; Komber, H.; Sommer, J. U.; Kiriy, A. Random Catalyst Walking along Polymerized Poly(3-Hexylthiophene) Chains in Kumada Catalyst-Transfer Polycondensation. *J. Am. Chem. Soc.* **2010**, *132*, 7803–7810.
- (75) Kohn, P.; Huettner, S.; Komber, H.; Senkovskyy, V.; Tkachov, R.; Kiriy, A.; Friend, R. H.; Steiner, U.; Huck, W. T. S.; Sommer, J.-U. U.; *et al.* On the Role of Single Regiodefects and Polydispersity in Regioregular poly(3-Hexylthiophene): Defect Distribution, Synthesis of Defect-Free Chains, and a Simple Model for the Determination of Crystallinity. *J. Am. Chem. Soc.* **2012**, *134*, 4790–4805.
- (76) Nojima, M.; Ohta, Y.; Yokozawa, T. Structural Requirements for Palladium Catalyst Transfer on a Carbon–Carbon Double Bond. *J. Am. Chem. Soc.* **2015**, *137*, 5682–5685.
- (77) Kochemba, W. M.; Kilbey, S. M.; Pickel, D. L. End-Group Composition of poly(3-Hexylthiophene)s Prepared by in Situ Quenching of the Grignard Metathesis Polymerization: Influence of Additives and Reaction Conditions. *J. Polym. Sci. Part A Polym. Chem.* **2012**, *50*, 2762–2769.
- (78) Sontag, S. K.; Bilbrey, J. A.; Huddleston, N. E.; Sheppard, G. R.; Allen, W. D.; Locklin, J. II-Complexation in Nickel-Catalyzed Cross-Coupling Reactions. *J. Org. Chem.* **2014**, *79*, 1836–1841.
- (79) Khlaifia, D.; Ewels, C. P.; Massuyeau, F.; Chemek, M.; Faulques, E.; Duvail, J.-L. L.; Alimi, K.; Xiao, G.; Guo, Y.; Lin, Y.; *et al.* Unraveling the Real Structures of Solution-Based and Surface-Bound poly(3-Hexylthiophene) (P3HT) Oligomers: A Combined Theoretical and Experimental Study. *RSC Adv.* **2016**, *6*, 56174–56182.
- (80) Hardeman, T.; Koeckelberghs, G. Steering Poly(thiophene) Properties by Incorporation of Phenyl Groups. *Macromolecules* **2014**, *47*, 8618–8624.
- (81) Okada, T.; Ogata, T.; Ueda, M. Synthesis and Characterization of Regiocontrolled Poly(2,5-Di-*N*-Butoxy-1,4-Phenylene) by Oxovanadium-Catalyzed Oxidative Coupling

Polymerization. *Macromolecules* **1996**, 29, 7645–7650.

## Chapter 4

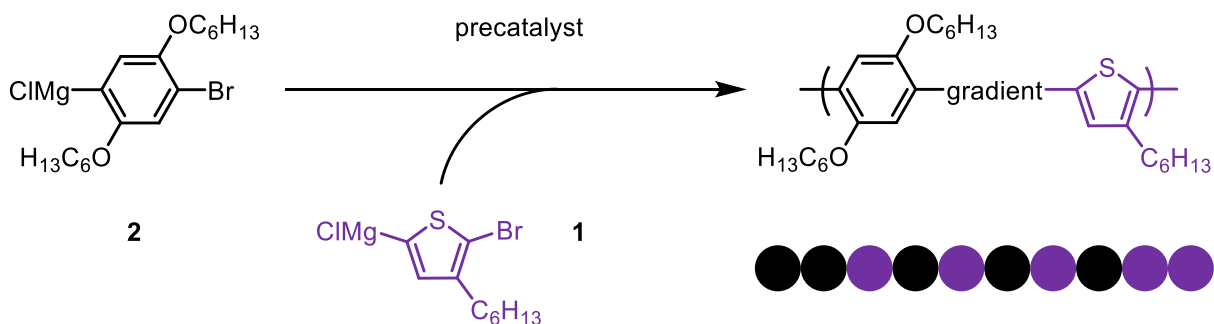
### Optimizing NHC-precatalysts for end-functionalized (co)polymers

#### Introduction

Conjugated polymers' unique combination of optical, conductive, and mechanical properties makes them attractive materials for light-emitting diodes,<sup>1</sup> field-effect transistors,<sup>2</sup> photovoltaic devices,<sup>3</sup> and sensors.<sup>4</sup> Dramatic improvements in performance have been realized through greater control over solid-state organization, but the optimized morphology of active layer blends can quickly deteriorate due to phase separation.<sup>5,6</sup> Several recent examples have highlighted the ability of conjugated copolymers to influence solid-state organization and reduce macro-phase separation.<sup>7-12</sup> Domain size of the homopolymer blends could be tuned in the hundreds of micrometers by adding 5–20 wt% poly(3-hexylthiophene-co-3-bromohexylthiophene). It was further revealed that gradient copolymers, where the copolymer composition changes gradually from monomer A to monomer B, yielded blends with the smallest domains (compared to block and random sequences).<sup>13</sup> Gradient copolymers are particularly proficient phase compatibilizers because they create a gradual interface between immiscible polymer blends.<sup>14</sup> However, there are no guiding principles for designing conjugated gradient copolymers due to the limited examples using chemically similar monomers.<sup>8,9,13,15,16</sup> The optimal gradient copolymer likely varies with each application, but a basic method to optimize copolymers would expedite screening the hundreds of possible gradient copolymers. Electronically and morphologically differentiated monomers would amplify subtle changes in bulk properties when changing sequence, composition,  $M_n$ , etc. of the copolymers—facilitating quantitative comparisons. Building an understanding of how  $\pi$ -conjugated gradient copolymers influence blend properties should guide their application in organic electronics.

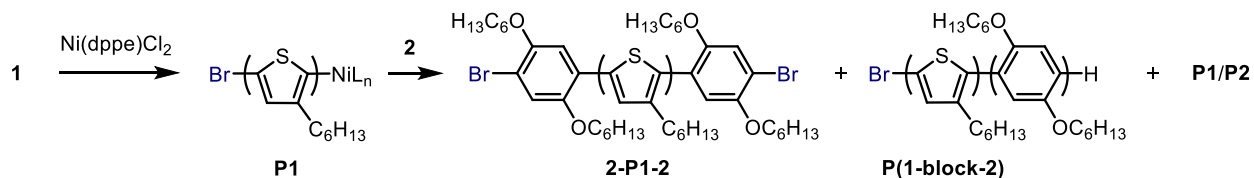
Gradient copolymers require a living, chain-growth polymerization, where one of the monomers is typically added over time (Scheme 4-1).<sup>8,13,15,16</sup> Gradient copolymers are rare because

the majority of conjugated polymers are synthesized by a step-growth mechanism that precludes sequence control. Catalyst-transfer condensation polymerization (CTCP) is a chain-growth method for synthesizing conjugated polymers, however, polymerizations are often independently optimized for precatalyst, monomer, and additives such that a universal set of conditions does not exist.



**Scheme 4-1.** Gradient sequence copolymer prepared via a semi-batch polymerization where **1** is added to a solution of **2** and precatalyst.

Copolymerizations can be challenging even when both monomers can be polymerized under similar conditions. In the simplest case, block copolymerizations require only one cross-propagation step where both repeat units are bound to catalyst at the same time. Catalyst-transfer from the first monomer to the second monomer enables block extension, but the order of monomer addition to generate the block copolymer can be critical.<sup>17–22</sup> Block copolymers from (5-bromo-4-hexylthiophen-2-yl)magnesium chloride (**1**) and 5-bromo-1,4-bis(hexyloxy)phenylmagnesium chloride (**2**) were successfully prepared using Ni(dppe)Cl<sub>2</sub> if **2** was polymerized first, and then **1** was added (dppe = 1,2-bis(diphenylphosphino)ethane). However, if the first block was **P1**, then adding **2** yielded a mixture of **P1**, **P2**, and **P(1-block-2)** (Scheme 4-2).<sup>21</sup> End-group analysis of the reaction mixture by MALDI-TOF MS revealed that many of the **P1** chains had two units of **2**.<sup>23</sup> This surprising result suggests that catalyst initially reacts with **2**, but the Ni-polymer  $\pi$ -complex sticks to **P1** after reductive elimination. The catalyst migrates across **P1** to react with **2** at the  $\alpha$  terminus, but again intramolecular transfer to **2** does not occur. The resultant polymer has reactive C-Br bonds at both ends, but preferential  $\pi$ -binding with the **P1** core (relative to **2**) prevents catalyst-transfer for block copolymerization.

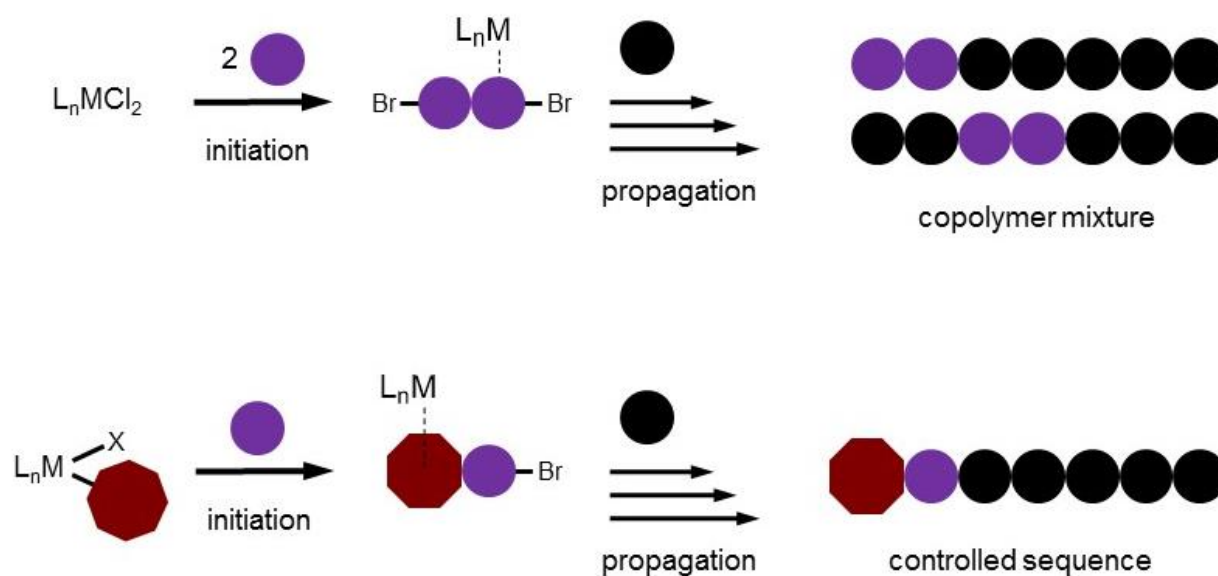


**Scheme 4-2.** Block copolymerizing **1** (**P1**  $M_n = 4.1$  kDa,  $\bar{D} = 1.33$ ) then **2** ( $M_n = 6.7$  kDa,  $\bar{D} = 1.44$ ) yields **P(1-block-2)** and **2-P1-2** as the major species.<sup>23</sup>

Efforts to overcome poor cross-propagation by changing the electronic character of the phosphine ligands have been unsuccessful. When polymerizing **2**, increasing the electron-donating ability of phosphine ligands improves molecular weight control by stabilizing the Ni-polymer  $\pi$ -complex and/or increasing the rate of oxidative addition.<sup>24,25</sup> Using precatalysts with more electron-rich ligands in block copolymerizations yielded no improvement in the dispersity of **P(1-block-2)**. Alternatively, precatalysts with more electron-poor ligands could decrease the magnitude of  $\pi$ -complex stabilization, reducing the thermodynamic preference for **1** over **2** and permitting catalyst-transfer between repeat units. However, precatalysts with more electron-poor ligands showed worse performance for both blocks as demonstrated by elevated dispersities.<sup>26</sup> Prompted by the inability to tailor Ni phosphine precatalysts to copolymerize **1** and **2**, we and others<sup>27–30</sup> investigated other types of precatalysts for CTCP.

The block copolymerization of **1** and **2** from either direction was reported in 2012 using  $\text{IPrPd}(\text{3-chloropyridine})\text{Cl}_2$  as the precatalyst ( $\text{IPr} = 1,3\text{-bis}(2,6\text{-di-}i\text{-propylphenyl})\text{imidazol-2-ylidene}$ ).<sup>31</sup> The single cross-propagation event where catalyst transfer from **P1** to **2** is promising, but other copolymer sequences (e.g., random or gradient) require many cross-propagation events. Batch copolymerizing **1** and **2** using precatalyst **3a** yield copolymers with moderate molecular weight and low dispersity, with **1** being consumed much more rapidly into the statistical copolymer than **2** (Appendix 3). The efficient cross-propagation of **1** and **2** is a significant breakthrough for CTCP catalyst reactivity, but it does not guarantee a route to sequence controlled copolymers. As discussed in Chapter 2 and Chapter 3, end-to-end catalyst migration can occur over more than 60 or 18 repeat units of **1** or **2**, respectively, enabling propagation from both polymer ends. Propagation from both ends would scramble the desired polymer sequence, and would be difficult to identify using NMR spectroscopy or physical properties. Therefore, we endeavored to

synthesize a precatalyst with the highly desirable reactivity of **3a** but cannot propagate from both polymer ends (Scheme 4-3). Detailed herein are our efforts to prepare a precatalyst that would transfer a reactive ligand to the polymer during initiation. The reactive ligand-terminated polymer can only propagate in a single direction—even if catalyst migration occurs, the polymer is only reactive at the  $\omega$  end. We evaluated precatalysts for living, chain-growth polymerization of **1** and **2** (separately), targeting a low dispersity. High dispersities—reflecting slow initiation, chain-transfer/dissociation, or termination—result in polymer growth at different feed compositions due to the constantly evolving reaction mixture. Therefore, dispersity provides a measure of both the molecular weight and compositional heterogeneity, which can both influence polymer properties.<sup>32–36</sup> End-group transfer was evaluated for precatalysts that fulfilled these initial criteria, and copolymerizations were performed to ensure cross-propagation of monomers **1** and **2**.

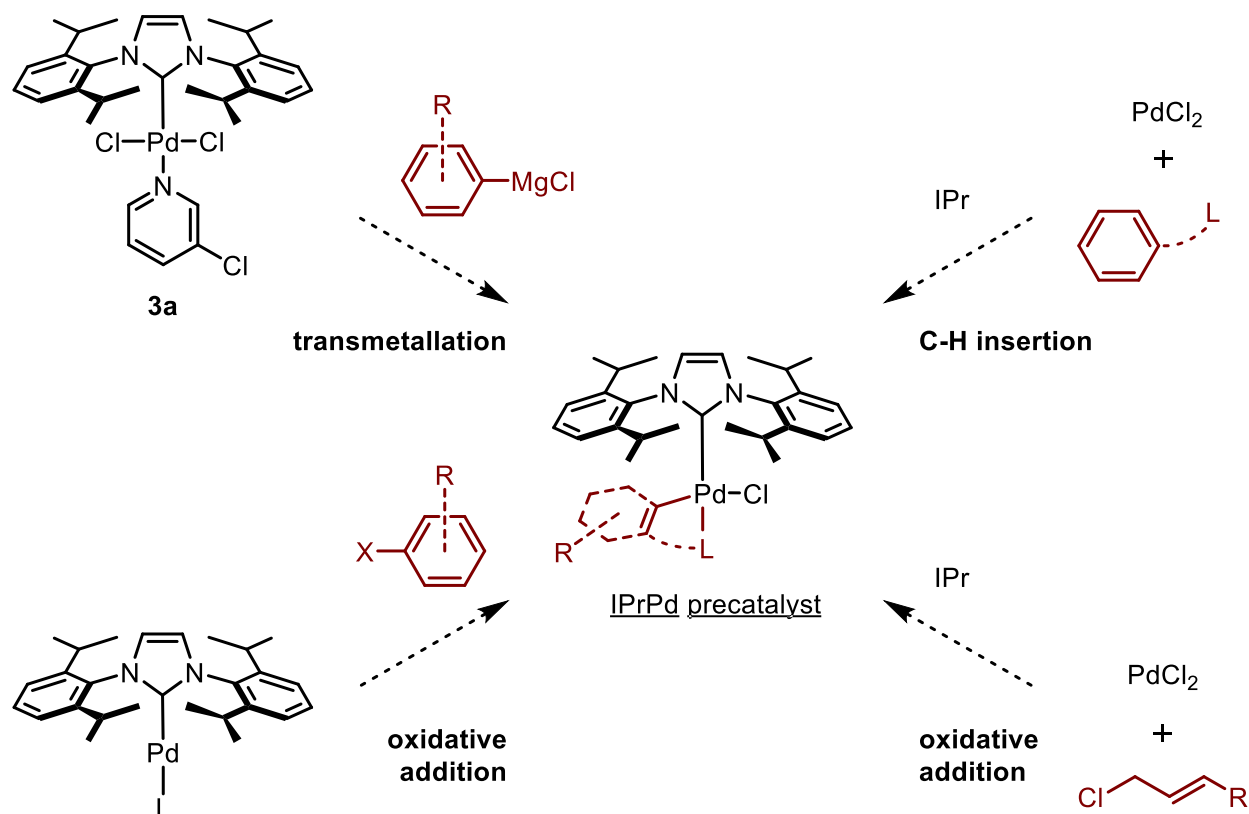


**Scheme 4-3.** General products from initiation and propagation using precatalysts. Dihalide precatalysts (top) generate a polymer that could propagate from both C-Br to yield ill-defined copolymers. Functionalized precatalysts (bottom) transfer a reactive ligand (●) to the polymer to prevent propagation from the  $\alpha$  end.

## Results and Discussion

Precatalysts were screened in multiple reactions on multiple days under multiple conditions (e.g., monomer concentration) unless noted, with some variability in the  $\bar{D}$  and monomer conversion. As such,  $M_n$  and  $\bar{D}$  for single experiments are presented. Precatalyst trends were

consistent between runs (each run evaluated several precatalysts/conditions against each other), and were used to select the most promising precatalysts prepared using four main routes (Scheme 4-4). Polymerizations using  $\text{IPrPd}(\text{3-chloropyridine})\text{Cl}_2$  were run as a control to benchmark precatalyst performance and identify issues unrelated to the precatalyst (e.g., monomer side-reactions).



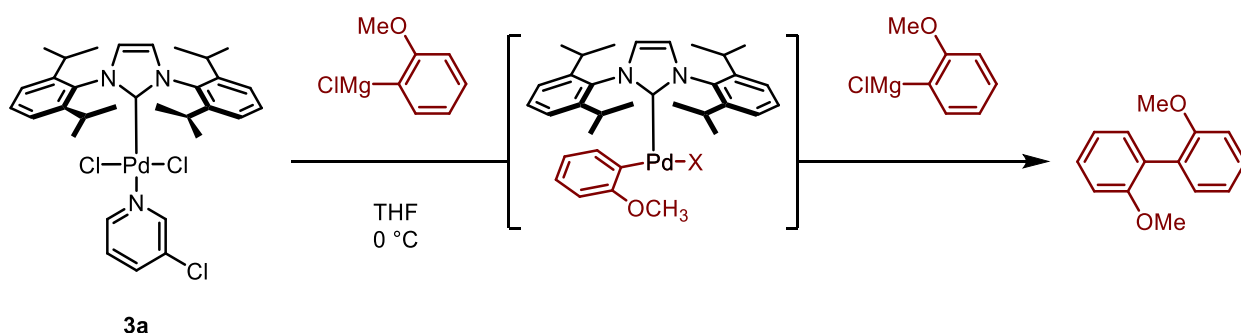
**Scheme 4-4.** General routes to an IPrPd precatalyst with a reactive ligand (red).

#### *Transmetallation from 3a*

Our initial attempt to prepare IPrPd-based precatalysts targeted transmetallation of **3a**, which would be straightforward to prepare from commercially available reagents. A related transmetallation route was used to generate Ni(aryl)X species for CTCP with monodentate<sup>37,38</sup> and bidentate phosphines.<sup>25,38</sup> Aryl reactive ligands were targeted because aryl-monomer reductive elimination exhibits faster reductive elimination rates (relative to alkyl).<sup>39-41</sup> Ortho-substituted aryl Grignard reagents should reduce the second transmetallation rate with  $\text{IPrPd}(\text{3-chloropyridine})(\text{aryl})\text{Cl}$ . Furthermore, ortho-substituted aryls can stabilize precatalysts via



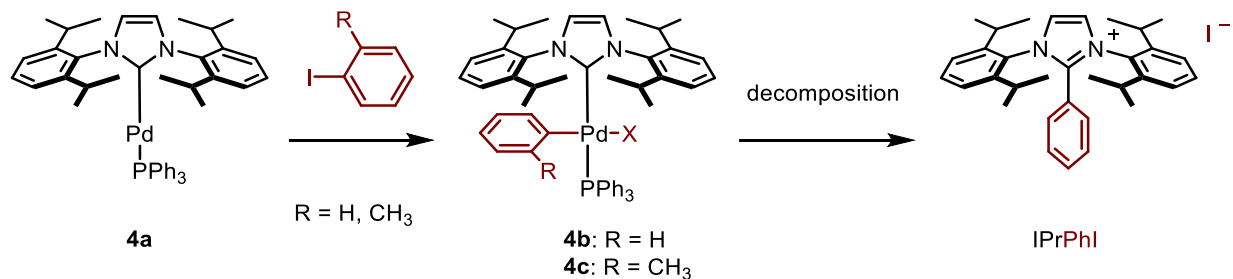
interaction with the  $d_z$  orbitals of the transition metal.<sup>42</sup> Unfortunately, we were unable to limit Grignard reactivity nor isolate a stable precatalyst. Reaction of **3a** with one equivalent of *o*-methoxyphenylmagnesium chloride generated several species by <sup>1</sup>H NMR spectroscopy, but none were stable to isolation (Scheme 4-5). Transmetalation occurred zero, one, or multiple times, as indicated by the large amount of recovered starting materials and bi-aryl coupling products. Cooling the reaction to -30 °C did not prevent multiple transmetalations, but no reaction was observed at -42 °C (Appendix 3).



**Scheme 4-5.** Transmetalating **3a** with 2-methoxyphenylmagnesium chloride to generate the bi-aryl coupling product observed by <sup>1</sup>H NMR spectroscopy.

#### *Oxidative addition from Pd<sup>0</sup>*

A second strategy to generate IPrPd(aryl)X is oxidative addition of an aryl halide into a Pd<sup>0</sup> precatalyst. We were inspired by a report where IPrPd(PPh<sub>3</sub>)(phenyl)Cl was prepared and isolated, although this complex was susceptible to decomposition in halogenated solvents.<sup>43</sup> However, we were unable to prepare IPrPd(PPh<sub>3</sub>)(phenyl)Cl via the reported ligand exchange procedure. We pursued an alternative strategy by preparing IPrPdPPh<sub>3</sub>, then generate the desired complex via oxidative addition of iodobenzene (Scheme 4-6).<sup>44</sup> An excess of aryl halide was used to accelerate this transformation before the precatalyst decomposes. Mixing IPrPdPPh<sub>3</sub> with iodobenzene yielded the reported decomposition product, IPrPhI, but we reasoned that increasing the steric bulk using *o*-iodotoluene could retard reductive elimination. We discovered that IPrPd(PPh<sub>3</sub>)(*o*-tolyl)I, **4c**, could be generated with minimal side-products by running the reaction in toluene, but polymerizing **1** with **4c** yielded only oligomers (Appendix 3). Due to the difficulty in purifying **4c** and poor performance, only one polymerization screen was performed.



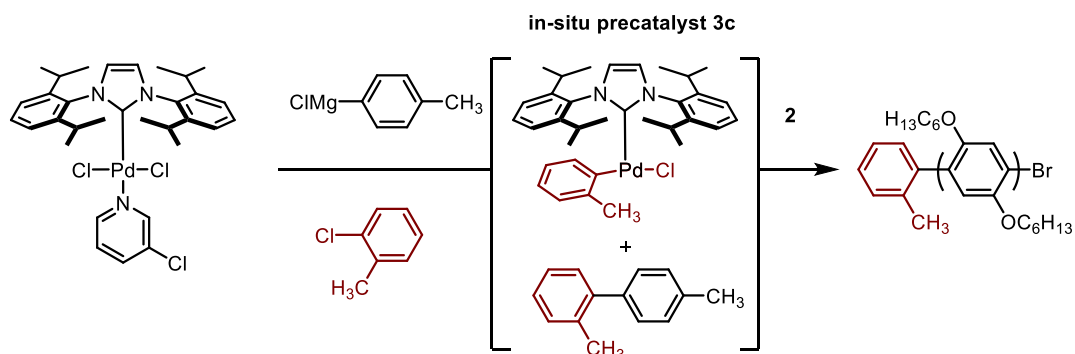
**Scheme 4-6.** Oxidative addition of iodobenzene or *o*-iodotoluene into **4a** to yield **4b/4c**. When R = H, the precatalyst decomposed to yield IPrPhI

### *In situ cross-coupling using 3a*

The difficulty in isolating an aryl-functionalized precatalyst that is highly active in polymerizations prompted us to prepare precatalysts in situ. Reaction stoichiometry for transmetalation was difficult to control precisely, and the mixture of recovered **3a** with coupling products suggests that achieving a single transmetalation for all precatalysts was unfeasible. It is possible that some of the desired precatalyst was generated in situ, but concentration and work-up conditions could facilitate disproportionation.

An alternative and simpler route is to generate the desired precatalyst in situ under cross-coupling conditions before adding monomer to initiate the polymerization. Adding *p*-tolylmagnesium chloride (4 equiv) and *o*-chlorotoluene (10 equiv) should initiate all precatalysts (1 equiv). The cross-coupling should proceed until all the Grignard is consumed then stall at the desired IPrPd(3-chloropyridine)(*o*-tolyl)Cl due to an excess of *o*-chlorotoluene (10 equiv). A similar strategy was used effectively for end-functionalized polymers produced by Suzuki CTCP.<sup>45,46</sup> Importantly, excess aryl halide in the polymerization solution does not affect polymer

molecular weight or dispersity (Appendix 1).<sup>31,47,48</sup> This in situ approach avoids stoichiometric and isolation issues discussed in previous sections.



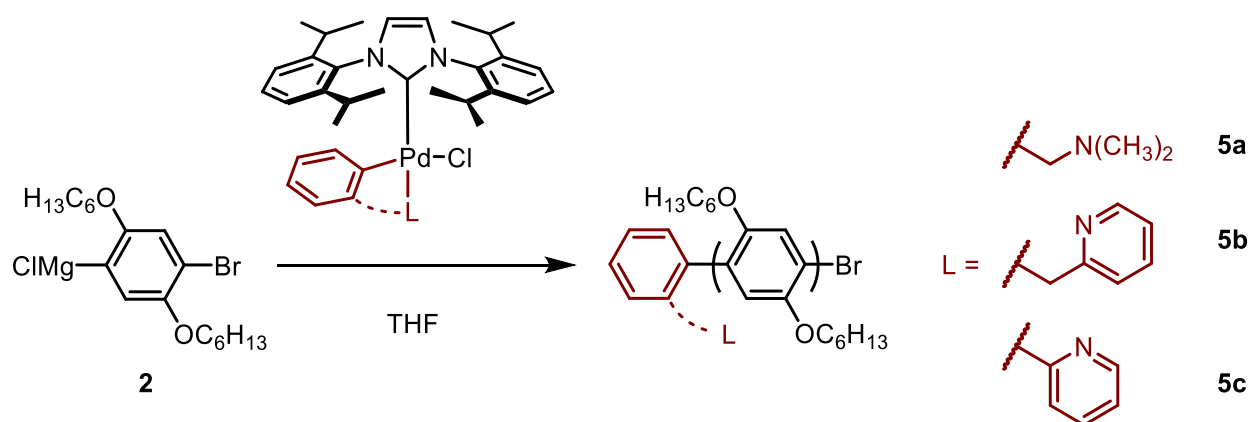
**Scheme 4-7.** Proposed in situ generation of **3c** from **3a** using *p*-tolylmagnesium chloride and *o*-chlorotoluene (biaryl cross-coupling products also shown). Adding **2** would initiate the polymerization, transferring the *o*-tolyl reactive ligand to the polymer

We tested this in situ cross-coupling approach using *p*-tolylmagnesium chloride and *o*-chlorotoluene. While aryl chlorides can be challenging substrates for traditional catalysts due to slower oxidative addition, numerous reports document successful cross-coupling of aryl chlorides using **3a** as the precatalyst.<sup>49–53</sup> Mixing 4 equiv of *p*-tolylmagnesium chloride and 10 equiv of *p*-chlorotoluene with **3a** for 1, 10, or 90 min, followed by adding **2** generated polymer with low dispersity (Appendix 3). However, there was no evidence for *o*-tolyl terminated **P2** by matrix-assisted laser desorption/ionization time-of-flight mass spectrometry (MALDI-TOF MS). The MALDI-TOF spectrum revealed that Br/H terminated **P2** was produced almost exclusively—suggesting a living polymerization but without reactive ligand transfer. Disproportionation or incomplete consumption of *p*-tolylmagnesium chloride could each explain the observed products.

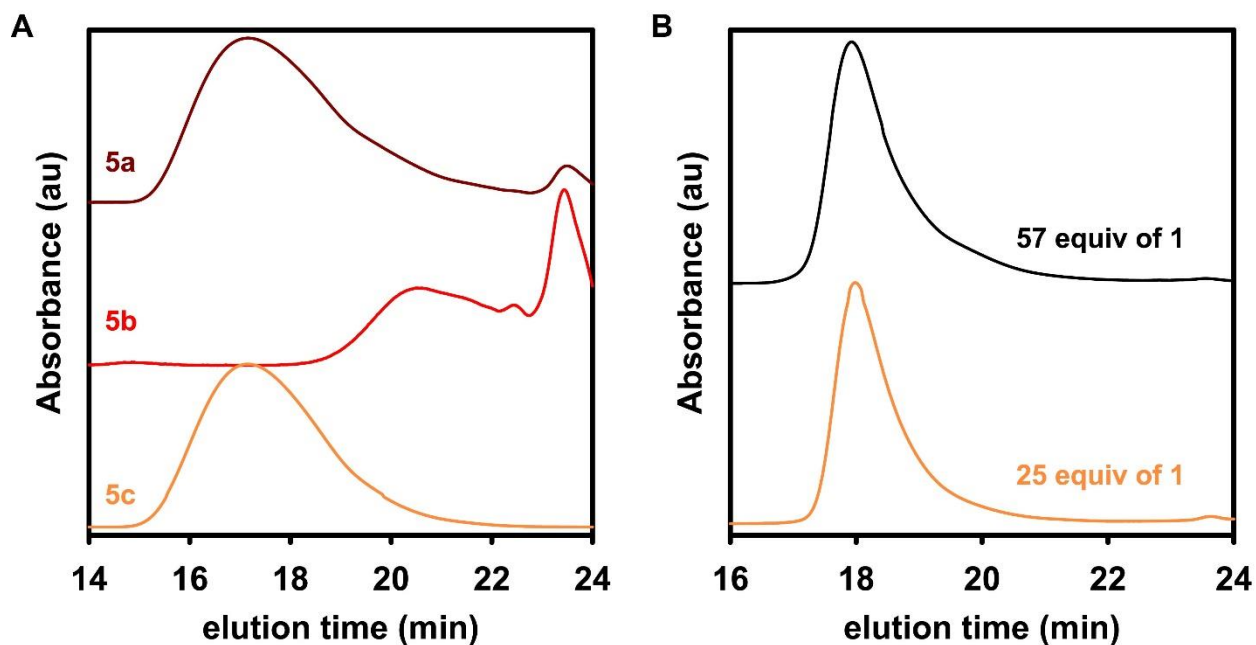
#### *Palladacycle precatalysts*

Stable, aryl-functionalized precatalysts can be prepared using a bidentate aryl ligand. Although examples of these complexes promoting Kumada cross-couplings are scarce, they have demonstrated high activity in Suzuki,<sup>54</sup> Negishi,<sup>55</sup> Heck,<sup>56</sup> and Buchwald-Hartwig<sup>55</sup> reactions. Initiating the precatalyst should append the reactive ligand onto one end of the growing polymer and restrict propagation to a single direction. Palladacycle precatalysts bearing an amine or pyridine L-type ligand were synthesized and evaluated for polymerizing **1** or **2**. Polymerizing **2** using precatalyst **5a** or **5c** resulted in polymers with a  $M_n$  that was ~8 times higher than predicted

by the  $[\text{monomer}]_0/[\text{precatalyst}]_0$  despite monomer conversion of only 30% or 66%, respectively (Scheme 4-8). The broad peak in the GPC chromatogram suggests that precatalyst was still initiating when the reaction was quenched after 1 h (Figure 4-1). Precatalyst that is initiated at early on would react for the longest amount of time to produce high molecular weight polymer, but consume only a small amount of monomer. Continuous initiation during the reaction activates catalysts that polymerize for decreasing amounts of time (and at lower monomer concentrations) to yield a broad molecular weight distribution. While termination reactions could have a similar effect, the high molecular weight achieved using **5a** and **5c** suggests that catalysts can incorporate hundreds of monomers into a single chain, which is inconsistent with prominent termination reactions at tens of repeat units.



**Scheme 4-8.** Polymerizing **2** with **5a–c**.

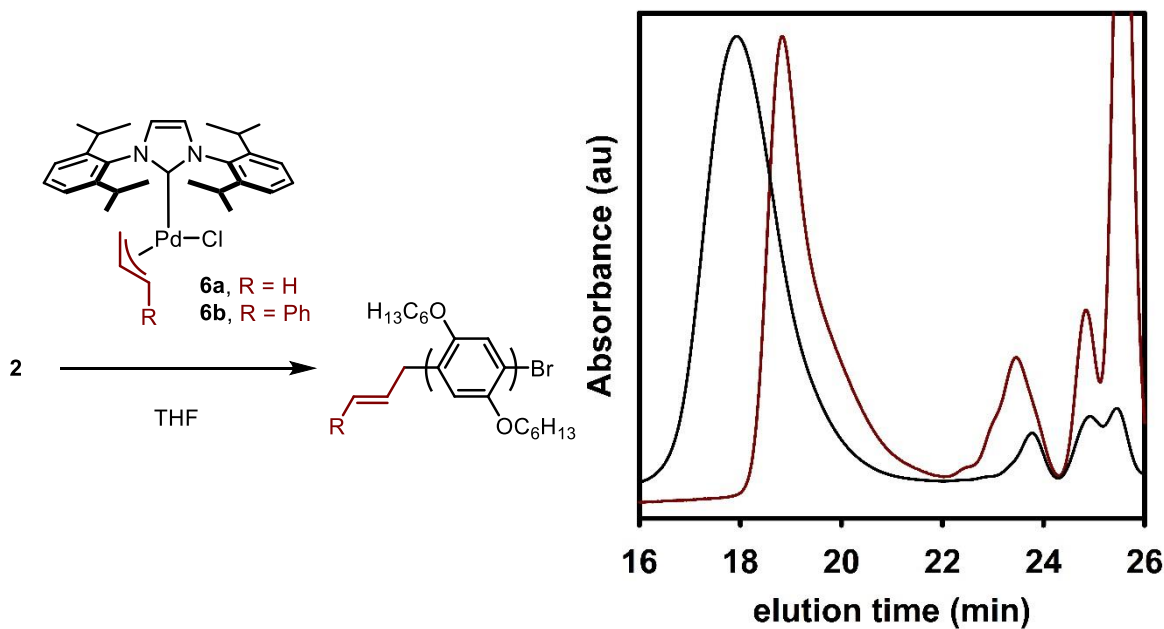


**Figure 4-1.** GPC chromatogram of (A) **P2** catalyzed by **5a** (—), **5b** (—), or **5c** (—) or (B) **P1** catalyzed by **5a** using 57 (—) or 25 (—) equiv of **1** relative to **5a**.

Switching to **1** could accelerate initiation by increasing the transmetallation rate (due to increased electron density) and/or reductive elimination rate (due to reduced steric congestion in the products), although the rate-determining step is not known. Polymerizing **1** using **5a** yielded  $M_n$  closer to the predicted values, and the dispersity was reduced to 1.73. However, the low molecular weight portion of the GPC chromatogram suggests that not all precatalysts were initiated at the beginning of the polymerization. Adding one equivalent of 3-chloropyridine further reduced the observed  $M_n$  and lowered the dispersity to 1.37. This result, which coincided with a slower consumption of **1**, suggests that 3-chloropyridine lowers dispersity by slowing propagation. The initiation rate could become more competitive with propagation, which would lead to a more narrow distribution of polymer lengths.<sup>57</sup> The slow initiation of the palladacycle precatalysts tested is especially problematic for gradient copolymerizations, where a second monomer is added to the reaction mixture while the first monomer is consumed. If this addition occurs prior to initiating all precatalysts, then the composition of the copolymers generated would vary widely. Therefore, the IPr palladacycle precatalysts **5a–c** are not suitable precatalysts for gradient copolymerizations of **1** and **2**.

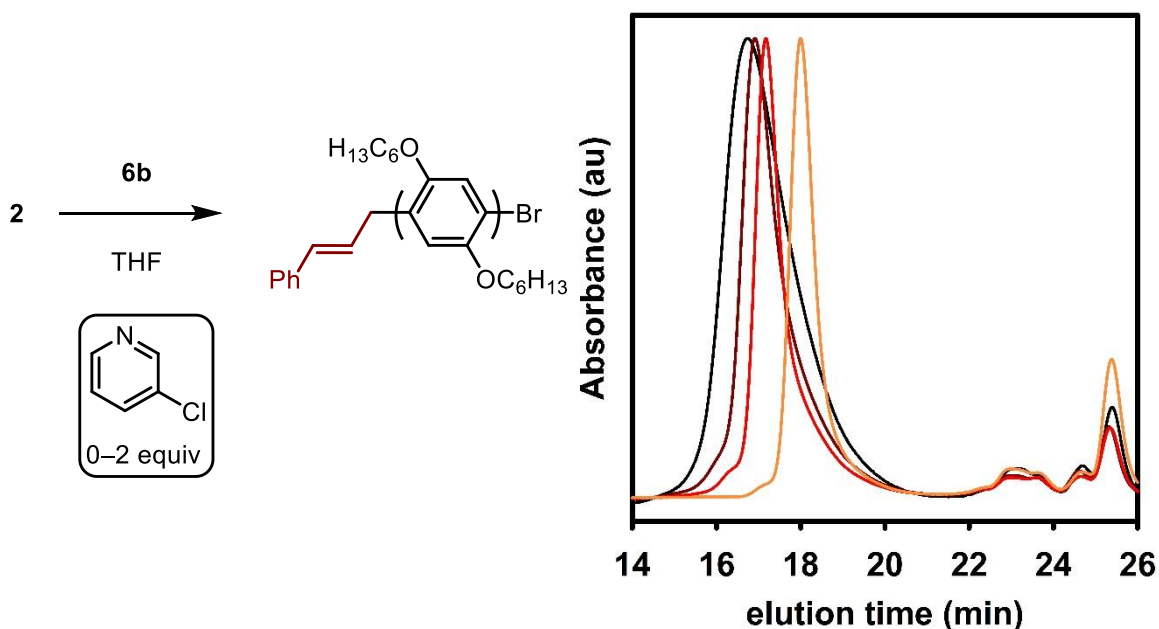
### Allyl reactive ligands

Allyl-functionalized precatalysts were also explored due to their use in a variety of cross-couplings, especially Buchwald-Hartwig and Suzuki methods.<sup>58-61</sup> Initiation studies have been carried out for IPrPd(allyl)Cl, **6a**, with KO<sup>t</sup>Bu in iPrOH, and for other Pd precatalysts in Tsuji-Trost allylations.<sup>59,62-64</sup> It was proposed that iPrOK, generated in situ, transmetalates with the precatalyst to generate IPrPd(allyl)(OiPr) which undergoes reductive elimination to yield allyl-OiPr (detected by GC-MS). We reasoned that transmetalation with monomer could yield a similar result, capping the  $\alpha$  chain-end with a vinyl substituent. Polymerizing **2** using **6a** gave higher yields and lower dispersities than any of the aforementioned precatalysts, although molecular weight control and dispersity were imperfect (Scheme 4-9). Again, we hypothesized that the elevated dispersity and poor molecular weight control (relative to **3a**) was due to slow precatalyst initiation. Substituted allyl derivatives have been shown to accelerate initiation and give higher yields in challenging cross-couplings.<sup>60,65</sup> Consistent with the hypothesis of slow initiation, switching to IPrPd(cinnamyl)Cl, **6b**, further improved molecular weight control and lowered dispersity (Scheme 4-9).



**Scheme 4-9.** GPC chromatogram and scheme of **P2** catalyzed by **6a** (—) or **6b** (—).

After initiation, the main difference between **3a** and **6b** is the 3-chloropyridine ligand. Commonly referred to as a “throw-away ligand”, recent reports suggest that it could play a vital role in initiation, catalyst stability, and participate in the catalytic cycle.<sup>66-69</sup> We systematically investigated the role of 3-chloropyridine in polymerizing **2** using **6b** as the precatalyst. Gratifyingly, increasing the equiv of 3-chloropyridine decreased dispersity, and the molecular weight at 1.0 equiv matched theoretical values given by the monomer to precatalyst ratio. However, 2 equiv of 3-chloropyridine retarded the polymerization, yielding polymers with lower molecular weight and lower conversion (Figure 4-2). We hypothesized that added 3-chloropyridine was reversibly binding to IPrPd(polymer) to form a less active or inactive intermediate.<sup>69</sup> This binding equilibrium to 3-chloropyridine would improve molecular weight control and dispersity by reducing propagation rates while precatalysts were still initiating. Adding 3-chloropyridine is not expected to affect initiation rates because the precatalyst does not have any accessible coordination sites. We determined that a slight excess of 3-chloropyridine (1.1 equiv relative to **6b**) provided a suitable balance between slowing propagation and achieving high polymer yields.

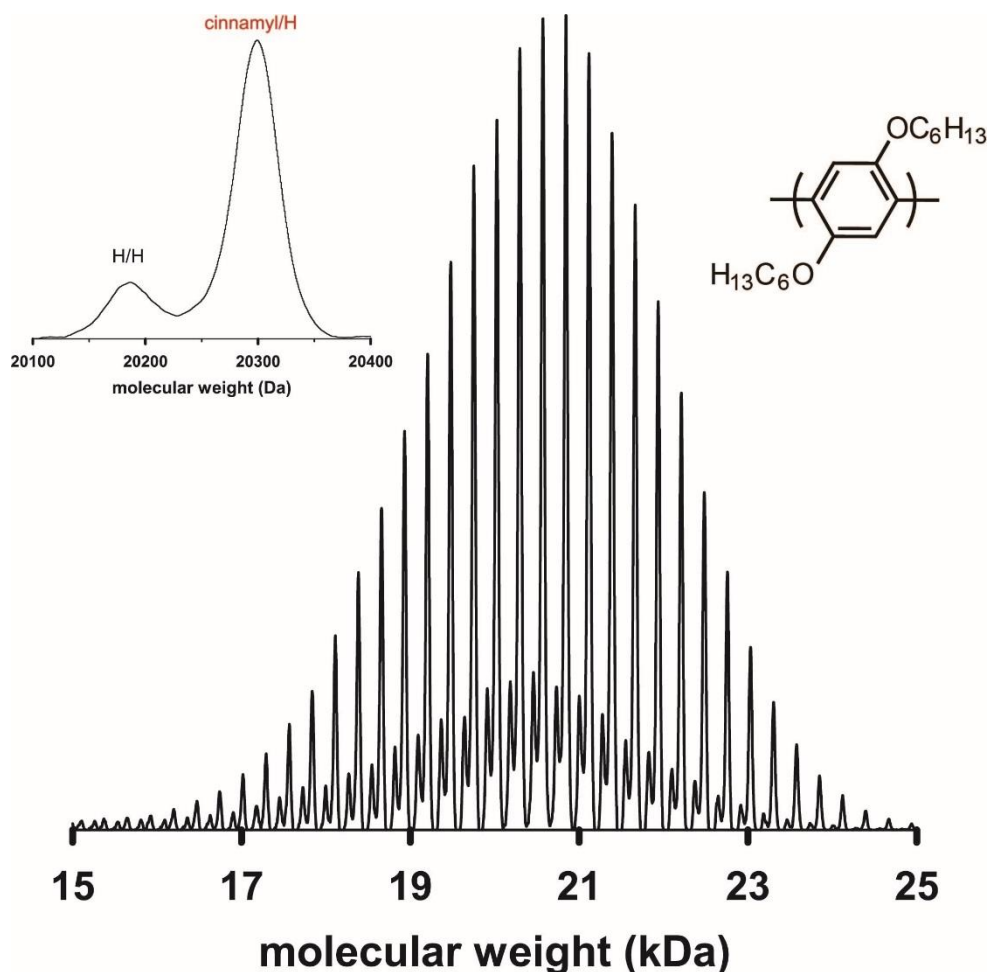


**Figure 4-2.** GPC chromatogram and scheme of **P2** produced by **6b** with 0 equiv (—), 0.5 equiv (—), 1 equiv (—), or 2 equiv (—) of 3-chloropyridine (relative to precatalyst).

With polymerization conditions optimized to yield **P2** with controlled molecular weight and low dispersities, we investigated initiation and cinnamyl transfer to the polymer. Model experiments identified that initiation should produce the linear reaction product,<sup>64,70</sup> with an <sup>1</sup>H chemical shift that was distinct from H/Br terminated **P2** (Appendix 3). End-group analysis by <sup>1</sup>H NMR spectroscopy verified that this peak was present in **P2** produced by **6b**, albeit in smaller ratios than expected based on the calculated molecular weight of the sample. The MALDI-TOF mass spectrum was consistent with this result—cinnamyl/H was the major peak series but H/H end-groups were also observed. Oxidative addition of IPrPd<sup>0</sup> into **2**, followed by a chain-growth polymerization could generate H/H end-groups.

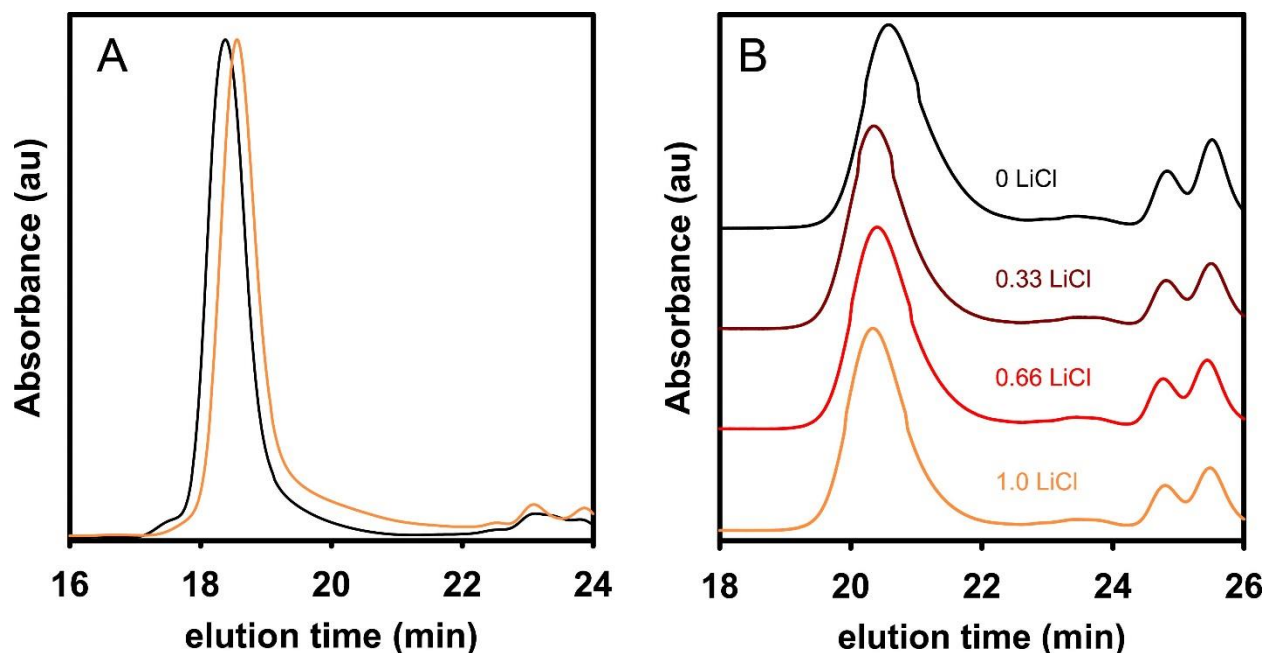
To investigate when end-group fidelity was lost, monomer **2** was polymerized at different [monomer]<sub>0</sub>/[precatalyst]<sub>0</sub> to target different molecular weights (and therefore different numbers of catalyst turnovers). The end-group fidelity of cinnamyl/H was compared as a function of chain-length to determine whether end-group ratios diminished during the polymerization. Cinnamyl/H end-groups were 81% at DP of 15, and were maintained above 80% through 90 repeat units. Clearly, the major loss of end-group control occurs early on and likely stems from initiation. Once initiated, the cinnamyl end-group is maintained over 90 catalyst turnovers.





**Figure 4-3.** MALDI-TOF mass spectrum of **P2** produced by **6b** with 1 equiv of 3-chloropyridine. Inset shows a zoomed in view at DP = 73 with cinnamyl/H (83% area ratio) and H/H (17 % area ratio) end-groups.

With a promising precatalyst identified, we adjusted the polymerization conditions to further improve molecular weight control and end-group transfer. Lithium chloride is a common additive to modify the aggregation state, selectivity, and reactivity of Grignard reagents.<sup>71,72</sup> Because precatalyst initiation begins with transmetalation, we investigated whether altering the reactivity of **2** would affect end-group transfer from the precatalyst. Oligomerizations were performed using **2** prepared with differing amounts of LiCl. Adding LiCl resulted in a slight increase in molecular weight and decrease in dispersity, but end-group transfer did not follow a similar trend (Figure 4-4). Slight improvements in cinnamyl group transfer were observed with 0.33 equiv of LiCl added (relative to *i*PrMgCl), but end-group transfer diminished when 1 equivalent was added. These results suggest that LiCl influences initiating **6b**, but the overall effect is small.



**Figure 4-4.** GPC chromatogram of **P2** produced by **6b** with (A) 65 equiv of **2** without LiCl (—) or with 1.0 equiv LiCl (—). (B) 18 equiv of **2** with 0 equiv LiCl (—), 0.33 equiv LiCl (—), 0.66 equiv LiCl (—), or 1.0 equiv LiCl (—). Equiv LiCl is relative to *i*PrMgCl used to generate **2**.

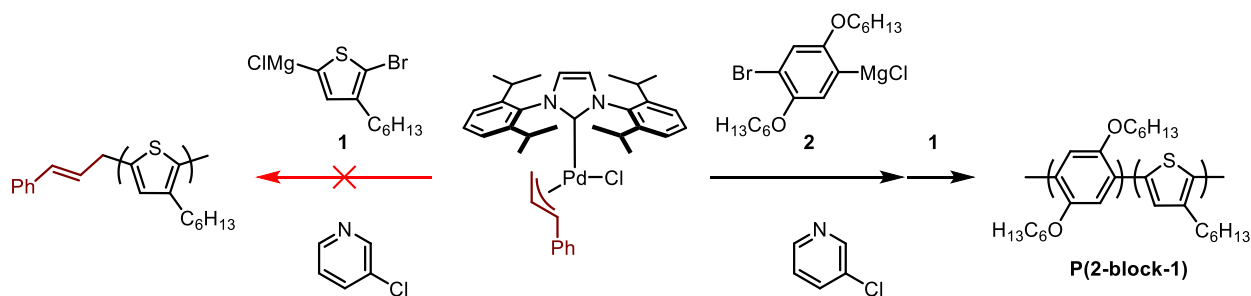
Equiv LiCl <sup>a</sup>	End-groups (%)	
	H/H	cinnamyl/H
0	17	77
0.33	15	77
0.66	14	81
1.0	16	67

**Table 4-1.** Percent end-groups of **P2** produced by **6b** as determined by MALDI-TOF MS.  $M_n$  and dispersity for **P2** ranged from 3.7–4.6 kDa and 1.16–1.17, respectively, and are plotted in Figure 4-4B. <sup>a</sup>Equiv LiCl is relative to *i*PrMgCl used to generate **2**.

### Copolymerizations using **6b**

Precatalyst screening was primarily optimized by polymerizing **2**, but the target is copolymerizing **1** and **2**. Initial copolymerizations using **3a**, which served as the basis for investigating IPrPd precatalysts, demonstrated that **1** is consumed more rapidly than **2** (Appendix 3). The reactivity difference results from **1** outcompeting **2** during transmetalation with the catalyst. Although the semi-batch methods to prepare copolymers are better suited for initiating with the less reactive monomer, the incomplete end-group transfer to **P2** during initiation prompted

us to investigate the initiation process with **1**. Mixing **1** with **6b** resulted in low conversion of **1** and almost no polymer formation. These results are especially surprising given reports of faster, more controlled polymerizations of **1** relative to **2** using Ni and Pd precatalysts.<sup>31,73,74</sup> To verify that **6b** could polymerize **1**, the block copolymerization of **2** then **1** was performed. After precatalyst was initiated using **2**, **P2** was successfully extended by adding **1** to yield **P(2-block-1)**. Block copolymer formation was confirmed by near-identical overlap of GPC traces at 254 nm (both **P1** and **P2** segments absorb) and at 427 nm (only **P1** absorbs, Appendix 3). These results indicate **6b** is not initiated efficiently using **1**, but propagation can occur if the precatalyst is pre-initiated (e.g., semi-batch copolymerization). Therefore, **2** must be used to initiate **6b**, so copolymerizations of **1** and **2** are expected to have the same end-group loss (~20%) as **P2**. The polymers without a cinnamyl group would be reactive at both termini, resulting in copolymer sequence scrambling due to catalyst migration. The large amount of potential impurity precludes copolymer sequence control of **1** and **2** using **6b**.



**Scheme 4-10.** Polymerizing **1** using **6b** and added 3-chloropyridine failed to yield the expected **P1**. Block copolymerization of **2** then **1** extended **P2** to yield **P(2-block-1)**, demonstrating that the propagation of **1** can occur.

## Conclusions

I<sub>Pr</sub>Pd-based precatalysts were explored for their unique ability to cross-propagate between monomers **1** and **2**. However, catalyst migration (Chapter 2 and Chapter 3) precludes access to sequence-controlled polymers from precatalyst **3a**. Precatalysts that could transfer a reactive ligand to the polymer to limit propagation to a single chain-end were screened for polymerizing **2**. Precatalysts generated via oxidative addition with aryl halides or transmetalation with aryl Grignards were unstable towards isolation, and generating them in situ did not result in end-group transfer to polymers. Therefore, we focused on alternative strategies to generate stable precatalysts by employing bidentate X,L-type ligands. The palladacycle complexes screened produced **P2** in

low yields with little molecular weight control and high dispersity. Switching to allyl-coordinated precatalysts improved all three criteria and were further optimized by changing the allyl to cinnamyl. Employing polymerization additives (3-chloropyridine and LiCl) lowered dispersity, but reactive ligand transfer to the polymer was only ~80% and was largely unaffected by the additives. Polymerization studies revealed that the major loss of cinnamyl terminated **P2** occurs early on, likely during precatalyst initiation. Surprising, **6b** is not initiated by **1**, but copolymerization can occur if **2** and **1** are present. In summary, none of the precatalysts fit our criterion to transfer a reactive ligand during initiation with targeted  $M_n$  and low dispersity. **6b** was identified as the most promising precatalyst, but end-group transfer was insufficient for obtaining sequence-specific copolymers. Other allyl derivatives or NHCs could be evaluated to increase end-group fidelity by directing intramolecular oxidative addition during initiation.

## References

- (1) Grimsdale, A. C.; Chan, K. L.; Martin, R. E.; Jokisz, P. G.; Holmes, A. B. Synthesis of Light-Emitting Conjugated Polymers for Applications in Electroluminescent Devices. *Chem. Rev.* **2009**, *109*, 897–1091.
- (2) Wang, C.; Dong, H.; Hu, W.; Liu, Y.; Zhu, D. Semiconducting  $\pi$ -Conjugated Systems in Field-Effect Transistors: A Material Odyssey of Organic Electronics. *Chem. Rev.* **2012**, *112*, 2208–2267.
- (3) Kularatne, R. S.; Magurudeniya, H. D.; Sista, P.; Biewer, M. C.; Stefan, M. C. Donor-Acceptor Semiconducting Polymers for Organic Solar Cells. *J. Polym. Sci. Part A Polym. Chem.* **2013**, *51*, 743–768.
- (4) Kim, H. N.; Guo, Z.; Zhu, W.; Yoon, J.; Tian, H. Recent Progress on Polymer-Based Fluorescent and Colorimetric Chemosensors. *Chem. Soc. Rev.* **2011**, *40*, 79–93.
- (5) Ro, H. W.; Akgun, B.; O'Connor, B. T.; Hammond, M.; Kline, R. J.; Snyder, C. R.; Satija, S. K.; Ayzner, A. L.; Toney, M. F.; Soles, C. L.; *et al.* Poly(3-Hexylthiophene) and [6,6]-Phenyl-C 61 -Butyric Acid Methyl Ester Mixing in Organic Solar Cells. *Macromolecules* **2012**, *45*, 6587–6599.
- (6) Zhao, J.; Swinnen, A.; Van Assche, G.; Manca, J.; Vanderzande, D.; Van Mele, B. Phase Diagram of P3HT/PCBM Blends and Its Implication for the Stability of Morphology. *J. Phys. Chem. B* **2009**, *113*, 1587–1591.
- (7) Gao, D.; Hollinger, J.; Seferos, D. S. Selenophene-Thiophene Block Copolymer Solar Cells with Thermostable Nanostructures. *ACS Nano* **2012**, *6*, 7114–7121.
- (8) Palermo, E. F.; Darling, S. B.; McNeil, A. J.  $\pi$ -Conjugated Gradient Copolymers Suppress Phase Separation and Improve Stability in Bulk Heterojunction Solar Cells. *J. Mater. Chem. C* **2014**, *2*, 3401–3406.
- (9) Amonoo, J. a.; Li, A.; Purdum, G. E.; Sykes, M. E.; Huang, B.; Palermo, E. F.; McNeil, A. J.; Shtein, M.; Loo, Y.-L.; Green, P. F. An All-Conjugated Gradient Copolymer Approach for Morphological Control of Polymer Solar Cells. *J. Mater. Chem. A* **2015**, *3*, 20174–20184.
- (10) Mulherin, R. C.; Jung, S.; Huettner, S.; Johnson, K.; Kohn, P.; Sommer, M.; Allard, S.; Scherf, U.; Greenham, N. C. Ternary Photovoltaic Blends Incorporating an All-Conjugated Donor-Acceptor Diblock Copolymer. *Nano Lett.* **2011**, *11*, 4846–4851.
- (11) Lombeck, F.; Sepe, A.; Thomann, R.; Friend, R. H.; Sommer, M. Compatibilization of All-Conjugated Polymer Blends for Organic Photovoltaics. *ACS Nano* **2016**, *10*, 8087–8096.
- (12) Nakabayashi, K.; Mori, H. All-Polymer Solar Cells Based on Fully Conjugated Block Copolymers Composed of Poly(3-Hexylthiophene) and Poly(naphthalene Bisimide) Segments. *Macromolecules* **2012**, *45*, 9618–9625.
- (13) Palermo, E. F.; van der Laan, H. L.; McNeil, A. J. Impact of  $\pi$ -Conjugated Gradient Sequence Copolymers on Polymer Blend Morphology. *Polym. Chem.* **2013**, *4*, 4606–4611.
- (14) Kim, J.; Gray, M. K.; Zhou, H.; Nguyen, S. T.; Torkelson, J. M. Polymer Blend

- Compatibilization by Gradient Copolymer Addition during Melt Processing: Stabilization of Dispersed Phase to Static Coarsening. *Macromolecules* **2005**, *38*, 1037–1040.
- (15) Locke, J. R.; McNeil, A. J. Syntheses of Gradient  $\pi$ -Conjugated Copolymers of Thiophene. *Macromolecules* **2010**, *43*, 8709–8710.
- (16) Palermo, E. F.; McNeil, A. J. Impact of Copolymer Sequence on Solid-State Properties for Random, Gradient and Block Copolymers Containing Thiophene and Selenophene. *Macromolecules* **2012**, *45*, 5948–5955.
- (17) Javier, A. E.; Varshney, S. R.; McCullough, R. D. Chain-Growth Synthesis of Polyfluorenes with Low Polydispersities, Block Copolymers of Fluorene, and End-Capped Polyfluorenes: Toward New Optoelectronic Materials. *Macromolecules* **2010**, *43*, 3233–3237.
- (18) Yokoyama, A.; Kato, A.; Miyakoshi, R.; Yokozawa, T. Precision Synthesis of Poly(N-Hexylpyrrole) and Its Diblock Copolymer with Poly(p-Phenylene) via Catalyst-Transfer Polycondensation. *Macromolecules* **2008**, *41*, 7271–7273.
- (19) Lanni, E. L.; Locke, J. R.; Gleave, C. M.; McNeil, A. J. Ligand-Based Steric Effects in Ni-Catalyzed Chain-Growth Polymerizations Using Bis(dialkylphosphino)ethanes. *Macromolecules* **2011**, *44*, 5136–5145.
- (20) Willot, P.; Govaerts, S.; Koeckelberghs, G. The Controlled Polymerization of Poly(cyclopentadithiophene)s and Their All-Conjugated Block Copolymers. *Macromolecules* **2013**, *46*, 8888–8895.
- (21) Miyakoshi, R.; Yokoyama, A.; Yokozawa, T. Importance of the Order of Successive Catalyst-Transfer Condensation Polymerization in the Synthesis of Block Copolymers of Polythiophene and Poly(p-Phenylene). *Chem. Lett.* **2008**, *37*, 1022–1023.
- (22) Ohshimizu, K.; Takahashi, A.; Higashihara, T.; Ueda, M. Synthesis of Poly(m-Phenylene) and Poly(m-Phenylene)-Block- poly(3-Hexylthiophene) with Low Polydispersities. *J. Polym. Sci. Part A Polym. Chem.* **2011**, *49*, 2709–2714.
- (23) Wu, S.; Bu, L.; Huang, L.; Yu, X.; Han, Y.; Geng, Y.; Wang, F. Synthesis and Characterization of Phenylene-Thiophene All-Conjugated Diblock Copolymers. *Polymer* **2009**, *50*, 6245–6251.
- (24) Lee, S. R.; Bryan, Z. J.; Wagner, A. M.; McNeil, A. J. Effect of Ligand Electronic Properties on Precatalyst Initiation and Propagation in Ni-Catalyzed Cross-Coupling Polymerizations. *Chem. Sci.* **2012**, *3*, 1562–1566.
- (25) Bryan, Z. J.; McNeil, A. J. Evidence for a Preferential Intramolecular Oxidative Addition in Ni-Catalyzed Cross-Coupling Reactions and Their Impact on Chain-Growth Polymerizations. *Chem. Sci.* **2013**, *4*, 1620–1624.
- (26) Locke, J. R.  $\pi$ -Conjugated Copolymers of Controlled Sequence, University of Michigan, 2012.
- (27) Bridges, C. R.; Yan, H.; Pollit, A. A.; Seferos, D. S. Controlled Synthesis of Fully  $\pi$ -Conjugated Donor–Acceptor Block Copolymers Using a Ni(II) Diimine Catalyst. *ACS Macro Lett.* **2014**, *3*, 671–674.
- (28) Yokozawa, T.; Suzuki, R.; Nojima, M.; Ohta, Y.; Yokoyama, A. Precision Synthesis of

- poly(3-Hexylthiophene) from Catalyst-Transfer Suzuki-Miyaura Coupling Polymerization. *Macromol. Rapid Commun.* **2011**, *32*, 801–806.
- (29) Fujita, K.; Sumino, Y.; Ide, K.; Tamba, S.; Shono, K.; Shen, J.; Nishino, T.; Mori, A.; Yasuda, T. Synthesis of Poly(3-Substituted Thiophene)s of Remarkably High Solubility in Hydrocarbon via Nickel-Catalyzed Deprotonative Cross-Coupling Polycondensation. *Macromolecules* **2016**, *49*, 1259–1269.
- (30) Elmalem, E.; Kiriya, A.; Huck, W. T. S. Chain-Growth Suzuki – Miyaura Condensation Polymerization of Fluorene Co-Polymers. *Macromolecules* **2011**, *44*, 9057–9061.
- (31) Bryan, Z. J.; Smith, M. L.; McNeil, A. J. Chain-Growth Polymerization of Aryl Grignards Initiated by a Stabilized NHC-Pd Precatalyst. *Macromol. Rapid Commun.* **2012**, *33*, 842–847.
- (32) Sanchez, I. C. Irreversible Anionic Polymerization Kinetics Revisited. *Ind. Eng. Chem. Res.* **2010**, *49*, 11890–11895.
- (33) Ganesan, V.; Kumar, N. A.; Pryamitsyn, V. Blockiness and Sequence Polydispersity Effects on the Phase Behavior and Interfacial Properties of Gradient Copolymers. *Macromolecules* **2012**, *45*, 6281–6297.
- (34) Atanase, L. I.; Bistac, S.; Riess, G. Effect of Poly(vinyl Alcohol-Co-Vinyl Acetate) Copolymer Blockiness on the Dynamic Interfacial Tension and Dilational Viscoelasticity of Polymer–anionic Surfactant Complex at the water–1-Chlorobutane Interface. *Soft Matter* **2015**, *11*, 2665–2672.
- (35) Jiang, R.; Wang, Z.; Yin, Y.; Li, B.; Shi, A.-C. Effects of Compositional Polydispersity on Gradient Copolymer Melts. *J. Chem. Phys.* **2013**, *138*, 74906.
- (36) Elsen, A. M.; Li, Y.; Li, Q.; Sheiko, S. S.; Matyjaszewski, K. Exploring Quality in Gradient Copolymers. *Macromol. Rapid Commun.* **2014**, *35*, 133–140.
- (37) Doubina, N.; Ho, A.; Jen, A. K.-Y. Y.; Luscombe, C. K. Effect of Initiators on the Kumada Catalyst-Transfer Polycondensation Reaction. *Macromolecules* **2009**, *42*, 7670–7677.
- (38) Standley, E. A.; Smith, S. J.; Müller, P.; Jamison, T. F. A Broadly Applicable Strategy for Entry into Homogeneous Nickel(0) Catalysts from Air-Stable Nickel(II) Complexes. *Organometallics* **2014**, *33*, 2012–2018.
- (39) Hartwig, J. F. Electronic Effects on Reductive Elimination To Form Carbon–Carbon and Carbon–Heteroatom Bonds from Palladium(II) Complexes. *Inorg. Chem.* **2007**, *46*, 1936–1947.
- (40) Low, J. J.; Goddard, W. A. Theoretical Studies of Oxidative Addition and Reductive Elimination. 3. Carbon-Hydrogen and Carbon-Carbon Reductive Coupling from Palladium and Platinum Bis(phosphine) Complexes. *J. Am. Chem. Soc.* **1986**, *108*, 6115–6128.
- (41) García-Melchor, M.; Braga, A. A. C.; Lledós, A.; Ujaque, G.; Maseras, F. Computational Perspective on Pd-Catalyzed C–C Cross-Coupling Reaction Mechanisms. *Acc. Chem. Res.* **2013**, *46*, 2626–2634.
- (42) Doubina, N.; Paniagua, S. a.; Soldatova, A. V.; Jen, A. K. Y.; Marder, S. R.; Luscombe, C. K. Steric Effects of the Initiator Substituent Position on the Externally Initiated

- Polymerization of 2-Bromo-5-Iodo-3-Hexylthiophene. *Macromolecules* **2011**, *44*, 512–520.
- (43) Marshall, W. J.; Grushin, V. V. Synthesis, Structure, and Reductive Elimination Reactions of the First ( $\sigma$ -Aryl)palladium Complex Stabilized by IPr N-Heterocyclic Carbene †. *Organometallics* **2003**, *22*, 1591–1593.
- (44) Lee, J.-H. H.; Jeon, H. T.; Kim, Y. J.; Lee, K.-E. E.; Ok Jang, Y.; Lee, S. W. Facile Oxidative Addition of Organic Halides to Heteroleptic and Homoleptic Pd<sup>0</sup>-N-Heterocyclic Carbene Complexes. *Eur. J. Inorg. Chem.* **2011**, *2011*, 1750–1761.
- (45) Zhang, H.; Xing, C.; Tsemo, G. B.; Hu, Q. T -Bu<sub>3</sub>P-Coordinated 2-Phenylaniline-Based Palladacycle Complex as a Precatalyst for the Suzuki Cross-Coupling Polymerization of Aryl Dibromides with Aryldiboronic Acids. *ACS Macro Lett.* **2013**, *9*, 10–13.
- (46) Zhang, H.-H.; Peng, W.; Dong, J.; Hu, Q.-S. T -Bu<sub>3</sub>P-Coordinated 2-Phenylaniline-Based Palladacycle Complex/ArBr as Robust Initiators for Controlled Pd(0)/ T -Bu<sub>3</sub>P-Catalyzed Suzuki Cross-Coupling Polymerization of AB-Type Monomers. *ACS Macro Lett.* **2016**, *5*, 656–660.
- (47) Yokoyama, A.; Suzuki, H.; Kubota, Y.; Ohuchi, K.; Higashimura, H.; Yokozawa, T. Chain-Growth Polymerization for the Synthesis of Polyfluorene via Suzuki–Miyaura Coupling Reaction from an Externally Added Initiator Unit. *J. Am. Chem. Soc.* **2007**, *129*, 7236–7237.
- (48) Beryozkina, T.; Senkovskyy, V.; Kaul, E.; Kiriya, A. Kumada Catalyst-Transfer Polycondensation of Thiophene-Based Oligomers: Robustness of a Chain-Growth Mechanism. *Macromolecules* **2008**, *41*, 7817–7823.
- (49) Valente, C.; Çalimsiz, S.; Hoi, K. H.; Mallik, D.; Sayah, M.; Organ, M. G. The Development of Bulky Palladium NHC Complexes for the Most-Challenging Cross-Coupling Reactions. *Angew. Chemie Int. Ed.* **2012**, *51*, 3314–3332.
- (50) Lee, D.-H. H.; Jin, M.-J. J. An Extremely Active and General Catalyst for Suzuki Coupling Reaction of Unreactive Aryl Chlorides. *Org. Lett.* **2011**, *13*, 252–255.
- (51) Gooßen, L. J.; Paetzold, J.; Briel, O.; Rivas-Nass, a.; Karch, R.; Kayser, B. Buchwald-Hartwig Aminations of Aryl Chlorides: A Practical Protocol Based on Commercially Available Pd(0)-NHC Catalysts. *Synlett* **2005**, 275–278.
- (52) Heravi, M. M.; Hajiabbasi, P. Recent Advances in Kumada-Tamao-Corriu Cross-Coupling Reaction Catalyzed by Different Ligands. *Monatshefte für Chemie - Chem. Mon.* **2012**, *143*, 1575–1592.
- (53) Organ, M. G.; Chass, G. A.; Fang, D.-C. C.; Hopkinson, A. C.; Valente, C. Pd-NHC (PEPPSI) Complexes: Synthetic Utility and Computational Studies into Their Reactivity. *Synthesis* **2008**, *21*, 2776–2797.
- (54) Peh, G.-R.; Kantchev, E. A. B.; Er, J.-C.; Ying, J. Y. Rational Exploration of N-Heterocyclic Carbene (NHC) Palladacycle Diversity: A Highly Active and Versatile Precatalyst for Suzuki-Miyaura Coupling Reactions of Deactivated Aryl and Alkyl Substrates. *Chemistry* **2010**, *16*, 4010–4017.
- (55) Kantchev, E. A. B.; O'Brien, C. J.; Organ, M. G. Palladium Complexes of N-Heterocyclic



Carbenes as Catalysts for Cross-Coupling Reactions--a Synthetic Chemist's Perspective. *Angew. Chem., Int. Ed.* **2007**, *46*, 2768–2813.

- (56) Peh, G.-R.; Kantchev, E. A. B.; Zhang, C.; Ying, J. Y. N-Heterocycle Carbene (NHC)-Ligated Cyclopalladated N,N-Dimethylbenzylamine: A Highly Active, Practical and Versatile Catalyst for the Heck-Mizoroki Reaction. *Org. Biomol. Chem.* **2009**, *7*, 2110–2119.
- (57) Odian, G. Principles of Polymerization. In *Principles of Polymerization*; John Wiley & Sons, Inc.: Hoboken, NJ, USA, 2004; pp. 372–463.
- (58) Viciu, M. S.; Germaneau, R. F.; Nolan, S. P. Well-Defined, Air-Stable (NHC)Pd(Allyl)Cl (NHC = N-Heterocyclic Carbene) Catalysts for the Arylation of Ketones. *Org. Lett.* **2002**, *4*, 4053–4056.
- (59) Viciu, M. S.; Navarro, O.; Germaneau, R. F.; Kelly, R. A.; Sommer, W.; Marion, N.; Stevens, E. D.; Cavallo, L.; Nolan, S. P. Synthetic and Structural Studies of (NHC)Pd(allyl)Cl Complexes (NHC = N-Heterocyclic Carbene). *Organometallics* **2004**, *23*, 1629–1635.
- (60) Marion, N.; Navarro, O.; Mei, J.; Stevens, E. D.; Scott, N. M.; Nolan, S. P. Modified (NHC)Pd(allyl)Cl (NHC = N-Heterocyclic Carbene) Complexes for Room-Temperature Suzuki-Miyaura and Buchwald-Hartwig Reactions. *J. Am. Chem. Soc.* **2006**, *128*, 4101–4111.
- (61) Chartoire, A.; Lesieur, M.; Falivene, L.; Slawin, A. M. Z.; Cavallo, L.; Cazin, C. S. J.; Nolan, S. P. [Pd(IPr\*)(cinnamyl)Cl]: An Efficient Pre-Catalyst for the Preparation of Tetra-Ortho-Substituted Biaryls by Suzuki-Miyaura Cross-Coupling. *Chemistry* **2012**, *18*, 4517–4521.
- (62) Viciu, M. S.; Kelly, R. A.; Stevens, E. D.; Naud, F.; Studer, M.; Nolan, S. P. Synthesis, Characterization, and Catalytic Activity of N-Heterocyclic Carbene (NHC) Palladacycle Complexes. *Org. Lett.* **2003**, *5*, 1479–1482.
- (63) Viciu, M. S.; Germaneau, R. F.; Navarro-Fernandez, O.; Stevens, E. D.; Nolan, S. P. Activation and Reactivity of (NHC)Pd(allyl)Cl (NHC = N-Heterocyclic Carbene) Complexes in Cross-Coupling Reactions. *Organometallics* **2002**, *21*, 5470–5472.
- (64) Poli, G.; Prestat, G.; Kammerer-pentier, C. *Transition Metal Catalyzed Enantioselective Allylic Substitution in Organic Synthesis*; Kazmaier, U., Ed.; Topics in Organometallic Chemistry; Springer Berlin Heidelberg: Berlin, Heidelberg, 2012; Vol. 38.
- (65) Hruszkewycz, D. P.; Balcells, D.; Guard, L. M.; Hazari, N.; Tilset, M. Insight into the Efficiency of Cinnamyl-Supported Precatalysts for the Suzuki-Miyaura Reaction: Observation of Pd(I) Dimers with Bridging Allyl Ligands during Catalysis. *J. Am. Chem. Soc.* **2014**, *136*, 7300–7316.
- (66) Chen, M.; Vicic, D. A.; Turner, M. L.; Navarro, O. (N-Heterocyclic Carbene)PdCl<sub>2</sub> (TEA) Complexes: Studies on the Effect of the “Throw-Away” Ligand in Catalytic Activity. *Organometallics* **2011**, *30*, 5052–5056.
- (67) Guest, D.; Chen, M. T.; Tizzard, G. J.; Coles, S. J.; Turner, M. L.; Navarro, O. “Throwing Away” a Different Ancillary Ligand To Enhance the Catalytic Activity At Room

- Temperature. *Eur. J. Inorg. Chem.* **2014**, *2*, 2200–2203.
- (68) Nasielski, J.; Hadei, N.; Achonduh, G.; Kantchev, E. A. B.; O'Brien, C. J.; Lough, A.; Organ, M. G. Structure-Activity Relationship Analysis of Pd-PEPPSI Complexes in Cross-Couplings: A Close Inspection of the Catalytic Cycle and the Precatalyst Activation Model. *Chem. - A Eur. J.* **2010**, *16*, 10844–10853.
- (69) Zhao, Y.; Nett, A. J.; McNeil, A. J.; Zimmerman, P. M. Computational Mechanism for Initiation and Growth of Poly(3-Hexylthiophene) Using Palladium N-Heterocyclic Carbene Precatalysts. *Macromolecules* **2016**, *49*, 7632–7641.
- (70) Kim, B.-S.; Hussain, M. M.; Norrby, P.-O.; Walsh, P. J. Breaking Conjugation: Unusual Regioselectivity with 2-Substituted Allylic Substrates in the Tsuji–Trost Reaction. *Chem. Sci.* **2014**, *5*, 1241–1250.
- (71) Wu, S.; Huang, L.; Tian, H.; Geng, Y.; Wang, F. LiCl-Promoted Chain Growth Kumada Catalyst-Transfer Polycondensation of The “reversed” thiophene Monomer. *Macromolecules* **2011**, *44*, 7558–7567.
- (72) Lanni, E. L.; McNeil, A. J. Evidence for Ligand-Dependent Mechanistic Changes in Nickel-Catalyzed Chain-Growth Polymerizations. *Macromolecules* **2010**, *43*, 8039–8044.
- (73) Lanni, E. L.; McNeil, A. J. Mechanistic Studies on Ni(dppe)Cl<sub>2</sub>-Catalyzed Chain-Growth Polymerizations: Evidence for Rate-Determining Reductive Elimination. *J. Am. Chem. Soc.* **2009**, *131*, 16573–16579.
- (74) Bryan, Z. J.; McNeil, A. J. Conjugated Polymer Synthesis via Catalyst-Transfer Polycondensation (CTP): Mechanism, Scope, and Applications. *Macromolecules* **2013**, *46*, 8395–8405.

## Chapter 5

### Conclusions and future directions

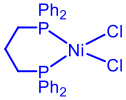
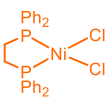

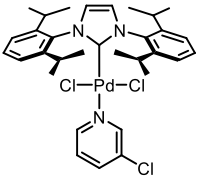
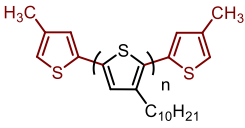
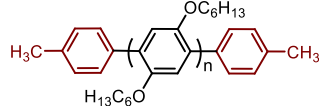
The demand for cheap, portable, and high-performing electronics is accelerating as more people that are not connected to the grid desire access to the internet and communication networks. Roll-to-roll printing provides a scalable, high-throughput method for organic photovoltaic (OPV) manufacture, and these light weight devices could be easily transported and installed without the need for additional building supports.<sup>1,2</sup> The ambitious goals for OPVs have not been realized to date due to low power conversion efficiencies and relatively short lifetimes.<sup>3-5</sup> Recent developments in conjugated polymer (CP) solar cells have generated inspiring results—polymer/polymer blend solar cells efficiencies have more than quadrupled in the past five years<sup>6</sup> and new small molecule electron acceptors<sup>7-10</sup> surpass the efficiency of fullerenes at >12% efficiencies.<sup>10</sup> Modifying both electron donor and acceptor components exponentially increases the design space for polymer solar cells that used to be pinned to the energy levels, solubility, and miscibility of fullerenes. The ability to affect further improvements and translate lab-scale devices to large-scale deployment will rely on new synthetic strategies to develop donor/acceptor materials, additives, and/or interfacial layers that provide stable morphological control.<sup>3,11-13</sup> While CPs are suitable for fulfilling all the roles listed above, synthetic methods for conjugated polymers, copolymers, and other advanced architectures are still in their infancy. The electronics of CPs for OPVs can be tuned using the broad substrate scope of step-growth polymerizations, but control over  $M_n$ ,  $\bar{D}$ , and copolymer sequence via chain-growth methods is desired. Thorough mechanistic studies of living, chain-growth polymerizations for conjugated polymers are necessary to bridge the gap between these two methods by expanding the monomer scope as well as copolymerization capabilities of chain-growth polymerizations.

### End-capping experiment results

We used end-group labeling to investigate the characteristics of the catalyst-polymer  $\pi$ -complex, which is the main feature that distinguishes catalyst-transfer condensation

polymerization (CTCP) from other cross-coupling methods. By employing an excess of competitive agent, we confidently assigned the reaction products to two separate pathways— (1) catalysts that formed strong  $\pi$ -complexes and could also migrate along the polymer via chain-walking yielded the migration product, while (2) weaker binding or less mobile catalysts dissociated from the polymer to afford the dissociation product. All high-performing CTCP catalysts generated the migration products with high selectivity (>85%) when migrating across poly(3-decylthiophene), suggesting that the  $\pi$ -complex is robust and tolerant of different ligands and/or transition metals.

We adapted the end-capping model system to investigate the  $\pi$ -complex with poly(2,5-bis(hexyloxy)phenylene), which produced dramatically different results. Despite similarities in the molecular weight and dispersity of control polymerizations, migration varied significantly depending on the ligand and/or transition metal (Chart 5-1). The mixture of products obtained using the Ni phosphine catalysts and IPrPd(3-chloropyridine)Cl<sub>2</sub> was sensitive to DP—more migration was observed across shorter polymers.

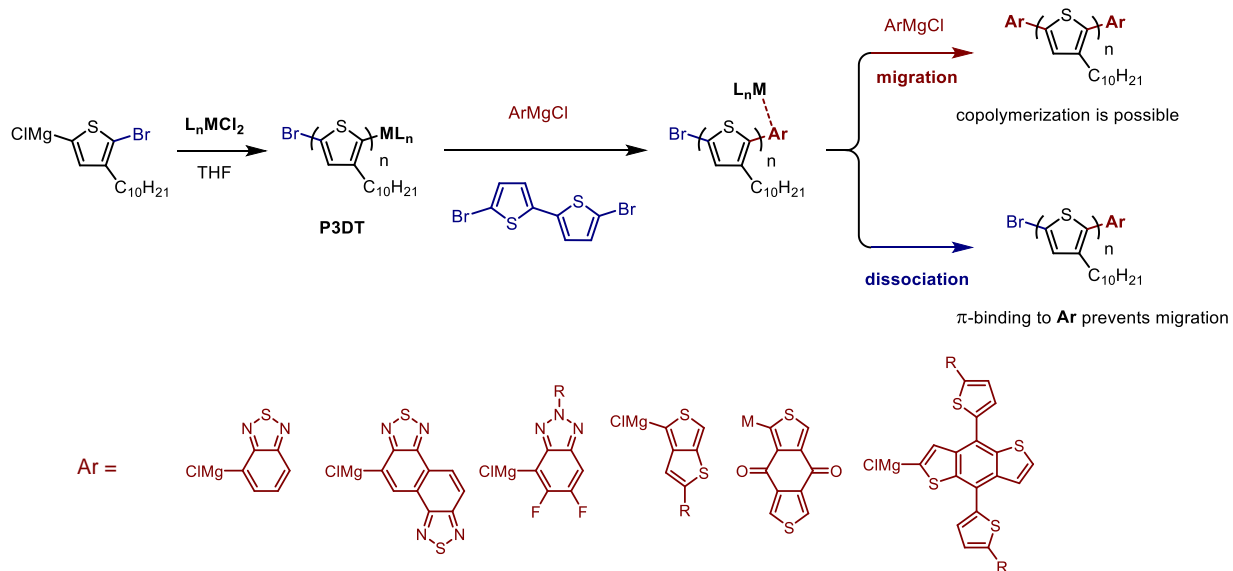
	 Ni(dppp)Cl <sub>2</sub> <b>4a</b>	 Ni(dppe)Cl <sub>2</sub> <b>4b</b>	 IPrNi(PPh <sub>3</sub> )Cl <sub>2</sub> <b>4c</b>	 IPrPd(3-chloropyridine)Cl <sub>2</sub> <b>4d</b>	
	89	97	100	100	migration (%) at DP = 50
	N/A	2	>41	12	maximum DP with >50% migration

**Chart 5-1.** Maximum DP where the migration percent was over 50% for poly(2,5-bis(hexyloxy)phenylene) or the migration percent at DP = 50 for poly(3-decylthiophene) sorted by catalyst as determined from MALDI-TOF MS analysis.

The differences in catalyst chain-walking across polythiophene and polyphenylene are noteworthy considering that batch copolymerizing thiophene and phenylene monomers fail with Ni(dppe)Cl<sub>2</sub> and Ni(dppp)Cl<sub>2</sub> as the catalyst, and only block copolymers prepared using poly(phenylene) as the macroinitiator have been successful. However, thiophene/phenylene

copolymerizations are successful using  $\text{IPrPd}(3\text{-chloropyridine})\text{Cl}_2$ , which exhibits intermediate migration across phenylene. Future work could investigate whether dramatically different migration behavior is predictive of poor copolymerization results and whether catalyst that is highly mobile across each homopolymer performs better in copolymerizations. In related work, a versatile copolymerization catalyst/monomer system developed by Koeckelberghs used an unassociated (and highly mobile) catalyst to prepare conjugated ABC tri-block copolymers<sup>14</sup> and gradient copolymers,<sup>15</sup> although most polymers had low molecular weight ( $<10$  kDa) and medium dispersity ( $>1.5$ ). The higher dispersities are likely due to the exceptionally weak or absent  $\pi$ -complex, which calculations showed to be higher in energy than free Pd phosphine catalyst and monomer.

Precatalyst  $\text{IPrNi}(\text{PPh}_3)\text{Cl}_2$  demonstrated prominent migration across both monomers in our experiments, and thiophene/phenylene copolymerizations have been conducted by other groups ( $M_n$  and  $\text{Đ}$  were not reported).<sup>16,17</sup> Future work could leverage the capacity for  $\text{IPrNi}(\text{PPh}_3)\text{Cl}_2$  to migrate across electronically distinct monomers to expand copolymerization scope, ideally maintaining  $M_n$  control and low  $\text{Đ}$ . Polymerizing multiple, differentiated comonomers using a living, chain-growth method would be a great step forward—high-performing CPs are typically synthesized from two or more monomers using a step-growth method. The end-capping experiments could also provide a general route to quickly screen for possible comonomer combinations with CTCP—migration product indicates that the catalyst could transfer between repeat units (Scheme 5-1). Kiriy used a similar concept to identify incompatibility between benzothiadiazole and thiophene using a reactive ligand on Ni, but his approach required a multi-step synthesis.<sup>18</sup> Capping agents can be prepared from simple starting materials that (1) do not require selective metalation like a monomer,<sup>19,20</sup> (2) avoid self-oligomerization issues that can arise from  $\text{S}_{\text{RN}}1$  reactions between bifunctional monomers (i.e., halogen and magnesium halide),<sup>21–23</sup> and (3) do not require side-chains so that a large set of commercially available reagents could be used. Additionally, only one of the comonomers (e.g., (5-bromo-4-hexylthiophen-2-yl)magnesium chloride) needs to have an established polymerization procedure. A rapid method to screen for copolymerization potential, by quickly ruling out  $\pi$ -binding incompatibilities, should accelerate development of CTCP copolymerizations and provide access to a broader range of opto-electronic properties.

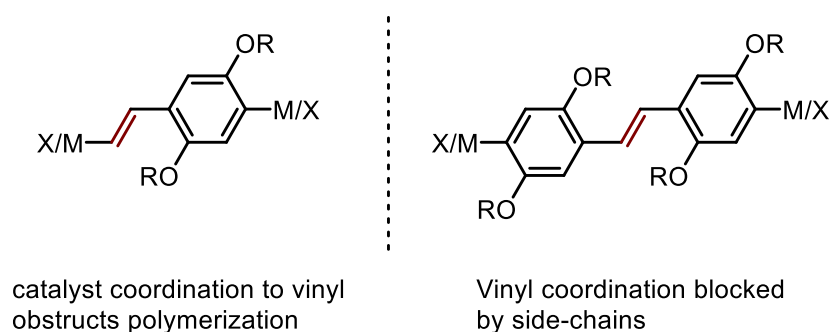


**Scheme 5-1.** End-capping to screen building blocks used in high-efficiency solar cells<sup>24–27</sup> for  $\pi$ -binding issues that could occur during copolymerizations.

### Translating end-capping experiments to polymerization behavior

Kiryi has shown that polymerizing extended thiophene monomers that incorporate multiple aryl groups can challenge CTCP catalysts and lead to a broadening of dispersity.<sup>28</sup> Changing the catalyst from  $\text{Ni}(\text{PPh}_3)_2(\text{Ph})\text{Br}$  to  $\text{Ni}(\text{dppp})\text{Cl}_2$  enabled the polymerization of quarterthiophene derivatives with the same dispersity as thiophene monomer with a single aryl unit.<sup>29</sup> Migration across multiple aryl units has enabled access to polymers with specifically tuned sequences and precise amounts of comonomer incorporation.<sup>29–32</sup> These small changes can have a large impact on thin-film morphology and performance, but major advantage of migration across multiple aryls is to produce donor-acceptor polymers. Ubiquitous in high performance devices, examples of alternating donor-acceptor polymers remain scarce in CTCP and focus on  $\text{Ni}(\text{dppp})\text{Cl}_2$  as the precatalyst.<sup>33,34</sup> New catalyst/monomer combinations that perform these challenging polymerizations could integrate the powerful tools of molecular weight and sequence control with the band-gap engineering critical to solar cell performance. Our end-capping experiments uncovered that  $\text{IPrNi}(\text{PPh}_3)\text{Cl}_2$  can migrate across both thiophene and phenylene—we anticipate that this more general migration behavior could be applied to extended monomers that incorporate repeat units that cannot be polymerized individually. For example, poly(phenylenevinylene) has many commercial applications, but catalyst coordination to the vinyl group of phenylenevinylene monomers can stall CTCP polymerizations or facilitate chain-transfer.<sup>35</sup> Much higher molecule

weights are achieved if the vinyl substituent is flanked by alkoxyphenylene on both ends (Figure 5-1).<sup>36</sup> Coordination to the vinyl group is partially blocked, leading to more efficient catalyst-transfer to react at the phenyl termini. Similarly, leveraging the demonstrated reactivity of thiophene or phenylene monomers on both ends of an electronically desirable functional group and general migration behavior (revealed through the end-capping experiments) could lead to new chain-growth polymerizations. Pairing opto-electronic and molecular weight control in CTCP would facilitate determining structure-property relationships for polymer solar cells, and reduce the batch-to-batch variability that can be a major determinant of performance.<sup>37–39</sup>



**Figure 5-1.** Multi-aryl monomers could be used to block coordination to groups (like vinyl) that are perform poorly in CTCP.

### Catalyst development for sequence-controlled copolymerizations

The unique copolymerization capability of  $\text{IPrPd}(3\text{-chloropyridine})\text{Cl}_2$  with thiophene and phenylene make it a promising scaffold for sequence-controlled copolymerizations, but catalyst migration is problematic for synthesizing di-block and gradient copolymers<sup>40</sup>—polymerizing from both ends scrambles the desired sequence. We pursued four main routes to access an  $\text{IPrPd}$ -based precatalyst that could transfer a reactive ligand to the polymer during initiation, thereby restricting propagation to only one direction. Reacting  $\text{IPrPd}(3\text{-chloropyridine})\text{Cl}_2$  with aryl Grignards to form a stable  $\text{IPrPd}(\text{aryl})\text{Cl}$  was unsuccessful due to the difficulty in achieving only a single transmetalation. In situ formation of a similar species via a cross-coupling (with excess aryl halide), then polymerizing phenylene gave targeted  $M_n$  and low dispersity but without any end-group incorporation. We therefore switched strategies to evaluate stable precatalysts with precedence for high activities in small-molecule cross-couplings. Initiation from these air stable palladacycles was slow when polymerizing phenylene, but showed some improvement after switching to thiophene. The most promising polymerization results were obtained from

IPrPd(cinnamyl)Cl, where phenylene could be polymerized with targeted  $M_n$  and low  $\mathcal{D}$  when 3-chloropyridine was present as an additive. However, the cinnamyl group was only transferred to 70–80% of poly(2,5-bis(hexyloxy)phenylene). Oligomerization studies identified that the polymer end groups did not change significantly throughout the polymerization, suggesting that incomplete end-group transfer occurred during initiation.

The unsuccessful attempts to generate a functionalized IPrPd precatalyst illustrated the importance of initiation on polymer molecular weight and end-group transfer. Precatalysts with allyl-based reactive ligands remain a promising approach. Recent work has identified Pd(I) dimers as potential side-reaction when activating allyl-based IPrPd precatalysts, and these species could reduce reactive ligand transfer to polymer.<sup>41,42</sup> Precatalysts with a 1-<sup>t</sup>Bu-indenyl reactive ligand are unable to form this dimer, so each metal center could transfer a reactive ligand to the polymer. Promising copolymerization behavior has been also observed using Ni-diimine catalysts where block copolymerizations of thiophene and benzotriazole could be performed from either order of addition.<sup>43</sup> Switching from IPrPd precatalysts may allow new synthetic routes that would expedite the discovery of a copolymerization precatalyst.

Preparing electronically and sterically differentiated conjugated copolymers with well-defined sequences could be a breakthrough for CTCP. Copolymers are used extensively as templates, additives, or single-components to achieve a range of solution or solid state properties. Fundamental studies are initially required to identify how changing  $M_n$ ,  $\mathcal{D}$ , and copolymer sequence influences the copolymer properties, and their subsequent effect on polymer blends. Using these insights as the foundation, conjugated copolymers could find use in a myriad of applications. In OPVs, balanced mixing/separation in the active layer facilitates charge generation/charge transport, but the morphology can evolve over time.<sup>44–47</sup> Copolymer additives can stabilize the blend morphology to increase the lifetime of the solar cell—one of the main limits to their widespread use.<sup>46</sup>

The work described in this thesis takes a mechanistic approach towards understanding the complexities of CTCP with a focus on the catalyst-polymer  $\pi$ -complex. The behavior of this fundamental intermediate has wide-ranging implications for living, chain-growth polymerizations of conjugated monomers. We studied popular catalysts with poly(3-decylthiophene) and poly(2,5-bis(hexyloxy)phenylene), and explored precatalysts to direct their copolymerization. The end-



capping model system revealed  $\pi$ -binding/catalyst mobility that was dependent on both monomer identity and precatalyst. The vast distances that  $\text{IPrNi}(\text{PPh}_3)\text{Cl}_2$  can migrate across both thiophene and phenylene make it a promising candidate for polymerizing extended monomers with various aryl groups, and different monomer combinations in copolymerizations. Continued efforts to prepare reactive ligand functionalized precatalysts could enable new gradient copolymers. Advances in both monomer scope and copolymerization ability would be a powerful combination that could expand the utility of CTCP to many applications where  $M_n$ ,  $\text{Đ}$ , and copolymer sequence effects have a dramatic effect on film morphology.

## References

- (1) Andersen, T. R.; Dam, H. F.; Hösel, M.; Helgesen, M.; Carlé, J. E.; Larsen-Olsen, T. T.; Gevorgyan, S. a.; Andreasen, J. W.; Adams, J.; Li, N.; *et al.* Scalable, Ambient Atmosphere Roll-to-Roll Manufacture of Encapsulated Large Area, Flexible Organic Tandem Solar Cell Modules. *Energy Environ. Sci.* **2014**, *7*, 2925–2933.
- (2) Osedach, T. P.; Andrew, T. L.; Bulović, V. Effect of Synthetic Accessibility on the Commercial Viability of Organic Photovoltaics. *Energy Environ. Sci.* **2013**, *6*, 711–718.
- (3) Liu, K.; Larsen-Olsen, T. T.; Lin, Y.; Beliatas, M.; Bundgaard, E.; Jørgensen, M.; Krebs, F. C.; Zhan, X. Roll-Coating Fabrication of Flexible Organic Solar Cells: Comparison of Fullerene and Fullerene-Free Systems. *J. Mater. Chem. A* **2016**, *4*, 1044–1051.
- (4) Agbomahena, M.; Douhéret, O.; Kounouhewa, B.; Vianou, A.; Awanou, N.; Lazzaroni, R. Ageing of Organic Photovoltaic Devices in Benin Environment (South-Sudanese Climate). *Sol. Energy Mater. Sol. Cells* **2013**, *117*, 93–97.
- (5) Emmott, C. J. M.; Moia, D.; Sandwell, P.; Ekins-Daukes, N.; Hösel, M.; Lukoschek, L.; Amarasinghe, C.; Krebs, F. C.; Nelson, J. In-Situ, Long-Term Operational Stability of Organic Photovoltaics for off-Grid Applications in Africa. *Sol. Energy Mater. Sol. Cells* **2016**, *149*, 284–293.
- (6) Benten, H.; Mori, D.; Ohkita, H.; Ito, S.; Søndergaard, R.; Hösel, M.; Angmo, D.; Larsen-Olsen, T. T.; Krebs, F. C.; Darling, S. B.; *et al.* Recent Research Progress of Polymer Donor/Polymer Acceptor Blend Solar Cells. *J. Mater. Chem. A* **2016**, *4*, 5340–5365.
- (7) Liu, F.; Zhou, Z.; Zhang, C.; Vergote, T.; Fan, H.; Liu, F.; Zhu, X. A Thieno[3,4 - B ]Thiophene-Based Non-Fullerene Electron Acceptor for High-Performance Bulk-Heterojunction Organic Solar Cells. *J. Am. Chem. Soc.* **2016**, *138*, 4–7.
- (8) Lin, Y.; Wang, J.; Zhang, Z.; Bai, H.; Li, Y.; Zhu, D.; Zhan, X. An Electron Acceptor Challenging Fullerenes for Efficient Polymer Solar Cells. *Adv. Mater.* **2015**, *27*, 1170–1174.
- (9) Holliday, S.; Ashraf, R. S.; Wadsworth, A.; Baran, D.; Yousaf, S. A.; Nielsen, C. B.; Tan, C.-H.; Dimitrov, S. D.; Shang, Z.; Gasparini, N.; *et al.* High-Efficiency and Air-Stable P3HT-Based Polymer Solar Cells with a New Non-Fullerene Acceptor. *Nat. Commun.* **2016**, *7*, 11585.
- (10) Li, S.; Ye, L.; Zhao, W.; Zhang, S.; Mukherjee, S.; Ade, H.; Hou, J. Energy-Level Modulation of Small-Molecule Electron Acceptors to Achieve over 12% Efficiency in Polymer Solar Cells. *Adv. Mater.* **2016**, *28*, 9423–9429.
- (11) Po, R.; Bernardi, A.; Calabrese, A.; Carbonera, C.; Corso, G.; Pellegrino, A. From Lab to Fab: How Must the Polymer Solar Cell Materials Design Change? – an Industrial Perspective. *Energy Environ. Sci.* **2014**, *7*, 925–943.
- (12) Cao, B.; He, X.; Fetterly, C. R.; Olsen, B. C.; Lubber, E. J.; Buriak, J. M. Role of Interfacial Layers in Organic Solar Cells: Energy Level Pinning versus Phase Segregation. *ACS Appl. Mater. Interfaces* **2016**, *8*, 18238–18248.
- (13) Shao, S.; Liu, J.; Zhang, J.; Zhang, B.; Xie, Z.; Geng, Y.; Wang, L. Interface-Induced

- Crystalline Ordering and Favorable Morphology for Efficient Annealing-Free poly(3-Hexylthiophene): Fullerene Derivative Solar Cells. *ACS Appl. Mater. Interfaces* **2012**, *4*, 5704–5710.
- (14) Verswyvel, M.; Steverlynck, J.; Hadj Mohamed, S.; Trabelsi, M.; Champagne, B.; Koeckelberghs, G. All-Conjugated ABC-Block-Copolymer Formation with a Varying Sequence via an Unassociated Catalyst. *Macromolecules* **2014**, *47*, 4668–4675.
  - (15) Hardeman, T.; Koeckelberghs, G. The Synthesis of Poly(thiophene-Co-Fluorene) Gradient Copolymers. *Macromolecules* **2015**, *48*, 6987–6993.
  - (16) Mikami, K.; Nojima, M.; Masumoto, Y.; Mizukoshi, Y.; Takita, R.; Yokozawa, T.; Uchiyama, M. Catalyst-Dependent Intrinsic Ring-Walking Behavior on  $\pi$ -Face of Conjugated Polymers. *Polym. Chem.* **2017**, *8*, 1708–1713.
  - (17) Hardeman, T.; De Becker, J.; Koeckelberghs, G. Influence of the Halogen and Organometallic Function in a KCTP (Co)polymerization. *J. Polym. Sci. Part A Polym. Chem.* **2016**, *54*, 3701–3706.
  - (18) Komber, H.; Senkovskyy, V.; Tkachov, R.; Johnson, K.; Kiriya, A.; Huck, W. T. S.; Sommer, M. Ring Walking versus Trapping of Nickel(0) during Kumada Catalyst Transfer Polycondensation Using Externally Initiated Electron-Accepting Thiophene–Benzothiadiazole–Thiophene Precursors. *Macromolecules* **2011**, *44*, 9164–9172.
  - (19) Verswyvel, M.; Hoebels, C.; De Winter, J.; Gerbaux, P.; Koeckelberghs, G. Study of the Controlled Chain-Growth Polymerization of poly(3,6-Phenanthrene). *J. Polym. Sci. Part A Polym. Chem.* **2013**, *51*, 5067–5074.
  - (20) Bedi, A.; De Winter, J.; Gerbaux, P.; Koeckelberghs, G. Detrimental Ni(0) Transfer in Kumada Catalyst Transfer Polycondensation of benzo[2,1-b:3,4-b']dithiophene. *J. Polym. Sci. Part A Polym. Chem.* **2016**, *54*, 1706–1712.
  - (21) Smith, M. L.; Leone, A. K.; Zimmerman, P. M.; McNeil, A. J. Impact of Preferential  $\pi$ -Binding in Catalyst-Transfer Polycondensation of Thiazole Derivatives. *ACS Macro Lett.* **2016**, *5*, 1411–1415.
  - (22) Murarka, S.; Studer, A. Radical/Anionic SRN1-Type Polymerization for Preparation of Oligoarenes. *Angew. Chemie Int. Ed.* **2012**, *51*, 12362–12366.
  - (23) Haines, B. E.; Wiest, O. SET-Induced Biaryl Cross-Coupling: An SRN1 Reaction. *J. Org. Chem.* **2014**, *79*, 2771–2774.
  - (24) Zhao, W.; Qian, D.; Zhang, S.; Li, S.; Inganäs, O.; Gao, F.; Hou, J. Fullerene-Free Polymer Solar Cells with over 11% Efficiency and Excellent Thermal Stability. *Adv. Mater.* **2016**, *28*, 4734–4739.
  - (25) Zhang, S.; Ye, L.; Hou, J. Breaking the 10% Efficiency Barrier in Organic Photovoltaics: Morphology and Device Optimization of Well-Known PBDTTT Polymers. *Adv. Energy Mater.* **2016**, *6*, 1502529.
  - (26) Liu, Y.; Zhao, J.; Li, Z.; Mu, C.; Ma, W.; Hu, H.; Jiang, K.; Lin, H.; Ade, H.; Yan, H. Aggregation and Morphology Control Enables Multiple Cases of High-Efficiency Polymer Solar Cells. *Nat. Commun.* **2014**, *5*, 5293.

- (27) Li, Z.; Jiang, K.; Yang, G.; Lai, J. Y. L.; Ma, T.; Zhao, J.; Ma, W.; Yan, H. Donor Polymer Design Enables Efficient Non-Fullerene Organic Solar Cells. *Nat. Commun.* **2016**, *7*, 13094.
- (28) Beryozkina, T.; Senkovskyy, V.; Kaul, E.; Kiriya, A. Kumada Catalyst-Transfer Polycondensation of Thiophene-Based Oligomers: Robustness of a Chain-Growth Mechanism. *Macromolecules* **2008**, *41*, 7817–7823.
- (29) Tsai, C.-H.; Fortney, A.; Qiu, Y.; Gil, R. R.; Yaron, D.; Kowalewski, T.; Noonan, K. J. T. Conjugated Polymers with Repeated Sequences of Group 16 Heterocycles Synthesized through Catalyst-Transfer Polycondensation. *J. Am. Chem. Soc.* **2016**, *138*, 6798–6804.
- (30) Hardeman, T.; Koeckelberghs, G. Steering Poly(thiophene) Properties by Incorporation of Phenyl Groups. *Macromolecules* **2014**, *47*, 8618–8624.
- (31) Blaskovits, J. T.; Bura, T.; Beaupré, S.; Lopez, S. A.; Roy, C.; de Goes Soares, J.; Oh, A.; Quinn, J.; Li, Y.; Aspuru-Guzik, A.; *et al.* A Study of the Degree of Fluorination in Regioregular Poly(3-Hexylthiophene). *Macromolecules* **2017**, *50*, 162–174.
- (32) Qiu, Y.; Fortney, A.; Tsai, C.-H. H.; Baker, M. A.; Gil, R. R.; Kowalewski, T.; Noonan, K. J. T. Synthesis of Polyfuran and Thiophene-Furan Alternating Copolymers Using Catalyst-Transfer Polycondensation. *ACS Macro Lett.* **2016**, *5*, 332–336.
- (33) Todd, A. D.; Bielawski, C. W. Controlled Synthesis of an Alternating Donor–Acceptor Conjugated Polymer via Kumada Catalyst-Transfer Polycondensation. *ACS Macro Lett.* **2015**, *4*, 1254–1258.
- (34) Qiu, Y.; Worch, J. C.; Fortney, A.; Gayathri, C.; Gil, R. R.; Noonan, K. J. T. Nickel-Catalyzed Suzuki Polycondensation for Controlled Synthesis of Ester-Functionalized Conjugated Polymers. *Macromolecules* **2016**, *49*, 4757–4762.
- (35) Yokozawa, T.; Nanashima, Y.; Nojima, M.; Ohta, Y. Catalyst-Transfer Condensation Polymerization of Acceptor Aromatic Monomers and of Donor Carbon-Carbon Double Bond-Containing Monomers. *Macromol. Symp.* **2015**, *350*, 22–33.
- (36) Nojima, M.; Ohta, Y.; Yokozawa, T. Additive-Controlled Switching from Abnormal to Normal Unstoichiometric Suzuki–Miyaura Polycondensation for Poly(biphenylenevinylene). *Chem. Lett.* **2017**, *46*, 35–37.
- (37) Vangerven, T.; Verstappen, P.; Drijkoningen, J.; Dierckx, W.; Himmelberger, S.; Salleo, A.; Vanderzande, D.; Maes, W.; Manca, J. V. Molar Mass versus Polymer Solar Cell Performance: Highlighting the Role of Homocouplings. *Chem. Mater.* **2015**, *27*, 3726–3732.
- (38) Gao, M.; Subbiah, J.; Geraghty, P. B.; Chen, M.; Purushothaman, B.; Chen, X.; Qin, T.; Vak, D.; Scholes, F. H.; Watkins, S. E.; *et al.* Development of a High-Performance Donor–Acceptor Conjugated Polymer: Synergy in Materials and Device Optimization. *Chem. Mater.* **2016**, *28*, 3481–3487.
- (39) Lee, H. K. H.; Li, Z.; Constantinou, I.; So, F.; Tsang, S. W.; So, S. K. Batch-to-Batch Variation of Polymeric Photovoltaic Materials: Its Origin and Impacts on Charge Carrier Transport and Device Performances. *Adv. Energy Mater.* **2014**, *4*, 1400768.
- (40) Verswyvel, M.; Monnaie, F.; Koeckelberghs, G. AB Block Copoly(3-Alkylthiophenes):

Synthesis and Chiroptical Behavior. *Macromolecules* **2011**, *44*, 9489–9498.

- (41) Melvin, P. R.; Balcells, D.; Hazari, N.; Nova, A. Understanding Precatalyst Activation in Cross-Coupling Reactions: Alcohol Facilitated Reduction from Pd(II) to Pd(0) in Precatalysts of the Type ( $\eta^3$ -allyl)Pd(L)(Cl) and ( $\eta^3$ -indenyl)Pd(L)(Cl). *ACS Catal.* **2015**, *5*, 5596–5606.
- (42) Melvin, P. R.; Nova, A.; Balcells, D.; Dai, W.; Hazari, N.; Hruszkewycz, D. P.; Shah, H. P.; Tudge, M. T. Design of a Versatile and Improved Precatalyst Scaffold for Palladium-Catalyzed Cross-Coupling: ( $\eta^3$ -1-tBu-indenyl) $2(\mu$ -Cl) $2$ Pd $2$ . *ACS Catal.* **2015**, *5*, 3680–3688.
- (43) Bridges, C. R.; Yan, H.; Pollit, A. A.; Seferos, D. S. Controlled Synthesis of Fully  $\pi$ -Conjugated Donor–Acceptor Block Copolymers Using a Ni(II) Diimine Catalyst. *ACS Macro Lett.* **2014**, *3*, 671–674.
- (44) Liao, M.-H.; Tsai, C.-E.; Lai, Y.-Y.; Cao, F.-Y.; Wu, J.-S.; Wang, C.-L.; Hsu, C.-S.; Liao, I.; Cheng, Y.-J. Morphological Stabilization by Supramolecular Perfluorophenyl-C 60 Interactions Leading to Efficient and Thermally Stable Organic Photovoltaics. *Adv. Funct. Mater.* **2014**, *24*, 1418–1429.
- (45) Kim, H. J.; Kim, J.-H. H.; Ryu, J. H.; Kim, Y.; Kang, H.; Lee, W. B.; Kim, T.-S. S.; Kim, B. J. Architectural Engineering of Rod–Coil Compatibilizers for Producing Mechanically and Thermally Stable Polymer Solar Cells. *ACS Nano* **2014**, *8*, 10461–10470.
- (46) Palermo, E. F.; Darling, S. B.; McNeil, A. J.  $\pi$ -Conjugated Gradient Copolymers Suppress Phase Separation and Improve Stability in Bulk Heterojunction Solar Cells. *J. Mater. Chem. C* **2014**, *2*, 3401–3406.
- (47) Lee, C.; Li, Y.; Lee, W.; Lee, Y.; Choi, J.; Kim, T.; Wang, C.; Gomez, E. D.; Woo, H. Y.; Kim, B. J. Correlation between Phase-Separated Domain Sizes of Active Layer and Photovoltaic Performances in All-Polymer Solar Cells. *Macromolecules* **2016**, *49*, 5051–5058.

## Appendix 1

### Supporting Information for Chapter 2

#### Long-distance catalyst migration across poly(3-alkylthiophene)

<b>I.</b>	<b>Materials</b>	<b>110</b>
<b>II.</b>	<b>General experimental</b>	<b>111</b>
<b>III.</b>	<b>Synthetic procedures</b>	<b>113</b>
<b>IV.</b>	<b>NMR spectra</b>	<b>115</b>
<b>V.</b>	<b>Reactivity of the competitive agent using all catalysts</b>	<b>116</b>
<b>VI.</b>	<b>Effect of competitive agent on polymerizing 1</b>	<b>118</b>
<b>VII.</b>	<b>End-capping model experiments</b>	<b>125</b>
<b>VIII.</b>	<b>Catalyst migration (%)</b>	<b>149</b>
<b>IX.</b>	<b>Random-walking calculations</b>	<b>151</b>
<b>X.</b>	<b>References</b>	<b>157</b>

## I. Materials

Flash chromatography was performed on SiliCycle silica gel (40–63  $\mu\text{m}$ ). Thin layer chromatography was performed on Merck TLC plates (pre-coated with silica gel 60 F254). 2,5-dibromo-3-decylthiophene was purchased from TCI America and purified via column chromatography with hexanes as eluent prior to use.  $\text{IPrNi}(\text{PPh}_3)\text{Cl}_2$  was purchased from TCI America.  $\text{iPrMgCl}$  (2 M in THF), 5,5'-dibromo-2,2'-bithiophene,  $\text{Ni}(\text{dppe})\text{Cl}_2$ ,  $\text{Ni}(\text{dppp})\text{Cl}_2$ ,  $\text{IPrPd}(\text{3-chloropyridine})\text{Cl}_2$ , and  $\text{Ni}(\text{PPh}_3)_2\text{Cl}_2$  were purchased from Sigma-Aldrich. All other reagent grade materials and solvents were purchased from Sigma-Aldrich, Acros, or Fisher and were used without further purification unless otherwise noted. THF was dried and deoxygenated using an Innovative Technology (IT) solvent system composed of activated alumina, copper catalyst, and molecular sieves. *N*-Bromosuccinimide was recrystallized from hot water and dried over  $\text{P}_2\text{O}_5$ . The glovebox in which specified procedures were carried out was an MBraun LABmaster 130 with a  $\text{N}_2$  atmosphere and  $\text{H}_2\text{O}$  levels below 4 ppm. Compounds **2a**<sup>1</sup> and **S1**<sup>2</sup> were prepared using modified literature procedures.

## II. General experimental

NMR Spectroscopy: Unless otherwise noted,  $^1\text{H}$ , and  $^{13}\text{C}$  NMR spectra for all compounds were acquired at rt in  $\text{CDCl}_3$  on a Varian MR400 Spectrometer operating at 400 and 100 MHz, respectively. Chemical shift data are reported in units of  $\delta$  (ppm) relative to tetramethylsilane (TMS) and referenced with residual solvent. Multiplicities are reported as follows: doublet (d), triplet (t), multiplet (m).

Mass Spectrometry: High-resolution mass spectrometry data were obtained on a Micromass AutoSpec Ultima Magnetic Sector mass spectrometer.

Gel-Permeation Chromatography: Polymer molecular weights were determined by comparison with polystyrene standards (Varian, EasiCal PS-2 MW 580–377,400) at 40 °C in THF on a Malvern Viscotek GPCMax VE2001 equipped with two Viscotek LT-5000L columns (8 mm (ID)  $\times$  300 mm (L)) and analyzed with Viscotek TDA 305 (with RI, UV-PDA Detector Model 2600 (190–500 nm), RALS/LALS, and viscometer). All presented data correspond to the absorbance at 254 nm normalized to the highest peak. Samples were dissolved in THF (with mild heating), and passed through a 0.2  $\mu\text{m}$  PTFE filter prior to analysis.

Gas Chromatography: Gas chromatography was carried out using a Shimadzu GC 2010 containing a Shimadzu SHRX5 column (crossbound 5% diphenyl–95% dimethyl polysiloxane; 15 m, 0.25 mm ID, 0.25  $\mu\text{m}$  df).

Titrations of the Grignard Reagents: An accurately weighed sample of salicylaldehyde phenylhydrazone<sup>3</sup> (typically between 170–200 mg) was dissolved in 10.00 mL of THF. This solution was added dropwise using a 500  $\mu\text{L}$  syringe to 0.10 mL of  $\text{ArMgCl}$ . The initial  $\text{ArMgCl}$  solution is pale yellow, turns bright orange, and then returns to pale yellow at the end-point.

Precatalyst stock solutions: Precatalyst **4d** (~55 mg) was weighed into a 5 mL volumetric flask in a glovebox, and then diluted with THF. These stocks solutions were stored in the freezer, and remain stable for several weeks or longer.

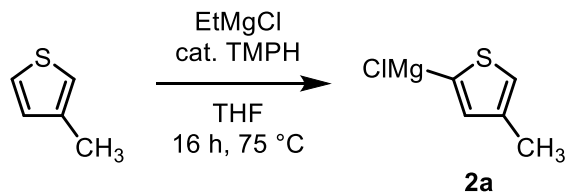


Precatalyst **4c** (~5 mg) was weighed into a 1 mL volumetric flask in a glovebox, and then diluted with THF immediately before use. If stored, the violet solution would turn blue over the course of several h.

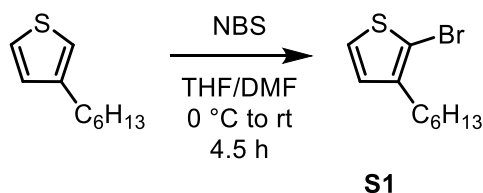
*MALDI-TOF MS*: Matrix-assisted laser desorption/ionization time-of-flight mass spectrometry was performed on a Bruker Autoflex Speed. Positive ion spectra were obtained in reflectron mode. Polymer samples (~1 mg) were dissolved in CHCl<sub>3</sub> (~3 mL) and mixed in a 1:1 (v/v) ratio with 0.1 M trans-2-[3-(4-tert-butylphenyl)-2-methyl-2-propenylidene]malononitrile (DTCB) solution in CHCl<sub>3</sub> then spotted. Serial dilutions (~five-fold) were performed to access a wide range of sample concentrations, and the spot yielding the highest signal/noise was subsequently analyzed. Molecular weight of HCl quenched **P3DT** with Br/H end groups was referenced to a series of low MW peptide standards. This **P3DT** was then used to calibrate the full MW range of the sample (~2–15 kDa).

Raw data was processed in flexAnalysis Version 3.4. Peak smoothing was performed using one cycle of the SavitskyGolay algorithm to a peak width of five m/z, and baseline subtraction was performed using TopHat. Peak picking was performed using the centroid method for peaks with signal/noise greater than one. Migration percent was calculated at each DP where both migration (cap/cap end-groups) and dissociation (cap/Br end-groups) product peaks were found by peak picking. For spectra where no dissociation product peaks were detected at any DP, migration is reported as 100% for all peaks with signal/noise above five.

### III. Synthetic procedures

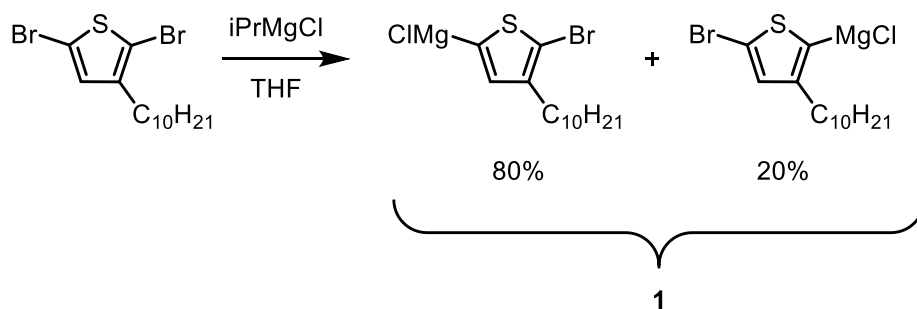


**4-methyl-2-chloromagnesiothiophene (2a).**<sup>1</sup> In a glovebox, 3-methylthiophene (1.00 g, 10.0 mmol, 1.40 equiv) and 2,2,6,6-tetramethylpiperidine (0.10 g, 0.73 mmol, 0.10 equiv) were added to a 25 mL Schlenk flask and diluted with THF (4.17 mL). With stirring, EtMgCl (7.16 mL of 1.015 M in Et<sub>2</sub>O solution, 7.27 mmol, 1.00 equiv) was added slowly over 5 min. A reflux condenser was added and then the combined setup was removed from the glovebox. A N<sub>2</sub> line was added and the solution was heated to 75 °C for 16 h. After cooling, the solution was transferred via cannula to a Schlenk tube and returned to the glovebox. <sup>1</sup>H NMR spectroscopic analysis confirmed complete consumption of the EtMgCl. The solution was further diluted with THF (~10 mL) and titrated prior to use (~0.2 M).



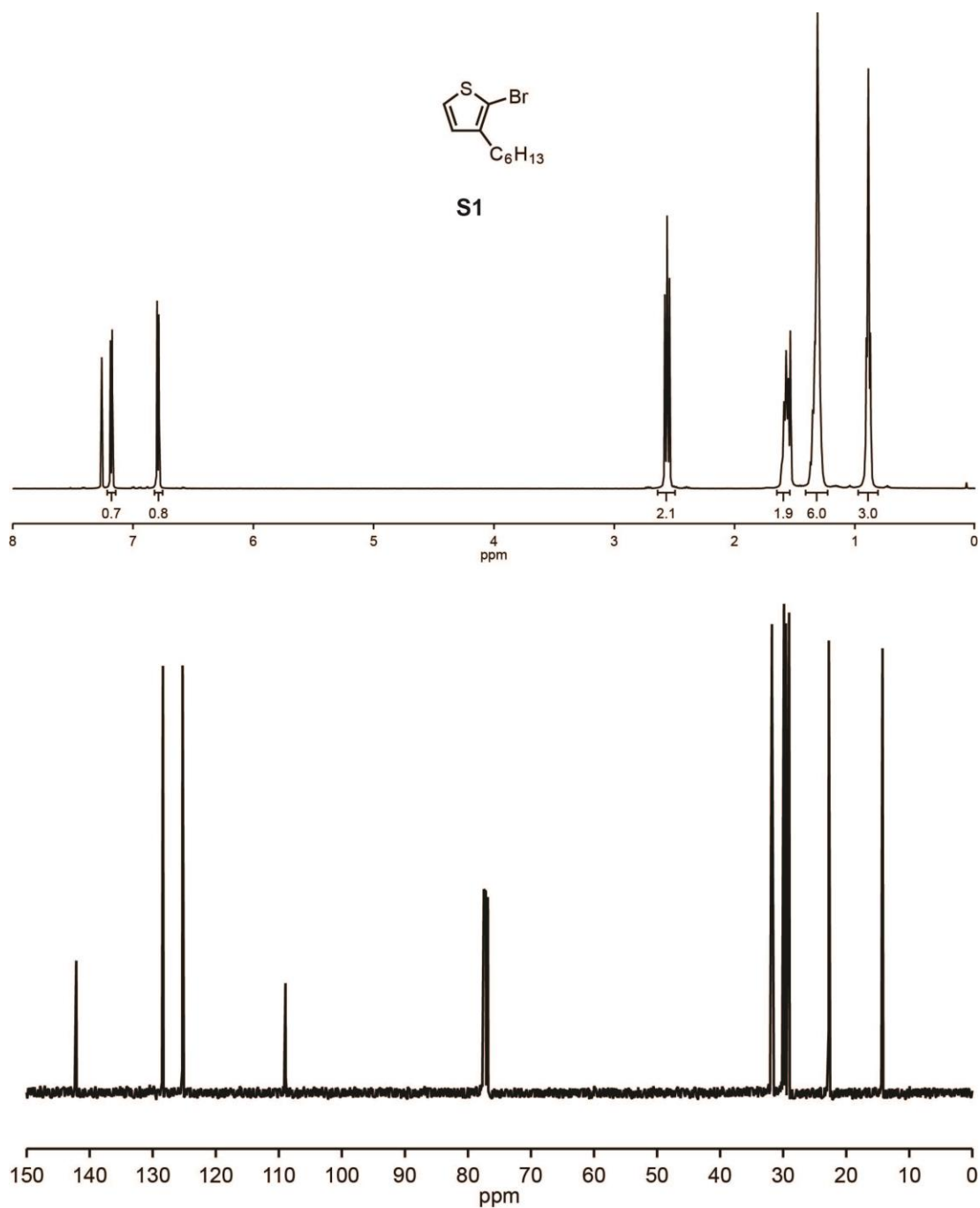
**2-bromo-3-hexylthiophene (S1).**<sup>2</sup> In a 200 mL Schlenk flask equipped with a stir bar, 3-hexylthiophene (5.0 g, 30. mmol, 1.0 equiv) was added and 3 evacuation/N<sub>2</sub> backfill cycles were performed. Under N<sub>2</sub> pressure, THF (50 mL) and DMF (10 mL) were added with stirring and the flask was cooled in an ice bath and covered with aluminum foil. N-bromosuccinimide (5.50 g, 30.9 mmol, 1.04 equiv) was added quickly in one portion. The reaction slowly warmed to rt over the first 3 h, and was quenched after 4.5 h with 20 mL aq. sat. Na<sub>2</sub>S<sub>2</sub>O<sub>3</sub>. The mixture was extracted with hexanes (4 x 20 mL), and the combined organic layers were washed with H<sub>2</sub>O (2 x 20 mL) and brine (1 x 20 mL). The solution was dried over MgSO<sub>4</sub>, filtered, and then condensed to a

slightly yellow oil using a rotary evaporator. The oil was filtered through a silica gel column (~50 mL) with hexanes (~250 mL) as the eluent to remove any color, collecting the entire sample in one portion. The mother liquor was condensed to a colorless oil, and then a fractional distillation under high vacuum with heating gave 5.23 g of **S1** as a colorless oil (71% yield). HRMS (EI+): Calcd. for C<sub>10</sub>H<sub>15</sub>BrS [M+H]<sup>+</sup> 246.0078; found 246.0087.



**1.**<sup>2</sup> In a glovebox, 2,5-dibromo-3-decylthiophene (0.978 g, 2.56 mmol, 1.00 equiv) was added to a 20 mL vial equipped with a stir bar and diluted with THF (~15 mL). A small amount of C<sub>22</sub>H<sub>44</sub> (~20 mg) was added as an internal standard, and then *i*PrMgCl (1.05 mL of a 1.98 M solution in THF, 2.07 mmol, 0.809 equiv). The mixture was stirred for 30 minutes. An aliquot of the solution was removed from the glovebox and quenched with conc. HCl (~0.5 mL). The aliquot was extracted with CHCl<sub>3</sub> (2 x 1 mL), washed with H<sub>2</sub>O (1 x 1 mL), brine (1 x 1 mL), and dried over MgSO<sub>4</sub>. The mixture was filtered, and the mother liquor analyzed by GC to show a mixture of regioisomers at 80% and 20%, respectively.

#### IV. NMR spectra

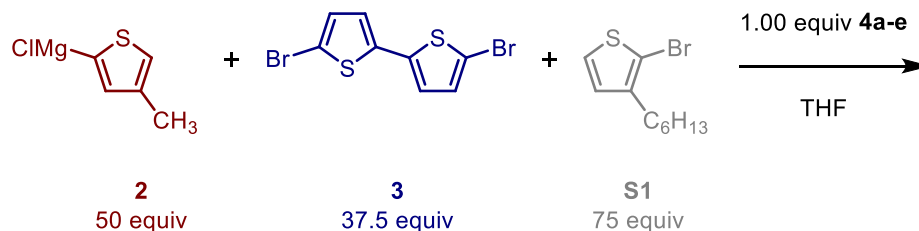


**Figure A1-1.** <sup>1</sup>H and <sup>13</sup>C NMR spectra for **S1**.

<sup>1</sup>H NMR (400 MHz, CDCl<sub>3</sub>) δ 7.18 (d, *J* = 5.6 Hz, 1H), 6.79 (d, *J* = 5.6 Hz, 1H), 2.56 (t, *J* = 7.5 Hz, 2H), 1.60–1.54 (m, 2H), 1.33–1.29 (m, 6H), 0.94–0.83 (m, 3H).

<sup>13</sup>C NMR (100 MHz, CDCl<sub>3</sub>) δ 142.13, 128.38, 125.26, 108.94, 31.78, 29.86, 29.56, 29.06, 22.76, 14.24.

## V. Reactivity of the competitive agent using all catalysts



aryl halide conversion monitored by GC

### General procedure for the cross-coupling of 5,5'-dibromo-2,2'-bithiophene (**3**) and 2-bromo-3-hexylthiophene (**S1**) with **2** catalyzed by **4a-e**.

*Solution A.* In a glovebox, **3** (2.21 mL of a 0.168 M solution in THF, 0.372 mmol) and 2-bromo-3-hexylthiophene (2.24 mL of a 0.333 M solution, 0.744 mmol) were added to a 20 mL vial with a stir bar and C<sub>22</sub>H<sub>46</sub> (~30 mg). An aliquot (~0.1 mL) was removed from the glovebox and quenched with conc. HCl (~1 mL) as the time zero point.

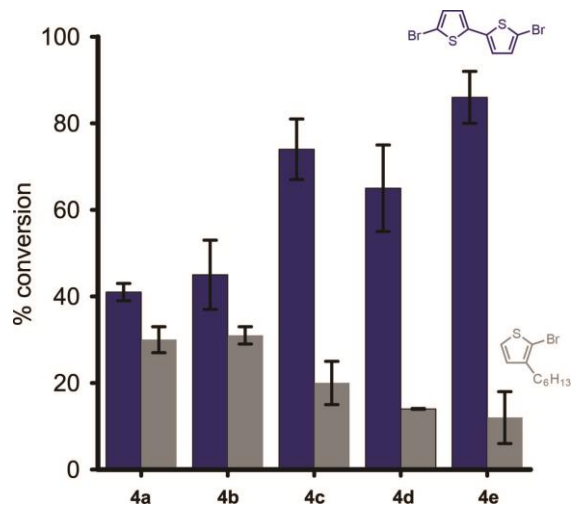
Separately, the insoluble precatalysts (**4a**, **4b**, and **4e**) were each weighed (~1–1.4 mg) into a 4 mL vial and diluted with THF (~1–1.4 mL) to achieve a precatalyst concentration of 0.00075 M during the reaction. For precatalysts soluble in THF (**4c** and **4d**), stock solutions (~0.1 mL of a 0.015 M solution in THF) of each were diluted with THF (~0.7 mL) in a 4 mL vial equipped with a stir bar to achieve a precatalyst concentration of 0.00075 M during the reaction.

Next, *Solution A* (~0.7–1 mL, 75 equiv of each heteroaryl bromide\*) was added to the precatalyst solutions and the combined mixture was stirred for 2 min. Then **2** (0.34–0.50 mL of a 0.221 M solution in THF, 50 equiv) was added with stirring. The reaction turned yellow within 20 s, and this color persisted for the next 1 h before quenching.

The reaction mixture was removed from the glovebox and quenched with conc. HCl (~2 mL). The quenched mixture was extracted with CHCl<sub>3</sub> (3 x 0.5 mL) with heating using a heat gun. The combined organic layers were washed with H<sub>2</sub>O (1 x 2 mL) and brine (1 x 2 mL) before drying over MgSO<sub>4</sub>. The solution was filtered, and then diluted with DCM (~1 mL) for GC analysis.

Conversion of the aryl halides was determined by GC from the change in peak area ratio with C<sub>22</sub>H<sub>46</sub> internal standard.

\*1 mol of **3** was treated as 2 equiv of heteroaryl bromide.

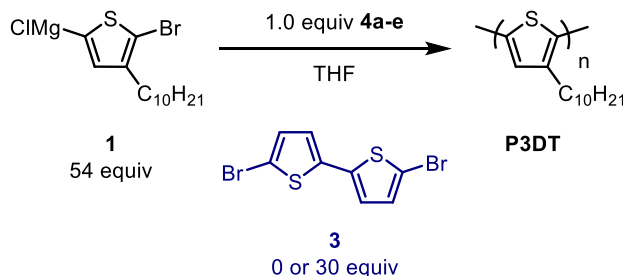


**Figure A1-2.** Average percent conversion of **3** (■), and 2-bromo-3-hexylthiophene (■) in cross-coupling competition experiments with **2** sorted by precatalyst. Error bars represent one standard deviation.

Precatalyst	Conversion (%)							
	3				S1			
	Run 1	Run 2	Average	STD	Run 1	Run 2	Average	STD
<b>4a</b>	42	40	41	2	32	32	30	3
<b>4b</b>	51	39	45	8	29	29	31	2
<b>4c</b>	69	79	74	7	24	24	20	5
<b>4d</b>	58	73	65	10	14	14	14	0
<b>4e</b>	82	91	86	6	17	17	12	6

**Table A1-1.** Conversion data plotted in Figure A1-2.

## VI. Effect of competitive agent on polymerizing **1**



### Polymerizing **1** in the presence of **3**.

**4c and 4d.** Precatalyst from a stock solution (~0.1 mL of a ~0.015 M solution in THF, 0.0015 mmol, 1.0 equiv) was added to a 10 mL Schleck flask equipped with a stir bar and diluted with THF (~1.2 mL) to achieve a precatalyst concentration of 0.00075 M during the polymerization. For each precatalyst, a flask was prepared with **3** (0.14 mL of a 0.33 M solution in THF, 0.045 mmol, 30 equiv) or without. The flasks were sealed with a rubber septum before removing from the glovebox and placed under N<sub>2</sub>. Previously prepared **1** (0.65 mL of a 0.12 M solution in THF, 0.81 mmol, 54 equiv) was added to initiate the polymerization. The reaction was quenched after 30 min by adding conc. HCl (~2 mL).

**4a, 4b, and 4e.** Precatalyst was weighed (~4 mg) into 20 mL vials equipped with a stir bar and diluted with THF (~6 mL) to achieve a precatalyst concentration of 0.00075 M during the polymerization. For each precatalyst, a vial was prepared with **3** (~0.3 mL of a 0.13 M solution in THF, 30 equiv) or without. Previously prepared **1** (~1 mL of a 0.12 M solution in THF, 0.81 mmol, 54 equiv) was added to initiate the polymerization. The reaction was quenched after 30 min by adding conc. HCl (~2 mL).

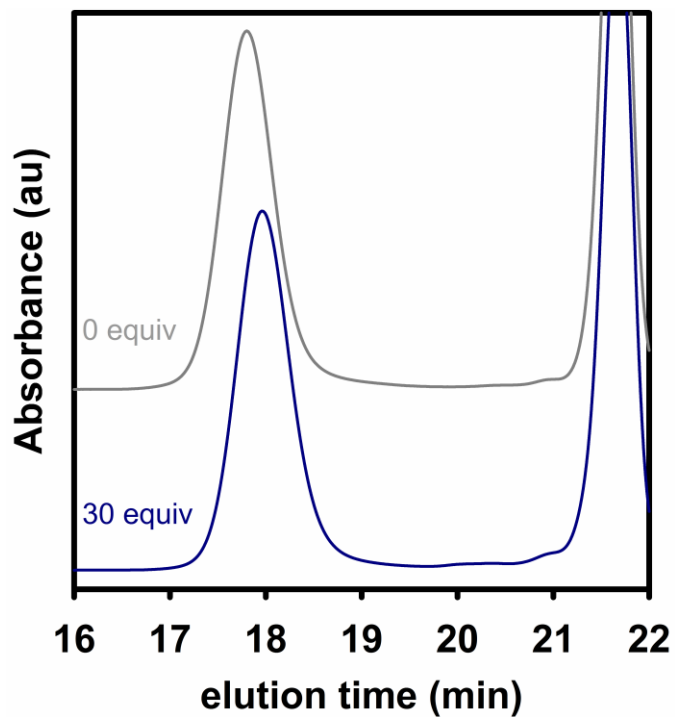
All quenched reactions were extracted with CHCl<sub>3</sub> (3 x 1 mL) with heating using a heat gun. The combined organic layers were washed with H<sub>2</sub>O (1 x 2 mL) and brine (1 x 2 mL). The solvent was then removed via rotary evaporation and the solids were re-dissolved with heating in THF (~10 mL). After cooling to rt, MgSO<sub>4</sub> (~10 mg) was added and the mixture was filtered through a PTFE syringe filter (0.2 μm). A small portion was removed for GC and GPC analysis, and the remaining liquid was removed using a rotary evaporator to yield a purple solid. The solid was dissolved in minimal CHCl<sub>3</sub> (~0.2 mL), and then precipitated into MeOH (10 mL) in a centrifuge

tube and centrifuged at 4500 rpm for 30 min. The supernatant was decanted and the solid polymer was dried under high vacuum for 4 h.

The solids (~2 mg) were dissolved in  $\text{CDCl}_3$  (2 mL) and analyzed by  $^1\text{H}$  NMR spectroscopy. Next, the NMR solutions were filtered through a pipette column (basic, acidic, then neutral alumina with a KimWipe plug) and rinsed with  $\text{CHCl}_3$  (~0.5 mL). The resultant polymer solution (2.5  $\mu\text{L}$ ) was mixed with DCTB matrix (2.5  $\mu\text{L}$  of a 0.1 M solution in  $\text{CHCl}_3$ ) in an Eppendorf tube. The polymer/matrix solution (~1.5  $\mu\text{L}$ ) was spotted onto the MALDI 96-well target, and the remaining solution in the Eppendorf tube was diluted five-fold with additional DCTB matrix (2.5  $\mu\text{L}$  of a 0.1 M solution in  $\text{CHCl}_3$ ). The diluted sample was spotted onto the MALDI target in the same manner, and further five-fold dilutions (with DCTB matrix solution) were performed and spotted to yield four spots for each polymer sample.



Precatalyst **4a**

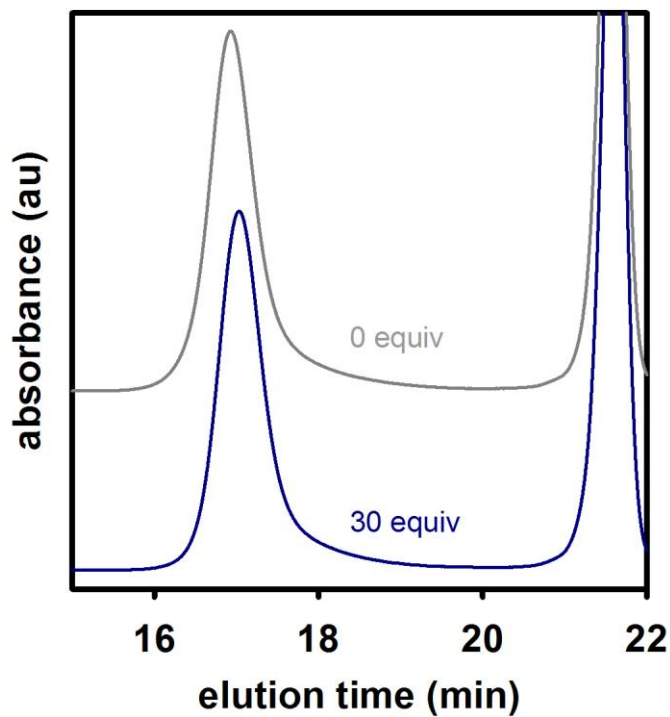


**Figure A1-3.** GPC chromatogram (prior to precipitation) of **P3DT** produced by **4a** with 0 (—) or 30 equiv (—) of **3**.

<b>Equiv of 3</b>	<b>Conversion of 1 (%)<sup>a</sup></b>	<b><math>M_n</math> (kDa)<sup>b</sup></b>	<b><math>\bar{D}^b</math></b>	<b>Br/H end-groups (%)<sup>c</sup></b>
0	94.6	12.8	1.16	92
30	92.5	10.5	1.12	87

**Table A1-2.** Data for **P3DT** produced by **4a** with 0 or 30 equiv of **3**. <sup>a</sup>Determined by GC analysis. <sup>b</sup>Determined by GPC analysis. <sup>c</sup>Calculated from the average peak area ratios (at each DP) from the five most intense peaks observed by MALDI-TOF MS analysis.

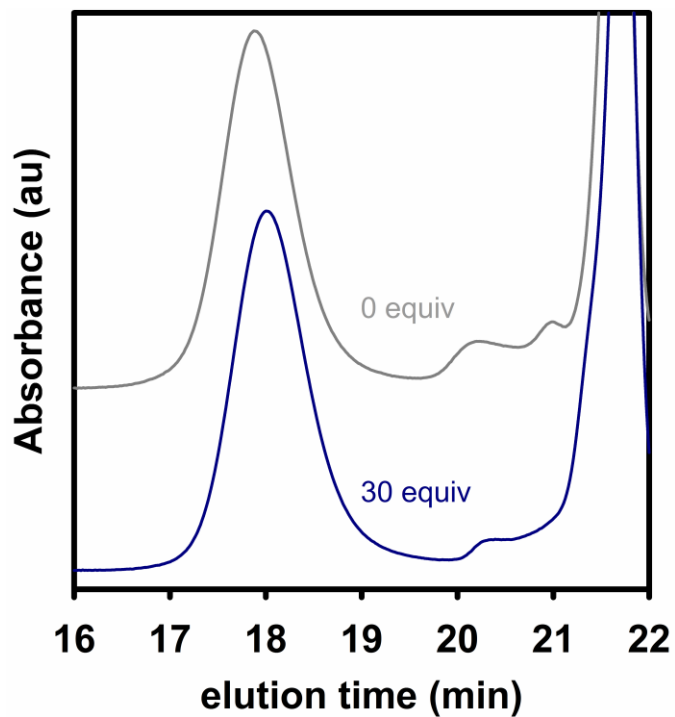
Precatalyst **4b**



**Figure A1-4.** GPC chromatogram (prior to precipitation) of **P3DT** produced by **4b** with 0 (—) or 30 equiv (—) of **3**.

<b>Equiv of 3</b>	<b>Conversion of 1 (%)<sup>a</sup></b>	<b><math>M_n</math> (kDa)<sup>b</sup></b>	<b><math>\mathcal{D}^b</math></b>	<b>Br/H end-groups (%)<sup>c</sup></b>
0	95.2	22.6	1.31	85
30	94.7	20.8	1.30	81

**Table A1-3.** Data for **P3DT** produced by **4b** with 0 or 30 equiv of **3**. <sup>a</sup>Determined by GC analysis. <sup>b</sup>Determined by GPC analysis. <sup>c</sup>Calculated from the average peak area ratios (at each DP) from the five most intense peaks observed by MALDI-TOF MS analysis.

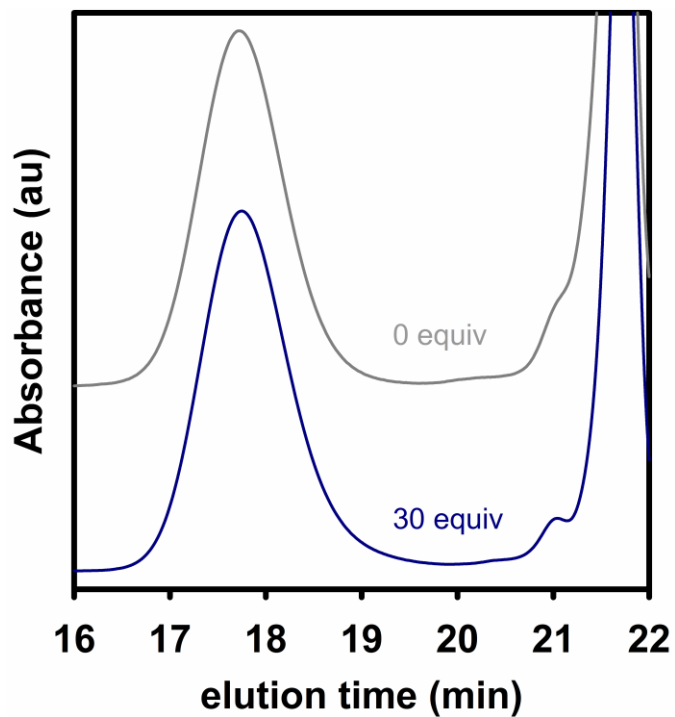


**Figure A1-5.** GPC chromatogram (prior to precipitation) of **P3DT** produced by **4c** with 0 (—) or 30 equiv (—) of **3**.

<b>Equiv of 3</b>	<b>Conversion of 1 (%)<sup>a</sup></b>	<b><math>M_n</math> (kDa)<sup>b</sup></b>	<b><math>\bar{D}^b</math></b>	<b>Br/H end-groups (%)<sup>c</sup></b>
0	> 98	11.8	1.19	70
30	> 98	10.1	1.22	65

**Table A1-4.** Data for **P3DT** produced by **4c** with 0 or 30 equiv of **3**. <sup>a</sup>Determined by GC analysis. <sup>b</sup>Determined by GPC analysis. <sup>c</sup>Calculated from the average peak area ratios (at each DP) from the five most intense peaks observed by MALDI-TOF MS analysis.

Precatalyst **4d**

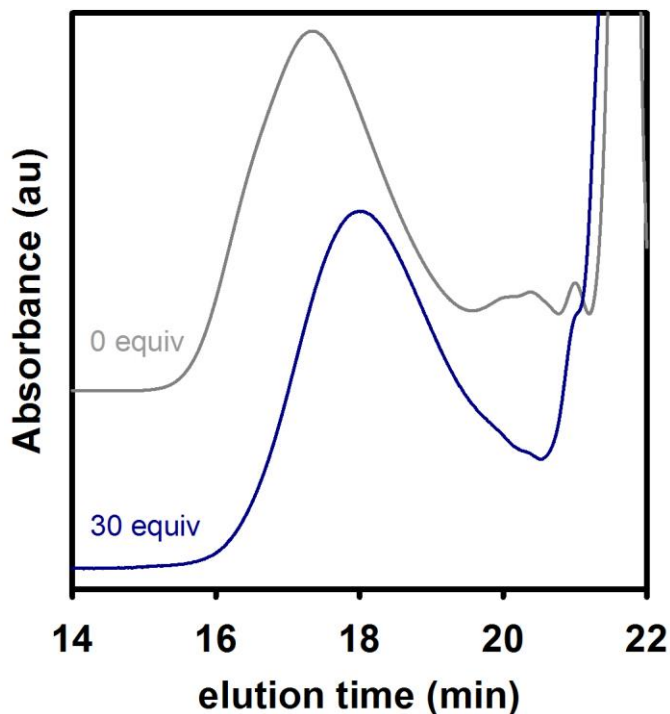


**Figure A1-6.** GPC chromatogram (prior to precipitation) of **P3DT** produced by **4d** with 0 (—) or 30 equiv (—) of **3**.

<b>Equiv of 3</b>	<b>Conversion of 1 (%)<sup>a</sup></b>	<b><math>M_n</math> (kDa)<sup>b</sup></b>	<b><math>\mathcal{D}^b</math></b>	<b>Br/H end-groups (%)<sup>c</sup></b>
0	95.4	14.1	1.23	66
30	86.9	16.1	1.26	82

**Table A1-5.** Data for **P3DT** produced by **4d** with 0 or 30 equiv of **3**. <sup>a</sup>Determined by GC analysis. <sup>b</sup>Determined by GPC analysis. <sup>c</sup>Calculated from the average peak area ratios (at each DP) from the five most intense peaks observed by MALDI-TOF MS analysis.

Precatalyst **4e**

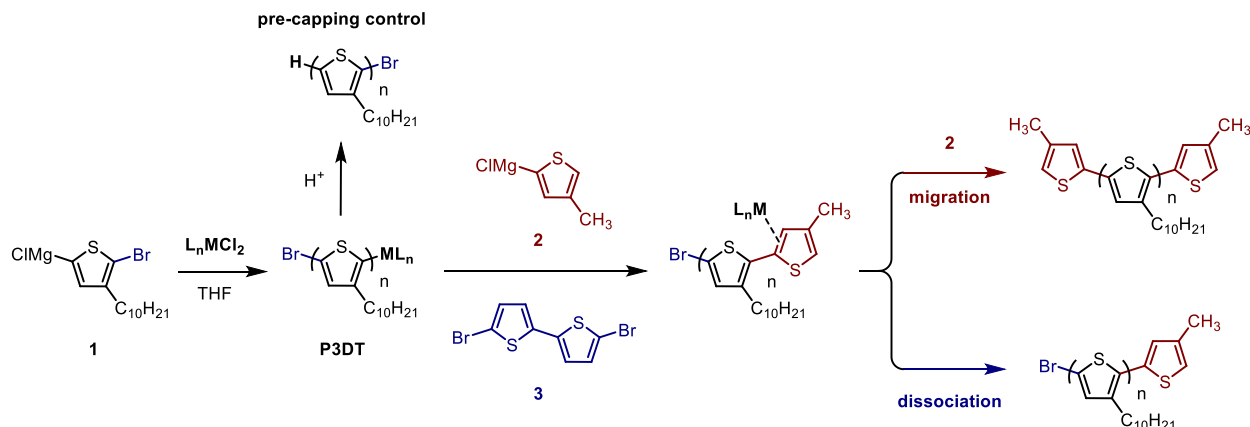


**Figure A1-7.** GPC chromatogram (prior to precipitation) of **P3DT** produced by **4e** with 0 (—) or 30 equiv (—) of **3**.

<b>Equiv of 3</b>	<b>Conversion of 1 (%)<sup>a</sup></b>	<b><math>M_n</math> (kDa)<sup>b</sup></b>	<b><math>\mathcal{D}^b</math></b>	<b>Br/H end-groups (%)<sup>c</sup></b>
0	78	6.0	3.83	33
30	83	5.4	2.52	28

**Table A1-6.** Data for **P3DT** produced by **4e** with 0 or 30 equiv of **3**. <sup>a</sup>Determined by GC analysis. <sup>b</sup>Determined by GPC analysis. <sup>c</sup>Calculated from the average peak area ratios (at each DP) from the five most intense peaks observed by MALDI-TOF MS analysis. The major end-group for both conditions was Br/Br.

## VII. End-capping model experiments



### Representative procedure for end-capping P3DT.

#### *Polymerization (on Schlenk line)*

**4c and 4d.** In a glovebox, precatalyst from a stock solution (~0.10 mL of a ~0.015 M solution in THF, 0.0015 mmol, 1.0 equiv) was added to a 10 mL Schleck flask equipped with a stir bar and diluted with THF (~1.2 mL) to achieve a precatalyst concentration of 0.00075 M during the polymerization. The flasks were sealed with a rubber septum before removing from the glovebox and placed under  $\text{N}_2$ . Previously prepared **1** (0.65 mL of a 0.12 M solution in THF, 0.81 mmol, 54 equiv) was added to initiate the polymerization.

#### *End-capping (on Schlenk line)*

After 30 minutes, an aliquot of the polymerization solution (1.0 mL, 0.00075 mmol catalyst, 1.0 equiv) was transferred to a 25 mL Schlenk tube containing **2** (0.051 mL of a 0.22 M solution in THF/ $\text{Et}_2\text{O}$ , 0.011 mmol, 15 equiv) and **3** (0.135 mL of a 0.17 M solution in THF, 0.023 mmol, 30 equiv) with stirring. The remaining polymerization solution was quenched with conc. HCl (~1 mL) immediately after the aliquot was drawn. After 1 h of end-capping, the solution was quenched by adding conc. HCl (~1 mL).

### *Polymerization (in a glovebox)*

**4a**, **4b**, and **4e**. Precatalyst was weighed (~4 mg) into 20 mL vials equipped with a stir bar and diluted with THF (~6 mL) to achieve a precatalyst concentration of 0.00075 M during the polymerization. Previously prepared **1** (~1 mL of a 0.12 M solution in THF, 0.81 mmol, 54 equiv) was added to initiate the polymerization.

### *End-capping*

After 30 minutes, an aliquot of the polymerization solution (1.0 mL, 0.00075 mmol catalyst, 1.0 equiv) was transferred to a 4 mL vial containing **2** (0.051 mL of a 0.22 M solution in THF/Et<sub>2</sub>O, 0.011 mmol, 15 equiv) and **3** (0.135 mL of a 0.17 M solution in THF, 0.023 mmol, 30 equiv) with stirring. The remaining polymerization solution was removed from the glovebox and quenched with conc. HCl (~1 mL) immediately after the aliquot was drawn. After 1 h of end-capping, the solution was removed from the glovebox and quenched by adding conc. HCl (~1 mL).

All quenched reactions were extracted with CHCl<sub>3</sub> (3 x 1 mL) with heating using a heat gun. The combined organic layers were washed with H<sub>2</sub>O (1 x 2 mL) and brine (1 x 2 mL). The solvent was then removed via rotary evaporation and the solids were re-dissolved with heating in THF (~10 mL). After cooling to rt, MgSO<sub>4</sub> (~10 mg) was added and the mixture was filtered through a PTFE syringe filter (0.2 μm). A small portion was removed for GC and GPC analysis, and the remaining liquid was removed using a rotary evaporator to yield a purple solid. The solid was dissolved in minimal CHCl<sub>3</sub> (~0.2 mL), and then precipitated into MeOH (10 mL) in a centrifuge tube and centrifuged at 4500 rpm for 30 min. The supernatant was decanted and the solid polymer was dried under high vacuum for 4 h.

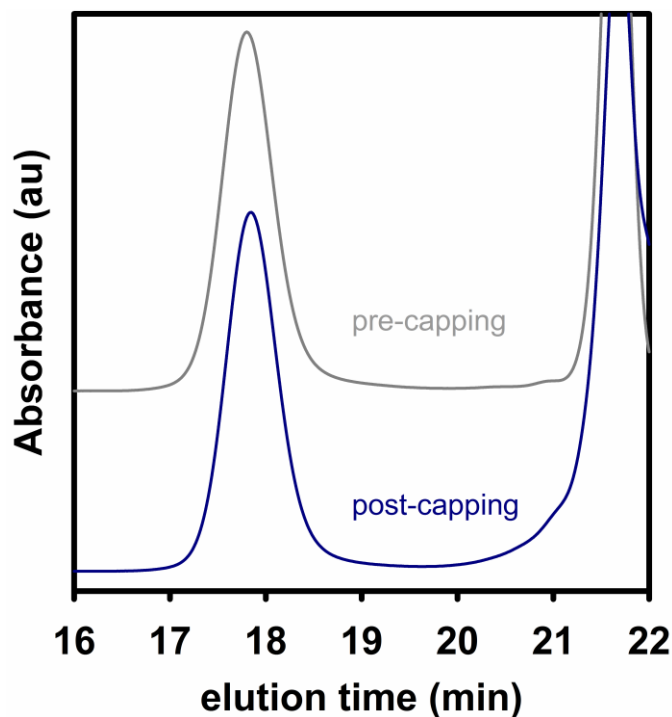
The solids (~2 mg) were dissolved in CDCl<sub>3</sub> (2 mL) and analyzed by <sup>1</sup>H NMR spectroscopy. Next, the NMR solutions were filtered through a pipette column (basic, acidic, then neutral alumina with a KimWipe plug) and rinsed with CHCl<sub>3</sub> (~0.5 mL). The resultant polymer solution (2.5 μL) was mixed with DCTB matrix (2.5 μL of a 0.1 M solution in CHCl<sub>3</sub>) in an Eppendorf tube. The polymer/matrix solution (~1.5 μL) was spotted onto the MALDI 96-well target, and the remaining solution in the Eppendorf tube was diluted five-fold with additional DCTB matrix (2.5 μL of a 0.1

M solution in  $\text{CHCl}_3$ ). The diluted sample was spotted onto the MALDI target in the same manner, and further five-fold dilutions (with DCTB matrix solution) were performed and spotted to yield four spots for each polymer sample.



## Representative analysis

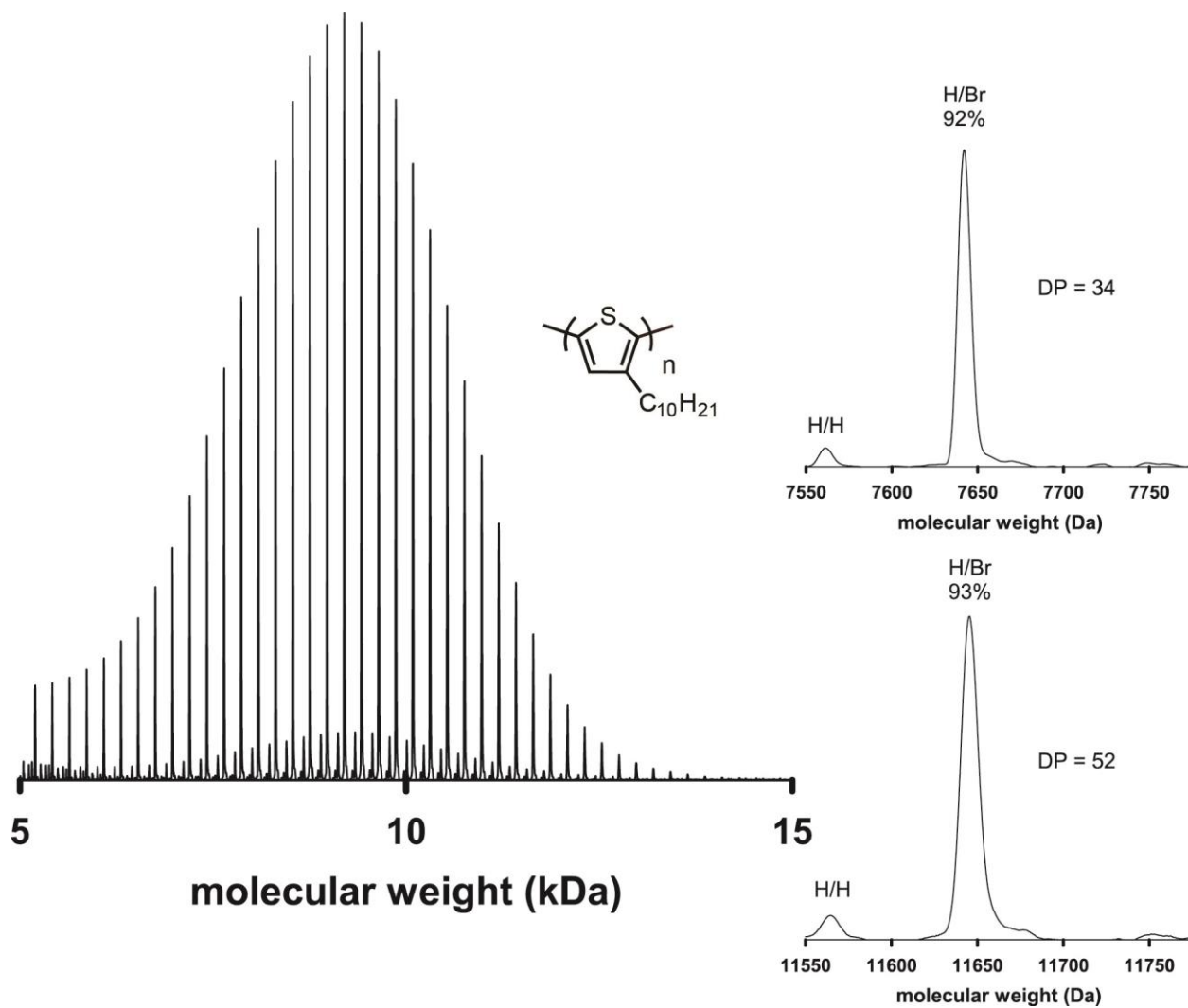
### Precatalyst **4a**



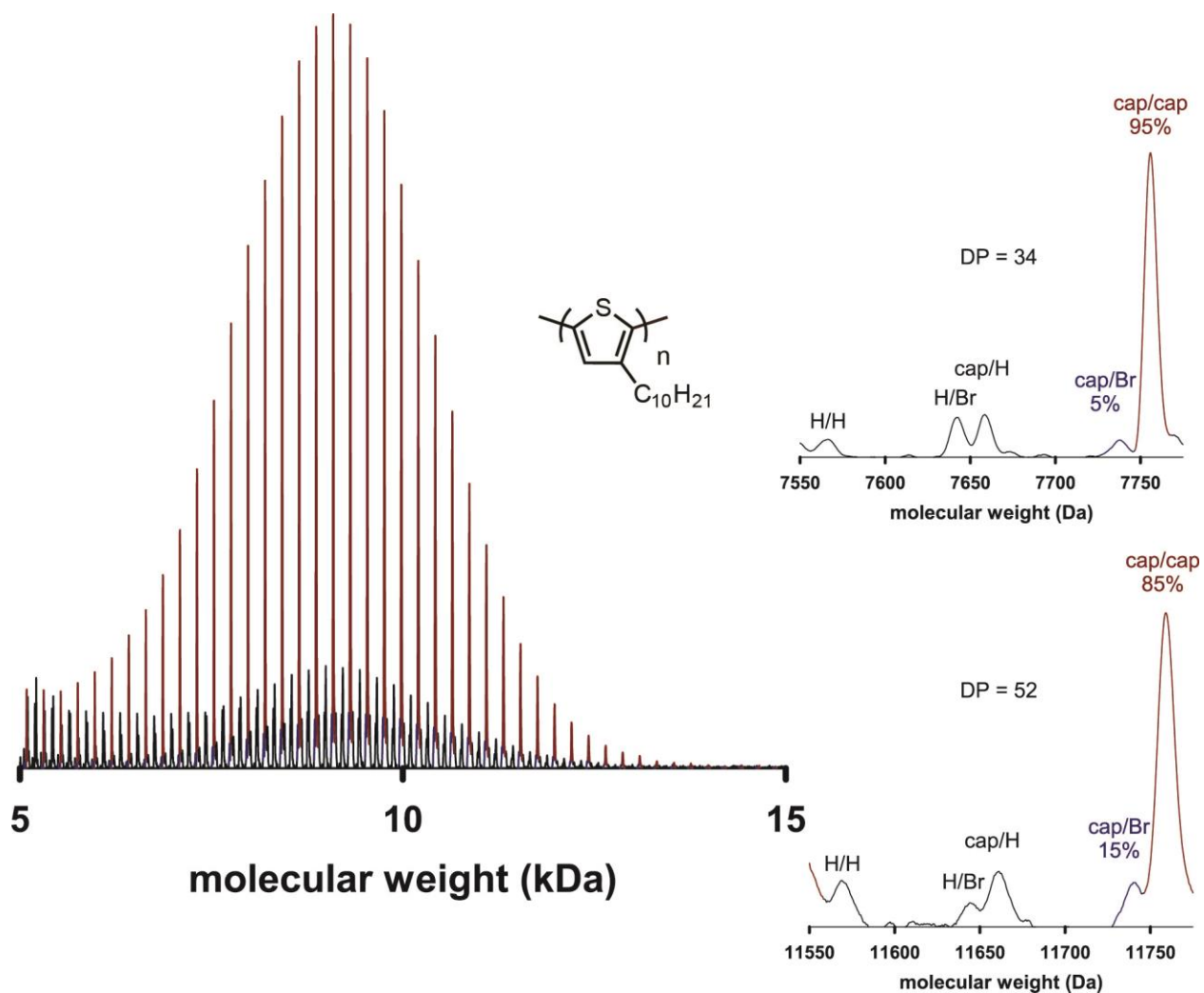
**Figure A1-8.** GPC chromatogram of **P3DT** produced by **4a** pre (—) or post (—) end-capping with **2** (15 equiv) and **3** (30 equiv).

Condition	Conversion of <b>1</b> (%) <sup>a</sup>	$M_n$ (kDa) <sup>b</sup>	$\bar{D}$ <sup>b</sup>	End-groups (%) <sup>c</sup>
pre-capping	95	12.8	1.16	92 (Br/H)
post-capping	96	12.2	1.15	91 (cap/cap)

**Table A1-7.** Data for **P3DT** produced by **4a** pre or post end-capping with **2** (15 equiv) and **3** (30 equiv). <sup>a</sup>Determined by GC analysis. <sup>b</sup>Determined by GPC analysis. <sup>c</sup>Calculated from the average peak area ratios (at each DP) from the five most intense peaks observed by MALDI-TOF MS analysis.



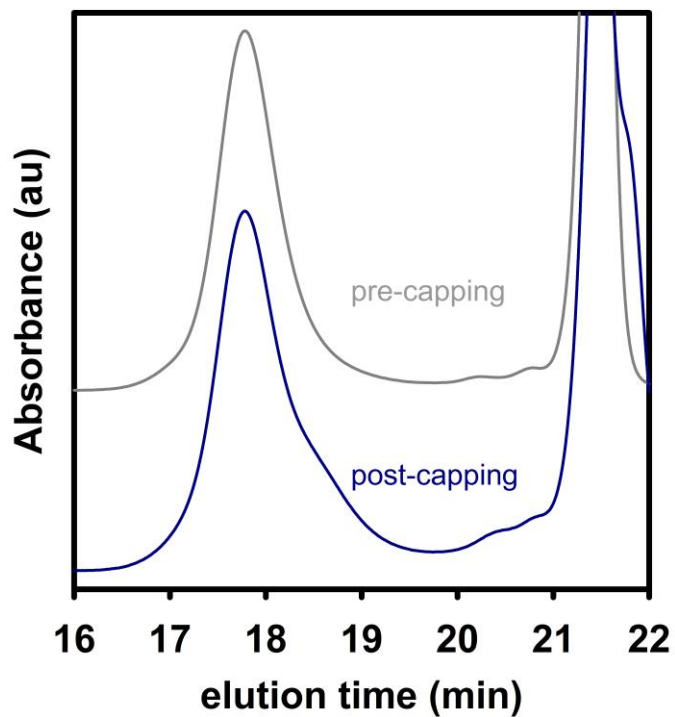
**Figure A1-9.** MALDI-TOF mass spectra of **P3DT** produced by **4a** pre end-capping (—). Insets (right) show **P3DT** end-groups at DP = 34 (top) and DP = 52 (bottom).



**Figure A1-10.** MALDI-TOF mass spectra of **P3DT** produced by **4a** post end-capping with **2** (15 equiv) and **3** (30 equiv). Migration (cap/cap, —) and dissociation (cap/Br, —) product peaks are highlighted from all other masses ( — ). Insets (right) show **P3DT** end-groups at DP = 34 (top) and DP = 52 (bottom).

m/z of migration product (Da)	DP	Catalyst migration (%)					
		Run 1	Run 2	Run 3	Run 4	Avg.	SD
5532	24				98		
5754	25				98		
5976	26				98		
6199	27				98		
6421	28				97		
6644	29				97		
6866	30			94	97	96	2
7088	31			95	97	96	2
7311	32			95	97	96	2
7533	33			95	96	96	1
7756	34			95	96	96	1
7978	35			94	96	95	1
8200	36		95	94	96	95	1
8423	37	94	95	94	95	95	1
8645	38	94	95	94	95	94	1
8868	39	93	96	93	94	94	1
9090	40	93	95	93	93	94	1
9312	41	92	95	93		93	1
9535	42	93	94	93		93	1
9757	43	92	94	92		93	1
9979	44	92	93	92		92	1
10202	45	90	93	91		92	1
10424	46	90	93	91		91	1
10647	47	90	93	90		91	2
10869	48	90	94	89		91	2
11091	49	91	94	89		91	2
11314	50	90		88		89	1
11536	51			88			
11759	52			85			

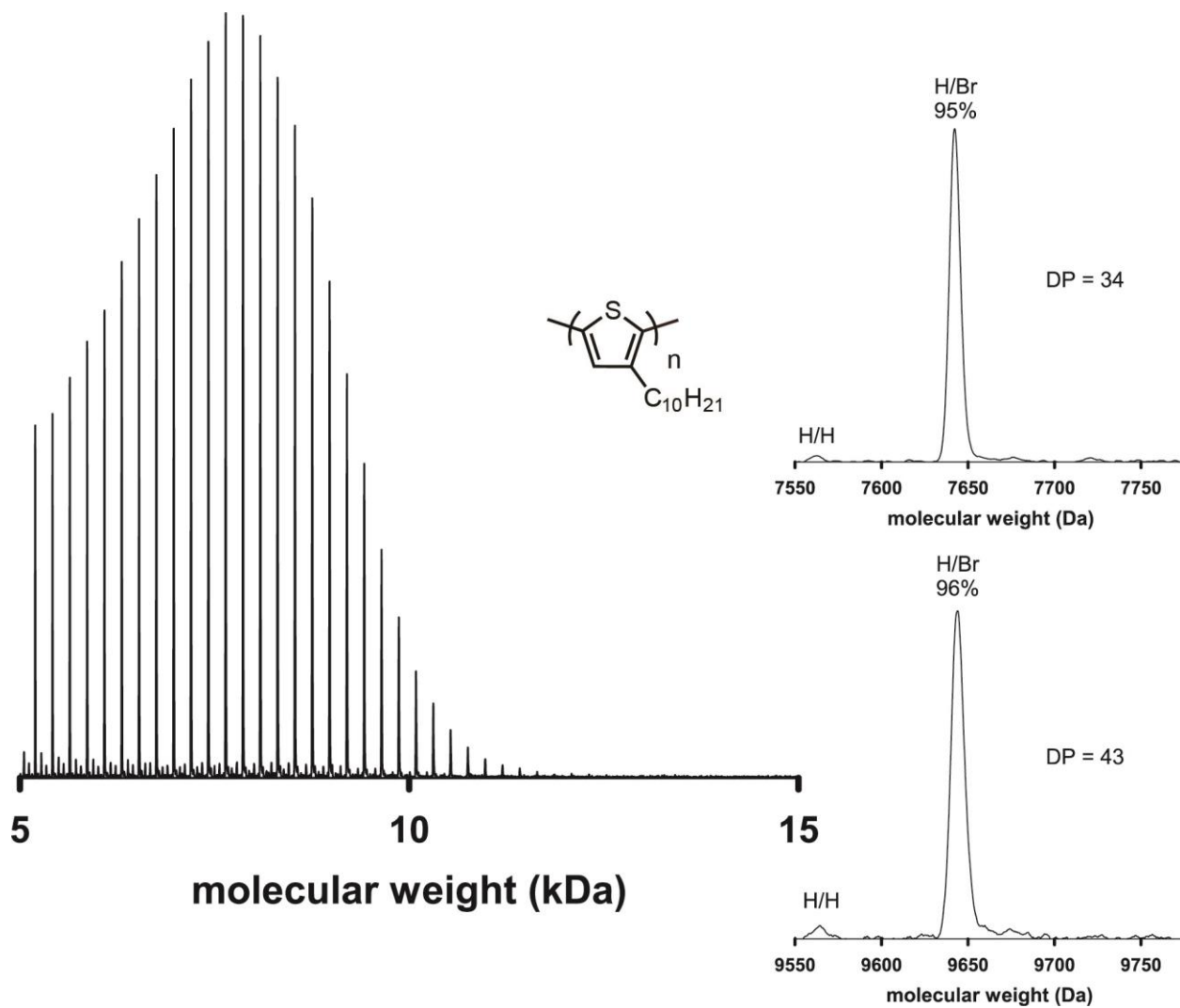
**Table A1-8.** Catalyst migration values for **4a** from Run 1–4. Avg and STD values are plotted in Figure A1-23.



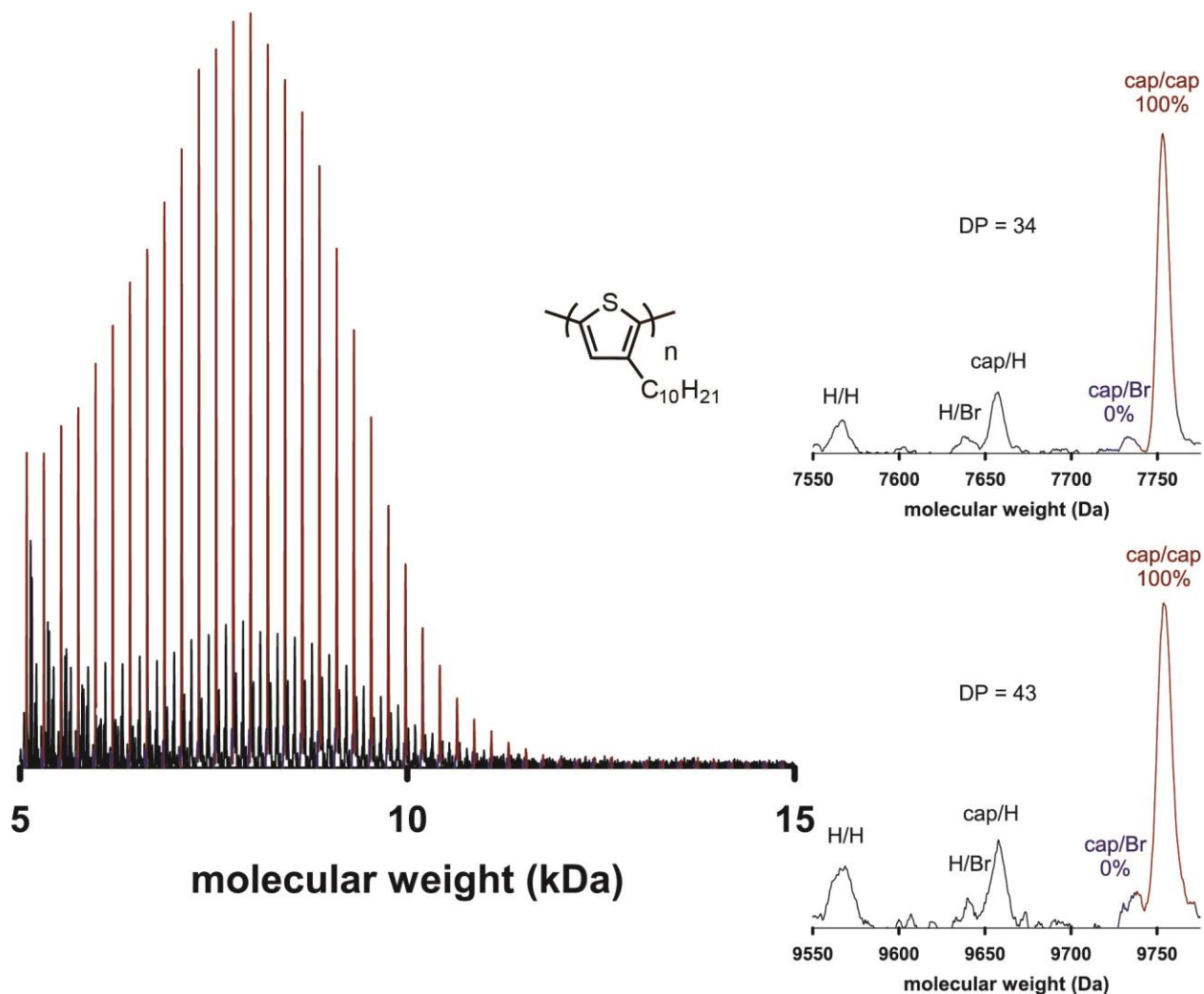
**Figure A1-11.** GPC chromatogram of **P3DT** produced by **4b** pre (—) or post (—) end-capping with **2** (15 equiv) and **3** (30 equiv).

Condition	Conversion of <b>1</b> (%) <sup>a</sup>	$M_n$ (kDa) <sup>b</sup>	$\bar{D}^b$	End-groups (%) <sup>c</sup>
pre-capping	> 98	10.5	1.22	95 (Br/H)
post-capping	> 98	9.5	1.26	100 (cap/cap)

**Table A1-9.** Data for **P3DT** produced by **4b** pre or post end-capping with **2** (15 equiv) and **3** (30 equiv). <sup>a</sup>Determined by GC analysis. <sup>b</sup>Determined by GPC analysis. <sup>c</sup>Calculated from the average peak area ratios (at each DP) from the five most intense peaks observed by MALDI-TOF MS analysis.



**Figure A1-12.** MALDI-TOF mass spectra of **P3DT** produced by **4b** pre end-capping (—). Insets (right) show **P3DT** end-groups at DP = 34 (top) and DP = 43 (bottom).



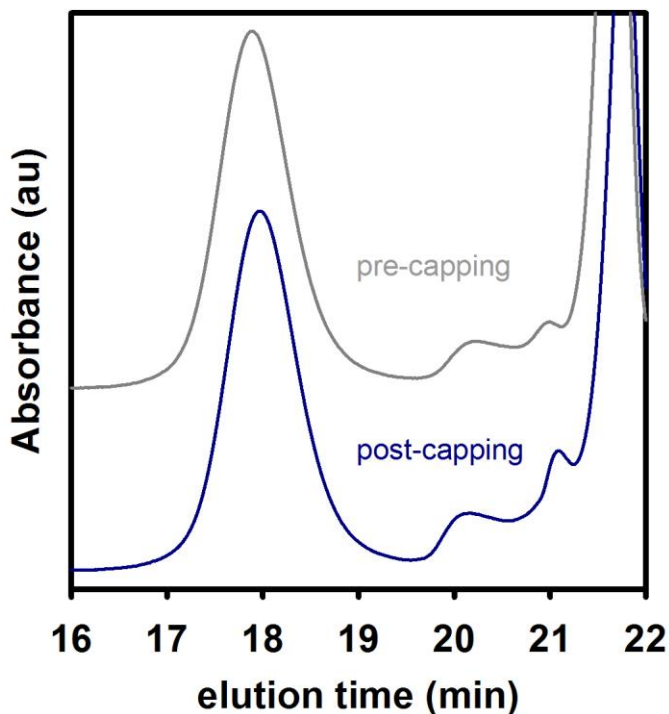
**Figure A1-13.** MALDI-TOF mass spectra of **P3DT** produced by **4b** post end-capping with **2** (15 equiv) and **3** (30 equiv). Migration (cap/cap, —) and dissociation (cap/Br, —) product peaks are highlighted from all other masses (—). Insets (right) show **P3DT** end-groups at DP = 34 (top) and DP = 43 (bottom).

m/z of migration product (Da)	DP	Catalyst migration (%)					
		Run 1	Run 2	Run 3	Run 4	Avg.	SD
5532	24			100	100	100	0
5754	25			100	100	100	0
5976	26			100	100	100	0
6199	27			100	100	100	0
6421	28			100	100	100	0
6644	29			100	100	100	0
6866	30			100	100	100	0
7088	31			100	100	100	0
7311	32			100	100	100	0
7533	33			100	100	100	0
7756	34		100	100	100	100	0
7978	35		100	100	100	100	0
8200	36		100	100	100	100	0
8423	37		100	100	100	100	0
8645	38		100	100	100	100	0
8868	39		100	100	100	100	0
9090	40		100	100	100	100	0
9312	41		100	100		100	0
9535	42		100	100		100	0
9757	43	95	100	100		98	3
9979	44	100	100			100	0
10202	45	96	100			98	3
10424	46	94	100			97	5
10647	47	94	100			97	4
10869	48	96	100			98	3
11091	49	95	100			97	4
11314	50	94	100			97	4
11536	51		100				
11759	52		100				
11981	53		100				
12203	54		100				
12426	55		100				
12648	56		100				
12871	57		100				
13093	58		100				
13315	59		100				
13538	60		100				
13760	61		100				
13982	62		100				
14205	63		100				
14427	64		100				



14650	65		100				
14872	66		100				
15094	67		100				
15317	68		100				

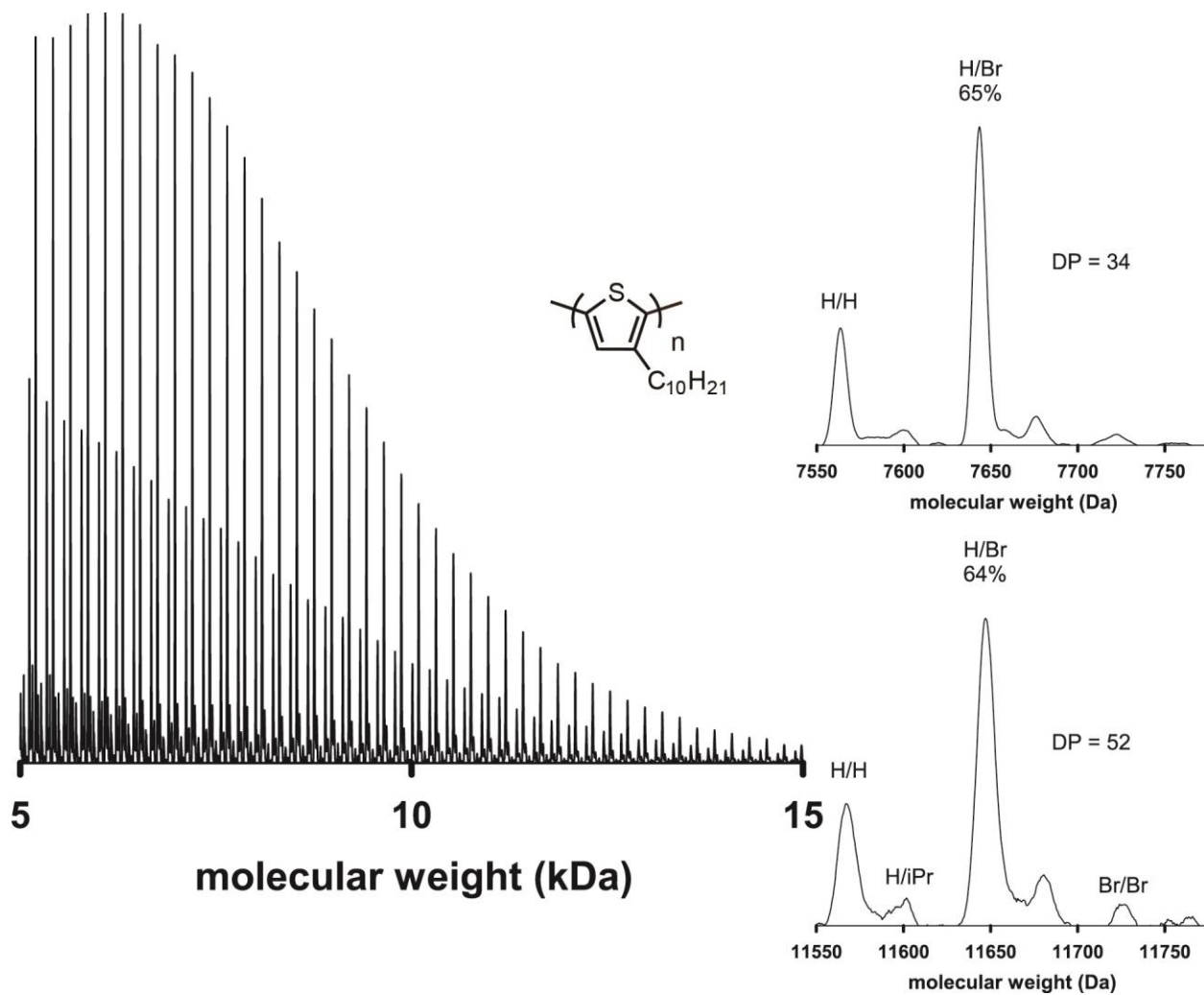
**Table A1-10.** Catalyst migration values for **4b** from Run 1–4. Avg and STD values are plotted in Figure A1-23.



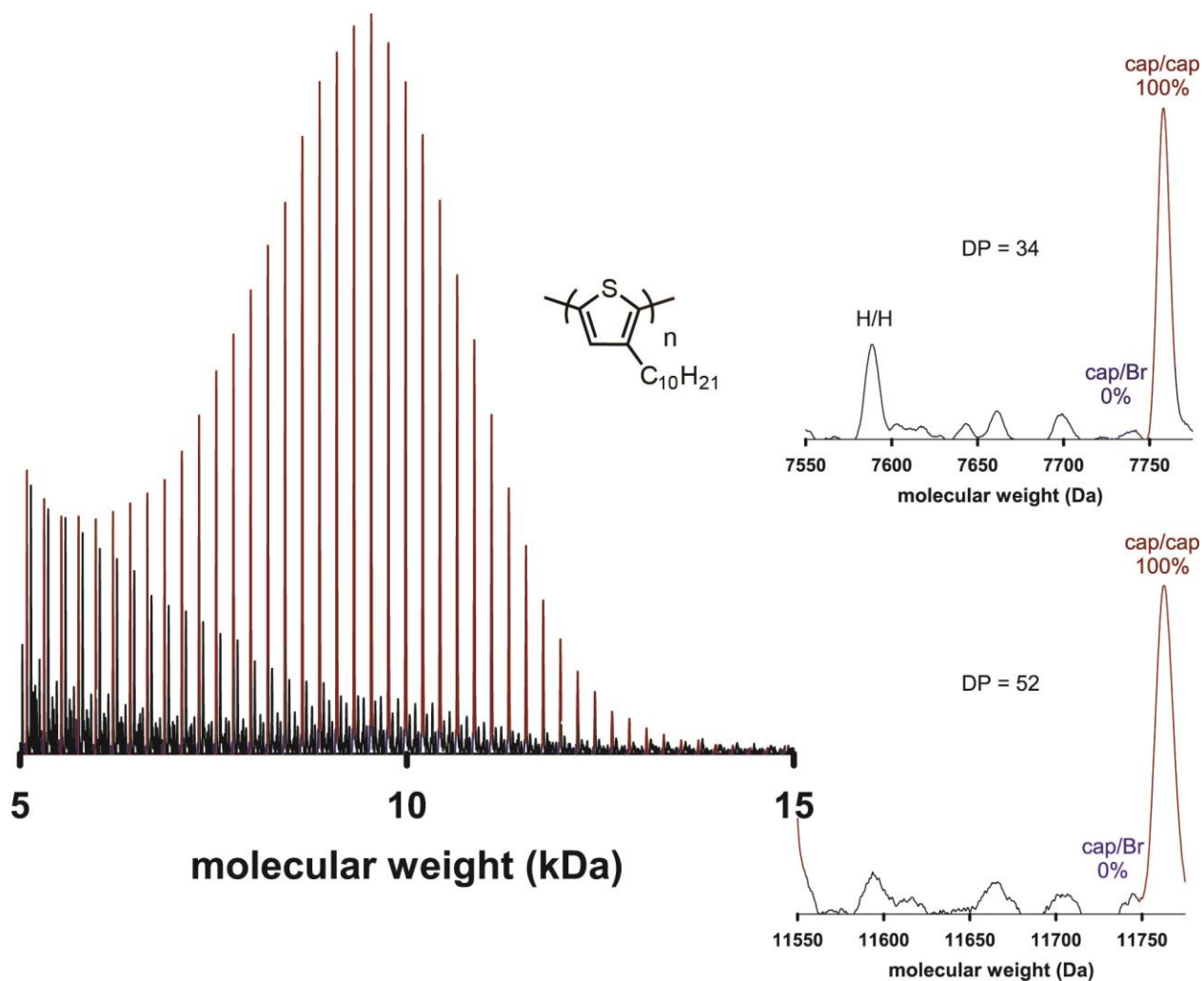
**Figure A1-14.** GPC chromatogram of **P3DT** produced by **4c** pre (—) or post (—) end-capping with **2** (15 equiv) and **3** (30 equiv).

Condition	Conversion of <b>1</b> (%) <sup>a</sup>	$M_n$ (kDa) <sup>b</sup>	$\bar{D}$ <sup>b</sup>	End-groups (%) <sup>c</sup>
pre-capping	> 98	11.8	1.19	65 (Br/H)
post-capping	> 98	12.1	1.22	93 (cap/cap)

**Table A1-11.** Data for **P3DT** produced by **4c** pre or post end-capping with **2** (15 equiv) and **3** (30 equiv). <sup>a</sup>Determined by GC analysis. <sup>b</sup>Determined by GPC analysis. <sup>c</sup>Calculated from the average peak area ratios (at each DP) from the five most intense peaks observed by MALDI-TOF MS analysis.



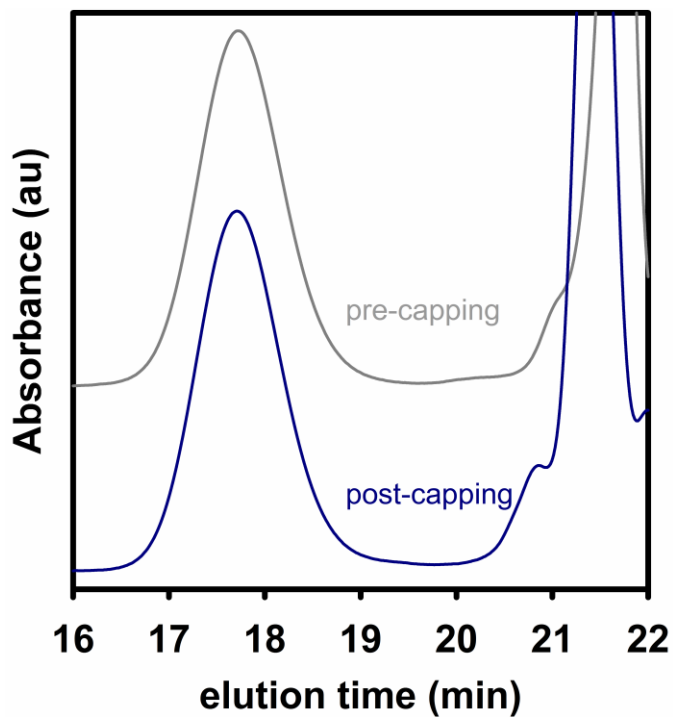
**Figure A1-15.** MALDI-TOF mass spectra of **P3DT** produced by **4c** pre end-capping (—). Insets (right) show **P3DT** end-groups at DP = 34 (top) and DP = 52 (bottom).



**Figure A1-16.** MALDI-TOF mass spectra of **P3DT** produced by **4c** post end-capping with **2** (15 equiv) and **3** (30 equiv). Migration (cap/cap, —) and dissociation (cap/Br, —) product peaks are highlighted from all other masses (—). Insets (right) show **P3DT** end-groups at DP = 34 (top) and DP = 52 (bottom).

m/z of migration product (Da)	DP	Catalyst migration (%)		
		Run 1	Avg.	SD
8868	39	100	100	N/A
9090	40	100	100	N/A
9312	41	100	100	N/A
9535	42	100	100	N/A
9757	43	100	100	N/A
9979	44	100	100	N/A
10202	45	100	100	N/A
10424	46	100	100	N/A
10647	47	100	100	N/A
10869	48	100	100	N/A
11091	49	100	100	N/A
11314	50	100	100	N/A
11536	51	100	100	N/A
11759	52	100	100	N/A
11981	53	100	100	N/A
12203	54	100	100	N/A
12426	55	100	100	N/A

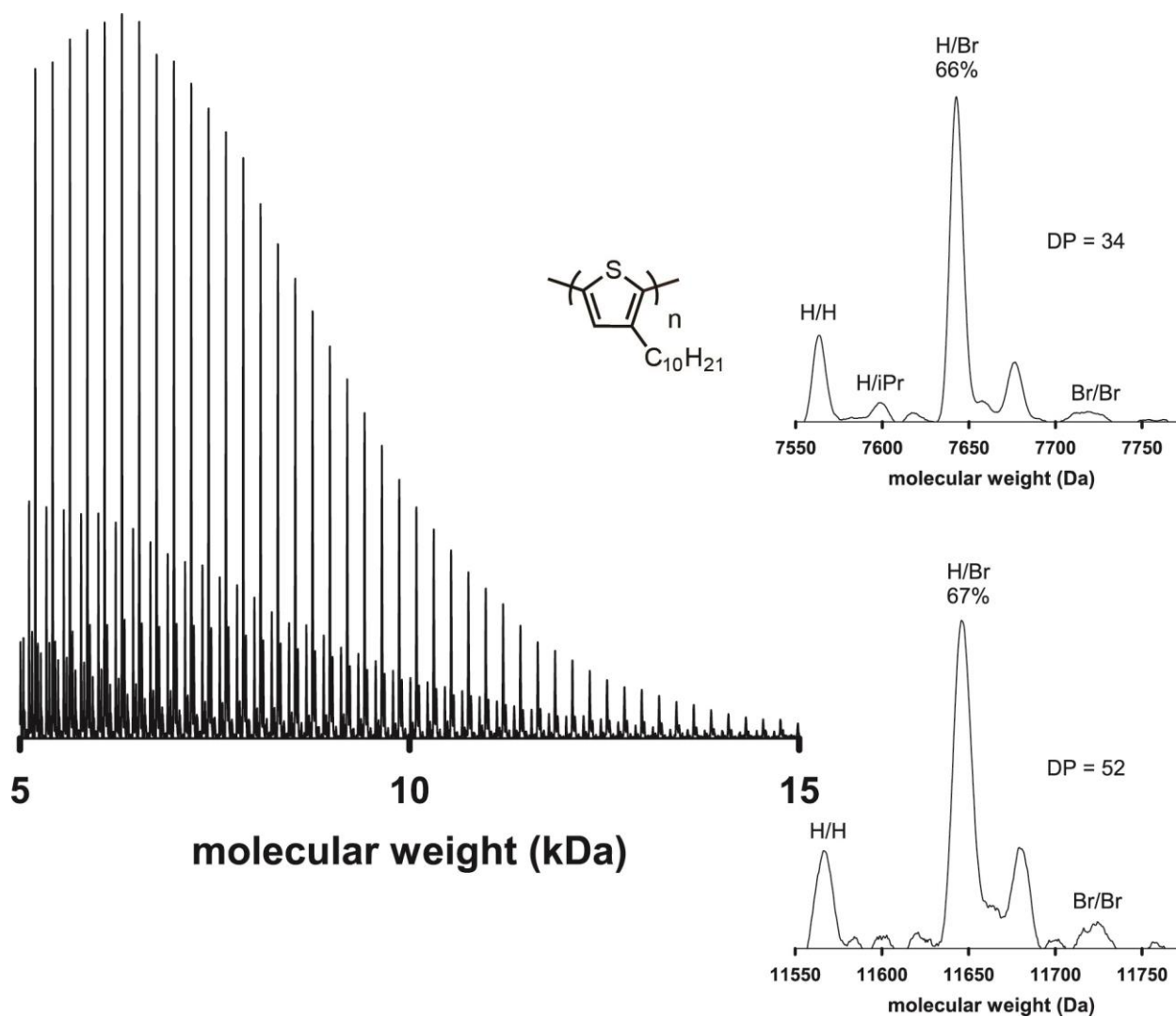
**Table A1-12.** Catalyst migration values for **4c** from Run 1. Avg and STD values are plotted in Figure A1-23.



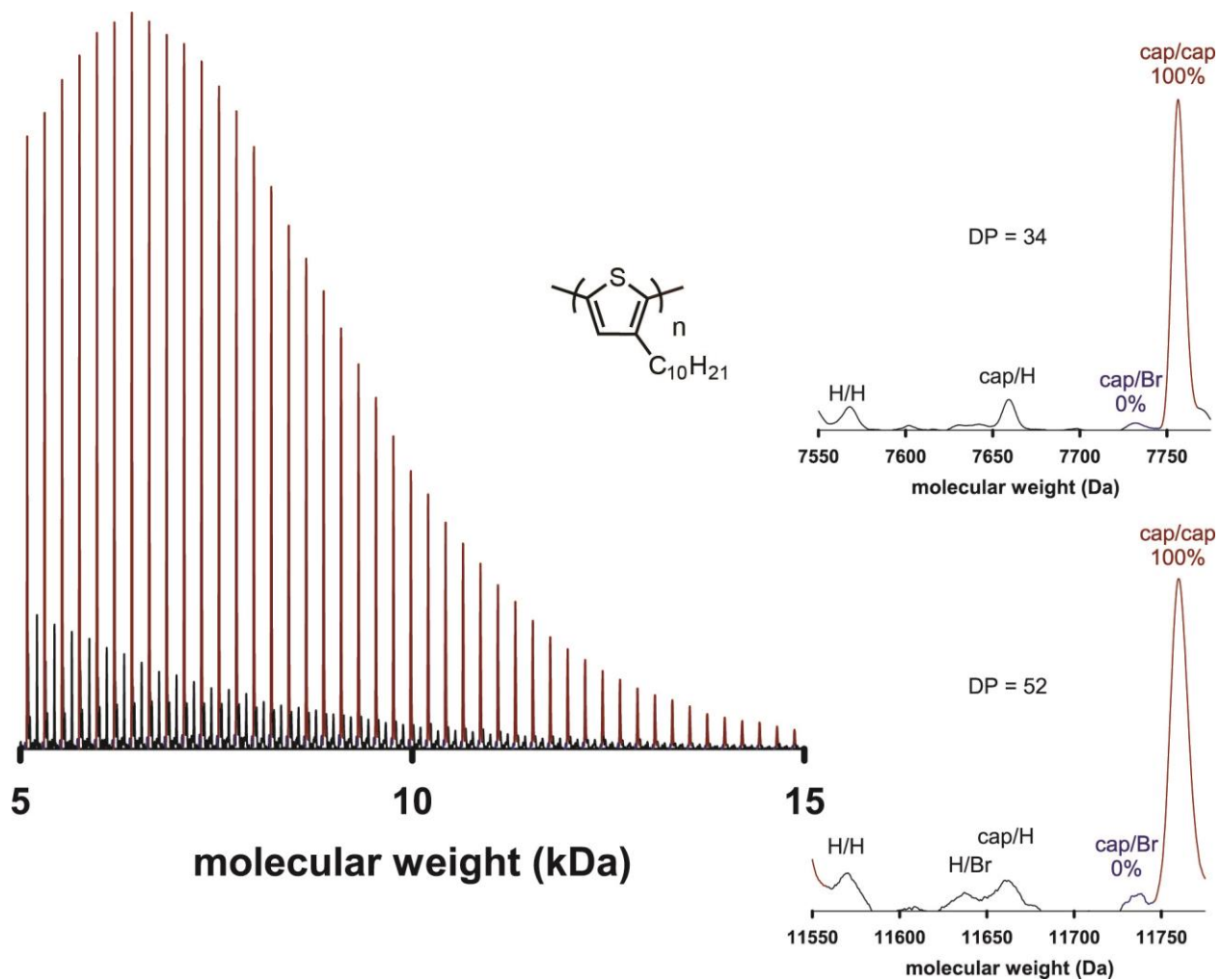
**Figure A1-17.** GPC chromatogram of **P3DT** produced by **4d** pre (—) or post (—) end-capping with **2** (15 equiv) and **3** (30 equiv).

Condition	Conversion of <b>1</b> (%) <sup>a</sup>	$M_n$ (kDa) <sup>b</sup>	$\bar{D}$ <sup>b</sup>	Br/H end-groups (%) <sup>c</sup>
pre-capping	95	14.1	1.23	66 (Br/H)
post-capping	98	13.6	1.23	100 (cap/cap)

**Table A1-13.** Data for **P3DT** produced by **4d** pre or post end-capping with **2** (15 equiv) and **3** (30 equiv). <sup>a</sup>Determined by GC analysis. <sup>b</sup>Determined by GPC analysis. <sup>c</sup>Calculated from the average peak area ratios (at each DP) from the five most intense peaks observed by MALDI-TOF MS analysis.



**Figure A1-18.** MALDI-TOF mass spectra of **P3DT** produced by **4d** pre end-capping (—). Insets (right) show **P3DT** end-groups at DP = 34 (top) and DP = 52 (bottom).

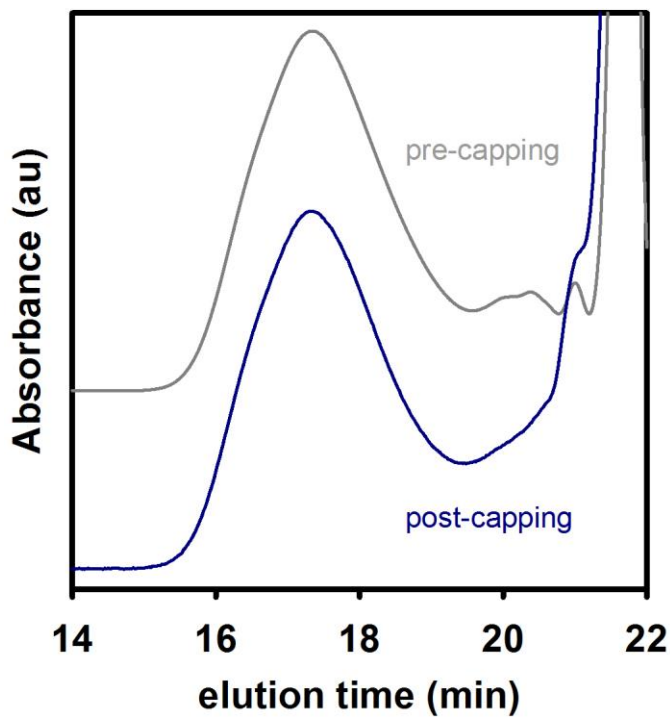


**Figure A1-19.** MALDI-TOF mass spectra of **P3DT** from end-capping model system using **4d**. Migration (cap/cap, —) and dissociation (cap/Br, —) product peaks are highlighted from all other masses (—). Insets (right) show **P3DT** end-groups at DP = 34 (top) and DP = 52 (bottom).



m/z of migration product (Da)	DP	Catalyst migration (%)		
		Run 1	Avg.	SD
7978	35	100	100	N/A
8200	36	100	100	N/A
8423	37	100	100	N/A
8645	38	100	100	N/A
8868	39	100	100	N/A
9090	40	100	100	N/A
9312	41	100	100	N/A
9535	42	100	100	N/A
9757	43	100	100	N/A
9979	44	100	100	N/A
10202	45	100	100	N/A
10424	46	100	100	N/A
10647	47	100	100	N/A
10869	48	100	100	N/A
11091	49	100	100	N/A
11314	50	100	100	N/A
11536	51	100	100	N/A
11759	52	100	100	N/A
11981	53	100	100	N/A
12203	54	100	100	N/A
12426	55	100	100	N/A
12648	56	100	100	N/A
12871	57	100	100	N/A
13093	58	100	100	N/A
13315	59	100	100	N/A
13538	60	100	100	N/A
13760	61	100	100	N/A
13982	62	100	100	N/A
14205	63	100	100	N/A
14427	64	100	100	N/A

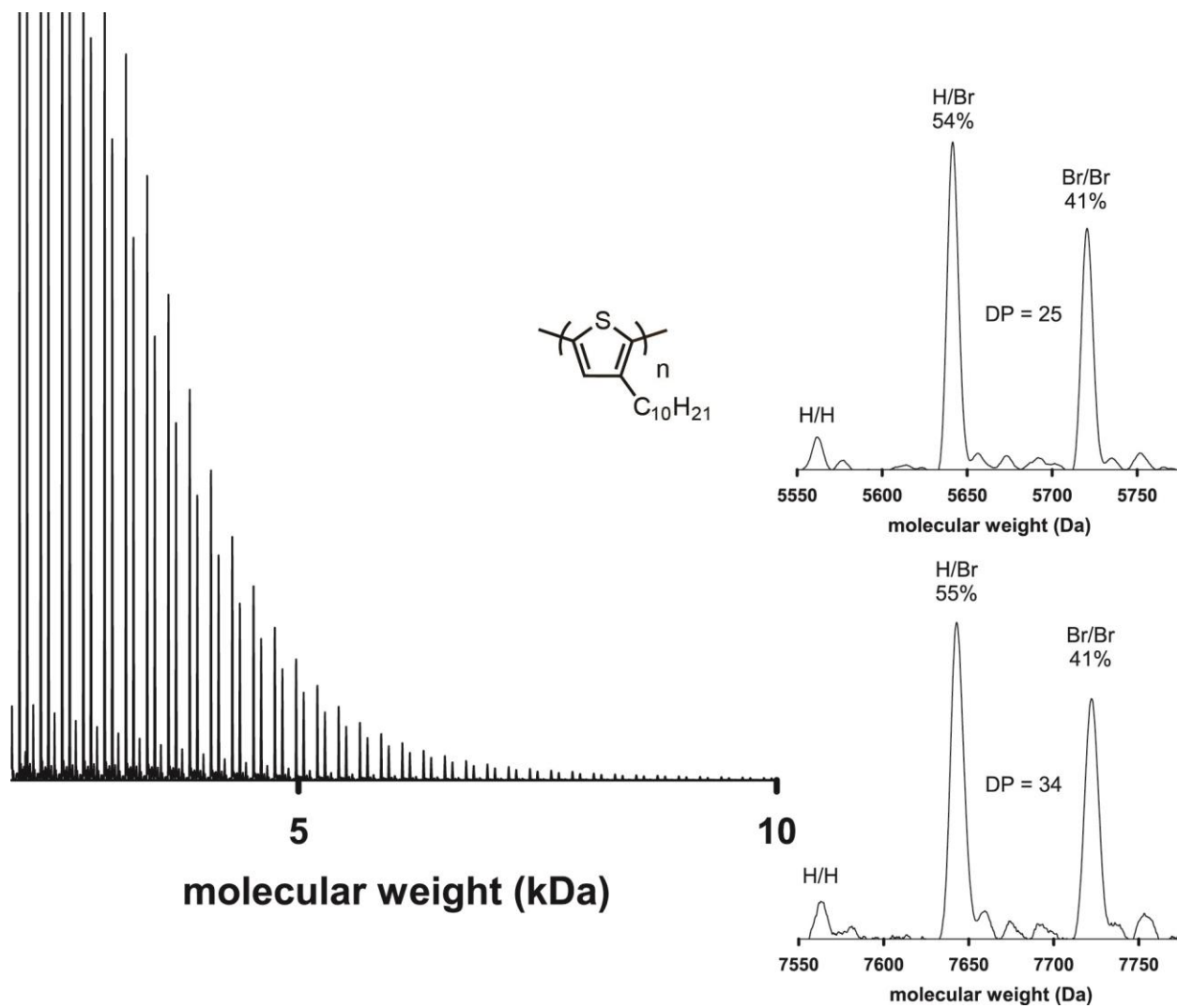
**Table A1-14.** Catalyst migration values for **4d** from Run 1. Avg and STD values are plotted in Figure A1-23.



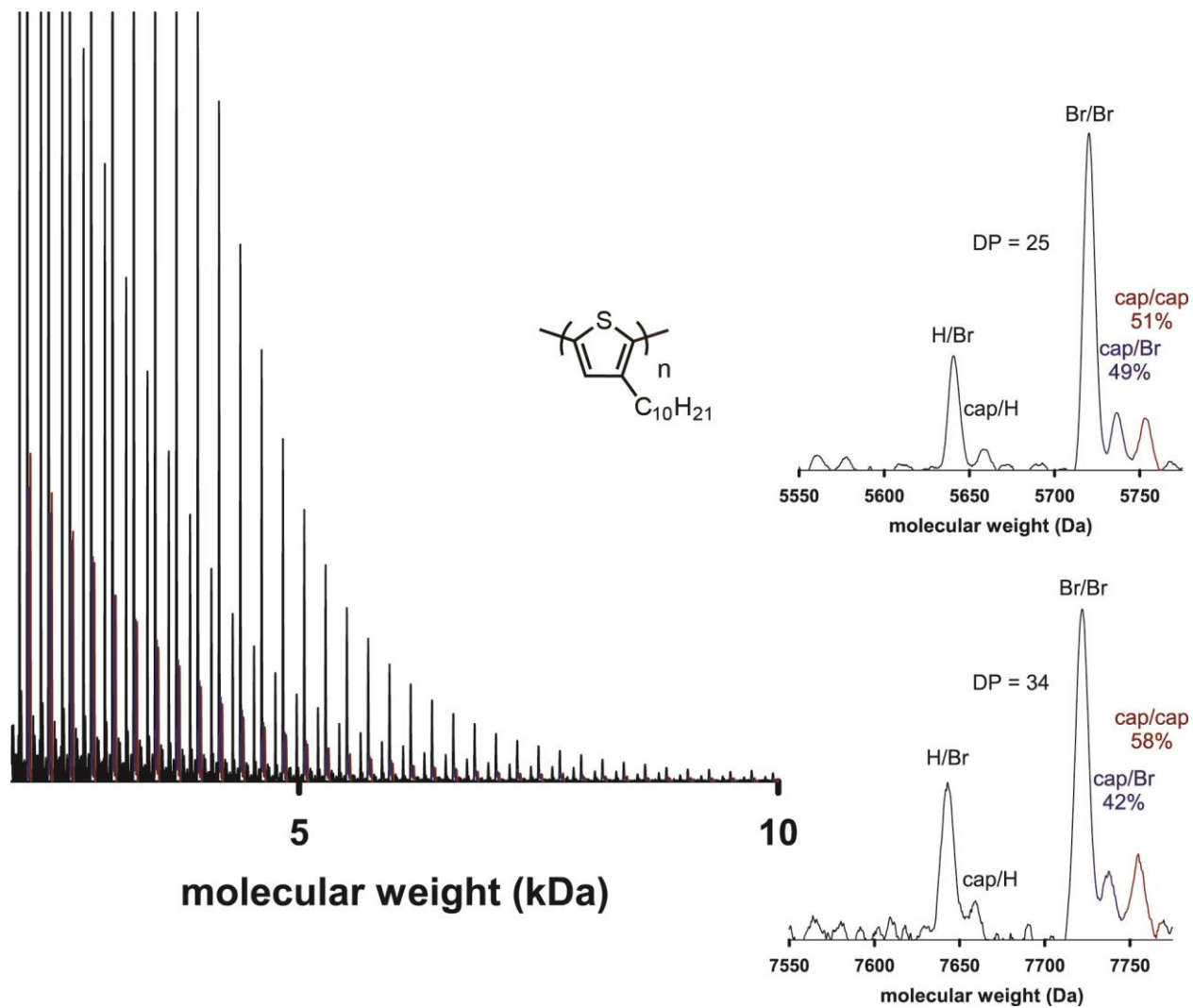
**Figure A1-20.** GPC chromatogram of **P3DT** produced by **4e** pre (—) or post (—) end-capping with **2** (15 equiv) and **3** (30 equiv).

Condition	Conversion of <b>1</b> (%) <sup>a</sup>	$M_n$ (kDa) <sup>b</sup>	$\bar{D}$ <sup>b</sup>	Br/H end-groups (%) <sup>c</sup>
pre-capping	78	6.0	3.83	54 (Br/H) 41 (Br/Br)
post-capping	84	5.2	4.16	52 (cap/cap)

**Table A1-15.** Data for **P3DT** produced by **4e** pre or post end-capping with **2** (15 equiv) and **3** (30 equiv). <sup>a</sup>Determined by GC analysis. <sup>b</sup>Determined by GPC analysis. <sup>c</sup>Calculated from the average peak area ratios (at each DP) from the five most intense peaks observed by MALDI-TOF MS analysis.



**Figure A1-21.** MALDI-TOF mass spectra of **P3DT** produced by **4e** pre end-capping (—). Insets (right) show **P3DT** end-groups at DP = 25 (top) and DP = 34 (bottom).



**Figure A1-22.** MALDI-TOF mass spectra of **P3DT** from end-capping model system using **4e**. Migration (cap/cap, **—**) and dissociation (cap/Br, **—**) product peaks are highlighted from all other masses (**—**). Insets (right) show **P3DT** end-groups at DP = 25 (top) and DP = 34 (bottom).

m/z of migration product (Da)	DP	Catalyst migration (%)		
		Run 1	Avg.	SD
5087	22	49	49	N/A
5309	23	50	50	N/A
5532	24	50	50	N/A
5754	25	49	49	N/A
5976	26	48	48	N/A
6199	27	50	50	N/A
6421	28	47	47	N/A
6644	29	51	51	N/A
6866	30	49	49	N/A
7088	31	51	51	N/A
7311	32	59	59	N/A
7533	33	57	57	N/A
7756	34	58	58	N/A

**Table A1-16.** Catalyst migration values for **4e** from Run 1. Avg and STD values are plotted in Figure A1-23.

### VIII. Catalyst migration (%)

Catalyst migration was determined using the peak areas (A) for cap/cap ( $A_{\text{cap/cap}}$ ) and cap/Br ( $A_{\text{cap/Br}}$ ) peaks at each DP. Catalyst migration was only calculated at DP where both peaks are detected by peak picking (see MALDI general procedures, pg. 2), except for **4c** and **4d** where cap/Br was not identified at any m/z.

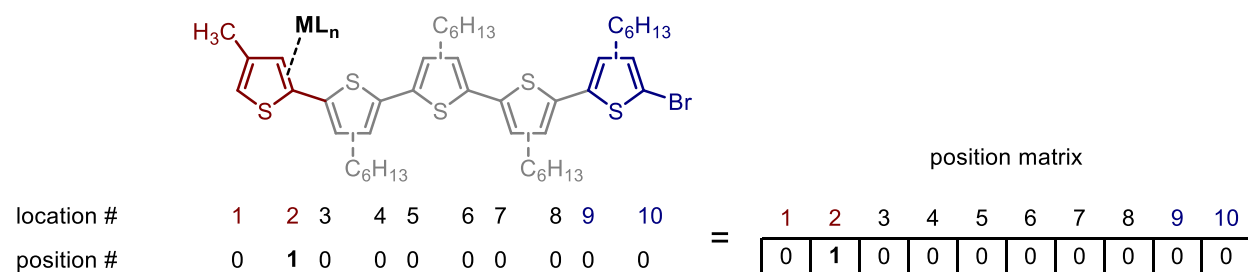
While cap/H end-groups also correspond to the migration pathway, these end-groups could also be generated from non-ideal reaction pathways (which give rise to H/H end-groups during acid quenching of typical polymerizations). Cap/H, although present in small amounts, was not included in this calculation to eliminate any possible contribution from this undesired pathway.

$$\text{catalyst migration} = A_{\text{cap/cap}} / (A_{\text{cap/cap}} + A_{\text{cap/Br}})$$



## IX. Random-walking calculations

In the end-capping experiments, a typical polymerization of **1** is terminated by adding **2** and **3**. All catalysts should initially transmetallate with **3**, forming catalyst-**P3DT**  $\pi$ -complex following reductive elimination. Using the most thermodynamically favorable  $\eta$ -2 coordination mode, there are two coordination sites on each monomer (and the cap).<sup>4,5</sup> The  $\pi$ -complex initially forms between the catalyst and cap, placing the catalyst one step away from the capped end and eight linear steps away from the C-Br terminus. This starting configuration can be represented by the position matrix [0,1,0,0,0,0,0,0,0], and is identified as location 2 (Figure A1-24).



**Figure A1-24.** Numerical representation of catalyst binding to the cap of **P3DT** (DP = 4) with cap/Br end-groups for use in the random-walking calculations. Zeroes represent unoccupied  $\pi$ -binding sites, while a one identifies the catalyst location in the position matrix.

Literature reports on catalyst migration in CTP use a random-walking model to describe end-to-end migration.<sup>6,7</sup> We employed a purely random-walk for all positions on the polymer chain (besides the chain ends) where the catalyst has an equal probability (1/2) of walking one unit towards either chain end. At the capped end, chain-walking always occurs towards the middle of the chain. Catalyst is assumed to react quantitatively when it reaches the C-Br terminus (i.e., after reaching the C-Br end, it stays there). These parameters result in the following transition matrix (Table A1-17).



0	1	0	0	0	0	0	0	0	0
1/2	0	1/2	0	0	0	0	0	0	0
0	1/2	0	1/2	0	0	0	0	0	0
0	0	1/2	0	1/2	0	0	0	0	0
0	0	0	1/2	0	1/2	0	0	0	0
0	0	0	0	1/2	0	1/2	0	0	0
0	0	0	0	0	1/2	0	1/2	0	0
0	0	0	0	0	0	1/2	0	1/2	0
0	0	0	0	0	0	0	1/2	0	1/2
0	0	0	0	0	0	0	0	0	1

**Table A1-17.** Transition matrix for a random walk with 10 linear steps from chain-end to chain-end (i.e., DP = 4 with cap/Br end-groups).

Calculations were performed in Wolfram Mathematica, Version 10.4. The random distribution function *DiscreteMarkovProcess* was used to calculate the products of the position and transition matrices to identify all the possible routes that a catalyst could take to migrate back and forth along the polymer (starting from location 2).

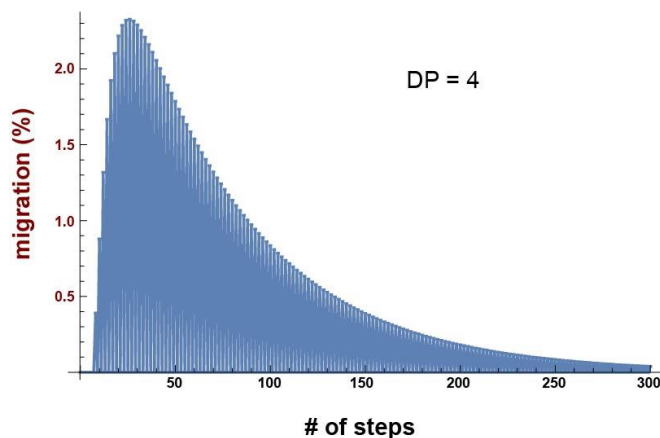
$$A = \text{DiscreteMarkovProcess}[\text{position matrix } x \text{ transition matrix}]$$

Because catalyst is assumed to react quantitatively when it reaches the  $\alpha$  terminus (position 10 when DP = 4), we were interested in the number of steps that it takes for a catalyst to randomly walk from location 2 to location 10. We use the *first passage time distribution* function to determine the number of steps for the catalyst to reach the chain-end (location 10) for the first time.

$$D = \text{FirstPassageTimeDistribution}[A, 10];$$

Thus far, all calculations interrogate the number of steps for 100% catalyst migration, but our end-capping experiments reveal that migration is not quantitative. We use the probability distribution function to identify how many steps are required for the catalyst to reach position 10 once. For example, there is only one possible way for the catalyst to migrate from location 2 to 10 in eight steps (migrate exclusively from left to right along the position matrix), but there are eight possible ways to migrate in ten steps (and so on). The probability for any catalyst to reach the  $\alpha$  end in each number of steps increases initially, then slowly decreases (Figure A1-25).

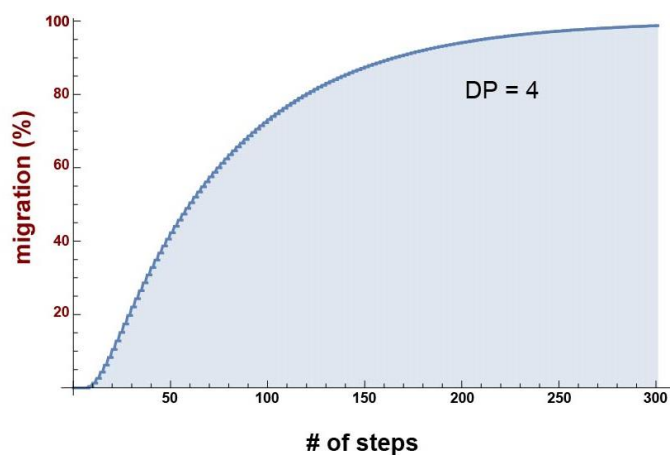
$PDF[D, k]; DiscretePlot[%, \{k, 0, 300\}, ExtentSize \rightarrow Right]$



**Figure A1-25.** Plot of the probability distribution function of the *first passage distribution* for a purely random walk across 10 locations (corresponding to a DP of 4).

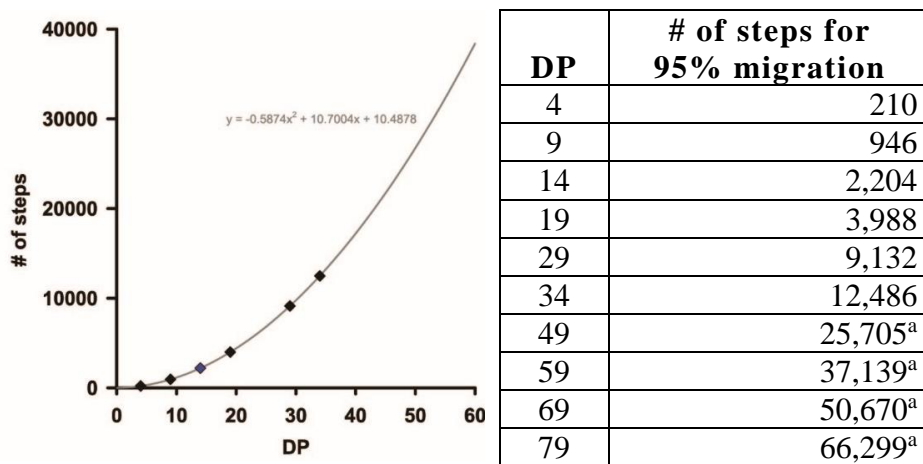
Calculating the integral of the probability distribution function (i.e., the cumulative distribution function) yields the cumulative percent of catalysts that migrated across the polymer within a given number of steps (Figure A1-26). This cumulative percent at a given number of steps is analogous to the migration percent determined experimentally. For a polymer with  $DP = 4$ , the number of steps would vary from 60 to 268 by selecting a migration from 50% to 98%.

$CDF[D, k]; DiscretePlot[%, \{k, 0, 300\}, ExtentSize \rightarrow Right]$



**Figure A1-26.** Plot of the cumulative distribution function of the *first passage distribution* for a purely random walk across 10 locations (corresponding to a DP of 4).

We calculated the cumulative distribution function at numerous points between DP = 4–34 in the same manner identified above. Calculating the random walking process at higher DP simply expands the transition and position matrices (the starting point is always location 2), but the catalyst can still only walk one unit left or right for each step. The same cumulative distribution function at each DP can be used with the experimental data from all precatalysts. We calculated the *number of steps* at 95% migration at select DP from 4–34, fit this with a quadratic equation, then extrapolated for DP > 34. Because precatalysts **4b–4d** yielded predominately migration products and were insensitive to DP, the values at 95% migration were applied to all catalysts.



**Figure A1-27.** The number of steps calculated from the cumulative distribution functions are plotted versus DP (◆). A quadratic fit (—,  $r^2 = 1.0000$ , (# of steps =  $-0.5874 \times \text{DP}^2 + 10.7004 \times \text{DP} + 10.4878$ ) is used to extrapolate the number of steps due to the high computational workload required at high DP. <sup>a</sup>Steps were calculated from the quadratic fit.

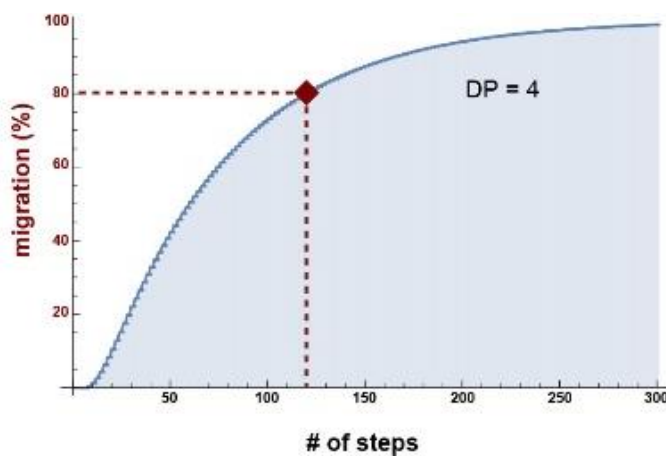
The output from these calculations is the *number of steps* required to achieve a migration percent that matches experimental data (for each catalyst at each DP). Although the random-walking model doesn't directly calculate chain-transfer/dissociation, the number of steps is linearly correlated to chain-transfer/dissociation in the end-capping experiments if the probability for chain-transfer/dissociation is constant across all polymer lengths. Given the high solubility, rod conformation, and effective conjugation length of ~10 repeat units of **P3DT**, we expect that the catalyst-**P3DT**  $\pi$ -complex is similar for all DP > 10. Therefore, the probability of chain-transfer/dissociation at each step should be independent of chain-length, and the cumulative probability of chain-transfer/dissociation is correlated to the total number of steps. The nearly exclusive migration products obtained in the end-capping experiments across the long **P3DT** for

**4b–4d** required an extraordinary number of steps, making the probability of chain-transfer/dissociation at each step extremely low.

For **4a**, the decrease in percent migration with increasing DP allows us to evaluate the validity of the random-walking calculation by fitting it to experimental data—does the decay in percent migration (experimental) with DP correlate to a similar number of calculated steps at each DP? If the random walking process is representative of catalyst migration in the end-capping experiments, we would expect a similar number of steps for each catalyst over the full range of DPs. In other words, the number of steps is correlated to the probability of dissociation at each step. Each catalyst should have a distinct probability of dissociation, but this value should remain constant for all DP (as discussed above). Using the number of chain-walking steps as a proxy for the probability of dissociation, we can fit the experimental data to the random-walking model. We identified the number of steps for **4a** to migrate by iterating the number of steps ( $S$ ) until the cumulative probability ( $M$ ) matched the experimentally determined migration percent. An arbitrary example for 80% migration when  $DP = 4$  is shown below (calculated to 3 significant digits, Figure A1-28).

$$N[CDF[D,S],3] = M$$

$$N[CDF[D,118],3] = 0.796$$



**Figure A1-28.** Plot of the cumulative distribution function of the *first passage distribution* for a purely random walk across 10 locations (corresponding to a DP of 4). The number of steps required to match 80% migration is 118.

We observe a wide variation in the number of steps at different DP for **4a**, suggesting that the simple random chain-walking model is insufficient to describe the migration behavior (Table A1-18).

<b>DP</b>	<b>Migration (%)</b>	<b>Calculated # of steps</b>
36	95	13977
42	93	17056
47	91	19369
50	89	20514

**Table A1-18.** Percent migration (experimental data) and calculated # of steps at each DP for **4a**.

## X. References

- (1) Asselin, S. M.; Bio, M. M.; Langille, N. F.; Ngai, K. Y. Practical Access to Metallo Thiophenes: Regioselective Synthesis of 2,4-Disubstituted Thiophenes. *Org. Process Res. Dev.* **2010**, *14*, 1427–1431.
- (2) Locke, J. R.; McNeil, A. J. Syntheses of Gradient  $\pi$ -Conjugated Copolymers of Thiophene. *Macromolecules* **2010**, *43*, 8709–8710.
- (3) Love, B. E.; Jones, E. G. The Use of Salicylaldehyde Phenylhydrazone as an Indicator for the Titration of Organometallic Reagents. *J. Org. Chem.* **1999**, *64*, 3755–3756.
- (4) Zhao, Y.; Nett, A. J.; McNeil, A. J.; Zimmerman, P. M. Computational Mechanism for Initiation and Growth of Poly(3-Hexylthiophene) Using Palladium N-Heterocyclic Carbene Precatalysts. *Macromolecules* **2016**, *49*, 7632–7641.
- (5) Mikami, K.; Nojima, M.; Masumoto, Y.; Mizukoshi, Y.; Takita, R.; Yokozawa, T.; Uchiyama, M. Catalyst-Dependent Intrinsic Ring-Walking Behavior on  $\pi$ -Face of Conjugated Polymers. *Polym. Chem.* **2017**, *8*, 1708–1713.
- (6) Tkachov, R.; Senkovskyy, V.; Komber, H.; Sommer, J. U.; Kiriya, A. Random Catalyst Walking along Polymerized Poly(3-Hexylthiophene) Chains in Kumada Catalyst-Transfer Polycondensation. *J. Am. Chem. Soc.* **2010**, *132*, 7803–7810.
- (7) Kohn, P.; Huettner, S.; Komber, H.; Senkovskyy, V.; Tkachov, R.; Kiriya, A.; Friend, R. H.; Steiner, U.; Huck, W. T. S.; Sommer, J.-U. U.; *et al.* On the Role of Single Regiodefects and Polydispersity in Regioregular poly(3-Hexylthiophene): Defect Distribution, Synthesis of Defect-Free Chains, and a Simple Model for the Determination of Crystallinity. *J. Am. Chem. Soc.* **2012**, *134*, 4790–4805.

## Appendix 2

### Supporting Information for Chapter 3

#### Catalyst-dependent migration in poly(phenylene) synthesis

<b>I.</b>	<b>Materials</b>	<b>159</b>
<b>II.</b>	<b>General experimental</b>	<b>160</b>
<b>III.</b>	<b>Synthetic procedures</b>	<b>162</b>
<b>IV.</b>	<b>NMR spectra</b>	<b>164</b>
<b>V.</b>	<b>Competitive agent screening</b>	<b>166</b>
<b>VI.</b>	<b>End-capping experiments</b>	<b>168</b>
<b>VII.</b>	<b>Catalyst migration</b>	<b>189</b>
<b>VIII.</b>	<b>Random-walking calculations</b>	<b>191</b>
<b>IX.</b>	<b>References</b>	<b>199</b>

## I. Materials

Flash chromatography was performed on SiliCycle silica gel (40–63  $\mu\text{m}$ ). Thin layer chromatography was performed on Merck TLC plates (pre-coated with silica gel 60 F254).  $i\text{PrMgCl}$  (2 M in THF) was purchased in 100 mL quantities from Sigma Aldrich.  $\text{IPrNi}(\text{PPh}_3)\text{Cl}_2$  was purchased from TCI America,  $\text{Ni}(\text{dppp})\text{Cl}_2$ ,  $\text{Ni}(\text{dppe})\text{Cl}_2$ ,  $\text{Ni}(\text{PPh}_3)_2\text{Cl}_2$ , and  $\text{IPrPd}(\text{3-chloropyridine})\text{Cl}_2$  were purchased from Sigma-Aldrich ( $\text{IPr}$  = 1,3-bis(2,6-diisopropylphenyl)imidazol-2-ylidene,  $\text{PPh}_3$  = triphenylphosphine,  $\text{dppp}$  = 1,3-bis(diphenylphosphino)propane, and  $\text{dppe}$  = 1,2-bis(diphenylphosphino)ethane). All other reagent grade materials and solvents were purchased from Sigma-Aldrich, Acros, or Fisher and were used without further purification unless otherwise noted. THF was dried and deoxygenated using an Innovative Technology (IT) solvent system composed of activated alumina, copper catalyst, and molecular sieves. *N*-Bromosuccinimide was recrystallized from hot  $\text{H}_2\text{O}$  and dried over  $\text{P}_2\text{O}_5$ . The glovebox in which specified procedures were carried out was an MBraun LABmaster 130 with a  $\text{N}_2$  atmosphere and  $\text{H}_2\text{O}$  levels below 4 ppm. Compounds **S1**,<sup>1</sup> **S2**,<sup>1</sup> and **2**<sup>1</sup> were prepared using modified literature procedures.



## II. General experimental

NMR Spectroscopy: Unless otherwise noted,  $^1\text{H}$  and  $^{13}\text{C}$  NMR spectra for all compounds were acquired at rt in  $\text{CDCl}_3$  on a Varian vnmrs 700 spectrometer operating at 700 and 176 MHz, respectively, Varian vnmrs 500 spectrometer operating at 500 and 126 MHz, respectively or Varian MR400 Spectrometer operating at 400 and 100 MHz, respectively. Chemical shift data are reported in units of  $\delta$  (ppm) relative to tetramethylsilane (TMS) and referenced with residual solvent. Multiplicities are reported as follows: singlet (s), triplet (t), doublet of triplets (dt), or multiplet (m). Residual  $\text{H}_2\text{O}$  is denoted by an \*.

Mass Spectrometry: High-resolution mass spectrometry data were obtained on a Micromass AutoSpec Ultima Magnetic Sector mass spectrometer.

Gel-Permeation Chromatography: Polymer molecular weights were determined by comparison with polystyrene standards (Varian, EasiCal PS-2 MW 580–377,400) at 40 °C in THF on a Malvern Viscotek GPCMax VE2001 equipped with two Viscotek LT-5000L columns (8 mm (ID)  $\times$  300 mm (L)) and analyzed with Viscotek TDA 305 (with RI, UV-PDA Detector Model 2600 (190–500 nm), RALS/LALS, and viscometer). All presented data correspond to the absorbance at 254 nm normalized to the highest peak. Samples were dissolved in THF (with mild heating), and passed through a 0.2  $\mu\text{m}$  PTFE filter prior to analysis.

Gas Chromatography: Gas chromatography was carried out using a Shimadzu GC 2010 containing a Shimadzu SHRX5 column (crossbound 5% diphenyl – 95% dimethyl polysiloxane; 15 m, 0.25 mm ID, 0.25  $\mu\text{m}$  df).

Titrations of the Grignard Reagents: An accurately weighed sample of salicylaldehyde phenylhydrazone<sup>2</sup> (typically between 170–200 mg) was dissolved in 10.00 mL of THF. This solution was added dropwise using a 0.5 mL syringe to 0.10 mL of (aryl)MgCl. The initial (aryl)MgCl solution is pale yellow, turns bright orange, and then returns to pale yellow at the endpoint.

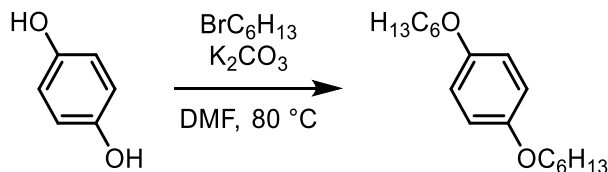
Precatalyst stock solutions: Precatalyst **4d** (~55 mg) was weighed into a 5 mL volumetric flask in a glovebox, and then diluted with THF. These stocks solutions were stored in the freezer, and remain stable for several weeks or longer.

Precatalyst **4c** (~5 mg) was weight into a 1 mL volumetric flask in a glovebox, and then diluted with THF immediately before use. If stored, the violet solution would turn blue over the course of several h.

MALDI-TOF MS: Matrix-assisted laser desorption/ionization time-of-flight mass spectrometry was performed on a Bruker Autoflex Speed. Positive ion spectra were obtained in reflectron mode. Polymer samples (~1 mg) were dissolved in CHCl<sub>3</sub> (~3 mL) and mixed in a 1:1 (v/v) ratio with 0.1 M trans-2-[3-(4-tert-butylphenyl)-2-methyl-2-propenylidene]malononitrile (DTCB) solution in CHCl<sub>3</sub> then spotted. Serial dilutions (~five-fold) were performed to access a wide range of sample concentrations, and the spot yielding the highest signal/noise was subsequently analyzed. Molecular weight of HCl quenched **P1** with Br/H end groups was referenced to a series of low MW peptide standards. The referenced **P1** was then used to calibrate the full MW range of the sample.

Raw data was processed in flexAnalysis Version 3.4. Baseline subtraction was performed using TopHat, and for polymer samples with a maximum m/z <10,000, peak smoothing was performed using one cycle of the SavitskyGolay algorithm to a peak width of 0.1 m/z and peak picking was performed using the SNAP method for peaks with signal/noise greater than two. For polymer samples with a maximum m/z >10,000, peak smoothing was performed using one cycle of the SavitskyGolay algorithm to a peak width of 5 m/z and peak picking was performed using the centroid method for peaks with signal/noise greater than one. End-group percentages were calculated by comparing the signal areas of picked peaks at each DP. Migration percent was calculated at each DP where both migration (cap/cap end-groups) and dissociation (cap/Br end-groups) product peaks were found by peak picking.

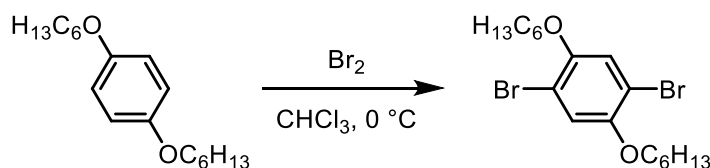
### III. Synthetic procedures



**S1**

**1,4-bis(hexyloxy)phenylene (S1).**<sup>1</sup> A 500 mL flask was equipped with a stir bar, then hydroquinone (20 g, 0.20 mol, 1.0 equiv), DMF (120 mL), potassium carbonate (63 g, 0.45 mol, 2.5 equiv), and 1-bromohexane (63 mL, 0.45 mol, 2.5 equiv) were added sequentially. The reaction mixture was stirred under N<sub>2</sub> at 80 °C for 5 d. The reaction mixture was cooled to rt, then poured into H<sub>2</sub>O (400 mL). The mixture was extracted with hexanes (3 x 200 mL) and the organic layer was washed with H<sub>2</sub>O (2 x 200 mL) and brine (1 x 200 mL), before drying over MgSO<sub>4</sub>. The brown mixture was filtered, and concentrated in vacuo. The resulting oil was passed through silica gel using DCM as the eluent. Recrystallization from hot MeOH gave a white, crystalline solid (29 g, 57% yield). HRMS (EI): [M<sup>+</sup>] Calcd. for C<sub>16</sub>H<sub>30</sub>O<sub>2</sub>, 224.1599; found, 224.1597.

---



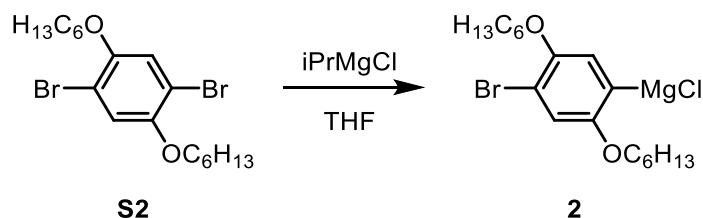
**S1**

**S2**

**1,4-bis(hexyloxy)-2,5-dibromophenylene (S2).**<sup>1</sup> A 500 mL flask was equipped with a stir bar, then **S1** (24 g, 0.86 mol, 1.0 equiv) and CHCl<sub>3</sub> (98 mL) were added. The flask was cooled to 0 °C in an ice/water bath and fitted with an addition funnel. Bromine (11 mL, 0.21 mol, 2.5 equiv) was added dropwise under N<sub>2</sub> over 10 min and the pressure was vented through an aq. solution of 10% Na<sub>2</sub>SO<sub>3</sub> (~ 150 mL). After 3 h, the reaction was quenched with an aq. sat. solution of Na<sub>2</sub>SO<sub>3</sub> and vigorously stirred until colorless. The aqueous mixture was extracted with DCM (3 x 100 mL) and the combined organic layers were washed with H<sub>2</sub>O (2 x 100 mL) and brine (1 x 100 mL), then dried over MgSO<sub>4</sub>, filtered, and concentrated in vacuo. The residue was dissolved in CHCl<sub>3</sub> (~10

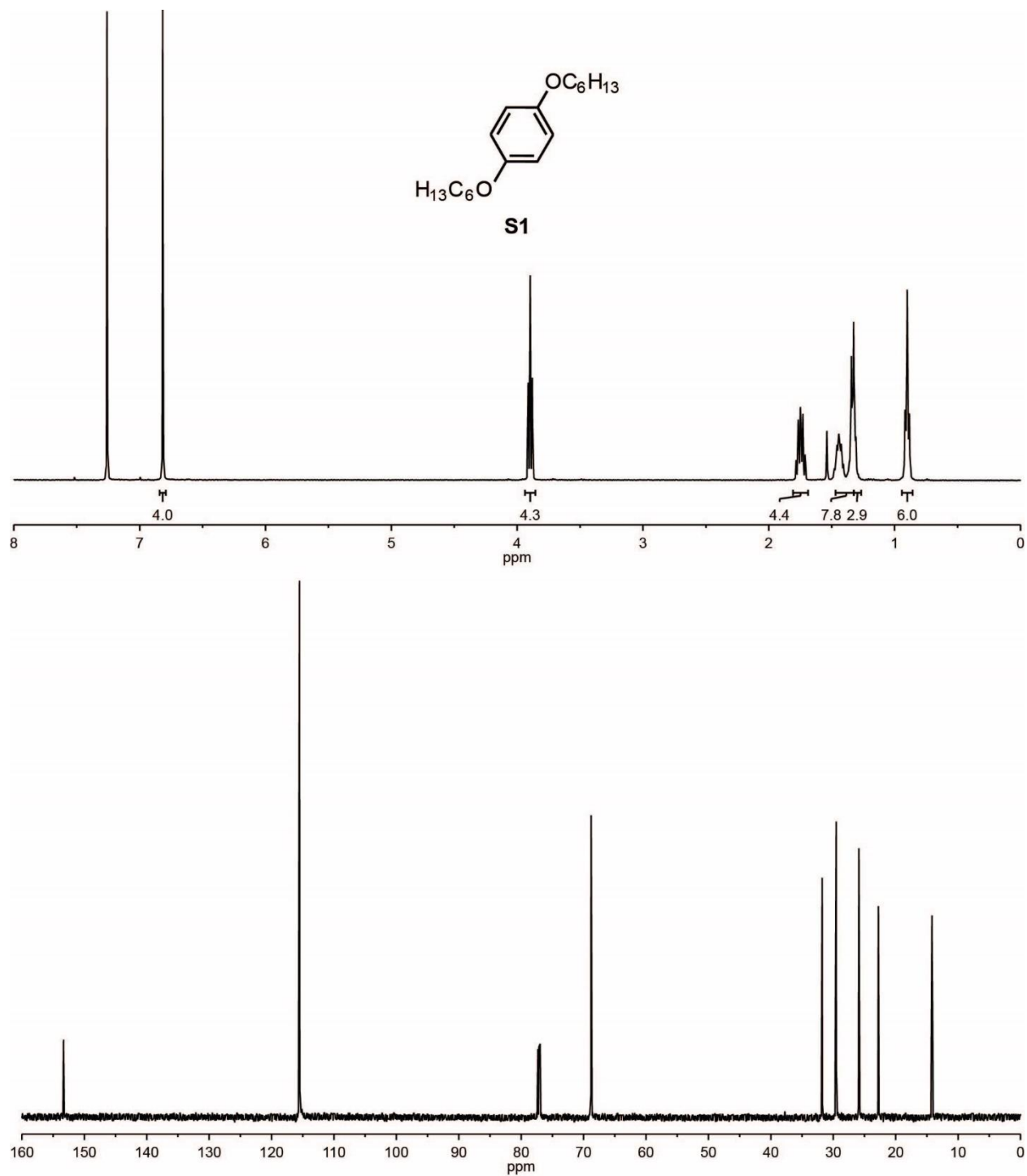
mL), then MeOH (~100 mL) was layered on top to recrystallize overnight. The solids were filtered to afford white crystals (29 g, 77% yield). HRMS (EI): [M<sup>+</sup>] Calcd. for C<sub>16</sub>H<sub>28</sub>Br<sub>2</sub>O<sub>2</sub>, 434.0456; found, 434.0455.

---



**(4-bromo-2,5-bis(hexyloxy)phenyl)magnesium chloride (2).**<sup>1</sup> In a glovebox, **S2** (0.109 g, 0.250 mmol, 1.00 equiv) was added to a 4 mL vial equipped with a stir bar. A small amount of C<sub>22</sub>H<sub>46</sub> (~ 5 mg) was added and the mixture was diluted with THF (1.1 mL). Next, iPrMgCl (0.11 mL of a 2 M solution in THF, 0.22 mmol, 0.88 equiv) was added and the solution was stirred for 16 h before titrating (0.15 M, see pg. 3).

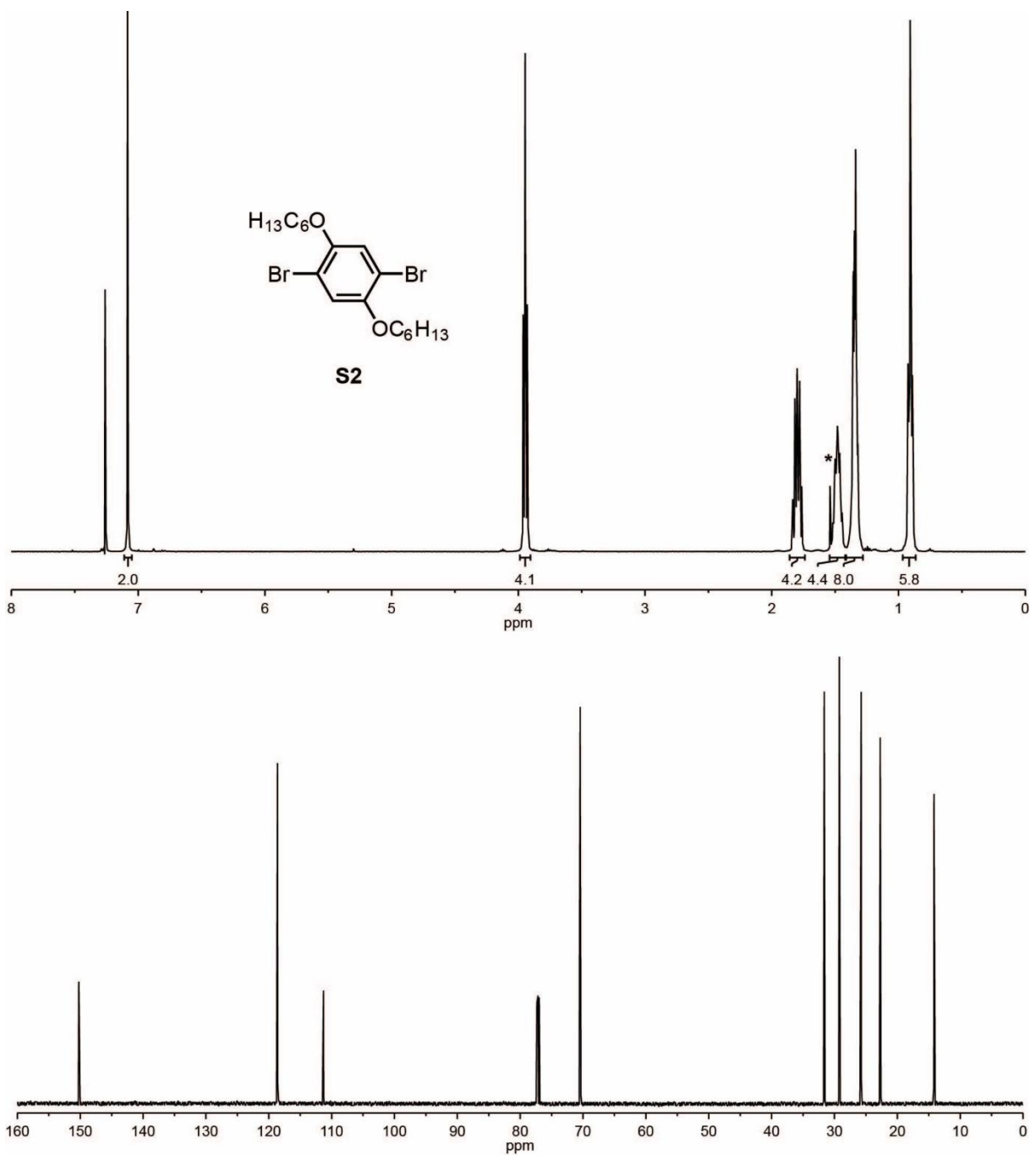
#### IV. NMR spectra



**Figure A2-1.**  $^1\text{H}$  and  $^{13}\text{C}$  NMR spectra for S1.

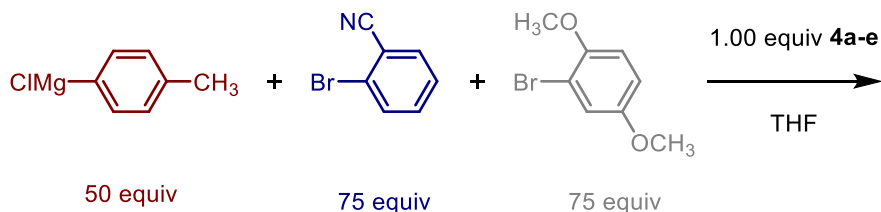
$^1\text{H}$  NMR (400 MHz,  $\text{CDCl}_3$ )  $\delta$  6.82 (s, 4H), 3.90 (t,  $J = 6.6$  Hz, 4H), 1.75 (dt,  $J = 14.7, 6.7$  Hz, 4H), 1.49–1.39 (m, 8H), 1.38–1.27 (m, 4H), 0.90 (t,  $J = 6.9$  Hz, 6H).

$^{13}\text{C}$  NMR (176 MHz,  $\text{CDCl}_3$ )  $\delta$  153.34, 115.53, 68.80, 31.77, 29.53, 25.90, 22.77, 14.19.



**Figure A2-2.** <sup>1</sup>H and <sup>13</sup>C NMR spectra for **S2**.  
<sup>1</sup>H NMR (500 MHz, CDCl<sub>3</sub>) δ 7.08 (s, 2H), 3.95 (t, *J* = 6.5 Hz, 4H), 1.80 (dt, *J* = 14.8, 6.7 Hz, 4H), 1.53–1.44 (m, 4H), 1.39–1.28 (m, 8H), 0.91 (t, *J* = 6.9 Hz, 6H).  
<sup>13</sup>C NMR (176 MHz, CDCl<sub>3</sub>) δ 150.22, 118.62, 111.28, 70.46, 31.63, 29.23, 25.76, 22.72

## V. Competitive agent screening



aryl halide conversion monitored by GC

### General procedure for the cross-coupling of 2-bromobenzonitrile, and 2-bromo-1,4-bis(methoxy)phenylene with **3a** catalyzed by **4a–e**.

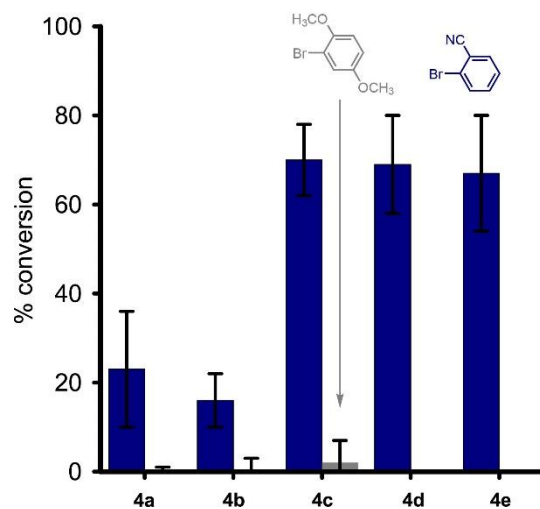
*Solution A.* In a glovebox, 2-bromobenzonitrile (2.23 mL of a 0.333 M solution, 0.744 mmol) and 2-bromo-1,4-bis(methoxy)phenylene (2.24 mL of a 0.333 M solution, 0.744 mmol) were added to a 20 mL vial with a stir bar and C<sub>22</sub>H<sub>46</sub> (~30 mg). An aliquot (~0.1 mL) was removed from the glovebox and quenched with conc. HCl (~1 mL) as the time zero point.

Separately, the insoluble precatalysts (**4a**, **4b**, and **4e**) were each weighed (~1–1.4 mg) into a 4 mL vial and diluted with THF (~1–1.4 mL) to achieve a catalyst concentration of 0.00075 M during the reaction. For precatalysts soluble in THF (**4c** and **4d**), stock solutions (~0.1 mL of a 0.015 M solution in THF) of each were diluted with THF (~0.7 mL) in a 4 mL vial equipped with a stir bar to achieve a catalyst concentration of 0.00075 M during the reaction.

Next, *Solution A* (~0.7–1 mL, 75 equiv of each heteroaryl bromide) was added to the catalyst solutions and the combined mixture was stirred for 2 min. Then **3a** (~0.34–0.5 mL of a 0.25 M solution in THF, 50 equiv) was added and the solution was stirred for 2 h before quenching.

The reaction mixture was removed from the glovebox and quenched with conc. HCl (~2 mL). The quenched mixture was extracted with CHCl<sub>3</sub> (3 x 0.5 mL) with heating. The combined organic layers were washed with H<sub>2</sub>O (1 x 2 mL) and brine (1 x 2 mL) before drying over MgSO<sub>4</sub>. The solution was filtered, and then diluted with DCM (~1 mL) for GC analysis.

Conversion of the aryl halides was determined by GC from the change in peak area ratio with C<sub>22</sub>H<sub>46</sub> internal standard.



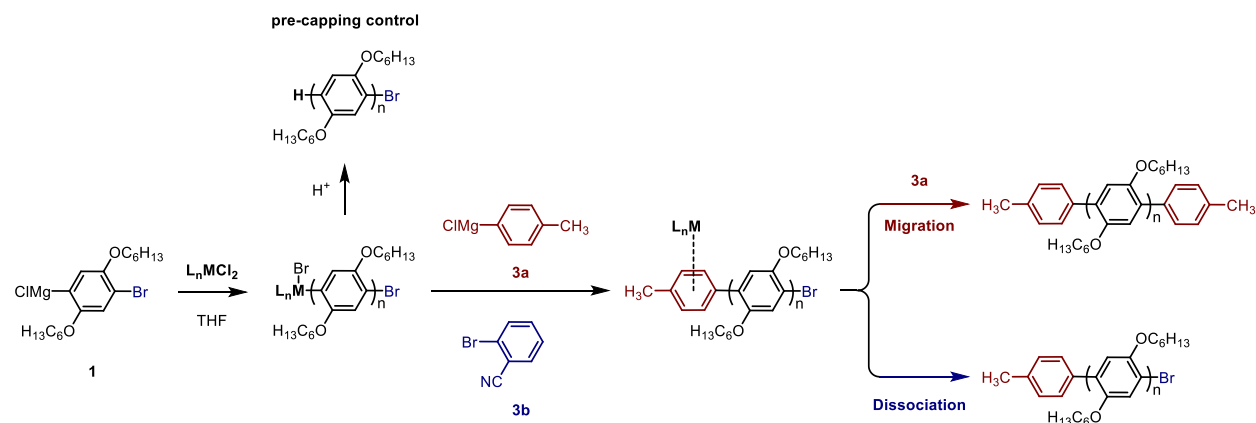
**Figure A2-3.** Percent conversion of **3b** (■), and 2-bromo-1,4-bis(methoxy)phenylene (■) in cross-coupling competition experiments with **3a** sorted by catalyst.

Precatalyst	Conversion (%)							
	3b				2-bromo-1,4-bis(methoxy)phenylene			
	Run 1	Run 2	Avg.	STD	Run 1	Run 2	Avg.	STD
<b>4a</b>	32	13	23	13	0	0	0	0
<b>4b</b>	20	12	16	6	2	0	0	1
<b>4c</b>	64	76	70	8	6	0	3	4
<b>4d</b>	61	77	69	11	0	0	0	0
<b>4e</b>	58	76	67	13	0	0	0	0

**Table A2-1.** Conversion data plotted in Figure A2-3.



## VI. End-capping experiments



### Representative procedure for end-capping 1

#### Polymerization

**4c/4d.** Precatalyst from a stock solution (~0.1 mL of a ~0.0015 M solution in THF, 0.0015 mmol, 1.0 equiv) was each added to a 10 mL Schleck flask equipped with a stir bar and diluted with THF (~1.2 mL) to achieve a catalyst concentration of 0.00075 M during the polymerization. The flasks were sealed with a rubber septum before removing from the glovebox and placed under  $N_2$ . Previously prepared **1** was added in the following amounts to initiate the polymerization:

to **4c**: 40 equiv **1** (0.50 mL of a 0.12 M solution in THF, 0.060 mmol).

to **4d**: 20 equiv **1** (0.25 mL of a 0.12 M solution in THF, 0.060 mmol).

**4a, 4b,** and **4e.** Precatalyst was weighed (~3 mg) into a 20 mL vial equipped with a stir bar and diluted with THF (~6 mL) to achieve a catalyst concentration of 0.00075 M during the polymerization. Previously prepared **1** was added in the following amounts to initiate the polymerization:

to **4a/b**: 6.0 equiv **1** (0.28 mL of a 0.12 M solution in THF, 0.034 mmol).

to **4e**: 20 equiv **1** (1.0 mL of a 0.12 M solution in THF, 0.12 mmol).

#### End-capping

After polymerizing for 45 min, an aliquot of the polymerization solution (1.0 mL) was added to 4 mL vials containing **3a** (0.046 mL of a 0.25 M in THF, 0.011 mmol, 15 equiv) and **3b** (0.10 mL

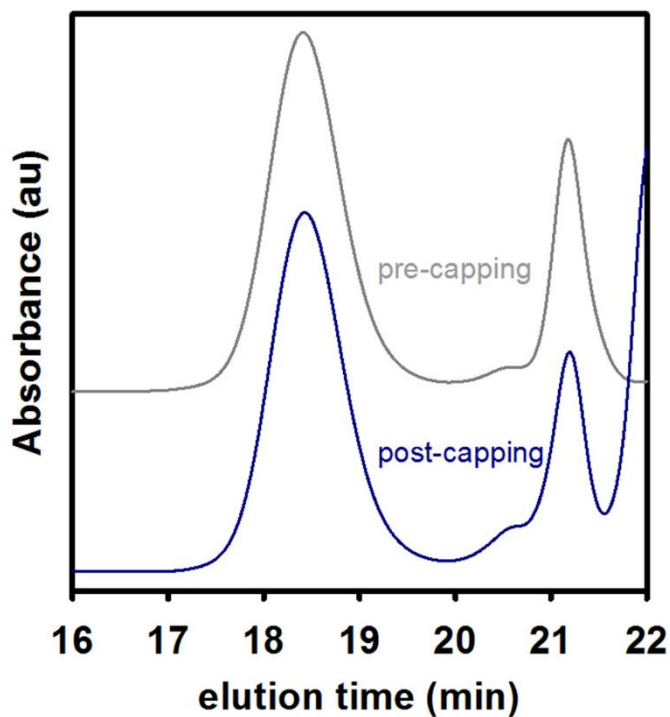
of a 0.385 M solution in THF, 0.038 mmol, 50 equiv). The remainder of the polymerization solution was immediately removed from the glovebox and quenched with conc. HCl (~1 mL). End-capping solutions were stirred for an additional 2 h before removing from the glovebox and quenching with conc. HCl (~1 mL).

The quenched reactions were extracted with CHCl<sub>3</sub> (3 x 1 mL) with heating. The combined organic layers were washed with H<sub>2</sub>O (1 x 2 mL) and brine (1 x 2 mL). The solvent was then removed via rotary evaporation and the solids were re-dissolved with heating in THF (~10 mL). After cooling to rt, MgSO<sub>4</sub> (~10 mg) was added and the mixture was filtered through a PTFE syringe filter (0.2 μm). A small portion was removed for GC and GPC analysis, and the remaining liquid was removed using a rotary evaporator to yield a white solid. The solid was dissolved in minimal CHCl<sub>3</sub> (~0.2 mL), and then precipitated into MeOH (10 mL) in a centrifuge tube and centrifuged at 4500 rpm for 30 min. The supernatant was decanted and the solid polymer was dried under high vacuum for 4 h.

The solids (~2 mg) were dissolved in CDCl<sub>3</sub> (2 mL) and analyzed by <sup>1</sup>H NMR spectroscopy. Next, the NMR solutions were filtered through a pipette column (basic, acidic, then neutral alumina with a KimWipe plug) and rinsed with CHCl<sub>3</sub> (~0.5 mL). The resultant polymer solution (2.5 μL) was mixed with DCTB matrix (2.5 μL of a 0.1 M solution in CHCl<sub>3</sub>) in an Eppendorf tube. The polymer/matrix solution (~1.5 μL) was spotted onto the MALDI 96-well target, and the remaining solution in the Eppendorf tube was diluted five-fold with additional DCTB matrix (2.5 μL of a 0.1 M solution in CHCl<sub>3</sub>). The diluted sample was spotted onto the MALDI target in the same manner, and further five-fold dilutions (with DCTB matrix solution) were performed and spotted to yield four spots for each polymer sample.

## Representative analysis

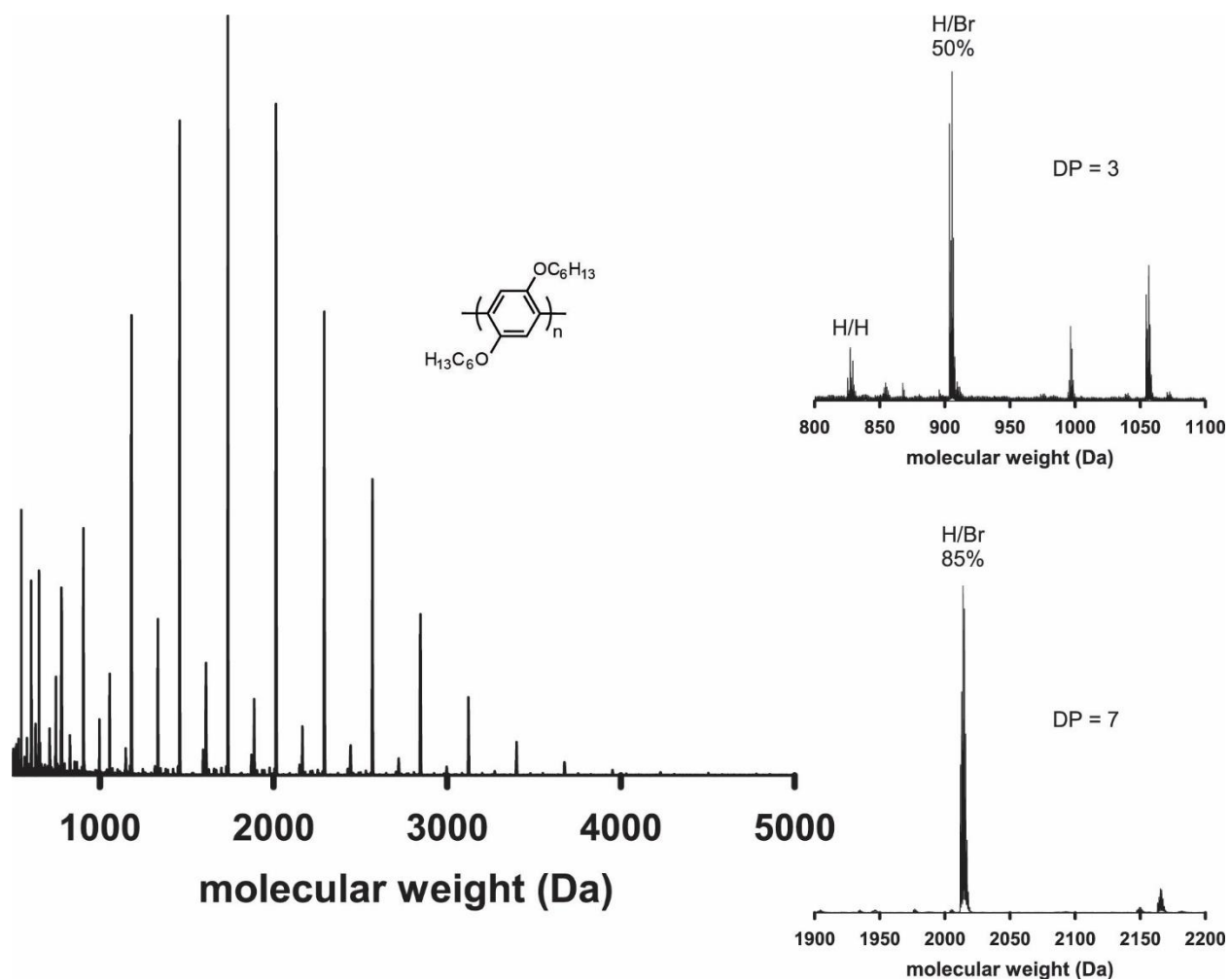
### Precatalyst **4a**



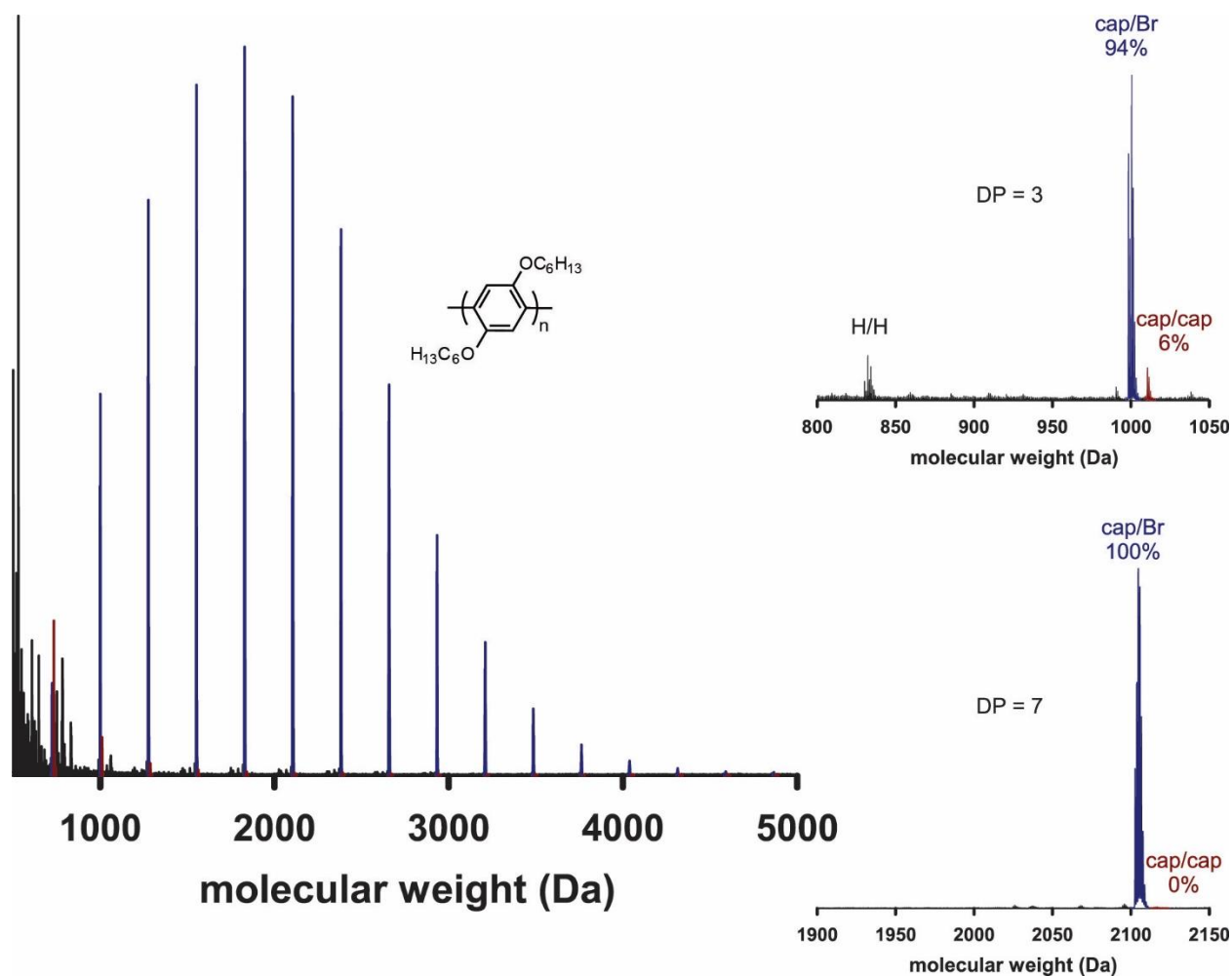
**Figure A2-4.** GPC chromatogram of **P1** produced by **4a** pre (—) or post (—) end-capping with **3a** (15 equiv) and **3b** (50 equiv).

Condition	Conversion of <b>1</b> (%) <sup>a</sup>	$M_n$ (kDa) <sup>b</sup>	$\bar{D}$ <sup>b</sup>	End-groups (%)
pre-capping	68	1.4	1.36	78 (Br/H) <sup>c</sup>
post-capping	68	1.8	1.18	Mostly cap/Br

**Table A2-2.** Data for **P1** produced by **4a** pre or post end-capping with **3a** (15 equiv) and **3b** (50 equiv). <sup>a</sup>Determined by GC analysis. <sup>b</sup>Determined by GPC analysis. <sup>c</sup>Calculated from the average peak area ratios (at each DP) from the five most intense peaks observed by MALDI-TOF MS analysis.



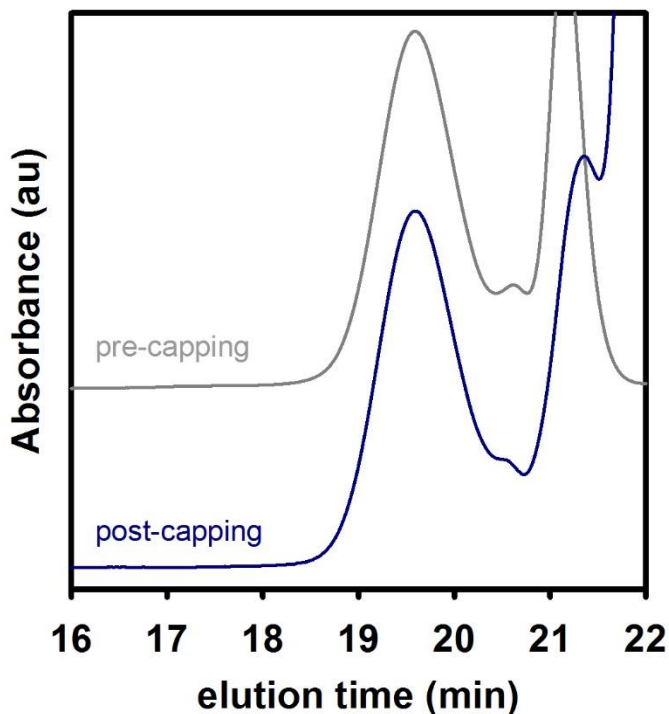
**Figure A2-5.** MALDI-TOF mass spectra of **P1** produced by **4a** before end-capping. Insets (right) show **P1** end-groups at DP = 3 (top) and DP = 7 (bottom).



**Figure A2-6.** MALDI-TOF mass spectra of **P1** produced by **4a** after end-capping with **3a** (15 equiv) and **3b** (50 equiv). Migration (cap/cap, ■) and dissociation (cap/Br, ■) product peaks are highlighted from all other masses (■). Insets (right) show **P1** end-groups at DP = 3 (top) and DP = 7 (bottom).

m/z of migration product (Da)	Catalyst migration (%)					
	DP	Run 1	Run 2	Run 3	Avg.	SD
735	2	52	48	46	49	3
1012	3	6	5	6	6	0
1288	4	2	2	2	2	0
1564	5	1	1	1	1	0
1841	6	1		1	1	0

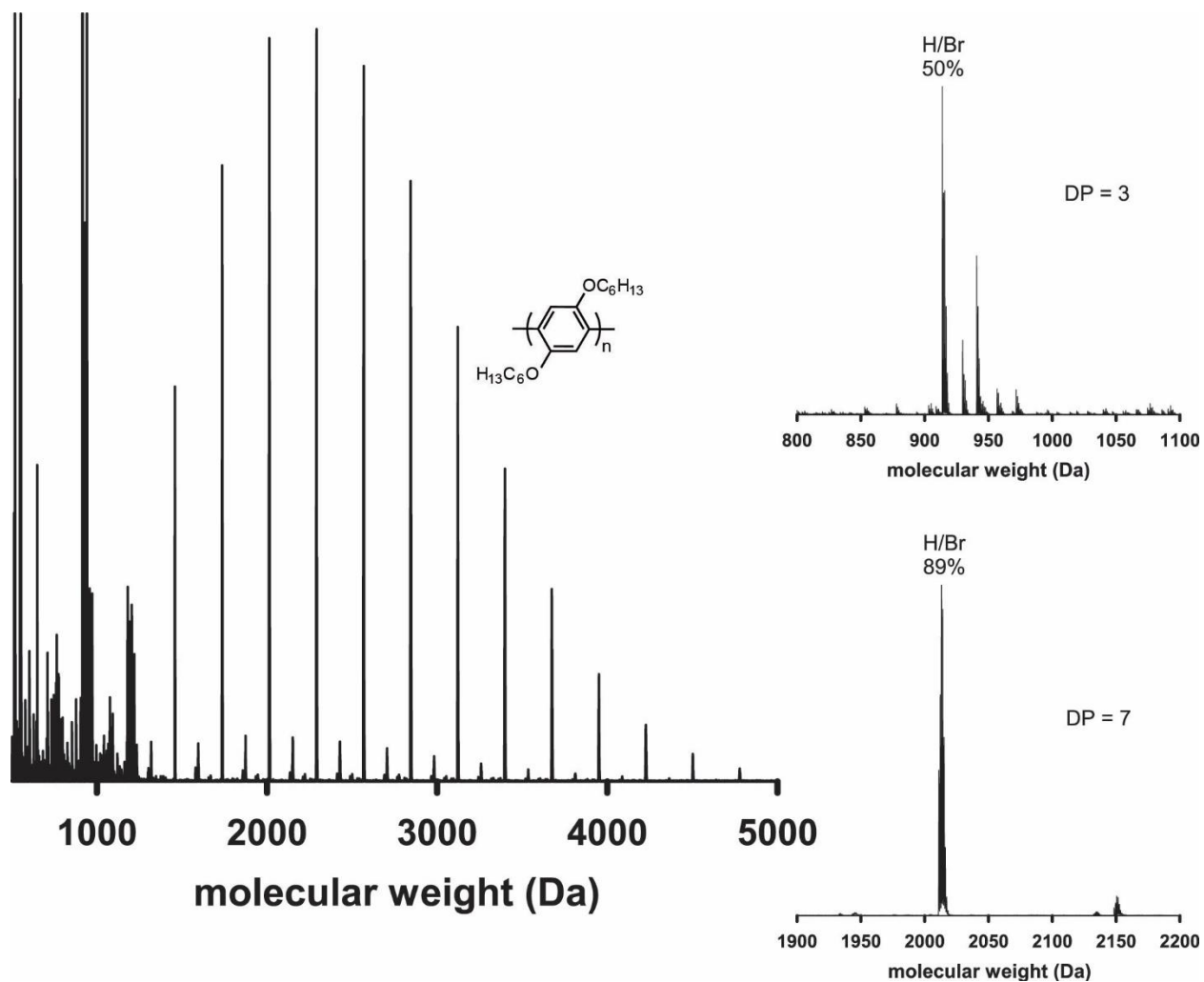
**Table A2-3.** Catalyst migration values for **4a** from Run 1–3. Avg and STD values are plotted in Figure A2-19.



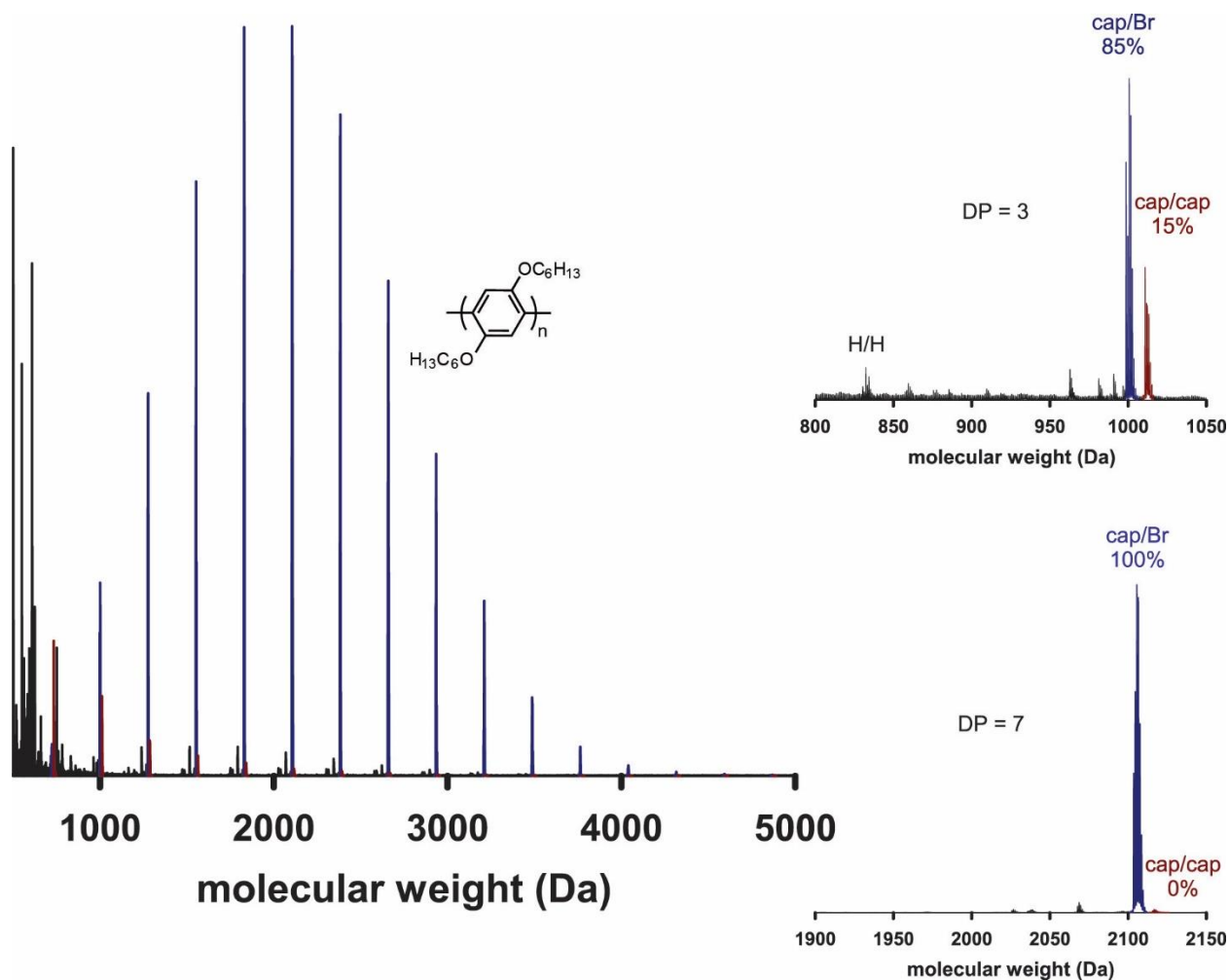
**Figure A2-7.** GPC chromatogram of **P1** produced by **4b** pre (—) or post (—) end-capping with **3a** (15 equiv) and **3b** (50 equiv).

Condition	Conversion of <b>1</b> (%) <sup>a</sup>	$M_n$ (kDa) <sup>b</sup>	$\bar{D}$ <sup>b</sup>	End-groups (%)
pre-capping	80	1.7	1.31	89 (Br/H) <sup>c</sup>
post-capping	81	1.7	1.30	Mostly cap/Br

**Table A2-4.** Data for **P1** produced by **4a** pre or post end-capping with **3a** (15 equiv) and **3b** (50 equiv). <sup>a</sup>Determined by GC analysis. <sup>b</sup>Determined by GPC analysis. <sup>c</sup>Calculated from the average peak area ratios (at each DP) from the five most intense peaks observed by MALDI-TOF MS analysis.



**Figure A2-8.** MALDI-TOF mass spectra of **P1** produced by **4b** before end-capping. Insets (right) show **P1** end-groups at DP = 3 (top) and DP = 7 (bottom).

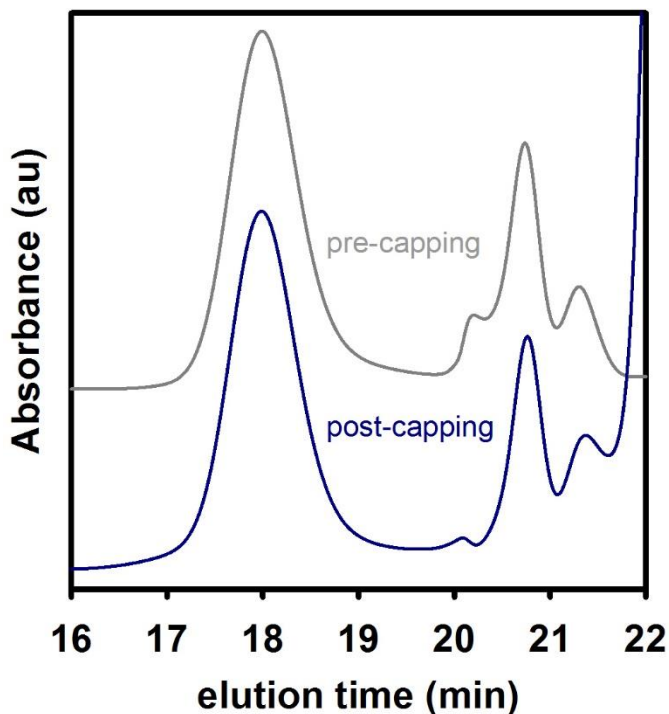


**Figure A2-9.** MALDI-TOF mass spectra of **P1** produced by **4b** after end-capping with **3a** (15 equiv) and **3b** (50 equiv). Migration (cap/cap, —) and dissociation (cap/Br, —) product peaks are highlighted from all other masses (—). Insets (right) show **P1** end-groups at DP = 3 (top) and DP = 7 (bottom).



m/z of migration product (Da)	Catalyst migration (%)							
	DP	Run 1	Run 2	Run 3	Run 4	Run 5	Avg.	SD
735	2	46	50	71	82	72	64	15
1012	3	15	16	32	16	17	19	7
1288	4	7	8	9	7	6	7	1
1564	5	3	2	3	3	2	3	1
1841	6	2	1	2	2	1	2	0
2117	7	1	1	1	1	1	1	0
2394	8	1		1	1	1	1	0
2670	9			1	1		1	0
2946	10			1				

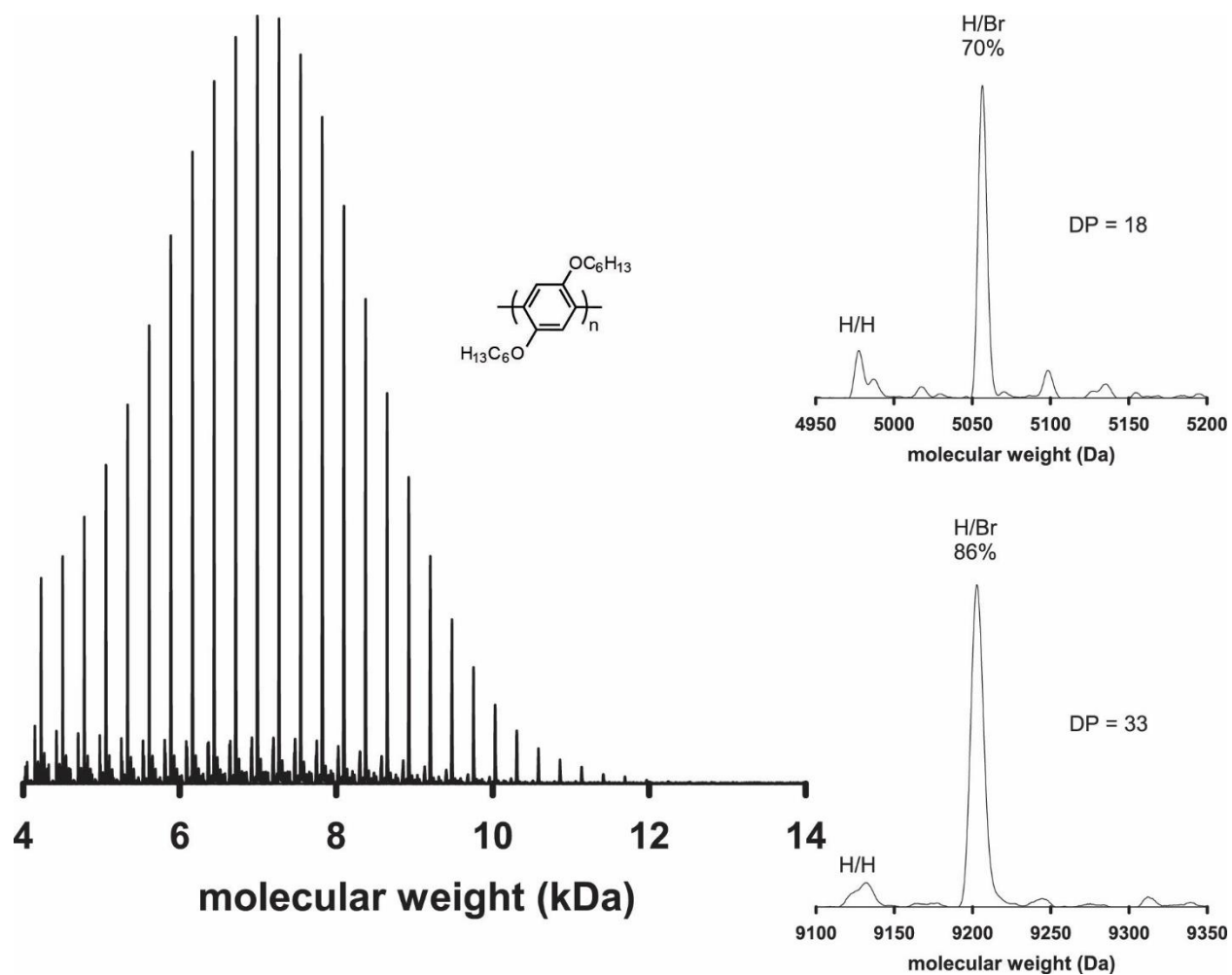
**Table A2-5.** Catalyst migration values for **4b** from Run 1–5. Avg and STD values are plotted in Figure A2-19.



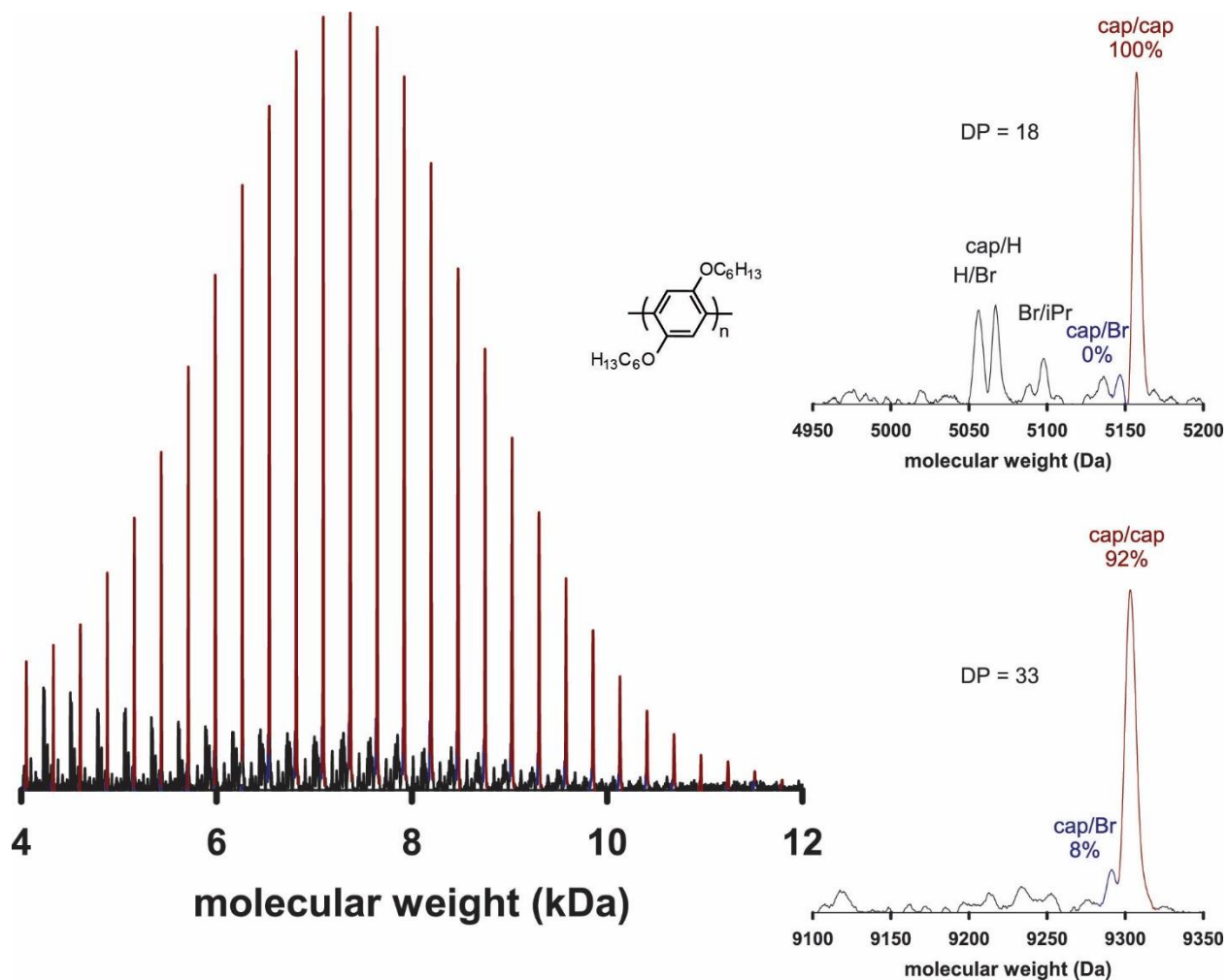
**Figure A2-10.** GPC chromatogram of **P1** produced by **4c** pre (—) or post (—) end-capping with **3a** (15 equiv) and **3b** (50 equiv).

Condition	Conversion of <b>1</b> (%) <sup>a</sup>	$M_n$ (kDa) <sup>b</sup>	$\mathcal{D}^b$	End-groups (%) <sup>c</sup>
pre-capping	93.1	8.8	1.24	83 (Br/H)
post-capping	93.1	9.2	1.34	93 (cap/cap)

**Table A2-6.** Data for **P1** produced by **4c** pre or post end-capping with **3a** (15 equiv) and **3b** (50 equiv). <sup>a</sup>Determined by GC analysis. <sup>b</sup>Determined by GPC analysis. <sup>c</sup>Calculated from the average peak area ratios (at each DP) from the five most intense peaks observed by MALDI-TOF MS analysis.



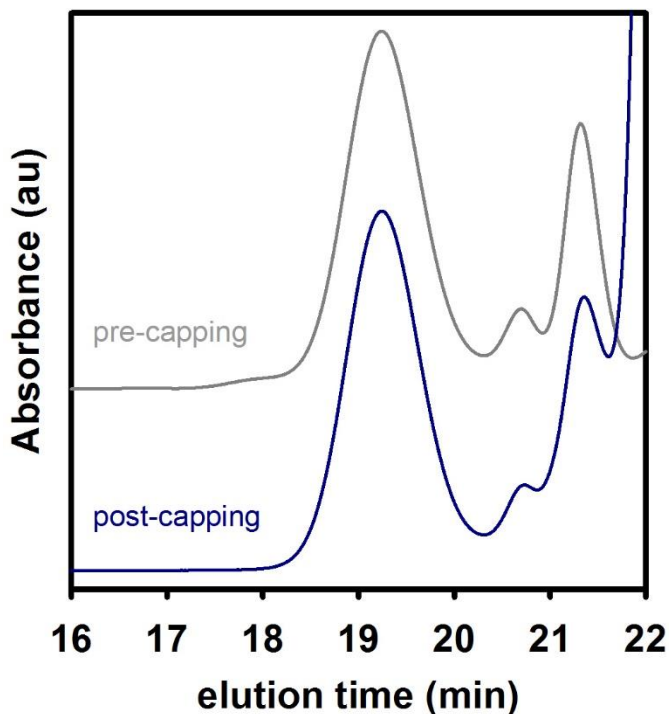
**Figure A2-11.** MALDI-TOF mass spectra of **P1** produced by **4c** before end-capping. Insets (right) show **P1** end-groups at DP = 18 (top) and DP = 33 (bottom).



**Figure A2-12.** MALDI-TOF mass spectra of **P1** produced by **4c** after end-capping with **3a** (15 equiv) and **3b** (50 equiv). Migration (cap/cap, —) and dissociation (cap/Br, —) product peaks are highlighted from all other masses (—). Insets (right) show **P1** end-groups at DP = 18 (top) and DP = 33 (bottom).

m/z of migration product (Da)	Catalyst migration (%)					
	DP	Run 1	Run 2	Run 3	Avg.	SD
5711	20	95	95		95	0
5987	21	93	94		94	0
6264	22	94	94		94	0
6540	23	94	93		94	0
6816	24	94	94		94	0
7093	25	93	93		93	0
7369	26	92	93		93	0
7646	27	93	94		93	1
7922	28	93	92		93	1
8198	29	92	92		92	0
8475	30	92	93		93	0
8751	31	92	91		92	1
9028	32	89	92		90	2
9304	33	92	92		92	0
9581	34		92		92	N/A
9857	35		91	93	92	1
10133	36			93		
10410	37			96		
10686	38			92		
10963	39			94		
11231	40			92		

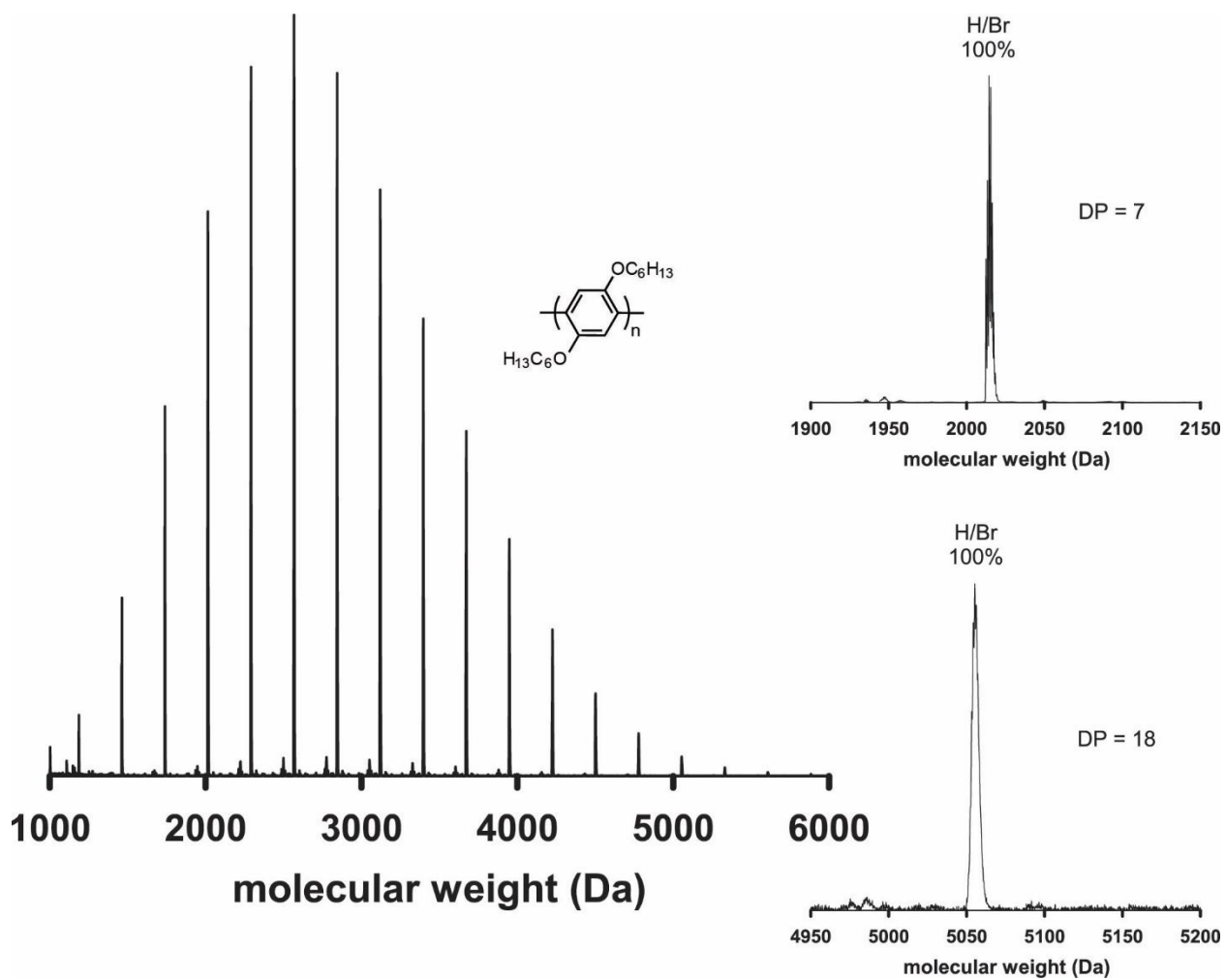
**Table A2-7.** Catalyst migration values for **4c** from Run 1–3. Avg and STD values are plotted in Figure A2-19.



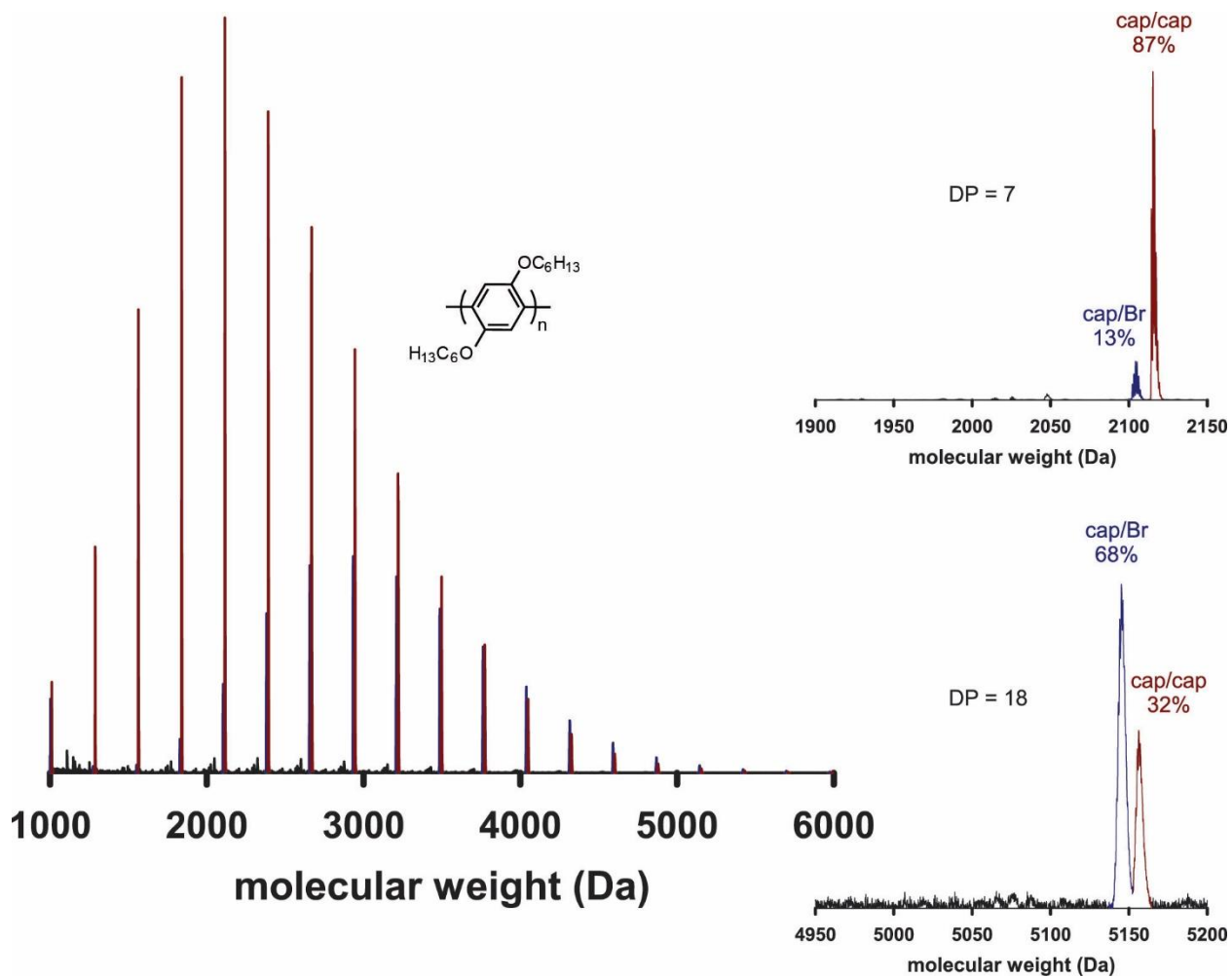
**Figure A2-13.** GPC chromatogram of **P1** produced **4d** pre (—) or post (—) end-capping with **3a** (15 equiv) and **3b** (50 equiv).

Condition	Conversion of <b>1</b> (%) <sup>a</sup>	$M_n$ (kDa) <sup>b</sup>	$\mathcal{D}^b$	End-groups (%)
pre-capping	69	3.0	1.18	94 (Br/H) <sup>c</sup>
post-capping	71	2.9	1.22	53 at DP = 12 (cap/cap)

**Table A2-8.** Data for **P1** produced by **4d** pre or post end-capping with **3a** (15 equiv) and **3b** (50 equiv). <sup>a</sup>Determined by GC analysis. <sup>b</sup>Determined by GPC analysis. <sup>c</sup>Calculated from the average peak area ratios (at each DP) from the five most intense peaks observed by MALDI-TOF MS analysis.



**Figure A2-14.** MALDI-TOF mass spectra of **P1** produced by **4d** before end-capping. Insets (right) show **P1** end-groups at DP = 7 (top) and DP = 18 (bottom).

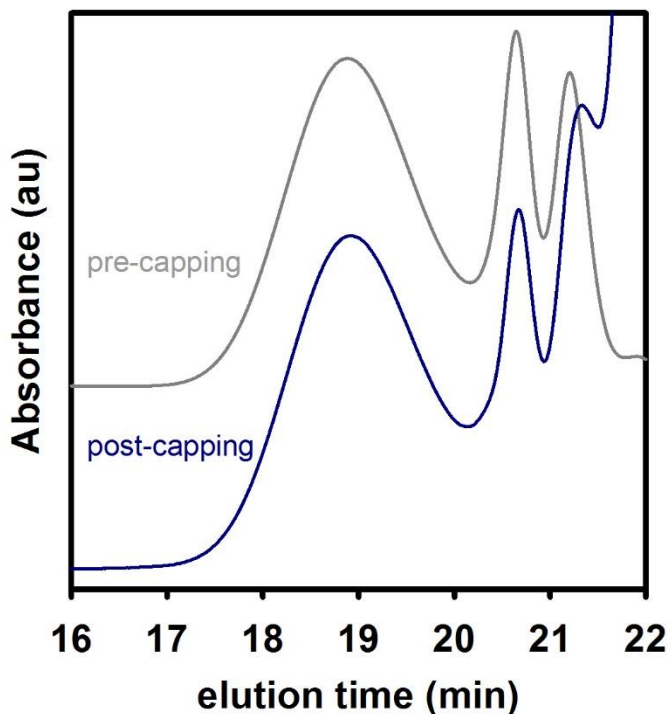


**Figure A2-15.** MALDI-TOF mass spectra of **P1** produced by **4d** after end-capping with **3a** (15 equiv) and **3b** (50 equiv). Migration (cap/cap, —) and dissociation (cap/Br, —) product peaks are highlighted from all other masses (—). Insets (right) show **P1** end-groups at DP = 7 (top) and DP = 18 (bottom).



m/z of migration product (Da)	Catalyst migration (%)					
	DP	Run 1	Run 2	Run 3	Avg.	SD
1564	5		98	98	98	0
1841	6	88	94	95	92	4
2117	7	80	87	89	86	5
2394	8	77	79	81	79	2
2670	9	68	70	72	70	2
2946	10	62	63	65	63	1
3223	11	56	59	57	57	2
3499	12	50	53	52	52	1
3776	13	47	48	47	47	1
4052	14	42	44	43	43	1
4329	15	38	40	39	39	1
4605	16	35	37	36	36	1
4881	17	32	34	33	33	1
5158	18	30	32	31	31	1
5434	19	28	31	31	30	2
5711	20	26				
5987	21	25				
6264	22	24				
6540	23	23				

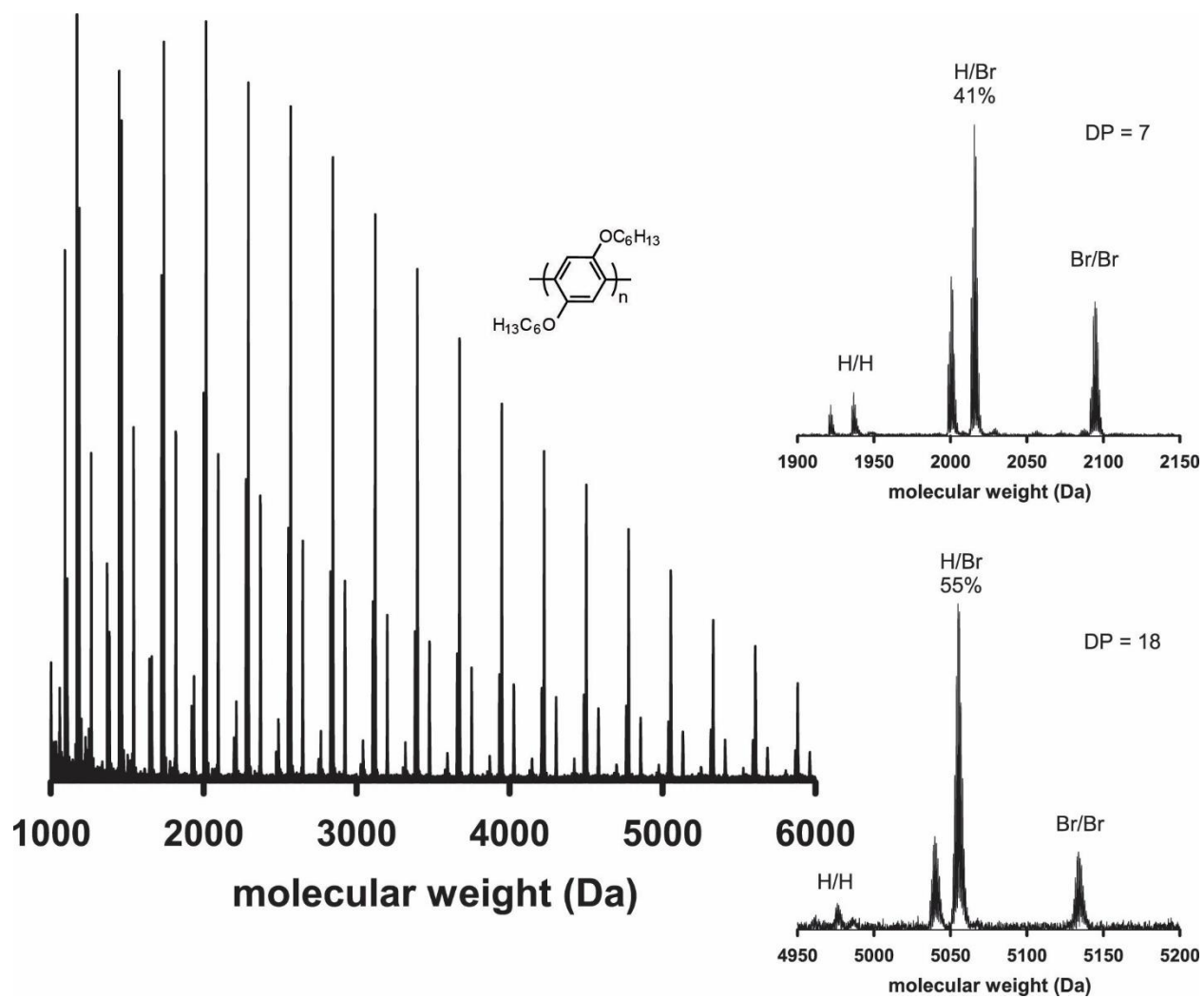
**Table A2-9.** Catalyst migration values for **4d** from Run 1–3. Avg and STD values are plotted in Figure A2-19.



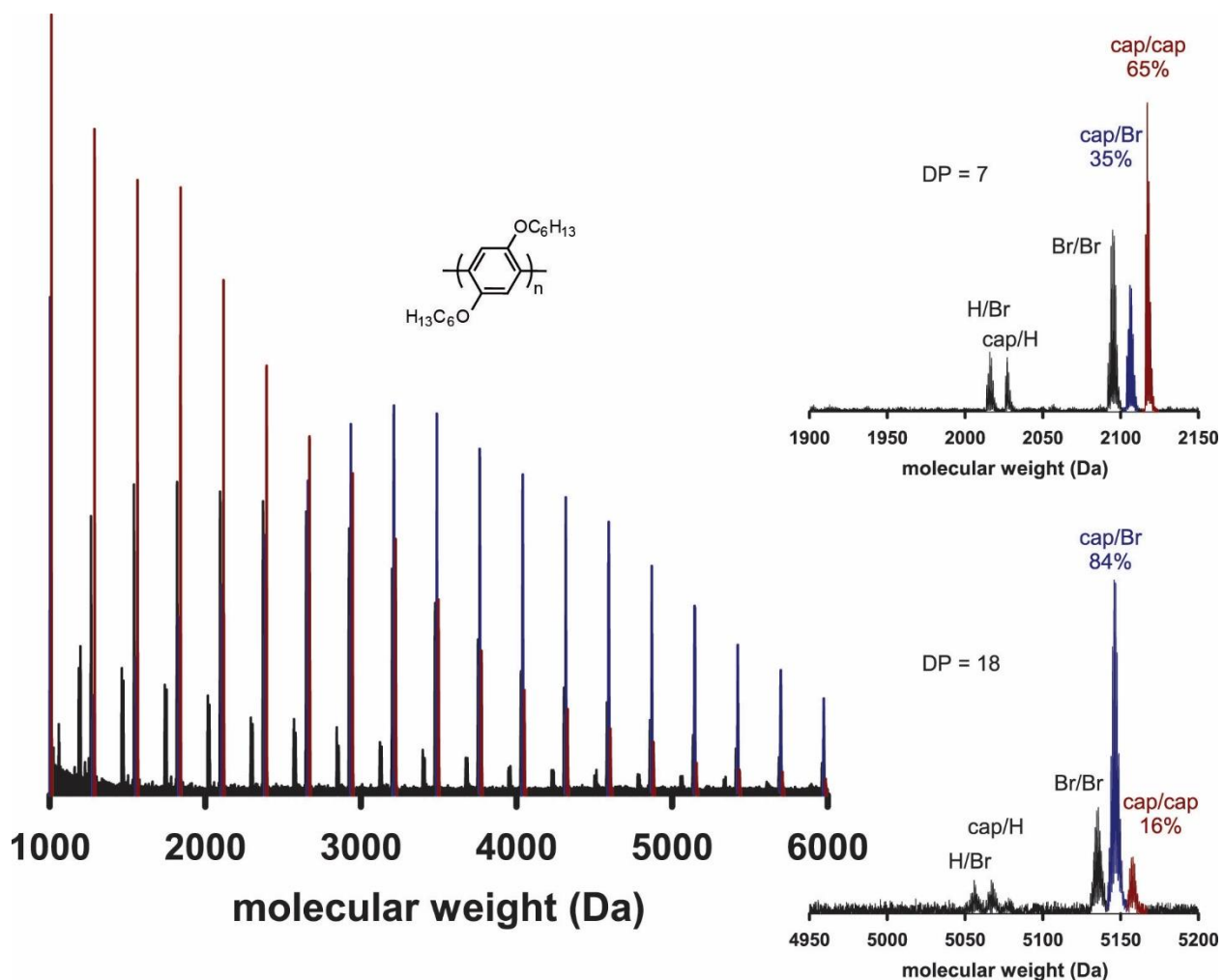
**Figure A2-16.** GPC chromatogram of **P1** produced **4e** pre (—) or post (—) end-capping with **3a** (15 equiv) and **3b** (50 equiv).

Condition	Conversion of <b>1</b> (%) <sup>a</sup>	$M_n$ (kDa) <sup>b</sup>	$\mathcal{D}^b$	End-groups (%)
pre-capping	81	5.3	1.42	48 (Br/H) <sup>c</sup>
post-capping	81	3.4	1.52	54 at DP = 9 (cap/cap)

**Table A2-10.** Data for **P1** produced by **4e** pre or post end-capping with **3a** (15 equiv) and **3b** (50 equiv). <sup>a</sup>Determined by GC analysis. <sup>b</sup>Determined by GPC analysis. <sup>c</sup>Calculated from the average peak area ratios (at each DP) from the five most intense peaks observed by MALDI-TOF MS analysis.



**Figure A2-17.** MALDI-TOF mass spectra of **P1** produced by **4e** before end-capping. Insets (right) show **P1** end-groups at DP = 7 (top) and DP = 18 (bottom).



**Figure A2-18.** MALDI-TOF mass spectra of **P1** produced by **4e** after end-capping with **3a** (15 equiv) and **3b** (50 equiv). Migration (cap/cap, —) and dissociation (cap/Br, —) product peaks are highlighted from all other masses (—). Insets (right) show **P1** end-groups at DP = 7 (top) and DP = 18 (bottom).

m/z of migration product (Da)	Catalyst migration (%)						
	DP	Run 1	Run 2	Run 3	Run 4	Avg.	SD
1564	5	86	80	82	82	83	2
1841	6	80	71	72	70	73	4
2117	7	72	60	65	60	64	6
2394	8	65	55	52	59	58	6
2670	9	59	49	50	52	53	5
2946	10	54	40	43	47	46	6
3223	11	46	36	37	40	40	5
3499	12	40	31	32	34	34	4
3776	13	35	26	28	31	30	4
4052	14	30	22	22	23	24	4
4329	15	26	18	20	22	22	3
4605	16	24	17	20	23	21	3
4881	17	22	15	18	17	18	3
5158	18	20	13	17	19	17	3
5434	19	17	11		14	14	3
5711	20	16					
5987	21	15					
6264	22	12					

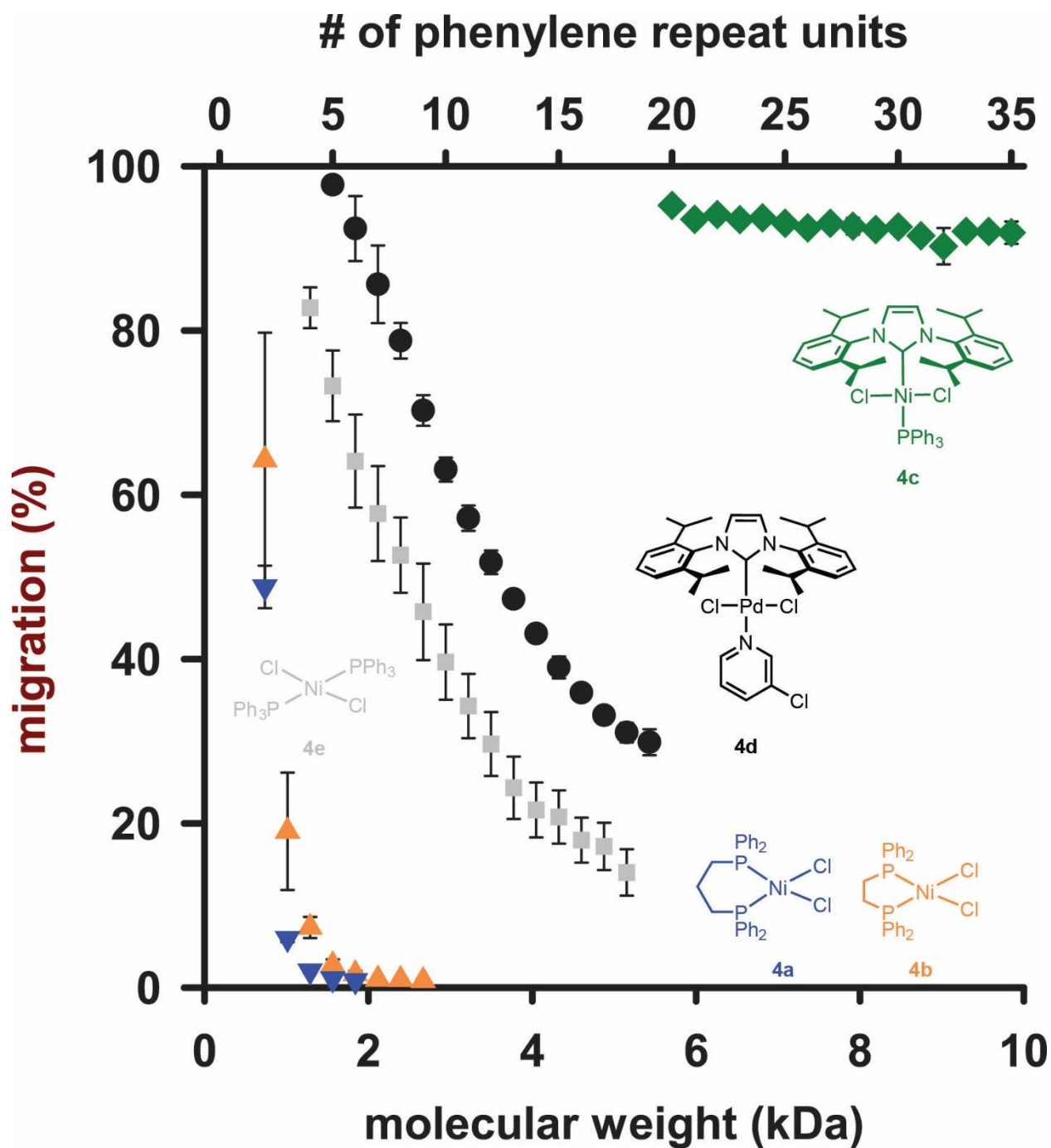
**Table A2-11.** Catalyst migration values for **4e** from Run 1–4. Avg and STD values are plotted in Figure A2-19.

## VII. Catalyst migration

Catalyst migration was determined using the peak areas (A) for cap/cap ( $A_{\text{cap/cap}}$ ) and cap/Br ( $A_{\text{cap/Br}}$ ) peaks at each DP. Catalyst migration was only calculated at DP where both peaks are detected by peak picking (see MALDI general procedures, pg. 2).

While cap/H end-groups also correspond to the migration pathway, these end-groups could also be generated from non-ideal reaction pathways (which give rise to H/H end-groups during acid quenching of typical polymerizations). Cap/H, although present in small amounts, was not included in this calculation to eliminate any possible contribution from this undesired pathway.

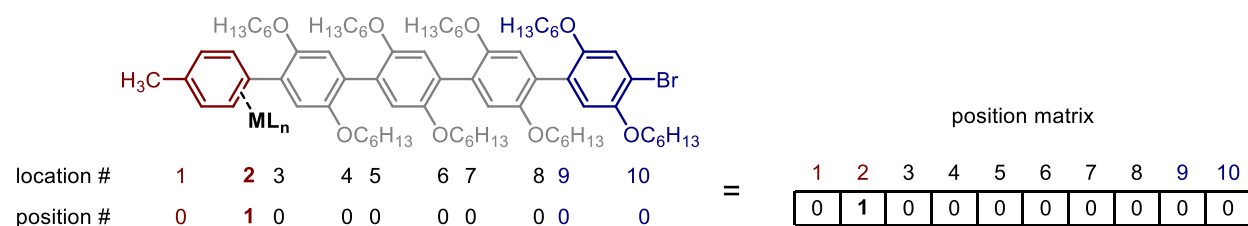
$$\text{catalyst migration} = A_{\text{cap/cap}} / (A_{\text{cap/cap}} + A_{\text{cap/Br}})$$



**Figure A2-19.** Migration pathway percent calculated at each DP for precatalysts **4a–e** across **P1** in the end-capping model experiments. Migration pathway percent was calculated from peak areas determined by MALDI-TOF MS. Error bars represent one standard deviation.

## VIII. Random-walking calculations

In the end-capping experiments, a typical polymerization of **1** is terminated by adding **3a** and **3b**. All catalysts should initially transmetallate with **3a**, forming a catalyst-**P1**  $\pi$ -complex following reductive elimination. Using the most thermodynamically favorable  $\eta$ -2 coordination mode, there are two coordination sites on each monomer (and the cap).<sup>3,4</sup> The  $\pi$ -complex initially forms between the catalyst and cap, placing the catalyst one step away from the capped end and eight linear steps away from the C-Br terminus. This starting configuration can be represented by the position matrix [0,1,0,0,0,0,0,0,0], and is identified as location 2 (Figure A2-20).



**Figure A2-20.** Numerical representation of catalyst binding to the cap of **P1** (DP = 4) with cap/Br end-groups for use in the random-walking calculations. Zeroes represent unoccupied  $\pi$ -binding sites, while a one identifies the catalyst location in the position matrix.

Literature reports on catalyst migration in CTP use a random-walking model to describe end-to-end migration.<sup>5,6</sup> We employed a purely random-walk for all positions on the polymer chain (besides the chain ends) where the catalyst has an equal probability (1/2) of walking one unit towards either chain end. At the capped end, chain-walking always occurs towards the middle of the chain. Catalyst is assumed to react quantitatively when it reaches the C-Br terminus (i.e., after reaching the C-Br end, it stays there). These parameters result in the following transition matrix (Table A2-12).



0	1	0	0	0	0	0	0	0	0
1/2	0	1/2	0	0	0	0	0	0	0
0	1/2	0	1/2	0	0	0	0	0	0
0	0	1/2	0	1/2	0	0	0	0	0
0	0	0	1/2	0	1/2	0	0	0	0
0	0	0	0	1/2	0	1/2	0	0	0
0	0	0	0	0	1/2	0	1/2	0	0
0	0	0	0	0	0	1/2	0	1/2	0
0	0	0	0	0	0	0	1/2	0	1/2
0	0	0	0	0	0	0	0	0	1

**Table A2-12.** Transition matrix for a random walk with 10 linear steps from chain-end to chain-end (i.e., DP = 4 with cap/Br end-groups).

Calculations were performed in Wolfram Mathematica, Version 10.4. The random distribution function *DiscreteMarkovProcess* was used to calculate the products of the position and transition matrices to identify all the possible routes that a catalyst could take to migrate back and forth along the polymer (starting from location 2).

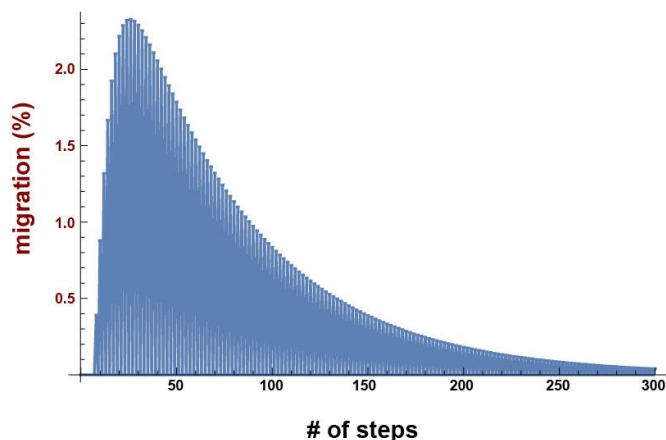
$$A = \text{DiscreteMarkovProcess}[\text{position matrix } x \text{ transition matrix}]$$

Because catalyst is assumed to react quantitatively when it reaches the  $\alpha$  terminus (position 10 when DP = 4), we were interested in the number of steps that it takes for a catalyst to randomly walk from location 2 to location 10. We use the *first passage time distribution* function to determine the number of steps for the catalyst to reach the chain-end (location 10) for the first time.

$$D = \text{FirstPassageTimeDistribution}[A, 10];$$

Thus far, all calculations interrogate the number of steps for 100% catalyst migration, but our end-capping experiments reveal that migration is not quantitative. We use the probability distribution function to identify how many steps are required for the catalyst to reach position 10 once. For example, there is only one possible way for the catalyst to migrate from location 2 to 10 in eight steps (migrate exclusively from left to right along the position matrix), but there are eight possible ways to migrate in ten steps (and so on). The probability for any catalyst to reach the  $\alpha$  end in each number of steps increases initially, then slowly decreases (Figure A2-21).

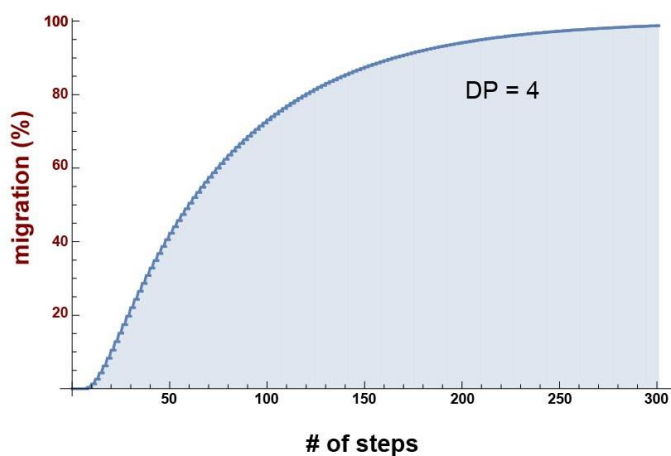
$$\text{PDF}[D, k]; \text{DiscretePlot}[\%, \{k, 0, 300\}, \text{ExtentSize} \rightarrow \text{Right}]$$



**Figure A2-21.** Plot of the probability distribution function of the *first passage distribution* for a purely random walk across 10 locations (corresponding to a DP of 4).

Calculating the integral of the probability distribution function (i.e., the cumulative distribution function) yields the cumulative percent of catalysts that migrated across the polymer within a given number of steps (Figure A2-22). This cumulative percent at a given number of steps is analogous to the migration percent determined experimentally. For a polymer with DP = 4, the number of steps would vary from 60 to 268 by selecting a migration from 50% to 98%.

`CDF[D, k]; DiscretePlot[%, {k, 0, 300}, ExtentSize -> Right]`



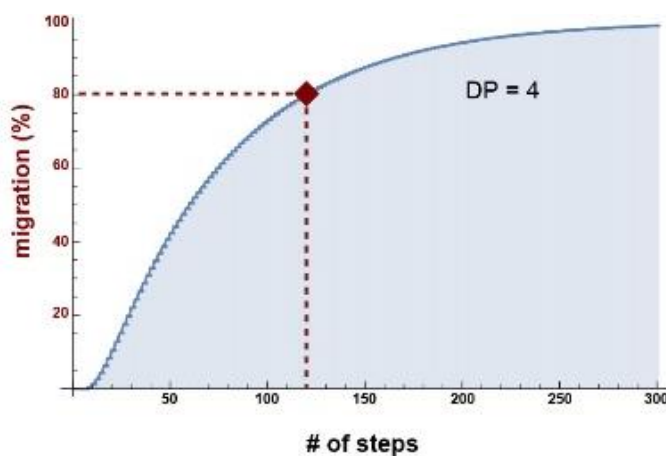
**Figure A2-22.** Plot of the cumulative distribution function of the *first passage distribution* for a purely random walk across 10 locations (corresponding to a DP of 4).

We calculated the cumulative distribution function at numerous points between DP = 4–34 in the same manner identified above. Calculating the random walking process at higher DP simply expands the transition and position matrices, but the catalyst can still only walk one unit left or

right for each step. The same cumulative distribution functions can be used with the experimental data from all catalysts. We identified the number of steps for each catalyst to migrate by iterating the number of steps ( $S$ ) until the cumulative probability ( $M$ ) matched the experimentally determined migration percent. An arbitrary example for 80% migration when  $DP = 4$  is shown below (calculated to 3 significant digits, Figure A2-23).

$$N[CDF[D,S],3] = M$$

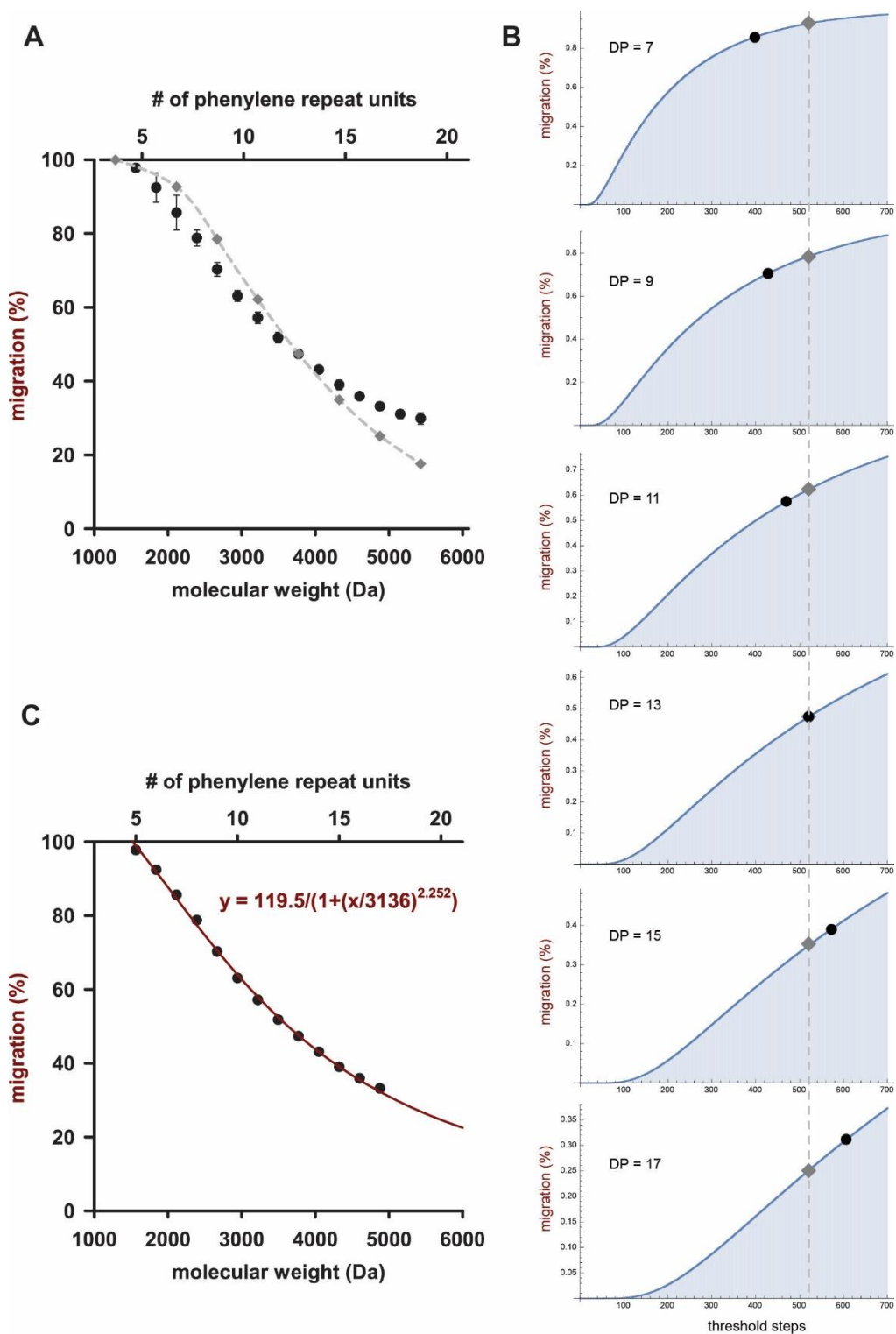
$$N[CDF[D,118],3] = 0.796$$



**Figure A2-23.** Plot of the cumulative distribution function of the *first passage distribution* for a purely random walk across 10 locations (corresponding to a DP of 4). The number of steps required to match 80% migration is 118.

The output from these calculations is the *number of steps* required to achieve a migration percent that matches experimental data (for each catalyst at each DP). Although the random-walking model doesn't directly calculate chain-transfer/dissociation, the number of steps is linearly correlated to chain-transfer/dissociation in the end-capping experiments if the probability for chain-transfer/dissociation is constant across all polymer lengths. Given the high solubility, rigid-rod conformation, and relatively short effective conjugation length for **P1**, we expect that the catalyst-**P1**  $\pi$ -complex is similar for all  $DP > 5$ . Therefore, the probability of chain-transfer/dissociation at each step should be independent of chain-length, and the cumulative probability of chain-transfer/dissociation is correlated to the total number of steps. If the random walking process is representative of catalyst migration in the end-capping experiments, we would expect a similar number of steps for each catalyst over the full range of DPs. In other words, the number of steps is correlated to the probability of dissociation at each step. Each catalyst should have a distinct probability of dissociation that remains constant for all DP (as discussed above).

Using the number of chain-walking steps as a proxy for the probability of dissociation, we can fit the experimental data to the random-walking model. If a catalyst can migrate 520 steps before dissociation, the migration percent would be 93% when  $DP = 7$ , but fall to 25% when  $DP = 17$ . We observe a wide variation in the number of steps at different DP for **4d**, suggesting that the simple random chain-walking model is insufficient to describe the migration behavior (Figure A2-24).



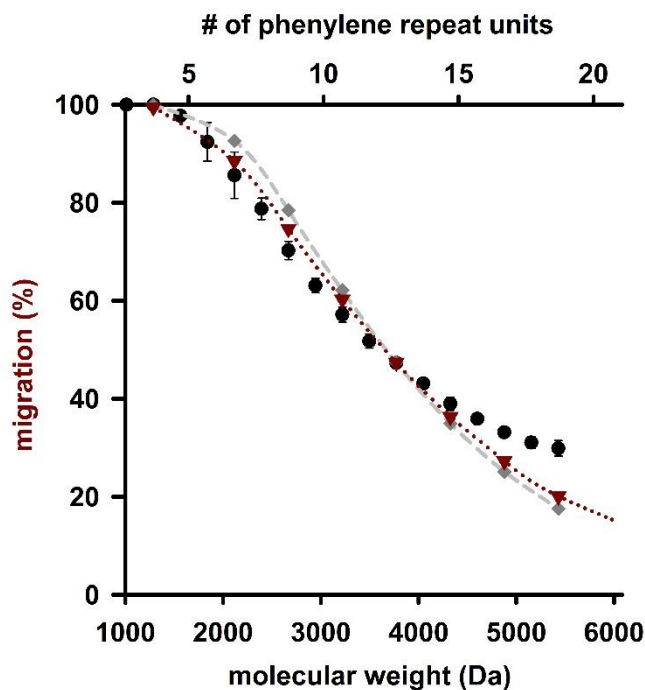
**Figure A2-24.** (A) Experimental values for the migration pathway are plotted against molecular weight/DP for **4d** (●) and statistical calculations (◆) at 520 steps. (B) Plots of cumulative distribution function for DP = 7, 9, 11, 13, 15, and 17 for 0–700 steps are overlaid with the end-capping data [plotted in (A)] from **4d** (●) and the statistical calculations points (◆). A reference line at 520 steps (---) is provided to illustrate the experimental deviation from the random-walking calculation. (C) Logistic function fit to migration percent across DP = 5–18 for **4d**.

Other groups have suggested that an additional parameter, termed *stickiness*, should be used to account for the different electronic and steric environment when the catalyst is one unit away from the chain-end (i.e., location 3 and location 7 represented in Figure A2-20).<sup>5,6</sup> We verified that *stickiness* plays a minor role in random walking for **4d** by comparing three binding affinities to the cap; one where the catalyst is repelled by the cap ( $C = 1$ ), one where chain-walking is purely random ( $C = 2$ ), and another where the catalyst is attracted to the cap ( $C = 3$ ). Independently, we evaluated *stickiness* to the phenylene-Br chain-end ( $B$ ) using the same range of values ( $B = 1, 2, \text{ or } 3$ ). These parameters result in the following 10 x 10 transition matrix:

0	1	0	0	0	0	0	0	0	0
1/2	0	1/2	0	0	0	0	0	0	0
0	$C/4$	0	$(4-C)/4$	0	0	0	0	0	0
0	0	1/2	0	1/2	0	0	0	0	0
0	0	0	1/2	0	1/2	0	0	0	0
0	0	0	0	1/2	0	1/2	0	0	0
0	0	0	0	0	1/2	0	1/2	0	0
0	0	0	0	0	0	$(4-B)/4$	0	$B/4$	0
0	0	0	0	0	0	0	1/2	0	1/2
0	0	0	0	0	0	0	0	0	1

**Table A2-13.** Transition matrix used for DP = 4 to account for *sticky*, *neutral*, or *repulsive* chain-ends ( $C$  = cap end, Br = phenylene-Br end) where B/C could each have values of 3, 2, or 1.

We calculated all nine combinations of *sticky/repulsive* chain-ends, observing that a sticky cap ( $C = 3$ ) and neutral phenylene-Br ( $B = 2$ ) improves the fit to experimental data but does not capture the curvature at high or low migration percentages (Figure A2-25, note that  $C = 2, B = 1$  yields the same results as  $C = 3, B = 2$ ). Therefore, end-group effects do not fully account for the observed discrepancy between experimental results (from **4d**) and the random-walking calculations. For migration using **4a/4b**, end-group *stickiness/repulsion* dominates the migration calculation due to the very small number of repeating units. Alternatively, the ratio of migration product is insensitive to DP when precatalyst **4c** is used, so no fitting can be performed.



**Figure A2-25.** Experimental values for the migration pathway are plotted against molecular weight/DP for **4d** (●) and statistical calculations for a purely random walk (520 steps, ◆) or a random walk that is biased towards the cap ( $C = 3$ ) and neutral to phenylene-Br ( $B = 2$ ) (816 steps, ▼).

m/z of migration product (Da)	Migration (%)		
	experimental	random	biased
1564	98	100	100
1841	92		
2117	86	93	88
2394	79		
2670	70	78	75
2946	63		
3223	57	62	60
3499	52		
3776	47	47	47
4052	43		
4329	39	35	36
4605	36		
4881	33	25	27
5158	31		
5434	30	18	20

**Table A2-14.** Migration and molecular weight values plotted in Figure A2-25.

## IX. References

- (1) Lanni, E. L.; McNeil, A. J. Mechanistic Studies on Ni(dppe)Cl<sub>2</sub>-Catalyzed Chain-Growth Polymerizations: Evidence for Rate-Determining Reductive Elimination. *J. Am. Chem. Soc.* **2009**, *131*, 16573–16579.
- (2) Love, B. E.; Jones, E. G. The Use of Salicylaldehyde Phenylhydrazone as an Indicator for the Titration of Organometallic Reagents. *J. Org. Chem.* **1999**, *64*, 3755–3756.
- (3) Zhao, Y.; Nett, A. J.; McNeil, A. J.; Zimmerman, P. M. Computational Mechanism for Initiation and Growth of Poly(3-Hexylthiophene) Using Palladium N-Heterocyclic Carbene Precatalysts. *Macromolecules* **2016**, *49*, 7632–7641.
- (4) Mikami, K.; Nojima, M.; Masumoto, Y.; Mizukoshi, Y.; Takita, R.; Yokozawa, T.; Uchiyama, M. Catalyst-Dependent Intrinsic Ring-Walking Behavior on  $\pi$ -Face of Conjugated Polymers. *Polym. Chem.* **2017**, *8*, 1708–1713.
- (5) Tkachov, R.; Senkovskyy, V.; Komber, H.; Sommer, J. U.; Kiriya, A. Random Catalyst Walking along Polymerized Poly(3-Hexylthiophene) Chains in Kumada Catalyst-Transfer Polycondensation. *J. Am. Chem. Soc.* **2010**, *132*, 7803–7810.
- (6) Kohn, P.; Huettner, S.; Komber, H.; Senkovskyy, V.; Tkachov, R.; Kiriya, A.; Friend, R. H.; Steiner, U.; Huck, W. T. S.; Sommer, J.-U. U.; *et al.* On the Role of Single Regiodefects and Polydispersity in Regioregular poly(3-Hexylthiophene): Defect Distribution, Synthesis of Defect-Free Chains, and a Simple Model for the Determination of Crystallinity. *J. Am. Chem. Soc.* **2012**, *134*, 4790–4805.



## Appendix 3

### Supporting Information for Chapter 4

#### Optimizing NHC-precatalysts for end-functionalized (co)polymers

<b>I.</b>	<b>Materials</b>	<b>201</b>
<b>II.</b>	<b>General experimental</b>	<b>202</b>
<b>III.</b>	<b>Synthetic procedures</b>	<b>204</b>
<b>IV.</b>	<b>NMR spectra</b>	<b>214</b>
<b>V.</b>	<b>Copolymerizing 1 and 2 with 3a.</b>	<b>226</b>
<b>VI.</b>	<b>Attempted transmetallation to yield IPrPd(aryl)Cl</b>	<b>229</b>
<b>VII.</b>	<b>Oxidative addition to yield IPrPd(aryl)I</b>	<b>235</b>
<b>VIII.</b>	<b>In situ cross-coupling to generate IPrPd(aryl)X, then polymerizing 2</b>	<b>245</b>
<b>IX.</b>	<b>Polymerizing 1 and 2 with precatalyst 5a–c</b>	<b>250</b>
<b>X.</b>	<b>Polymerizing 2 with precatalyst 6a/6b</b>	<b>256</b>
<b>XI.</b>	<b>Effect of 3-chloropyridine on polymerizing 2 with precatalyst 6b</b>	<b>258</b>
<b>XII.</b>	<b>Effect of LiCl on polymerizing 2 with precatalyst 6b</b>	<b>265</b>
<b>XIII.</b>	<b>References</b>	<b>275</b>

## I. Materials

Flash chromatography was performed on SiliCycle silica gel (40–63  $\mu\text{m}$ ). Thin layer chromatography was performed on Merck TLC plates (pre-coated with silica gel 60 F254).  $i\text{PrMgCl}$  (2 M in THF) was purchased in 100 mL quantities from Sigma-Aldrich. Palladium(II) dichloride and  $\text{IPrPd(allyl)Cl}$  (**6a**) were purchased from Strem (IPr = 1,3-bis(2,6-diisopropylphenyl)imidazol-2-ylidene). All other reagent grade materials and solvents were purchased from Sigma-Aldrich, Acros, or Fisher and were used without further purification unless otherwise noted. THF was dried and deoxygenated using an Innovative Technology (IT) solvent system composed of activated alumina, copper catalyst, and molecular sieves. *N*-Bromosuccinimide was recrystallized from hot  $\text{H}_2\text{O}$  and dried over  $\text{P}_2\text{O}_5$ . The glovebox in which specified procedures were carried out was an MBraun LABmaster 130 with a  $\text{N}_2$  atmosphere and  $\text{H}_2\text{O}$  levels below 4 ppm. Compounds **S1**,<sup>1</sup> **S2**,<sup>1</sup> **2**,<sup>1</sup> **S3**,<sup>2</sup> **1**,<sup>2</sup> **S4**,<sup>3</sup> **S5**,<sup>3</sup> **3a**,<sup>4</sup> **5a**,<sup>5</sup> **5b**,<sup>5</sup> **5c**,<sup>5</sup> and **6b**<sup>6</sup> were prepared using modified literature procedures.

## II. General experimental

NMR Spectroscopy: Unless otherwise noted,  $^1\text{H}$ ,  $^{13}\text{C}$ , and  $^{31}\text{P}$  NMR spectra for all compounds were acquired at rt in  $\text{CDCl}_3$  on a Varian vnmrs 700 spectrometer operating at 700 and 176 MHz, respectively, Varian vnmrs 500 spectrometer operating at 500, 162, and 126 MHz, respectively or Varian MR400 Spectrometer operating at 400 and 100 MHz, respectively. Chemical shift data are reported in units of  $\delta$  (ppm) relative to tetramethylsilane (TMS) and referenced with residual solvent. Multiplicities are reported as follows: singlet (s), doublet (d), triplet (t), doublet of doublets (dd), triplet of doublets (td), pentet (p), heptet (h), or multiplet (m). Residual  $\text{H}_2\text{O}$  is denoted by an \*.

Mass Spectrometry: High-resolution mass spectrometry data were obtained on a Micromass AutoSpec Ultima Magnetic Sector mass spectrometer.

Gel-Permeation Chromatography: Polymer molecular weights were determined by comparison with polystyrene standards (Varian, EasiCal PS-2 MW 580–377,400) at 40 °C in THF on a Malvern Viscotek GPCMax VE2001 equipped with two Viscotek LT-5000L columns (8 mm (ID)  $\times$  300 mm (L)) and analyzed with Viscotek TDA 305 (with RI, UV-PDA Detector Model 2600 (190–500 nm), RALS/LALS, and viscometer) or a Waters 1515 HPLC instrument equipped with Waters Styragel® (7.8 x 300 mm) THF HR 0.5, THF HR 1, and THF HR 4 type columns in sequence and analyzed with Waters 2487 dual absorbance detector (254 nm). Samples were dissolved in THF (with mild heating), and passed through a 0.2  $\mu\text{m}$  PTFE filter prior to analysis. All presented data correspond to the absorbance at 254 nm normalized to the highest peak.

Gas Chromatography: Gas chromatography was carried out using a Shimadzu GC 2010 containing a Shimadzu SHRX5 column (crossbound 5% diphenyl–95% dimethyl polysiloxane; 15 m, 0.25 mm ID, 0.25  $\mu\text{m}$  df).

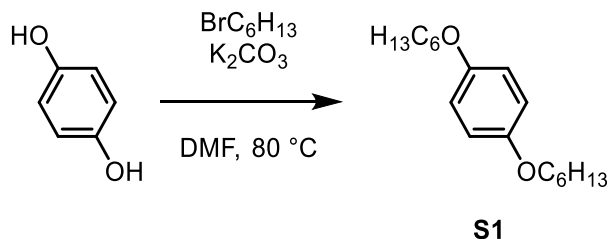
Titration of the Grignard Reagents: An accurately weighed sample of salicylaldehyde phenylhydrazone<sup>7</sup> (typically between 170–200 mg) was dissolved in 10.00 mL of THF. This solution was added dropwise using a 0.5 mL syringe to 0.10 mL of (aryl)MgCl. The initial

(aryl)MgCl solution is pale yellow, turns bright orange, and then returns to pale yellow at the end-point.

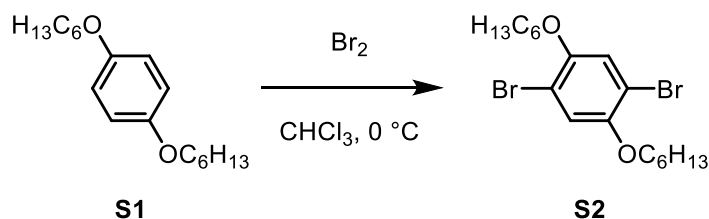
*MALDI-TOF MS*: Matrix-assisted laser desorption/ionization time-of-flight mass spectrometry was performed on a Bruker Autoflex Speed. Positive ion spectra were obtained in reflectron mode. Polymer samples (~1 mg) were dissolved in CHCl<sub>3</sub> (~3 mL) and mixed in a 1:1 (v/v) ratio with 0.1 M trans-2-[3-(4-tert-butylphenyl)-2-methyl-2-propenylidene]malononitrile (DTCB) solution in CHCl<sub>3</sub> then spotted. Serial dilutions (~five-fold) were performed to access a wide range of sample concentrations, and the spot yielding the highest signal/noise was subsequently analyzed. Molecular weight of HCl quenched **P1** or **P2** with Br/H end groups was referenced to a series of low MW peptide standards. The referenced polymer was then used to calibrate the full MW range of the sample.

Raw data was processed in flexAnalysis Version 3.4, with baseline subtraction performed using TopHat. For polymer samples with a maximum m/z <10,000, peak smoothing was performed using one cycle of the SavitskyGolay algorithm to a peak width of 0.1 m/z and peak picking was performed using the SNAP method for peaks with signal/noise greater than two. For polymer samples with a maximum m/z >10,000, peak smoothing was performed using one cycle of the SavitskyGolay algorithm to a peak width of 5-15 m/z and peak picking was performed using the centroid method for peaks with signal/noise greater than one. End-group percentages were calculated by comparing the signal areas of picked peaks at each DP, then averaged across at least five DPs. End-group percentages were independent of DP unless otherwise noted.

### III. Synthetic procedures



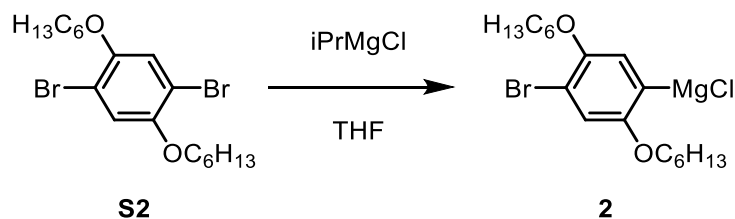
**1,4-bis(hexyloxy)benzene (S1).**<sup>1</sup> A 500 mL flask was equipped with a stir bar, then hydroquinone (20 g, 0.20 mol, 1.0 equiv), DMF (120 mL), potassium carbonate (63 g, 0.45 mol, 2.5 equiv), and 1-bromohexane (63 mL, 0.45 mol, 2.5 equiv) were added sequentially. The reaction mixture was stirred under  $\text{N}_2$  at  $80\text{ }^\circ\text{C}$  for 5 d. The reaction mixture was cooled to rt, then poured into  $\text{H}_2\text{O}$  (400 mL). The mixture was extracted with hexanes (3 x 200 mL) and the organic layer was washed with  $\text{H}_2\text{O}$  (2 x 200 mL) and brine (1 x 200 mL), before drying over  $\text{MgSO}_4$ . The brown mixture was filtered, and concentrated in vacuo. The resulting oil was passed through silica gel using DCM as the eluent. Recrystallization from hot methanol gave a white, crystalline solid (29 g, 57% yield).



**1,4-bis(hexyloxy)-2,5-dibromobenzene (S2).**<sup>1</sup> A 500 mL flask was equipped with a stir bar, then **S1** (24 g, 0.086 mol, 1.0 equiv) and  $\text{CHCl}_3$  (98 mL) were added. The flask was cooled to  $0\text{ }^\circ\text{C}$  in an ice/water bath and fitted with an addition funnel. Bromine (11 mL, 0.21 mol, 2.5 equiv) was added dropwise under  $\text{N}_2$  over 10 min and the pressure was vented through an aq. solution of 10%  $\text{Na}_2\text{SO}_3$  (~150 mL). After 3 h, the reaction was quenched with an aq. sat. solution of  $\text{Na}_2\text{SO}_3$  and vigorously stirred until colorless. The aqueous mixture was extracted with DCM (3 x 100 mL) and the combined organic layers were washed with  $\text{H}_2\text{O}$  (2 x 100 mL) and brine (1 x 100 mL), then

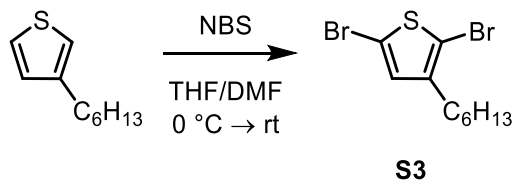
dried over  $\text{MgSO}_4$ , filtered, and concentrated in vacuo. The residue was recrystallized overnight from  $\text{CHCl}_3/\text{MeOH}$  and filtered to afford white crystals (29 g, 77% yield).

---



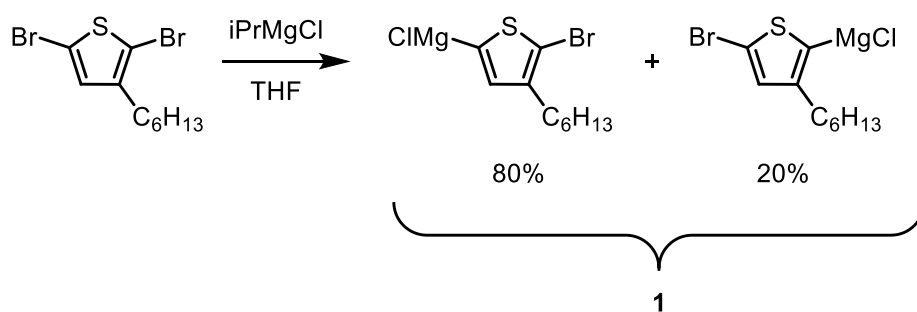
**(4-bromo-2,5-bis(hexyloxy)phenyl)magnesium chloride (2).**<sup>1</sup> In a glovebox, **S2** (0.109 g, 0.25 mmol, 1 equiv) was added to a 4 mL vial equipped with a stir bar. A small amount of  $\text{C}_{22}\text{H}_{46}$  (~5 mg) was added and the mixture was diluted with THF (1.1 mL). Next,  $\text{iPrMgCl}$  (0.11 mL of a 2 M solution in THF, 0.22 mmol, 0.88 equiv) was added and the solution was stirred for 16 h before titrating (0.15 M, see pg. S3).

---

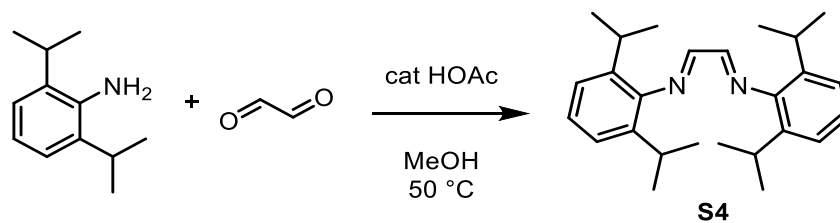


**2,5-dibromo-3-hexylthiophene (S3).**<sup>2</sup> In a 200 mL Schlenk flask equipped with a stir bar, 3-hexylthiophene (5.0 g, 30. mmol, 1.0 equiv) was added and 3 evacuation/ $\text{N}_2$  backfill cycles were performed. Under  $\text{N}_2$  pressure, THF (50 mL) and DMF (10 mL) were added with stirring and the flask was cooled in an ice bath and covered with aluminum foil. N-Bromosuccinimide (11.6 g, 65.3 mmol, 2.20 equiv) was added quickly in one portion. The reaction slowly warmed to rt over the first 3 h, and quenched after 4.5 h with aq. sat.  $\text{Na}_2\text{S}_2\text{O}_3$  (20 mL). The mixture was extracted with hexanes (4 x 20 mL), and the combined organic layers were washed with  $\text{H}_2\text{O}$  (2 x 20 mL) and

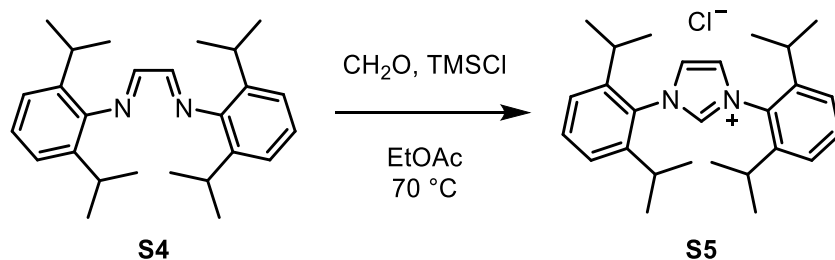
brine (1 x 20 mL). The solution was dried over MgSO<sub>4</sub>, filtered, and then concentrated to a slightly yellow oil using a rotary evaporator. The oil was filtered through a silica gel column (~50 mL) with hexanes (~250 mL) as the eluent to remove any color, collecting the entire sample as in one portion. The solution was concentrated to a colorless oil, which was fractionally distilled under high vacuum with heating (7.5 g, 76% yield).



**1.**<sup>2</sup> In a glovebox, 2,5-dibromo-3-hexylthiophene (0.834 g, 2.56 mmol, 1.00 equiv) was added to a 20 mL vial equipped with a stir bar and diluted with THF (~15 mL). A small amount of C<sub>22</sub>H<sub>44</sub> (~20 mg) was added as an internal standard, and then iPrMgCl (1.1 mL of a 1.98 M solution in THF, 2.1 mmol, 0.81 equiv). The mixture was stirred for 30 min. An aliquot of the solution was removed from the glovebox and quenched with conc. HCl (~0.5 mL). The aliquot was extracted with CHCl<sub>3</sub> (2 x 1 mL), washed with H<sub>2</sub>O (1 x 1 mL), brine (1 x 1 mL), and dried over MgSO<sub>4</sub>. The mixture was filtered, and the mother liquor analyzed by GC to show a mixture of regioisomers at 80% and 20%, respectively.

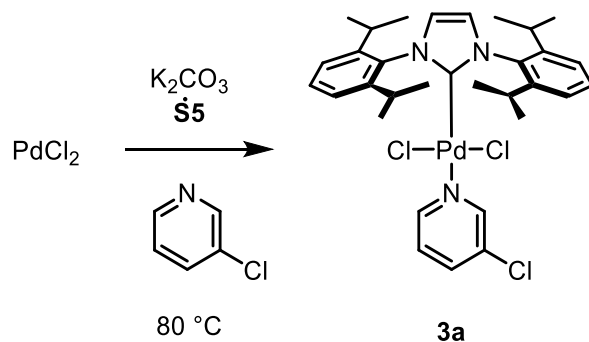


**(1E,2E)-N<sup>1</sup>,N<sup>2</sup>-bis(2,6-di-isopropylphenyl)ethane-1,2-diimine (S4).**<sup>3</sup> A 500 mL round-bottom flask was equipped with a stir bar, then 2,6-diisopropylaniline (100 g, 0.60 mol, 2.0 equiv) and HOAc (0.60 mL, 8.9 mmol, 0.035 equiv) were dissolved in MeOH (135 mL) then heated to 50 °C. Next, glyoxal (39 g of a 40% solution in H<sub>2</sub>O, 0.27 mol, 1.0 equiv) was added to cause an immediate change from colorless to orange-yellow. The reaction mixture was stirred at 50 °C for 15 min over which time the mixture solidified. Additional MeOH (50 mL) was added to enable stirring, which proceeded for an extra 10 h before filtering. The filter cake was washed with cold MeOH (2 x 50 mL) and dried in vacuo to give a yellow solid (94.8 g, 84 % yield).

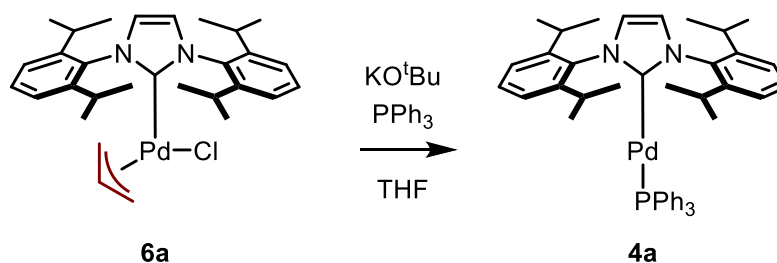


**1,3-bis(2,6-di-isopropylphenyl)imidazolium chloride (S5).**<sup>3</sup> In air, **S4** (50.0 g, 133 mmol, 1.00 equiv) and paraformaldehyde (4.01 g, 133 mmol, 1.00 equiv) were combined with EtOAc (1.2 L) and heated to 70 °C. A solution of TMSCl (16.9 mL, 0.479 mmol, 1.03 equiv) in EtOAc (25 mL) was added dropwise over 45 min with vigorous stirring, and then stirred for an additional 3 h. The reaction mixture was cooled to 0 °C overnight. The solids were filtered, washed with EtOAc (3 x 100 mL), and dried in vacuo to afford a fine white powder (44.4 g, 78% yield).



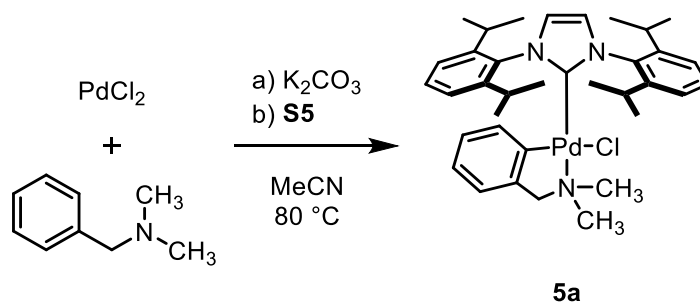


**[1,3-bis(2,6-diisopropylphenyl)imidazol-2-ylidene](3-chloropyridyl)palladium(II) dichloride (3a).**<sup>4</sup> Palladium(II) chloride (0.177 g, 0.100 mmol, 1.00 equiv), **S5** (0.467 g, 0.110 mmol, 1.10 equiv),  $\text{K}_2\text{CO}_3$  (0.69 g, 0.50 mmol, 5.0 equiv), and 3-chloropyridine (4.0 mL) were added to a 15 mL pressure tube equipped with a stir bar. The pressure tube was sealed, and the solution was heated to 80 °C for 16 h. After cooling to rt, the mixture was subjected to a silica gel column with a celite pad at the top. The compound was eluted with a DCM/EtOAc gradient (100/0 to 50/50), and the combined fractions were concentrated using a rotary evaporator. The solids were redissolved in minimal DCM (~0.2 mL), then hexanes (~5 mL) were carefully layered on top and the mixture was placed in the freezer overnight. Yellow crystals were collected by filtration and rinsed with hexanes (~1 mL). The sample was dried under high vacuum for 8 h to yield **3a** (0.463 g, 68%). Elemental Analysis: Calcd for  $\text{C}_{32}\text{H}_{40}\text{Cl}_3\text{N}_3\text{Pd}$ . C, 56.57; H, 5.93; N, 6.18; Found C, 56.40; H, 5.98; N, 6.02.



**[1,3-bis(2,6-di-isopropylphenyl)imidazol-2-ylidene](triphenylphosphino)palladium(0) (4a).<sup>8</sup>**

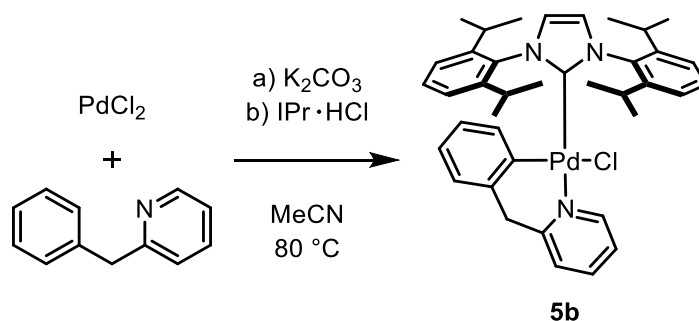
In a glovebox, **6a** (0.190 g, 0.332 mmol, 1.00 equiv) and potassium tert-butoxide (0.038 g, 0.36 mmol, 1.1 equiv) were added to a 50 mL pressure tube and *i*PrOH (5 mL) was added with stirring. Next, triphenylphosphine (0.091 g, 0.35 mmol, 1.1 equiv) was added to the cloudy tan solution and the tube was sealed. Quickly, the solution turned to a cloudy, neon yellow, and was stirred for a total of 2 h. The solids were collected via filtration and the filter cake washed with cold *i*PrOH (~3 mL), cold hexanes (~1 mL), and then dried in vacuo for 6 h to yield a neon yellow solid (0.185 g, 72 % yield).



**Chloro{2-[(dimethylamino)methyl]phenyl}[1,3-bis(2,6-di-isopropylphenyl)imidazol-2-ylidene]palladium(II) (5a).<sup>5</sup>**

Palladium(II) chloride (0.177 g, 0.100 mmol, 1.00 equiv), *N,N*-dimethyl-1-phenylmethanamine (0.148 g, 0.110 mmol, 1.10 equiv), and MeCN (3 mL) were added to a 15 mL pressure tube equipped with a stir bar. The solution was heated to 80 °C (open to air) for 30 min to yield an orange solution, and then  $K_2CO_3$  (0.69 g, 0.50 mmol, 5.0 equiv) was added. The reaction was stirred for an additional 10 min to yield a canary yellow solution, then **S5** (0.467 g, 0.110 mmol, 1.10 equiv) and MeCN (2 mL) were added. The pressure tube was sealed, and the

solution was stirred for an additional 16 h. After cooling to rt, the entire mixture was subjected to a silica gel column with a celite pad at the top. The column was eluted with a DCM/EtOAc gradient (100/0 to 50/50), and the desired fractions were concentrated using a rotary evaporator. The solids were redissolved in minimal DCM (~0.2 mL), then hexanes (~5 mL) were carefully layered on top and the mixture was placed in the freezer overnight. Light yellow/green crystals were collected by filtration and rinsed with hexanes (~1 mL). The sample was dried under high vacuum for 8 h to yield **5a** (0.352 g, 53%).

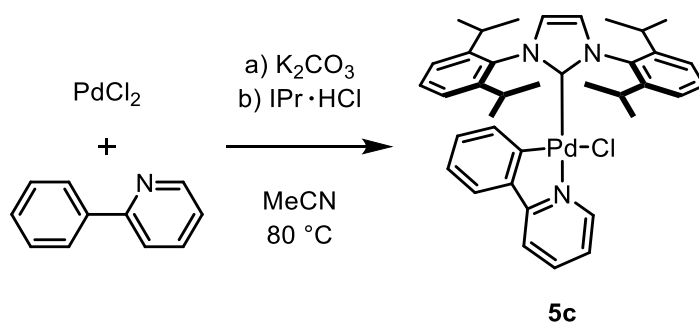


**Chloro[2-(benzyl)pyridine][1,3-bis(2,6-di-isopropylphenyl)imidazol-2-**

**ylidene]palladium(II) (**5b**).**<sup>5</sup> Palladium(II) chloride (0.177 g, 0.100 mmol, 1.00 equiv), 2-benzylpyridine (0.186 g, 0.110 mmol, 1.10 equiv), and MeCN (3 mL) were added to a 15 mL pressure tube equipped with a stir bar. The solution was heated to 80 °C (open to air) for 30 min to yield an orange solution, and then K<sub>2</sub>CO<sub>3</sub> (0.69 g, 0.50 mmol, 5.0 equiv) was added. The reaction was stirred for an additional 10 min to yield a canary yellow solution, then **S5** (0.467 g, 0.110 mmol, 1.10 equiv) and MeCN (2 mL) were added. The pressure tube was sealed, and the solution was stirred for an additional 16 h. After cooling to rt, the entire mixture was subjected to a silica gel column with a celite pad at the top. The column was eluted with a DCM/EtOAc gradient (100/0 to 50/50), and the desired fractions were concentrated using a rotary evaporator. The solids were redissolved in minimal DCM (~0.2 mL), then hexanes (~5 mL) were carefully layered on top and the mixture was placed in the freezer overnight. A white powder was collected by filtration and

rinsed with hexanes (~1 mL). The sample was dried under high vacuum for 8 h to yield **5b** (0.286 g, 41%).

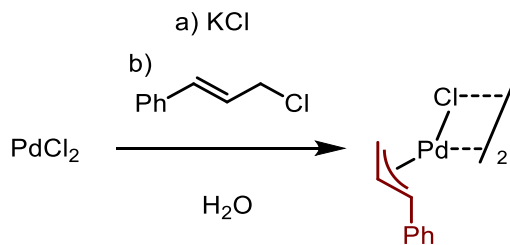
---



**Chloro[2-(phenyl)pyridine][1,3-bis(2,6-di-isopropylphenyl)imidazol-2-**

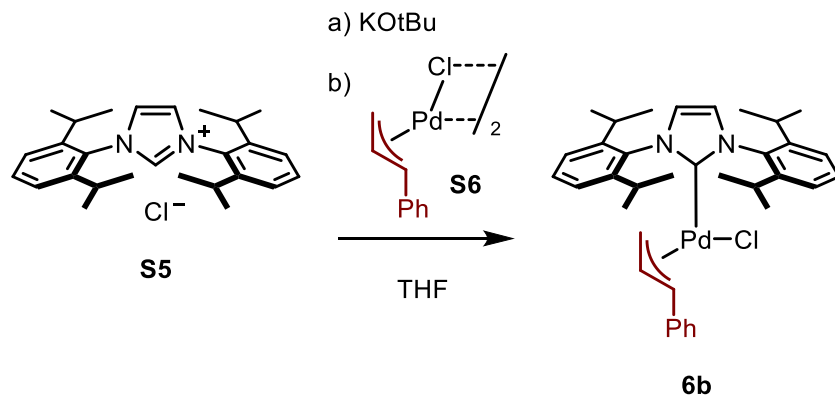
**ylidene]palladium(II) (**5c**).**<sup>5</sup> Palladium(II) chloride (0.177 g, 0.100 mmol, 1.00 equiv), 2-phenylpyridine (0.171 g, 0.110 mmol, 1.10 equiv), and MeCN (3 mL) were added to a 15 mL pressure tube equipped with a stir bar. The solution was heated to  $80\text{ }^\circ\text{C}$  (open to air) for 30 min to yield an orange solution, and then  $\text{K}_2\text{CO}_3$  (0.69 g, 0.50 mmol, 5.0 equiv) was added. The reaction was stirred for an additional 10 min to yield a canary yellow solution, then **S5** (0.467 g, 0.110 mmol, 1.10 equiv) and MeCN (2 mL) were added. The pressure tube was sealed, and the solution was stirred for an additional 16 h. After cooling to rt, the entire mixture was subjected to a silica gel column with a celite pad at the top. The column was eluted with a DCM/EtOAc gradient (100/0 to 50/50), and the desired fractions were concentrated using a rotary evaporator. The solids were redissolved in minimal DCM (~0.2 mL), then hexanes (~5 mL) were carefully layered on top and the mixture was placed in the freezer overnight. A white powder was collected by filtration and rinsed with hexanes (~1 mL). The sample was dried under high vacuum for 8 h to yield **5c** (0.458 g, 67%). Elemental Analysis: Calcd for  $\text{C}_{38}\text{H}_{44}\text{ClN}_3\text{Pd}$ . C, 66.66; H, 6.48; N, 6.14; Found C, 66.86; H, 6.78; N, 6.111.

---



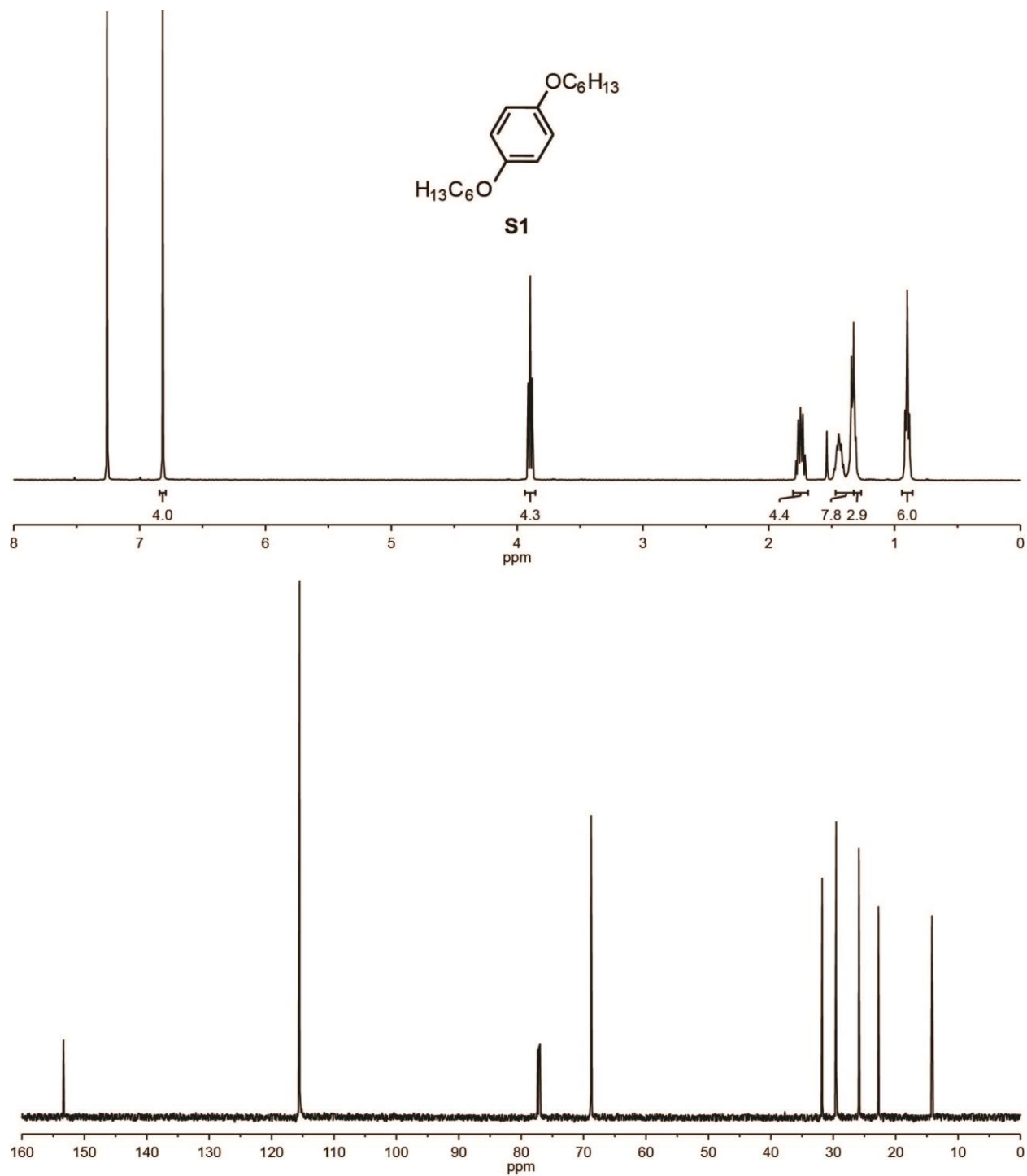
**S6**

**Di- $\mu$ -chlorobis[(1,2,3- $\eta$ )-1-phenyl-2-propenyl]dipalladium(II) (S6).**<sup>9</sup> Palladium(II) chloride (0.53 g, 0.30 mmol, 1.0 equiv) and KCl (0.43 g, 0.60 mmol, 2.0 equiv) were added to a 50 mL round bottom flask with a stir bar and sealed with a rubber septum. Degassed H<sub>2</sub>O (25 mL) was added, and the mixture slowly dissolved to yield a clear, orange-brown solution. After stirring for 1 h, cinnamyl chloride (1.4 g, 0.90 mmol, 3.0 equiv) was added and the mixture was stirred for an additional 24 h. The mixture was extracted with CHCl<sub>3</sub> (5 x 10 mL), washed with H<sub>2</sub>O (1 x 15 mL), and dried over MgSO<sub>4</sub> (~0.1 g). The mixture was filtered and the filtrate was rinsed with CHCl<sub>3</sub> (~2 mL) to remove all yellow color. The mother liquor was concentrated to yield a golden oil. The oil was diluted in DCM (~0.2 mL), then hexanes (5 mL) was slowly layered on and the solution was placed in the freezer. Yellow crystals were collected via filtration, then recrystallized from DCM/Hexanes overnight in the same manner as above. The mixture was filtered, and the filtrate dried under high vacuum for 8 h (0.52 g, 64%). Elemental Analysis: Calcd for C<sub>18</sub>H<sub>18</sub>Cl<sub>2</sub>Pd<sub>2</sub>. C, 41.73; H, 3.50; Found C, 41.70; H, 3.53.



**Chloro[(1,2,3- $\eta$ )-3-phenyl-2-propenyl][1,3-bis(2,6-di-isopropylphenyl)imidazol-2-ylidene]palladium(II) (6b).**<sup>6</sup> In a glovebox, **S5** (0.327 g, 0.771 mmol, 2.03 equiv) and KO<sup>t</sup>Bu (0.0959 g, 0.859 mmol, 2.26 equiv) were added to a 20 mL vial equipped with a stir bar and THF (23 mL) was added. The homogenous solution was stirred for 4.5 h, then **S6** (0.210 g, 0.0380 mmol, 1.00 equiv) was added and the mixture was stirred for an additional 4 h. The solution was removed from the glovebox, then filtered through celite and the mother liquor was concentrated to a dark tan oil that was purified via column chromatography using silica gel (~30 mL) with Hex/EtOAc (7/3 v/v) as eluent. Combined fractions were concentrated to a yellow solid, then redissolved in minimal DCM (~0.2 mL) and hexanes (~5 mL) were carefully layered on top. The mixture was placed in the freezer overnight, and the yellow crystals were collected by filtration and rinsed with hexanes (~1 mL). The sample was dried under high vacuum for 8 h to yield **6b** (0.198 g, 34%).

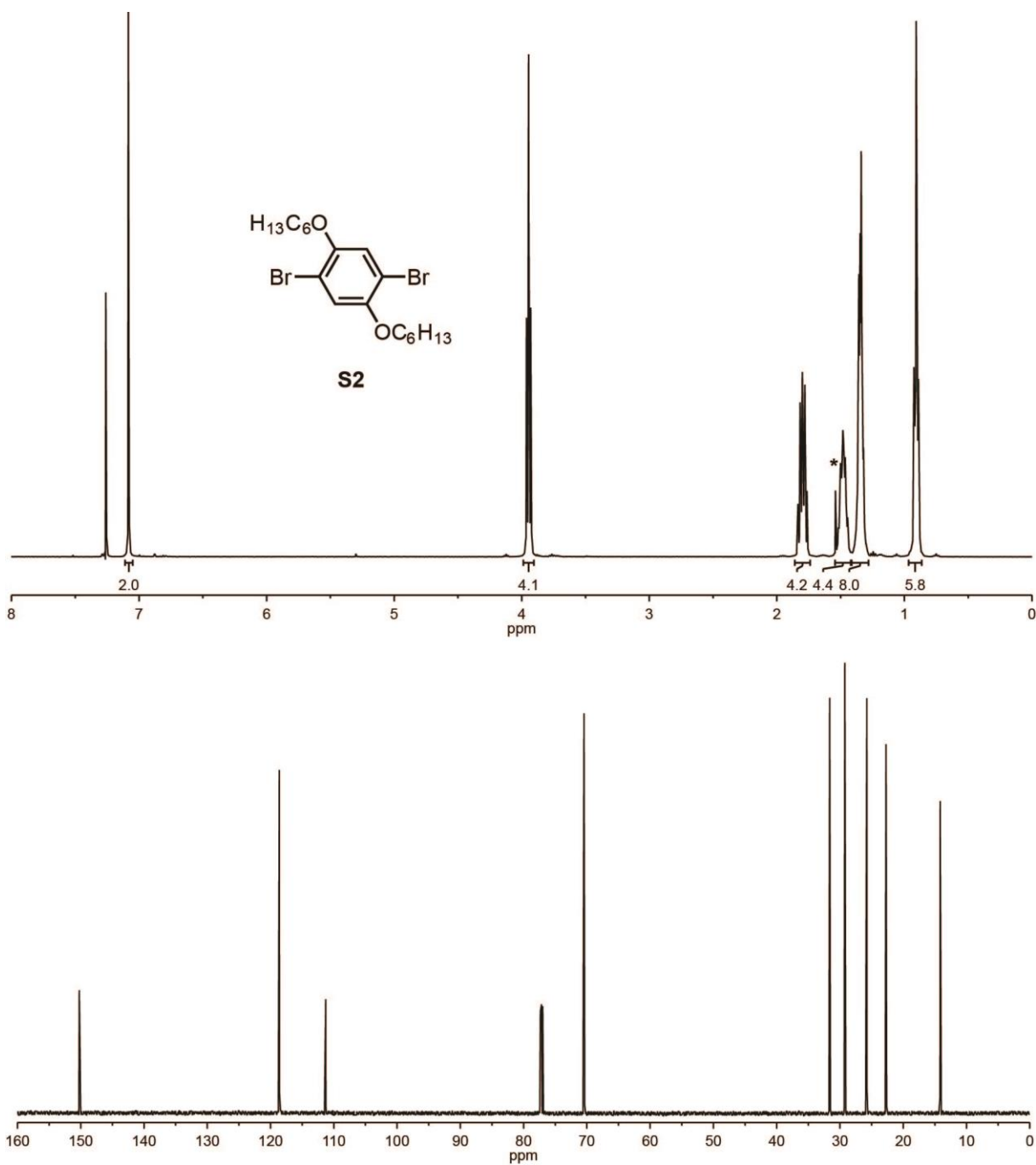
#### IV. NMR spectra



**Figure A3-1.** <sup>1</sup>H and <sup>13</sup>C NMR spectra for **S1**.

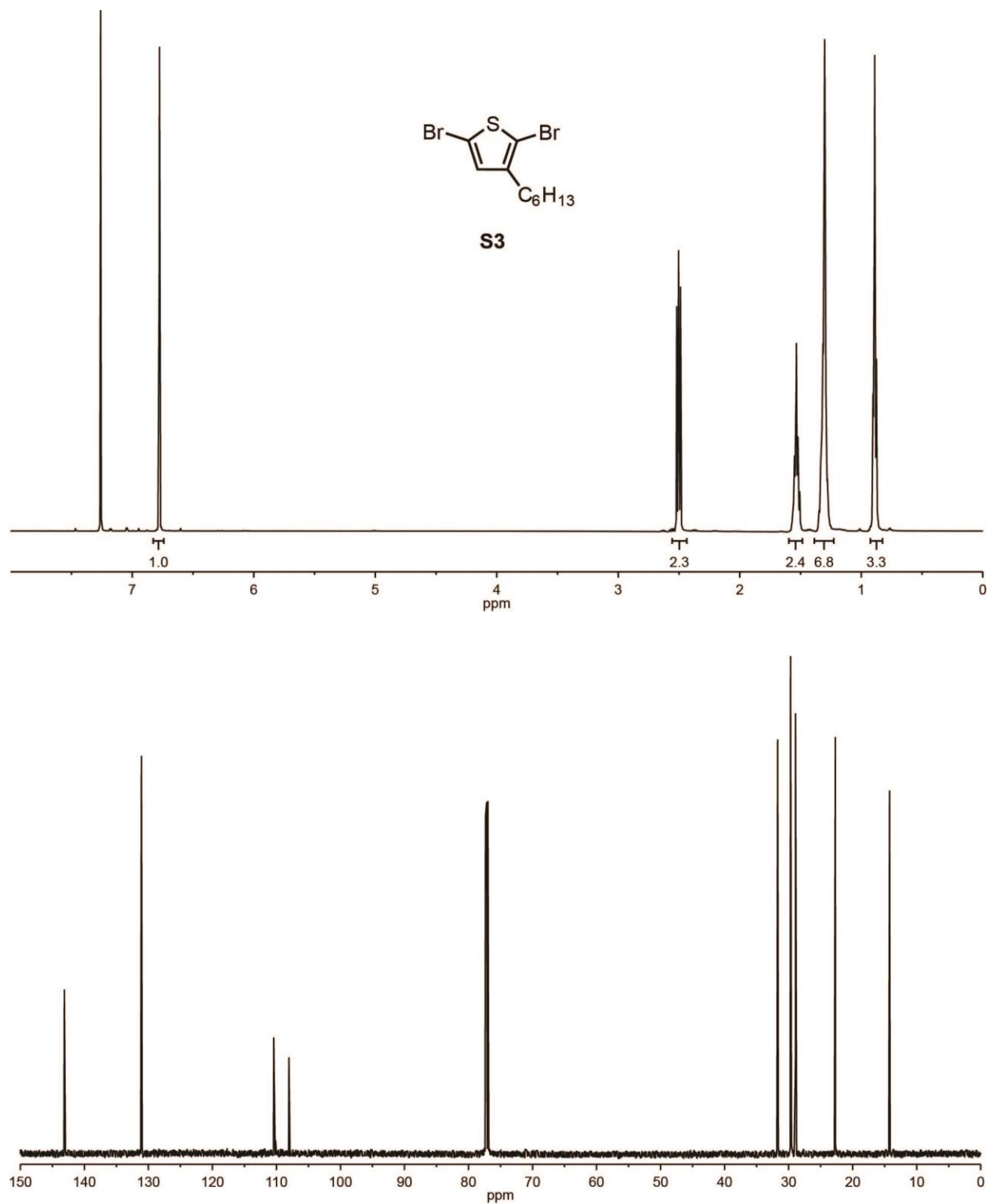
<sup>1</sup>H NMR (400 MHz, CDCl<sub>3</sub>) δ 6.82 (s, 4H), 3.90 (t, *J* = 6.6 Hz, 4H), 1.75 (dt, *J* = 14.7, 6.7 Hz, 4H), 1.49–1.39 (m, 8H), 1.38–1.27 (m, 4H), 0.90 (t, *J* = 6.9 Hz, 6H).

<sup>13</sup>C NMR (176 MHz, CDCl<sub>3</sub>) δ 153.34, 115.53, 68.80, 31.77, 29.53, 25.90, 22.77, 14.19.



**Figure A3-2.** <sup>1</sup>H and <sup>13</sup>C NMR spectra for **S2**.  
<sup>1</sup>H NMR (500 MHz, CDCl<sub>3</sub>) δ 7.08 (s, 2H), 3.95 (t, *J* = 6.5 Hz, 4H), 1.80 (dt, *J* = 14.8, 6.7 Hz, 4H), 1.53–1.44 (m, 4H), 1.39–1.28 (m, 8H), 0.91 (t, *J* = 6.9 Hz, 6H).  
<sup>13</sup>C NMR (176 MHz, CDCl<sub>3</sub>) δ 150.22, 118.62, 111.28, 70.46, 31.63, 29.23, 25.76, 22.72, 14.16

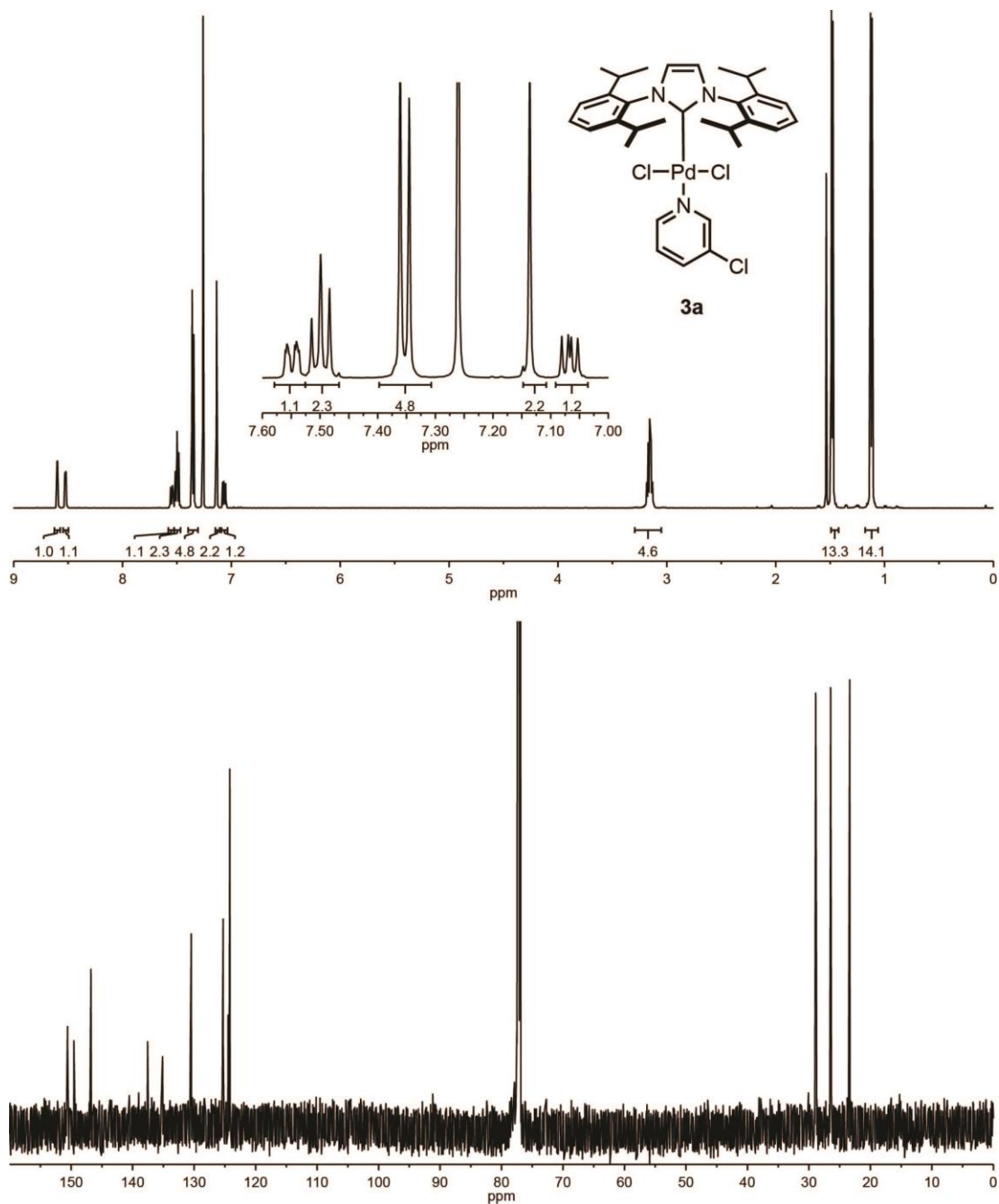




**Figure A3-3.** <sup>1</sup>H and <sup>13</sup>C NMR spectra for **S3**.

<sup>1</sup>H NMR (500 MHz, CDCl<sub>3</sub>) δ 6.78 (s, 1H), 2.60–2.42 (m, 2H), 1.62–1.47 (m, 2H), 1.37–1.23 (m, 6H), 0.89 (t, J = 6.9 Hz, 3H).

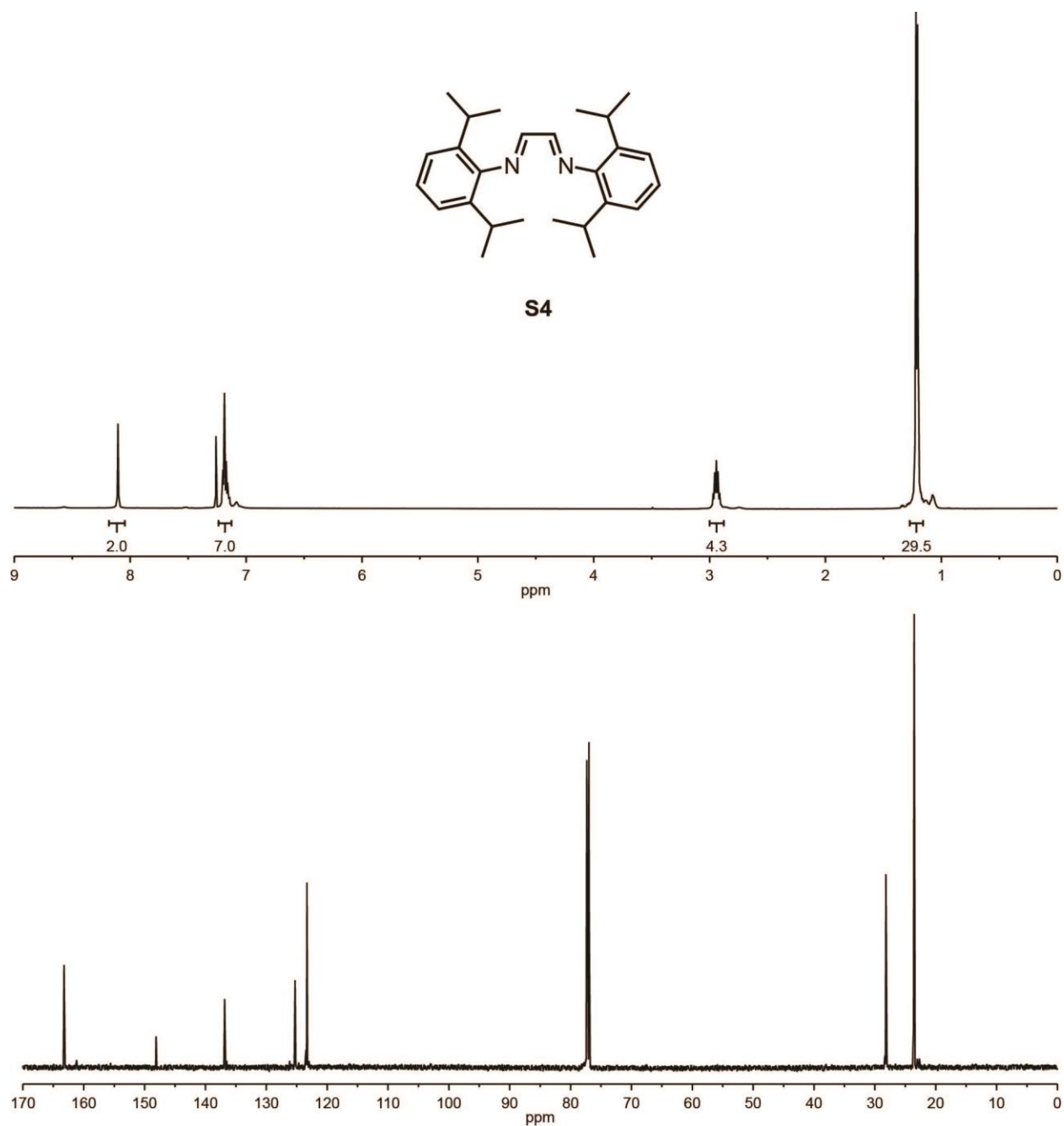
<sup>13</sup>C NMR (176 MHz, CDCl<sub>3</sub>) δ 143.13, 131.09, 110.42, 108.04, 31.71, 29.70, 29.64, 28.93, 22.72, 14.24.



**Figure A3-4.** <sup>1</sup>H and <sup>13</sup>C NMR spectra for **3a**.

<sup>1</sup>H NMR (500 MHz, CDCl<sub>3</sub>) δ 8.60 (d, *J* = 2.3 Hz, 1H), 8.52 (dd, *J* = 5.6, 1.3 Hz, 1H), 7.55 (ddd, *J* = 8.2, 2.4, 1.3 Hz, 1H), 7.50 (t, *J* = 7.8 Hz, 2H), 7.35 (d, *J* = 7.8 Hz, 4H), 7.14 (s, 2H), 7.07 (dd, *J* = 8.2, 5.6 Hz, 1H), 3.16 (hept, *J* = 6.9 Hz, 4H), 1.48 (d, *J* = 6.6 Hz, 12H), 1.12 (d, *J* = 6.9 Hz, 12H).

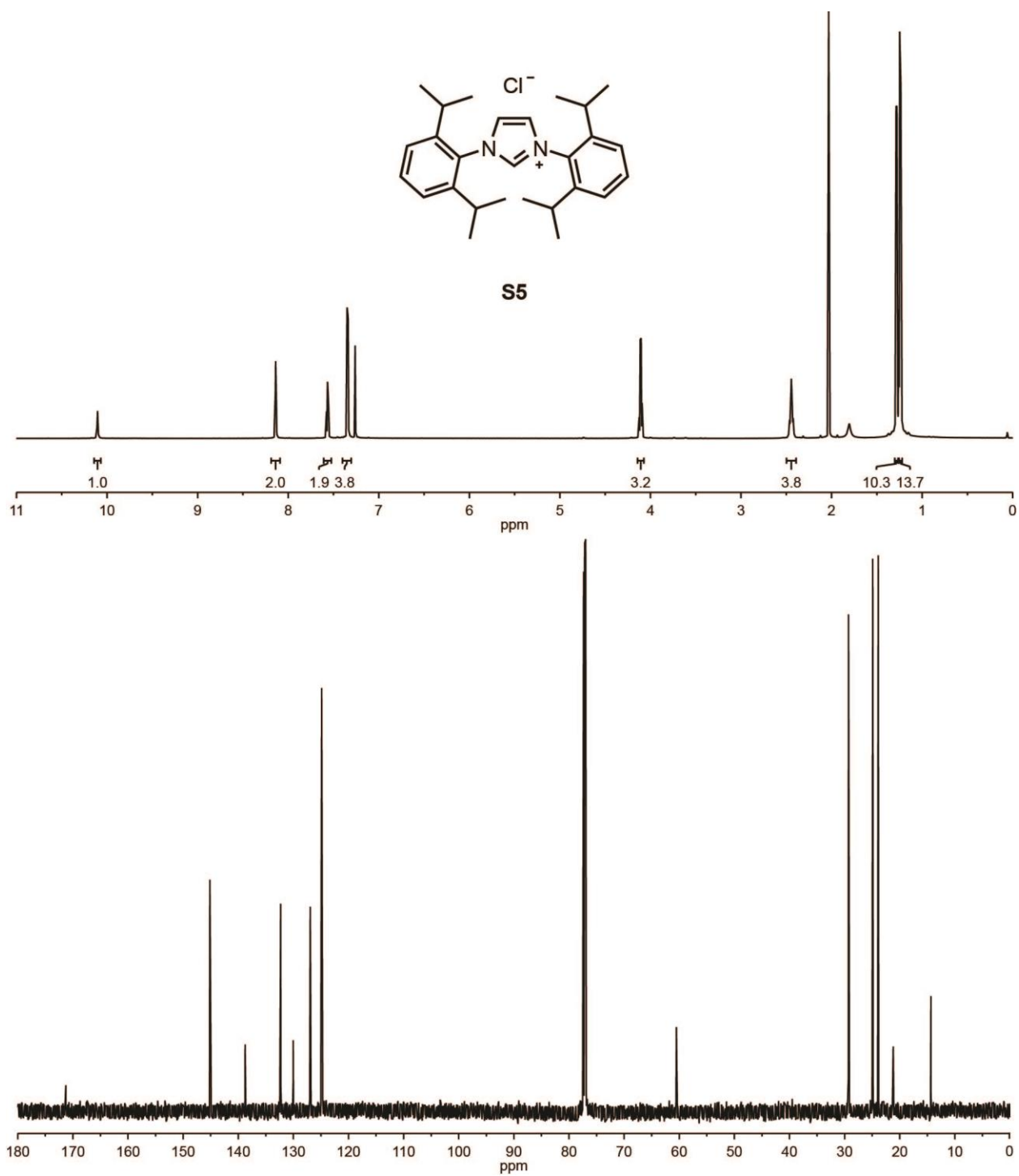
<sup>13</sup>C NMR (176 MHz, CDCl<sub>3</sub>) δ 150.59, 149.55, 146.79, 137.57, 135.13, 130.47, 125.28, 124.48, 124.20, 28.90, 26.46, 23.37.



**Figure A3-5.**  $^1\text{H}$  and  $^{13}\text{C}$  NMR spectra for S4.

$^1\text{H}$  NMR (500 MHz,  $\text{CDCl}_3$ )  $\delta$  8.11 (s, 2H), 7.22–7.13 (m, 6H), 2.94 (hept,  $J = 6.9$  Hz, 4H), 1.21 (d,  $J = 6.9$  Hz, 24H).

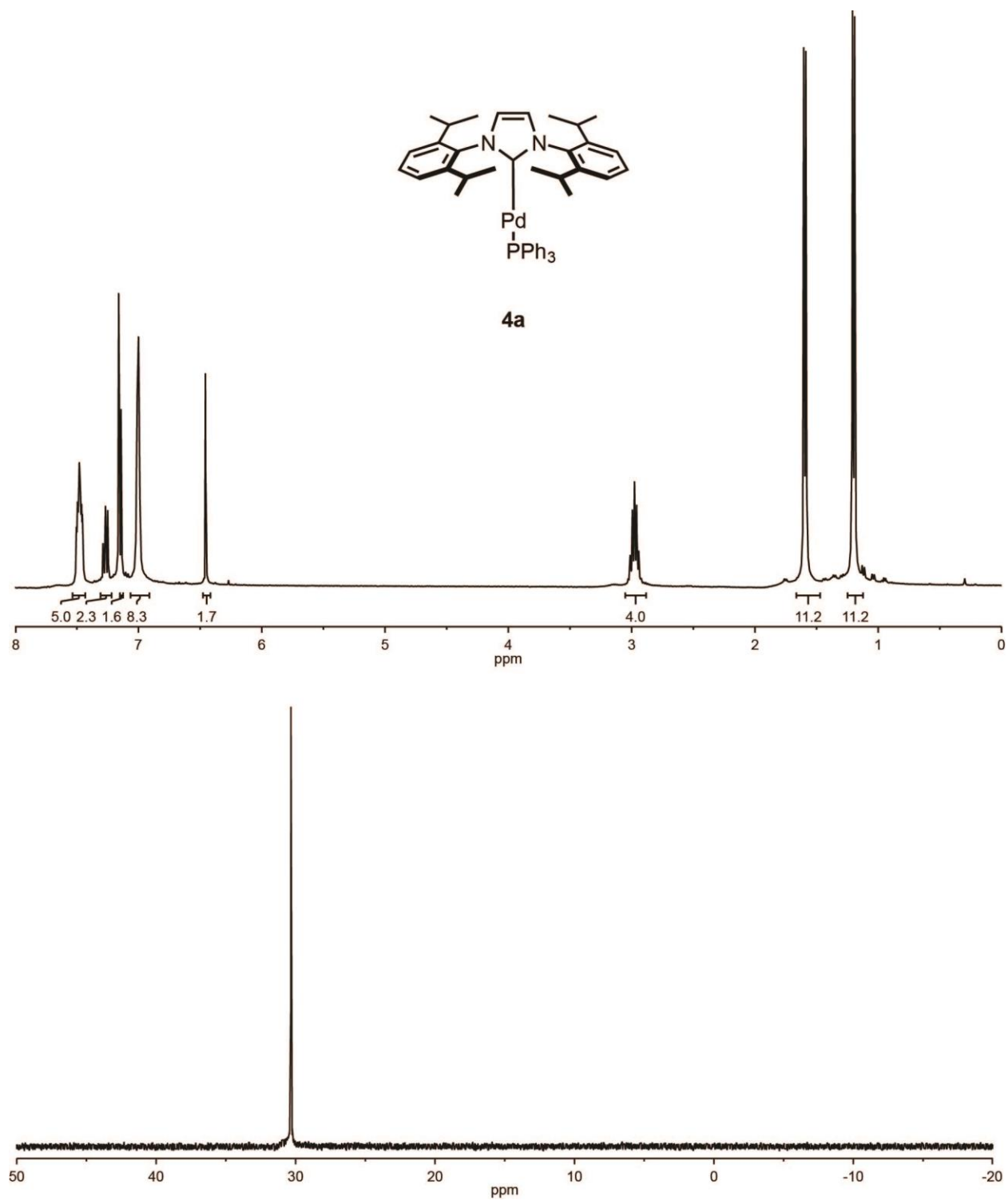
$^{13}\text{C}$  NMR (176 MHz,  $\text{CDCl}_3$ )  $\delta$  163.23, 148.11, 136.85, 136.51, 125.26, 123.32, 28.18, 22.68.



**Figure A3-6.**  $^1\text{H}$  and  $^{13}\text{C}$  NMR spectra for **S5**.

$^1\text{H}$  NMR (700 MHz,  $\text{CDCl}_3$ )  $\delta$  10.11 (s, 1H), 8.14 (s, 2H), 7.56 (t,  $J = 7.9$  Hz, 2H), 7.35 (dd,  $J = 7.8, 2.0$  Hz, 4H), 4.11 (q,  $J = 7.0$  Hz, 4H), 2.44 (hept,  $J = 6.7$  Hz, 4H), 1.28 (d,  $J = 6.8$  Hz, 12H), 1.24 (dd,  $J = 7.0, 2.1$  Hz, 12H).

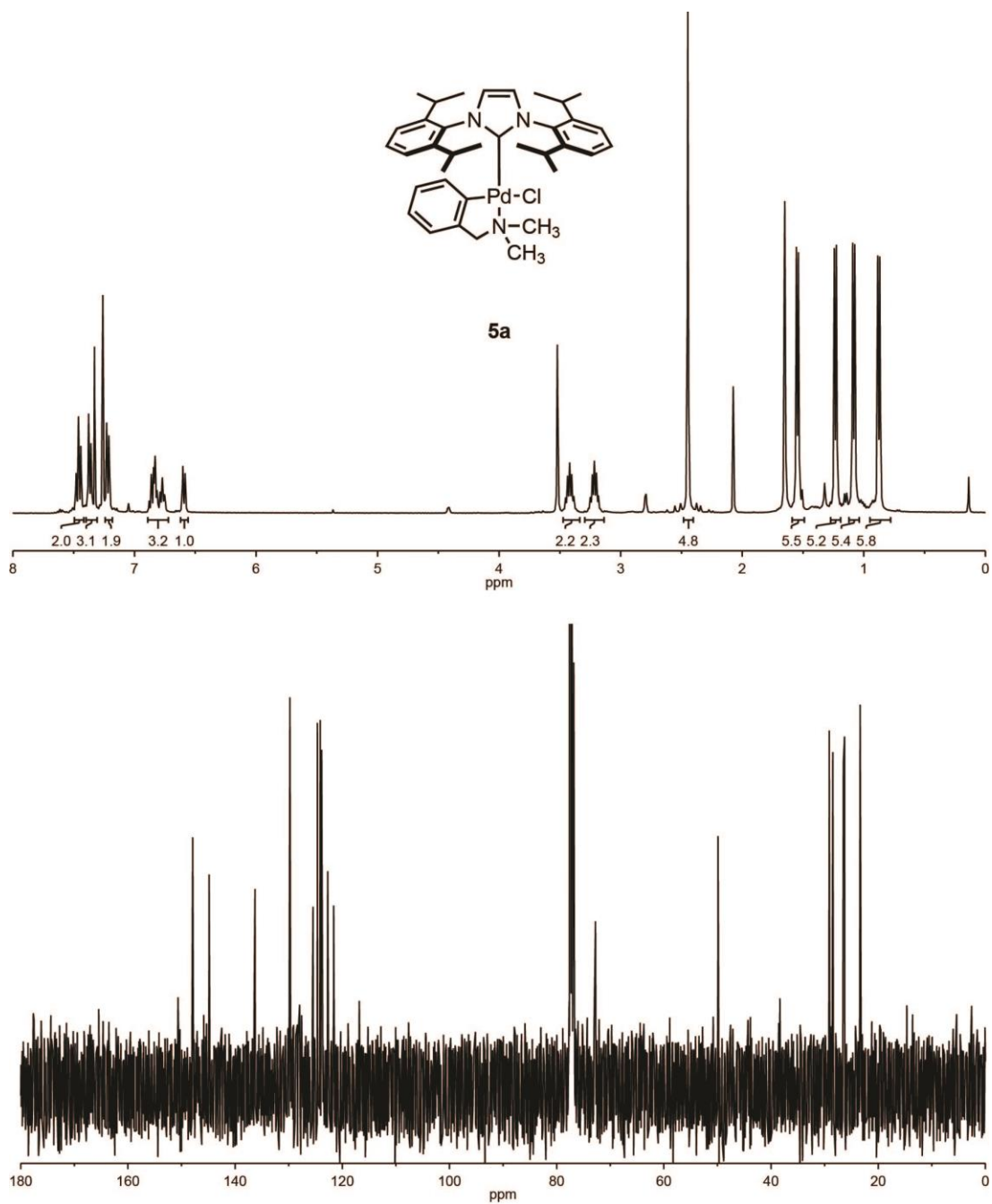
$^{13}\text{C}$  NMR (176 MHz,  $\text{CDCl}_3$ )  $\delta$  171.27, 145.15, 138.76, 132.30, 130.03, 126.94, 124.87, 29.29, 24.90, 23.89.



**Figure A3-7.** <sup>1</sup>H and <sup>31</sup>P NMR spectra for **4a**.

<sup>1</sup>H NMR (400 MHz, C<sub>6</sub>D<sub>6</sub>) δ 7.48 (m, 6H), 7.30–7.24 (m, 3H), 7.14 (s, 2H), 7.03–6.97 (m, 10H), 6.46 (s, 2H), 2.98 (hept, J = 6.9 Hz, 4H), 1.60 (d, J = 6.8 Hz, 12H), 1.20 (d, J = 6.9 Hz, 12H).

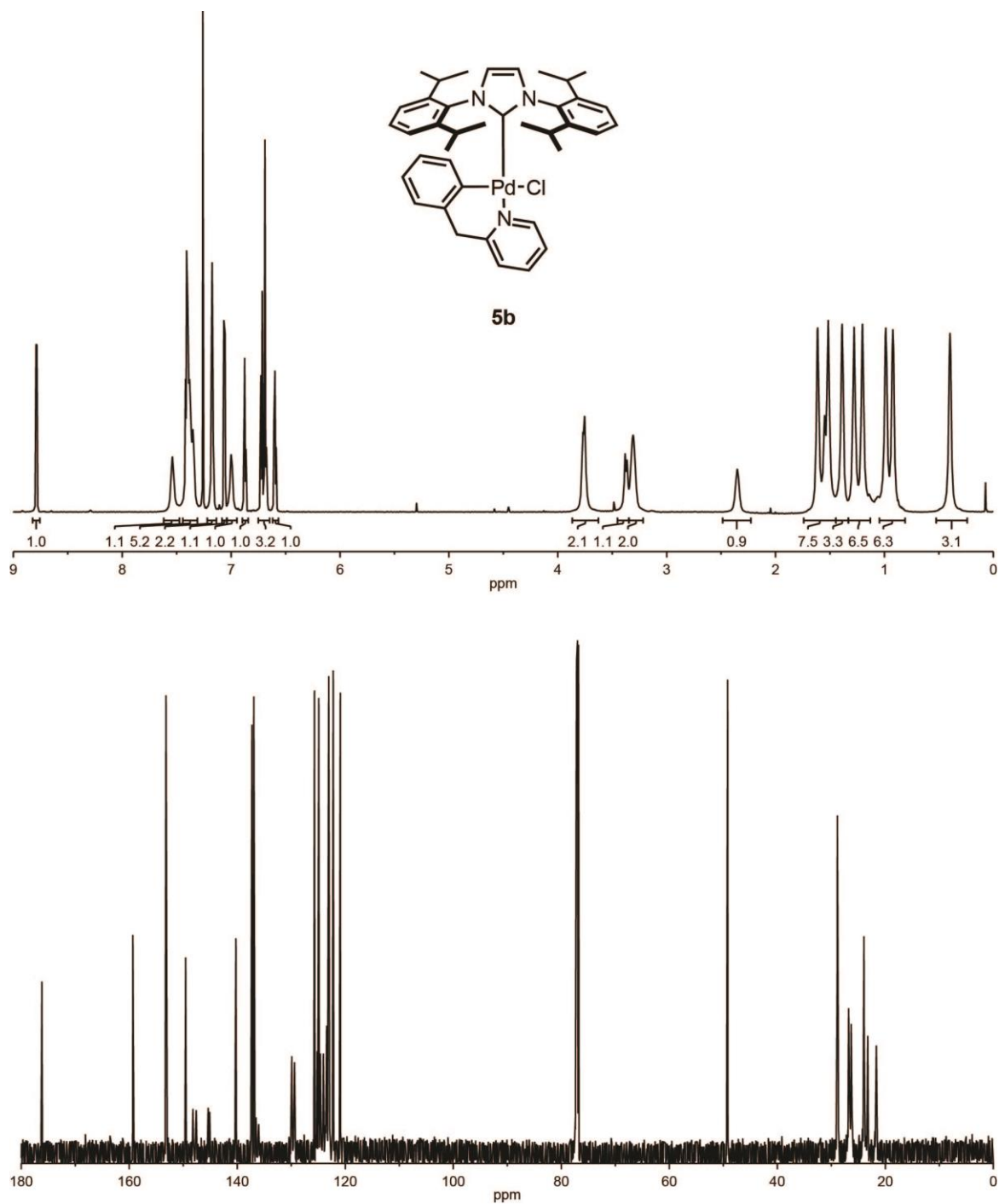
<sup>31</sup>P NMR (162 MHz, C<sub>6</sub>D<sub>6</sub>) δ 30.34.



**Figure A3-8.** <sup>1</sup>H and <sup>13</sup>C NMR spectra for **5a**.

<sup>1</sup>H NMR (400 MHz, CDCl<sub>3</sub>) δ 7.49–7.43 (m, 2H), 7.39–7.32 (m, 3H), 7.24–7.20 (m, 2H), 6.90–6.73 (m, 3H), 6.59 (d, *J* = 7.4 Hz, 1H), 3.42 (p, *J* = 6.7 Hz, 2H), 3.22 (p, *J* = 6.7 Hz, 2H), 2.45 (d, *J* = 1.2 Hz, 6H), 1.55 (dd, *J* = 6.6, 1.1 Hz, 6H), 1.23 (dd, *J* = 6.8, 1.2 Hz, 6H), 1.08 (dd, *J* = 6.9, 1.2 Hz, 6H), 0.88 (dd, *J* = 6.7, 1.2 Hz, 6H).

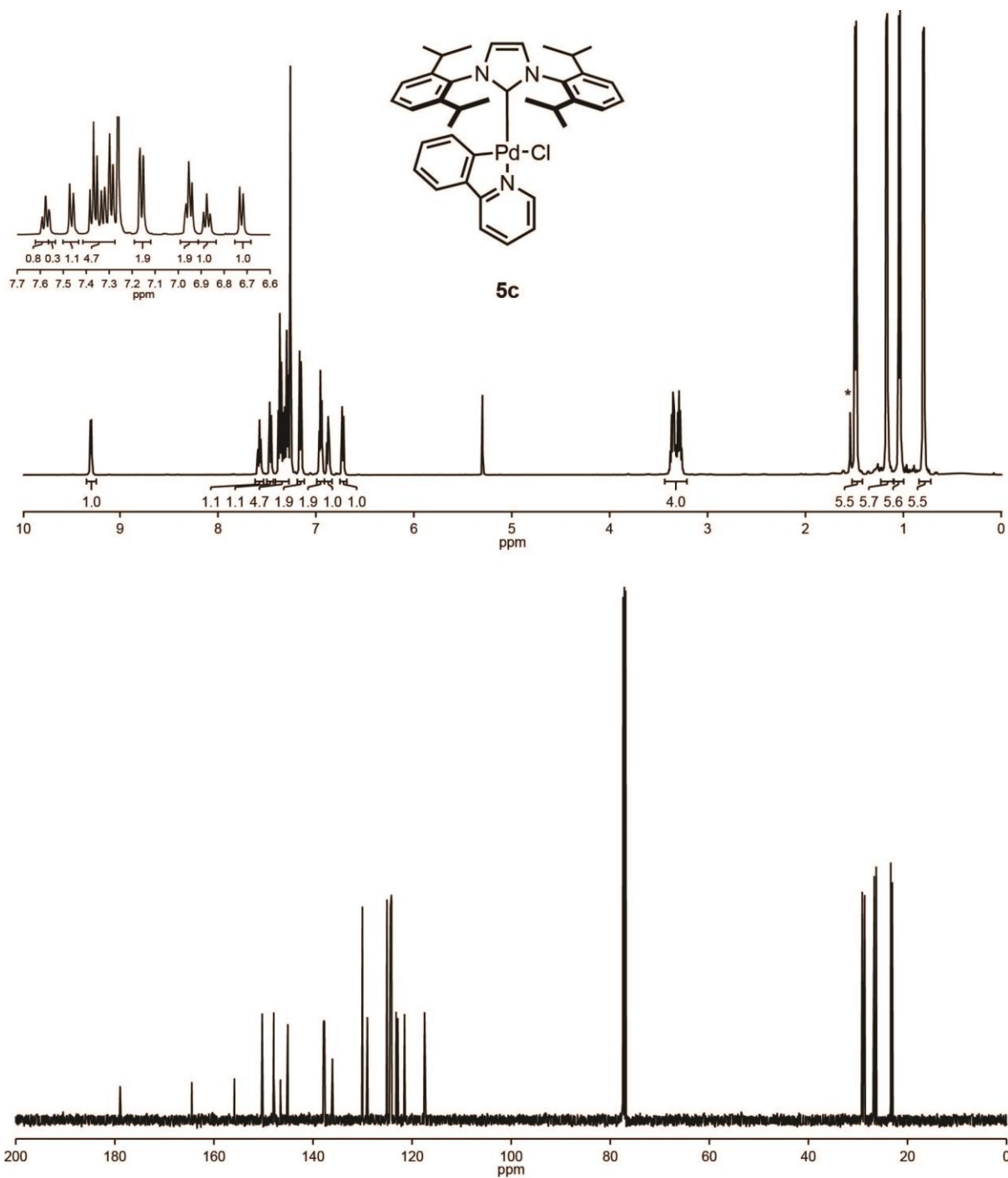
<sup>13</sup>C NMR (100 MHz, CDCl<sub>3</sub>) δ 147.91, 144.85, 136.29, 129.77, 125.46, 124.64, 124.11, 123.85, 122.71, 121.60, 72.75, 49.88, 29.14, 28.46, 26.49, 26.28, 23.37, 23.25.



**Figure A3-9.** <sup>1</sup>H and <sup>13</sup>C NMR spectra for **5b**.

<sup>1</sup>H NMR (700 MHz, CDCl<sub>3</sub>) δ 8.79 (d, *J* = 5.7 Hz, 1H), 7.54 (s, 1H), 7.44–7.33 (m, 5H), 7.17 (s, 2H), 7.06 (d, *J* = 7.7 Hz, 1H), 7.02–6.98 (m, 1H), 6.87 (dd, *J* = 7.4, 5.8 Hz, 1H), 6.72 (d, *J* = 7.4 Hz, 1H), 6.60 (td, *J* = 7.0, 2.2 Hz, 1H), 3.76 (d, *J* = 12.6 Hz, 2H), 3.37 (d, *J* = 13.3 Hz, 1H), 3.31 (s, 3H), 2.35 (s, 1H), 1.61 (s, 3H), 1.52 (s, 3H), 1.42–1.36 (m, 3H), 1.28 (s, 3H), 1.20 (d, *J* = 6.7 Hz, 3H), 1.02–0.97 (m, 3H), 0.95–0.90 (m, 3H), 0.42–0.37 (m, 3H).

<sup>13</sup>C NMR (176 MHz, CDCl<sub>3</sub>) δ 176.17, 159.34, 153.19, 149.56, 148.21, 147.60, 145.40, 145.11, 140.24, 137.28, 136.93, 136.52, 136.01, 129.92, 129.39, 125.70, 125.21, 124.90, 124.61, 124.06, 123.53, 123.44, 123.06, 122.97, 122.23, 120.91, 49.20, 28.88, 28.74, 26.75, 26.33, 26.21, 23.95, 23.24, 21.66.

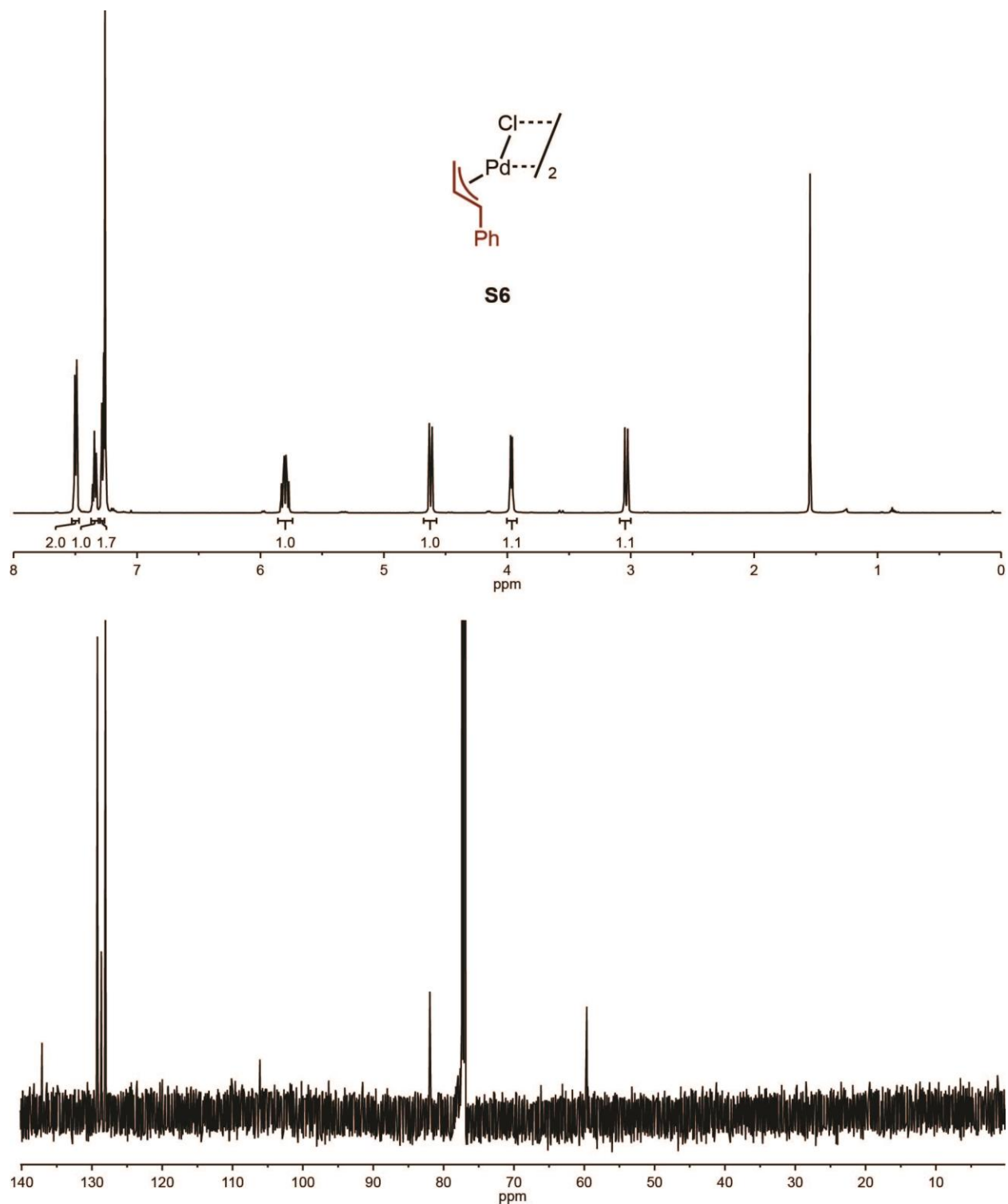


**Figure A3-10.** <sup>1</sup>H and <sup>13</sup>C NMR spectra for **5c**.

<sup>1</sup>H NMR (500 MHz, CDCl<sub>3</sub>) δ 9.30 (dd, *J* = 5.7, 1.6 Hz, 1H), 7.58 (td, *J* = 7.8, 1.7 Hz, 1H), 7.46 (d, *J* = 8.0 Hz, 1H), 7.39–7.33 (m, 6H), 7.16 (dd, *J* = 7.7, 1.5 Hz, 2H), 6.97–6.93 (m, 2H), 6.87 (td, *J* = 7.4, 1.5 Hz, 1H), 6.72 (d, *J* = 7.5 Hz, 1H), 3.36 (hept, *J* = 6.8 Hz, 2H), 3.28 (hept, *J* = 6.7 Hz, 2H), 1.49 (d, *J* = 6.5 Hz, 7H), 1.17 (d, *J* = 6.8 Hz, 6H), 1.04 (d, *J* = 6.9 Hz, 7H), 0.79 (d, *J* = 6.7 Hz, 6H).

<sup>13</sup>C NMR (126 MHz, CDCl<sub>3</sub>) δ 178.94, 164.49, 155.86, 150.27, 147.92, 146.58, 145.10, 137.88, 137.70, 136.09, 130.03, 129.04, 125.09, 124.37, 124.16, 123.23, 122.90, 121.55, 117.49, 77.16, 29.14, 28.65, 26.71, 26.32, 23.38, 23.08.

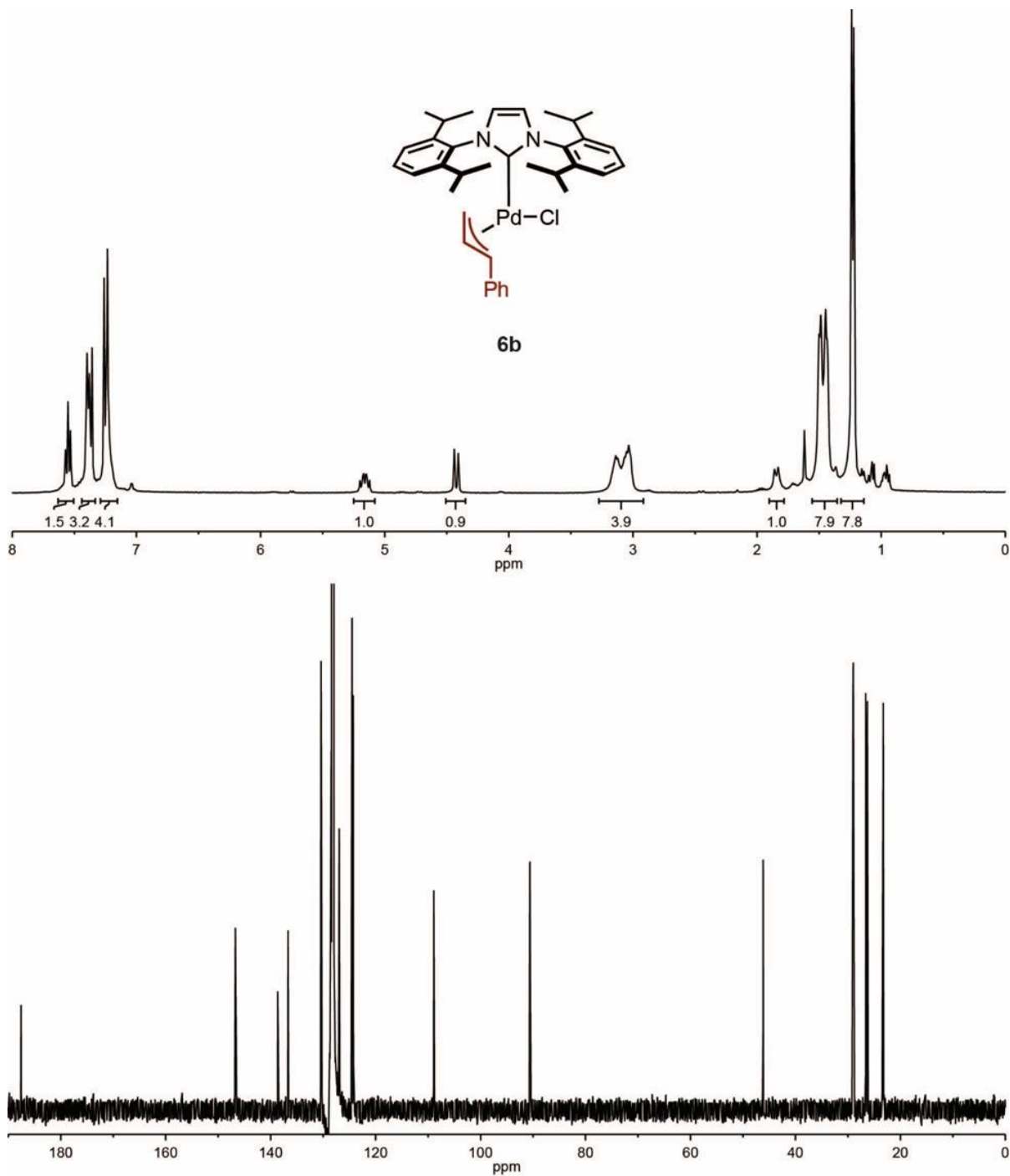




**Figure A3-11.** <sup>1</sup>H and <sup>13</sup>C NMR spectra for **S6**.

<sup>1</sup>H NMR (500 MHz, CDCl<sub>3</sub>) δ 7.49 (d, *J* = 7.4 Hz, 2H), 7.34 (t, *J* = 7.4 Hz, 1H), 7.28 (d, *J* = 7.6 Hz, 1H), 5.80 (td, *J* = 11.6, 6.8 Hz, 1H), 4.62 (d, *J* = 11.3 Hz, 1H), 3.97 (d, *J* = 6.8 Hz, 1H), 3.04 (d, *J* = 11.9 Hz, 1H).

<sup>13</sup>C NMR (176 MHz, CDCl<sub>3</sub>) δ 137.10, 129.21, 128.67, 128.09, 106.11, 81.96, 59.64.

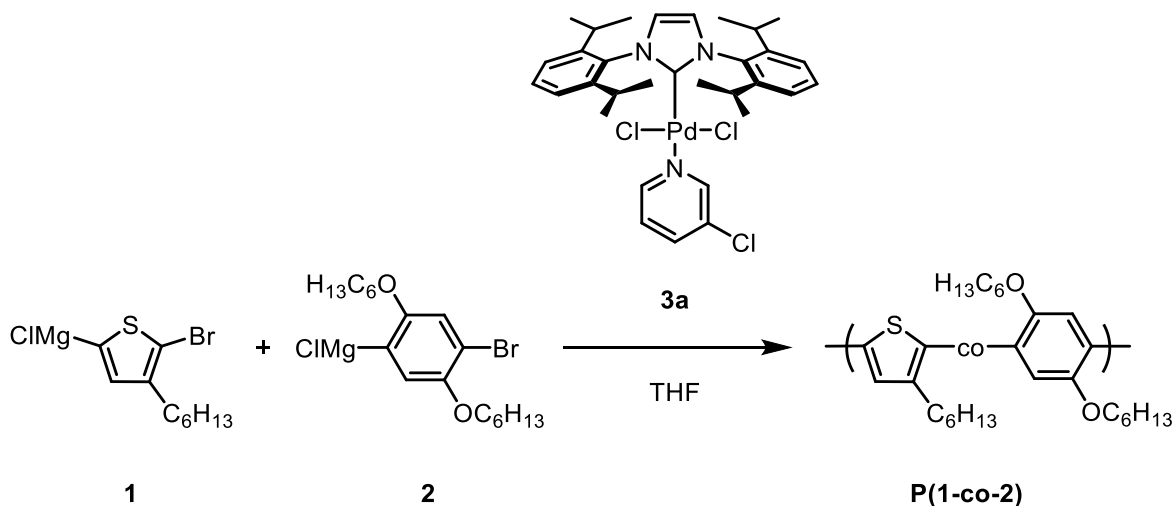


**Figure A3-12.**  $^1\text{H}$  and  $^{13}\text{C}$  NMR spectra for **6b**.

$^1\text{H}$  NMR (400 MHz,  $\text{C}_6\text{D}_6$ )  $\delta$  7.55 (t,  $J = 7.8$  Hz, 2H), 7.44–7.33 (m, 4H), 7.23 (s, 5H), 5.16 (dt,  $J = 12.7, 9.2$  Hz, 1H), 4.42 (d,  $J = 12.7$  Hz, 1H), 3.24–2.95 (m, 4H), 1.84 (d,  $J = 11.7$  Hz, 1H), 1.47 (dd,  $J = 21.5, 6.6$  Hz, 12H), 1.23 (d,  $J = 6.9$  Hz, 12H).

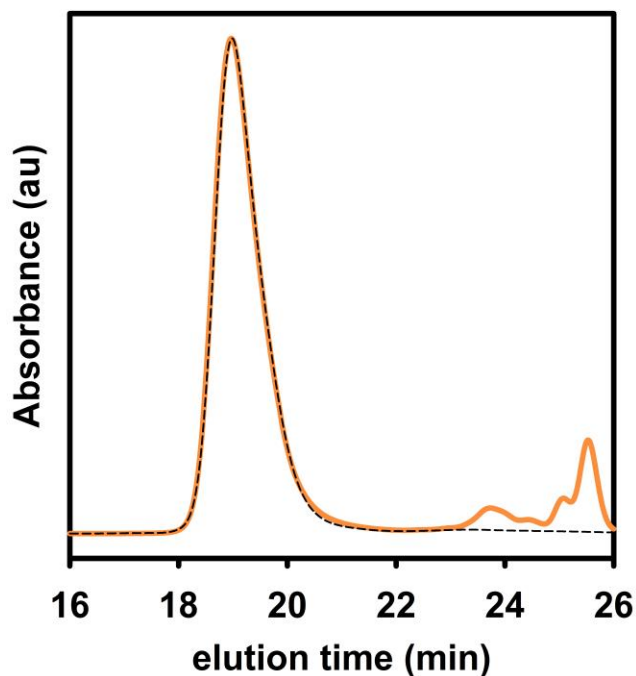
$^{13}\text{C}$  NMR (176 MHz,  $\text{C}_6\text{D}_6$ )  $\delta$  187.56, 146.77, 146.72, 138.64, 136.69, 130.40, 128.49, 128.44, 128.34, 128.26, 128.20, 128.16, 128.13, 128.06, 126.92, 124.50, 124.27, 124.25, 108.91, 90.60, 46.14, 29.01, 28.98, 26.60, 26.29, 23.38, 23.27.

## V. Copolymerizing **1** and **2** with **3a**.

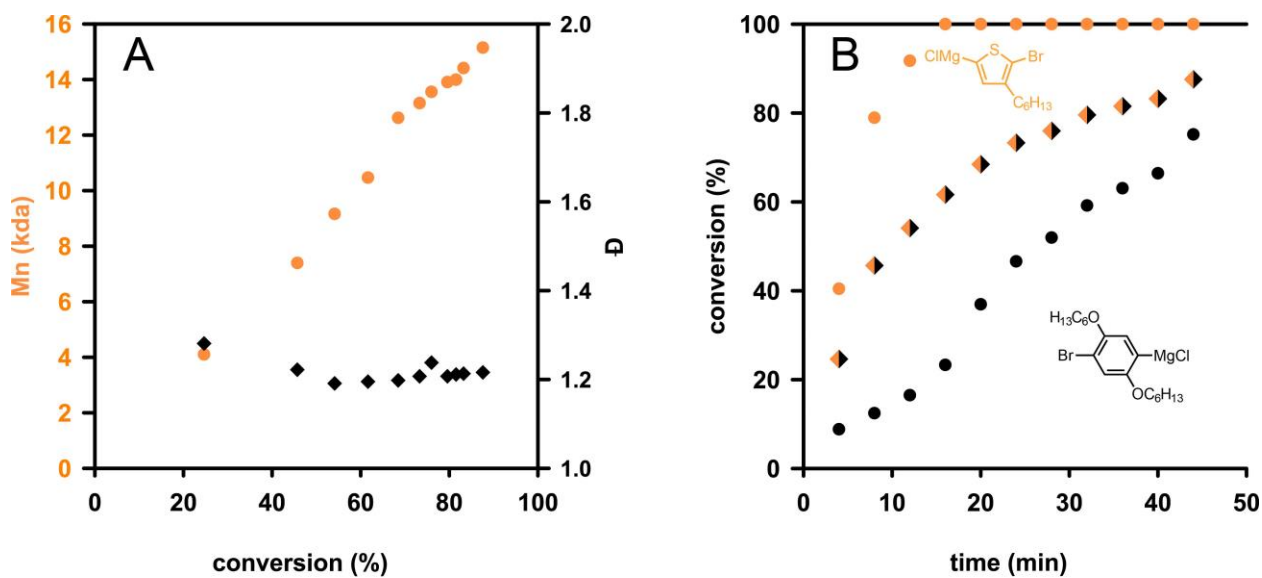


### Batch copolymerizing **1** and **2** with **3a**.

In a glovebox, **3a** (1.0 mL of a 0.0015 M solution in THF, 0.0015 mmol, 1.0 equiv) was added to a 10 mL Schlenk flask equipped with a stir bar and diluted with THF (~1.2 mL) to achieve a catalyst concentration of 0.00075 M during the polymerization. The flask was sealed with a rubber septum. Separately, **1** (1.36 mL of a ~0.48 M solution in THF) and **2** (1.36 mL of a ~0.41 M solution in THF) were combined in a Schlenk tube and sealed with a PTFE stopper and rubber septum. Both solutions were removed from the glovebox and placed under N<sub>2</sub>. The monomer solution (2.25 mL, 0.054 mmol **1** (36 equiv), 0.046 mmol **2** (31 equiv)) were added to the precatalyst solution and the combined mixture was stirred for 40 min. Aliquots (~0.3 mL) were drawn every 4 min from 0–44 min and quenched in conc. HCl (~0.5 mL). Aliquots were extracted with CHCl<sub>3</sub> (3 x 0.5 mL) with heating. The combined organic layers were then washed with H<sub>2</sub>O (1 x 1 mL) and brine (1 x 1 mL). The solvent was then removed via rotary evaporation and the solids were re-dissolved with heating in THF (~10 mL). After cooling to rt, MgSO<sub>4</sub> (~20 mg) was added and the mixture was filtered through a PTFE syringe filter (0.2 μm) and analyzed by GC and GPC.



**Figure A3-13.** GPC chromatogram of **P(1-co-2)** catalyzed by **3a** at 254 nm (—) and 427 nm (---). All aryl groups absorb light at 254 nm, but only **P1** segments absorb at 427 nm.

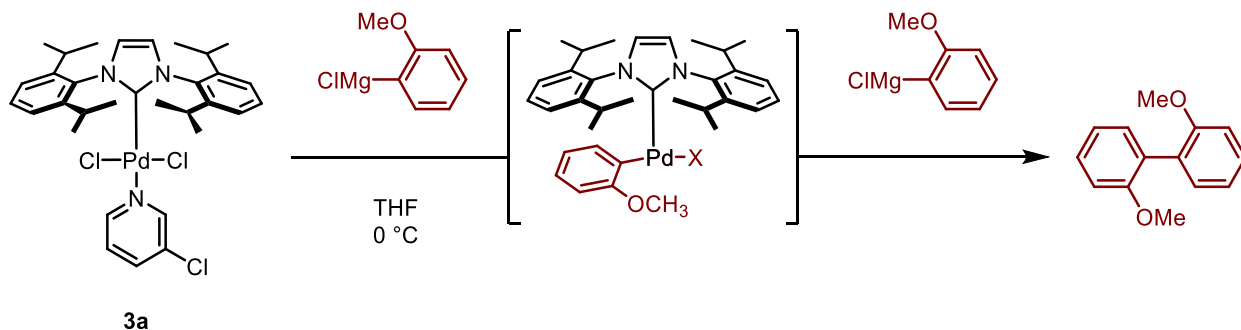


**Figure A3-14.** (A) number average molecular weight (●) and dispersity (◆) versus percent conversion (**1** and **2** combined) for the copolymerization of **1** and **2** using **3a**. (B) Percent total conversion (◆), conversion of **1** (●), and conversion of **2** (●) versus time.

<b>Time (min)</b>	<b>Conversion of 1 (%)</b>	<b>Conversion of 2 (%)</b>	<b>Total conversion (%)</b>	<b><math>M_n</math> (kDa)</b>	<b><math>\bar{D}</math></b>
4	41	0	0	4.1	1.28
8	79	9	25	7.4	1.22
12	92	12	46	9.2	1.19
16	>98	17	54	10.5	1.20
20	>98	23	62	12.6	1.20
24	>98	37	69	13.2	1.21
28	>98	47	73	13.6	1.24
32	>98	52	76	13.9	1.21
36	>98	59	80	14.0	1.21
40	>98	63	82	14.4	1.21
44	>98	66	83	15.1	1.22

**Table A3-1.** Molecular weight, dispersity, and conversion values as plotted in Figure A3-14.

## VI. Attempted transmetalation to yield IPrPd(aryl)Cl

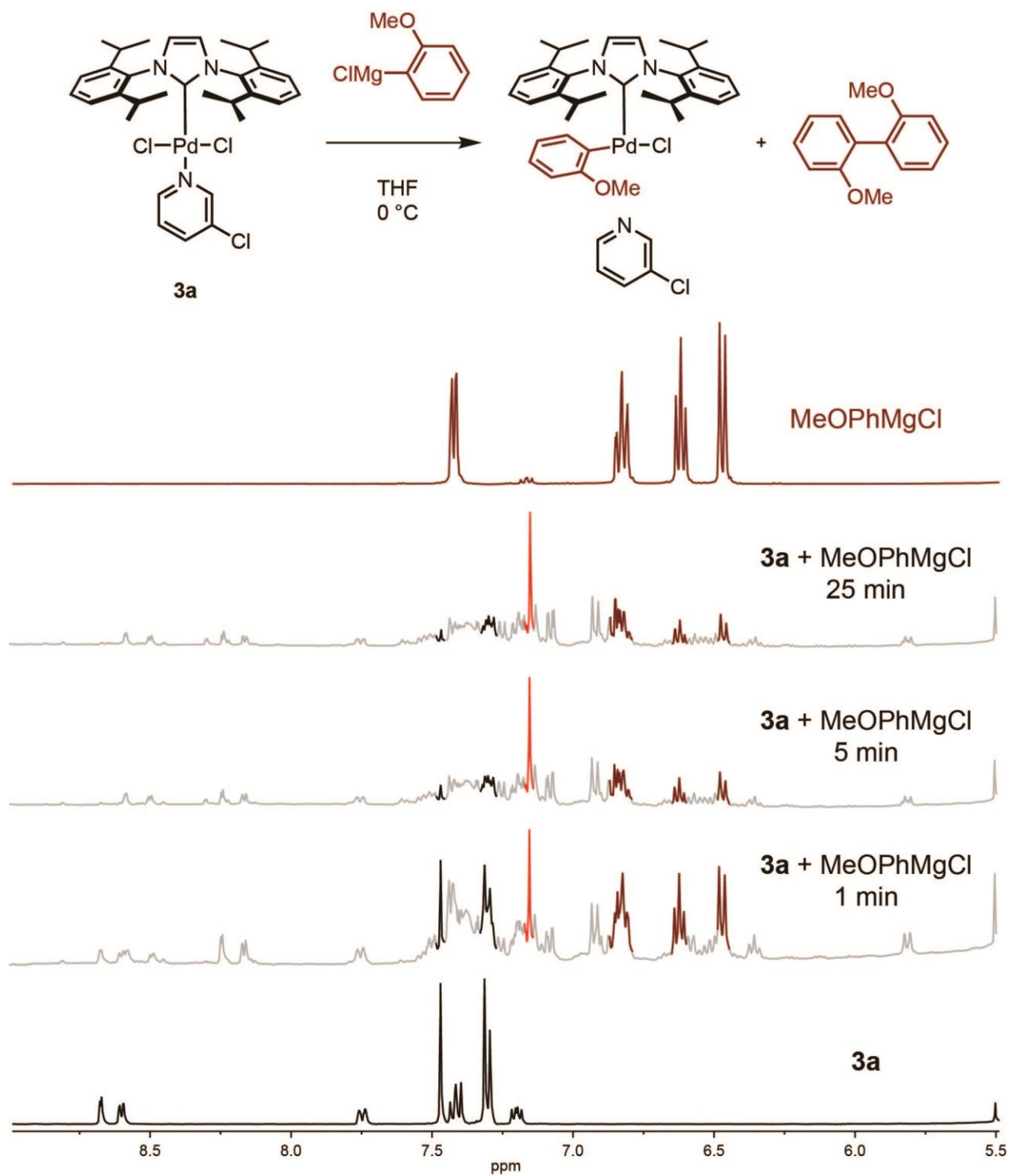


### Trial 1 at 0 °C monitored by NMR.

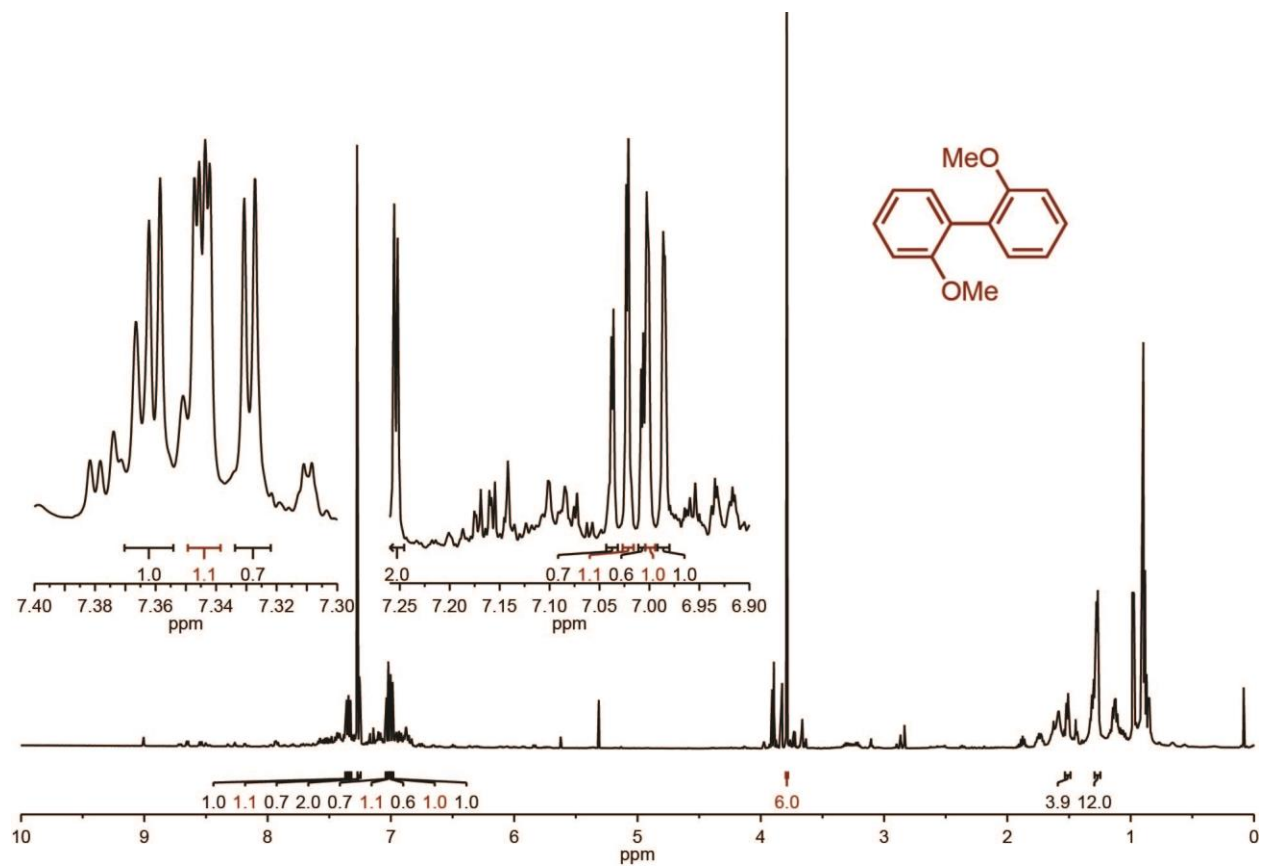
In a glovebox, **3a** (0.0147 g, 0.0220 mmol, 1.00 equiv) was diluted in THF (1.0 mL) then transferred to a J-Young NMR tube and sealed with a rubber septum. Separately, a solution of 2-methoxyphenylmagnesium chloride (MeOPhMgCl) was added to a J-Young NMR tube and sealed with a rubber septum.

Both NMR tubes were removed from the glovebox and immersed in a 0 °C ice bath for 15 min. After cooling, both **3a** and MeOPhMgCl were analyzed by  $^1\text{H}$  NMR spectroscopy at 0 °C. Next, MeOPhMgCl (0.20 mL of a 0.123 M solution in THF, 0.025 mmol, 1.0 equiv) was added to **3a** by syringe, shaken briefly, then loaded into the instrument to monitor the reaction at 0 °C by  $^1\text{H}$  NMR spectroscopy over 25 min.

The mixture was quenched with brine and extracted with hexanes (3 x 1 mL), before drying briefly over  $\text{MgSO}_4$ . The solids were removed by filtration, and the mother liquor was concentrated via rotary evaporation to yield a very small amount of off-white solid. The primary product was determined to be 2,2'-dimethoxybiphenyl (Figure A3-16). Prominent signals from  $^1\text{H}$  chemical shifts for **3a** or anisole are absent.



**Figure A3-15.** Selected regions of the  $^1\text{H}$  NMR spectra of Trial 1 in THF. Bottom (**3a**) and top (**MeOPhMgCl**) spectra correspond to the two starting materials prior to mixing. The middle three spectra show the reaction progress at 1, 5, and 25 min after mixing (bottom to top). Prominent peaks are highlighted in the reaction spectrum from the starting materials [**3a** (—), **MeOPhMgCl** (—)] and the reaction product (—)].



**Figure A3-16.** <sup>1</sup>H NMR spectrum in CDCl<sub>3</sub> of Trial 1 after workup. The integrals highlighted (dark red) correspond to 2,2'-dimethoxybiphenyl.



### **Trial 2 at -30 °C.**

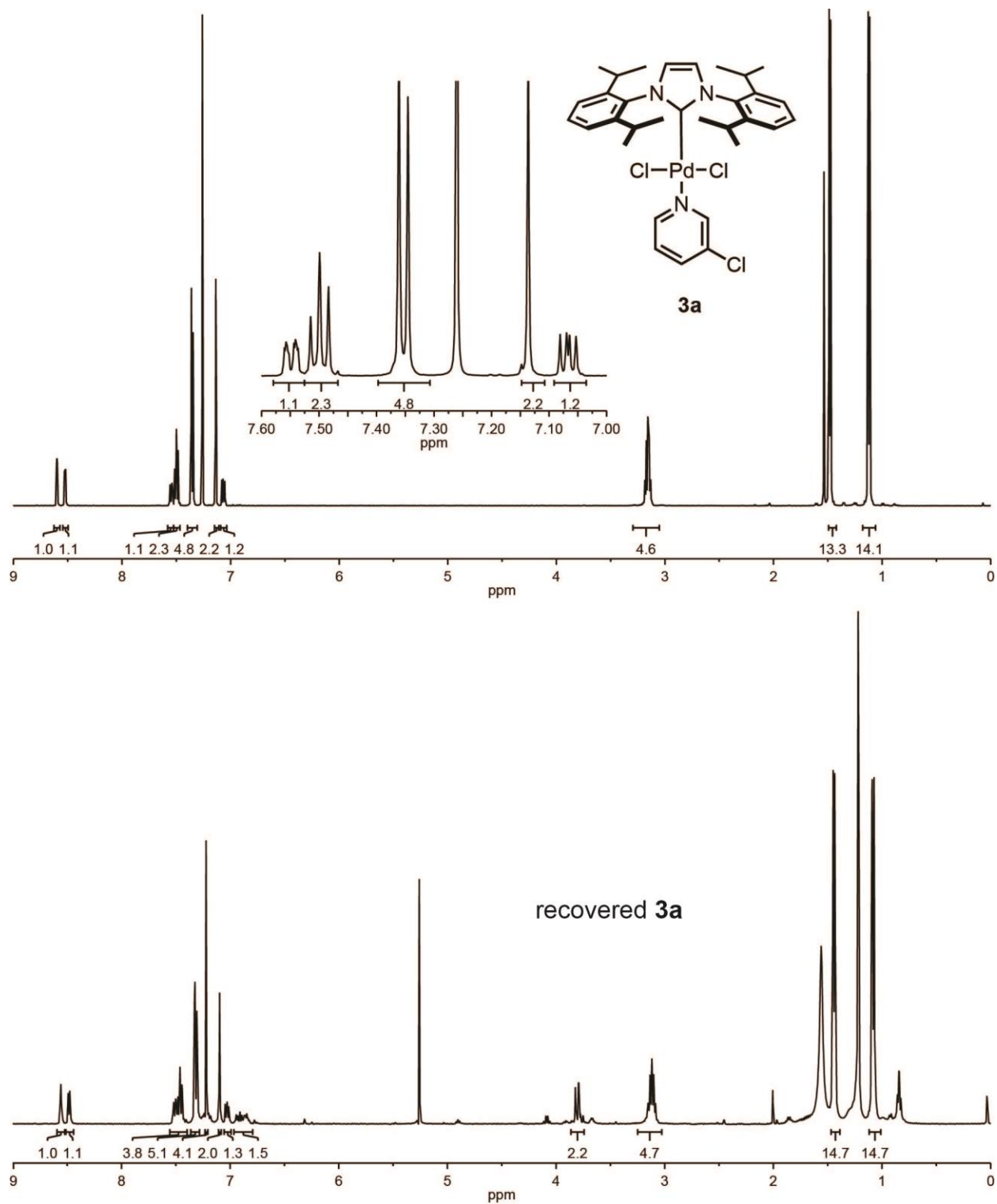
In a glovebox, **3a** (2.3 mL of a 0.0015 M solution in THF, 0.033 mmol, 1.0 equiv) was added to a 10 mL Schlenk tube, diluted with THF (2.75 mL), and sealed with a rubber septum. Separately, a solution of 2-methoxyphenylmagnesium chloride was added to a Schlenk tube and sealed with a rubber septum.

Both vessels were removed from the glovebox, placed under N<sub>2</sub>, and then immersed in a -30 °C ice/brine bath for 15 min. After cooling, 2-methoxyphenylmagnesium chloride (0.50 mL of a 0.074 M solution in THF, 0.036 mmol, 1.1 equiv) was added over 1 min. The mixture was stirred for 40 min at -30 °C, then warmed to rt for 1 h before quenching with brine. The mixture was extracted with hexanes (3 x 5 mL), then dried briefly over MgSO<sub>4</sub>. The solids were removed by filtration, and the mother liquor was concentrated via rotary evaporation to yield a very small amount of off-white residue and analyzed by <sup>1</sup>H NMR spectroscopy (matched the major peaks for 2,2'-dimethoxybiphenyl, Figure A3-16).

### **Trial 3 at -42 °C.**

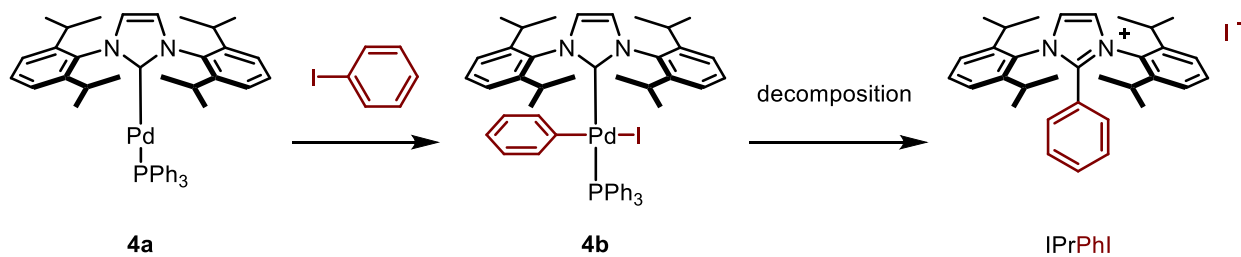
In a glovebox, **3a** (4.0 mL of a 0.0015 M solution in THF, 0.060 mmol, 1.0 equiv) was added to a 25 mL Schlenk tube, diluted with THF (3.0 mL), and sealed with a rubber septum. Separately, a solution of 2-methoxyphenylmagnesium chloride was added to a Schlenk tube and sealed with a rubber septum.

Both vessels were removed from the glovebox, placed under N<sub>2</sub>, then immersed in a -42 °C dry ice/acetone bath for 15 min. After cooling, 2-methoxyphenylmagnesium chloride (0.43 mL of a 0.15 M solution in THF, 0.060 mmol, 1.0 equiv) was added over 1 min. The mixture was stirred for 1 h at -42 °C, then warmed to rt for 1 h before quenching with brine. The mixture was extracted with hexanes (3 x 5 mL), then dried briefly over MgSO<sub>4</sub>. The solids were removed by filtration, and the mother liquor was concentrated via rotary evaporation to yield a yellow oil. Hexanes (~5 mL) was layered on top of the oil, and the mixture was placed in the freezer overnight. The mixture was filtered to yield a yellow powder, which matched **3a** by <sup>1</sup>H NMR spectroscopy.



**Figure A3-17.** <sup>1</sup>H NMR spectra in CDCl<sub>3</sub> of analytically pure **3a** (top) and recovered **3a** from Trial 3 (bottom).

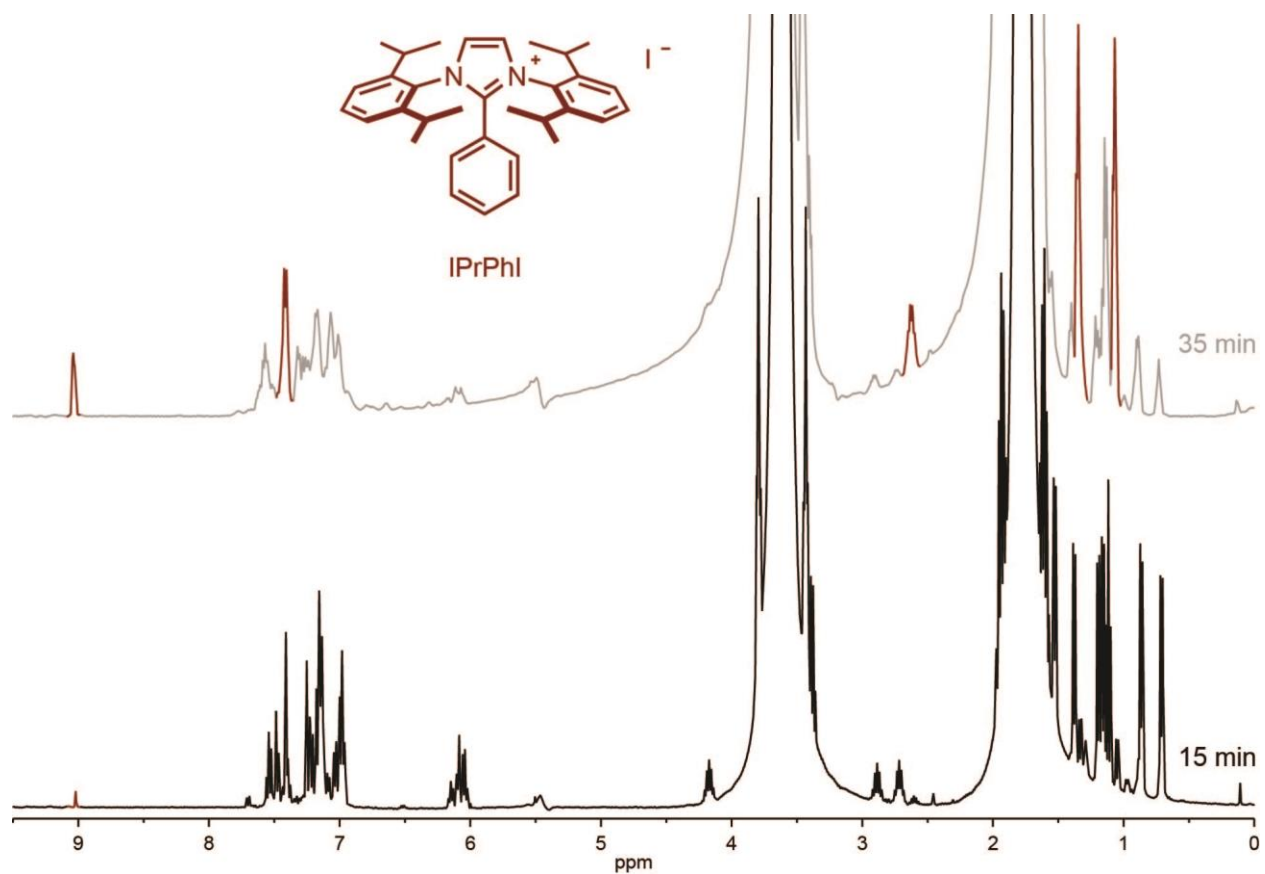
## VII. Oxidative addition to yield IPrPd(aryl)I



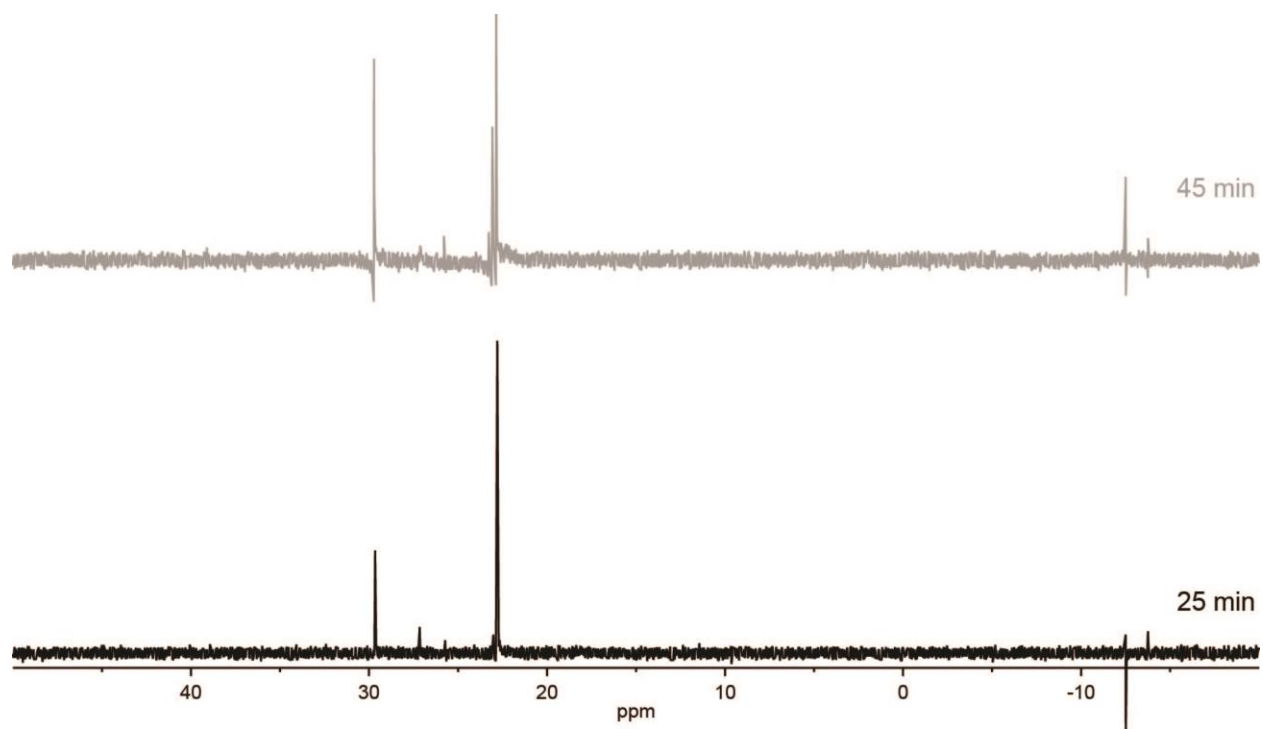
### Synthesis and decomposition of **4b** to yield IPrPhI.

In a glovebox, **4a** (0.50 mL of a 0.0015 M solution in THF, 0.00075 mmol, 1.0 equiv) was combined with iodobenzene (0.15 mL of a 0.051 M solution in THF, 0.00075 mmol, 1.0 equiv) in an NMR tube with a screw top, and shaken vigorously. The sample was removed from the glovebox and the reaction was monitored by <sup>1</sup>H and <sup>31</sup>P NMR spectroscopy for 1 h, over which time the solution went from cloudy yellow to dark maroon.

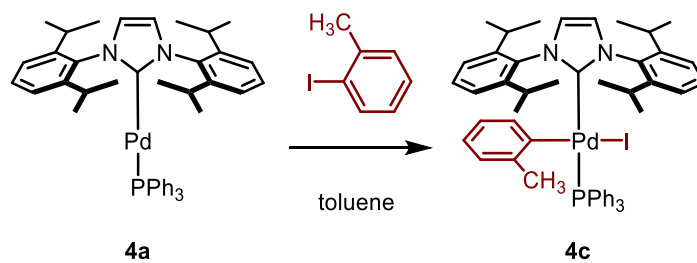
The sample was returned to the glovebox and hexanes (~1 mL) was layered on, but no solid was recovered.



**Figure A2 - 1:** <sup>1</sup>H NMR spectra of Synthesis and decomposition of 4b to yield IPrPhI after 15 min (—) and 35 min (—). The highlighted peaks (—) correspond to the decomposition product, IPrPhI.<sup>10</sup>

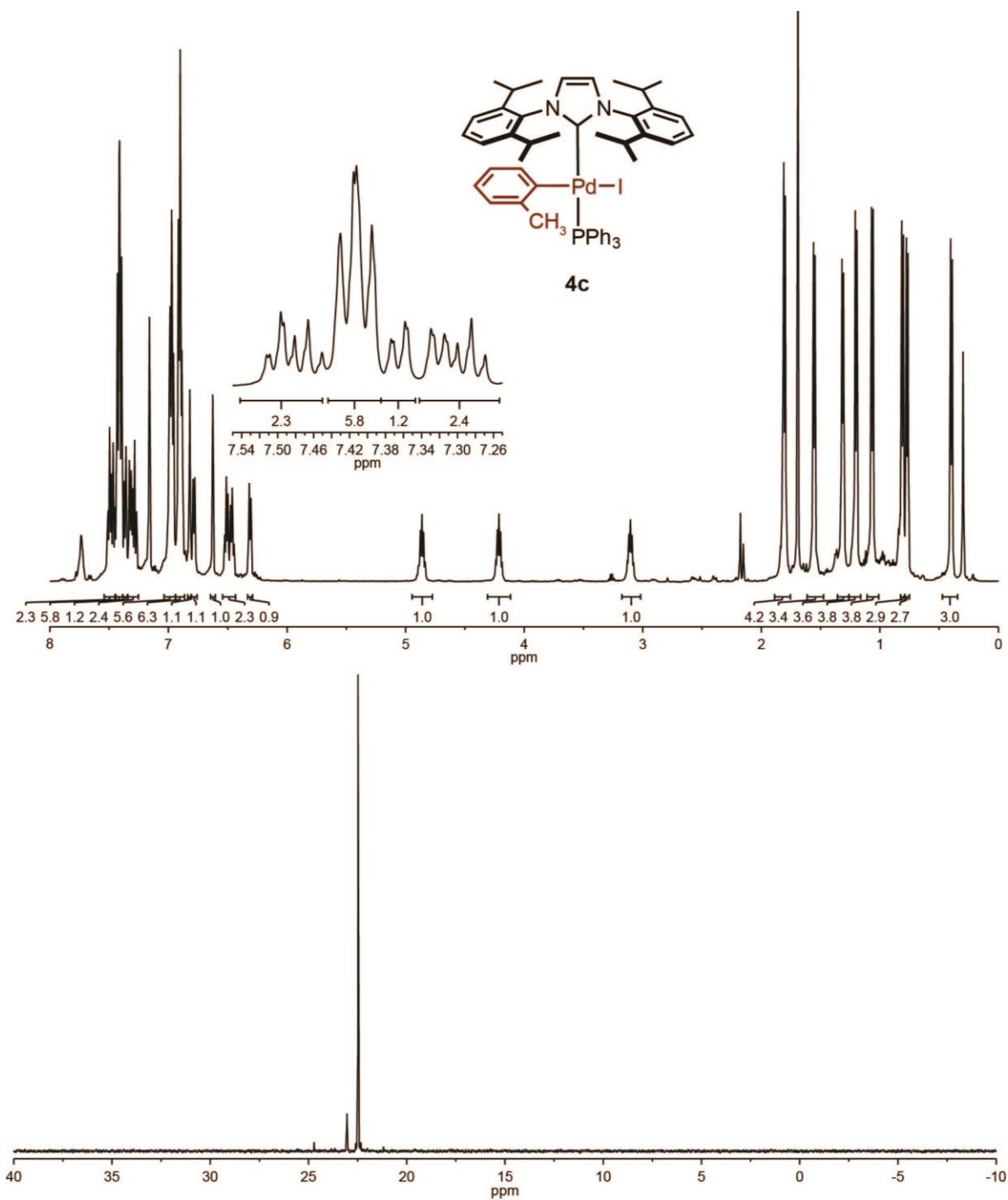


**Figure A2 - 2:**  $^{31}\text{P}$  NMR spectra of Synthesis and decomposition of 4b to yield IPrPhI after 25 min (—) and 45 min (—).



### Synthesis of IPrPd(PPh<sub>3</sub>)(*o*-tolyl)I, **4c**.

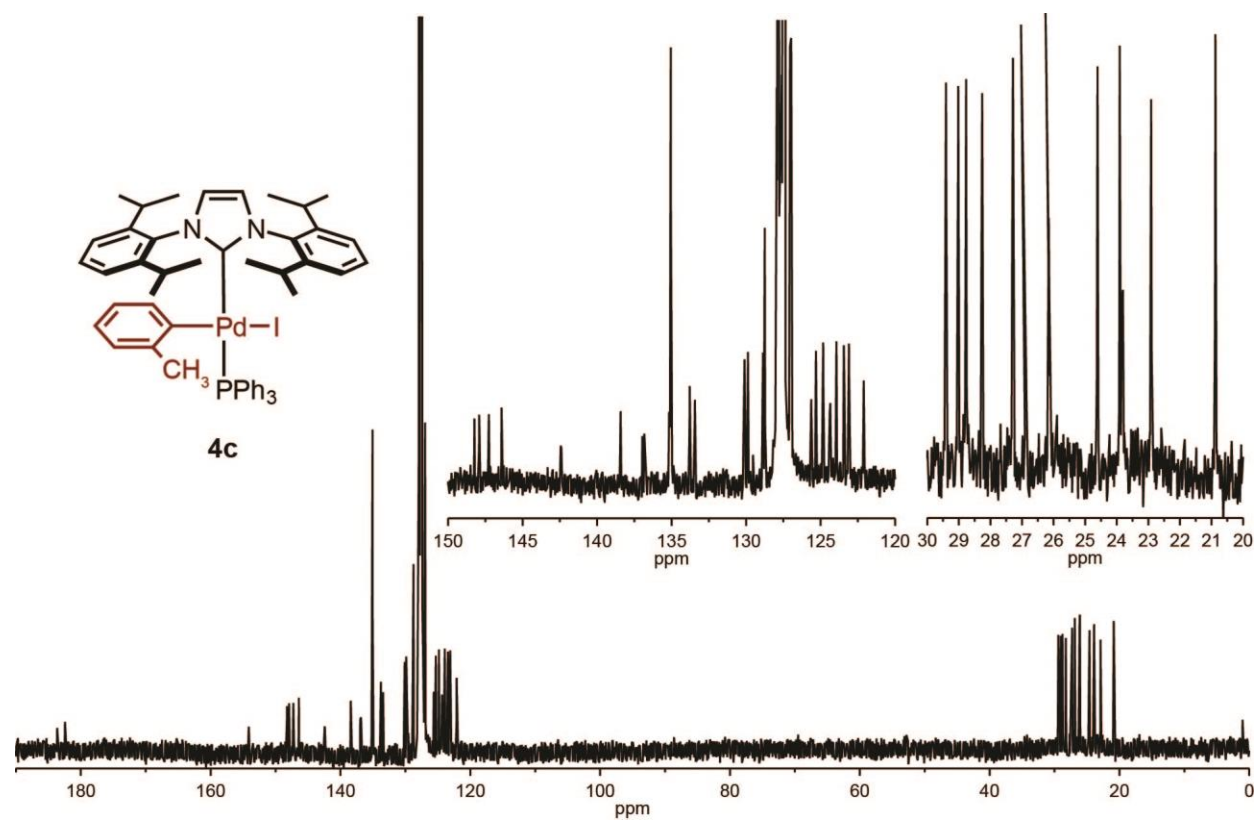
In a glovebox, **4a** (0.003 g, 0.003 mmol, 1 equiv) was added to a 20 mL vial equipped with a stir bar and diluted with toluene (1 mL) to yield a clear, intense neon yellow solution. Next, 2-iodotoluene (0.010 g, 0.046 mmol, 15 equiv) was added. The solution was stirred vigorously for 6 h, during which time the solution became less brightly colored. The volatiles were removed in vacuo for 6 h to yield a small amount of an off-white powder. The entire sample was analyzed by <sup>1</sup>H, <sup>13</sup>C, and <sup>31</sup>P NMR spectroscopy.



**Figure A3-18.**  $^1\text{H}$  and  $^{31}\text{P}$  spectra of **4c**.

$^1\text{H}$  NMR (500 MHz,  $\text{C}_6\text{D}_6$ )  $\delta$  7.53–7.46 (m, 2H), 7.45–7.38 (m, 5H), 7.36 (dd,  $J = 7.8, 1.7$  Hz, 1H), 7.34–7.24 (m, 2H), 7.01–6.94 (m, 5H), 6.93–6.88 (m, 6H), 6.82 (d,  $J = 1.3$  Hz, 1H), 6.79 (d,  $J = 7.3$  Hz, 1H), 6.63 (s, 1H), 6.49 (dtd,  $J = 25.2, 7.3, 1.7$  Hz, 2H), 6.31 (d,  $J = 7.4$  Hz, 1H), 4.86 (hept,  $J = 6.8$  Hz, 1H), 4.21 (h,  $J = 6.6$  Hz, 1H), 3.10 (hept,  $J = 6.6$  Hz, 1H), 1.81 (d,  $J = 6.7$  Hz, 3H), 1.56 (d,  $J = 6.4$  Hz, 4H), 1.32 (d,  $J = 6.4$  Hz, 3H), 1.20 (d,  $J = 6.7$  Hz, 3H), 1.07 (d,  $J = 6.8, 2.2$  Hz, 3H), 0.81 (d,  $J = 6.8$  Hz, 3H), 0.77 (d,  $J = 6.7$  Hz, 3H), 0.40 (d,  $J = 6.8$  Hz, 3H).  
 $^{31}\text{P}$  NMR (162 MHz,  $\text{C}_6\text{D}_6$ )  $\delta$  24.72, 23.04, 22.60, 22.51, 22.48, 22.45, 22.33.





**Figure A3-19.**  $^{13}\text{C}$  NMR spectrum of **4c**.

$^{13}\text{C}$  NMR (126 MHz,  $\text{C}_6\text{D}_6$ )  $\delta$  183.64, 182.43, 154.13, 148.23, 147.92, 147.26, 146.41, 142.44, 138.45, 138.42, 136.96, 136.83, 135.14, 135.10, 135.06, 135.00, 133.78, 133.44, 130.10, 129.88, 128.86, 128.76, 128.75, 127.94, 127.84, 127.73, 127.65, 127.54, 127.45, 127.05, 126.97, 125.66, 125.62, 125.31, 124.82, 124.39, 124.35, 123.94, 123.44, 123.10, 122.10, 29.41, 29.02, 28.77, 28.26, 27.29, 26.87, 26.14, 26.10, 24.61, 23.91, 23.84, 22.91, 20.88.

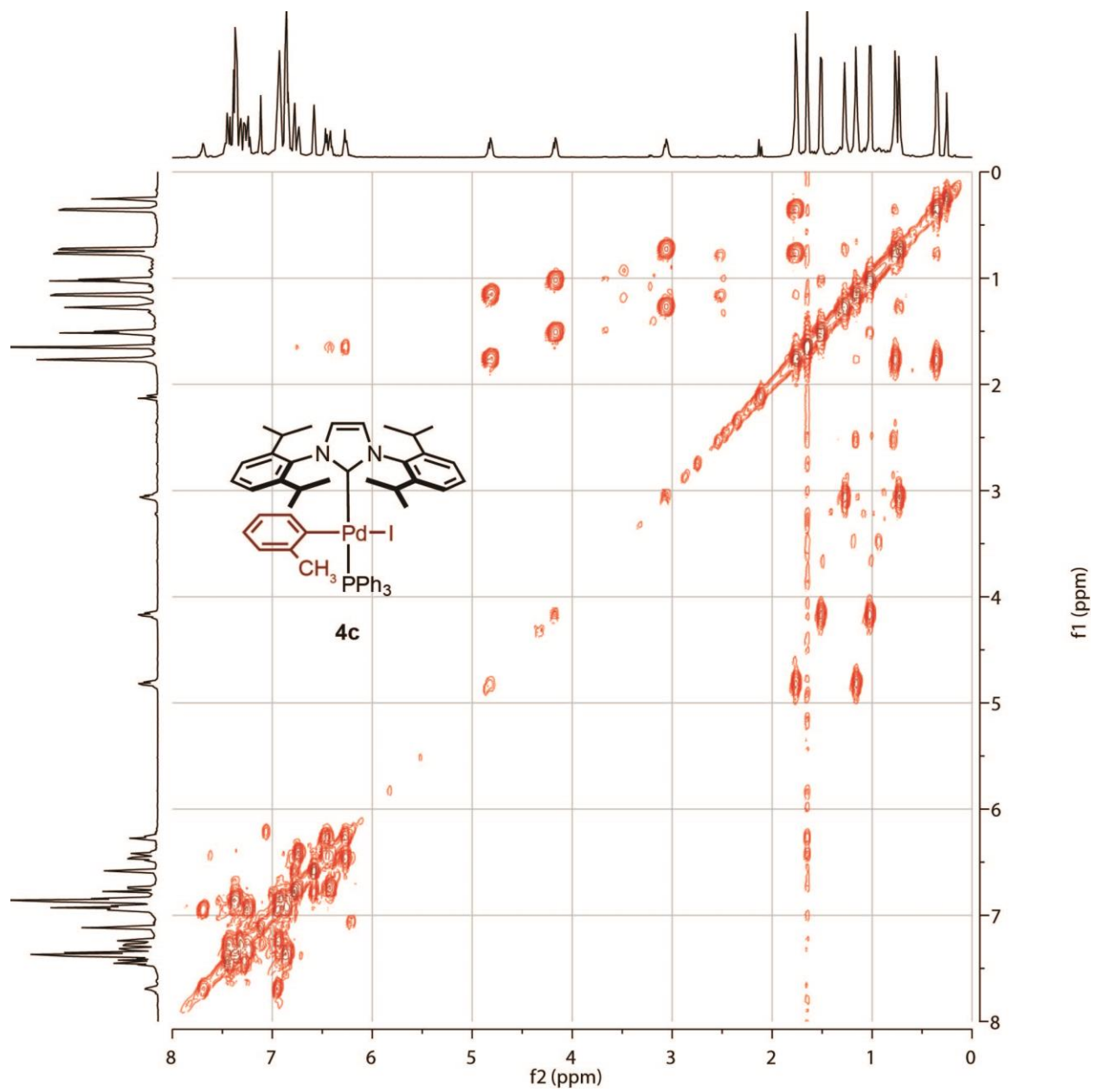
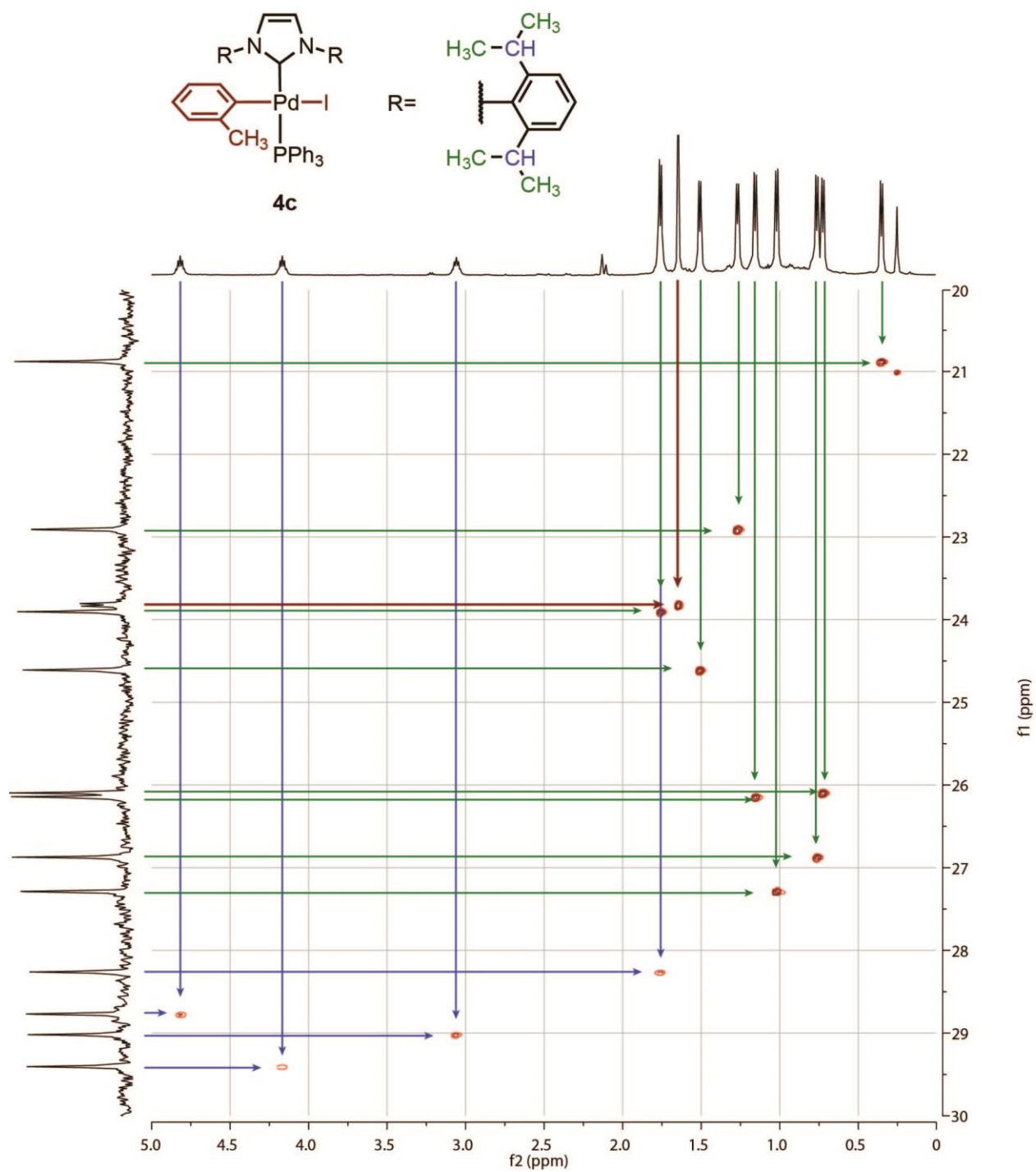
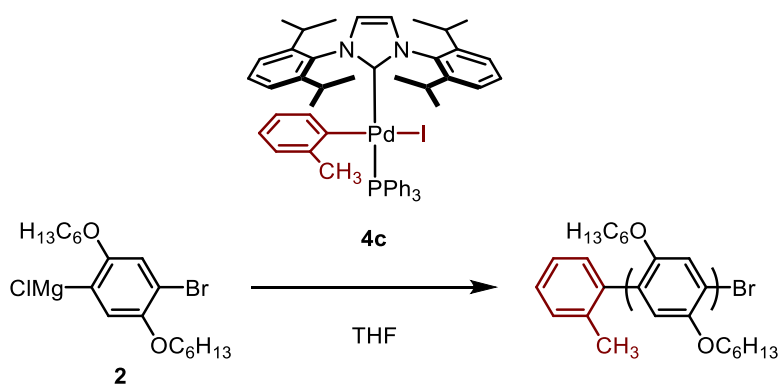


Figure A3-20. HSQCAD NMR spectrum of **4c**.



**Figure A3-21.** HSQCAD NMR spectrum highlighting the <sup>1</sup>H/<sup>13</sup>C correlations of the CH (—) and CH<sub>3</sub> (—) of the iPr groups on the IPrligand and CH<sub>3</sub> (—) of the tolyl ligand of **4c**.

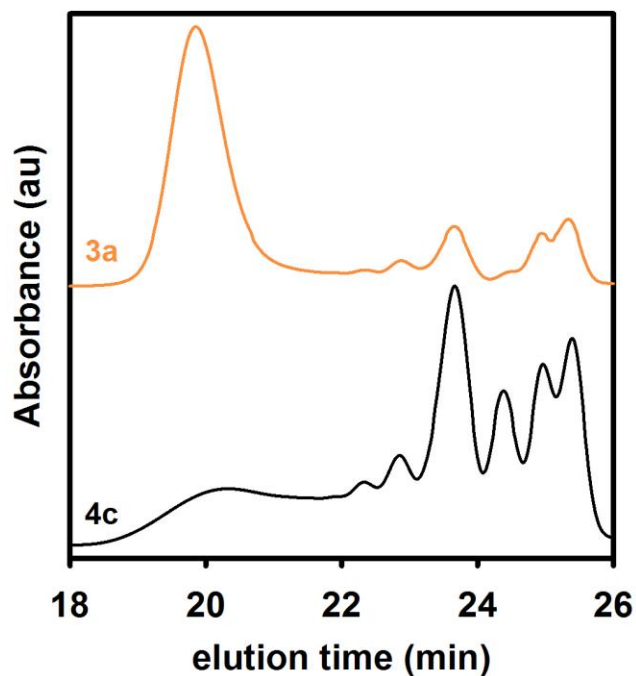


### Polymerizing **2** using **4c**.

**4c** (0.3 mL of a 0.005 M solution in benzene, 0.003 mmol, 1. equiv) was added to a 10 mL Schlenk flask equipped with a stir bar. Next, the solution was diluted with THF (1.2 mL) and the flask was sealed with a rubber septum, removed from the glovebox and placed under  $\text{N}_2$ .

As a reference, **3a** (0.20 mL of a 0.0015 M solution in THF, 0.0030 mmol, 1.0 equiv) was added to a 10 mL Schlenk flask equipped with a stir bar. Next, the solution was diluted with THF (1.2 mL) and the flask was sealed with a rubber septum, removed from the glovebox and placed under  $\text{N}_2$ .

Previously prepared **2** (0.30 mL of a 0.28 M solution in THF, 0.084 mmol, 28 equiv) was added to precatalyst solutions **3a** or **4c** to initiate each polymerization. The reaction was quenched after 1 h by adding conc. HCl (~2 mL). The quenched reactions were extracted with  $\text{CHCl}_3$  (3 x 1 mL) with heating. The combined organic layers were then washed with  $\text{H}_2\text{O}$  (1 x 2 mL) and brine (1 x 2 mL). The solvent was then removed via rotary evaporation and the solids were re-dissolved with heating in THF (~10 mL). After cooling to rt,  $\text{MgSO}_4$  (~20 mg) was added and the mixture was filtered through a PTFE syringe filter (0.2  $\mu\text{m}$ ). A small portion was removed for GC and GPC analysis, and the remaining liquid was removed using a rotary evaporator to yield a white solid (from **3a** or a small amount of oil from **4c**). The residue was dissolved in minimal  $\text{CHCl}_3$  (~0.2 mL), and then precipitated into MeOH (10 mL) in a centrifuge tube and centrifuged at 4500 rpm for 30 min. The supernatant was decanted and the solid polymer was dried under high vacuum for 4 h to afford 5 mg from **4c** (18% yield) or 15 mg from **3a** (61 % yield).

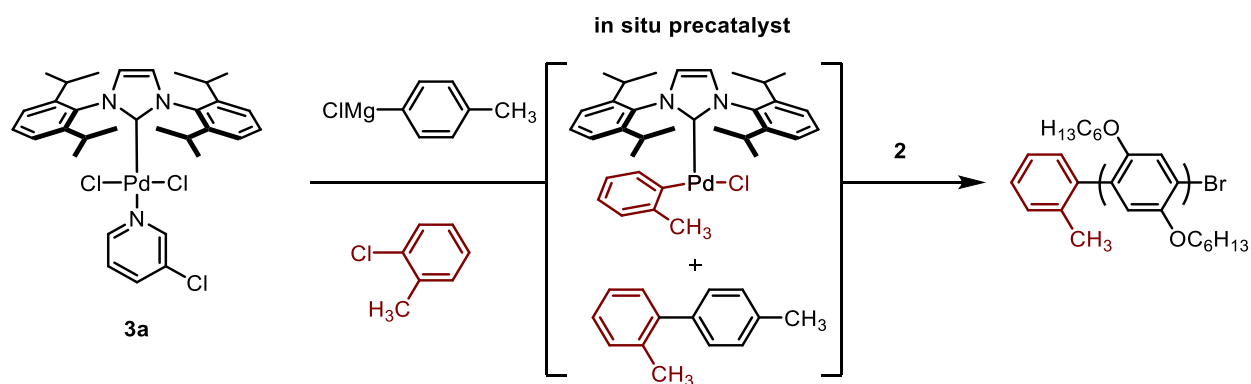


**Figure A3-22.** GPC chromatogram of **P2** catalyzed by **4c** (—) and **3a** (—).

Catalyst	$M_n$ (kDa)	$\bar{D}$	Conversion of <b>2</b> (%)
<b>3a</b>	6.5	1.14	77
<b>4c</b>	N/A <sup>a</sup>	N/A <sup>a</sup>	72

**Table A3-2.** Molecular weight, dispersity, and conversion values of **P2** catalyzed by **4c**.<sup>a</sup>  $M_n$  and  $\bar{D}$  could not be calculated due to the low molecular weight peak tail that extended beyond the lower limit of the GPC calibration curve.

## VIII. In situ cross-coupling to generate IPrPd(aryl)X, then polymerizing **2**



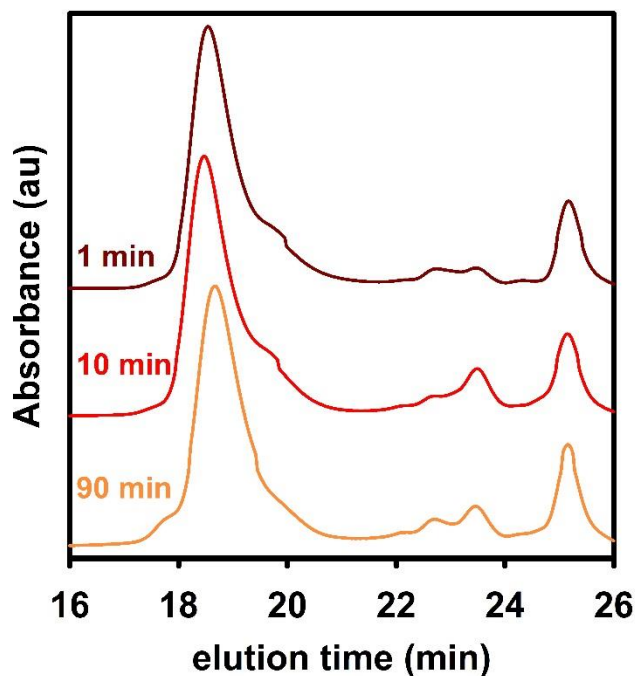
### Cross-coupling using **3a**, then polymerizing **2** from in situ precatalyst.

**3a** (0.5 mL of a 0.0015 M solution in THF, 0.00075 mmol, 1.0 equiv) was added to a 4 mL vial equipped with a stir bar. Next, 2-chlorotoluene (0.0092 g, 0.075 mmol, 10 equiv) was added and the solution was stirred. After 2 min, 4-tolylmagnesium chloride (0.00075 mL of a 2 M solution in THF, 0.021 mmol, 4.0 equiv) was added, then aliquots of the solution (0.1 mL, 0.0015 mmol) were added to three 10 mL Schlenk flasks and diluted with THF (1.6 mL) before sealing with a rubber septum. The flasks were removed from the glovebox and placed under N<sub>2</sub>.

Previously prepared **2** (0.25 mL of a 0.43 M solution in THF, 0.11 mmol, 72 equiv) was added to each solution containing precatalyst **3a** 1, 10, or 90 min after 4-tolylmagnesium chloride had been added. The reaction was quenched after 2 h by adding conc. HCl (~2 mL). The quenched reactions were extracted with CHCl<sub>3</sub> (3 x 1 mL) with heating. The combined organic layers were washed with H<sub>2</sub>O (1 x 2 mL) and brine (1 x 2 mL). The solvent was then removed via rotary evaporation and the solids were re-dissolved with heating in THF (~10 mL). After cooling to rt, MgSO<sub>4</sub> (~20 mg) was added and the mixture was filtered through a PTFE syringe filter (0.2 μm). A small portion was removed for GC and GPC analysis, and the remaining liquid was removed using a rotary evaporator to yield a tan solid. The solid was dissolved in minimal CHCl<sub>3</sub> (~0.2 mL), and then precipitated into MeOH (10 mL) in a centrifuge tube and centrifuged at 4500 rpm for 30 min. The supernatant was decanted and the solid material was dried under high vacuum for 4 h.

The solids (~2 mg) were dissolved in CDCl<sub>3</sub> (2 mL) and analyzed by <sup>1</sup>H NMR spectroscopy. Next, the NMR solutions were filtered through a pipette column (basic, acidic, then neutral alumina with

a KimWipe plug) and rinsed with  $\text{CHCl}_3$  (~0.5 mL). The resultant polymer solution (2.5  $\mu\text{L}$ ) was mixed with DCTB matrix (2.5  $\mu\text{L}$  of a 0.1 M solution in  $\text{CHCl}_3$ ) in an Eppendorf tube. The polymer/matrix solution (~1.5  $\mu\text{L}$ ) was spotted onto the MALDI 96-well target, and the remaining solution in the Eppendorf tube was diluted five-fold with additional DCTB matrix (2.5  $\mu\text{L}$  of a 0.1 M solution in  $\text{CHCl}_3$ ). The diluted sample was spotted onto the MALDI target in the same manner, and further five-fold dilutions (with DCTB matrix solution) were performed and spotted to yield four spots for each polymer sample.

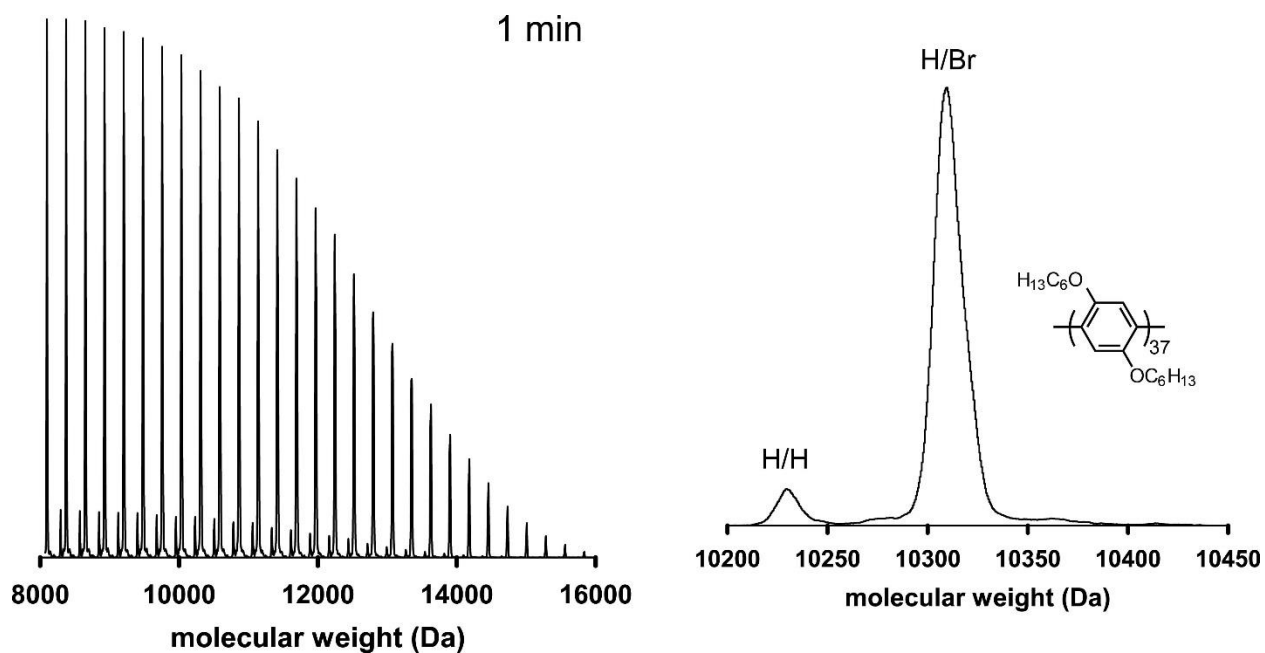


**Figure A3-23.** GPC chromatogram of **P2** catalyzed by **3c** after pre-initiating with 2-chlorotoluene (10 equiv) and *p*-tolylmagnesium chloride for 1 (—), 10 (—), or 90 (—) min.

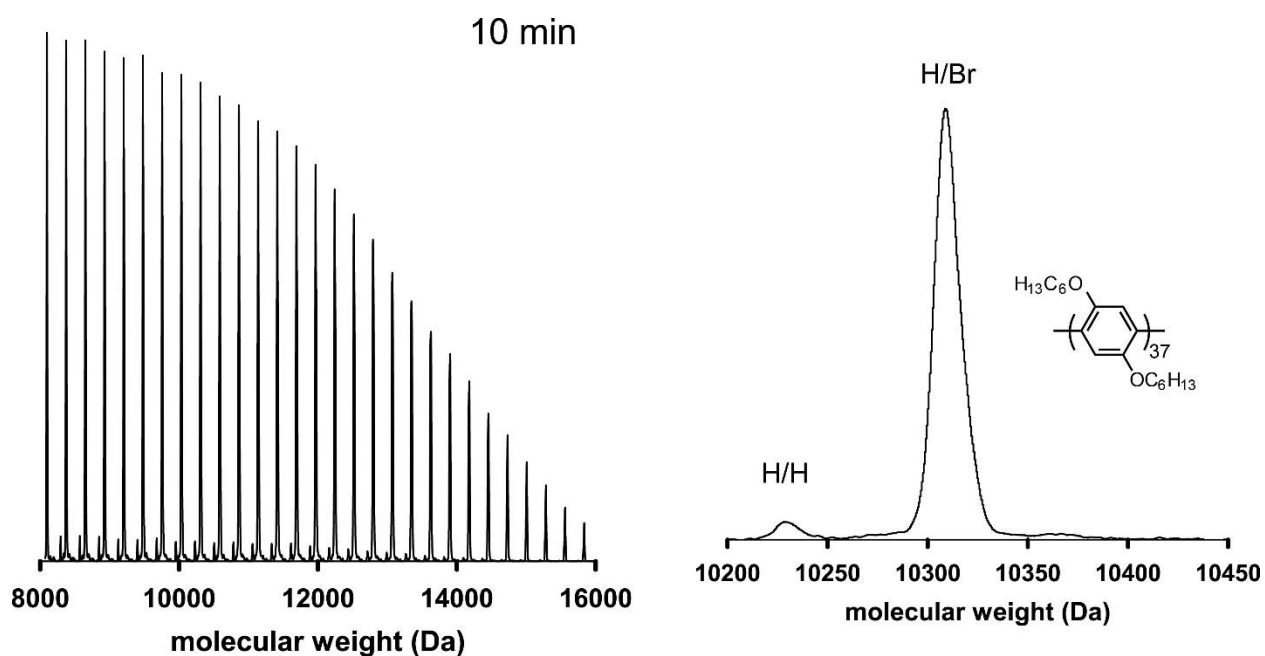
Time after preinitiation (min)	$M_n$ (kDa)	$\bar{D}$	Conversion of <b>2</b> (%)
1	17.8	1.37	53
10	19.3	1.35	65
90	18.6	1.30	58

**Table A3-3.** Molecular weight, dispersity, and conversion values for polymerizing **2** using **3c** as plotted in Figure A3-23.

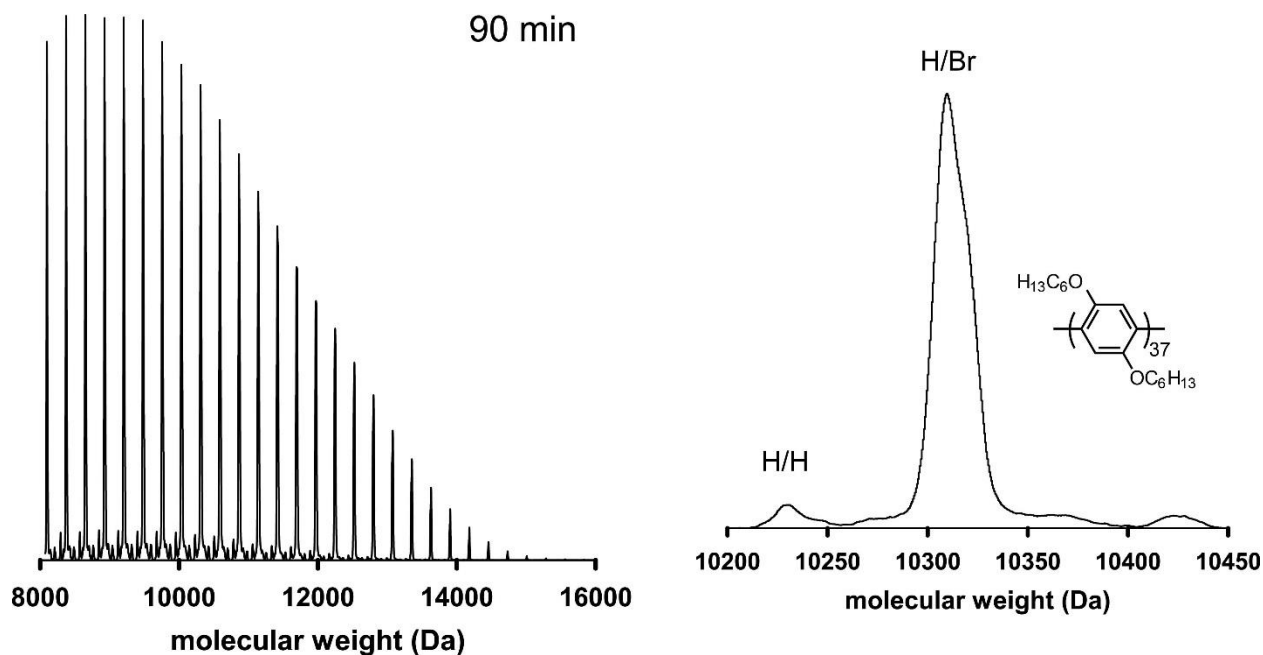




**Figure A3-24.** MALDI-TOF mass spectrum of **P2** produced by **3c** after pre-initiating for 1 min. Inset shows a zoomed in view at DP = 37.



**Figure A3-25.** MALDI-TOF mass spectrum of **P2** produced by **3c** after pre-initiating for 10 min. Inset shows a zoomed in view at DP = 37.

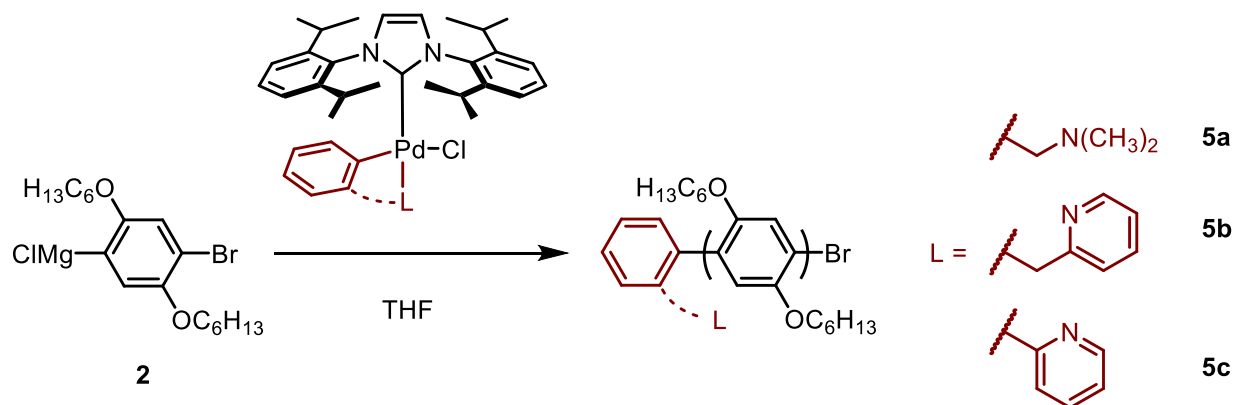


**Figure A3-26.** MALDI-TOF mass spectrum of **P2** produced by **3c** after pre-initiating for 90 min. Inset shows a zoomed in view at DP = 37.

Time after pre-initiation (min)	% End group	
	H/H	Br/H
1	7	91
10	4	96
90	4	92

**Table A3-4.** Percent end-groups for **P2** catalyzed by **3c** after pre-initiating with 2-chlorotoluene (10 equiv) and *p*-tolylmagnesium chloride for 1, 10, or 90 min as determined by MALDI-TOF MS and as plotted in Figure A3-24, Figure A3-25, and Figure A3-26.

## IX. Polymerizing 1 and 2 with precatalyst 5a–c



### Polymerizing 2 with 5a–c.

Precatalysts (~0.50 mL of a ~0.030 M solution in THF, 0.0015 mmol, 1.0 equiv) were added to a 10 mL Schlenk flask equipped with a stir bar and diluted with THF (~3 mL) to achieve a catalyst concentration of 0.0015 M during the polymerization. The flask was removed from the glovebox and placed under  $\text{N}_2$ .

Previously prepared **2** (1.0 mL of a 0.41 M solution in THF, 0.81 mmol, 50 equiv) was added to each precatalyst solution to initiate the polymerization. The reaction was quenched after 45 min by adding conc. HCl (~2 mL). The quenched reactions were extracted with  $\text{CHCl}_3$  (3 x 1 mL) with heating. The combined organic layers were then washed with  $\text{H}_2\text{O}$  (1 x 2 mL) and brine (1 x 2 mL). The solvent was then removed via rotary evaporation and the solids were re-dissolved with heating in THF (~10 mL). After cooling to rt,  $\text{MgSO}_4$  (~20 mg) was added and the mixture was filtered through a PTFE syringe filter (0.2  $\mu\text{m}$ ) and analyzed by GC and GPC.

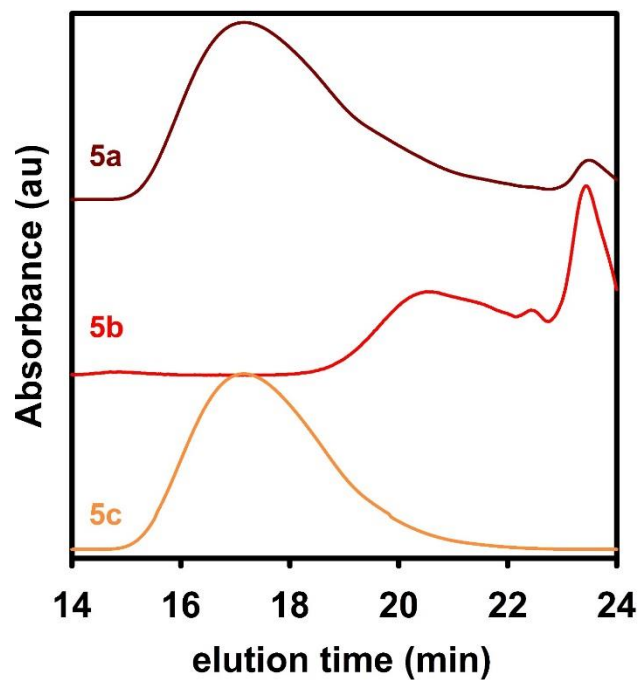
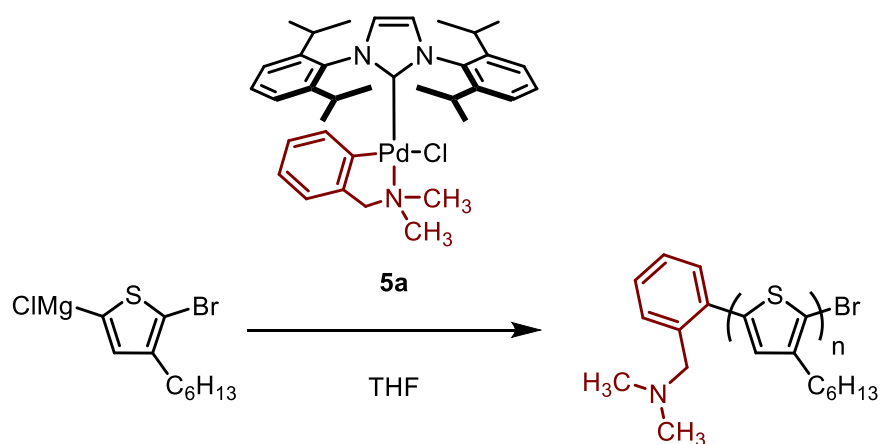


Figure A3-27. GPC chromatogram of P2 catalyzed by 5a (—), 5b (—), or 5c (—).

Catalyst	$M_n$ (kDa)	$\bar{D}$	Conversion of 2 (%)
5a	27.1	4.28	30
5b	1.4	2.58	11
5c	32.9	3.69	66

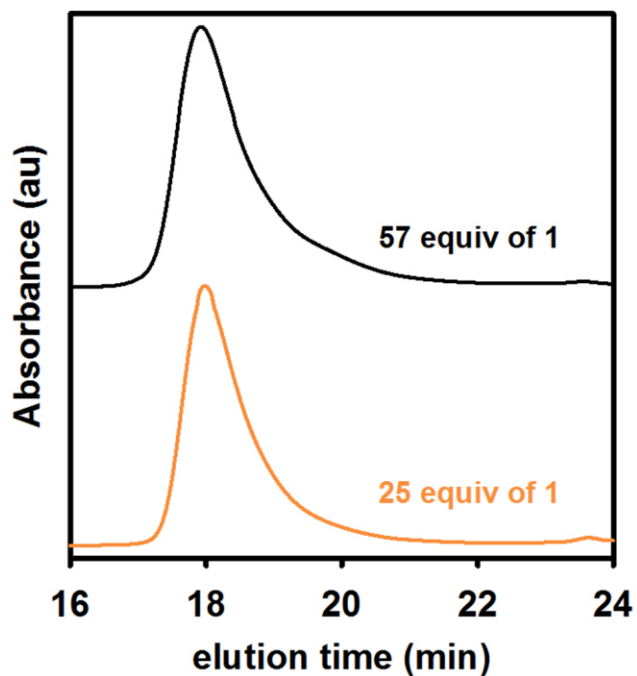
Table A3-5. Molecular weight, dispersity, and conversion values for polymerizing 2 using 5a, 5b, or 5c.



### Polymerizing **1** with **5a**.

**5a** (1.0 mL of a 0.0015 M solution in THF, 0.0015 mmol, 1.0 equiv) was added to 2 separate 25 mL Schlenk flasks equipped with a stir bar and diluted with THF (6.80 mL [*solution A*] or 8.0 mL [*solution B*]) to achieve a catalyst concentration of 0.0015 M during the polymerization. The flasks were removed from the glovebox and placed under N<sub>2</sub>.

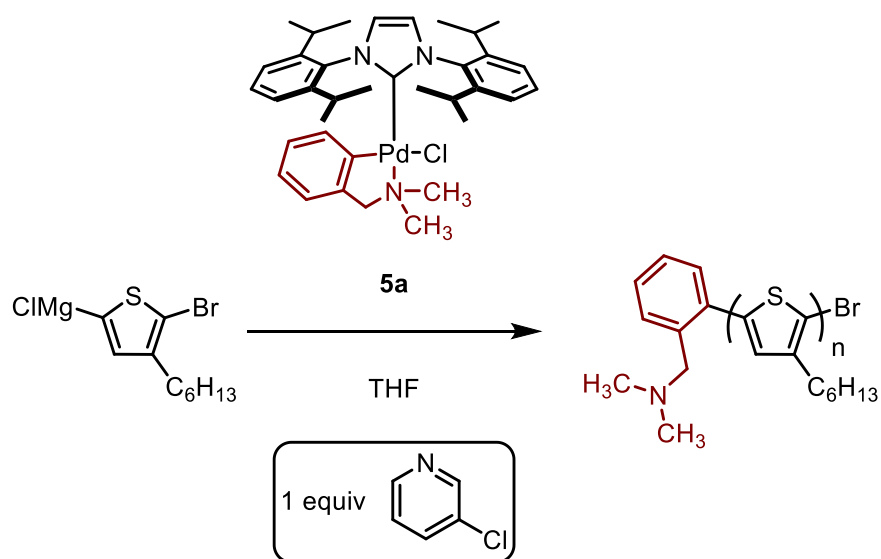
Previously prepared **1** (2.2 mL of a 0.40 M solution in THF, 0.085 mmol, 56 equiv) was added to *solution A* to initiate the polymerization. Separately, previously prepared **1** (0.93 mL of a 0.40 M solution in THF, 0.038 mmol, 25 equiv) was added to *solution B* to initiate the polymerization. The reactions were quenched after 45 min by adding conc. HCl (~2 mL). The quenched reactions were extracted with CHCl<sub>3</sub> (3 x 1 mL) with heating. The combined organic layers were then washed with H<sub>2</sub>O (1 x 2 mL) and brine (1 x 2 mL). The solvent was then removed via rotary evaporation and the solids were re-dissolved with heating in THF (~10 mL). After cooling to rt, MgSO<sub>4</sub> (~20 mg) was added and the mixture was filtered through a PTFE syringe filter (0.2 μm) and analyzed by GC and GPC.



**Figure A3-28.** GPC chromatogram of **P1** catalyzed by **5a** using 57 (—) or 25 (—) equiv of **1** relative to **5a**.

<b>Equiv of 1</b>	$M_n$ (kDa)	$\mathcal{D}$	<b>Conversion of 1 (%)</b>
57	23.6	1.73	92
25	26.5	1.49	93

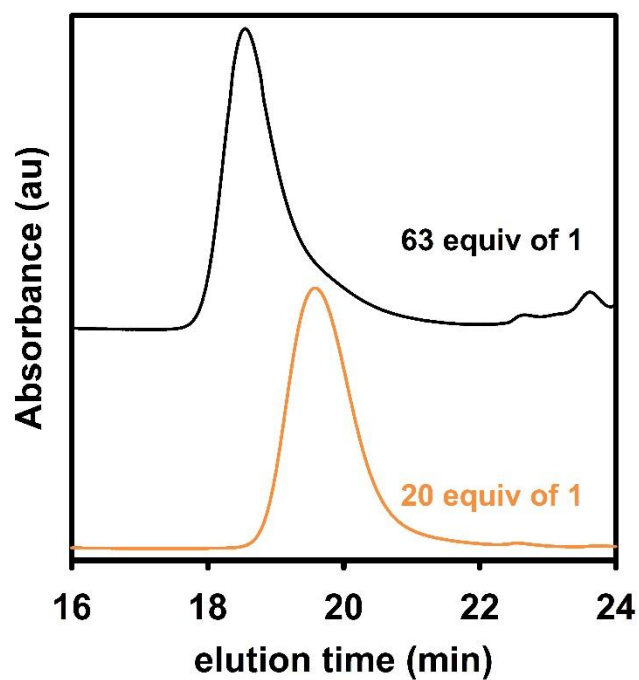
**Table A3-6.** Molecular weight, dispersity, and conversion values for polymerizing **1** using **5a** as plotted in Figure A3-28.



### Polymerizing **1** with **5a** and 3-chloropyridine.

**5a** (1.0 mL of a 0.0015 M solution in THF, 0.0015 mmol, 1.0 equiv) and 3-chloropyridine (0.33 mL of a 0.046 M solution in THF, 0.0015 mmol, 1.0 equiv) were each added to two separate 25 mL Schlenk flasks equipped with a stir bar and diluted with THF (6.80 mL [*solution A*] or 8.0 mL [*solution B*]) to achieve a catalyst concentration of 0.0015 M during the polymerization. The flasks were removed from the glovebox and placed under  $\text{N}_2$ .

Previously prepared **1** (2.3 mL of a 0.40 M solution in THF, 0.095 mmol, 63 equiv) was added to *solution A* to initiate the polymerization. Separately, previously prepared **1** (0.75 mL of a 0.40 M solution in THF, 0.030 mmol, 20 equiv) was added to *solution B* to initiate the polymerization. The reactions were quenched after 65 min by adding conc. HCl (~2 mL). The quenched reactions were extracted with  $\text{CHCl}_3$  (3 x 1 mL) with heating. The combined organic layers were then washed with  $\text{H}_2\text{O}$  (1 x 2 mL) and brine (1 x 2 mL). The solvent was then removed via rotary evaporation and the solids were re-dissolved with heating in THF (~10 mL). After cooling to rt,  $\text{MgSO}_4$  (~20 mg) was added and the mixture was filtered through a PTFE syringe filter (0.2  $\mu\text{m}$ ) and analyzed by GC and GPC.



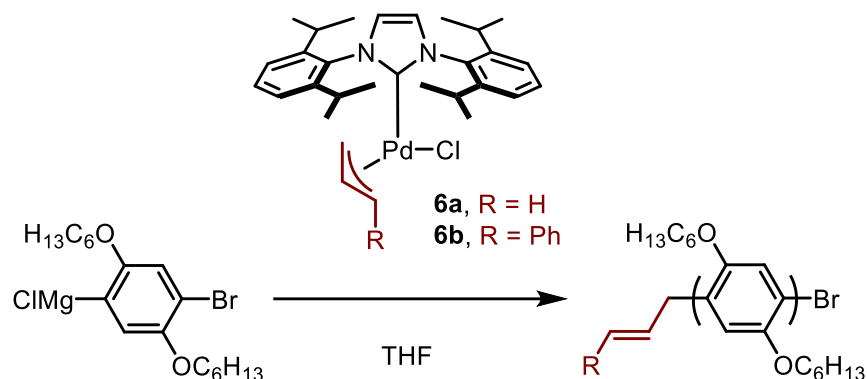
**Figure A3-29.** GPC chromatogram of **P1** catalyzed by **5a** with 1 equiv of 3-chloropyridine using 63 (—) or 20 (—) equiv of **1** relative to **5a**.

<b>Equiv of 1</b>	$M_n$ (kDa)	$\mathcal{D}$	<b>Conversion of 1 (%)</b>
63	17.7	1.36	88
20	9.7	1.20	72

**Table A3-7.** Molecular weight, dispersity, and conversion values for polymerizing **1** using **5a** as plotted in Figure A3-29.



## X. Polymerizing **2** with precatalyst **6a/6b**

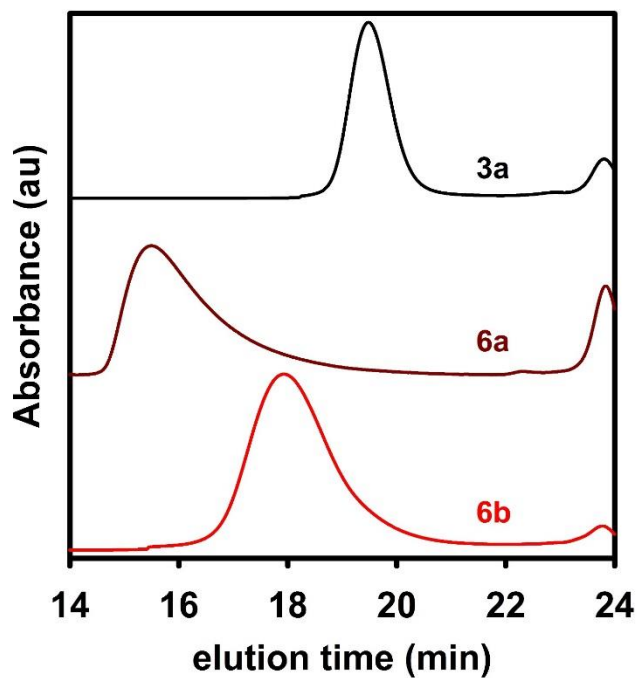


### Polymerizing **2** with **6a/6b**.

Catalyst **3a**<sup>a</sup>, **6a**, or **6b** (~0.20 mL of a ~0.0015 M solution in THF, 0.0030 mmol, 1.0 equiv) were added to a 10 mL Schlenk flask equipped with a stir bar and diluted with THF (~1.4 mL) to achieve a catalyst concentration of 0.0015 M during the polymerization. The flasks were removed from the glovebox and placed under N<sub>2</sub>.

Previously prepared **1** (0.20 mL of a 0.40 M solution in THF, 0.81 mmol, 54 equiv) was added to initiate the polymerization. The reaction was quenched after 1 h by adding conc. HCl (~2 mL). The quenched reactions were extracted with CHCl<sub>3</sub> (3 x 1 mL) with heating. The combined organic layers were then washed with H<sub>2</sub>O (1 x 2 mL) and brine (1 x 2 mL). The solvent was then removed via rotary evaporation and the solids were re-dissolved with heating in THF (~10 mL). After cooling to rt, MgSO<sub>4</sub> (~20 mg) was added and the mixture was filtered through a PTFE syringe filter (0.2 μm) and analyzed by GC and GPC.

<sup>a</sup> Polymerizing **2** with **3a** was performed as a reference.

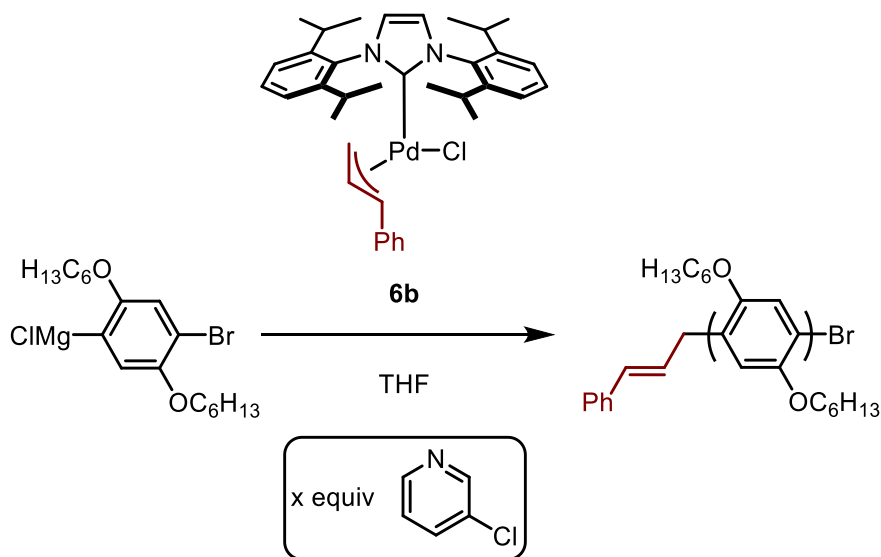


**Figure A3-30.** GPC chromatogram of **P2** catalyzed by **3a** (—), **6a** (—), or **6b** (—).

Catalyst	$M_n$ (kDa)	$\bar{D}$	Conversion of <b>2</b> (%)
<b>3a</b>	9.2	1.13	93
<b>6a</b>	129.3	2.66	55
<b>6b</b>	25.6	1.84	90

**Table A3-8.** Molecular weight, dispersity, and conversion values for polymerizing **2** using **3a**, **6a**, or **6b** as plotted in Figure A3-30.

## XI. Effect of 3-chloropyridine on polymerizing **2** with precatalyst **6b**



### Polymerizing **2** with **6b** and 3-chloropyridine (0–2 equiv).

**6b** (0.14 mL of a 0.00157 M solution in THF, 0.0015 mmol, 1.0 equiv) was added to 10 mL Schlenk flasks equipped with a stir bar, and 3-chloropyridine (0.13 M solution in THF, 0–2.0 equiv) was added in the amount specified below:

*Solution A*: 0 equiv 3-chloropyridine

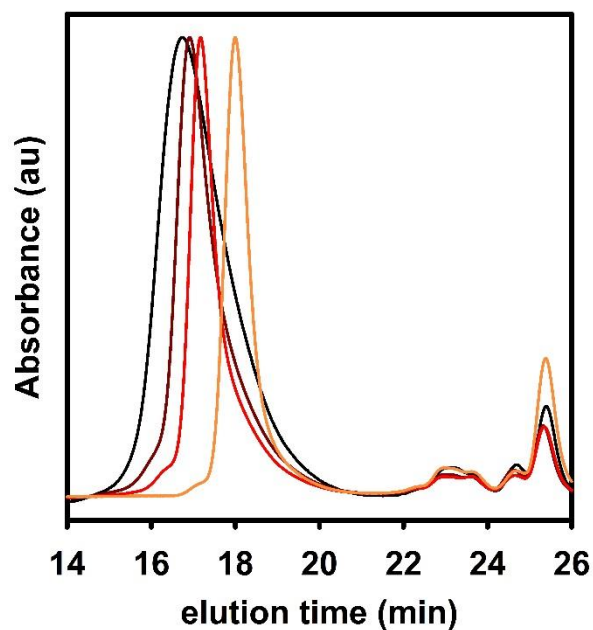
*Solution B*: 0.5 equiv 3-chloropyridine (0.0058 mL, 0.00075 mmol)

*Solution C*: 1.0 equiv 3-chloropyridine (0.012 mL, 0.0015 mmol)

*Solution D*: 2.0 equiv 3-chloropyridine (0.023 mL, 0.0030 mmol)

Each flask was diluted with THF (1.37 mL) to achieve a catalyst concentration of 0.00075 M during the polymerization. The flasks were removed from the glovebox and placed under  $N_2$ . Previously prepared **1** (0.48 mL of a 0.41 M solution in THF, 0.19 mmol, 130 equiv) was added to *solutions A–D* to initiate each polymerization. The reaction was quenched after 2 h by adding conc. HCl (~2 mL). The quenched reactions were extracted with  $CHCl_3$  (3 x 1 mL) with heating. The combined organic layers were then washed with  $H_2O$  (1 x 2 mL) and brine (1 x 2 mL). The solvent was then removed via rotary evaporation and the solids were re-dissolved with heating in

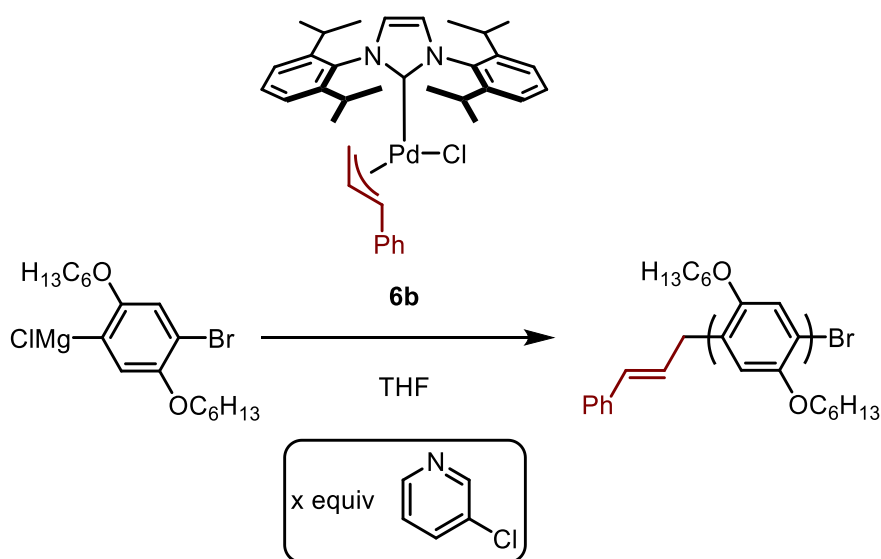
THF (~10 mL). After cooling to rt,  $\text{MgSO}_4$  (~20 mg) was added and the mixture was filtered through a PTFE syringe filter (0.2  $\mu\text{m}$ ) and analyzed by GC and GPC.



**Figure A3-31.** GPC chromatogram of **P2** produced by **6b** with 0 equiv (—), 0.5 equiv (—), 1 equiv (—), or 2 equiv (—) of 3-chloropyridine (relative to catalyst).

<b>Equiv of 3-chloropyridine</b>	<b><math>M_n</math> (kDa)</b>	<b><math>\mathcal{D}</math></b>	<b>Conversion of <b>2</b> (%)</b>
0	59.6	2.19	88
0.5	59.5	1.81	84
1.0	54.5	1.60	77
2.0	33.4	1.25	48

**Table A3-9.** Molecular weight, dispersity, and conversion of **2** for **P2** produced by **6b** with different amounts of 3-chloropyridine (relative to catalyst) as plotted in Figure A3-31.



### Polymerizing **2** with **6b** and 3-chloropyridine (0.5–1.1 equiv).

**6b** (0.22 mL of a 0.0135 M solution in THF, 0.0030 mmol, 1.0 equiv) was added to 10 mL Schlenk flasks equipped with a stir bar, and 3-chloropyridine (0.22 M solution in THF, 0.5–1.1 equiv) was added in the amount specified below:

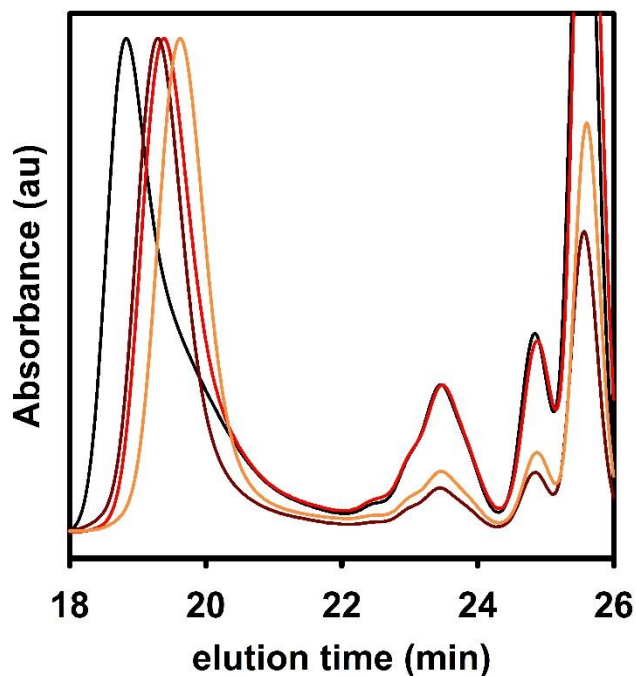
*Solution A*: 0.5 equiv 3-chloropyridine (0.0070 mL, 0.0015 mmol)

*Solution B*: 0.9 equiv 3-chloropyridine (0.0013 mL, 0.0027 mmol)

*Solution C*: 1.0 equiv 3-chloropyridine (0.0014 mL, 0.0030 mmol)

*Solution D*: 1.1 equiv 3-chloropyridine (0.0015 mL, 0.0033 mmol)

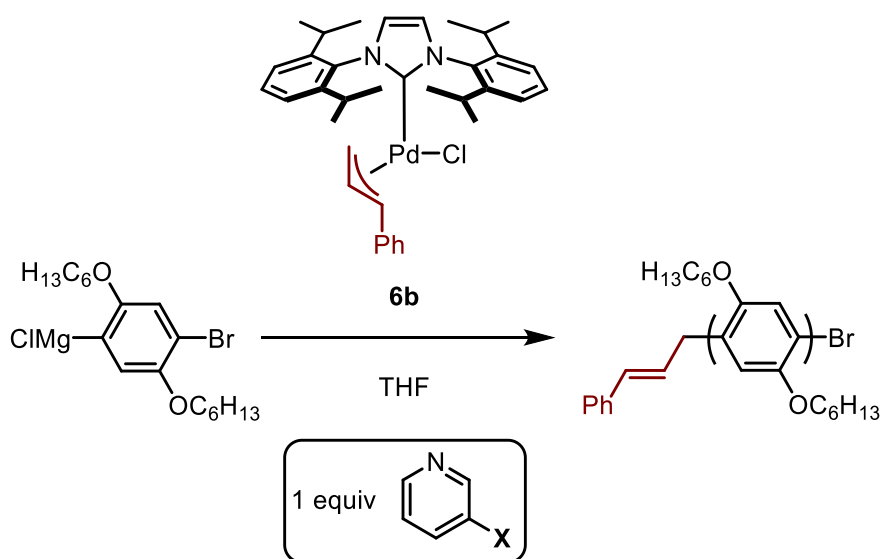
Each flask was diluted with THF (1.16 mL) to achieve a catalyst concentration of 0.0015 M during the polymerization. The flasks were removed from the glovebox and placed under  $\text{N}_2$ . Previously prepared **1** (0.48 mL of a 0.41 M solution in THF, 0.19 mmol, 130 equiv) was added to *solutions A–D* to initiate each polymerization. The reaction was quenched after 30 min by adding conc. HCl (~2 mL). The quenched reactions were extracted with  $\text{CHCl}_3$  (3 x 1 mL) with heating. The combined organic layers were then washed with  $\text{H}_2\text{O}$  (1 x 2 mL) and brine (1 x 2 mL). The solvent was then removed via rotary evaporation and the solids were re-dissolved with heating in THF (~10 mL). After cooling to rt,  $\text{MgSO}_4$  (~20 mg) was added and the mixture was filtered through a PTFE syringe filter (0.2  $\mu\text{m}$ ) and analyzed by GC and GPC.



**Figure A3-32.** GPC chromatogram of **P2** produced by **6b** with 0.5 equiv (—), 0.9 equiv (—), 1 equiv (—), or 1.1 equiv (—) of 3-chloropyridine (relative to catalyst).

<b>Equiv of 3-chloropyridine</b>	<b><math>M_n</math> (kDa)</b>	<b><math>\mathcal{D}</math></b>	<b>Conversion of <b>2</b> (%)</b>
0.5	11.34	1.42	43
0.9	10.6	1.23	32
1.0	9.1	1.20	31
1.1	8.5	1.15	25

**Table A3-10.** Molecular weight, dispersity, and conversion of **2** for **P2** produced by **6b** with different amounts of 3-chloropyridine (relative to catalyst) as plotted in Figure A3-32.



### Polymerizing **2** with **6b** and different pyridines.

**6b** (0.22 mL of a 0.0135 M solution in THF, 0.0030 mmol, 1.0 equiv) was added to 10 mL Schlenk flasks equipped with a stir bar, and various pyridines (0.0033 mmol, 1.05 equiv) were added in the amount specified below:

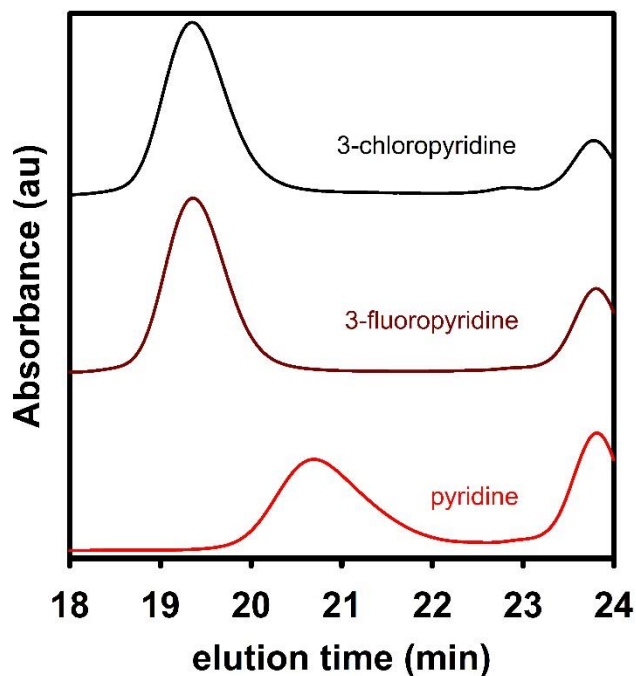
*Solution A:* 1.05 equiv 3-chloropyridine (0.0033 mL of a 0.93 M solution in THF)

*Solution B:* 1.05 equiv 3-fluoropyridine (0.0033 mL of a 0.95 M solution in THF)

*Solution C:* 1.05 equiv pyridine (0.0033 mL of a 0.94 M solution in THF)

Each flask was diluted with THF (1.3 mL) to achieve a catalyst concentration of 0.0015 M during the polymerization. The flasks were removed from the glovebox and placed under  $\text{N}_2$ . Previously prepared **1** (0.50 mL of a 0.41 M solution in THF, 0.21 mmol, 66 equiv) was added to *solutions A–C* to initiate each polymerization. The reaction was quenched after 65 min by adding conc. HCl (~2 mL). The quenched reactions were extracted with  $\text{CHCl}_3$  (3 x 1 mL) with heating. The combined organic layers were then washed with  $\text{H}_2\text{O}$  (1 x 2 mL) and brine (1 x 2 mL). The solvent was then removed via rotary evaporation and the solids were re-dissolved with heating in THF (~10 mL). After cooling to rt,  $\text{MgSO}_4$  (~20 mg) was added and the mixture was filtered through a PTFE syringe filter (0.2  $\mu\text{m}$ ) and analyzed by GC and GPC.



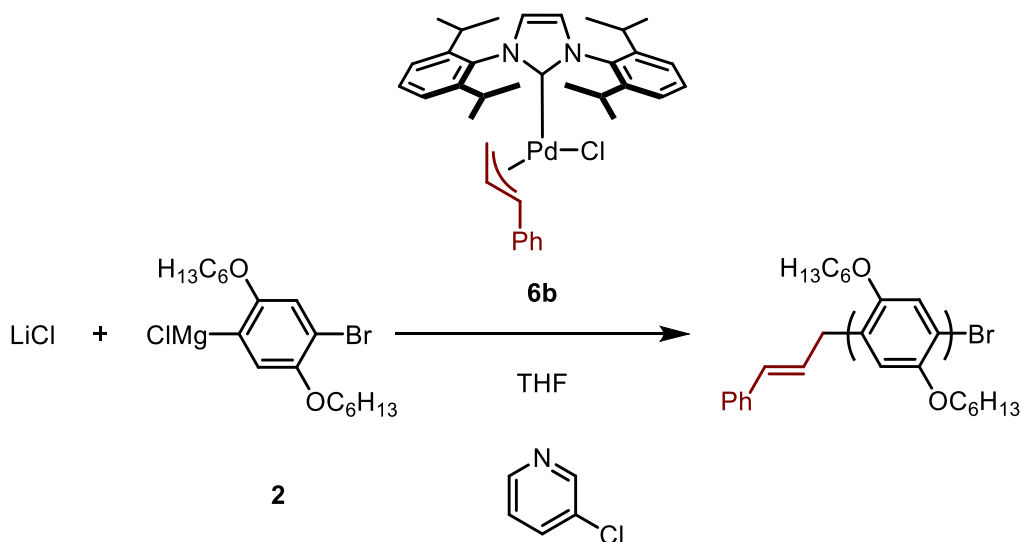


**Figure A3-33.** GPC chromatogram of **P2** produced by **6b** with 1.05 equiv of 3-chloropyridine (—), 3-fluoropyridine (—), or pyridine (—) (relative to catalyst).

<b>Pyridine</b>	<b><math>M_n</math> (kDa)</b>	<b><math>\mathcal{D}</math></b>	<b>Conversion of <b>2</b> (%)</b>
3-chloropyridine	11.3	1.14	79
3-fluoropyridine	10.4	1.14	76
pyridine	3.2	1.14	63

**Table A3-11.** Molecular weight, dispersity, and conversion of **2** for **P2** produced by **6b** with 1.05 equiv of 3-chloropyridine, 3-fluoropyridine, or pyridine as plotted in Figure A3-33.

## XII. Effect of LiCl on polymerizing **2** with precatalyst **6b**



### Polymerizing **2** with precatalyst **6b** and added LiCl.

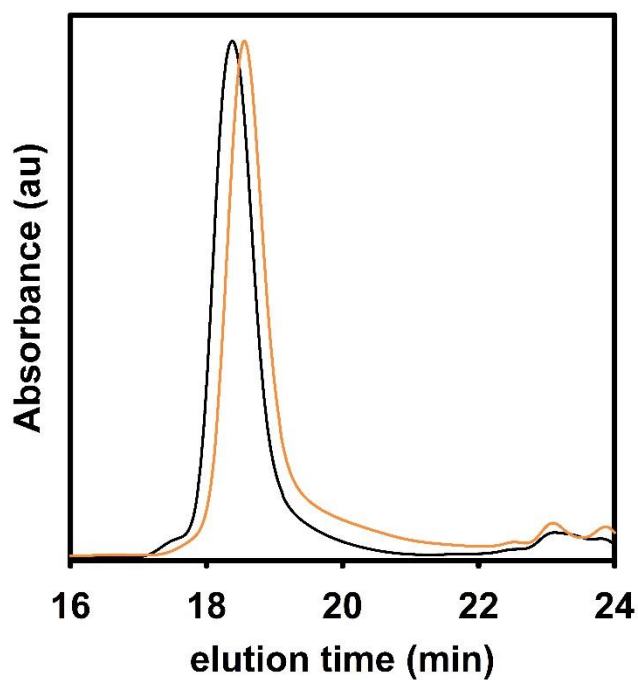
*Solution A.* In a glovebox, **S2** (0.45 g, 1.0 mmol, 1.0 equiv) was added to a 20 mL vial equipped with a stir bar. A small amount of C<sub>22</sub>H<sub>46</sub> (~25 mg) was added and the mixture was diluted with THF (1.1 mL). Next, iPrMgCl (0.47 mL of a 2 M solution in THF, 0.95 mmol, 0.90 equiv) was added and the solution was stirred for 26 h before titrating (0.41 M, see pg. 3). The solution was added to a 25 mL Schlenk tube, sealed with a PTFE stopcock and rubber septum, and then removed from the glovebox and placed under N<sub>2</sub>.

*Solution B.* In a glovebox, **S2** (0.90 g, 2.1 mmol, 1.0 equiv) and LiCl (0.087 g, 2.0 mmol, 1.0 equiv) was added to a 20 mL vial equipped with a stir bar. A small amount of C<sub>22</sub>H<sub>46</sub> (~25 mg) was added and the mixture was diluted with THF (1.1 mL). Next, iPrMgCl (0.94 mL of a 2 M solution in THF, 1.9 mmol, 0.90 equiv) was added and the solution was stirred for 26 h before titrating (0.40 M, see pg. 3). The solution was added to a 25 mL Schlenk tube, sealed with a PTFE stopcock and rubber septum, and then removed from the glovebox and placed under N<sub>2</sub>.

**6b** (1.0 mL of a 0.0135 M solution in THF, 0.014 mmol, 1.0 equiv) and 3-chloropyridine (0.014 mL of a 0.93 M solution in THF, 0.014 mmol, 1.0 equiv) were added to 25 mL Schlenk flasks equipped with a stir bar. Each flask was diluted with THF (6.8 mL) to achieve a catalyst

concentration of 0.0015 M during the polymerization. The flasks were removed from the glovebox and placed under N<sub>2</sub>.

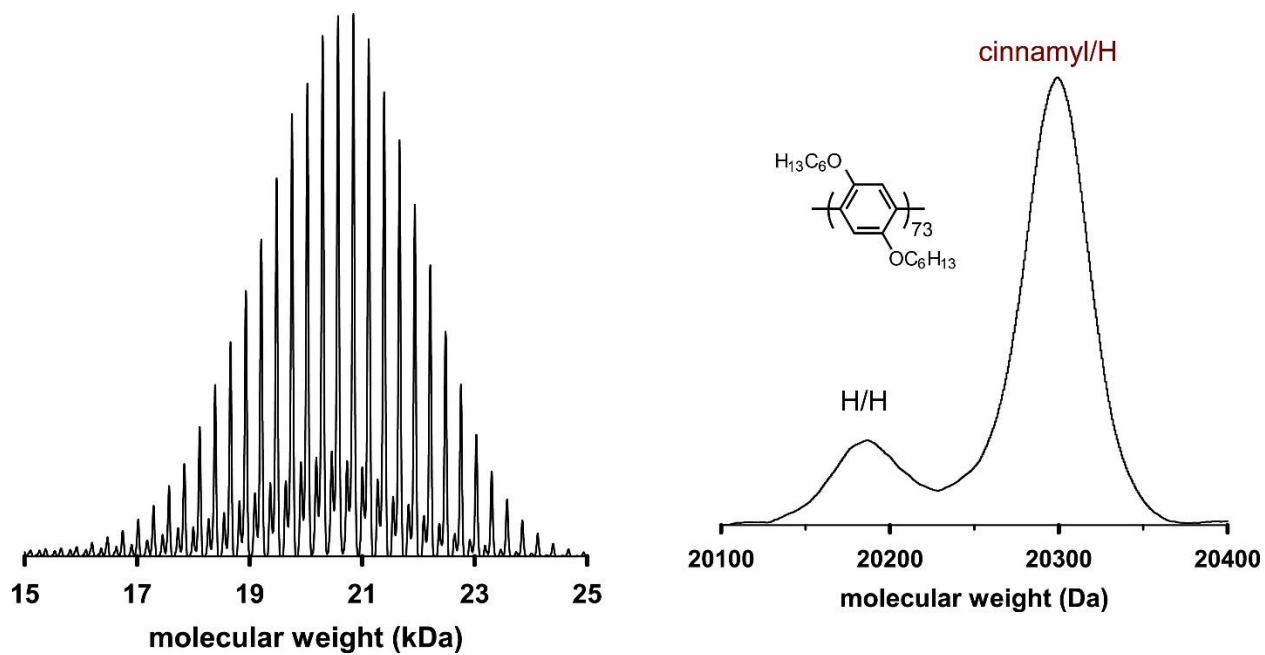
*Solution A* (2.15 mL of a 0.41 M solution in THF, 0.88 mmol, 65 equiv) was added to a 25 mL Schlenk flask with catalyst to initiate *polymerization A*, and *solution B* (2.2 mL of a 0.40 M solution in THF, 0.88 mmol, 65 equiv) was added to a 25 mL Schlenk flask with catalyst to initiate *polymerization B*. The reactions were quenched after 95 min by adding conc. HCl (~2 mL). The quenched reactions were extracted with CHCl<sub>3</sub> (3 x 1 mL) with heating. The combined organic layers were then washed with H<sub>2</sub>O (1 x 2 mL) and brine (1 x 2 mL). The solvent was then removed via rotary evaporation and the solids were re-dissolved with heating in THF (~10 mL). After cooling to rt, MgSO<sub>4</sub> (~20 mg) was added and the mixture was filtered through a PTFE syringe filter (0.2 μm) and analyzed by GC and GPC.



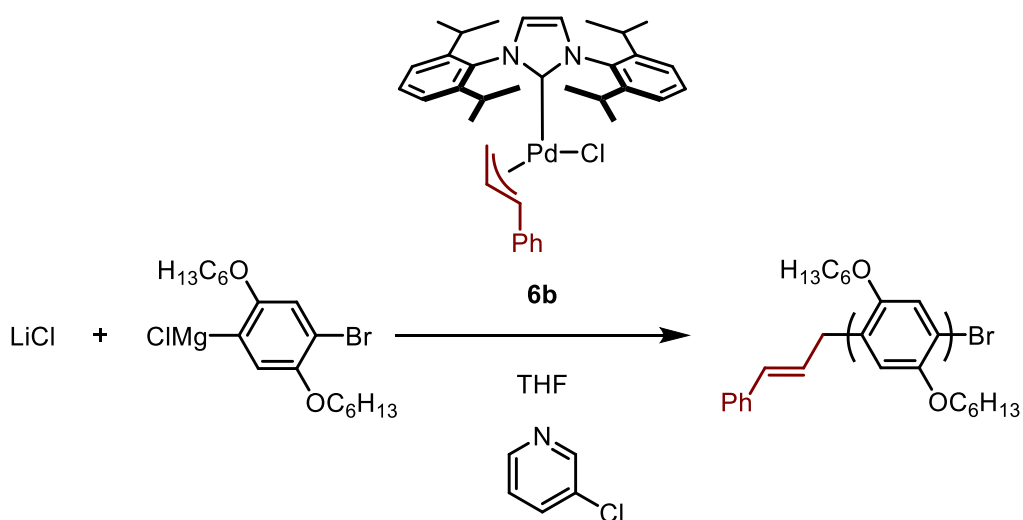
**Figure A3-34.** GPC chromatogram of **P2** produced by **6b** with 1.0 equiv LiCl (—) or without LiCl (—).

Equiv LiCl <sup>a</sup>	$M_n$ (kDa)	$\mathcal{D}$	Conversion of <b>2</b> (%)
0	23.5	1.19	53
1.0	16.8	1.32	54

**Table A3-12.** Molecular weight, dispersity, and conversion of **2** for **P2** produced by **6b** with or without added LiCl as plotted in Figure A3-34. <sup>a</sup> Equiv LiCl is relative to iPrMgCl used to generate **2**.



**Figure A3-35.** MALDI-TOF mass spectrum of **P2** produced by **6b** with 1 equiv of 3-chloropyridine. Inset shows a zoomed in view at DP = 73 with cinnamyl/H (83% area ratio) and H/H (17% area ratio) end-groups.



### Oligomerizing **2** with added $\text{LiCl}$ using **6b**.

In a glovebox, **S2** (0.25 g, 0.57 mmol, 1.0 equiv) was added to a 4 mL vial equipped with a stir bar. A small amount of  $\text{C}_{22}\text{H}_{46}$  (~15 mg) was added and the mixture was diluted with THF (0.6 mL). Next,  $\text{iPrMgCl}$  (0.26 mL of a 2 M solution in THF, 0.52 mmol, 0.90 equiv) was added and the solution was stirred for 16 h before titrating (0.43 M, see pg. 3). The remaining solution was divided into four separate 10 mL Schlenk flasks and the following solutions were added.

*oligomerization A*: 18 equiv  $\text{LiCl}$  (0.18 mL of a 0.3 M solution in THF, 0.054 mmol, 18.0 equiv) and THF (1.42 mL).

*oligomerization B*: 12 equiv  $\text{LiCl}$  (0.12 mL of a 0.3 M solution in THF, 0.036 mmol, 18.0 equiv) and THF (1.48 mL).

*oligomerization C*: 6 equiv  $\text{LiCl}$  (0.06 mL of a 0.3 M solution in THF, 0.018 mmol, 18.0 equiv) and THF (1.54 mL).

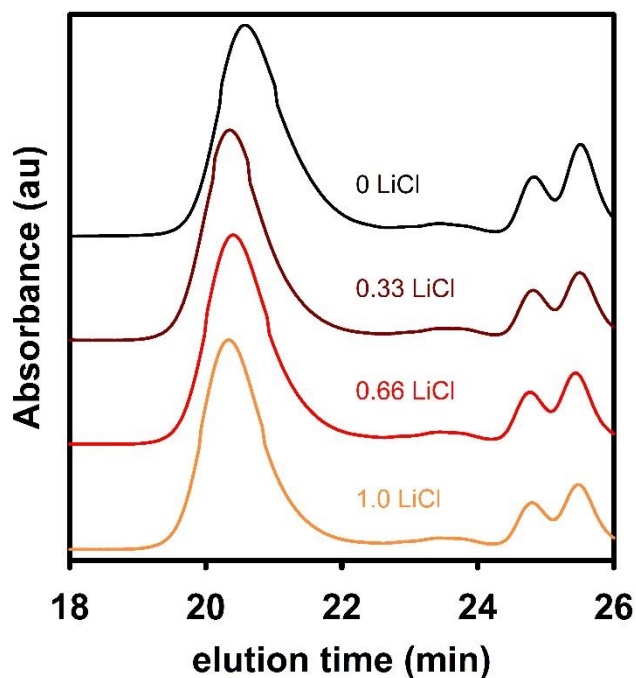
*oligomerization D*: THF (1.60 mL).

The Schlenk flasks were sealed with rubber septum, and then removed from the glovebox and placed under  $\text{N}_2$ .

**6b** (1.3 mL of a 0.0126 M solution in THF, 0.017 mmol, 1.0 equiv) and 3-chloropyridine (0.19 mL of a 0.093 M solution in THF, 0.018 mmol, 1.1 equiv) were added to a 25 mL Schlenk tube. The flasks were removed from the glovebox and placed under N<sub>2</sub>.

Precatalyst solution (0.24 mL, 0.0030 mmol, 1.0 equiv) was added to each 10 mL Schlenk flask to initiate *oligomerizations A-D*. The reactions were quenched after 60 min by adding conc. HCl (~2 mL). The quenched reactions were extracted with CHCl<sub>3</sub> (3 x 1 mL) with heating. The combined organic layers were then washed with H<sub>2</sub>O (1 x 2 mL) and brine (1 x 2 mL). The solvent was then removed via rotary evaporation and the solids were re-dissolved with heating in THF (~10 mL). After cooling to rt, MgSO<sub>4</sub> (~20 mg) was added and the mixture was filtered through a PTFE syringe filter (0.2 μm). A small portion was removed for GC and GPC analysis, and the remaining liquid was removed using a rotary evaporator to yield a tan solid. The solid was dissolved in minimal CHCl<sub>3</sub> (~0.2 mL), and then precipitated into MeOH (10 mL) in a centrifuge tube and centrifuged at 4500 rpm for 30 min. The supernatant was decanted and the solid polymer was dried under high vacuum for 4 h.

The solids (~2 mg) were dissolved in CDCl<sub>3</sub> (2 mL) and analyzed by <sup>1</sup>H NMR spectroscopy. Next, the NMR solutions were filtered through a pipette column (basic, acidic, then neutral alumina with a KimWipe plug) and rinsed with CHCl<sub>3</sub> (~0.5 mL). The resultant polymer solution (2.5 μL) was mixed with DCTB matrix (2.5 μL of a 0.1 M solution in CHCl<sub>3</sub>) in an Eppendorf tube. The polymer/matrix solution (~1.5 μL) was spotted onto the MALDI 96-well target, and the remaining solution in the Eppendorf tube was diluted five-fold with additional DCTB matrix (2.5 μL of a 0.1 M solution in CHCl<sub>3</sub>). The diluted sample was spotted onto the MALDI target in the same manner, and further five-fold dilutions (with DCTB matrix solution) were performed and spotted to yield four spots for each polymer sample.

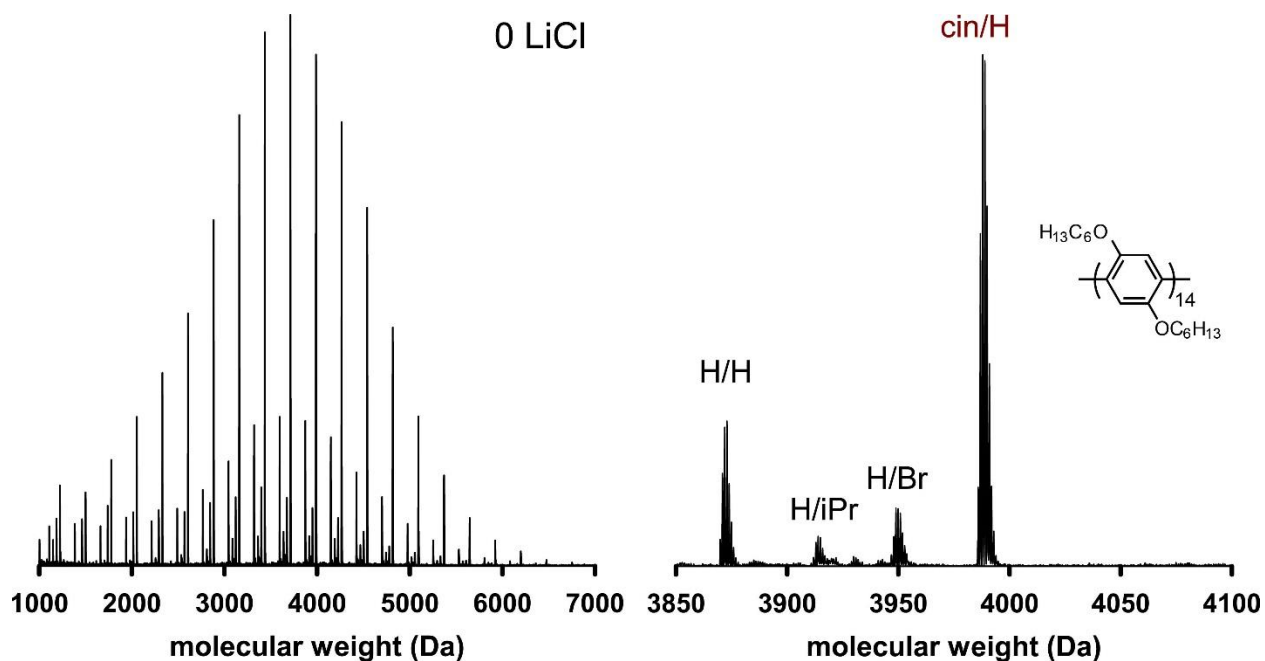


**Figure A3-36.** GPC chromatogram of **P2** produced by **6b** with 0 equiv LiCl (—), 0.33 equiv LiCl (—), 0.66 equiv LiCl (—), or 1 equiv LiCl (—).

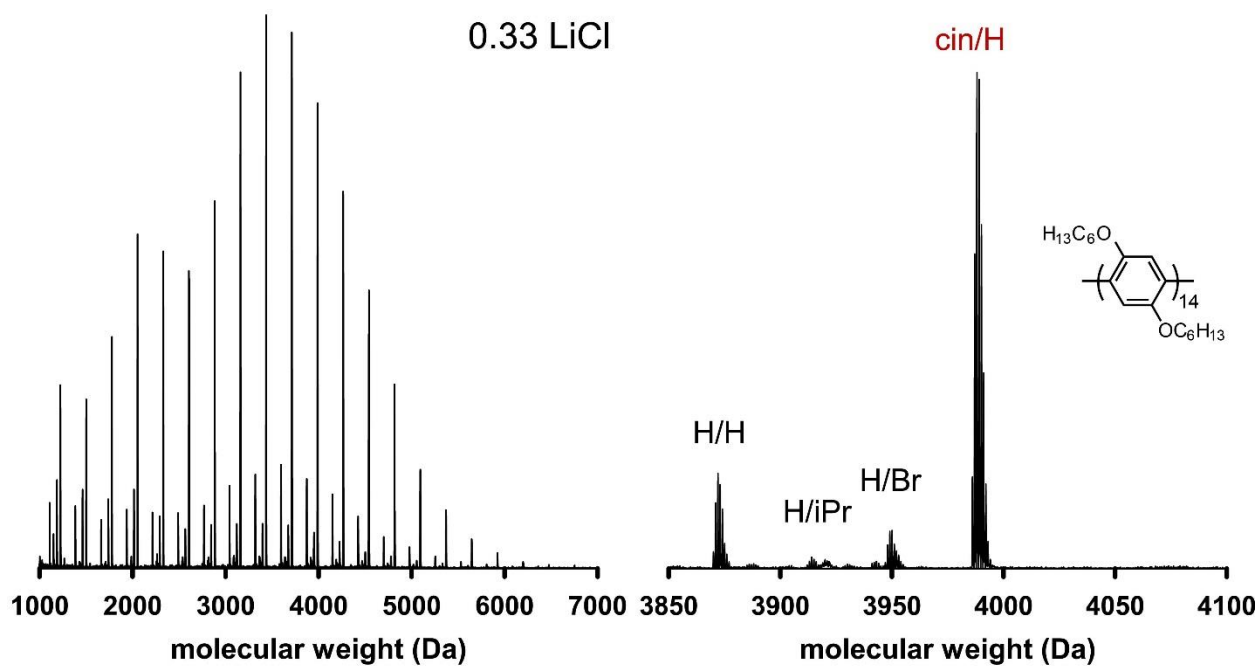
Equiv LiCl <sup>a</sup>	$M_n$ (kDa)	$\mathcal{D}$	Conversion of <b>2</b> (%)
0	3.7	1.16	55
0.33	4.5	1.17	54
0.66	4.3	1.16	54
1.0	4.6	1.16	46

**Table A3-13.** Molecular weight, dispersity, and conversion of **2** for **P2** produced by **6b** with or without added LiCl as plotted in Figure A3-36. <sup>a</sup> Equiv LiCl is relative to *i*PrMgCl used to generate **2**.

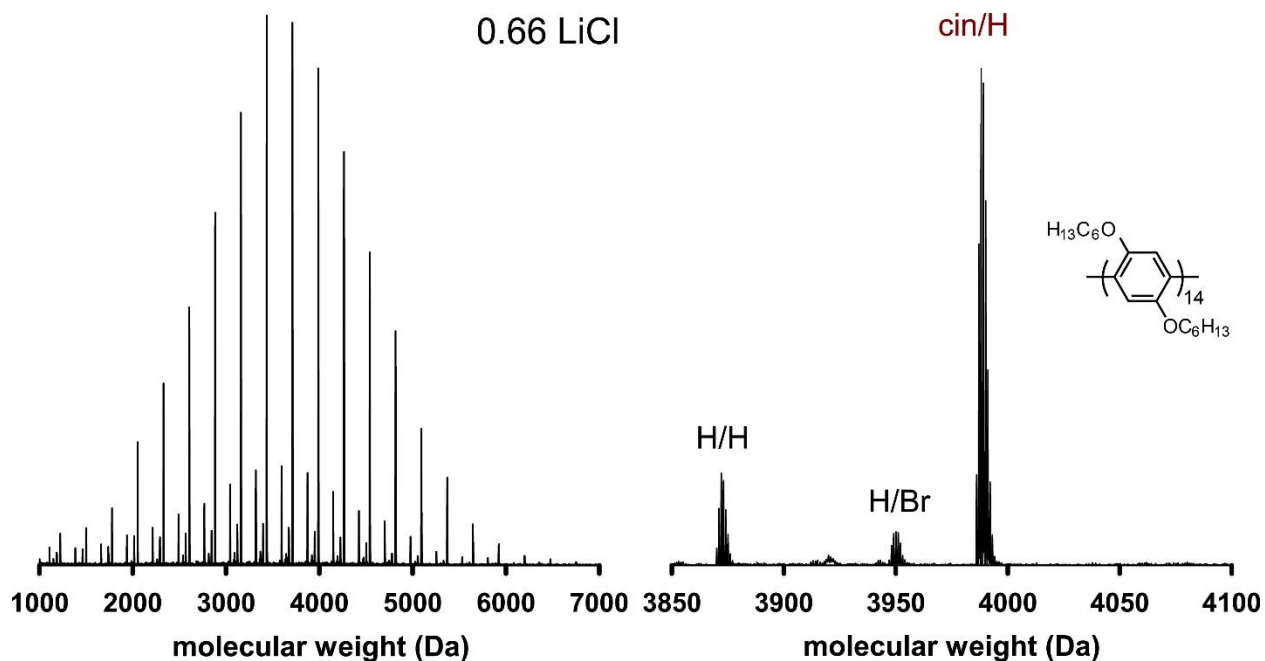




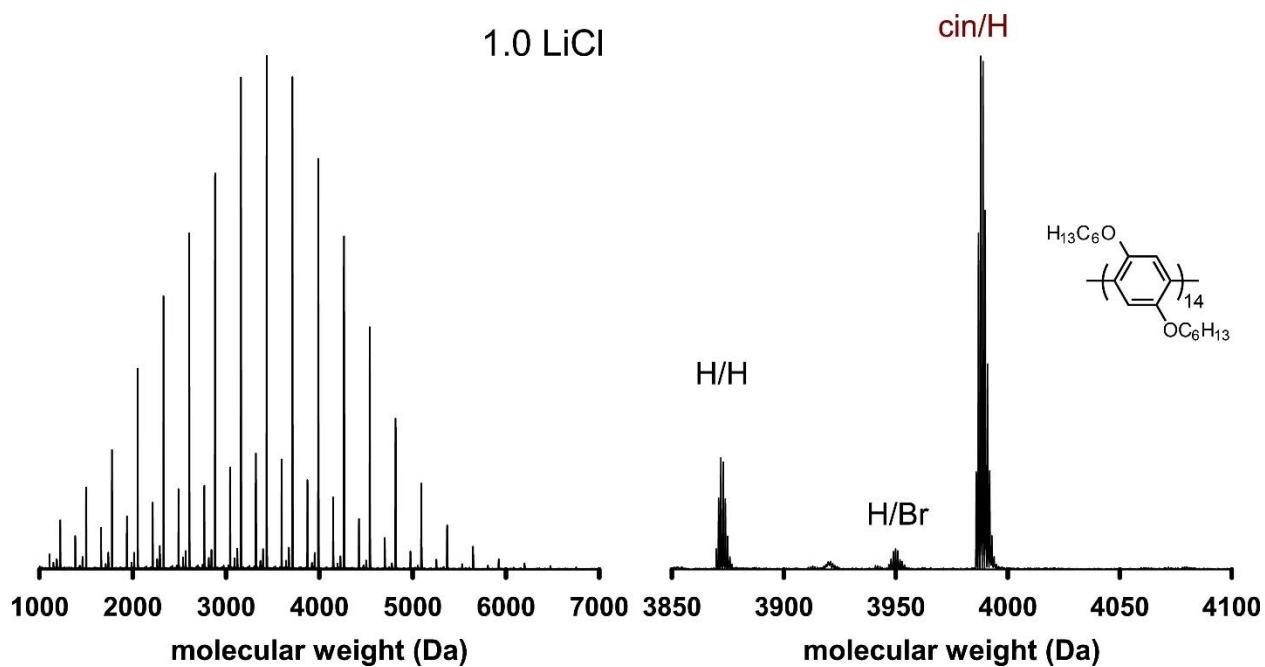
**Figure A3-37.** MALDI-TOF mass spectrum of **P2** produced by **6b** without LiCl. Inset shows a zoomed in view at DP = 14.



**Figure A3-38.** MALDI-TOF mass spectrum of **P2** produced by **6b** with 0.33 equiv LiCl (relative to *i*PrMgCl used to generate **2**). Inset shows a zoomed in view at DP = 14.



**Figure A3-39.** MALDI-TOF mass spectrum of **P2** produced by **6b** with 0.66 equiv LiCl (relative to *i*PrMgCl used to generate **2**). Inset shows a zoomed in view at DP = 14.



**Figure A3-40.** MALDI-TOF mass spectrum of **P2** produced by **6b** with 1.0 equiv LiCl (relative to *i*PrMgCl used to generate **2**). Inset shows a zoomed in view at DP = 14.

Equiv LiCl <sup>a</sup>	% End group			
	H/H	iPr/H	Br/H	Cin/H
0	17	2	4	77
0.33	15	1	5	77
0.66	14	2	7	81
1.0	16	3	14	67

**Table A3-14.** Percent end-groups of **P2** from polymerizing **2** with **6b** and added LiCl as determined by MALDI-TOF MS as plotted in Figure A3-37, Figure A3-38, Figure A3-39, and Figure A3-40.<sup>a</sup> Equiv LiCl is relative to iPrMgCl used to generate **2**.

### XIII. References

- (1) Lanni, E. L.; McNeil, A. J. Mechanistic Studies on Ni(dppe)Cl<sub>2</sub>-Catalyzed Chain-Growth Polymerizations: Evidence for Rate-Determining Reductive Elimination. *J. Am. Chem. Soc.* **2009**, *131*, 16573–16579.
- (2) Locke, J. R.; McNeil, A. J. Syntheses of Gradient  $\pi$ -Conjugated Copolymers of Thiophene. *Macromolecules* **2010**, *43*, 8709–8710.
- (3) Tang, P.; Wang, W.; Ritter, T. Deoxyfluorination of Phenols. *J. Am. Chem. Soc.* **2011**, *133*, 11482–11484.
- (4) O'Brien, C. J.; Kantchev, E. A. B.; Valente, C.; Hadei, N.; Chass, G. A.; Lough, A.; Hopkinson, A. C.; Organ, M. G. Easily Prepared Air- and Moisture-Stable Pd–NHC (NHC=N-Heterocyclic Carbene) Complexes: A Reliable, User-Friendly, Highly Active Palladium Precatalyst for the Suzuki–Miyaura Reaction. *Chem. Eur. J.* **2006**, *12*, 4743–4748.
- (5) Ying, J. Y.; Kantchev, E. A. B. N-Heterocyclic Carbene Metallacycle Catalysts and Methods. WO2008156451A1, 2008.
- (6) Song, Y.-J.; Jung, I. G.; Lee, H.; Lee, Y. T.; Chung, Y. K.; Jang, H.-Y. Cationic NHC–Pd (NHC=N-Heterocyclic Carbene) Complex-Catalyzed Cycloisomerization of Dienes. *Tetrahedron Lett.* **2007**, *48*, 6142–6146.
- (7) Love, B. E.; Jones, E. G. The Use of Salicylaldehyde Phenylhydrazone as an Indicator for the Titration of Organometallic Reagents. *J. Org. Chem.* **1999**, *64*, 3755–3756.
- (8) Fantasia, S.; Nolan, S. P. A General Synthetic Route to Mixed NHC-Phosphane Palladium(0) Complexes (NHC=N-Heterocyclic Carbene). *Chem. Eur. J.* **2008**, *14*, 6987–6993.
- (9) Marion, N.; Navarro, O.; Mei, J.; Stevens, E. D.; Scott, N. M.; Nolan, S. P. Modified (NHC)Pd(allyl)Cl (NHC = N-Heterocyclic Carbene) Complexes for Room-Temperature Suzuki–Miyaura and Buchwald–Hartwig Reactions. *J. Am. Chem. Soc.* **2006**, *128*, 4101–4111.
- (10) Marshall, W. J.; Grushin, V. V. Synthesis, Structure, and Reductive Elimination Reactions of the First ( $\sigma$ -Aryl)palladium Complex Stabilized by IPr N-Heterocyclic Carbene †. *Organometallics* **2003**, *22*, 1591–1593.